

---

# **Development of dual BET/HDAC inhibitors**

---

## **Dissertation**

zur Erlangung des Doktorgrades der Naturwissenschaften

vorgelegt beim Fachbereich 14

**der Johann Wolfgang Goethe-Universität in Frankfurt am Main**

von

**Tim Weiser**

aus Frankfurt Höchst

Frankfurt am Main 2021

D30

---

Tim Weiser

Geboren am 28.02.1989 in Frankfurt Höchst

Dekan: Prof. Dr. Clemens Glaubitz

Gutachter: Prof. Dr. Stefan Knapp

Prof. Dr. Eugen Proschak

Datum der Disputation: 13.04.2022, 14 Uhr

*If at first you don't succeed, try, try, try, try, try again.*

*Jack O'Neill*



# Content

List of abbreviations .....	II
List of figures.....	IV
List of tables .....	VI
List of schemes .....	VII
1. Introduction .....	1
1.1. Epigenetics.....	2
1.2. Bromodomain and extra terminal motif (BET) .....	3
1.2.1. Inhibition of BET proteins.....	5
1.3. Histone deacetylases (HDACs).....	7
1.3.1. Inhibition of HDAC proteins.....	8
1.4. Simultaneous administration of two inhibitors .....	10
1.5. Multi-target drugs .....	13
2. Objective .....	15
3. Methods.....	19
3.1. Synthetic strategy of the first generation .....	19
3.1.1. Optimization of the synthetic route of <b>14</b> .....	28
3.1.2. Additional JQ1-adduct.....	31
3.2. Synthetic strategy of the second generation.....	32
3.3. Synthetic strategy of the third generation .....	42
3.4. Characterization of the final compounds .....	50
3.4.1. Differential scanning fluorimetry assay .....	50
3.4.2. Isothermal titration calorimetry .....	51
3.4.3. Fluorogenic HDAC assay.....	53
3.4.4. NanoBRET assay.....	53
3.4.5. X-ray crystallography .....	54
3.4.6. Immunoblot analysis.....	55
3.4.7. Reverse transcription polymerase chain reaction .....	55
3.4.8. CellTiter Glo cell viability assay .....	55
3.4.9. Cell cycle analysis .....	56
3.4.10. Gene Set Enrichment Analysis.....	56
4. Results and discussion.....	57
4.1. Dual BET/HDAC inhibitors of the first generation.....	57
4.1.1. Crystal structures .....	58
4.1.2. DSF results .....	58

4.1.3.	ITC results.....	60
4.1.4.	Fluorogenic HDAC assay results.....	60
4.1.5.	NanoBRET assay results.....	61
4.1.6.	Expression behavior of PDAC cells treated with <b>14</b> .....	63
4.1.7.	Growth and viability of PDAC cells treated with <b>14</b> .....	65
4.1.8.	Combination of gemcitabine and <b>14</b> .....	68
4.1.9.	Transcriptomic profiling.....	71
4.1.10.	NUT midline carcinoma cells treated with <b>14</b> .....	75
4.2.	Dual BET/HDAC inhibitors of the second generation.....	77
4.2.1.	DSF results.....	78
4.2.2.	Fluorogenic HDAC and nanoBRET assay results.....	79
4.3.	Dual BET/HDAC inhibitors of the third generation.....	81
4.3.1.	DSF results.....	82
4.3.2.	Fluorogenic HDAC assay results.....	83
5.	Summary.....	85
6.	Zusammenfassung.....	90
7.	Experimental section.....	95
7.1.	General procedures.....	95
7.2.	Syntheses.....	96
8.	References.....	167
9.	Supplementary Information.....	174
9.1.	Analytical data.....	174
9.1.1.	Compound <b>14</b> .....	174
9.1.2.	Compound <b>15</b> .....	178
9.1.3.	Compound <b>16</b> .....	182
9.1.4.	Compound <b>62</b> .....	186
9.1.5.	Compound <b>18</b> .....	190
9.1.6.	Compound <b>19</b> .....	194
9.1.7.	Compound <b>20</b> .....	198
9.1.8.	Compound <b>21</b> .....	202
9.1.9.	Compound <b>22</b> .....	206
9.1.10.	Compound <b>25</b> .....	210
9.1.11.	Compound <b>26</b> .....	214
9.1.12.	Compound <b>27</b> .....	218
9.1.13.	Compound <b>28</b> .....	222
9.1.14.	Compound <b>29</b> .....	226

9.1.15.	Compound <b>30</b> .....	230
9.1.16.	Compound <b>31</b> .....	234
9.1.17.	Compound <b>32</b> .....	238
9.1.18.	Compound <b>33</b> .....	242
9.1.19.	Compound <b>37</b> .....	246





Whenever a figure, table or text is identical to a previous publication, it is stated explicitly in the thesis that copyright permission and/or co-author agreement has been obtained. The following parts of the thesis have been previously published:

Figures 4, 5, 9, 15, 30: Copyright obtained by Elsevier

Figures 7, 8, 14, 27: Copyright obtained by Springer Nature

Figure 13: Copyright obtained by AACR

Figure 16: Copyright obtained by ACS Publication

Figure 28, 29, 33: Not required to obtain permission to reuse this article, as it is an open access article distributed under the terms of the Creative Commons CC-BY license.

## List of abbreviations

ACN	Acetonitrile
Ac	Acetyl
AcOH	Acetic acid
ADP	Adenosine diphosphate
AML	acute myeloid leukemia
BD	binding domain
BET	bromodomain and extra terminal motif
Boc	<i>tert</i> -Butyloxycarbonyl protecting group
Boc <sub>2</sub> O	Di- <i>tert</i> -butyl dicarbonate
BRD	bromodomain containing protein
BRDi	BRD inhibitor
BRET	Bioluminescence Resonance Energy Transfer
CDK	cyclin-dependent kinase
CPB	CREB-binding protein
CREB	cAMP response element-binding protein
d (NMR)	doublet
DCE	Dichlorethane
DCM	Dichloromethane
dd (NMR)	doublet of doublet
DIPEA	N,N-Diisopropylethylamine
DMAP	4-dimethylaminopyridine
DME	Dimethoxyethane
DMF	Dimethylformamide
DML	designed multiple ligands
DMSO	Dimethyl sulfoxide
DNA	Deoxyribonucleic acid
DSF	Differential scanning fluorimetry
eq	equivalents
ESI	electrospray ionization
et al.	Et alii (and others)
EtOH	Ethanol
FBS	fetal bovine serum
FDA	United States Food and Drug Administration
Fmoc	Fluorenylmethyloxycarbonyl protecting group
GSEA	Gene set enrichment analysis
h	hours
HAT	histone acetyltransferases
HATU	Hexafluorophosphate Azabenzotriazole Tetramethyl Uronium
HCCA	$\alpha$ -cyano-4-hydroxycinnamic acid
HDAC	histone deacetylases
HDACi	HDAC inhibitor
HEPES	4-(2-Hydroxyethyl)-1-piperazineethanesulfonic acid
HOBt	Hydroxybenzotriazole

HPLC	high-performance liquid chromatography
HRMS	High-resolution mass spectrometry
ITC	Isothermal titration calorimetry
LiOH	Lithium hydroxide
m (NMR)	multiplet
MALDI	matrix-assisted laser desorption/ionization
MeOH	Methanol
min	minutes
MS	mass spectrometry
Nluc	Nanoluc
NMC	NUT midline carcinoma
NMR	nuclear magnetic resonance
NUT	nuclear protein in testis
OTX	2-(Aminooxy)tetrahydro-2 <i>H</i> -pyran
PDAC	pancreatic ductal adenocarcinoma
Ph	phenyl
ppm	parts per million
P-TEFb	positive transcription elongation factor
q (NMR)	quartet
RFU	relative fluorescent unit
RT	room temperature
RT-PCR	real-time polymerase chain reaction
s (NMR)	singlet
SAHA	Suberanolohydroxamic acid
sat.	saturated
SE	super-enhancer
t (NMR)	triplet
TCEP	Tris(2-carboxyethyl)phosphine
TEA	Triethylamine
TF	transcription factor
Tf <sub>2</sub> O	Trifluoromethanesulfonic anhydride
TFA	Trifluoroacetic acid
THF	Tetrahydrofuran
TLC	thin-layer chromatography
T <sub>m</sub>	melting temperature
TSA	Trichostatin A
UV	ultraviolet
Xphos	2-Dicyclohexylphosphin-2',4',6'-triisopropylbiphenyl

## List of figures

Figure 1: Cancer incidence and mortality .....	1
Figure 2: Gemcitabine and deoxycytidine. ....	2
Figure 3 Scheme of chromatin remodeling with DNA (black) and histones (blue). ....	3
Figure 4: Phylogenic tree of all 46 proteins containing 61 bromodomains. ....	3
Figure 5: Structure of BRD4 (1) in complex with a diacetylated histone peptide ligand.....	4
Figure 6: Four BRD inhibitors.....	5
Figure 7: Selectivity pattern of JQ1 determined by DSF.....	6
Figure 8: Phylogenic tree of all HDACs divided in their respective class .....	7
Figure 9: Crystal structure of HDAC2 in complex with SAHA .....	8
Figure 10: Structures of vorinostat <b>5</b> , belinostat <b>6</b> and panobinostat <b>7</b> and Romidepsin <b>8</b> .....	9
Figure 11:HDACis Trichostatin A ( <b>9</b> ) and Etinostat ( <b>10</b> ).....	9
Figure 12: Nanatinostat ( <b>11</b> ) and CI994 ( <b>12</b> ).....	10
Figure 13: Simultaneous treatment of AML cells with two inhibitors. ....	11
Figure 14: Simultaneous treatment of pancreatic cells with two inhibitors.....	12
Figure 15: Possible types of DML .....	13
Figure 16: Strategies for the development of DML. ....	14
Figure 17: Chemical structure of the planned JQ1-HDACi-adducts .....	15
Figure 18: Chemical structure of the first merged potential dual BET/HDAC inhibitor .....	16
Figure 19: Planned derivatives of <b>18</b> with a possibly higher selectivity. ....	16
Figure 20: Starting point of the third generation of dual BET/HDAC inhibitors. ....	17
Figure 21: Planned dual inhibitors of the third generation. ....	17
Figure 22: Structure of PLX51107 ( <b>36</b> ) and the planned potential dual inhibitor <b>37</b> .....	18
Figure 23: Structure of the precatalyst Xphos Pd Gen. 3 ( <b>78</b> ) and mode of activation of <b>78</b> ..	33
Figure 24: Catalytic cycle of a palladium catalyzed cross coupling reaction .....	34
Figure 25: Amines used in the nucleophilic aromatic substitution. ....	34

## List of figures

---

Figure 26: Directive effects of the substituents of <b>63</b> and <b>94</b> .....	43
Figure 27: Principle of DSF assay.....	51
Figure 28: Schematic representation of an isothermal titration calorimeter .....	52
Figure 29: Characteristic data of a titration experiment and integrated heat signals plotted against the molar ratio. ....	53
Figure 30: Schematic representation of BRET in living cells. ....	54
Figure 31: Dual BET/HDAC inhibitors of the first generation. ....	57
Figure 32: Superimposed crystal structures of dual inhibitors and JQ1 in complex with BRD4 1. ....	58
Figure 33: Sequence alignment of the BET BRDs.....	59
Figure 34: Quantitative RT-PCR analysis for MYC and HEXIM .....	63
Figure 35: Time- and dose-dependent immunoblots of PaTu 8988t cells.....	64
Figure 36: RT-PCR and washout experiment of PaTu 8998t cells. ....	65
Figure 37: CellTiter Glo cell viability assay with three different PDAC cell lines.....	66
Figure 38: Immunoblot analysis of cleaved caspase-3 in MIA PaCa-2 cells.....	66
Figure 39: Cell confluence measurement of MIA PaCa-2 cells.....	67
Figure 40: Cell confluence measurement with 1 $\mu$ M indicated inhibitor on day 1, 8 and 15 for 24 hours. ....	67
Figure 41: Combination response of HPAC cell.....	68
Figure 42: Colony formation assay for HPAC cells with different administration schedules. ....	69
Figure 43: Immunoblot analysis of p21 and cell-cycle analysis of HPAC cells. ....	69
Figure 44: Immunoblot analysis of phospho-CHK1 and cell cycle analysis of HPAC. ....	70
Figure 45: Immunoblot analysis of cleaved caspase-3 and phospho-CHK1.....	70
Figure 46: Cell-cycle analysis by flow cytometry of HPAC cells. ....	71
Figure 47: Hierarchical clustering of the differentially expressed genes in PANC-1 cells and Venn diagram of those genes.....	71
Figure 48: Gene ontology analysis of genes downregulated by <b>14</b> .....	72
Figure 49: GSEA plots, that compare the enrichment of pathways related to cell cycle. ....	73

---

Figure 50: GSEA plots comparing the enrichment of HDACi signature. ....	73
Figure 51: Enhancers in PANC-1 ranked based on the intensity of H3K27ac signal .....	74
Figure 52: Kaplan-Meier plot of the survival of pancreatic cancer patients.....	74
Figure 53: Quantitative RT-PCR analysis of FOSL1 gene in PANC-1 cells. ....	75
Figure 54: H3K27ac occupancy profiles at the FOSL1 gene in healthy pancreas compared to PANC-1 cells. ....	75
Figure 55: Morphological changes of HCC2429 cells.....	76
Figure 56: Quantitative RT-PCR analysis of three typical squamous tissue genes .....	76
Figure 57: Dual BET/HDAC inhibitors of the second generation.....	77
Figure 58: Dual BET/HDAC inhibitors of the third generation. ....	81
Figure 59: Transformation of the basic structure of the second-generation inhibitors.....	87
Figure 60: Additional derivates.....	88

## List of tables

Table 1: Reaction conditions for the synthesis of <b>39</b> .....	28
Table 2: Reaction conditions for the synthesis of <b>41</b> .....	29
Table 3: Reaction conditions for the synthesis of <b>42</b> .....	29
Table 4: Reaction conditions for the synthesis of <b>44</b> .....	30
Table 5: DSF assay results of the first generation. $\Delta T_m$ in $^{\circ}\text{C}$ .....	59
Table 6: $K_d$ values (in nM) obtained by ITC .....	60
Table 7: $IC_{50}$ values (in $\mu\text{M}$ ) obtained from cell-free fluorogenic HDAC assay.....	60
Table 8: $IC_{50}$ values (in $\mu\text{M}$ ) of the cellular BRD4 and HDAC1 activity of dual inhibitors determined by nanoBRET assay. ....	61
Table 9: DSF assay results of the second generation. $\Delta T_m$ in $^{\circ}\text{C}$ . ....	78
Table 10: Repetition of the DSF assay for compounds <b>20</b> and <b>22</b> . $\Delta T_m$ in $^{\circ}\text{C}$ . ....	78
Table 11: $IC_{50}$ values (in $\mu\text{M}$ ) obtained from cell-free fluorogenic HDAC assay and nanoBRET respectively. ....	79
Table 12: DSF assay results of the third generation. $\Delta T_m$ in $^{\circ}\text{C}$ .....	82

---

Table 13: IC <sub>50</sub> values (in $\mu\text{M}$ ) obtained from cell-free fluorogenic HDAC assay. ....	83
--	----

## List of schemes

Scheme 1: Reaction scheme for the synthesis of compound <b>13</b> . ....	19
Scheme 2: Selective protection of one amine of <b>38</b> .....	20
Scheme 3: Amide coupling reaction of <b>39</b> and <b>40</b> with HATU and DIPEA. ....	20
Scheme 4: Mechanism of N-acylation with HATU. <sup>[82]</sup> .....	21
Scheme 5: Removal of the Fmoc protection group with morpholine. ....	21
Scheme 6: Hydrolysis of JQ1 with LiOH. ....	22
Scheme 7: Amide coupling reaction of <b>42</b> and <b>43</b> with HATU and DIPEA. ....	22
Scheme 8: Removal of Boc protecting group with TFA. ....	22
Scheme 9: Reaction scheme for the synthesis of compound <b>14</b> . ....	23
Scheme 10: Amide coupling reaction of <b>25</b> with HATU and DIPEA. ....	24
Scheme 11: Reaction scheme for compound <b>49</b> . ....	24
Scheme 12: Reaction scheme for compound <b>15</b> . ....	24
Scheme 13: Direct conversion of the ester <b>49</b> to hydroxamic acid <b>15</b> . ....	25
Scheme 14: Reaction scheme for the synthesis of compound <b>15</b> . ....	25
Scheme 15: Reaction scheme of the Staudinger reaction. ....	26
Scheme 16: Mechanism of the Staudinger reaction. ....	26
Scheme 17: Reaction scheme for compound <b>16</b> . ....	27
Scheme 18: Direct conversion of the ester <b>55</b> to hydroxamic acid <b>16</b> . ....	27
Scheme 19: Reaction scheme for the synthesis of compound <b>62</b> . ....	31
Scheme 20: Reaction scheme for the first half dual inhibitors. ....	32
Scheme 21: Reaction scheme for the Suzuki reaction to obtain <b>64</b> . ....	33
Scheme 22: Nucleophilic aromatic substitution using the example of <b>79</b> to afford <b>65</b> . ....	35
Scheme 23: Reduction of nitrobenzene using the example of <b>65</b> to afford <b>68</b> . ....	35

---

Scheme 24: HATU reaction.....	35
Scheme 25: Attempted formation of aldehyde <b>72</b> with TFA.....	36
Scheme 26: Ring closure and removal of protecting group using the example of <b>73</b> to obtain <b>75</b> .....	36
Scheme 27: Reaction scheme for the synthesis of compound <b>18</b> . ....	37
Scheme 28: Reductive amination of <b>75</b> and <b>83</b> to form <b>84</b> .....	38
Scheme 29: Reaction scheme for the synthesis of compound <b>86</b> . ....	38
Scheme 30: Direct conversion of <b>84</b> to obtain final compound <b>18</b> .....	39
Scheme 31: Amide coupling reaction of <b>87</b> and <b>39</b> .....	39
Scheme 32: Synthesis of triflate <b>89</b> from phenol <b>88</b> .....	40
Scheme 33: Palladium catalyzed arylation of <b>75</b> .....	40
Scheme 34: HATU coupling reaction followed by the removal of the Boc-protecting group	41
Scheme 35: HATU reaction of <b>70</b> and <b>91</b> to obtain <b>92</b> .....	41
Scheme 36: HATU coupling reaction followed by the removal of the Boc-protecting group	41
Scheme 37: Reaction scheme for the first half dual inhibitors. ....	42
Scheme 38: Substitution reaction of <b>64</b> to obtain <b>96</b> . ....	43
Scheme 39: Reaction conditions that lead to double Boc protection.....	43
Scheme 40: Single protection of <b>96</b> to afford <b>97</b> . ....	44
Scheme 41: Reduction of <b>97</b> with Pd/C and H <sub>2</sub> followed by a HATU reaction.....	44
Scheme 42: Reaction of <b>99</b> in dioxane/4 N HCl to afford <b>100</b> and <b>101</b> . ....	44
Scheme 43: HATU reaction of <b>100</b> with <b>39</b> and deprotection of its product <b>121</b> to afford final compound <b>25</b> and direct conversion of <b>101</b> to obtain final compound <b>26</b> .....	45
Scheme 44: Nucleophilic aromatic substitution.....	45
Scheme 45: Result of the reduction of benzylamines with Pd/C and H <sub>2</sub> .....	45
Scheme 46: Reduction of the nitro group with SnCl <sub>2</sub> .....	46
Scheme 47: Reaction in dioxane/4 N HCl .....	46
Scheme 48: HATU reaction using the example of <b>114</b> .....	47

---



Scheme 49: Boc protection of the aniline <b>128</b> to afford <b>129</b> .....	47
Scheme 50: Suzuki reaction of <b>129</b> with boronic acids.....	47
Scheme 51: Reduction of <b>132</b> and <b>133</b> with SnCl <sub>2</sub> .....	48
Scheme 52: HATU reaction of <b>115</b> with <b>134</b> and <b>135</b> followed by the deprotection of both products .....	48
Scheme 53: Synthesis of <b>139</b> and <b>140</b> with HATU and TEA .....	49
Scheme 54: Microwave assisted Suzuki reaction.....	49
Scheme 55: HATU reaction of <b>36</b> with <b>39</b> followed by the deprotection of the product .....	50



## 1. Introduction

Noncommunicable diseases such as diabetes, cancer and heart disease are the main reason for global death in the 21<sup>st</sup> century.<sup>[1]</sup> Of these diseases cancer is estimated to rank high in the majority of countries and first all over the globe. In 2015 cancer was approximately at least the fourth leading cause of death before the age of 70 in 113 of 172 countries.<sup>[2]</sup> Because of this, a lot of research has been done in this field with some success. The 5-year survival rate of rectal, breast and colon cancer for example has risen continuously since 1995 especially in developed countries.<sup>[3]</sup> Nevertheless, there is one exception with pancreatic ductal adenocarcinoma (PDAC) often simply called pancreatic cancer since it is the most common form of this type of cancer.<sup>[4]</sup> Although this cancer type is relatively rare it is still the eighth leading cause of cancer death worldwide,<sup>[2,5]</sup> with a 5-year survival rate of approximately 6 % (Figure 1).

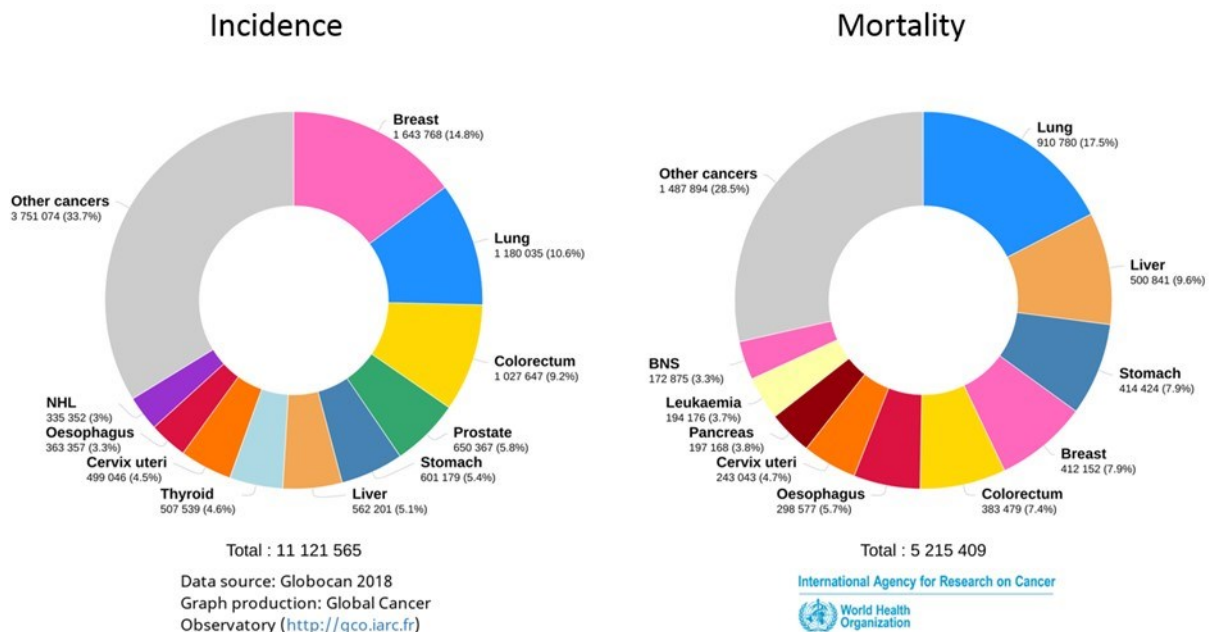


Figure 1: Cancer incidence and mortality of the 10 most common cancer types in 2018<sup>[5]</sup>.

This is due to the cancers tendency to quickly spread into the lymphatic system and distant organs. In addition, the cancer is resistant to targeted and conventional therapeutic approaches and therefore often incurable at the time of diagnosis.<sup>[6]</sup> The typical cancer medication, referred to as chemotherapy, includes cytotoxic agents for example gemcitabine (Figure 2, 1), a prodrug which is active after phosphorylation.<sup>[7]</sup> The mechanism of action of gemcitabine is based on its similarity to deoxycytidine (Figure 2, 2) and is therefore incorporated into the DNA, thereby blocking the replication resulting in subsequent cell death.<sup>[7]</sup> This mainly affects rapidly dividing cells, as is the case with cancer.<sup>[8]</sup> Unfortunately, there are also healthy rapidly dividing tissues such as the gastrointestinal mucosa, bone marrow and hair follicles.<sup>[9]</sup>

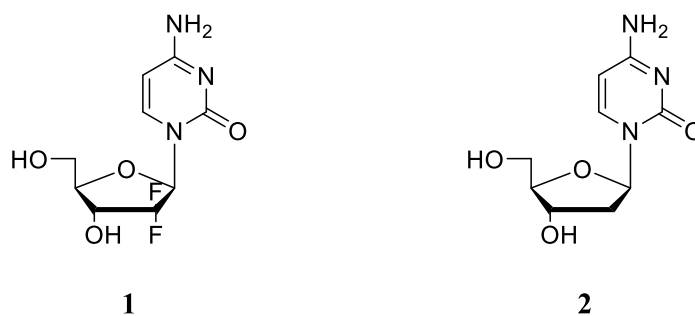


Figure 2: Gemcitabine and deoxycytidine.

This leads to a variety of side effects, the best known of which is probably hair loss.<sup>[10]</sup> However, in the specific case of PDAC, the cancer exhibits a high genetic heterogeneity, resulting in an equally high chemoresistance.<sup>[11]</sup> Thus, a new therapeutic strategy is necessary to reduce the lethal nature of PDAC. One upcoming new approach is the inhibition of specific epigenetic proteins because the initiation and progression of cancer is highly dependent on epigenetic mechanisms.<sup>[12]</sup>

## 1.1. Epigenetics

The term “epigenetics” is known since the 1942 and was introduced and defined by Conrad Waddington as the interactions between genes and therein encoded proteins which are responsible for the development of the phenotype.<sup>[13]</sup> With this definition Waddington included all molecular pathways that regulated the expression of a genotype into a specific phenotype.<sup>[14]</sup> Over the years as the research progressed and knowledge grew this definition changed and became more accurate. Today epigenetics refers to the study of meiotically and mitotically inheritable changes in the function of a gene without altering the DNA sequence.<sup>[15]</sup> These changes are DNA modifications primarily in form of methylation of cytosine bases<sup>[16]</sup> and histone modifications. While DNA modifications are limited to methylation histone modification include methylation as well as acetylation<sup>[17]</sup>, phosphorylation<sup>[18]</sup>, ADP ribosylation<sup>[19]</sup>, ubiquitylation<sup>[20]</sup> and SUMOylating.<sup>[21]</sup> The proteins involved in adding modifications are called “writers” while the “readers” recognize and the “erasers” remove those epigenetic marks again.<sup>[22]</sup> Acetylation marks, which occur on lysine residues,<sup>[14]</sup> for example are placed by histone acetyltransferases (HATs), whereas bromodomain containing proteins (BRDs) recognize and histone deacetylases (HDACs) remove this modification.<sup>[22]</sup> In terms of transcription acetylation marks play an important role since they neutralize the positive charge of the lysine residue and weaken their electrostatic interaction with the negatively charged DNA backbone.<sup>[23]</sup> Thus, the chromatin structure opens up and transcription factors can access promoters of targeted genes (Figure 3).<sup>[24]</sup>

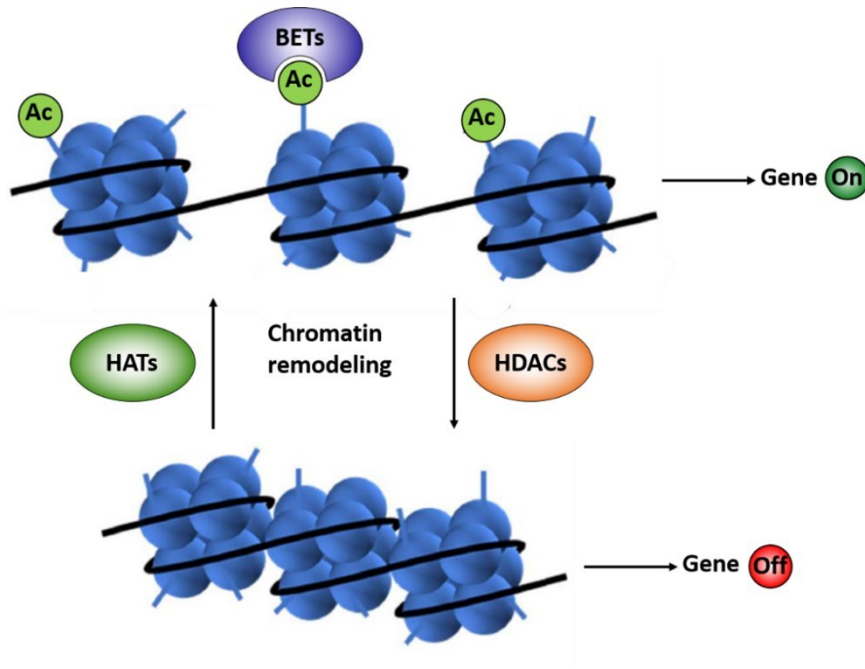


Figure 3 Scheme of chromatin remodeling with DNA (black) and histones (blue).

## 1.2. Bromodomain and extra terminal motif (BET)

The first bromodomain was reported the *Drosophila* protein brahma, which is the origin of its name, in the year 1992.<sup>[25]</sup> Since then 61 bromodomains were found distributed among 46 proteins which were divided into 8 major families (Figure 4).<sup>[26]</sup>

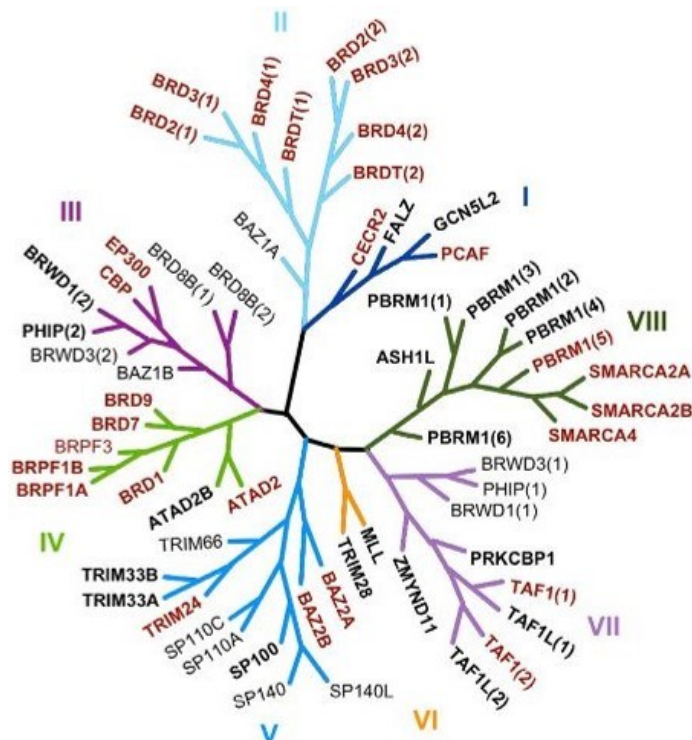


Figure 4: Phylogenetic tree of all 46 proteins containing 61 bromodomains. Numbers in brackets indicate the amount of bromodomains in this specific protein.<sup>[27]</sup>

BRDs are found in a variety of nuclear proteins including HATs (e.g. p300/CBP)<sup>[28]</sup>, HMTs (e.g. ASH1L)<sup>[29]</sup> and transcriptional coactivators (e.g. TAF1/TAF1L).<sup>[30]</sup> One of the most important family in regard of transcriptional activity is the bromodomain and extra terminal (BET) family which consists of BRD2, BRD3, BRD4 and BRDT. While BRDT is only found in male germ cells and the others are expressed ubiquitously. All of them contain two tandem bromodomains and one extra-terminal domain, as their name suggests.<sup>[31]</sup> The bromodomain itself is a conserved structure with approximately 110 amino acids that arrange in the form of four  $\alpha$ -helices ( $\alpha_Z$ ,  $\alpha_A$ ,  $\alpha_B$  and  $\alpha_C$ ) and two loops connecting  $\alpha_Z$  with  $\alpha_A$  and  $\alpha_B$  and  $\alpha_C$ , hence ZA-loop and BC-loop. These two loops are packed against one another to form a surface accessible hydrophobic pocket, which form the acetyl-lysine binding side (Figure 5).<sup>[27,32]</sup>

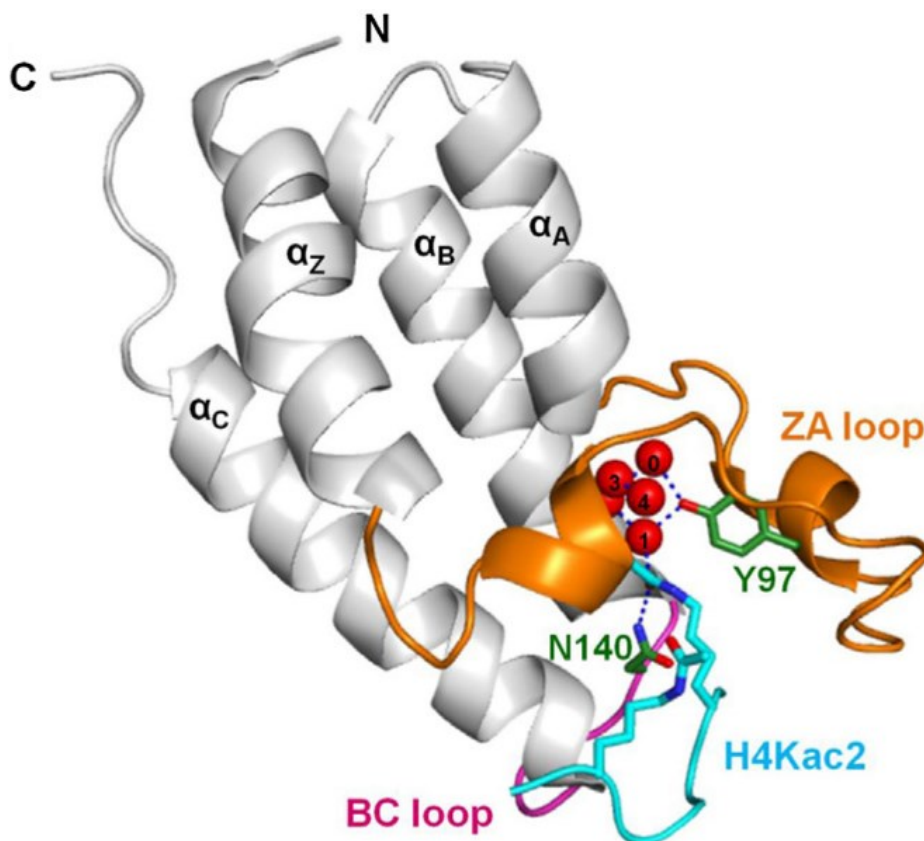


Figure 5: Structure of BRD4 (1) in complex with a diacetylated histone peptide ligand (H4K12acK16ac) with the four helices (grey), the loops BC (magenta) and ZA (orange) and the peptide ligand (cyan). The acetylated lysine forms a hydrogen bond with the highly conserved asparagine N140 (green) and a water-mediated bond with the tyrosine Y97 (green).<sup>[27]</sup> (PDB: 3UVX)

With these sides BET proteins recognize acetylated lysine residues on histone tails and recruit transcription factors. For example, BRD4 recruits the positive transcription elongation factor (P-TEFb) to the transcription start site, which then phosphorylates several other targets. This leads to the activation of paused RNA polymerase II and elongation of transcription.<sup>[27]</sup> As such

BET proteins play a crucial role in cellular proliferation and differentiation since they mainly control the expression of growth promoting genes like oncogene *MYC*.<sup>[33,34]</sup>

### 1.2.1. Inhibition of BET proteins

As described, BET proteins and BRD4 in particular control the progression of the cell cycle and thus cell proliferation and cell differentiation. Dysregulation of this progress leads to aberrant gene expression which is found in many diseases, cancer included.<sup>[35]</sup> In the majority of common cancer types BET proteins promote the overexpression of *MYC* oncogene.<sup>[36]</sup> For example, acute myeloid leukemia (AML) as well as solid tumors such as lung and pancreatic cancer show a high expression level of *MYC*.<sup>[37]</sup> Although several studies could show, that suppression of *MYC* expression is followed by tumor regression, a direct targeting approach has remained unsuccessful so far.<sup>[38,35]</sup> But since *MYC* transcription is dependent on BRD4s ability to bind to acetylated lysine residues the idea arose to target *MYC* indirectly by inhibiting BRD4 or BET proteins in general.<sup>[35]</sup> The first reported BRD inhibitors, for example MS2126 (**2a**) and MS0745 (**2b**) all shared the same structural motif of an acetylated amine (Figure 6, red) which is recognized by bromodomains. Although they have a rather weak affinity and thus showed their inapplicability in clinical trials, they proved that BRD inhibition is generally possible.<sup>[39]</sup>

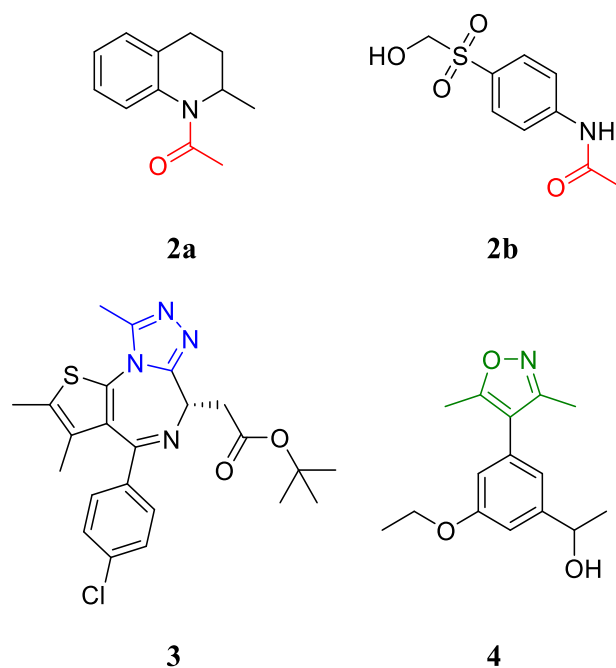


Figure 6: Four BRD inhibitors. Top: Examples of the first molecules that bind to the CBP BRD with MS2126 (2a) and MS0745 (2b). These molecules share the same structural motif of an acetylated amine (red). Bottom: Structure of JQ1 (3) and an unnamed BRD inhibitor. The triazole ring (blue) and the isoxazole (green) forms the same hydrogen bond with the conserved asparagine as the acetylated lysins.<sup>[39,40]</sup>

Subsequently more potential inhibitors were synthesized which resulted in the development of the thienotriazolodiazepine (+)-JQ1 (JQ1, **3**),<sup>[40]</sup> the first potent inhibitor for BET proteins with the highest affinity towards BRD4.

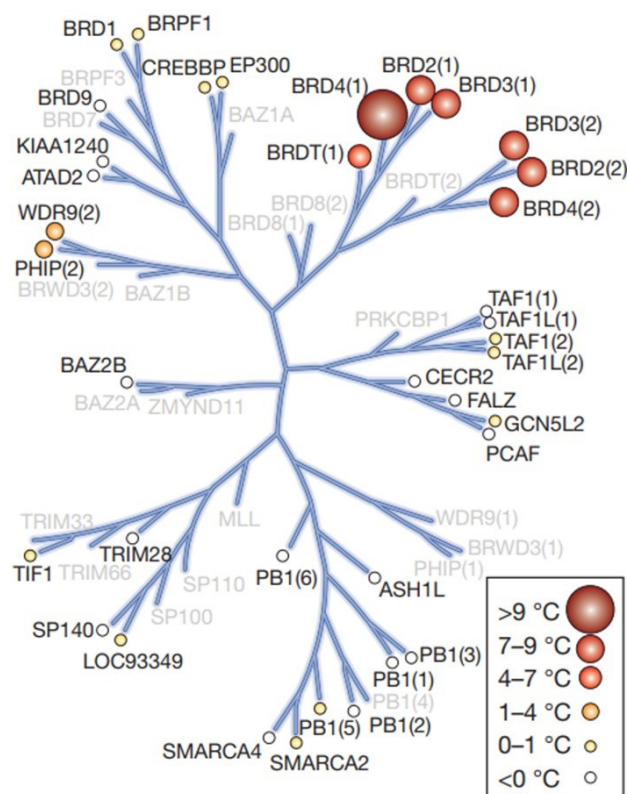


Figure 7: Selectivity pattern of JQ1 determined by DSF. Averaged temperature shifts are shown in °C upon binding of 10 μM JQ1. Temperature shifts are represented by spheres. Bromodomains not included in the panel are grey.<sup>[40]</sup>

The main reason for this affinity is the triazole ring (Figure 6, blue) which forms the same hydrogen bond with the conserved asparagine as the acetylated lysins.<sup>[40]</sup> The same applies to the 3,5-dimethylisoxazole unit (Figure 6, green) shown in the first but unnamed BRDi **4** with this moiety. Like the triazole in JQ1 the isoxazole is an acetyl-lysine bioisostere and binds to the described asparagine as well.<sup>[41]</sup> Of those inhibitors only JQ1 was tested in preclinical studies and showed promising characteristics in the treatment of several cancers, including but not limited to breast<sup>[42]</sup> and pancreatic cancer.<sup>[43]</sup> Unfortunately its short half-life of one hour prevents its clinical use and limits JQ1 to preclinical studies.<sup>[44]</sup> However, in those studies amplification of JQ1 resulted in reduced cell growth by inhibiting *MYC* transcription and even induced apoptosis.<sup>[34,45]</sup> Although the efficacy of the JQ1 treatment is highly dependent on the cell type the results show the importance of BET in cancer treatment especially in those with a pathological c-MYC activation.<sup>[34,35]</sup> Other BETi with a longer half-life were already tested in clinical trials mainly in phase I. Unfortunately, these trials only yielded mixed results so far.<sup>[46]</sup>



### 1.3. Histone deacetylases (HDACs)

As their name suggests HDAC are in charge of the elimination of the acetylation marks placed by HATs. This action restores the electromagnetic interaction between the histones and the DNA to repress the transcriptional activity. HDACs are known since 1969 when they were discovered in the calf thymus extract.<sup>[47]</sup> Since then 18 HDAC enzymes were found and divided into 4 classes (Figure 8).

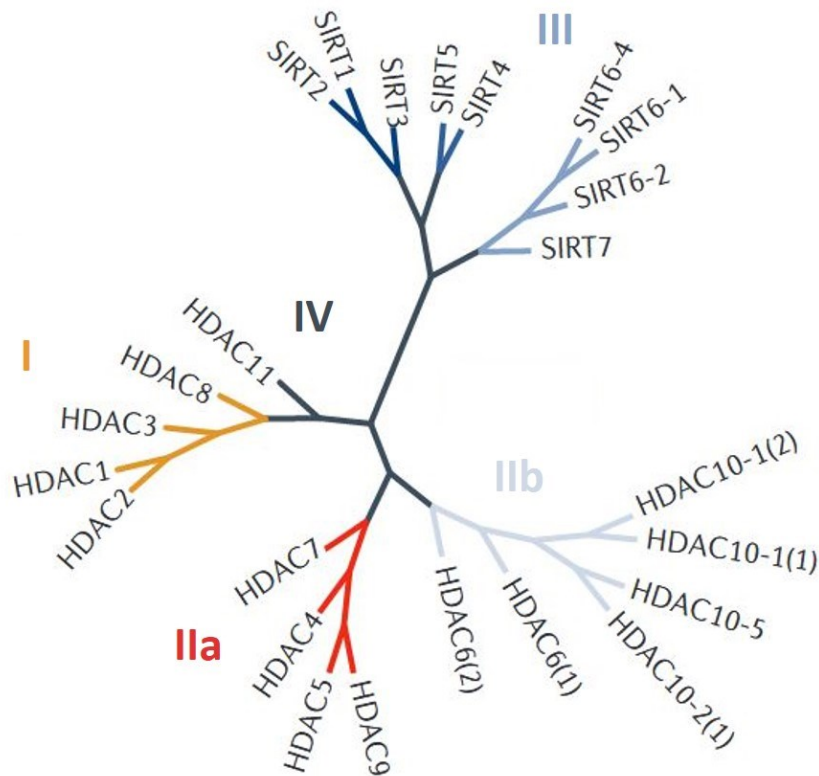


Figure 8: Phylogenetic tree of all HDACs divided in their respective class (modified).<sup>[48]</sup>

The first class of HDACs include HDAC1-3 and 8 (numbered in order of discovery) which are located mainly in the nucleus (HDAC 8 is also localized in the cytoplasm) and expressed ubiquitously. These HDACs play a central role regarding cell cycle control, tissue development and cell proliferation. One study for example showed that HDAC1-null mice display general growth retardation and serious proliferation defects. These mice died in early embryonic stages.<sup>[49]</sup> The second class of HDACs is subdivided into class IIa and IIb. The HDACs 4, 5, 7 and 9 belong to class IIa and are more tissue specific than the first class and are primarily expressed in the brain and muscles especially in the heart.<sup>[50]</sup> HDAC 6 and 10 are members of class IIb due to a unique presumably second catalytic domain both share.<sup>[51]</sup> They are primarily expressed in liver, kidney and testis and involved in differentiation.<sup>[52]</sup> HDAC11 cannot be assigned to class I or class II because its deacetylase domain shows homology to both classes.<sup>[53]</sup>

Therefore it is considered to be its own class and so far the only member of class IV. Like class II HDACs it is expressed in kidney, brain and testis but mostly nuclear as are the members of class I.<sup>[52]</sup> All these HDACs are called classical HDACs because they share one specific characteristic which is a  $Zn^{2+}$  ion deep inside the HDACs binding pocket.<sup>[54]</sup> Class III HDACs do not share this characteristic since they are  $NAD^+$  dependent enzymes and structurally unrelated to the other classes. Additionally because of the substituted  $Zn^{2+}$  ion they are not inhibited by the classical HDAC inhibitors (HDACi) and are therefore not further discussed.<sup>[55]</sup> The other HDACs also share a region of homology consisting of approximately 390 amino acids which is the deacetylase core. This catalytic side is tube-like shaped, and its walls are covered with hydrophobic and aromatic residues. The narrowest section of this pocket has a spacing of only 7.5 Å behind which the already mentioned  $Zn^{2+}$  ion is located (Figure 9).<sup>[56]</sup>

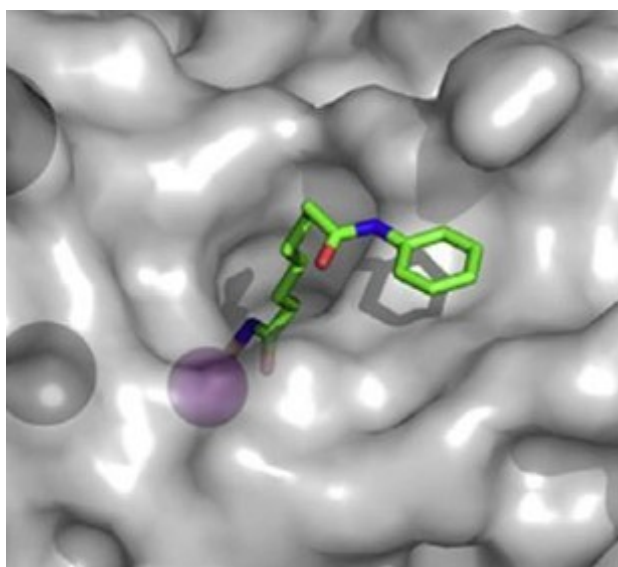


Figure 9: Crystal structure of HDAC2 in complex with SAHA (green) which chelates the zinc ion (purple) inside the catalytic side (PDB: 4LXZ).<sup>[57]</sup>

### 1.3.1. Inhibition of HDAC proteins

Due to the fact that histone modification affects gene expression by modulating chromatin structure it comes with no surprise that aberrant histone acetylation is correlated with cancer development and progression. Although HDACs are generally associated with gene silencing and therefore considered transcriptional repressors, deletion or inhibition of HDAC is often followed by a similar amount of up and down regulated genes.<sup>[58]</sup> Additionally, HDACs are also able to deacetylate non histone proteins for example the tumor suppressor protein p53 which is then accessible to ubiquitination followed by degradation.<sup>[59]</sup> These results contribute to the idea of targeting HDACs in cancer therapy as a supplement if not an alternative to chemotherapy.

And in fact, HDAC inhibition has antiproliferative effects by up-regulating cyclin-dependent kinase (CDK) inhibitors or down-regulating cyclins and CDKs and thus inducing cell cycle arrest.<sup>[60]</sup> In contrast to BETis the HDACis vorinostat (SAHA, **5**), belinostat (**6**), panobinostat (**7**) and romidepsin (**8**), were already approved by the FDA for the treatment of one specific cancer type each (Figure 10).

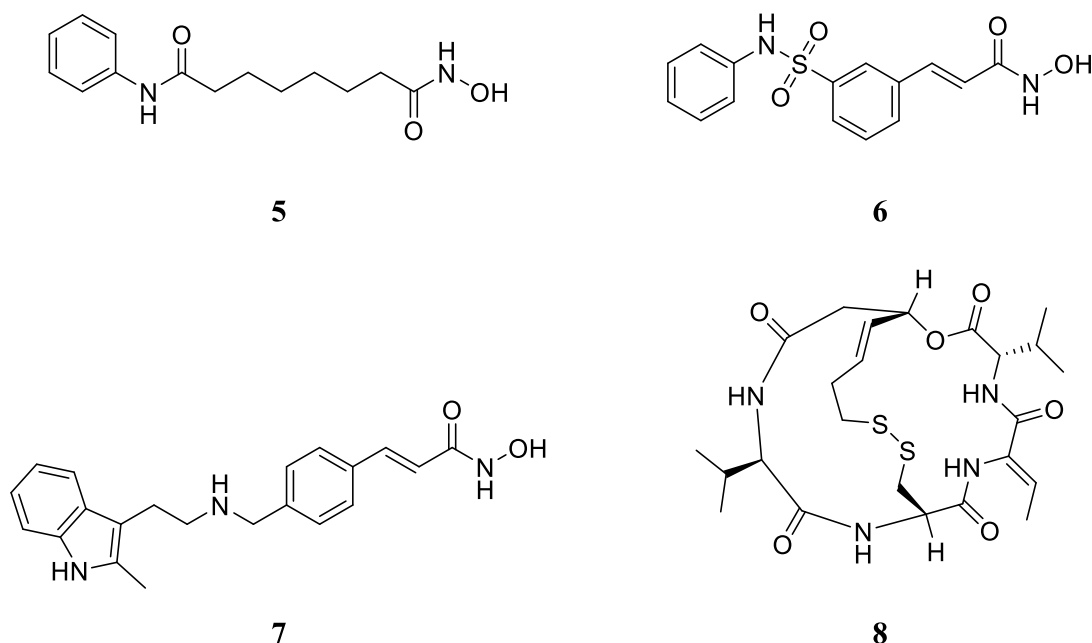


Figure 10: Structures of SAHA **5**, belinostat **6** and panobinostat **7** and romidepsin **8**, approved HDACi.

While vorinostat and Romidepsin are both approved for treatment of cutaneous T-cell lymphoma belinostat is applied to peripheral T-cell lymphoma. panobinostat on the other hand is approved for multiple myeloma which means that so far no HDACi is accepted for solid tumors.<sup>[61]</sup> Except for **8** most of the synthesized HDACi bear resemblance to the aliphatic acetyl-lysine substrate. These HDACi deliver a zinc-binding moiety either in form of a hydroxamic acid or a benzamine to chelate the  $Zn^{2+}$  ion deep inside the binding pocket. In order to reach this ion the zinc-binding group is followed by a hydrophobic linker which ends in the solvent-exposed capping group (Figure 11).<sup>[62]</sup>

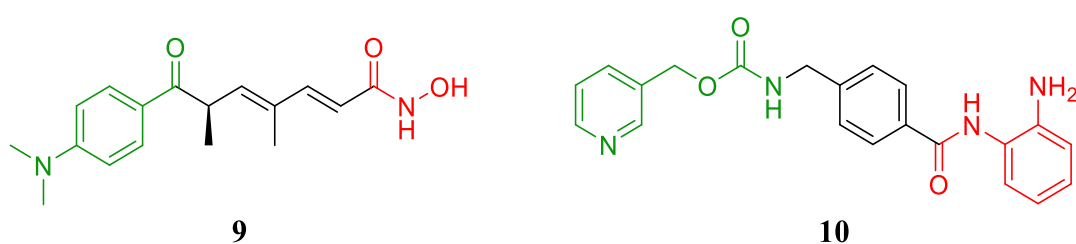


Figure 11: HDACi Trichostatin A (**9**) and Etinostat (**10**) with their zinc-binding group (red), the hydrophobic linker (black) and the capping group (green).

The different metal binding group has a major impact on the selectivity regarding the targeted proteins. Most of the HDACi with a hydroxamic acid inhibit all classical HDACs and are therefore called panHDACi as for example panobinostat and vorinostat. The exceptions of this rule contain an aromatic system near the zinc binding group which interacts with two phenylalanine residues only present in Class I and II at their slenderest section (Figure 12, left). The HDACi with a benzamine moiety on the other hand form an additional hydrogen bond which is only possible with HDACs of class I. This bond is formed between the amine NH and the CO of a glycine only present in HDACs of class I.<sup>[63]</sup> Another characteristic only present in class I is the so-called foot pocket next to the catalytic side which is also exploited by some HDACi to raise activity and selectivity. One example is the CI994 derivative **12** which has an additional thiophen group (Figure 12, right).<sup>[57]</sup> Compared to CI994 (**13**), this rather small change increases the activity on HDAC1 by a factor of 900.<sup>[64,65]</sup>

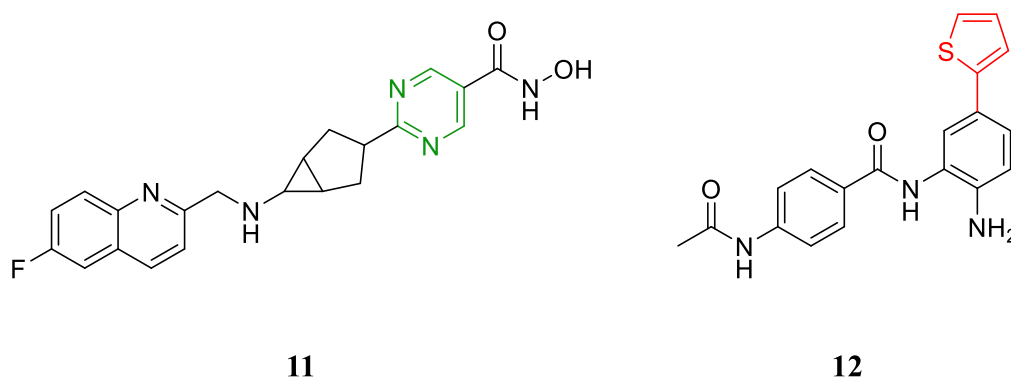


Figure 12: Nanatinostat (**11**) and CI994 (**12**). **11** is a class I selective HDACi probably due to the aromatic system (green) and a **12** a class I selective HDACi as well due to the thiophen (red) reaching in the foot pocket next to the active side.

#### 1.4. Simultaneous administration of two inhibitors

For a long time, drug development followed the old “one gene, one drug, one disease” paradigm. In the last years, this paradigm has been challenged due to the discovered compensatory signaling patterns that can counterbalance the effect of a drug, especially in cancer. The logical conclusion of this is to consider multitarget strategies over single-target approaches.<sup>[66]</sup> Thus, several clinical studies combined HDACis with other drugs for example cytotoxic agents like gemcitabine<sup>[67]</sup> and proteasome inhibitors.<sup>[68]</sup> Unfortunately the combination of gemcitabine with CI994 resulted in increased toxicity and no beneficial effects.<sup>[69]</sup> Regarding BETi only *in vivo* studies<sup>[6]</sup> were performed so far. In these studies, BETi were combined with targeted agents,<sup>[70]</sup> cell cycle inhibitors<sup>[71]</sup> and inhibitors of DNA damage repair<sup>[72]</sup> amongst others.

One rather new combination is the simultaneous usage of BETi and HDACi that shows synergistic effects in several *in vivo* studies. The combination of JQ1 and panobinostat for example was used to treat acute myeloid leukemia (AML) cells and showed a significant higher percentage of apoptosis and reduced cell growth compared to each inhibitor alone (Figure 13).<sup>[73]</sup>

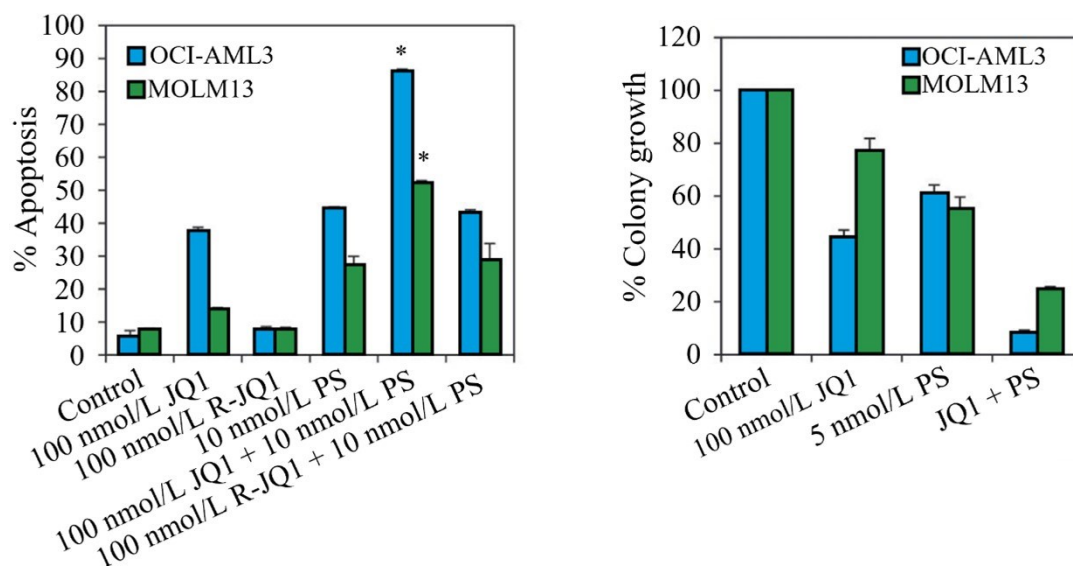


Figure 13: Simultaneous treatment of AML cells with two inhibitors. Left: OCI-AML3 (blue) and MOLM13 (green) cells were treated with the concentration of indicated inhibitors for 48 hours and then apoptotic cells (annexin V staining) were determined by flow cytometry. The \* indicates a significant higher value with combined treatment. Right: OCI-AML3 and MOLM13 cells were treated with the concentration of indicated inhibitors for 48 hours, then washed and cultured for 7-10 days. Again combined treatment shows higher impact than each inhibitor alone (both modified).<sup>[73]</sup>

JQ1 was also combined with SAHA (5) and used to treat pancreatic cell lines. The results again showed a significant synergistic effect on cell viability, demonstrating that this approach not only seems to work in solid tumors but also indicate the susceptibility of pancreatic cancer to the combination of epigenetic inhibitors (Figure 14).<sup>[74]</sup>

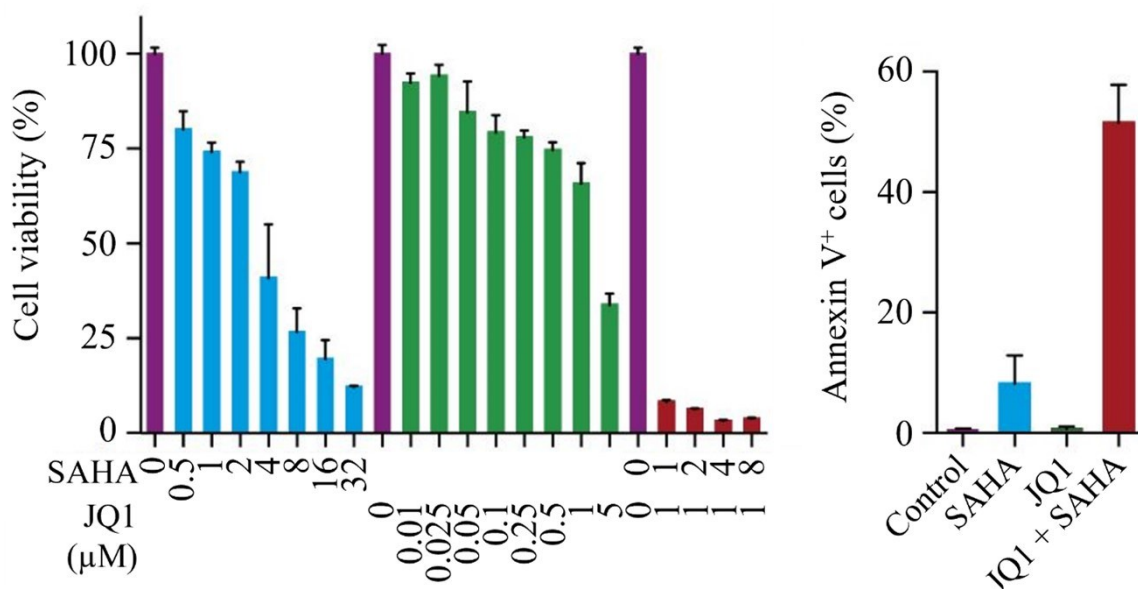


Figure 14: Simultaneous treatment of pancreatic cells with two inhibitors. Left: Cell viability assay with the effects of SAHA (blue), JQ1 (green) and combination of both (red) on DanG PDAC cells after 72 hours in comparison to untreated cells (purple). Right: Quantification of apoptotic cell death in DanG PDAC cells (annexin V staining) after treatment with SAHA (blue), JQ1 (green) and both combined (red) in comparison to untreated cells (purple) (both modified).<sup>[74]</sup>

It has been hypothesized that the reason for this synergy is due to hyperacetylation of histones induced by HDACis. Since HDACis attenuate the transcription of growth promoting proteins like c-MYC the hypothesis is that hyperacetylation of histones would increase the dependency of cancer cells on BET regulated proteins of which c-MYC is a member. In conclusion the application of HDACis renders cancer cells more susceptible to the activity of BETis.<sup>[73]</sup> Although these results are promising it is very difficult to transfer it to a living human being. Application of two drugs simultaneously always bears the risk of unwanted drug-drug interaction, complicates dosing scheduling as well as the pharmacokinetic properties. To bypass these problems it has been shown that multitarget drugs can accomplish the same goal but utilize a single compound, for example in the treatment of nonalcoholic steatohepatitis.<sup>[75]</sup> Regarding dual BET/HDAC inhibitors the idea of developing those is not new, already being investigated in 2013 by Atkinson *et al.*<sup>[76]</sup> and in 2017 by Amemiya *et al.*<sup>[77]</sup> Albeit both groups developed molecules capable of inhibiting both targets no increase in activity compared to the parent compounds could be observed.

## 1.5. Multi-target drugs

In order to synthesize a multi-target drug, there are basically only two different starting points: A knowledge-based approach and a screening approach. Knowledge-based approaches use existing data from known ligands that either bind to target A or target B, while the screening approach largely relies on serendipity to find appropriate starting points. To obtain designed multiple ligands (DML) especially when using the knowledge-based approach, two ligands that bind A and B, respectively, are connected by a (cleavable) linker or even overlap if structural similarities exist. The degree of overlap varies greatly from DML to DML but is always accompanied by a reduction in molar mass and reduced structural complexity.<sup>[78]</sup>

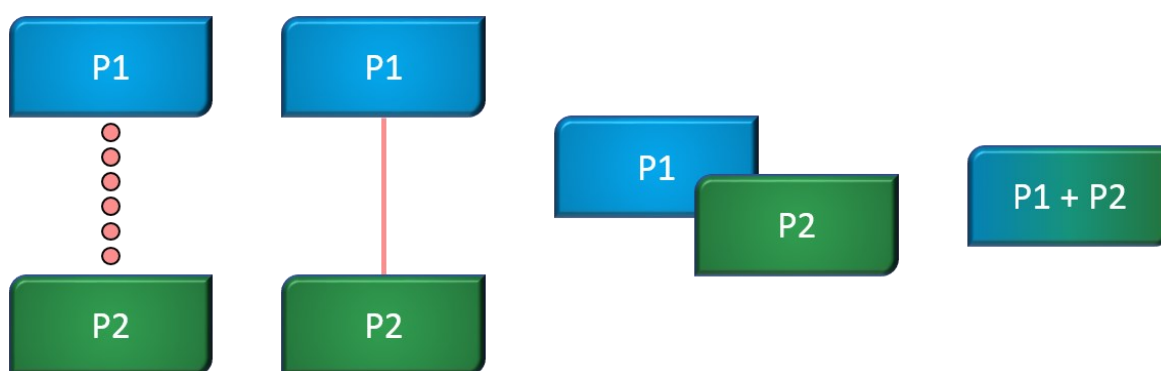


Figure 15: Possible types of DML: cleavable or non-cleavable linker, slightly overlapping or highly intermingled pharmacophores (P) (modified).<sup>[78]</sup>

Serendipitous approaches start with high-throughput screening of large, diverse compound libraries at one target. Each hit is then tested against the second target and even if there is only a low affinity, those compounds can be used as a starting point for DML development. In focused screening, a combination of the knowledge-based approach and screening approach, compounds with a known activity on one target are screened against the other one. Again, only weak activities are already a success. Regardless the approach, the identification of a compound with a balanced and appropriate activity on both targets is highly improbable. Instead, a so called “hit-to-lead” phase is required, in which the activity of the compound is enhanced, balanced or undesired activities on other targets are reduced, depending on what is necessary. The result of the lead generation phase is a compound that usually still misses the optimal ratio of *in vitro* activities and may also show unwanted affinities on different targets (Figure 16).

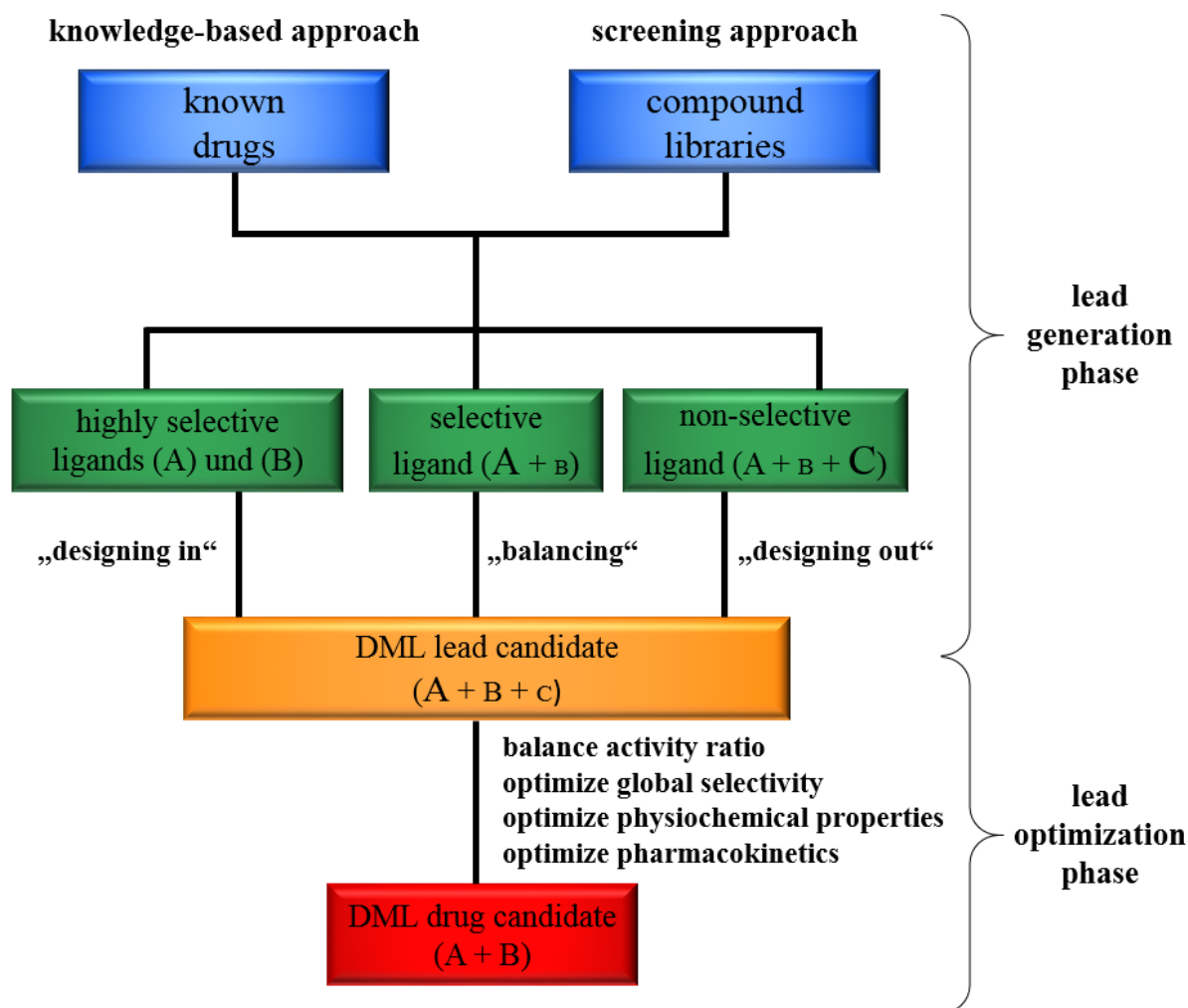


Figure 16: Strategies for the development of DML. In the lead generation phase starting compounds are provided using knowledge-based or screening approaches. Those compounds can be highly selective with no or little affinity at a second target or non-selective with one or more undesired activities. To obtain a DML lead candidate the following strategy consists of “designing in”, “balancing” and/or “designing out” activities. The subsequent lead optimization phase involves further challenges like global selectivity and pharmacokinetic optimization. A and B represent desired activity, C undesired. Size of letter indicates the affinity (modified).<sup>[79]</sup>

In the following lead optimization phase the selectivity is further enhanced and the ratio of *in vitro* activities is adjusted to obtain a well-balanced DML under the assumption that this is necessary for a similar level of receptor occupancy *in vivo*. The optimal ratio is ultimately clarified through the results of animal models and the feedback from clinical studies. Additionally, those results are also used to optimize the pharmacokinetic profile and the physiochemical properties to obtain a DML drug candidate.<sup>[79]</sup>



## 2. Objective

Although the already synthesized dual inhibitors show the possibility of targeting both proteins with a single compound, they still do not present an increased potency. Nevertheless, encouraged by these results, this work focuses on a different scaffold especially on a different BETi to achieve an increased activity towards BET and HDAC proteins. While the previous studies used either tetrahydroquinoline like I-BET726<sup>[76]</sup> or a rather new N<sup>6</sup>-benzoyladenine<sup>[77,80]</sup> structure as basis, JQ1 (**3**) will be part of the new generation of dual inhibitors connected to either CI994 (**13**), vorinostat (**5**) or panobinostat (**7**) (Figure 17).

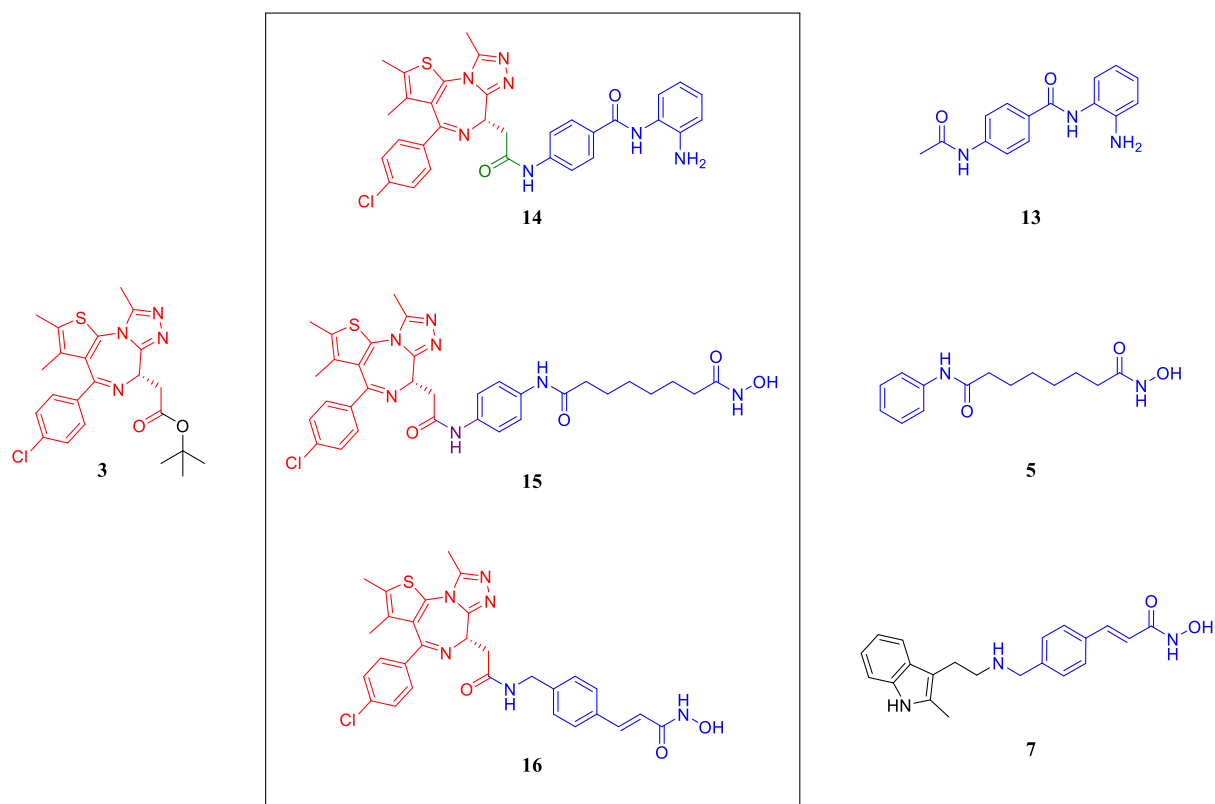


Figure 17: Chemical structure of the planned JQ1-HDACi-adducts with JQ1 (red), HDACi (blue), overlapping part (green), added linker (purple), and removed moieties (black).

The reason JQ1 (**3**) was picked is because of its high affinity towards the two binding domains of BRD4 with a  $K_d$  of 50 nM and 90 nM to its first and second bromodomain, respectively.<sup>[40]</sup> Additionally the *tert*-butyl ester of JQ1 is solvent exposed when bound which makes it destined to be substituted by a HDAC inhibiting moiety. Regarding the HDACis two already approved drugs were picked with **4** and **6**. The last one, CI994 (**13**), was chosen due to its different zinc-binding group and coherently its class I specificity. Furthermore, the resulting inhibitor **14** includes a small overlap (Figure 17, green) which is not present in **15** and **16**.

For the second generation of dual BET/HDAC inhibitors the goal was to merge the inhibitors instead of simply linking them. Since merging any HDACi with JQ1 seems to be impossible because of no structural similarities JQ1 needed to be replaced by other BRDis that have structural commonalities with HDACis. One inhibitor that fits that description is SGC-CBP30 (**17**)<sup>[81]</sup>, a compound that harbors a benzimidazole structure. That structure is very close to the indole structure of panobinostat, and therefore suitable for merging (Figure 18). **17** was selected despite the fact that it specifically binds to CREBBP (CBP) and EP300, two BRDs that are not part of the BET family. Nevertheless, **17** still shows some activity on BET and it could be possible to enhance that affinity by replacing the morpholine moiety (Figure 18, black) that seems to be responsible for the selectivity.

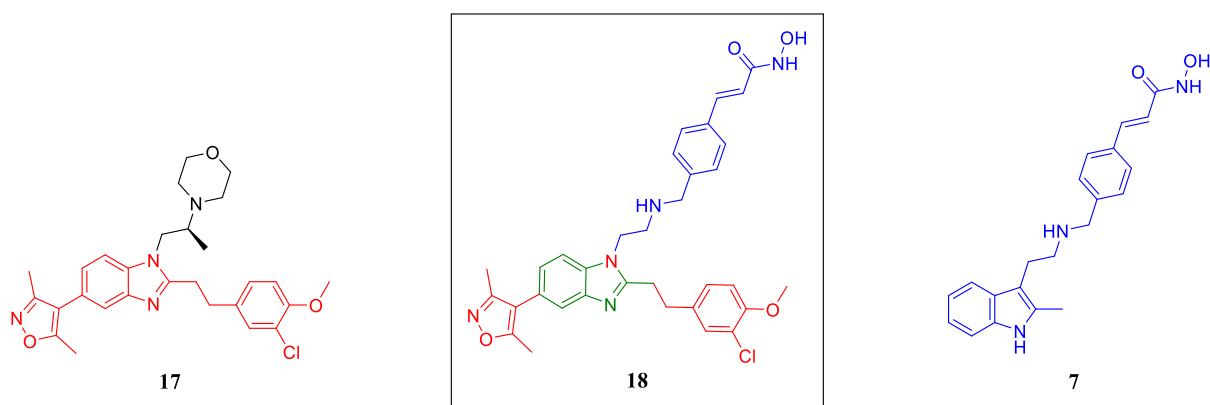


Figure 18: Chemical structure of the first merged potential dual BET/HDAC inhibitor **18** with SGC-CBP30 (red), panobinostat (blue) and overlapping structure (green) and removed moiety (black).

Additionally, the hydroxamic acid of **18** (Figure 18, blue) was replaced by the benzamine structure of either CI994 **13** or Etinostat **10** in order to gain class I selectivity, connected to the basic structure by an amine or an amide bond. Finally, the chlorine atom and the methoxy group were substituted by a hydrogen atom and a methyl group, respectively, which should increase the affinity towards the BET proteins.

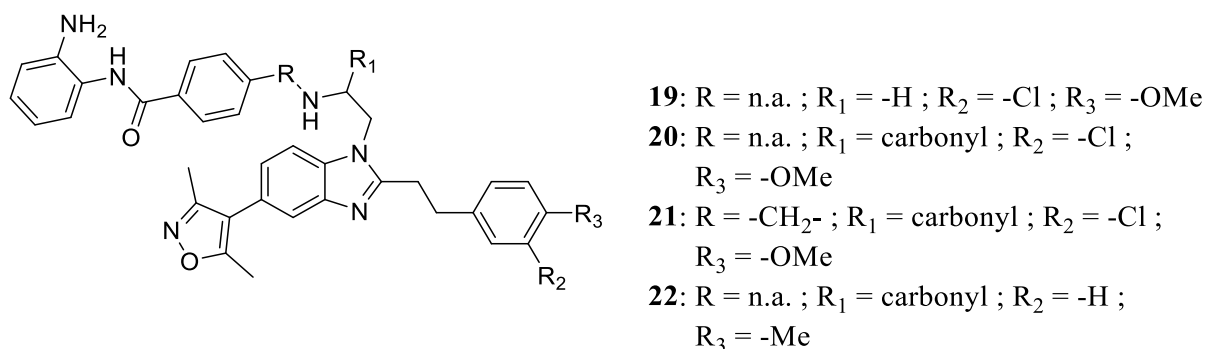


Figure 19: Planned derivatives of **18** with a possibly higher selectivity.

Since the compounds of the second generation are still quite large, there is hardly any room for optimization. In order to be able to optimize a smaller BETi that selectively binds BRD4(1) in the low three-digit nanomolar range was picked (Figure 20, **23**). Additionally, compound **24** was chosen as well due to potential synthetic problems with the nitrile group in **23**.

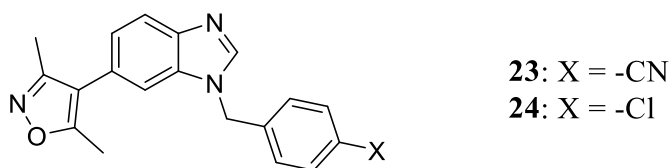


Figure 20: Starting point of the third generation of dual BET/HDAC inhibitors.

To integrate the HDAC activity, either a benzamine or a hydroxamic acid was added without a specific HDACi in mind. Naturally, the compounds incorporating benzamines still have a high similarity to CI994, due to its rather simple structure.

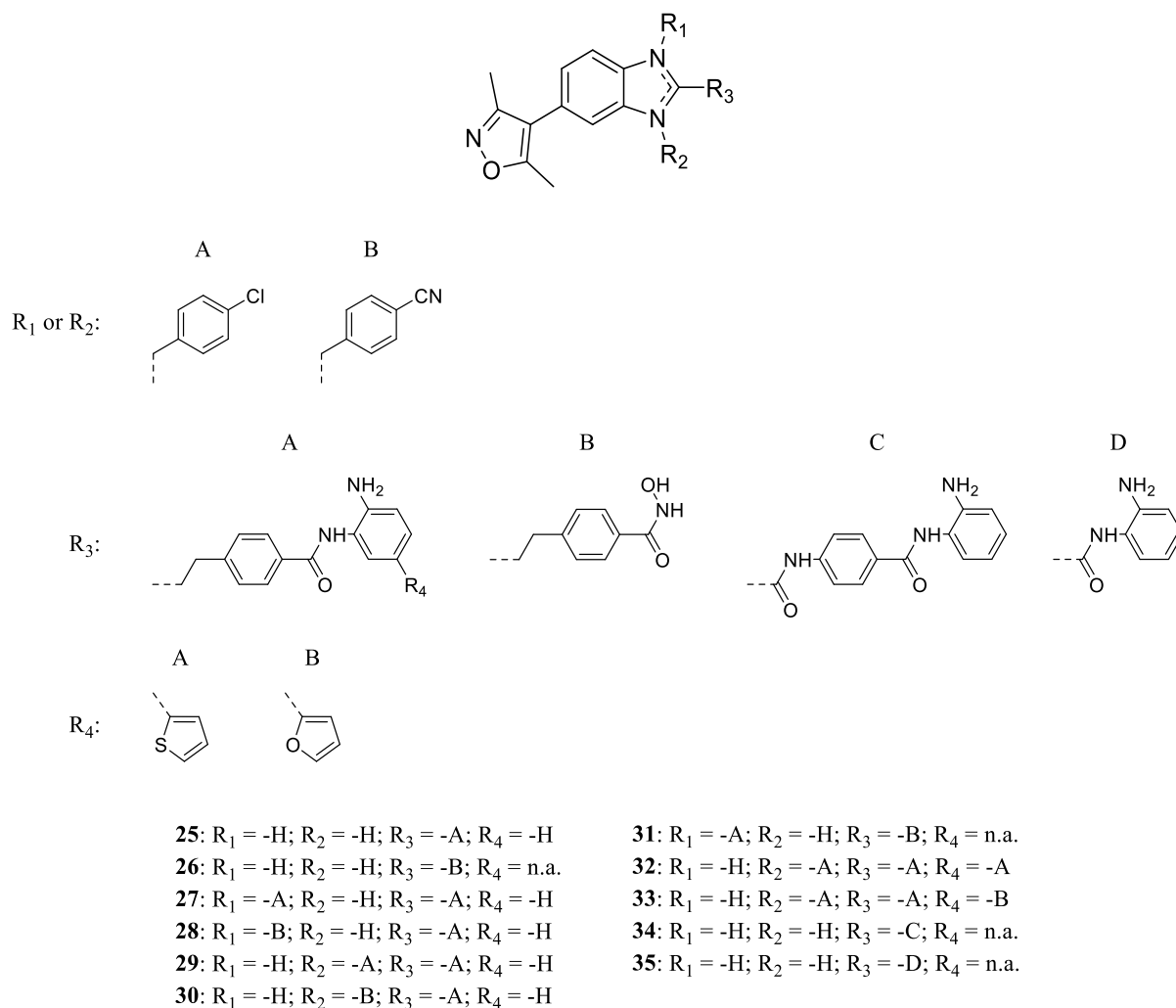


Figure 21: Planned dual inhibitors of the third generation.

At last, with PLX51107 (**36**) one more BETi was selected to be the basic structure of a dual inhibitor. The distinction between **36** and **23** is that **36** is a pyrrolo[3,2-b]pyridine and **23** is a benzimidazole, two different but rather similar structures. Apart from that, there are two more reasons for this selection, first its low nanomolar activity and second its exposed carboxylic acid similar to JQ1. A benzamine can be easily attached to this carboxylic acid to integrate the HDAC activity.

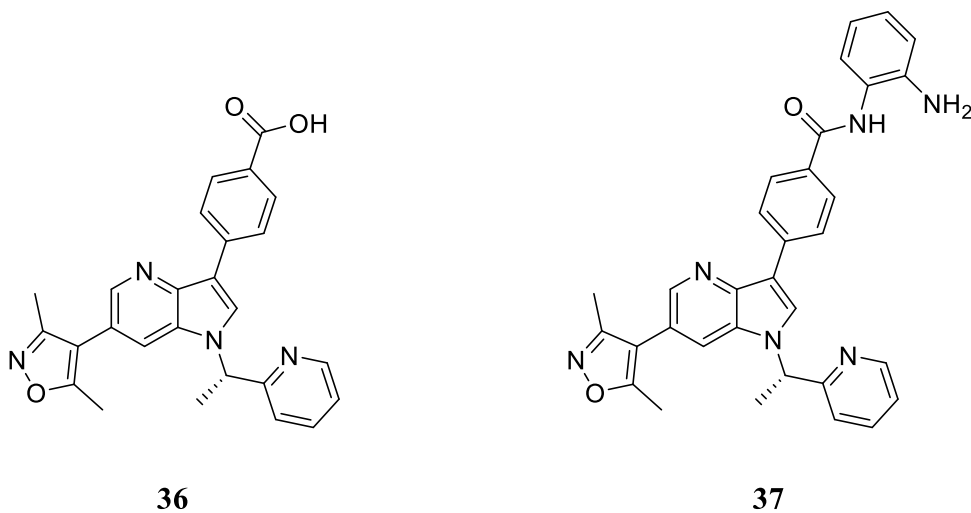
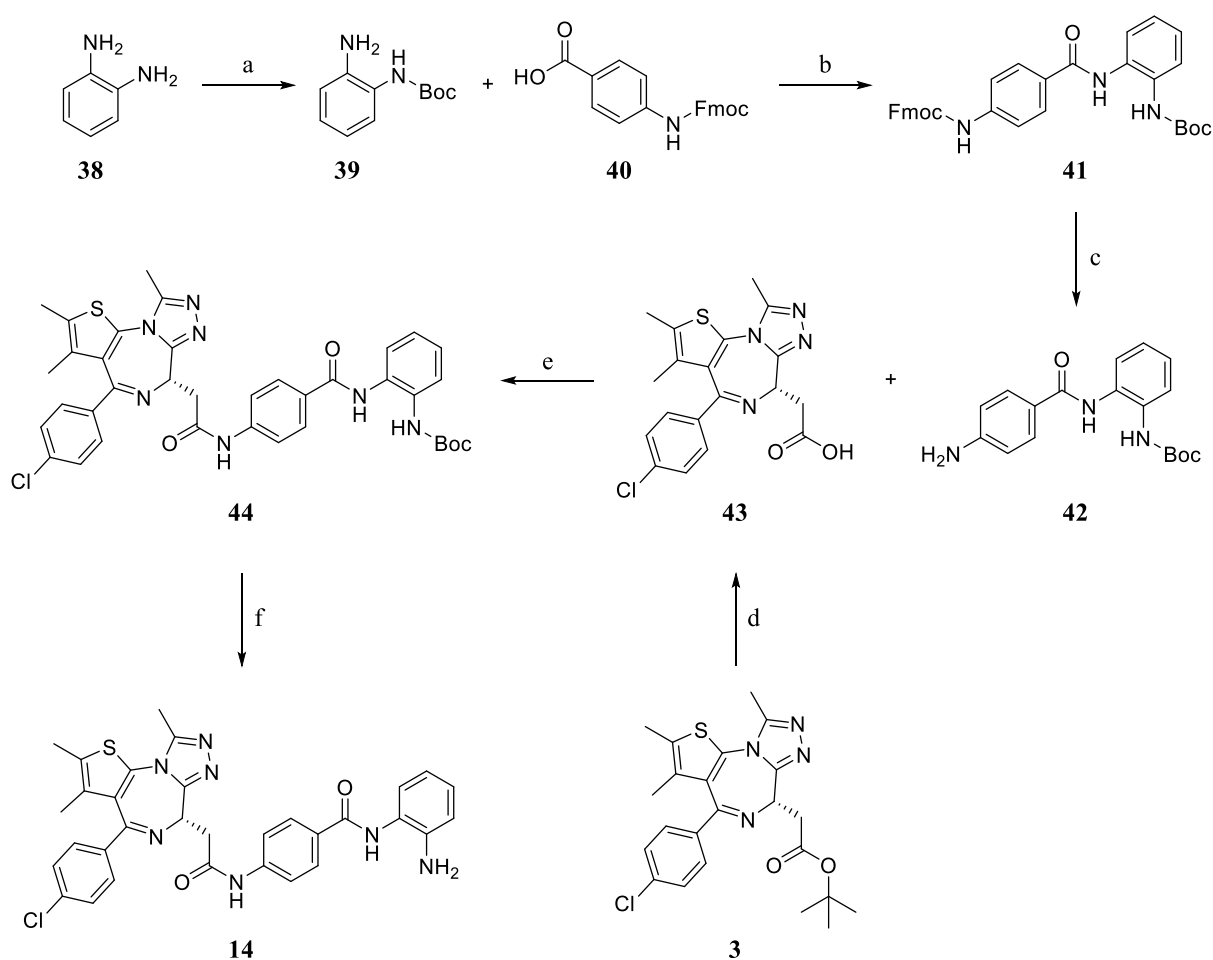


Figure 22: Structure of PLX51107 (**36**) and the planned potential dual inhibitor **37**.

### 3. Methods

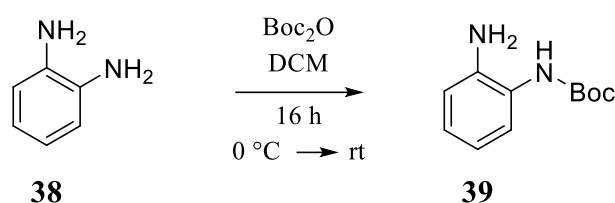
#### 3.1. Synthetic strategy of the first generation

Synthesis of the BETi part is relatively easy since JQ1 is commercially available and has to be hydrolyzed to obtain the desired carbonic acid **43**. The synthesis of the first HDACi begins with the introduction of a Boc-protecting group followed by a HATU coupling reaction with the commercially available carbonic acid **40**. Of the resulting compound **41** the Fmoc-protecting group needs to be removed to obtain **42** which is then ready to be coupled with **43**. In the final step, only the Boc protective group needs to be removed to obtain **14** (Scheme 1).



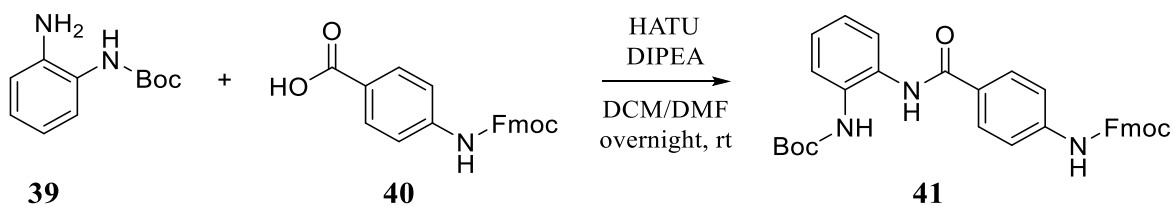
Scheme 1: Reaction scheme for the synthesis of compound 13. (a) DCM,  $\text{Boc}_2\text{O}$ , rt, 16 h ; (b) DCM/DMF, HATU, DIPEA, rt, 16 h ; (c) DCM, morpholine, rt, 30 min ; (d) THF/MeOH/ $\text{H}_2\text{O}$ , LiOH, rt, 16 h ; (e) DCM/DMF, HATU, DIPEA, rt, 16 h ; (f) DCM/TFA, rt, 45 min.

The first step of the synthetic route was to selectively protect one amine of compound **38**, whereas due to the symmetry no distinction between the two available amines was necessary. This reaction was performed with di-*tert*-butyl dicarbonate ( $\text{Boc}_2\text{O}$ ) dissolved in dichloromethane (DCM) and added dropwise to a solution of **38** in DCM without any catalytic amounts of a base and stirred for 16 hours (Scheme 2). In a first attempt of this reaction triethylamine (TEA) and 4-Dimethylaminopyridine (DMAP) was added which resulted in the protection of both amines. Depending on the expected yield, purification was performed either by column chromatography or recrystallisation which resulted in a relative yield of 77 % or 62 %, respectively.



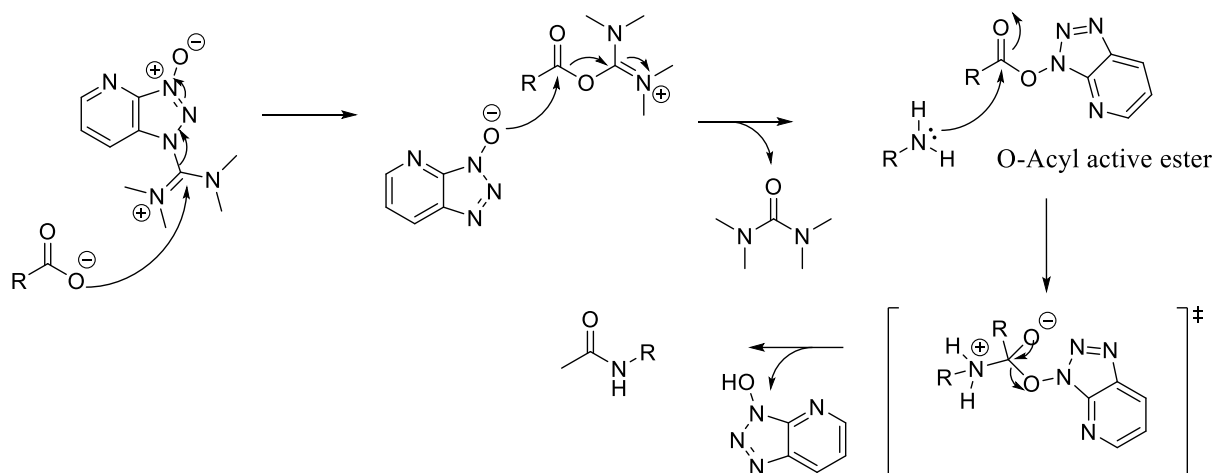
Scheme 2: Selective protection of one amine of **38** with a *tert*-butyloxycarbonyl protecting group.

The resulting compound **39** was reacted with the commercially available benzoic acid **40** in the presence of the coupling agent hexafluorophosphate azabenzotriazole tetramethyl uranium (HATU) and *N,N*-diisopropylethylamine (DIPEA) (Scheme 3).



Scheme 3: Amide coupling reaction of **39** and **40** with HATU and DIPEA.

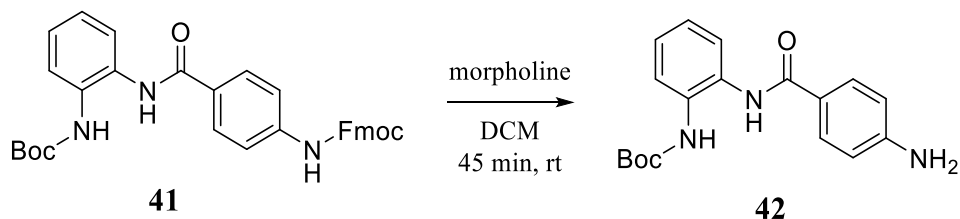
An important step in this reaction is not to add the amine immediately, but to wait so that the active ester can form (Scheme 4).<sup>[82]</sup>



Scheme 4: Mechanism of N-acylation with HATU.<sup>[82]</sup>

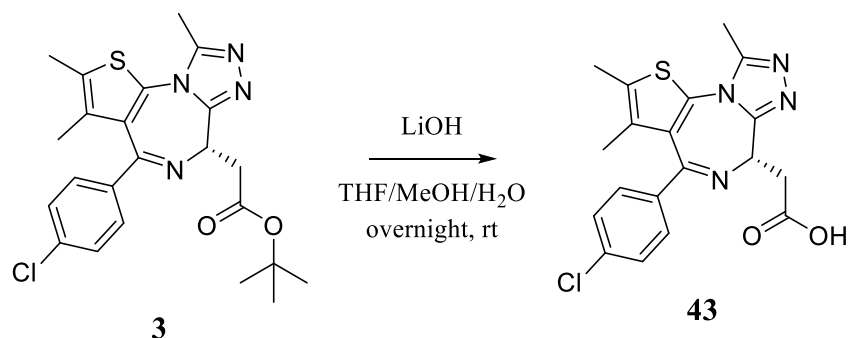
First the deprotonated acid function attacks the positively charged carbon of HATU and generates the reactive O-acyl active ester by rearrangement. The amine is then added and reacts with the active ester to form a peptide bond to give the desired product.

The following step included the removal of the Fmoc protective group (Scheme 5). Although this reaction is normally performed with piperidine it turned out that morpholine provides the significantly better yields here (86 % instead of 68 % or even 0 %).



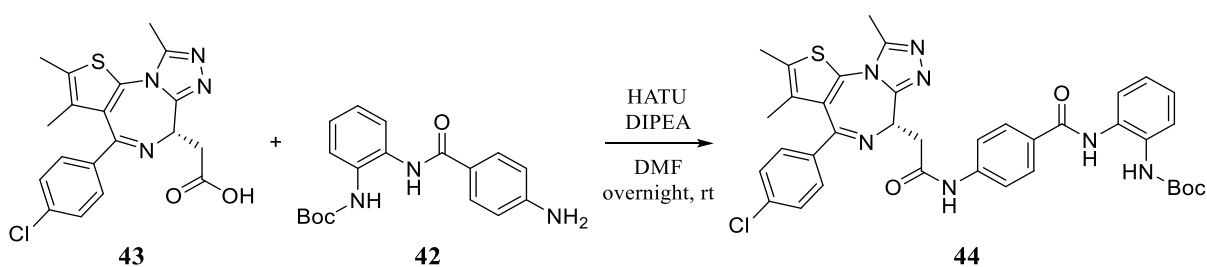
Scheme 5: Removal of the Fmoc protection group with morpholine.

In order to couple **42** to JQ1, JQ1 needed to be hydrolyzed to afford **43**. To do that, JQ1 was dissolved in a mixture of THF/MeOH/H<sub>2</sub>O and reacted with LiOH overnight (Scheme 6).



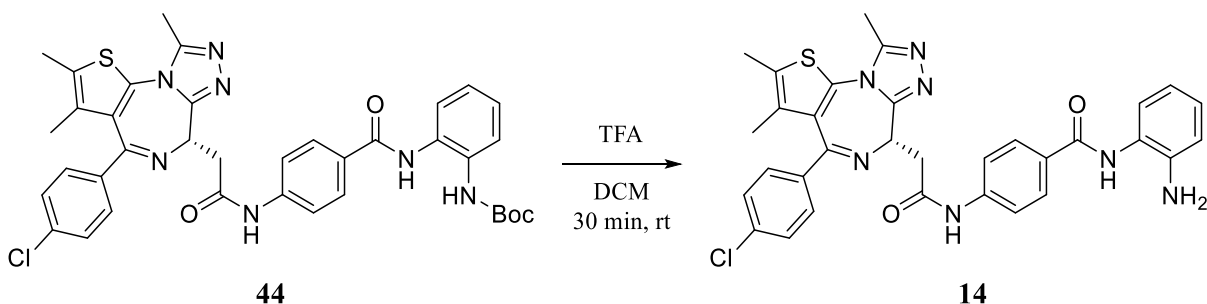
Scheme 6: Hydrolysis of JQ1 with LiOH.

The second to last step is the crucial one, because of its low yield of only 56 % after optimizing the reaction (Scheme 7).



Scheme 7: Amide coupling reaction of **42** and **43** with HATU and DIPEA.

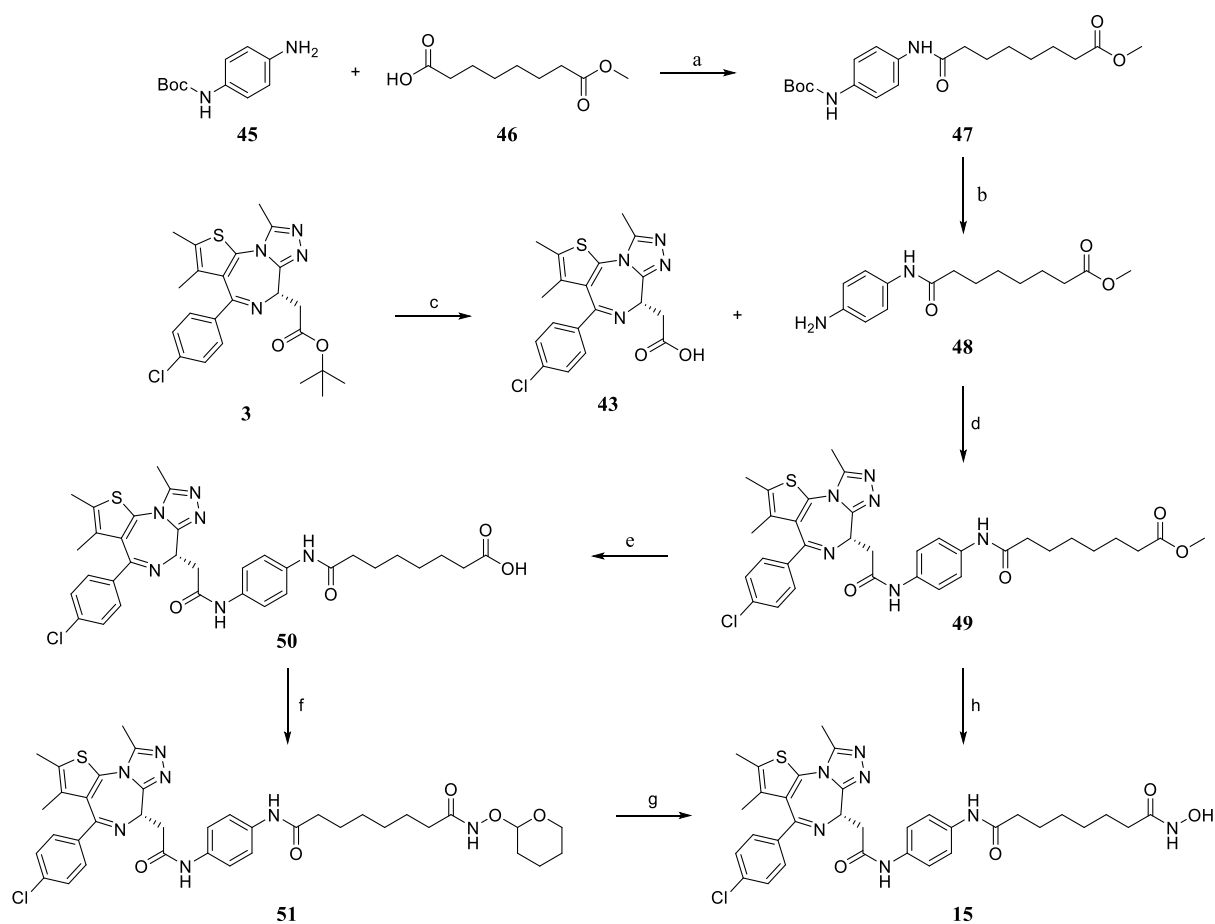
In the last step the Boc protecting group was removed with trifluoroacetic acid (TFA) to obtain the final compound **14** (Scheme 8). The yield here was 64 %, giving a yield of 8 % over all reactions.



Scheme 8: Removal of Boc protecting group with TFA.

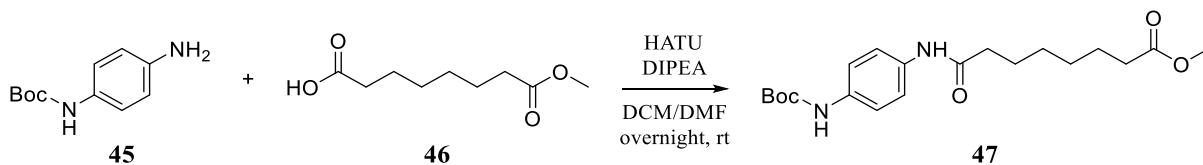


The synthesis of the second JQ1 adduct starts with another HATU coupling reaction to obtain compound **47** followed by the removal of the Boc protecting group. Then the JQ1 adduct is formed by yet another HATU coupling reaction. To reach the desired final stage with hydroxamic acid function there are at least two possibilities from this stage on. The first possibility starts with the hydrolysis of the ester followed by a coupling reaction with 2-(Aminoxy)tetrahydro-2H-pyran (OTX) and the deprotection to obtain the hydroxamic acid. The second possibility converts the ester directly into the hydroxamic acid under the use of hydroxylamine hydrochloride and sodium methoxide (Scheme 9).



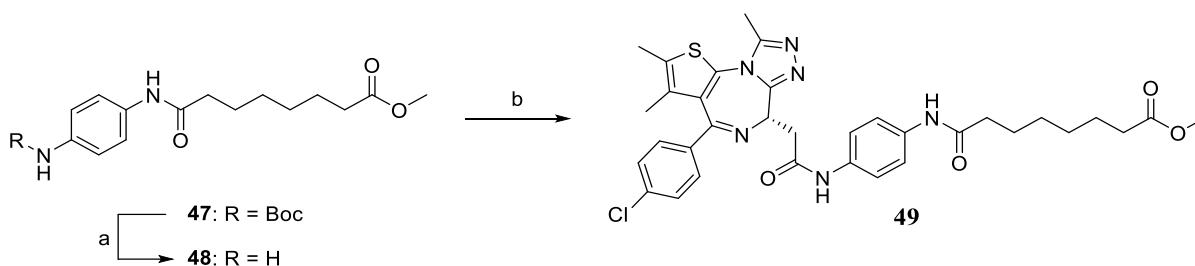
Scheme 9: Reaction scheme for the synthesis of compound **14**. (a) DCM/DMF, HATU, DIPEA, rt, 16 h ; (b) DCM/TFA, rt, 45 min ; (c) THF/MeOH/H<sub>2</sub>O, LiOH, rt, 16 h ; (d) DCM/DMF, HATU, DIPEA, rt, 16 h ; (e) THF/MeOH/H<sub>2</sub>O, LiOH, rt, 16 h ; (f) DCM/DMF, HATU, DIPEA, OTX, rt, 16 h ; (g) DCM/TFA, rt, 45 min ; (h) NH<sub>2</sub>OH·HCl, NaOMe, -78 °C, rt, 3 h.

This synthetic route started with a coupling reaction between the commercially available compounds **45** and **46** in the presence of HATU and DIPEA (Scheme 10).



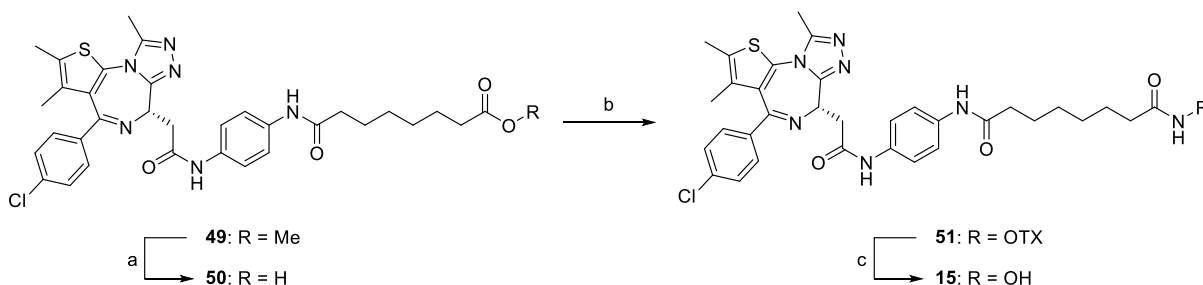
Scheme 10: Amide coupling reaction of **25** with HATU and DIPEA.

After removal of the Boc protection group the resulting compound **48** was coupled with **43** in the presence of HATU and DIPEA (Scheme 11).



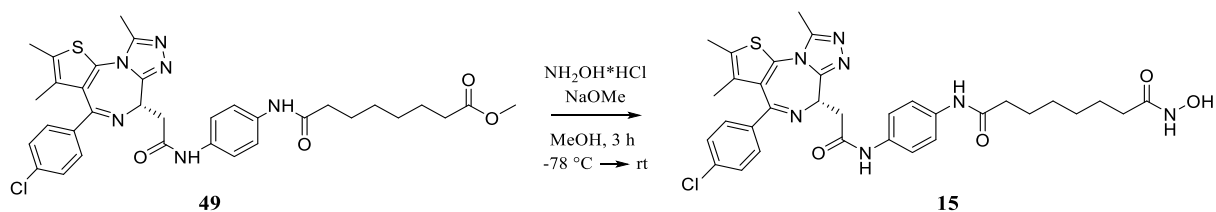
Scheme 11: Reaction scheme for compound **49**. (a) DCM/TFA, rt, 45 min ; (b) DCM/DMF, 16, HATU, DIPEA, rt, 16 h.

After obtaining compound **49** there are at least two possibilities to afford the desired compound **15**. The first possibility contains three reaction steps starting with the hydrolysis of the ester. The resulting carbonic acid is coupled with OTX in the presence of HATU and DIPEA to afford **51** which converts to the desired compound **15** after treatment with TFA (Scheme 12). The combined yield over all three steps was 18 %.

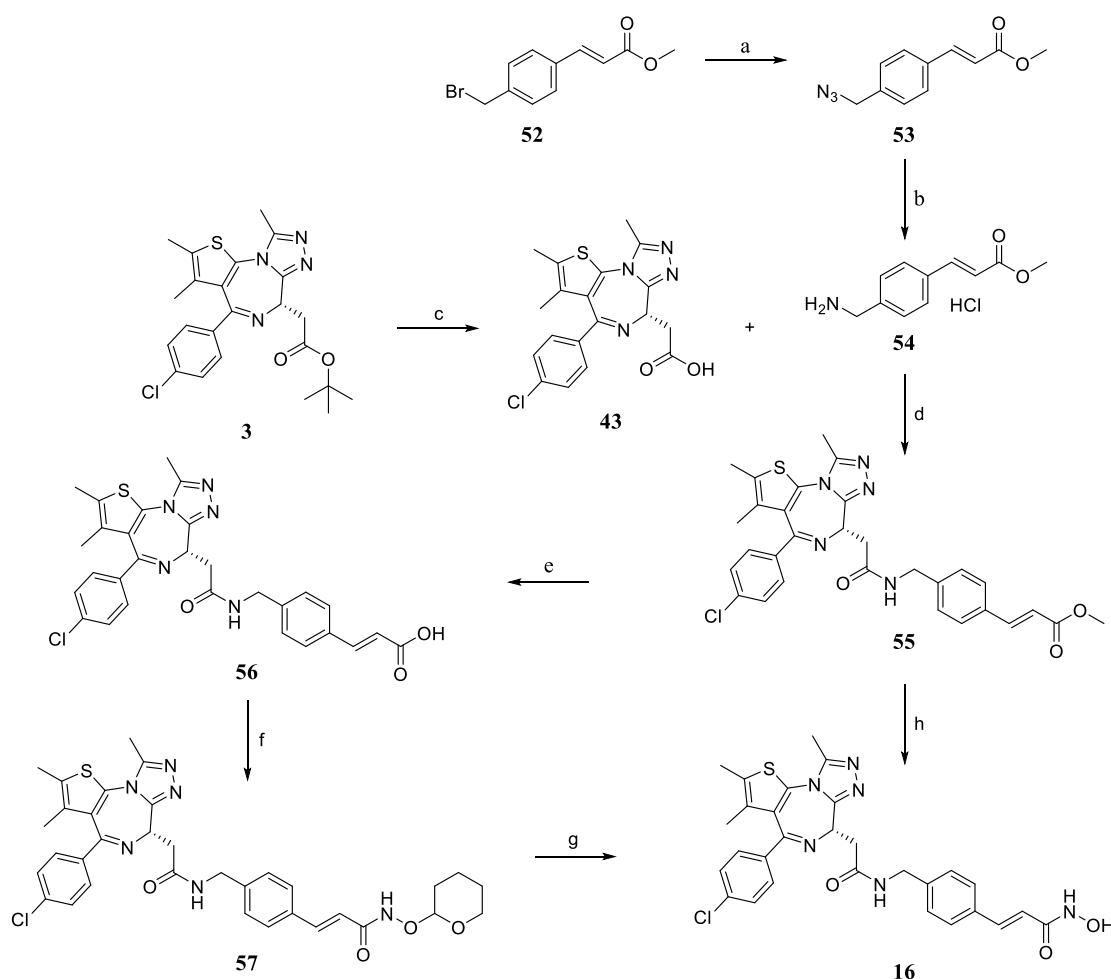


Scheme 12: Reaction scheme for compound **15**. (a) THF/MeOH/H<sub>2</sub>O, LiOH, rt, overnight ; (b) DCM/DMF, OTX, HATU, DIPEA, rt, 16 h ; (c) DCM/THF, rt, 45 min.

In contrast to the first, the second possible synthetic route contains only one step. Here compound **49** is converted directly into compound **15** with hydroxylamine hydrochloride and sodium methoxide. The reaction starts at -78 °C and is warmed to room temperature over the course of 3 hours. Although the route consists of only one step, the yield of 26 % is only slightly higher compared to the first one (Scheme 13).

Scheme 13: Direct conversion of the ester **49** to hydroxamic acid **15**.

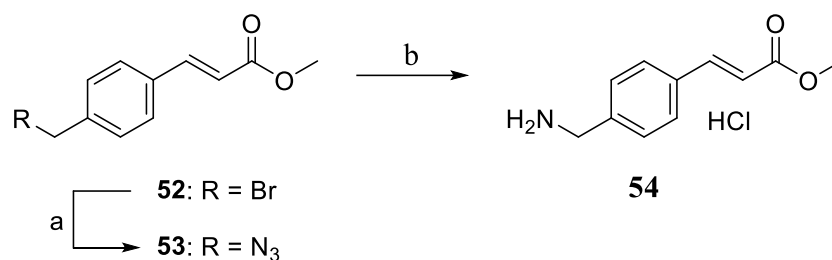
The synthetic route of the last JQ1 adduct starts with a Staudinger reaction to convert **52** into the required amine **53**. The here following steps are the same compared to the synthesis of compound **15**. First the coupling reaction with HATU and DIPEA to provide **55** succeeded by the two ways of forming the hydroxamic acid **16** (Scheme 14).



Scheme 14: Reaction scheme for the synthesis of compound **15**. (a) DMF, NaN<sub>3</sub>, 80 °C, 2 h ; (b) THF/H<sub>2</sub>O, PPh<sub>3</sub>, rt, overnight ; (c) THF/MeOH/H<sub>2</sub>O, LiOH, rt, 16 h ; (d) DCM/DMF, HATU, DIPEA, rt, 16 h ; (e) THF/MeOH/H<sub>2</sub>O, LiOH, rt, 16 h ; (f) DCM/DMF, HATU, DIPEA, OTX, rt, 16 h ; (g) DCM/TFA, rt, 45 min ; (h) NH<sub>2</sub>OH·HCl, NaOMe, -78 °C, rt, 3 h.

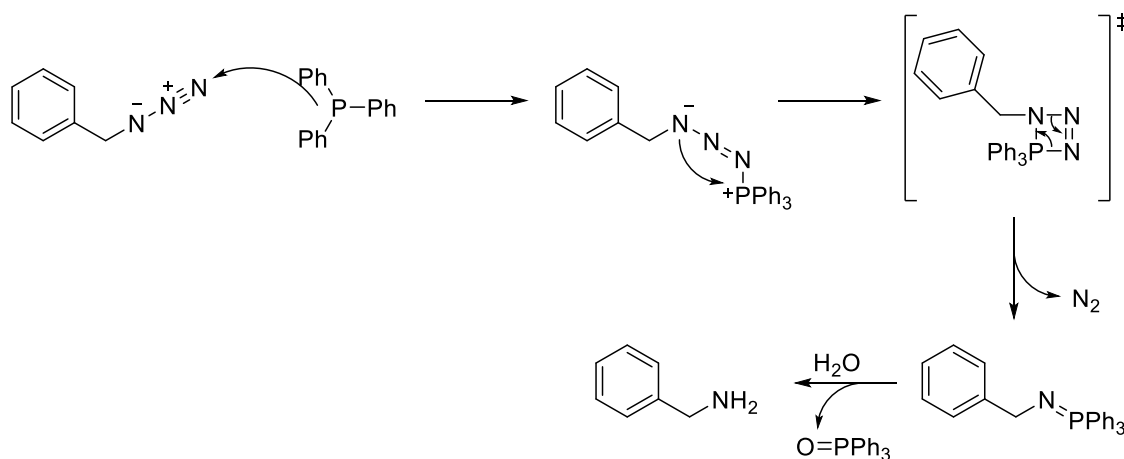
The first two reactions are part of the Staudinger reaction. The synthesis named after Hermann Staudinger is a method for the preparation of primary amines from halogen alkanes.<sup>[83]</sup> In the first step of this two-step synthesis, halogen alkanes react with sodium azide to replace the

halogen atom with an azide. The following reduction with triphenylphosphine and the subsequent aqueous preparation yields the desired primary amines. However, in this reaction the desired primary amine was precipitated with HCl dissolved in diethyl ether (Scheme 15).



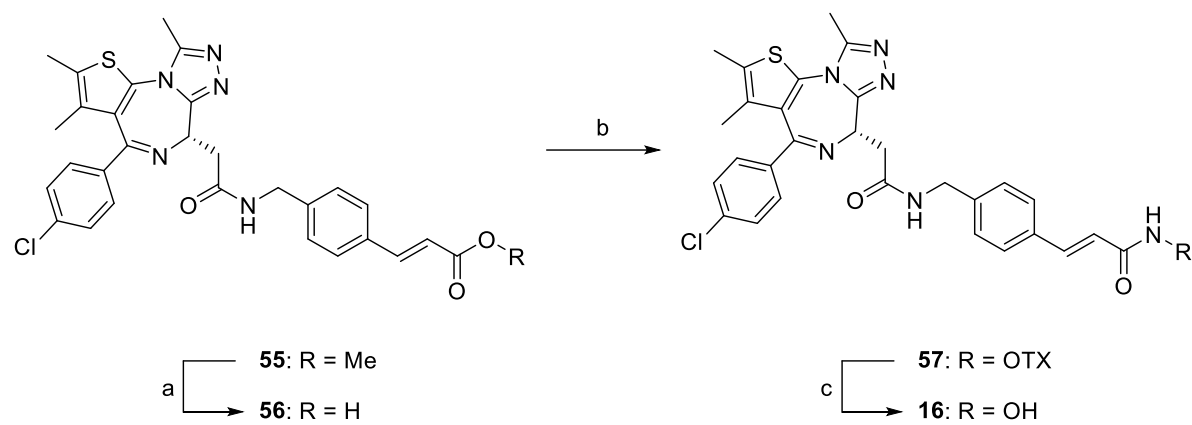
Scheme 15: Reaction scheme of the Staudinger reaction. (a) DMF, NaN<sub>3</sub>, 80 °C, 2 h ; (b) THF/H<sub>2</sub>O, PPh<sub>3</sub>, rt, overnight, HCl (1 M in diethyl ether).

The driving force of this reaction is the formation of elemental nitrogen and triphenylphosphine oxide. Yet, the Staudinger reaction is only suitable as a laboratory method, since triphenylphosphine oxide is formed stoichiometrically (Scheme 16).

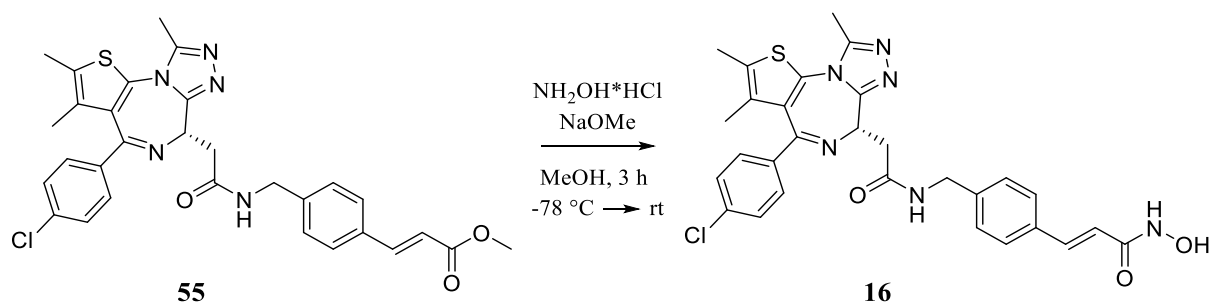


Scheme 16: Mechanism of the Staudinger reaction.

After obtaining compound **54** the now following steps are equivalent to the synthesis of **15**. After coupling to **43**, the resulting compound **55** can either be processed in the three steps described above (Scheme 17) or converted directly into the final product (Scheme 18).



Scheme 17: Reaction scheme for compound **16**. (a) THF/MeOH/H<sub>2</sub>O, LiOH, rt, overnight ; (b) DCM/DMF, OTX, HATU, DIPEA, rt, 16 h ; (c) DCM/THF, rt, 45 min.



Scheme 18: Direct conversion of the ester **55** to hydroxamic acid **16**.

### 3.1.1. Optimization of the synthetic route of **14**

Compound **14** showed very promising results (see chapter 4.1.) and was therefore synthesized multiple times. In order to obtain as much product as possible every reaction step was performed under several different conditions. For the first reaction (Scheme 2) the highest yield was obtained if no additional base was added while with TEA and DMAP both amines were eventually protected (Table 1). Although a yield of 77 % (or 62 % due to recrystallisation, respectively) is still not as high as it could be, the reaction is effortless to carry out and the educts are very favorable, so that further optimization is not necessary.

Table 1: Reaction conditions for the synthesis of **39**

Amount of <b>38</b> [g]	Solvent DCM [mL]	Bases	Absolute. yield [g]	Relative yield [%]
0.2	36	TEA/DMAP	0.065	17
0.2	18	TEA/DMAP	0.126	33
0.2	9	-	0.250	65
1.0	45	-	1.48	77
5.0	225	-	5.93	62

For the second reaction (Scheme 3) several different conditions were tested not only to optimize this reaction but also to obtain conditions worth testing for reaction number four, which is an amide coupling reaction as well (Table 2). The higher yields were obtained with the coupling reagent HATU in combination with DIPEA and an activation time of approximately 2 h. However, a larger batch size led to a dramatic loss of yield, despite the use of HATU and DIPEA. The probably best result of 86 % was achieved with a batch size of 0.5 g and DMF as the only solvent. The yield of 95 % is placed in parentheses because true yield was not definable since here the product still included minor impurities.

Table 2: Reaction conditions for the synthesis of **41**

Amount of <b>40</b> [g]	Solvent   proportion	Coupling agent	Base   eq	Activation [h]	Yield [%]
0.1	DCM/DMF   1:1	EDC/HOBt	DIPEA   1.2	1	-
0.1	DCM/DMF   1:1	EDC/HOBt	DIPEA   1.2	1	-
0.1	DCM/DMF   1:1	HATU	TEA   1.2	2	-
0.1	DMF	EDC/HOBt	DIPEA   2.4	2	17
0.1	DCM	HATU	DIPEA   1.2	1	68
0.1	DCM	HATU	DIPEA   1.2	1.5	74
0.1	DCM/DMF   1:1	HATU	DIPEA   2.4	1	76
0.1	DCM/DMF   1:1	HATU	DIPEA   2.4	2	77
1.0	DCM/DMF   1:1	HATU	DIPEA   2.4	2	27
1.0	DCM/DMF   1:1	HATU	DIPEA   2.4	2	45
0.5	DCM/DMF   1:1	HATU	DIPEA   2.4	2	(95)
0.5	DMF	HATU	DIPEA   2.4	2	86

Although the third reaction (Scheme 5) is a well-known deprotection step, the achievable yield may depend on the compound that needs to be deprotected and the base used. Here the deprotection with piperidine showed unreliable results from 0 % to 68 % yield but worked with morpholine even without additional solvent (Scheme 3).

Table 3: Reaction conditions for the synthesis of **42**

Solvent	Base	Proportion	Yield
DCM/DMF	Piperidine	5:4:1	68 %
DCM/DMF	Piperidine	2:2:1	25 %
DCM/DMF	Piperidine	2:2:1	64 %
DCM	Piperidine	1:1	-
DCM	Morpholine	1:1	80 %
-	Morpholine	-	86 %

As mentioned before beneficial conditions in the first amide coupling reaction were also tested in the next reaction (Scheme 7). Unfortunately, the outcome of this reaction is hard to predict and even with every condition the same the yield varies between 14 % (lowest) and 56 % (highest). In the end this reaction was not optimized further because enough product was eventually obtained (Table 4).

Table 4: Reaction conditions for the synthesis of **44**

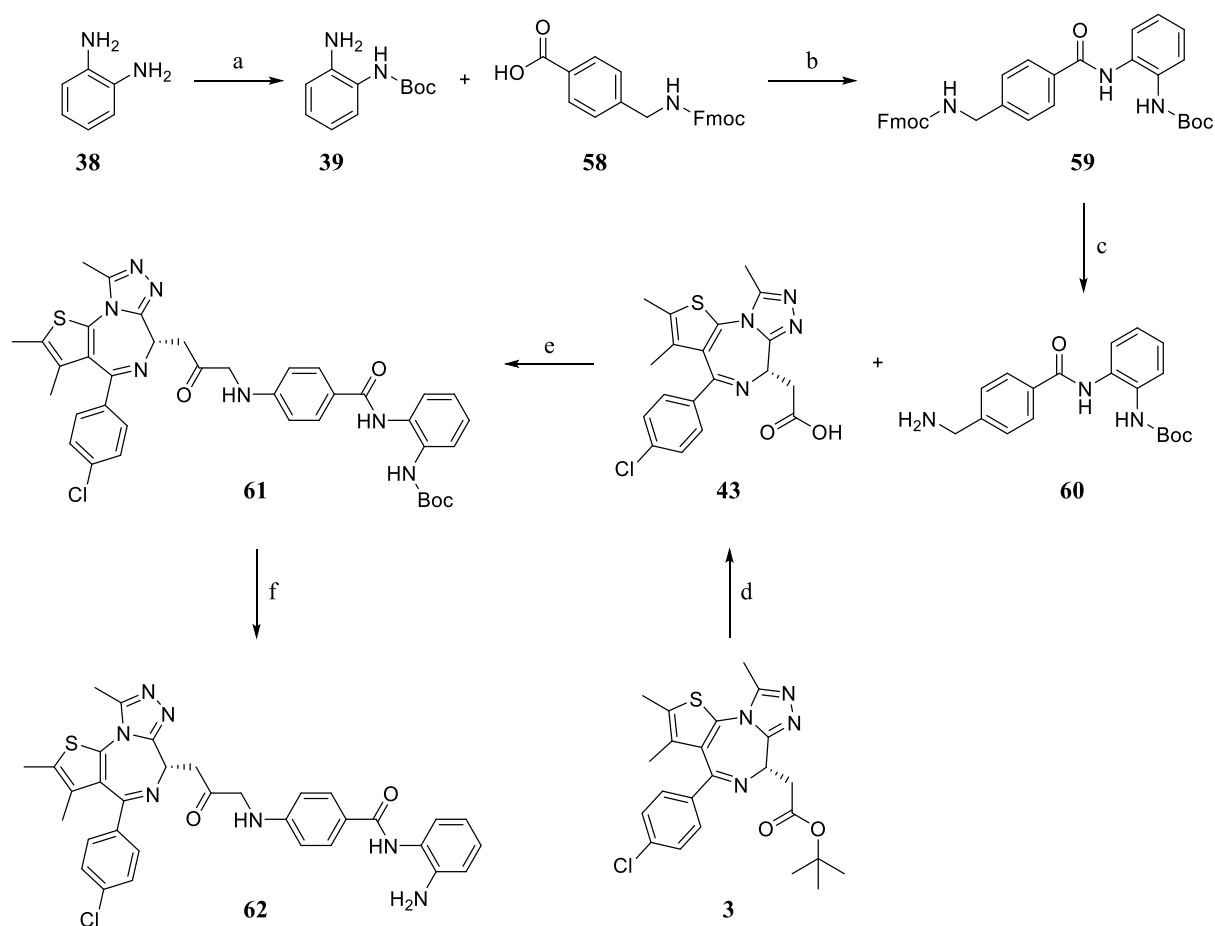
Amount of <b>16</b> [mg]	Solvent   proportion	Activation [h]	Base   eq	Yield %
102	DCM/DMF   1:1	1	DIPEA   1.1	38
133	DCM/DMF   1:1	1	DIPEA   2.4	40
200	DCM/DMF   1:1	0.5	DIPEA   2.4	40
50	DCM/DMF   1:1	2	DIPEA   2.4	50
131	DCM/DMF   1:1	2	DIPEA   2.4	55
100	DMF	0.5	DIPEA   1.2	56
100	DMF	0.5	DIPEA   1.2	48
100	DMF	0.5	DIEPA   1.2	14

The last reaction is the removal of the Boc group (Scheme 8) and due to its simplicity, there are hardly changeable conditions. The only condition changed was the temperature which was reduced from room temperature to 0 °C while adding TFA. This measure resulted in a yield increase from 60 % to 76 %. In total over all reactions, the yield was increased from 8 % to 24 %.



## 3.1.2. Additional JQ1-adduct.

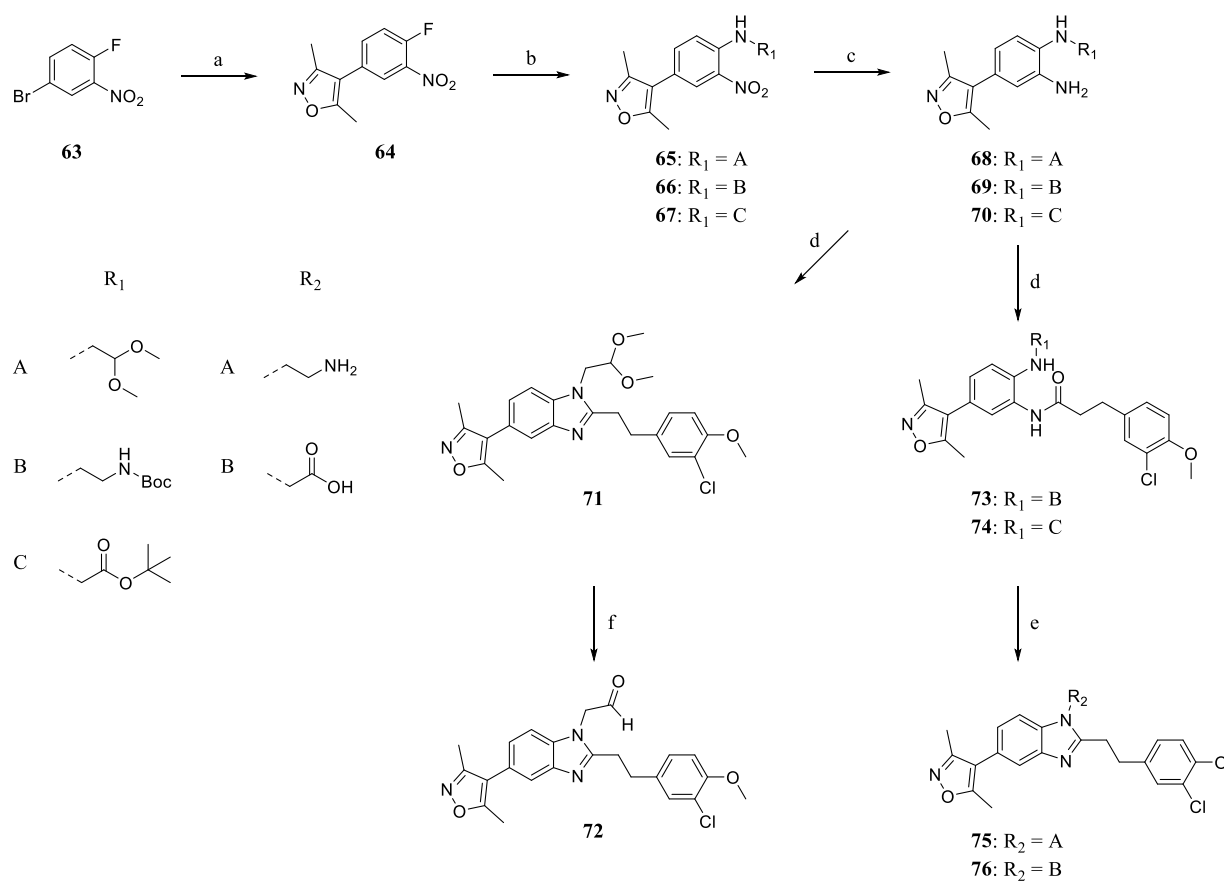
The relatively low yield in the fourth step of the synthesis could be due to the aniline **42** used, with which a higher yield may not be possible. In general anilines exhibit a lower basicity because the nitrogen lone pair is partly delocalized into the  $\pi$ -system. However, since a higher basicity is advantageous for the HATU coupling reaction, aniline **42** was replaced by benzylamine **60**, which should lead to a higher yield and hopefully maintains its inhibitory effect. The complete synthetic route is shown in Scheme 19.



Scheme 19: Reaction scheme for the synthesis of compound **62**. (a) DCM, Boc<sub>2</sub>O, rt, 16 h ; (b) DCM/DMF, HATU, DIPEA, rt, 16 h ; (c) DCM, morpholine, rt, 30 min ; (d) THF/MeOH/H<sub>2</sub>O, LiOH, rt, 16 h ; (e) DCM/DMF, HATU, DIPEA, rt, 16 h ; (f) DCM/TFA, rt, 45 min.

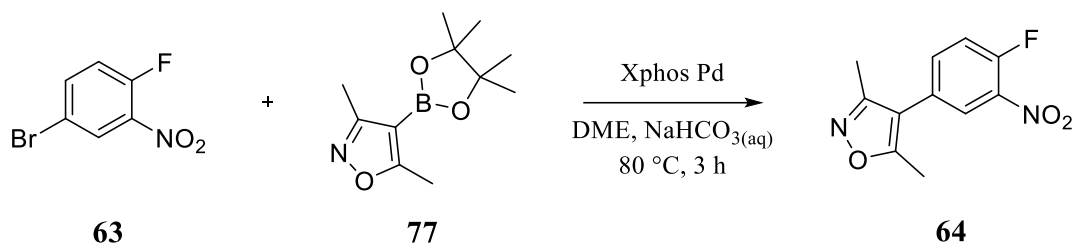
### 3.2. Synthetic strategy of the second generation

The first part of the synthetic route of these compounds started with a Suzuki reaction followed by a nucleophilic aromatic substitution at the fluorine with three different amines. In the next step the nitro group is reduced to the amine so it can be part of the following HATU reaction to form the amide. In case of **71** the ring closed itself during the HATU reaction and the last step here is to oxidize the acetal to form the aldehyde **72**. However, the ring closure was a separate reaction for **73** and **74** in which their respective protective groups were removed as well to obtain **75** and **76** (Scheme 20).



Scheme 20: Reaction scheme for the first half dual inhibitors. (a) DME,  $\text{NaHCO}_3(\text{aq})$ , **77**, Xphos palladacycle Gen 3, 80 °C, 3 h ; (b) THF, corresponding amine, DIPEA, rt, overnight ; (c) EtOH, EtOAc, Pd/C,  $\text{H}_2$ , rt, 1 h ; (d) DMF, HATU, DIPEA, **82**, rt, overnight ; (e) dioxane/4 N HCl, reflux, overnight ; (f) DCE,  $\text{H}_2\text{O}$ , TFA

The first step of this reaction route was a Suzuki reaction, which is a palladium catalyzed cross coupling reaction. Here it was used to react **63** with the boronic ester **77** to form **64** in a good yield of 83 %.



Scheme 21: Reaction scheme for the Suzuki reaction to obtain **64**.

In this reaction XPhos-G3-Palladacycle (Figure 23, **78**) is used as a precatalyst, which means that the active LPd(0) species is generated *in situ*.<sup>[84]</sup> The activation of the precatalyst is performed by a suitable base such as NaHCO<sub>3</sub> which deprotonates **78** and forms the key intermediate Pd(II) complex I. In the next step the reductive elimination occurs which produces the kinetically active LPd(0) species (Figure 23, bottom).<sup>[85]</sup>

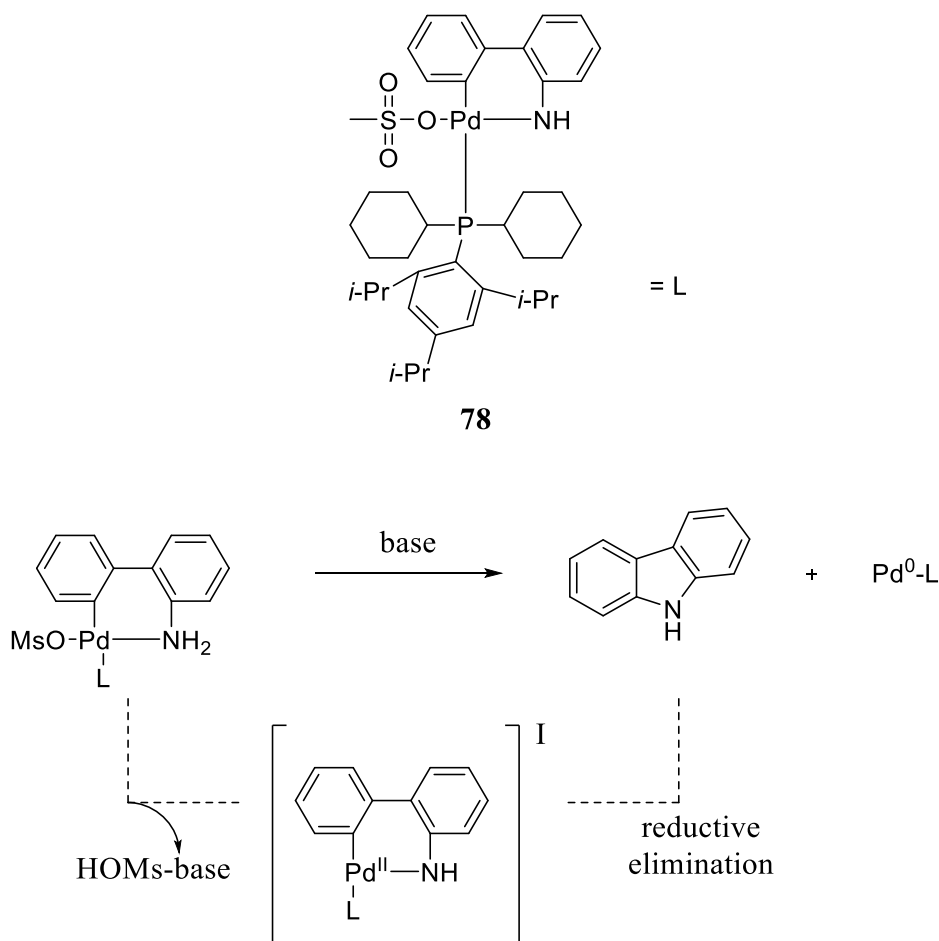


Figure 23: Structure of the precatalyst XPhos Pd Gen. 3 (**78**) and mode of activation of **78**.

Since the Suzuki reaction and other cross coupling reaction as well are palladium catalyzed the kinetically active  $\text{LPd}(0)$  species needs to be regenerated in a catalytic cycle (Figure 24). This cycle starts with the oxidative addition of an aryl halide to the  $\text{Pd}(0)$  species followed by the transmetalation in which a second aryl is transferred from a boron to the palladium. The last step completes the catalytic cycle and yields the desired biaryl and restores the  $\text{Pd}(0)$  species in a reductive elimination.<sup>[86]</sup>

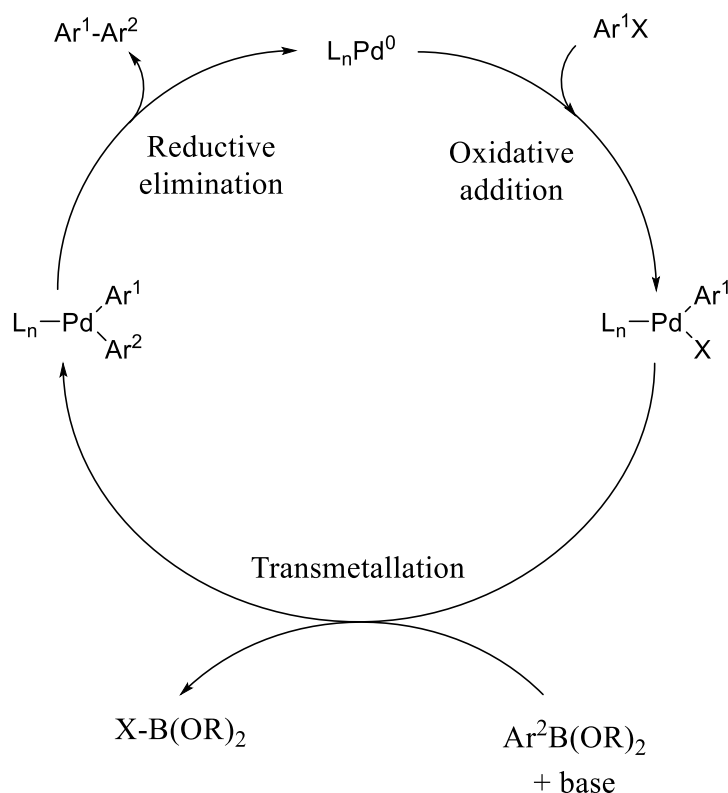


Figure 24: General catalytic cycle of a palladium catalyzed cross coupling reaction, X = halide  $\text{L}_n$  = ligand

The resulting compound **64** was then reacted with three different amines (Figure 25) in the presence of DIPEA (Scheme 22). This reaction is a nucleophilic aromatic substitution and affords the compounds **65**, **67** in high yields of 96 %. In case of **66** the yield is only 60 % probably due to the fact that the corresponding amine **80** was present as hydrochloride.

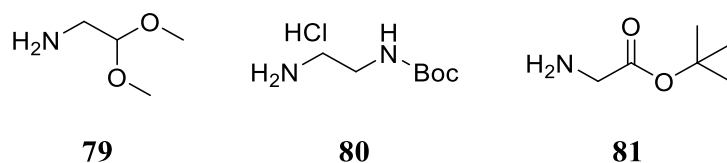
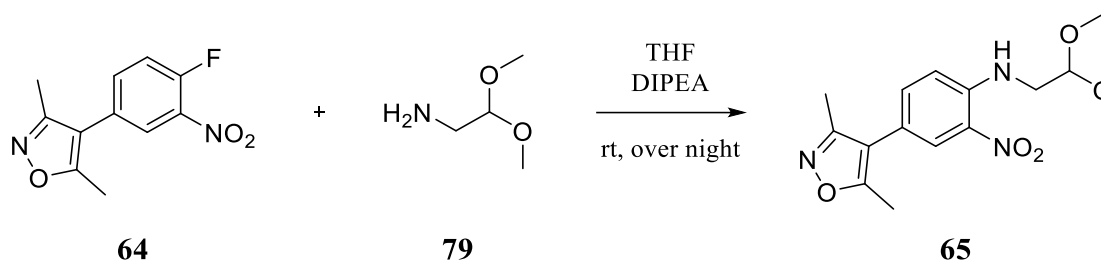
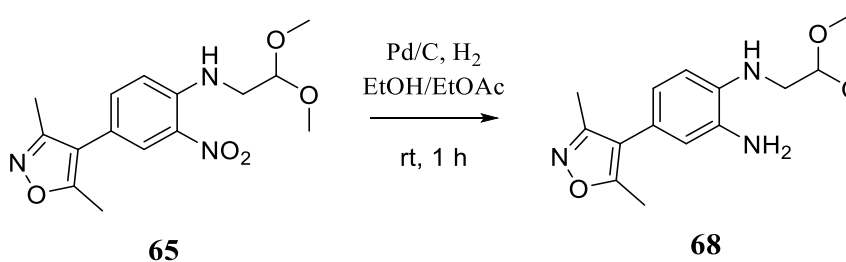


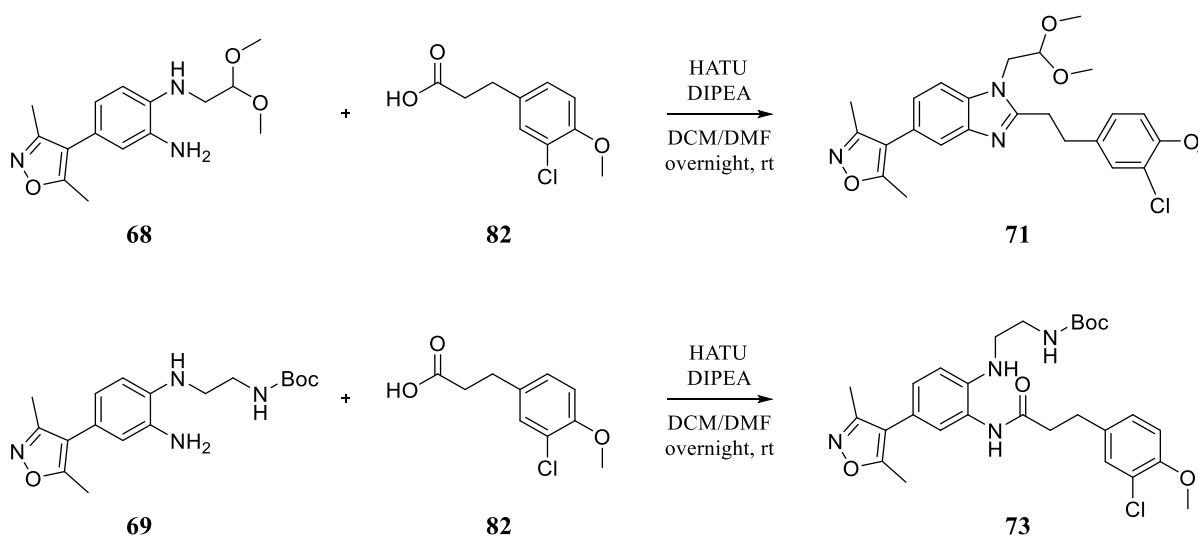
Figure 25: Amines used in the nucleophilic aromatic substitution.

Scheme 22: Nucleophilic aromatic substitution using the example of **79** to afford **65**.

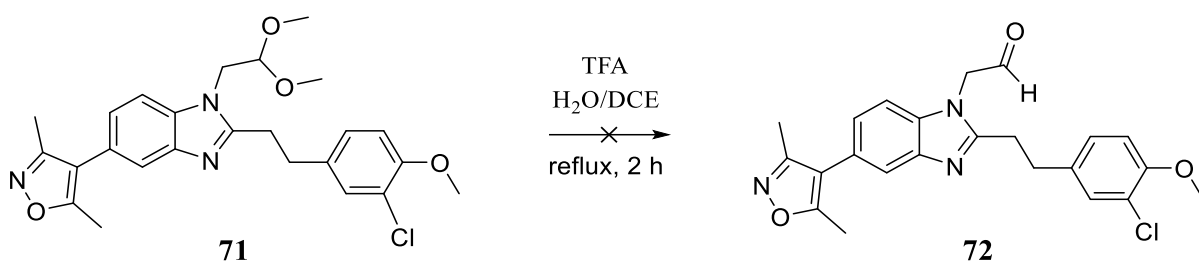
The following reaction is performed with hydrogen and palladium on carbon in order to reduce the nitro group (Scheme 23). For the success of this reaction, it is crucial not to let the reaction stir too long, even if educt is still present, otherwise the isoxazole will be reduced as well.

Scheme 23: Reduction of nitrobenzene using the example of **65** to afford **68**.

The resulting anilines **68-70** were reacted with **82** and HATU to form the desired amides in yields from 63 % to 83 %. In the case of **68**, the reaction did not stop at the amide stage, but rather completed the intramolecular conversion to the benzimidazole **71** already during this reaction in a yield of 84 % (Scheme 24).

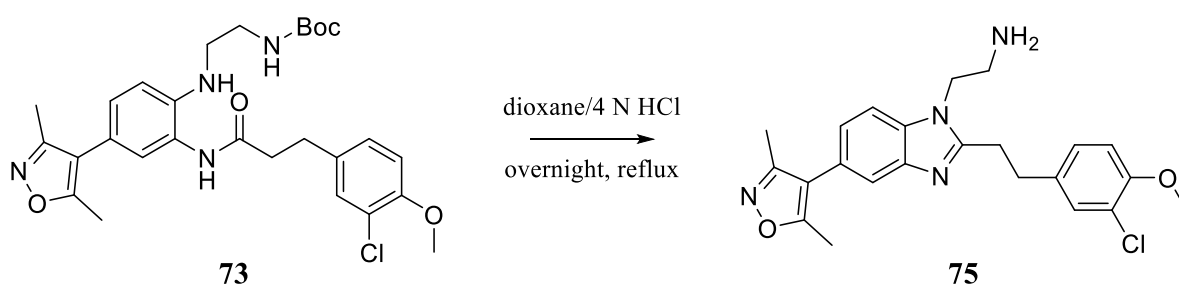
Scheme 24: HATU reaction using the example of **68** which directly converts to the benzimidazole **71** and HATU reaction using the example of **69** to obtain **73**.

Compound **71** was then treated with TFA in H<sub>2</sub>O/DCE which should result in the formation of the aldehyde **72** (Scheme 25). Although MS initially indicated the success of the reaction, the aldehyde **72** could neither be isolated nor used in the following reaction without purification, as the aldehyde was either oxidized to carboxylic acid or reduced to primary alcohol.



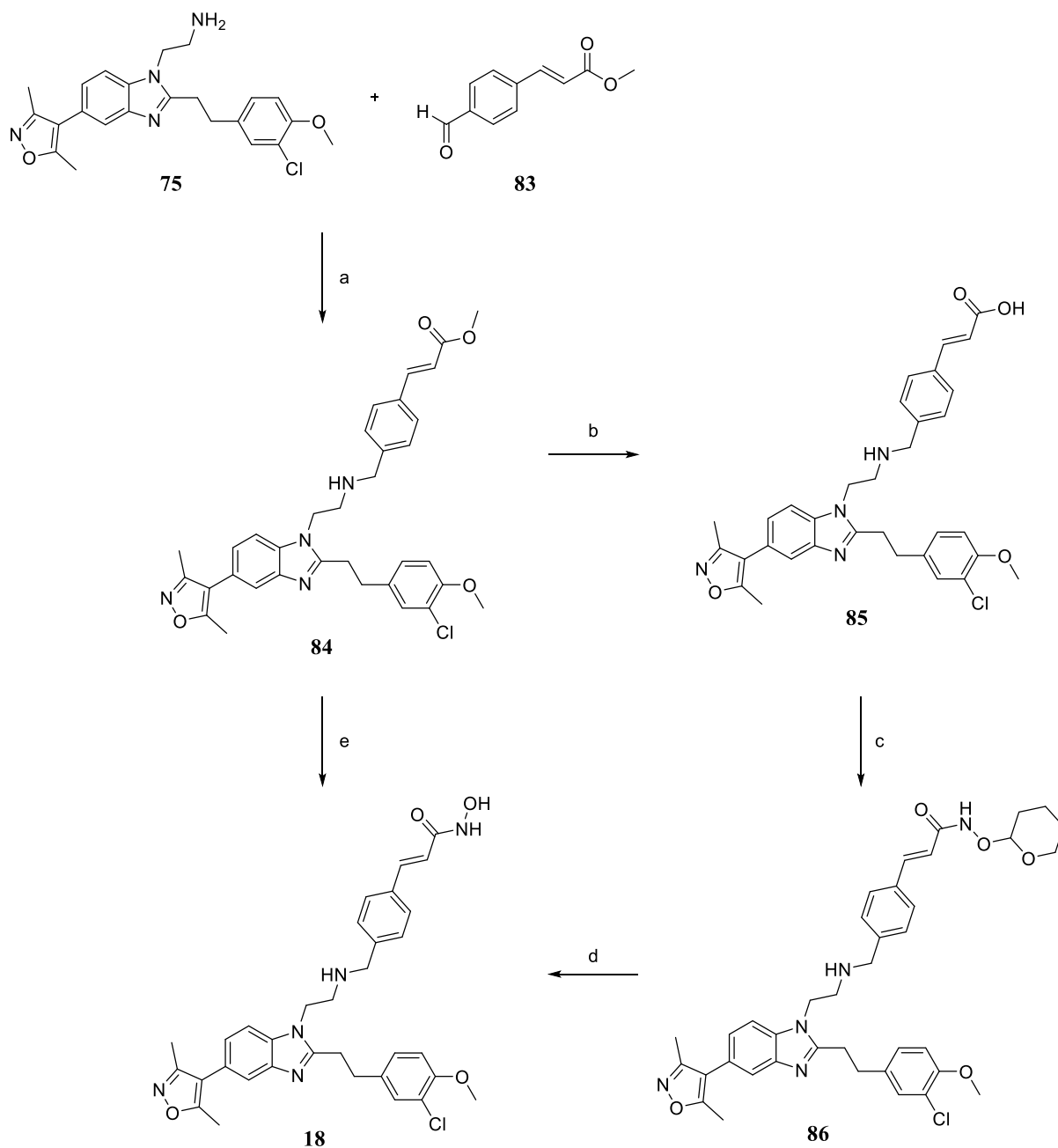
Scheme 25: Attempted formation of aldehyde **72** with TFA.

For this reason, the synthetic route was changed and **79** was replaced by **80** in order to obtain the amine **75** instead of the aldehyde **72**. In principle, this does not change the execution of this synthetic route except for a separate reaction to close the ring during which the protecting groups are removed as well (Scheme 26). The same applies if **81** is used to obtain the carboxylic acid **76**.



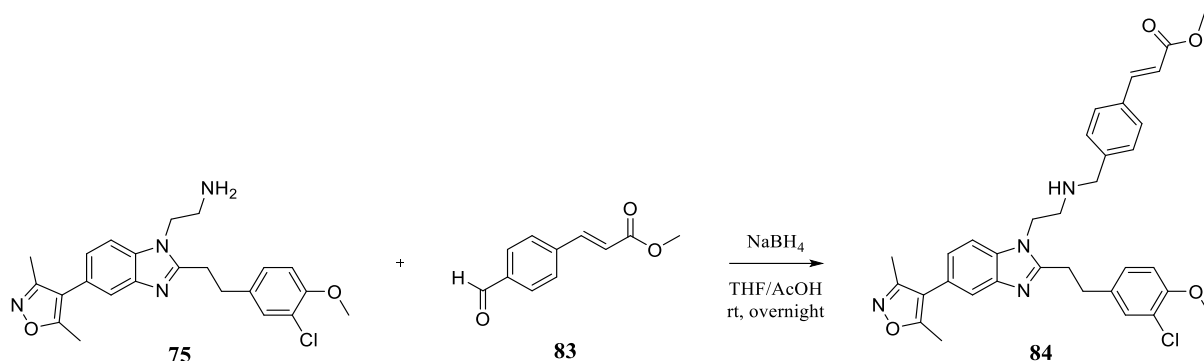
Scheme 26: Ring closure and removal of protecting group using the example of **73** to obtain **75**.

The second half of this synthetic route is to implement the HDAC inhibiting group. In the case of **18**, this is performed by a reductive amination which is the reason why it was possible to use **75** instead of **72** and still obtain the desired compound **84**. This reaction is again succeeded by the two possible ways of forming the hydroxamic acid to obtain the final compound **18** (Scheme 27).



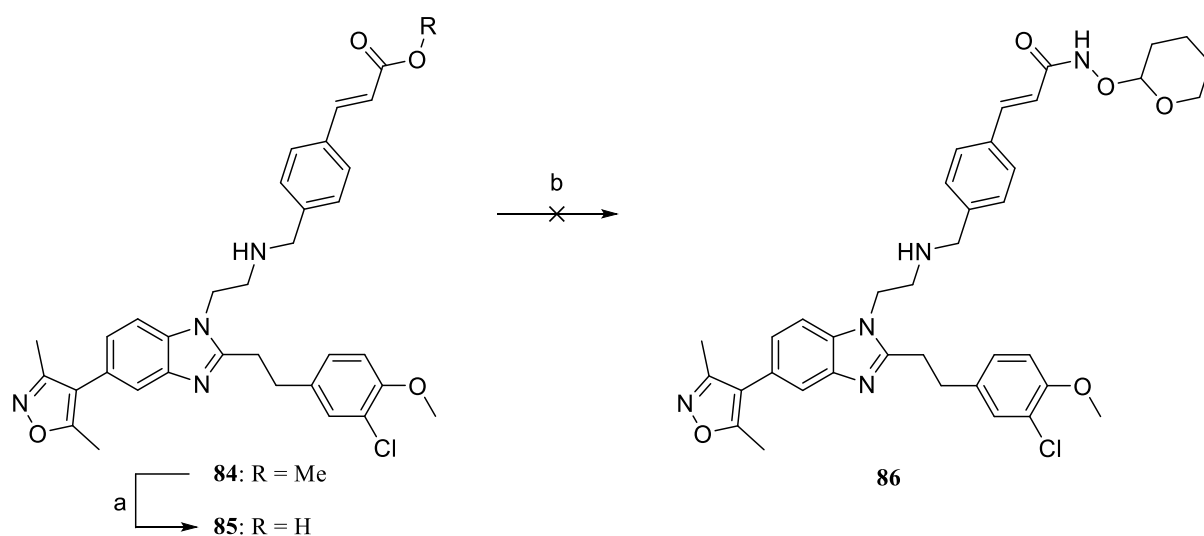
Scheme 27: Reaction scheme for the synthesis of compound **18**. (a) THF, AcOH, NaBH<sub>4</sub>, rt, overnight ; (b) THF/MeOH/H<sub>2</sub>O, LiOH, rt, 16 h ; (c) DCM/DMF, HATU, DIPEA, OTX, rt, 16 h ; (d) DCM/TFA, rt, 45 min ; (e) NH<sub>2</sub>OH·HCl, NaOMe, -78 °C, rt, 3 h.

The reductive amination between **75** and **83** was carried out multiple times with the yield varying between 22 % and 55 %. The best results were obtained when THF was mixed with a small amount of acetic acid and used as a solvent (Scheme 28). This is comparable to the Eschweiler-Clarke reaction, in which formic acid serves both as a proton source and as a hydrogenating agent.<sup>[87]</sup>



Scheme 28: Reductive amination of **75** and **83** to form **84**.

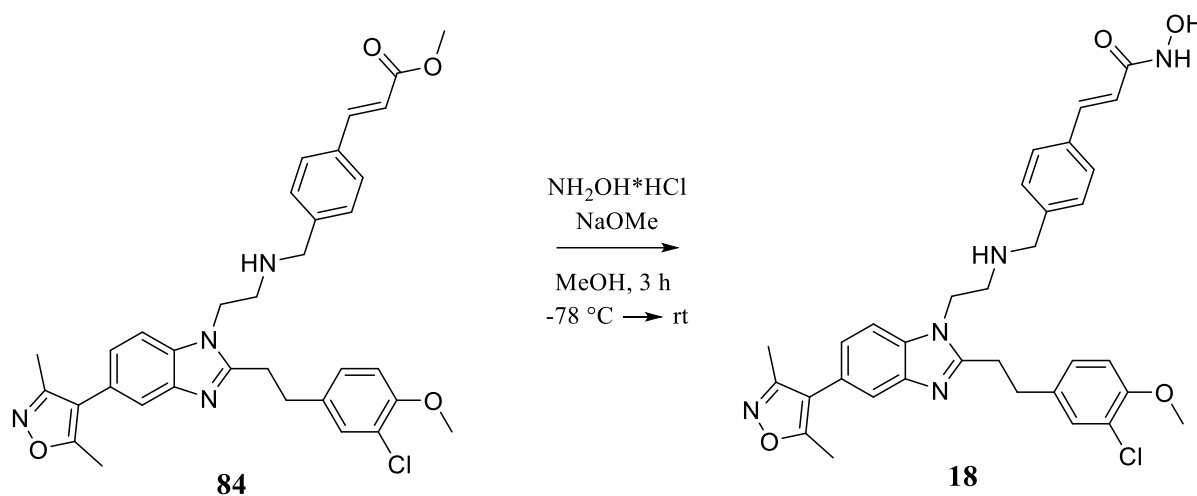
After the synthesis of **84** there are again the two previously described possibilities for the preparation of hydroxamic acid. However, the first possibility did not work here due to solubility issues, which is why a different synthetic route had to be found in the first place. After hydrolysis of the ester, the resulting compound **85** proved to be insoluble in DMF and hardly soluble in DMSO, so that the following HATU coupling reaction was impossible (Scheme 29).



Scheme 29: Reaction scheme for the synthesis of compound **86**. (a) THF/MeOH/H<sub>2</sub>O, LiOH, rt, 16 h; (b) DCM/DMF, HATU, DIPEA, OTX, rt, 16 h

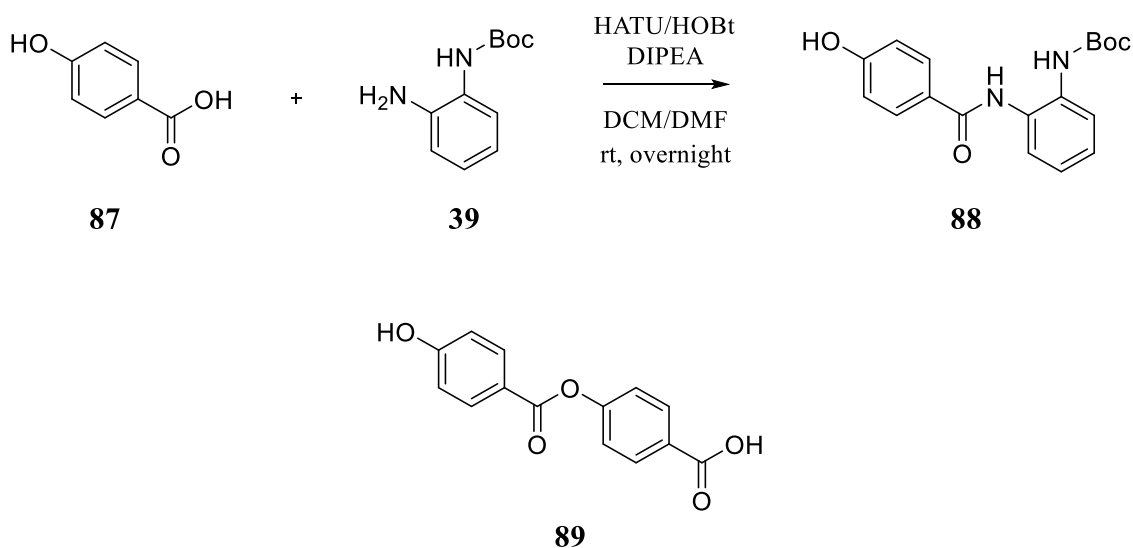


The alternative found was the direct conversion of the ester (Scheme 30) which is the better option in every way. Since it is only one reaction instead of three there is a huge time saving, and the yield is higher as well. For this reason, this reaction became the standard when synthesizing hydroxamic acids.



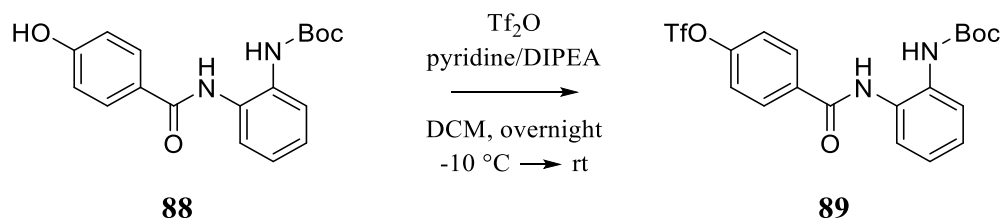
Scheme 30: Direct conversion of **84** to obtain final compound **18**.

Regarding the planned compounds **19-21** two of the required HDACi parts were already synthesized with **42** and **60**, respectively. The synthetic route for the still required HDACi part started with yet another HATU coupling reaction but this time the amine was added right from the start (Scheme 31, top). This measure was taken to minimize the formation of the ester **89** (Scheme 31, bottom) as a side product. Additionally, HOBt was added here which resulted in a higher yield.



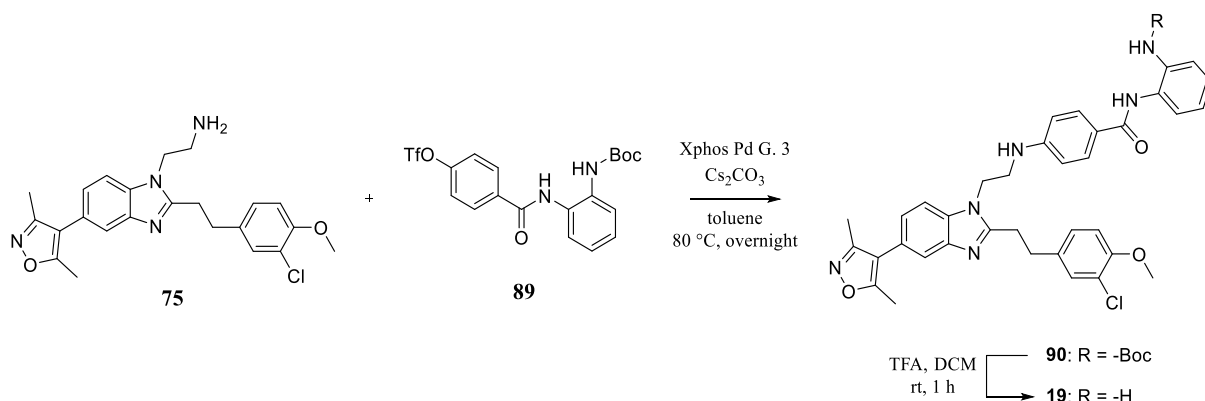
Scheme 31: Amide coupling reaction of **87** and **39** with HATU, HOBt and DIPEA with the potential side product **89** of the reaction above.

In the following step **88** was reacted with trifluoromethanesulfonic anhydride (Tf<sub>2</sub>O) in the present of pyridine and DMAP (Scheme 32). Through this reaction the hydroxy group gets replaced by a triflate which is the better leaving group and enables the arylation of **75**.



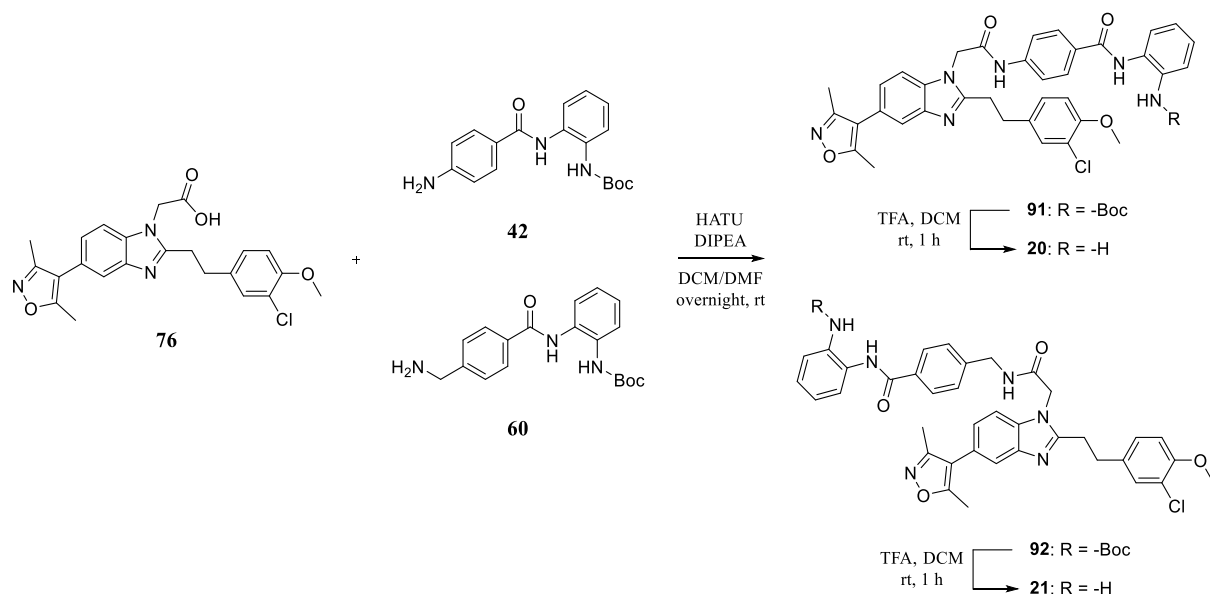
Scheme 32: Synthesis of triflate **89** from phenol **88**.

In the next reaction **75** is reacted with **89** in the presents of Xphos Pd Gen. 3 and cesium carbonate to obtain **90**. After this only the Boc group needs to be removed to obtain the final compound (Scheme 33).



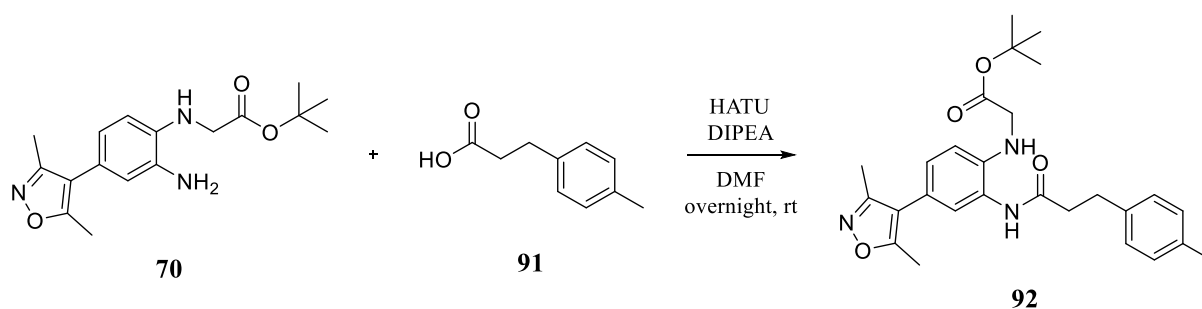
Scheme 33: Palladium catalyzed arylation of **75** followed by the removal of Boc-protecting group to obtain final compound **19**.

The next two compounds of this generation are synthesized the same way, whereby **76** is linked once with **42** and once with **60** in a HATU coupling reaction. Again, the last step is the deprotection of the amine which is performed with TFA in DCM (Scheme 34).



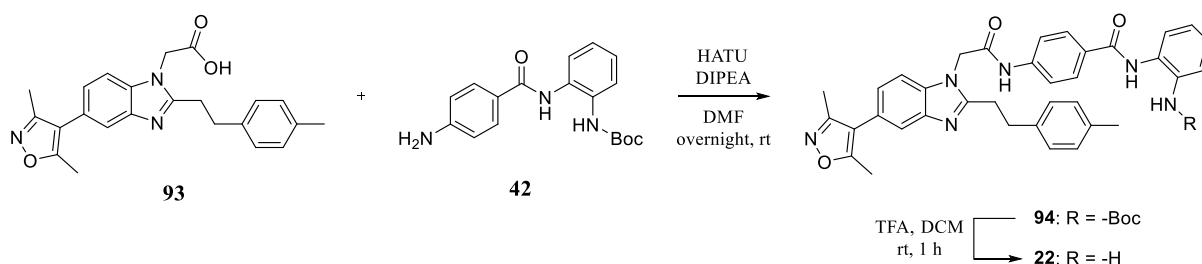
Scheme 34: HATU coupling reaction followed by the removal of the Boc-protecting group to obtain the final compounds **20** and **21**.

The last compound of the second generation is basically synthesized the same way, whereby **70** is linked to **91** instead of **82** (Scheme 35) in the fourth step of the synthetic route described in Scheme 20 with the difference that from now on only DMF is used as solvent.



Scheme 35: HATU reaction of **70** and **91** to obtain **92**.

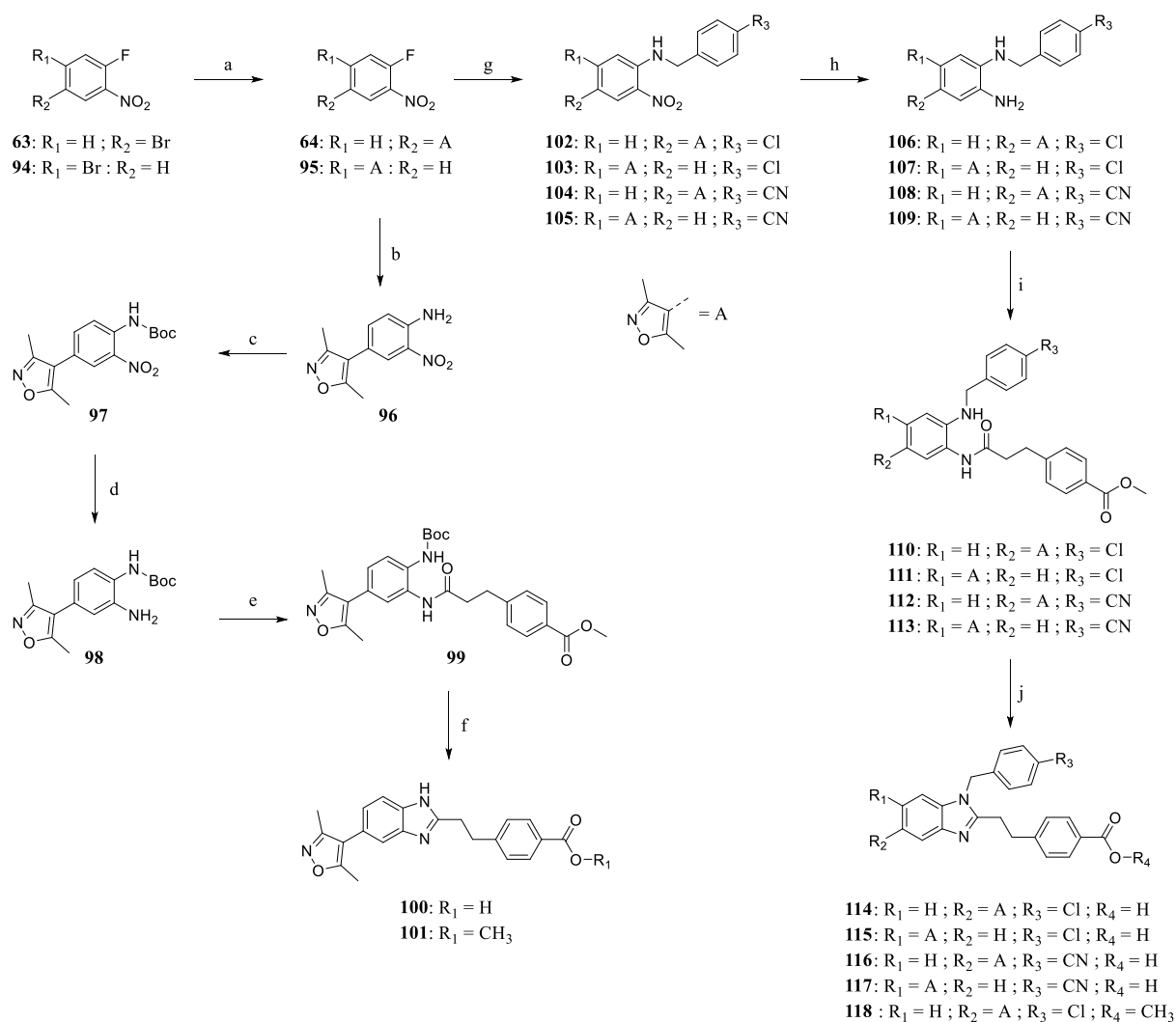
Following the same reactions as before the final compound **22** is obtained in the end. As HDACi part **42** was used again (Scheme 36), because the corresponding final compound **20** showed the most promising results in testing (see chapter 4.2.).



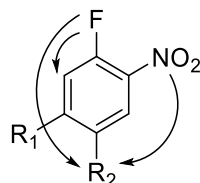
Scheme 36: HATU coupling reaction followed by the removal of the Boc-protecting group to obtain the final compound **22**.

### 3.3. Synthetic strategy of the third generation

The synthetic strategy of the third generation is partially same as for the second one (see chapter 3.2.). In order to obtain the compounds **25** - **33** the first half of this route starts again with a Suzuki reaction, this time with **63** and its constitutional isomer **94**. In the first of the two next possible steps the fluorine is replaced by an amine to afford **96** after which an additional reaction step of protection is necessary before the nitro group is reduced. Then, after another HATU coupling reaction to obtain **99**, the ring closure and removal of either both protecting groups or just the Boc group can be done in one reaction step to yield **100** and **101**. The other possible step after the Suzuki reaction and the steps after that are basically the same as for the second generation with one exception. The reduction step was no longer performed with palladium on carbon, but with tin(II) chloride.



Although the first reaction is basically the same as before it is still worth a closer look because with **94** the yield is only 45 % in comparison to 83 %. Since the only difference is the position of the bromine in relation to the other substitutes, the reason for the lower yield must be related to this. In fact, the reason is to be found in the directing effect of the nitro group and the fluorine. While a nitro group favors a substitution in meta position, a fluorine group directs in ortho and para position both from the point of view of the respective substituent. In case of **63** the bromine is in the right position, whereas in **94** it is the exact opposite (Figure 26).

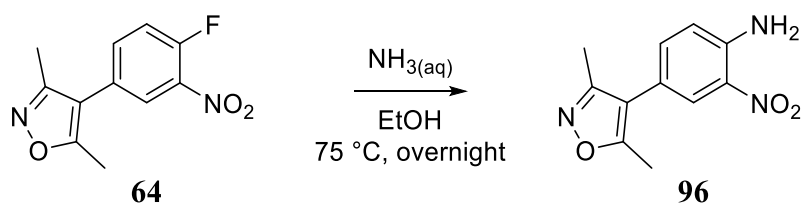


**63**:  $R_1 = H$  ;  $R_2 = Br$

**94**:  $R_1 = Br$  ;  $R_2 = H$

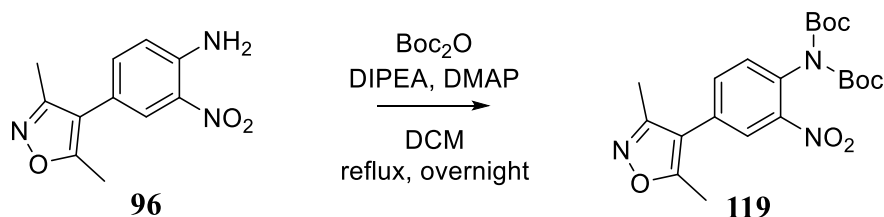
Figure 26: Directive effects of the substituents of **63** and **94**.

In the next step the fluorine is substituted by an amine, which is achieved with an excess amount of ammonia solution.



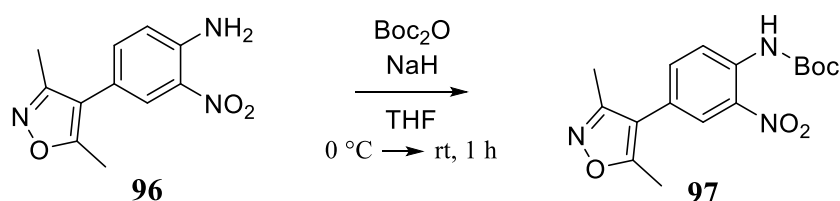
Scheme 38: Substitution reaction of **64** to obtain **96**.

Before the nitro group could be reduced the amine had to be protected. Despite its easy nature this reaction was rather challenging because the amine became protected twice as main product (76 %) which prevented the following reactions from working properly.



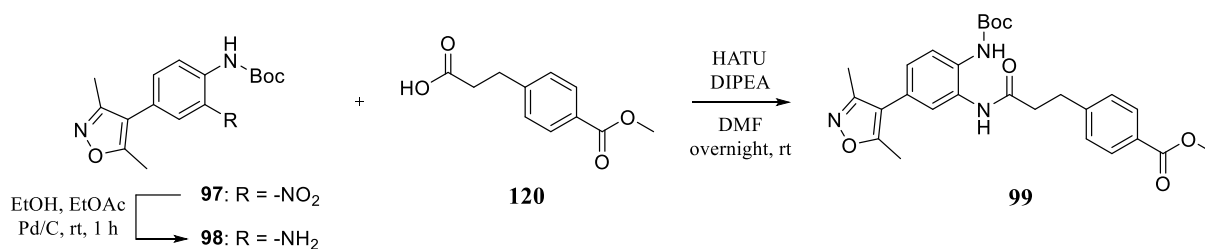
Scheme 39: Reaction conditions that lead to double Boc protection and yielded **119**.

First, the reaction was repeated with a smaller amount of  $\text{Boc}_2\text{O}$ , which increased the yield of the desired product from 25 % to 45 %, but still produced **119** as well and left educt behind. By using sodium hydride, an alternative route was found to produce the desired product with a yield of 79 % without the occurrence of double protection (Scheme 40).



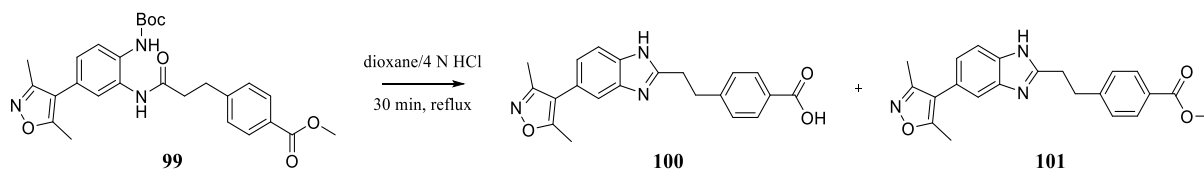
Scheme 40: Single protection of **96** to afford **97**.

The following reduction of the nitro group and the subsequent HATU reaction were performed as before.



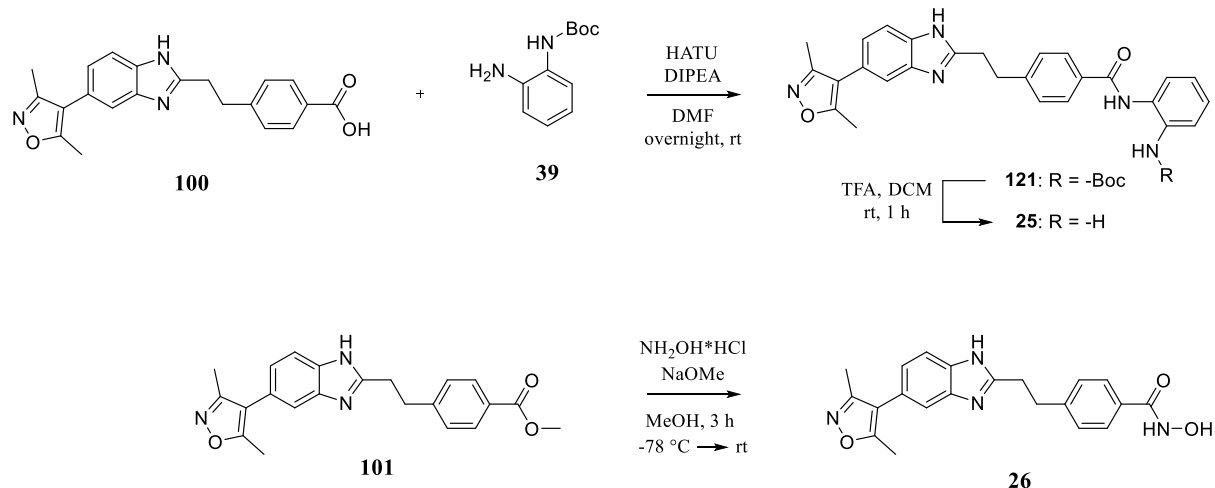
Scheme 41: Reduction of **97** with Pd/C and  $\text{H}_2$  followed by a HATU reaction to afford **99**.

Although the last step is the same as before, the outcome is slightly different. By closely observing the progress of the reaction and stopping it after 30 minutes two products the carboxylic acid **100** and the ester **101** could be obtained.



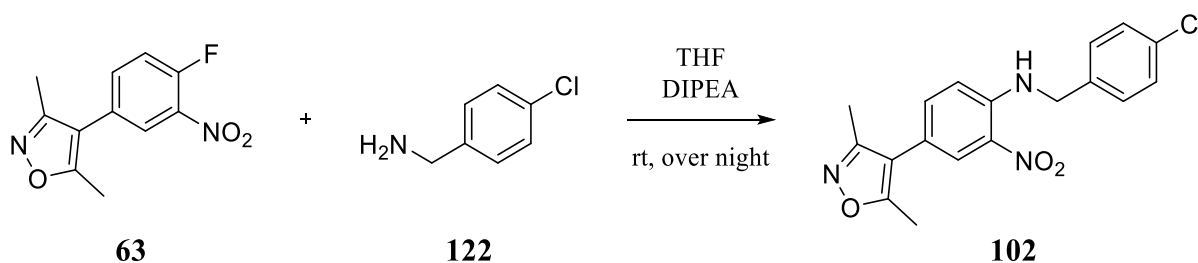
Scheme 42: Reaction of **99** in dioxane/4 N HCl to afford **100** and **101**.

In order to obtain the final compound **25** two reactions are left to perform, which are another HATU reaction and the subsequent deprotection. For **26** on the other hand the only reaction left is the direct conversion of the ester to the hydroxamic acid.



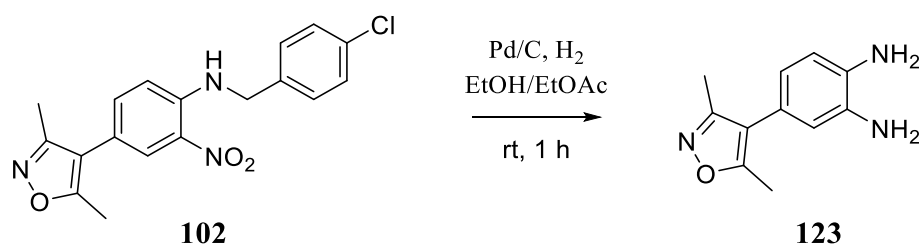
Scheme 43: HATU reaction of **100** with **39** and deprotection of its product **121** to afford final compound **25** and direct conversion of **101** to obtain final compound **26**.

Instead of the synthesis of the aniline **96** both educts **63** and **94** were also reacted with two different benzylamines in another nucleophilic aromatic substitution of which one reaction is shown as example in Scheme 44.



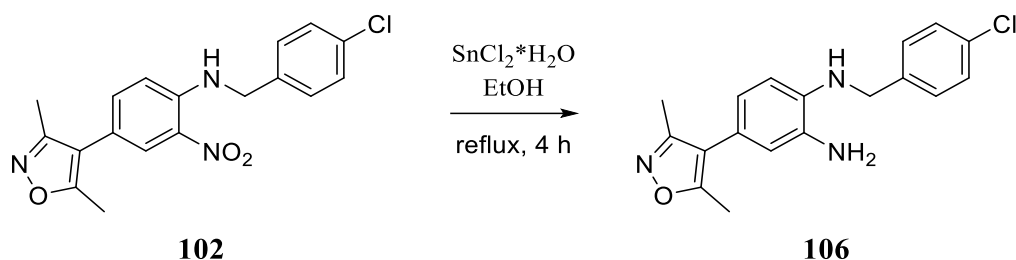
Scheme 44: Nucleophilic aromatic substitution using the example of **63** and **122** to obtain **102**.

The next reaction is the reduction step of the nitro group which had to be a different reaction than before. This is due to the benzyl amine which is basically a benzyl protecting group usually used to protect hydroxy groups and removed with palladium on carbon and hydrogen gas. Used in this reaction the main product would be a benzene-1,2-diamine **123** which is not the desired product.



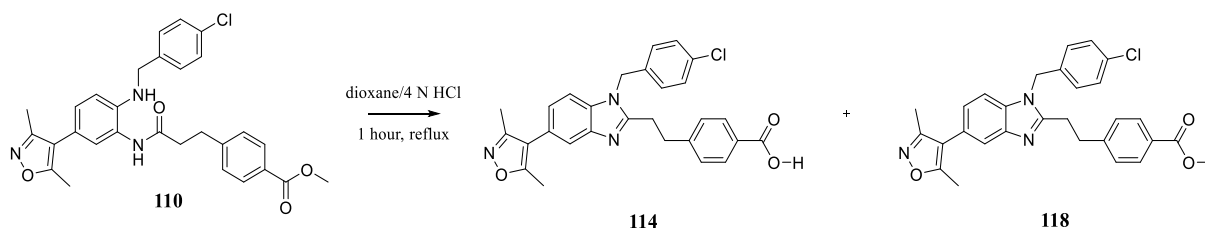
Scheme 45: Result of the reduction of benzylamines with Pd/C and  $\text{H}_2$  using the example of **102**.

To prevent the cleavage of benzylamines, a milder method had to be found that specifically reduces nitro groups even in the presence of other reducible groups. This is possible with tin(II) chloride, which became the standard reagent for reductions of this kind.



Scheme 46: Reduction of the nitro group with  $\text{SnCl}_2$  using the example of **102** to obtain **106**.

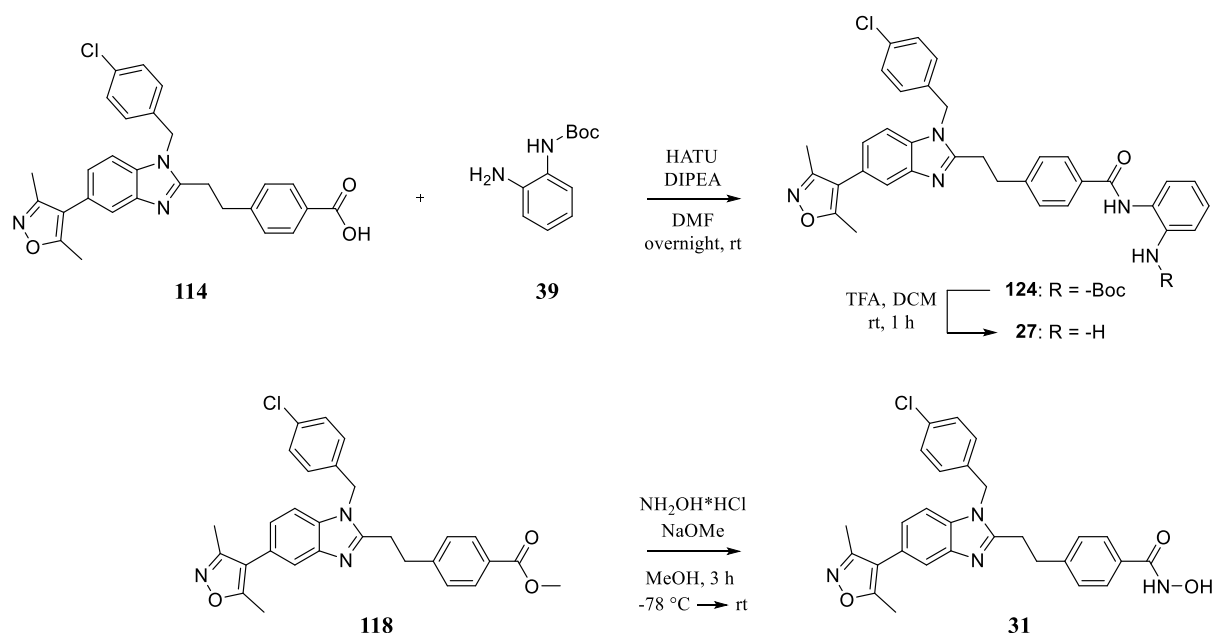
The last two missing reactions are the coupling reaction with HATU followed by reaction in dioxane/4 N HCl in which the five-membered ring closes and the ester is cleaved. Nevertheless, there is an exception with compound **110**, where at the end of the reaction the uncleaved ester **118** could be isolated as well.



Scheme 47: Reaction in dioxane/4 N HCl using the example of **110** to afford **114** and **118**.

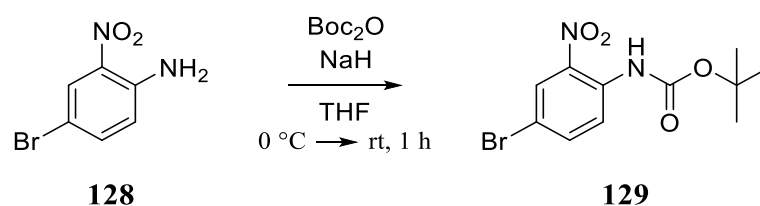
When this point is reached there are again two reactions left, HATU coupling and deprotection, in case of the carboxylic acids **114** - **117** while the ester **118** is converted directly to the final compound **31**. The intermediates **125** - **127**, which result in the final compounds **28** - **30** after deprotection, are not shown.





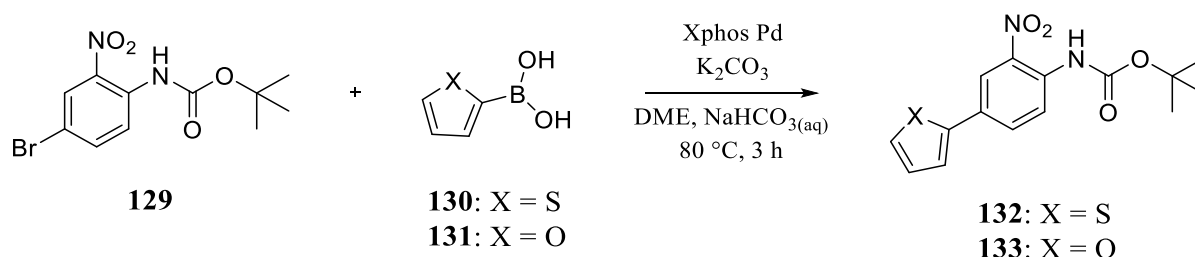
Scheme 48: HATU reaction using the example of **114** with **39** and deprotection of its product **124** to afford final compound **27** and direct conversion of **118** to obtain final compound **31**.

In order to obtain the final compounds **32** and **33** the modified HDAC inhibitory part had to be synthesized. The synthesis of these parts consists of three steps, starting with the protection of the aniline. This reaction was performed with sodium hydride on mineral oil to minimize the risk of double Boc protection.



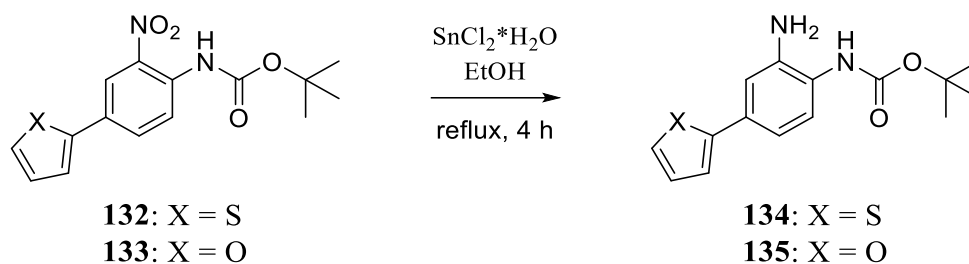
Scheme 49: Boc protection of the aniline **128** to afford **129**.

Regarding the Suzuki reaction there are two differences in the following compared to the previous one. The boron containing educt used here is a boronic acid instead of a pinacol ester and with potassium carbonate an additional base was added.



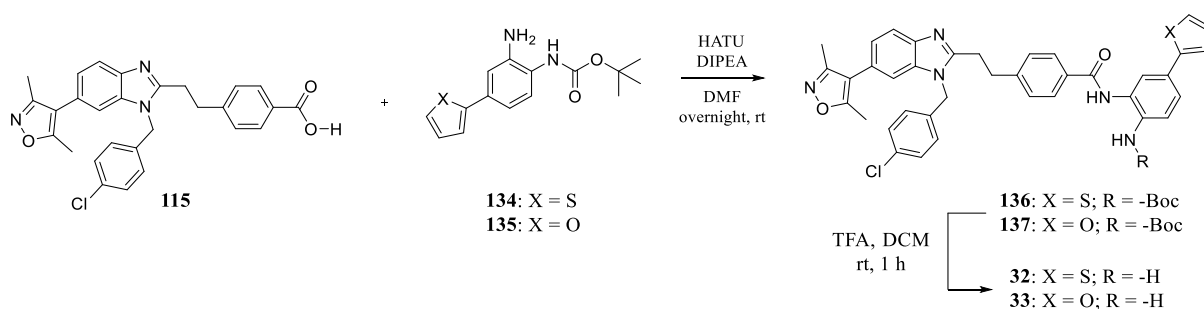
Scheme 50: Suzuki reaction of **129** with boronic acids **130** and **131** and additional base  $\text{K}_2\text{CO}_3$ .

In the last step the nitro group of **132** and **133** was reduced using the milder method with tin(II) chloride to afford the corresponding anilines **134** and **135** (Scheme 51).



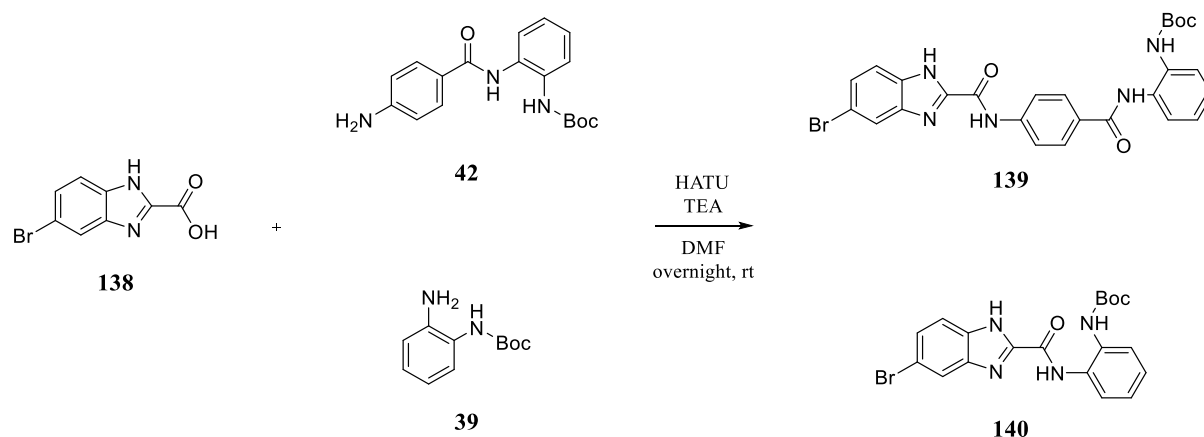
Scheme 51: Reduction of **132** and **133** with  $\text{SnCl}_2$  to afford **134** and **135**.

The two anilines are then coupled to **115** via HATU and subsequently deprotected using TFA to afford the final compounds **32** and **33** (Scheme 52).

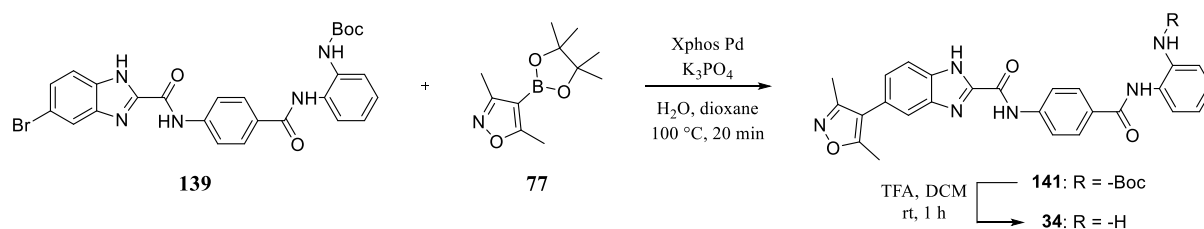


Scheme 52: HATU reaction of **115** with **134** and **135** followed by the deprotection of both products to afford the final compounds **32** and **33**.

Unfortunately, the next two compounds **34** and **35** could either not be purified or not synthesized at all. The planned synthesis itself is basically the same for both compounds starting with the formation of the amide with HATU, followed by a Suzuki reaction and the deprotection in the end. Already the first reaction did not work as planned since the educt **138** precipitated out of solution after addition of DIPEA. In order to obtain the desired compounds, the corresponding amines **39** and **42** were added right from the start and TEA had to be used as base.

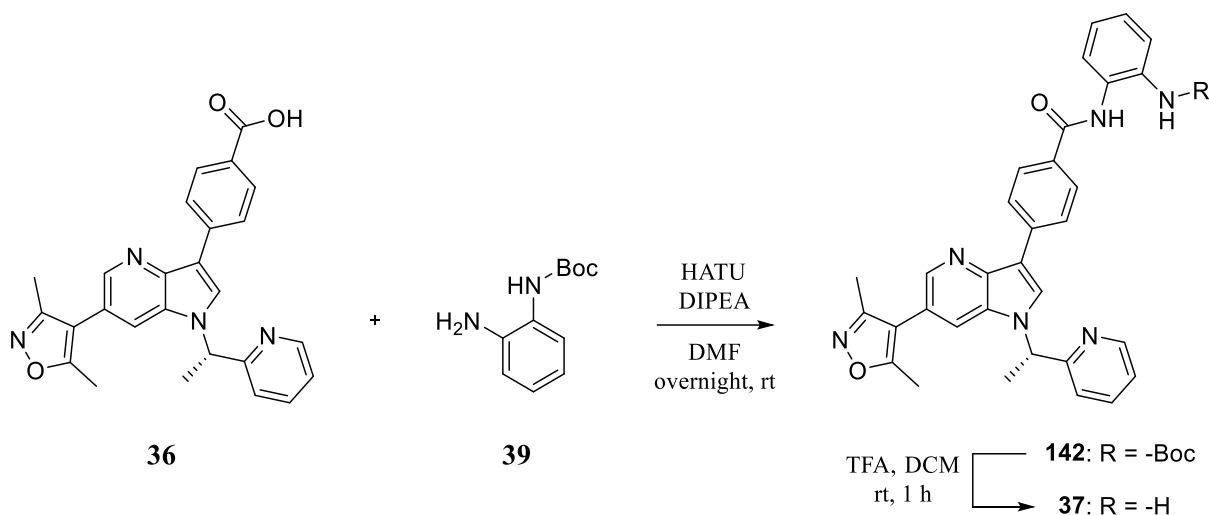
Scheme 53: Synthesis of **139** and **140** with HATU and TEA instead of DIPEA.

The following Suzuki reaction had to be modified as well since both compounds but especially **140** were hardly soluble in DME and water, the solvents used for the coupling reaction. Consequently, the solvents H<sub>2</sub>O and dioxane were used and the reaction was conducted in the microwave in order to overcome the solubility problems, which worked for **139** but not for **140**. For that reason, the synthesis for the final compound **35** was no longer pursued. Although **141** could be synthesized and the subsequent deprotection itself was not a problem, the final compound **34** could not be sufficiently purified and will therefore not be tested.



Scheme 54: Microwave assisted Suzuki reaction.

The last compound synthesized is a bit different than the other since its basic structure is not a benzimidazole. Instead PLX51107 is a pyrrolo[3,2-*b*]pyridine and an already known BET inhibitor with a low nanomolar activity. The only thing left to do here is to implement the HDAC activity which is performed by a HATU coupling reaction followed by the deprotection of the amine.



Scheme 55: HATU reaction of **36** with **39** followed by the deprotection of the product to afford the final compound **37**.

### 3.4. Characterization of the final compounds

#### 3.4.1. Differential scanning fluorimetry assay

The differential scanning fluorimetry (DSF) is an inexpensive and fast screening method to determine whether a ligand binds and stabilizes a protein.<sup>[88]</sup> The protein of interest is therefore heated in presence of a fluorescence dye and a ligand, which is the inhibitor to be tested. Starting the assay, the dye is quenched due to the aqueous solution. Upon heating the protein slowly unfolds giving access to its non-polar regions, which the dye binds to and starts to fluorescence. As the temperature rises the fluorescence rises as well until a peak is reached, which indicates that all proteins are unfolded. After that, the proteins aggregate, the dye dissociates and subsequently the fluorescence decreases again (Figure 27). The melting point of the protein is hidden in the inflection point of the curve and can be calculated by determine the maximum of the first derivative of the Boltzmann equation (1), which describes the obtained curve. In the equation UL and LL are the values of minimum and maximum intensities and a indicates the slope within the inflection point.

$$y = LL + \frac{(UL - LL)}{1 + \exp\left(\frac{T_m - x}{a}\right)} \quad (1)$$

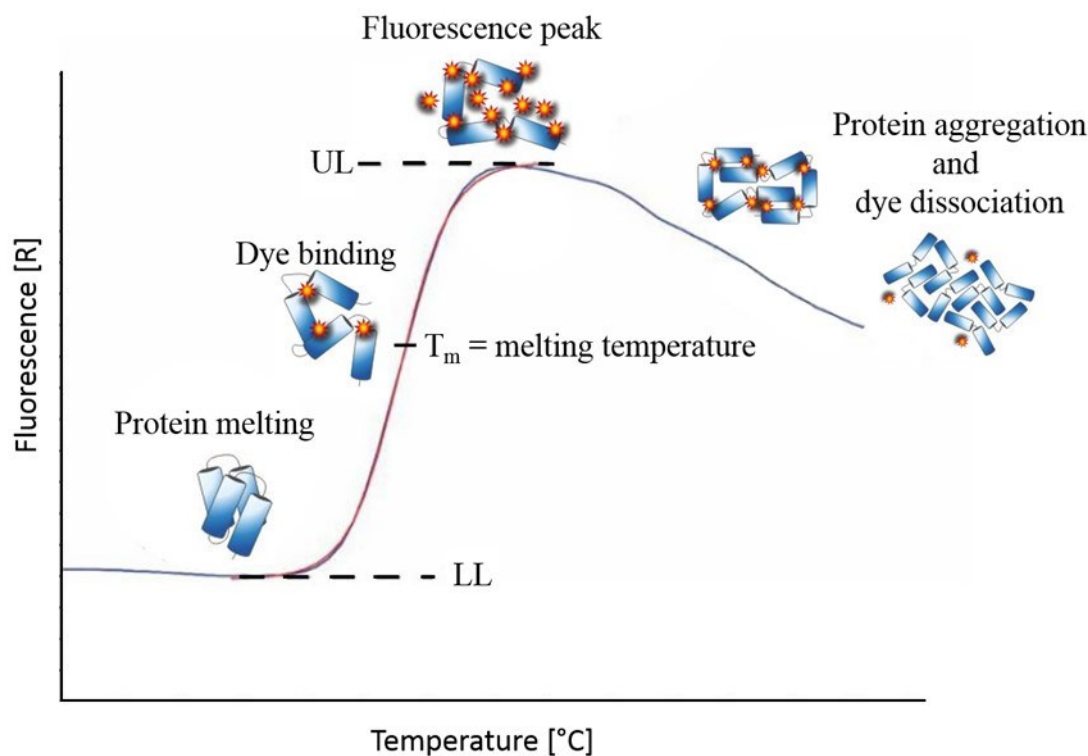


Figure 27: Principle of DSF assay. While heating, the protein unfolds, and the dye can bind. After binding, the dye fluoresces until the maximum is reached. Then the fluorescence level drops again due to protein aggregation and dye dissociation (modified).<sup>[88]</sup>

The melting point of the protein inhibitor complex can be compared to the melting point of the protein without any ligands, which should result in a temperature shift ( $\Delta T_m$ ). If an inhibitor binds the proteins stability should increase and therefore melt at a higher temperature.

### 3.4.2. Isothermal titration calorimetry

The isothermal titration calorimetry (ITC)<sup>[89]</sup> is a technic that allows to follow the energetics of a binding process, such as a ligand binding a protein. Therefore, the protein is titrated into a solution of a ligand (or vice versa), which results in a measurable heat change. Through this change it is possible to directly determine the enthalpy ( $\Delta H$ ), the binding affinity ( $K_A$ ), the stoichiometry and subsequently the entropy ( $\Delta S$ ) and the Gibbs free energy ( $\Delta G$ ). Those parameters are connected via the equation 2 and 3.

$$\Delta G = -RT \ln K_A \quad (2)$$

$$\Delta G = \Delta H - T\Delta S \quad (3)$$

The calorimeter itself consist of two cells, one for the sample and one as reference, surrounded by an adiabatic shield (Figure 28). While the reference cell is only filled with the solvent, usually water, the sample cell includes the ligand (or protein, depending on the method used)

as well. The other binding partner is loaded into a rotatable injection syringe which is able to add a precise amount of sample and distributes it by stirring. Both cells are kept at a constant and equal temperature throughout the experiment. Upon injection of the second binding partner the complex is formed which is accompanied by the absorption or release of heat, depending on whether the reaction is exothermic or endothermic.

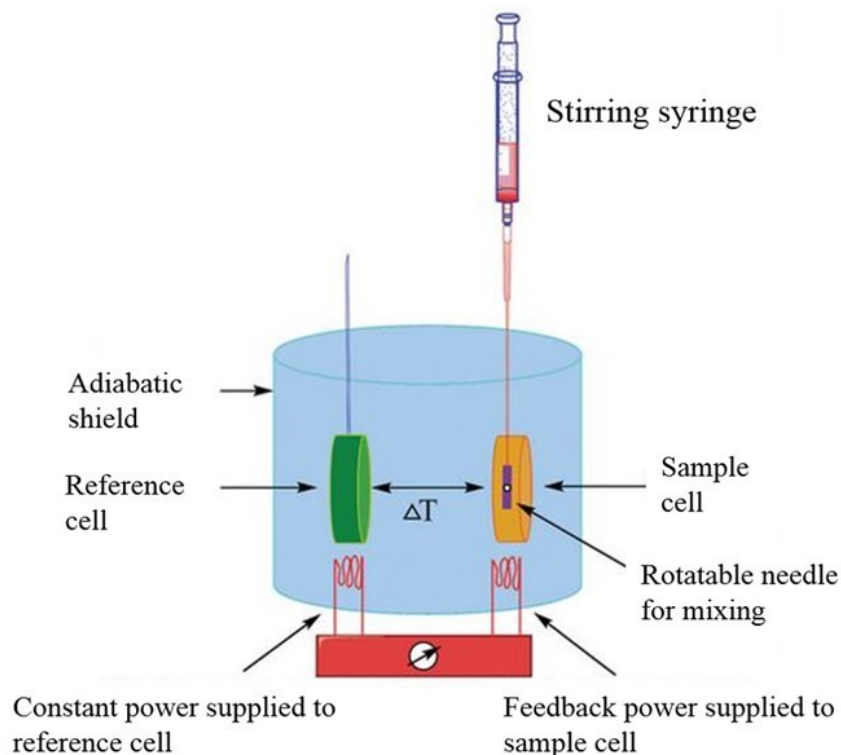


Figure 28: Schematic representation of an isothermal titration calorimeter (modified).<sup>[90]</sup>

These heat quantity changes are monitored by the calorimeter by measuring the difference in power of the cell heaters required to maintain the temperature difference of both cells at zero. The heat change is plotted against the time which results in the titration thermogram typical for ITC. To evaluate the ITC data the thermal impulses are integrated over time and normalized with respect to the concentration. Plotting the resulting values against the molar ratio of protein/ligand provides the titration curve after a non-linear regression fit. Using the appropriate binding model (for example one-site or two independent sites) the values for  $K_D$ ,  $n$  and  $\Delta H$  can be generated (Figure 29).

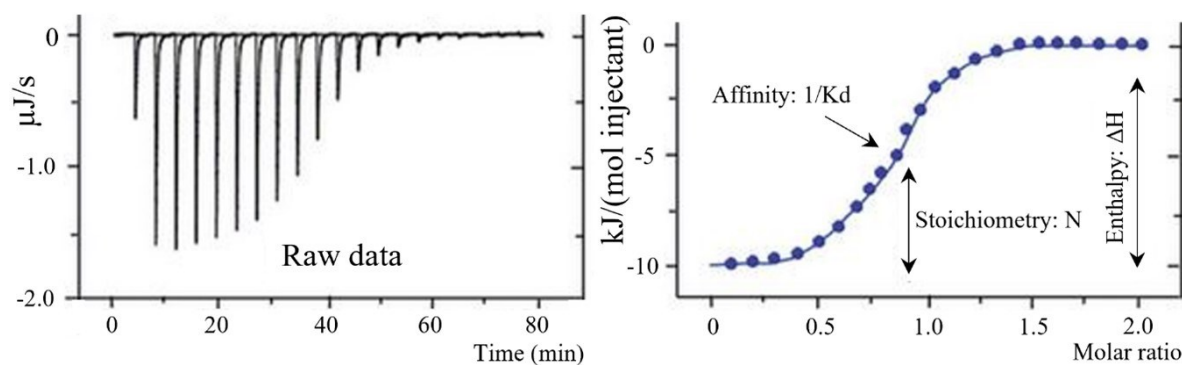


Figure 29: Characteristic data of a titration experiment and integrated heat signals plotted against the molar ratio. Circles represent experimental data and the line is the non-linear regression using a one-site binding model (modified).<sup>[90]</sup>

### 3.4.3. Fluorogenic HDAC assay

To determine the HDAC inhibitory activity a screening kit was used (Cayman Chemical Company, USA). This fluorescent-based assay makes use of an acetylated lysine as a substrate, which is sensitized through deacetylation by HDAC1. After that step, the HDAC developer provided in the kit, is added which reacts with the sensitized substrate and releases a fluorescent product. The fluorophore can be analyzed with a fluorescence plate reader with the wavelengths for excitation and emission of 360 nm and 465 nm, respectively. The collected data is then evaluated with GraphPad, which delivers a value for inhibition in percent as well as an  $\text{IC}_{50}$  value.

### 3.4.4. NanoBRET assay

BRET (Bioluminescence Resonance Energy Transfer) assays utilize an energy transfer between a bioluminescent donor and a fluorescent acceptor which occurs in close proximity ( $< 10$  nm). As donor acts the engineered Nanoluc (Nluc) luciferase which uses a novel coelenterazine derivative as substrate and produces high intensity luminescence. The small size (19 kDa) and high physical stability of Nluc are important for the use as a fusion tag, transmitting only a minimal influence when attached to other proteins. The acceptor is a chloroalkane derivative of nonchloro TOM (NCT) dye, which is attached to a ligand to form a tracer, that binds the protein of interest. Upon binding the proximity between donor and acceptor is close enough for the energy transfer (Figure 30).

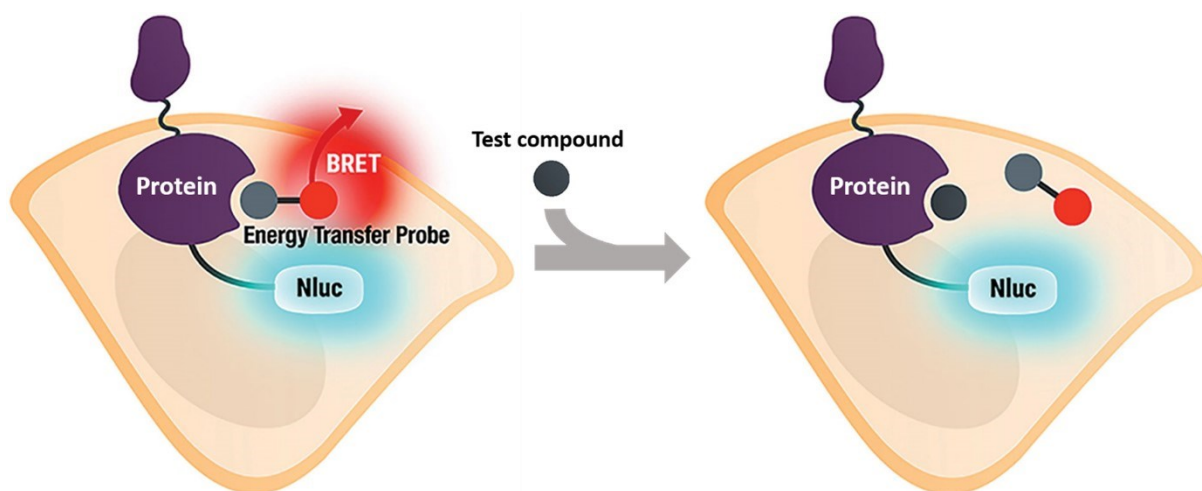


Figure 30: Schematic representation of BRET in living cells. The tracer binds reversibly the protein active site, which results in a BRET signal. After addition of a test compound the tracer gets replaced and the BRET signal attenuates (modified).<sup>[91]</sup>

The NanoBRET target engagement assay, which is a cell-based assay, uses BRET to provide the affinity of test compounds and subsequently their cell permeability. In the first step of a NanoBRET assay, the tracer is added to transfected cells, expressing the required Nluc fusion protein which results in an increased BRET signal. Upon introduction of a compound and the competitive displacement of the tracer the BRET signal decreases in a dose dependent manner. Furthermore, an extracellular Nluc inhibitor is added to ensure that the measured signals originate exclusively from inside a cell.<sup>[92]</sup> The assay was performed by Benedict-Tilman Berger.

### 3.4.5. X-ray crystallography

Crystallization of proteins or other large biological complexes depends on the creation of a solution that is supersaturated with the protein. However, this must not create conditions that significantly disturb the natural state of the protein. Supersaturation is achieved by adding mild precipitants such as neutral salts or polymers and by changing various physical parameters such as temperature and pH. The main technique is vapor diffusion, in which an unsaturated droplet containing the protein and precipitant is placed in a closed apparatus containing pure precipitant. There are two different arrangements in which the droplet is either on a plate (sitting droplet) or on the bottom of the lid (hanging droplet). In both cases, water vapor subsequently diffuses from the droplet into the reservoir until the osmolarity of the two is in equilibrium. As the water diffuses, the concentration of the protein and precipitant in the droplet increases, and once a critical concentration is reached, crystal growth begins.<sup>[93]</sup>



For the co-crystallization of protein and a compound, the latter is additionally in the droplet.<sup>[94]</sup> X-ray crystallography was performed by Deep Chatterjee and Dimitriou- Ilias Balourdas.

### 3.4.6. Immunoblot analysis

Immunoblotting is a rapid and reliable assay for the detection and characterization of proteins. For this purpose, the proteins of a cell lysate are first separated by molecular weight using SDS-polyacrylamide gels. The separated proteins are then transferred to a nitrocellulose membrane, and the blot is blocked with the primary antibodies that specifically bind to the proteins of interest. A secondary antibody coupled with an enzyme (usually horseradish peroxidase) is then used to bind to the primary antibodies. The peroxidase catalyzes the conversion of luminol to its oxidized form, allowing detection of luminescence and therefore the proteins of interest. The immunoblot analysis were performed by Tim Zegar.

### 3.4.7. Reverse transcription polymerase chain reaction

Reverse transcription polymerase chain reaction (RT-PCR) is a method for expression detection and selective amplification of RNA. RT-PCR consists essentially of three steps: First, the RNA is isolated, which is then transcribed into a complementary cDNA using a reverse transcriptase. Finally, the actual amplification takes place by PCR. The detour via the cDNA must be taken because conventional polymerases cannot amplify RNA. For quantitative detection of the expression of a gene, an internal standard or a reference gene must always be tested in parallel to verify the success of the assay. RT-PCR was performed by Tim Zegar.

### 3.4.8. CellTiter Glo cell viability assay

The CellTiter Glo cell viability assay is a method for determining the number of viable cells in cultures. The assay is based on the quantification of ATP, which signals the presence of metabolically active cells. These cells consume ATP in the conversion of luciferin to the luminescent oxyluciferin. The measured luminescence is directly proportional to the number of viable cells in the culture. The assay was performed by Tim Zegar.

### 3.4.9. Cell cycle analysis

Cell cycle analysis takes advantage of the fact that the amount of DNA in the cell nucleus doubles during the S phase. The DNA in the cell nucleus can be stained with special fluorescent dyes such as propidium iodide. Since the fluorescence of a cell is proportional to its DNA content, this staining can be used to determine the DNA content and thus the cell cycle status of an individual cell or cell population.

### 3.4.10. Gene Set Enrichment Analysis

Gene Set Enrichment Analysis (GSEA) is a computer-based method for evaluating microarray data at the level of specific gene sets. All genes in a set share certain common characteristics, for example an influence on the cell cycle. With GSEA one can determine whether members of a gene set are more likely to be at the top or bottom of a ranked gene list. If they cluster at either option, there is a correlation between the gene set used and phenotypic class differentiation.<sup>[95]</sup>

## 4. Results and discussion

### 4.1. Dual BET/HDAC inhibitors of the first generation

In total four potential dual BET/HDAC inhibitors are members of the first generation (Figure 31) and all of them are based on the BET inhibitor (+)-JQ1. In order to introduce the HDAC-inhibitory activity the *tert*-butyl ester of JQ1 was substituted by three different established HDACis which are CI994 (**13**), vorinostat (**5**) and panobinostat (**7**). While **5** and **13** are completely used in their respective compound (**14** and **15**) **7** was cut short due to its high molecular weight compared to the others. The last compound (**62**) was originally not planned but because of good test results of **14** in combination with the low yield of a crucial reaction step, an additional C-atom was introduced which results in a resemblance to Etinostat (**10**). The goal was to obtain higher yields while retaining the good characteristics of **14**.

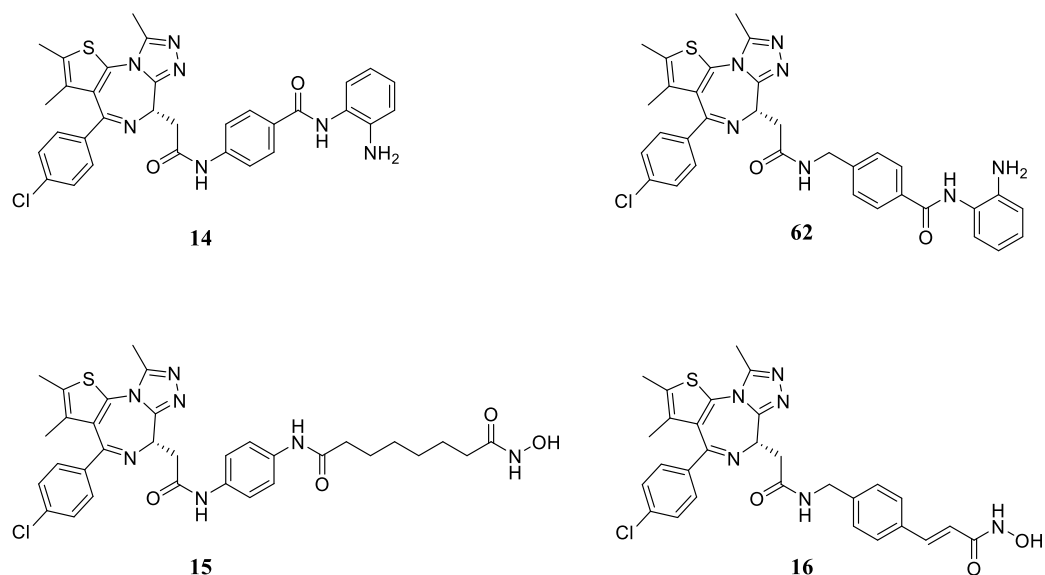


Figure 31: Dual BET/HDAC inhibitors of the first generation.

### 4.1.1. Crystal structures

Except for compound **62**, all dual inhibitors of the first generation were crystalized with the BRD4 1 at a resolution ranging from 1.05 to 1.25 Å. As expected, there was little to no difference in the binding mode of the JQ1 moiety of all three adducts compared to that of the parental compound JQ1. The HDAC moieties are all solvent-exposed and do not appear to affect the ability of JQ1 to bind to BRD4 1 (Figure 32).

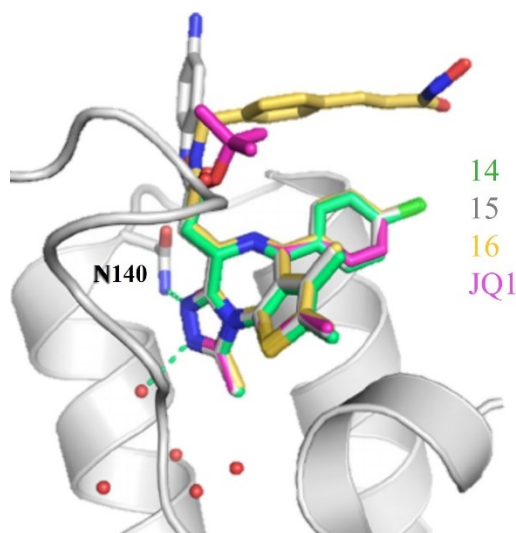


Figure 32: Superimposed crystal structures of dual inhibitors and JQ1 in complex with BRD4 1. The binding modes of all four JQ1 moieties is virtually the same. The hydrogen bond with the highly conserved N140 is highlighted. Due to interaction with a symmetry-related molecule in the crystal the HDAC substructure of **16** is visible, whereas the others were largely disordered and therefore deleted from the final model.

All the essential interactions with the bromodomain binding pocket are conserved, including the hydrogen bond of the highly conserved asparagine (N140) with the triazole moiety. The HDAC-inhibiting structures are all solvent-accessible and therefore may be able to interact with HDACs even when bound to a BET protein. Except for compound **16**, the HDAC substructures were disordered and thus deleted in the final crystal structure. In the case of **16**, however, the substructure of panobinostat is visible due to stabilization by crystal contacts.

### 4.1.2. DSF results

To evaluate the interaction of the synthesized compounds with the BET bromodomains, the thermal stability of a protein-compound adduct was determined by DSF. The potential dual inhibitors were tested in duplicates on both binding domains of every BET protein with the exception of compound **15**. Its results were obtained from a previous performance of the DSF

assay and are not necessarily comparable with the other results. In addition, the positive control JQ1 (**3**) was measured for verification purposes as well.

Table 5: DSF assay results of the first generation.  $\Delta T_m$  in °C

Nr.	BRD4 1	BRD4 2	BRD2 1	BRD2 2	BRD3 1	BRD3 2	BRDT 1	BRDT 2
<b>3</b>	11.6	14.2	9.4	11.2	9.1	10.6	7.9	6.5
<b>14</b>	7.0	12.6	4.6	10.8	4.4	4.7	3.0	5.5
<b>15*</b>	3.9	6.7	2.4	9.5	nt	nt	nt	nt
<b>16</b>	11.7	14.4	8.9	11.5	8.9	11.2	7.1	7.0
<b>62</b>	9.5	13.3	7.0	9.5	7.2	8.7	4.0	6.3

Fields are colored according to the measured thermal shift  $\Delta T_m$  whereas green indicates a low, yellow a mediocre and red a strong shift. nt = not tested and marked blue. Standard deviation is 0.8 °C or less.

\* Experimental data obtained from a previous performance of DSF assay.

Compared to the parental compound JQ1 all developed adducts show a similar inhibition pattern with **16** presenting the highest shift on all bromodomains in some cases even higher than JQ1 itself although not significantly. In any case, leaving BRDT aside, the highest shifts are always found on the second bromodomain of each protein. This result fits because the sequence alignment shows that the same BD in a different BET have a higher similarity to each other than the BD of the same protein (Figure 30). One major exception seems to be compound **15** with a shift of only 6.7 °C on the second bromodomain of BRD4 but this result originates from a previous DSF assay. During that assay BRD4 (BD2) experienced a shift of 6.8 °C when bound to JQ1 indicating that **15** stabilizes BRD4 (BD2) approximately as strongly as the other compounds. Nevertheless, the measured shift of **15** at the first bromodomain of both BRD4 and BRD2 is significantly lower, which could already disqualify **15** as a dual inhibitor. In general, these results were to be expected since the replaced ester group is solvent exposed and hardly contributes to the binding affinity. For the same reason, it might seem possible to replace this group with pretty much any HDACi without affecting JQ1 activity too much.

```

BRD2/BD1 97  WPFYRQPVDAVKLGLPDYHKI I KQPMDMGTI I KRRLENNYYWAASECMQDFNTMFTNCYI IYNKPTDDI VLMAQT
BRD2/BD2 370  WPFYKPVDAKALGLHDYHDI I KHPMDLSTVKKRKMENRDRDAQEFAADVRLMFSNCKYKYNPPD HDV VAMARK
BRD3/BD1 57  WPFYQPVDAIKLNLDPDYHKI I KNPMDMGTI I KKRLENNYYWSASECMQDFNTMFTNCYI IYNKPTDDI VLMAQA
BRD3/BD2 332  WPFYKPVDAEALGLHDYHDI I KHPMDLSTVKKRKM D GREYPDAQGFAADVRLMFSNCKYKYNPPD HEV VAMARK
BRD4/BD1 81  WPFYQPVDAVKLNLDPDYKI I KTPMDMGTI I KKRLENNYYWNAQECIQDFNTMFTNCYI IYKPGDDI VLMAEA
BRD4/BD2 374  WPFYKPVDAEALGLHDYCDI I KHPMDMSTI I KSKLEAREYRDAQEFGADVRLMFSNCKYKYNPPD HEV VAMARK
BRDT/BD1 50  WPFYRQPVDAVKLQLPDYTI I KNPMDLNTI I KKRLENKYAKASECIED FNTMFSNCKYLYNKPGDDI VLMAQA
BRDT/BD2 293  WPFYRQPVDAVKLGLHNYD VVKNPMDLGTI I KEKMDNQEYKDAYKFAADVRLMFMNCKYKYNPPD HEV VTMARM
    
```

Figure 33: Sequence alignment of the BET BRDs. Conserved residues (blue) and similar residues (yellow, red, green, purple) are highlighted. Alternating colors show a higher similarity between the BDs of different BETs (modified).<sup>[96]</sup>

### 4.1.3. ITC results

After the initial evaluation by DSF, the dissociation constants,  $K_d$ , of binding to both bromodomains of BRD4 were determined by ITC. Compound **62** was not measured by ITC because it was synthesized at a later date and discarded as a dual inhibitor by other assays.

Table 6:  $K_d$  values (in nM) obtained by ITC.

Protein	<b>3</b>	<b>14</b>	<b>15</b>	<b>16</b>
<b>BRD4 1</b>	51 ± 15	69 ± 9	52 ± 6	21 ± 4
<b>BRD4 2</b>	89 ± 13	231 ± 31	88 ± 15	54 ± 16

The results show that all three adducts bind the first bromodomain of BRD4 in a low nanomolar affinity, resulting in  $K_d$  values of 69, 52 and 21 nM, respectively, which is very similar to JQ1. Quite interesting is the measured  $K_d$  of compound **15** which is higher than expected, considering the results of the DSF assay (shift of only 3.9 °C compared to 11.6 °C of JQ1) but shows the limit of that assay. By DSF it is only possible to determine if an affinity exists not its proper level. This becomes even more clearer regarding the  $K_d$ 's of the second bromodomain of BRD4. In contrast to the DSF assay results the  $K_d$  values were all higher compared to BRD4 (1) spanning from 231 nM for compound **14** to 54 nM for compound **16**, including JQ1 with 89 nM. Nevertheless, the DSF assay did predict the high affinity of compound **16**, which is again higher than that of JQ1 itself. In summary, the ITC measurements confirm the excellent BET binding activity of the dual inhibitors, which is hardly reduced by the introduction of the HDAC inhibitor moiety, and in one case even increased.

### 4.1.4. Fluorogenic HDAC assay results

After confirming that the BET activity was still present, HDAC activity had to be assessed. Therefore, a cell-free fluorogenic HDAC assay was performed, and all adducts were tested in duplicates against HDAC1. Trichostatin A (TSA), included in the kit, was also measured for verification, and yielded an  $IC_{50}$  of 18.1 nM, which is within the desired range according to the manufacturer's protocol.

Table 7:  $IC_{50}$  values (in  $\mu$ M) obtained from cell-free fluorogenic HDAC assay.

Protein	<b>13*</b>	<b>14</b>	<b>62</b>	<b>5*</b>	<b>15</b>	<b>7*</b>	<b>16</b>
<b>HDAC 1</b>	1.2	1.9	4.8	0.01	1.3	0.005	3.4

Standard deviation is 1.2  $\mu$ M or lower. \*data obtained from literature<sup>[64]</sup>

These results show that all compounds are capable of inhibiting HDAC1 although the effectiveness is greatly reduced compared to their parental inhibitors. In particular, compound **16** ( $IC_{50} = 3.4 \mu\text{M}$ ) showed significant reduction in affinity by about 700-fold relative to panobinostat ( $IC_{50} = 0.005 \mu\text{M}$ , **7**). However, considering that only a relatively small segment of **7** is actually part of **16** this result is not too surprising. Nevertheless, even compound **15** ( $IC_{50} = 1.3 \mu\text{M}$ ), in which the whole structure of **5** ( $IC_{50} = 0.01 \mu\text{M}$ ) is present, has a reduced affinity, yet the highest of all tested compounds. The smallest discrepancy between parental molecule and dual inhibitor however is found in **13** and **14** in which the  $IC_{50}$  increases from  $1.2 \mu\text{M}$  to  $1.9 \mu\text{M}$ . This is further increased by introducing another  $-\text{CH}_2-$  group to obtain compound **62** ( $IC_{50} = 3.4 \mu\text{M}$ ), which already indicates the inferior binding properties compared to **14**.

#### 4.1.5. NanoBRET assay results

After confirming the activity on both targets, a nanoBRET assay was performed to determine the cellular activity on HDAC1, both BD of BRD4 and the full-length BRD4 protein (FL-BRD4) of all compounds. In addition, all parental molecules were included for purposes of both verification and comparison.

Table 8:  $IC_{50}$  values (in  $\mu\text{M}$ ) of the cellular BRD4 and HDAC1 activity of dual inhibitors determined by nanoBRET assay.

Protein	BRD4 1	BRD4 2	FL-BRD4	HDAC1
<b>13</b>	-	-	-	$0.96 \pm 0.17$
<b>14</b>	$0.72 \pm 0.09$	$0.074 \pm 0.010$	$0.64 \pm 0.09$	$0.29 \pm 0.04$
<b>5</b>	-	-	-	$0.52 \pm 0.08$
<b>15</b>	$4.53 \pm 0.26$	$11.0 \pm 3.0$	$6.85 \pm 1.04$	$1.11 \pm 0.36$
<b>7</b>	-	-	-	$0.19 \pm 0.10$
<b>16</b>	$1.35 \pm 0.15$	$1.58 \pm 0.54$	$1.43 \pm 0.07$	>20
<b>3</b>	$0.231 \pm 0.042$	$0.039 \pm 0.008$	$0.104 \pm 0.010$	-

Fields are colored according to the measured  $IC_{50}$  whereas red indicates a low, yellow a mediocre and green a high  $IC_{50}$ . - = not tested.

These results were highly unexpected and demonstrate the necessity of cell-based assays. Here compound **14** showed the highest BRD4-targeting activity on both BD of BRD4 with an  $IC_{50}$  of 720 nM on the first and 74 nM on the second domain. Both values are in the same order of magnitude as those of JQ1 and at least one order of magnitude lower compared to the other compounds.

With respect to BRD4 1, the  $IC_{50}$  value of **14** is twice and six times higher than those of compounds **15** and **16**, respectively. For BRD4 2, the discrepancy is even higher, with the  $IC_{50}$  value of **15** and **16** being 20 times and 150 times greater, respectively, than that of **14**. With relation to the ITC data, these results are quite counterintuitive, but the reason for the drastically reduced potency of **15** and **16** is most likely to be found in the reduced cellular uptake. In addition to testing the two BDs separately, the  $IC_{50}$ 's of the full-length protein, FL-BRD4, were measured as well. Here, as was to be expected, the values are always in between those determined for the two isolated domains.

The nanoBRET assay was also used to determine the cellular activity of the compounds against HDAC1, member of the second target protein class. Here compound **14** further showed its potential with an  $IC_{50}$  of 290 nM, a value even higher than that obtained from its parental HDACi **13** ( $IC_{50}$  = 960 nM). The other inhibitors **15** and **62** (not included in Table 8) displayed lower potency with 1.1  $\mu$ M and 1.7  $\mu$ M, respectively and **16** presented an even lower potency with an  $IC_{50}$  of >20  $\mu$ M. Compared to its parental compound **7**, this is equivalent to a potency that is more than three orders of magnitude lower. Based on these results, compound **14** was chosen as the most promising dual BET/HDAC inhibitor for further characterization in cancer cells.



#### 4.1.6. Expression behavior of PDAC cells treated with **14**

In order to characterize compound **14** in cancer cells immunoblots and expression analysis by RT-PCR were first performed. Here *MYC* and *HEXIM1* are commonly used as readout biomarkers for BETi activity<sup>[97]</sup>, whereas HDAC inhibitor activity can be assessed directly via the acetylated lysines 9 and 14 of histone H3. For comparison reasons the parental compounds were also tested, individually and partly in combination to see if synergistic effects occur. A first expression analysis of said BETi responsive genes showed a rapid (6 hours) downregulation of *MYC* and upregulation of *HEXIM1* by **14**. For comparison JQ1 had the same effect on *MYC* while a slightly lower effect on *HEXIM1* (Figure 34).

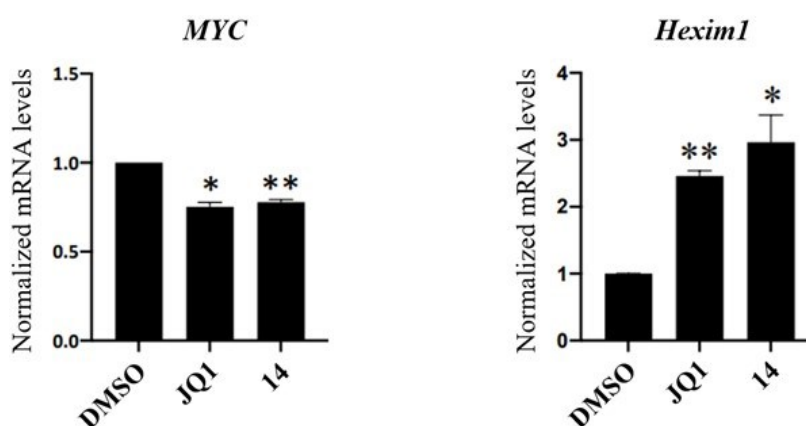


Figure 34: Quantitative RT-PCR analysis for *MYC* and *HEXIM1* (BETi responsive genes). PaTu 8988t cells were treated with 500 nM of indicated inhibitor and harvested after 6 h. \*\* $P \leq 0.01$ , \* $P \leq 0.05$ .

The initial immunoblot assays were performed with indicated compounds in a dose- and time-dependent manner (Figure 35, A and B). Again, the two immunoblots show, that JQ1 and **14** regulate *MYC* in a similar fashion regardless of whether dose or time dependence is considered. Acetylation of histone H3 on the other hand, although still dose- and time-dependent, is enhanced by **14** to a much greater extent compared to its parental HDAC inhibitor CI994 (made more apparent in Figure 35 C). This result is coherent with the results of the nanoBRET assay.

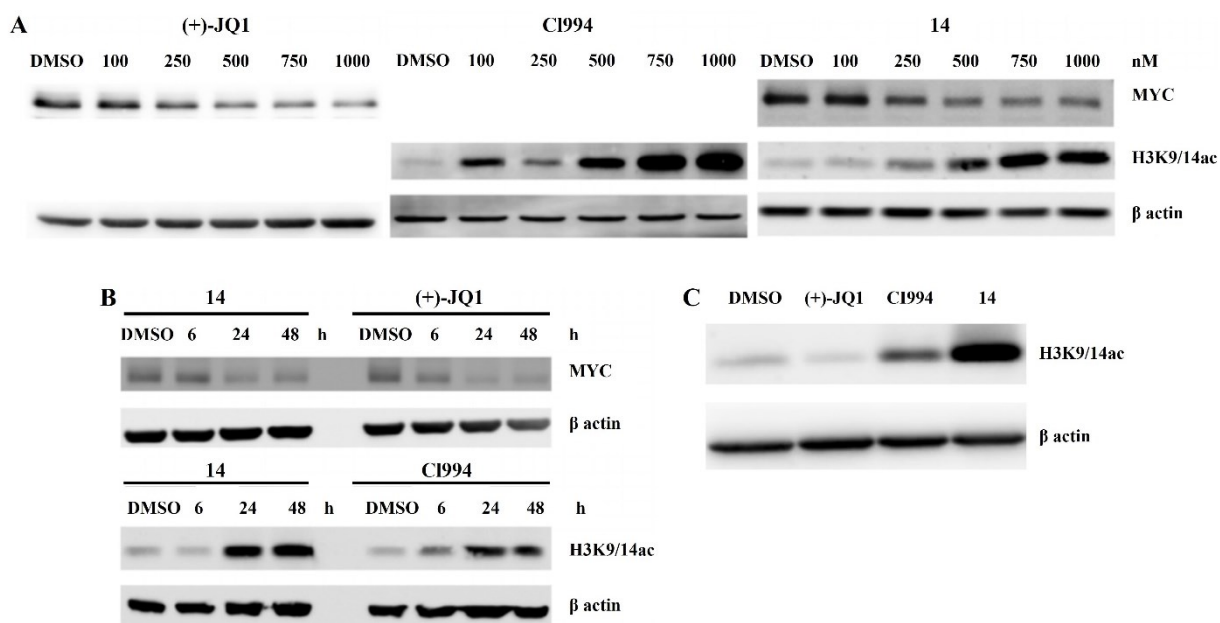


Figure 35: Time- and dose-dependent immunoblots of PaTu 8988t cells. A: Dose-dependent immunoblot of the proteins MYC and H3K9/14ac. PaTu 8988t cells were treated with the indicated doses of inhibitors for 48 hours. B: Time-dependent immunoblot of the proteins MYC and H3K9/14ac. PaTu 8988t cells were treated with 1 μM of indicated inhibitors and harvested at the indicated time points. C: Immunoblot analysis of PaTu 8988t cells treated with 1 μM of indicated inhibitor for 48 h next to each other to make the difference of CI994 and **14** more apparent.

Next, the cells were treated with an even higher dose of inhibitors (4 μM instead of 1 μM), which resulted in a more sustained suppression of MYC (Figure 36, A and B). Additionally the higher concentration of **14** also induced p57, a protein with known proapoptotic effects in several cell lines<sup>[98]</sup> and controlled by combined BET/HDAC inhibition<sup>[74]</sup>. Therefore, cells were treated with both inhibitors, JQ1 and CI994 separately and simultaneously. While CI994 alone had virtually no effect, regardless of concentration, JQ1 caused the mRNA level of p57 to increase sharply. Nevertheless, that increase is short-lived and independent of the used concentration as well (1 μM or 4 μM). Even the simultaneous administration of both inhibitors had little to no effect especially compared to those of compound **14**. The mRNA levels are at least doubled and remained at that level for at least three days. In every other case, the mRNA level was back to normal after this amount of time (Figure 36, C and D). Both the sustained suppression of MYC and induction of p57 suggest a longer-lasting BETi activity. In addition, persistent HDAC inhibitory activity was observed as well when washout experiments were performed. (1 day on and 2 days off). On day three increased histone H3 acetylation could still be observed even in cells treated with only 1 μM **14** (Figure 36, E and F)

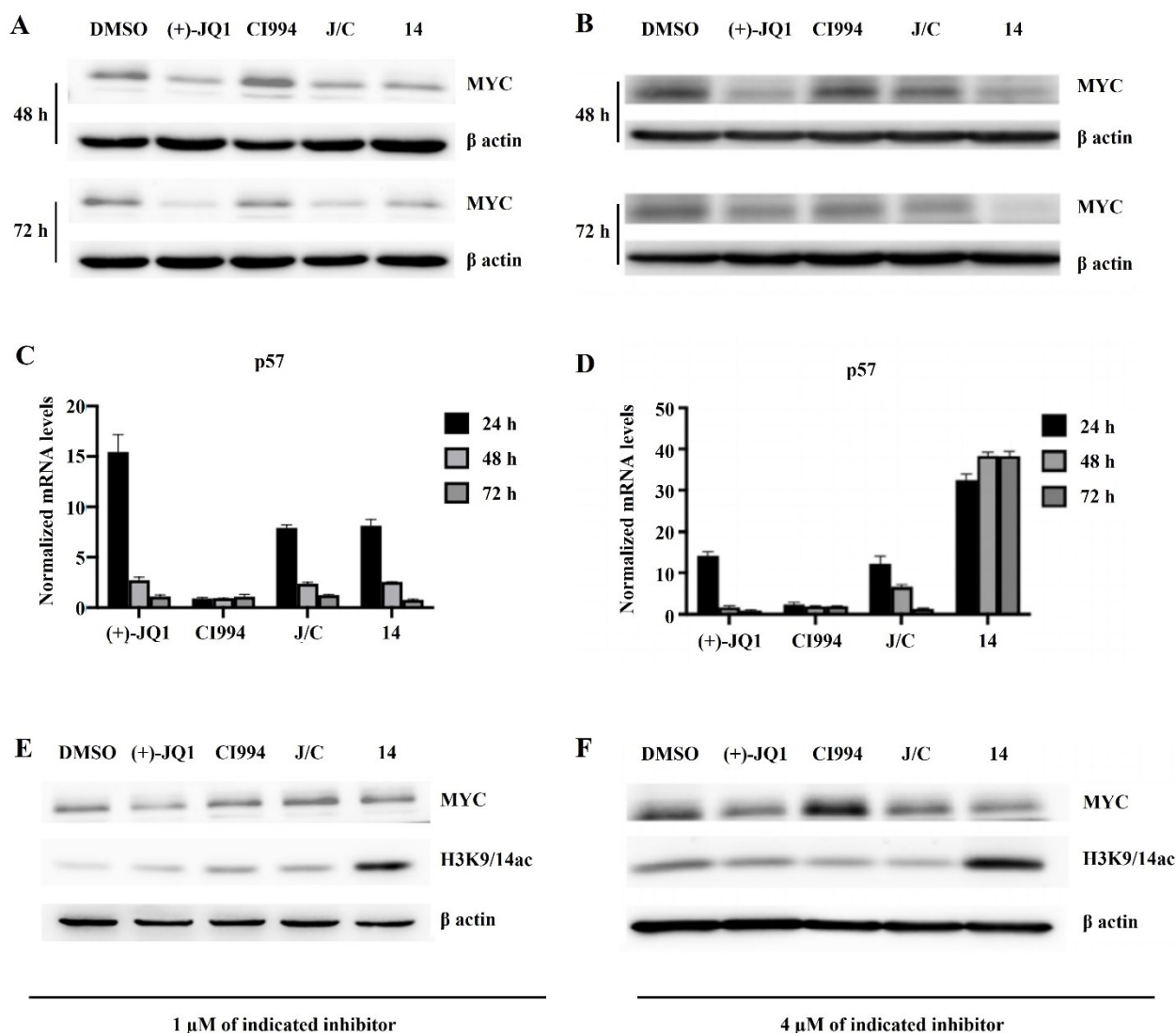


Figure 36: RT-PCR and washout experiment of PaTu 8988t cells. A and B: Time-course analysis of MYC protein levels by immunoblot. PaTu 8988t cells were treated with 1  $\mu$ M (A) or 4  $\mu$ M (B) of indicated inhibitor and harvested at the indicated time points. C and D: mRNA levels of *p57* by quantitative RT-PCR. PaTu 8988t cells were treated with 1  $\mu$ M (C) or 4  $\mu$ M (D) indicated inhibitors and harvested at the indicated time points. Mean  $\pm$  SEM from three independent experiments. E and F: Drug washout experiment by immunoblot. PaTu 8988t cells were treated with 1  $\mu$ M (E) or 4  $\mu$ M (F) indicated inhibitors (1 day on and 2 days off).

#### 4.1.7. Growth and viability of PDAC cells treated with 14

Next, cell viability assays were performed in a panel of different PDAC cell lines (MIA PaCa-2, DAN-G and HPAC, Figure 37). In all of them, 14 not only reduced cell survival in a dose-dependent manner, but also showed a more potent effect than the parental molecules, individually or combined. While the cell viability of MIA PaCa-2 cells is already halved at a concentration as low as 50 nM with a significant difference to JQ1, in the other cells a higher concentration of 0.5  $\mu$ M (HPAC) and 1  $\mu$ M (DAN-G) is needed, respectively. Interestingly,

CI994 alone or in combination with JQ1 had hardly any effect on cell survival and the only visible synergetic effect is found in DAN-G cells at 2  $\mu$ M.

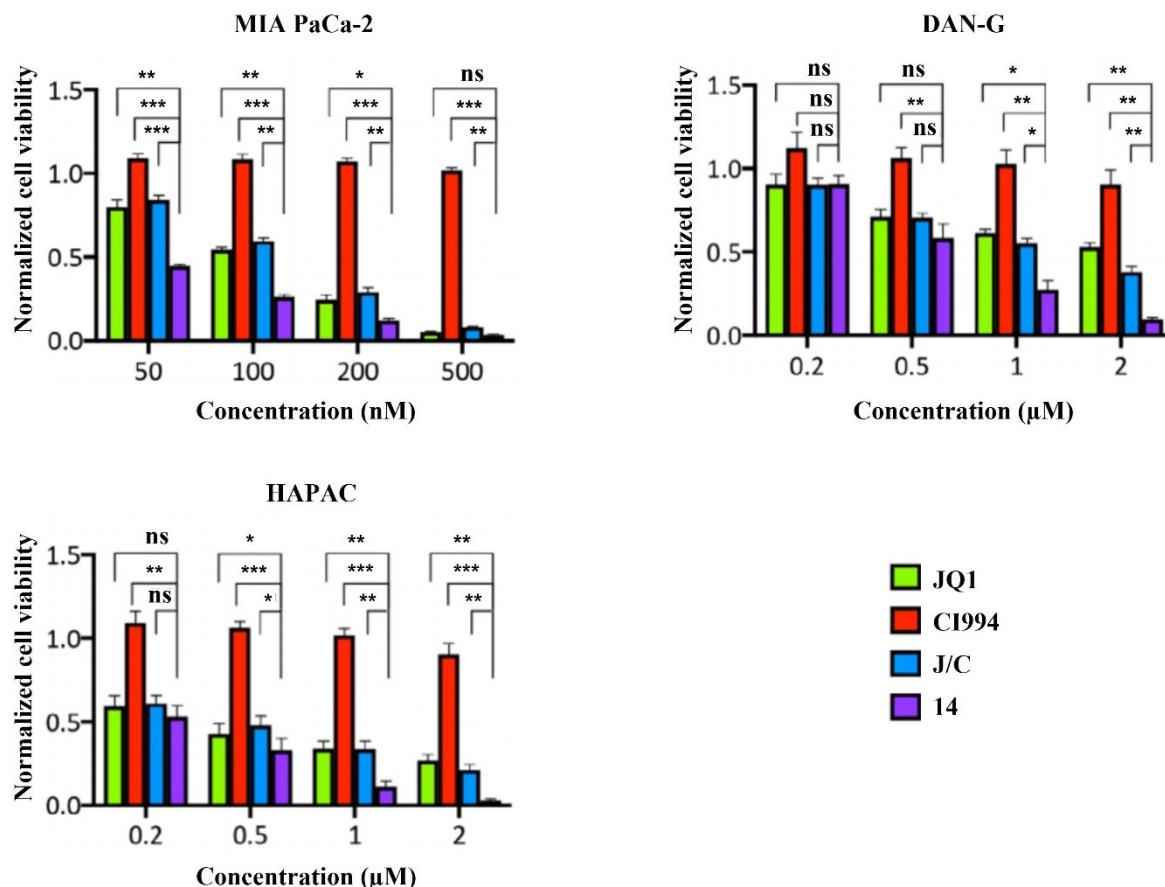


Figure 37: CellTiter Glo cell viability assay with three different PDAC cell lines. Cells were treated with indicated inhibitor with different doses for 5 days. Mean  $\pm$  SEM from three independent experiments, \*\*\* $P \leq 0.001$ , \*\* $P \leq 0.01$ , \* $P \leq 0.05$ , n.s.: not significant.

Subsequent immunoblot analysis of MIA-PaCa-2 cells showed that upon administration of compound **14**, the expression of cleaved caspase 3, present in apoptotic cells,<sup>[99]</sup> increased significantly. Interestingly, its expression is also visibly increased when cells were treated with both inhibitors combined, but probably not high enough to influence cell viability (Figure 38).

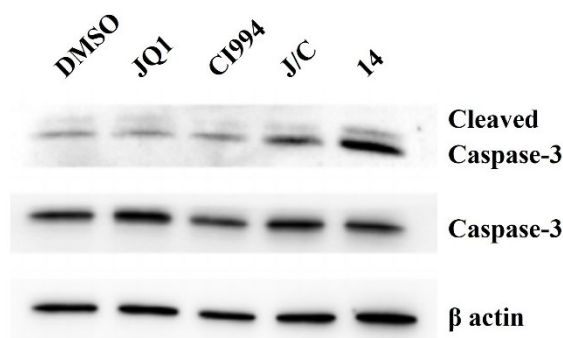


Figure 38: Immunoblot analysis of cleaved caspase-3 in MIA PaCa-2 cells. Cells were treated with 50 nM indicated inhibitors for 3 days. Expression increased when treated with **14** or with JQ1 and CI994 combined.

Next, the long-term effects on cell survival were evaluated so **14** was only administered once for a time period of 24 hours. This should help evaluating alternative scheduling strategies at an early stage, as single-agent BET inhibition is challenging due to unknown scheduling strategies in addition to limited efficacy and toxicity issues.<sup>[35]</sup> Again, compound **14** had a more sustained effect on suppressing cell growth than single-agent or combined treatment with indicated inhibitors. While cells treated with **14** did not begin to grow until day 10, JQ1 treated cells grew as early as day 6 and the others even earlier. On the 15<sup>th</sup> day, the cell confluence of **14** treated cells reached approximately 25 %, which is significantly lower than that of the cells treated with JQ1 (approx. 75 %) or the remaining treated cells (approx. 80 %) respectively.

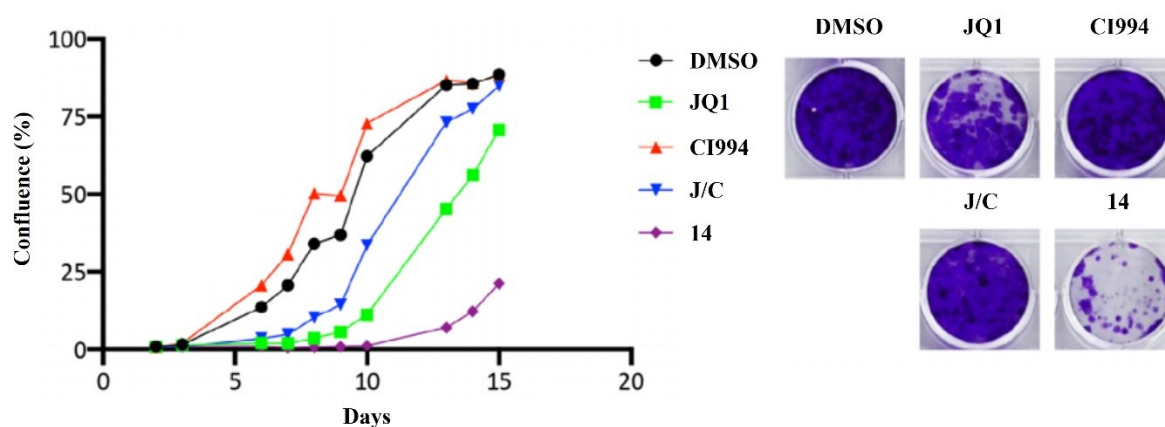


Figure 39: Cell confluence measurement of MIA PaCa-2 cells. Cells were treated with 1  $\mu$ M of indicated inhibitors for 24 hours by NYONE image cytometry and colony formation assay after 15 days.

In a different schedule (inhibitors on for 1 day and off for 6 in 3 cycles) the suppressive effects of **14** were further prolonged. After 15 days, cell confluence was approximately 85% for all cells except those treated with **14** (approx. 40%). This did not change much until the end.

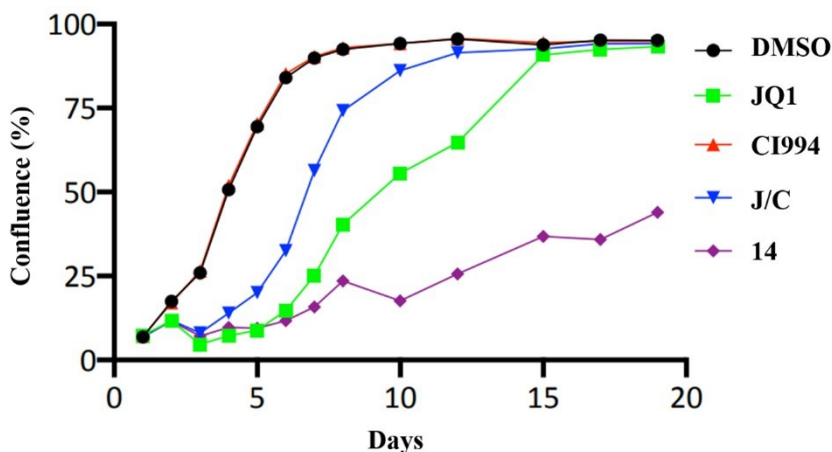


Figure 40: Cell confluence measurement with 1  $\mu$ M indicated inhibitor on day 1, 8 and 15 for 24 hours.

#### 4.1.8. Combination of gemcitabine and **14**

As a standard-of-care chemotherapeutic agent gemcitabine is used in the treatment of pancreatic cancer and was already tested in combination with CI994. As previously mentioned this combination did not prove as beneficial.<sup>[69]</sup> To see if the combination of **14** and gemcitabine is any better the efficacy of the combination was evaluated in different scheduling routes. Both drugs were either administered at the same time or consecutively. For this, combinations of serial dilutions of each compound were used to treat HPAC cells and the viability of these cells was measured. Those results were evaluated by SynergyFinder (synergyfinder.fimm.fi)<sup>[100]</sup> to find synergistic effects in the different scheduling (Figure 41).

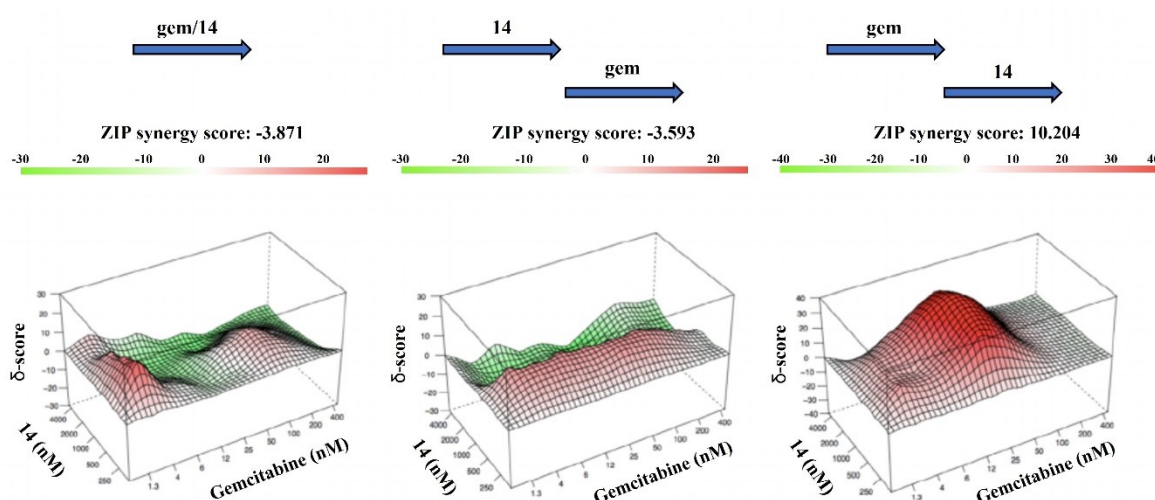


Figure 41: Combination response of HPAC cell, which were treated with **14** and gemcitabine in three different administration schedules: (1) administration of **14** and gemcitabine simultaneously for 24 hours and incubation for another 4 days; (2) first administration of **14** followed by gemcitabine (both for 24 hours) and incubation for another 3 days; (3) first administration of gemcitabine followed by **14** (both for 24 hours) and incubation for another 3 days. Cell viabilities for all indicated dose combination were measured by CellTiter Glo viability assay. Synergy effects were evaluated using SynergyFinder. ZIP synergy score is averaged over all dose combination cells.

Intriguingly, a synergistic effect is only observed, but strikingly high, when gemcitabine is administered first, followed by **14** 24 hours later. Here, the ZIP score is 10.20 which is significantly higher than that of both other possible combinations (-3.81 and -3.59, respectively). Additionally, gemcitabine was also combined with JQ1/CI994 which had a lower ZIP score (8.96) than the gemcitabine/**14** combination in the same scheduling, proving benefits of **14** as a dual inhibitor. Those results are consistent with the followed colony formation assay, in which again the gemcitabine first schedule showed the most promising results. Even regardless of the inhibitor used, gemcitabine must be administered first to obtain a good response (Figure 42).

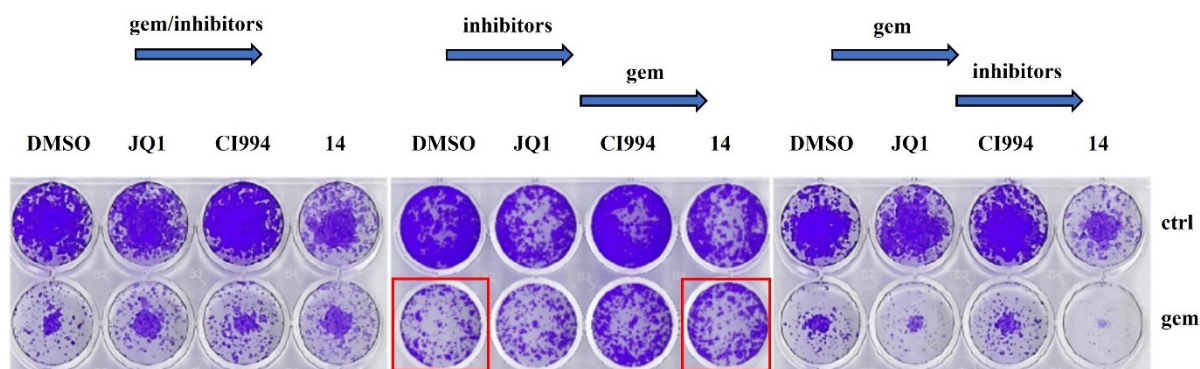


Figure 42: Colony formation assay for HPAC cells with different administration schedules. In general, 10 nM gemcitabine and 2  $\mu$ M of indicated inhibitor were used. Detrimental effect is highlighted (red box). More colonies grew, when **14** was administered before gemcitabine.

Interestingly, both simultaneous and **14**-first scheduling not only showed no combinatorial advantages, but even proved to be detrimental to colony formation. Looking at the red boxed colonies in Figure 42, colony formation is clearly less reduced when **14** is administered before gemcitabine compared to gemcitabine alone. Since the mechanism of action of gemcitabine is based on being incorporated into DNA<sup>[101]</sup> during S phase of the cell cycle this could indicate, that **14** prevents initiation of the S phase. Due to reports, that JQ1 induces accumulation of the cell cycle regulator p21<sup>[102]</sup> which causes cell cycle arrest in G1 and blocks entry into S phase<sup>[103]</sup> it was natural so see if **14** acts the same way. Indeed, immunoblot and cell-cycle analysis showed that p21 is highly expressed by **14** and transition from G1 to S phase is blocked (Figure 43).

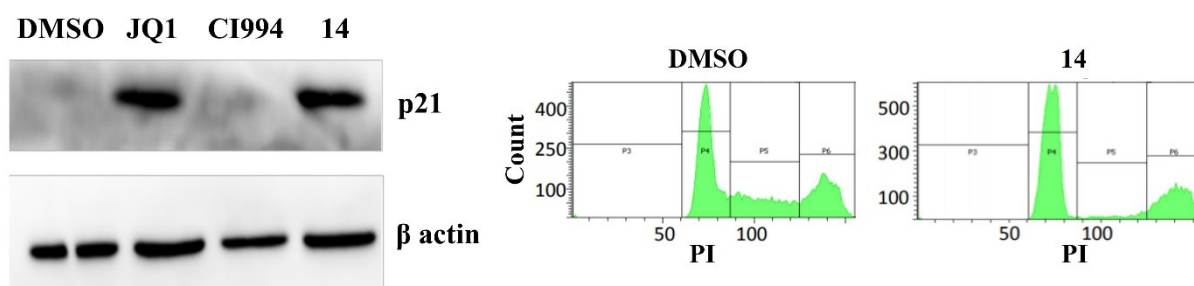


Figure 43: Immunoblot analysis of p21 and cell-cycle analysis of HPAC cells. HPAC cells were treated with 2  $\mu$ M of indicated inhibitor for 24 h and then harvested. Both JQ1 and **14** induce accumulation of p21, which leads to G1 arrest. For cell-cycle analysis of HPAC cells were treated with **14** for 24 hours and then harvested. After treatment with **14**, the number of cells in S phase is clearly reduced.

It is only logical that when **14** and gemcitabine are used simultaneously, more cells remain in G1 phase and thus gemcitabine cannot exert its effect. This effect also involves the induction of acute replication stress as indicated by induction of phospho-CHK1,<sup>[66]</sup> which is reduced by the simultaneous schedule as well (Figure 44).

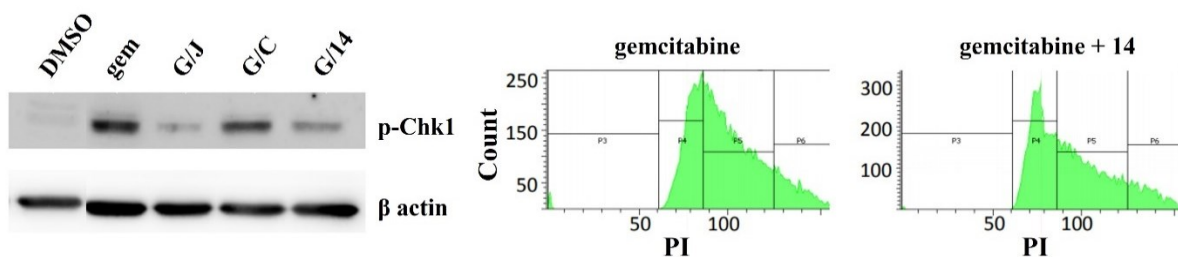


Figure 44: Immunoblot analysis of phospho-CHK1 and cell cycle analysis of HPAC. HPAC cells were treated with 2  $\mu$ M of indicated inhibitor together with 10 nM gemcitabine for 24 hours and then harvested. Simultaneous administration clearly reduces induction of p-CHK1 compared to gemcitabine alone. For cell cycle analysis by flow cytometry of HPAC cells, cells treated with 10 nM gemcitabine alone or simultaneously with 2  $\mu$ M 14. Simultaneous administration retains more cells in G1 phase compared to gemcitabine alone.

However, by changing the schedule to gemcitabine first the induced replication stress is not only on its normal level but even enhanced consistent with the increased expression of p-CHK1. Furthermore, cleaved caspase 3 is strongly expressed by this schedule, which supports highly increased apoptosis (Figure 45).

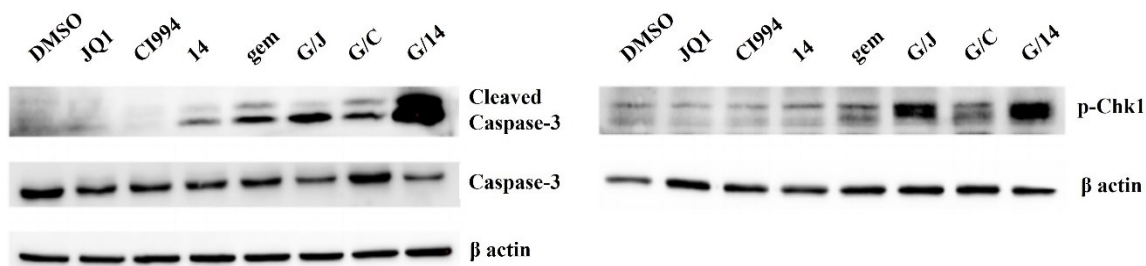


Figure 45: Immunoblot analysis of cleaved caspase-3 and phospho-CHK1. HPAC cells were sequentially treated with 10 nM gemcitabine and 2 $\mu$ M of indicated inhibitor. After removal of inhibitors cells were cultured for another day. Both, cleaved caspase-3 and p-CHK1 are highly expressed by this schedule.

Another effect of the gemcitabine first schedule is, that after gemcitabine was discontinued, the cells did not return to the normal cell cycle as usually but remained in S phase arrest. This is clearly visible in the cell-cycle analysis of HPAC cells that were treated sequentially with gemcitabine followed by 14 or gemcitabine alone. 48 hours after removal gemcitabine treated cells have returned to an almost normal cell-cycle distribution (Figure 46).



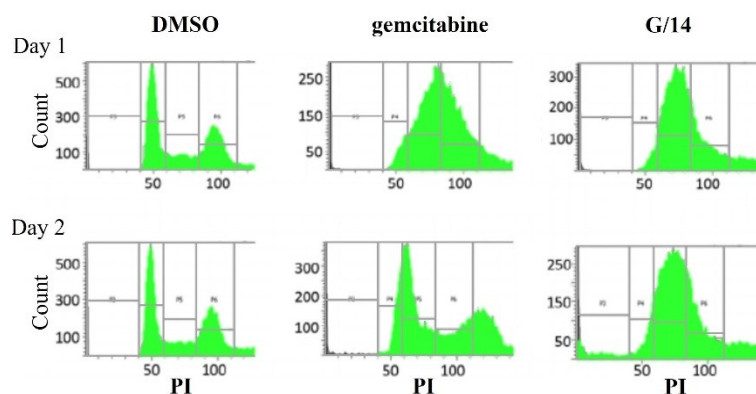


Figure 46: Cell-cycle analysis by flow cytometry of HPAC cells. Cells were treated with 10 nM gemcitabine alone or sequentially with 2  $\mu$ M of **14**. After 48 h gemcitabine treated cells are almost back to a normal cell-cycle distribution while sequentially treated cells remain in S-phase arrest.

In summary, this schedule shows the most prominent synergistic effects, by optimally exploiting the gemcitabine-induced replication stress and increased apoptosis.

#### 4.1.9. Transcriptomic profiling

The transcriptomic profiling was performed in the established PDAC line PANC-1 to explore the molecular mechanisms elicited by **14**. Hierarchical clustering revealed different gene expression profiles between **14** and JQ1 treated samples and untreated cells (Figure 47).

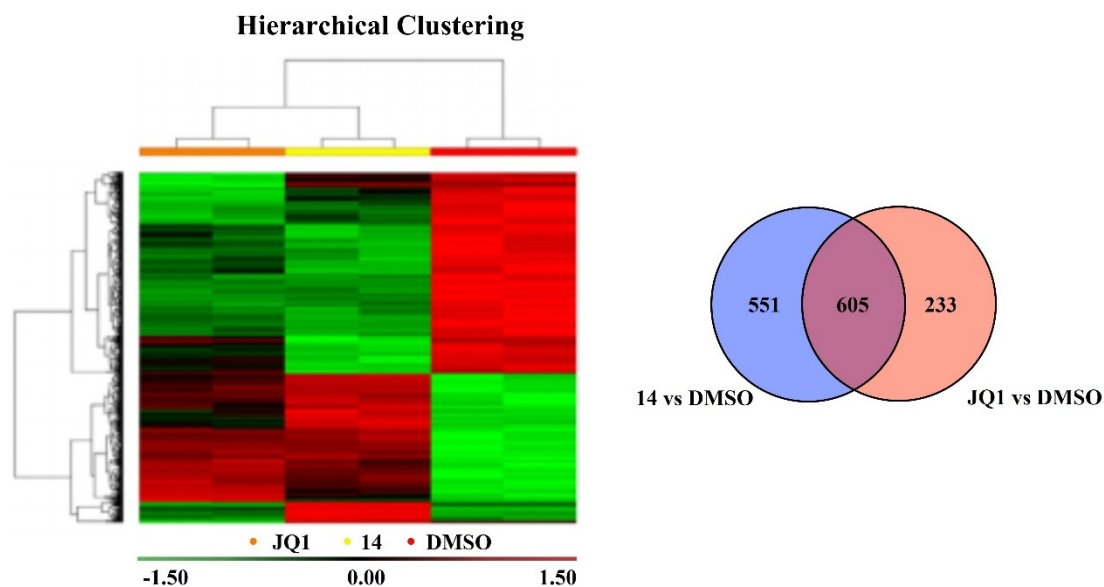


Figure 47: Hierarchical clustering of the differentially expressed genes in PANC-1 cells and Venn diagram of those genes. Cells were treated with either 1  $\mu$ M **14** or JQ1 for 24 hours compared to DMSO treatment. Each treatment was done in duplicate. Venn diagram analysis and hierarchical clustering show, that **14** deregulates most of the genes that JQ1 deregulates but additionally many more.

Compared to untreated cells, **14** seems to almost reverse the expression profile completely, while JQ1 had a similar effect but not quite to the extent. Nevertheless, approximately 70 % of the differentially expressed genes by JQ1 (838 genes absolute) were deregulated by **14** as well, but there were also 551 additional genes that are affected by **14** alone. To gain a deeper understanding of the gene expression patterns affected by **14**, Gene Ontology (GO) analysis was performed. This analysis revealed that most of the downregulated genes were connected to cell-cycle-related processes, cellular component organization and metabolic processes (Figure 48).

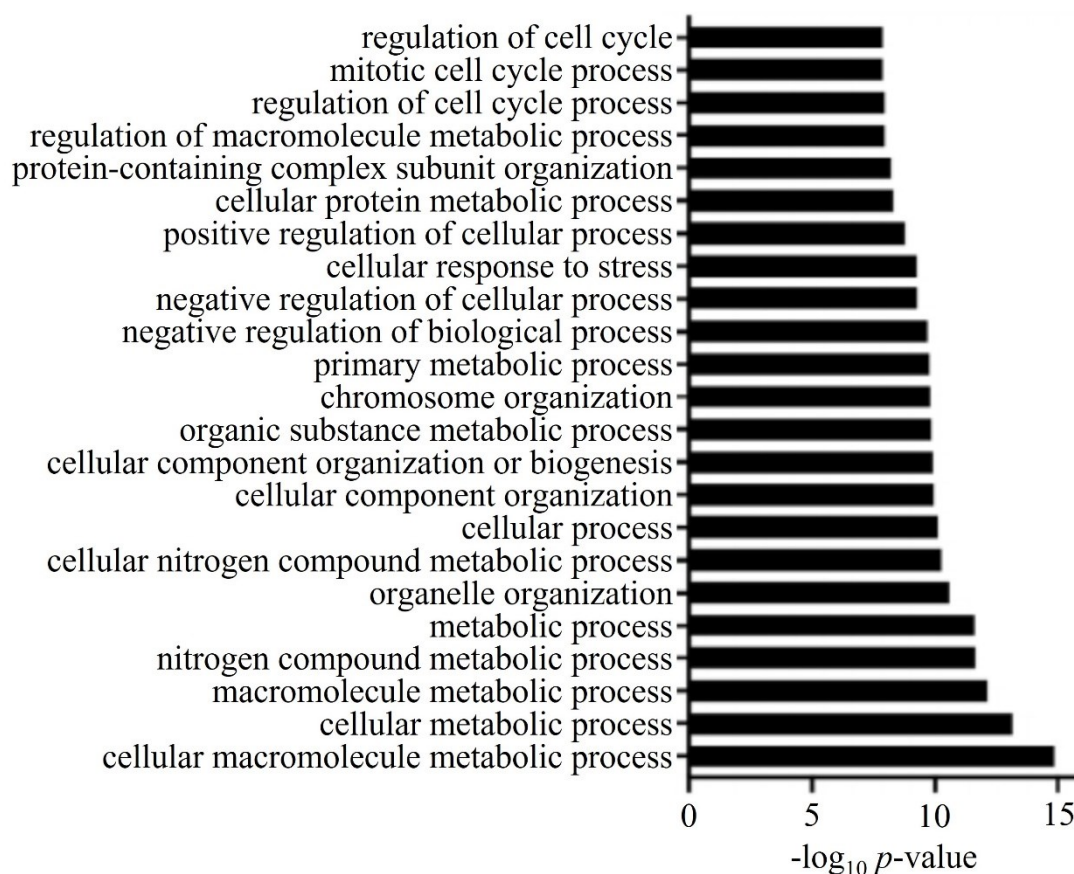


Figure 48: Gene ontology analysis of genes downregulated by **14**. The genes downregulated by **14** are mainly associated with cell-cycle-related processes, cellular component organization and metabolic processes.

The influence of **14** on cell-cycle progression was further confirmed by gene set enrichment analysis (GSEA). The gene sets used are called Kong\_E2F3\_Targets, Reactome\_Cell\_Cycle and Zhou\_Cell\_Cycle\_Genes\_in\_IR\_Response\_6HR which contain a total of 959 cell cycle related genes. GSEA revealed that those genes were downregulated by **14** compared to DMSO or JQ1 treatment (Figure 49).

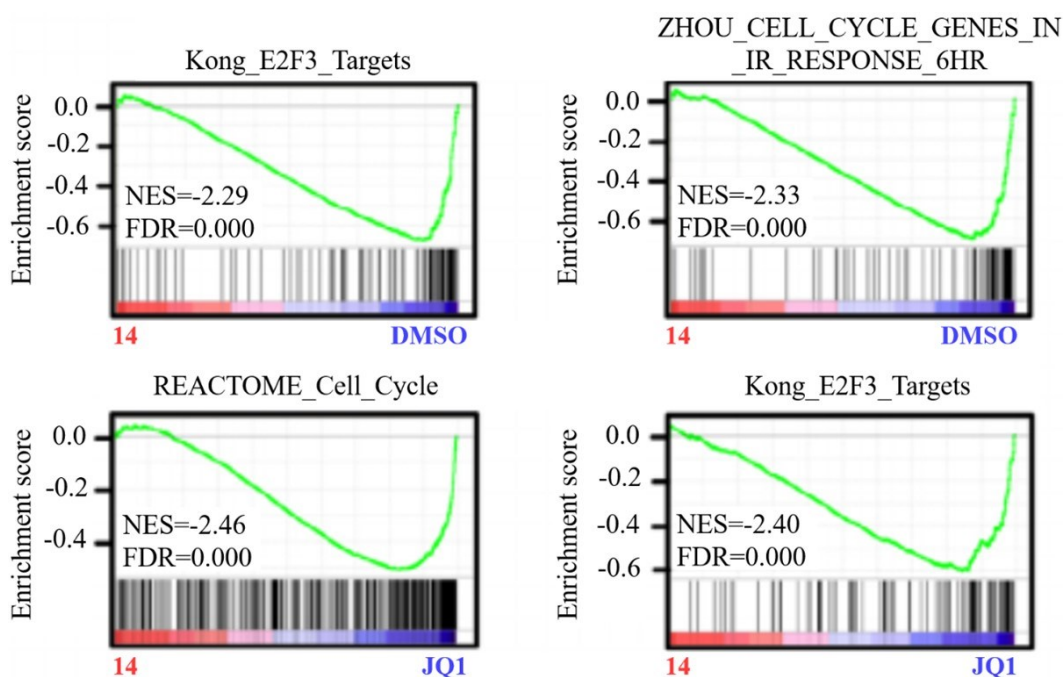


Figure 49: GSEA plots, that compare the enrichment of pathways related to cell cycle. Plots show that these pathways are downregulated by **14** in comparison with DMSO or JQ1 treatment.

GSEA was also performed with gene sets related to HDAC inhibition to see how those are regulated by **14**. The sets used were Heller\_HDAC\_Targets\_Up and Chiba\_Response\_To\_TSA which contain a total of 380 genes that are up regulated by TSA. GSEA revealed that those pathways were significantly enriched in cells treated with **14** as well, indicating that **14** also recapitulates the HDACi activity of CI994.

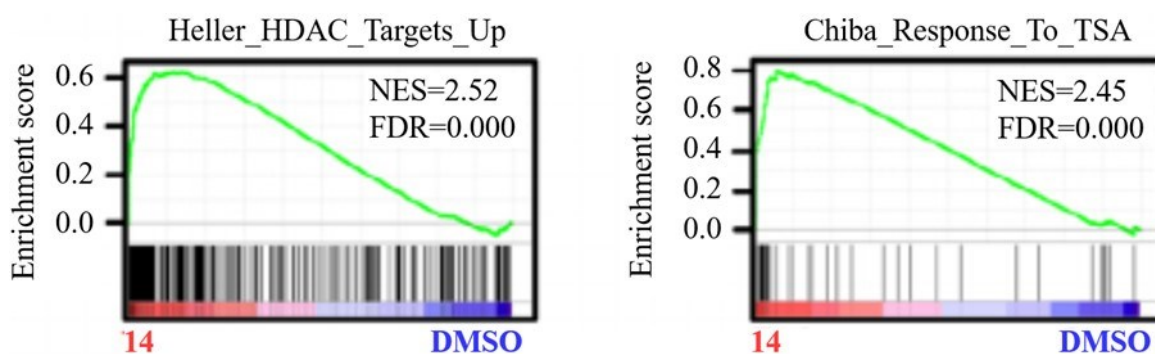


Figure 50: GSEA plots comparing the enrichment of HDACi signature. Plots show that these pathways are upregulated by **14**.

Next, master transcriptional regulators (TFs) had to be identified that control cell cycle progression. Since previous studies indicated that TFs could be driven by super-enhancers (SEs)<sup>[104]</sup> ChIP-seq using H3K27ac was performed to identify the genomic enhancer landscape. This resulted in the identification of a total of 453 SEs in PANC-1 cells. Next, the SE-associated gene expression of cells treated with JQ1 or **14** was analyzed and compared to controls. Of the

453 SEs found 41 are downregulated by **14** and compared to JQ1 12 SE-associated genes are selectively targeted by **14** including FOSL1 (Figure 51).

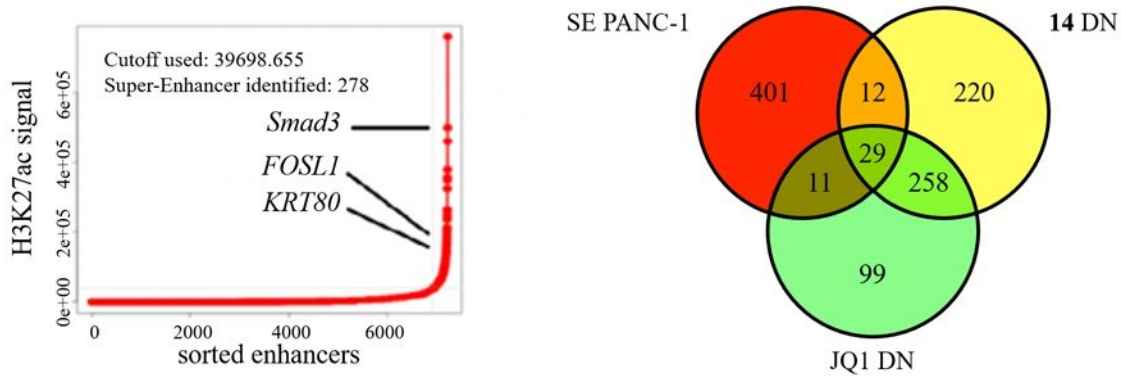


Figure 51: Enhancers in PANC-1 ranked based on the intensity of H3K27ac signal using ROSE algorithm defining 453 super-enhancers. Venn diagram analysis of super-enhancers shows that of 41 downregulated SEs 12 SEs are specific to **14**.

FOSL1 is a transcription factor and has been linked to KRAS-associated mitotic progression.<sup>[105]</sup> As revealed by a statistical analysis of a pancreatic cancer cohort from the Human Protein Atlas data set<sup>[106]</sup> high FOSL1 expression in KRAS pancreatic cancer has an extremely poor impact on patient survival (Figure 52).

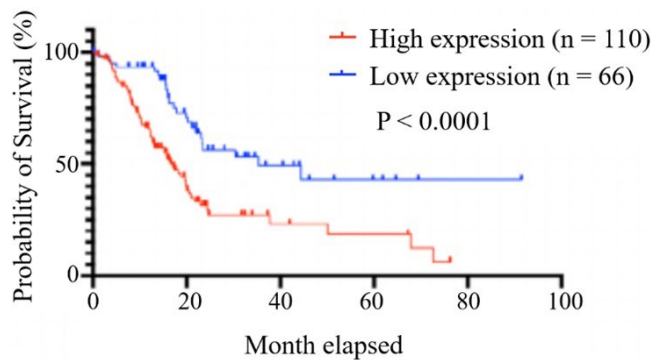


Figure 52: Kaplan-Meier plot of the survival of pancreatic cancer patients partitioned between high and low FOSL1 mRNA expression. Plot clearly shows that high FOSL1 expression decreases survival probability.

In order to confirm the **14**-dependent downregulation of FOSL1, which is detrimental to KRAS driven PDAC<sup>[105]</sup>, RT-PCR was performed. Results showed that FOSL1 was downregulated to a higher extent compared to DMSO control and even to JQ1, CI994 and the combined treatment (Figure 53, left). Furthermore, as revealed by GSEA, FOSL1 targets<sup>[105]</sup> are downregulated as well, indicating a dysregulation of the transcriptional program of FOSL1 by **14** (Figure 53, right).

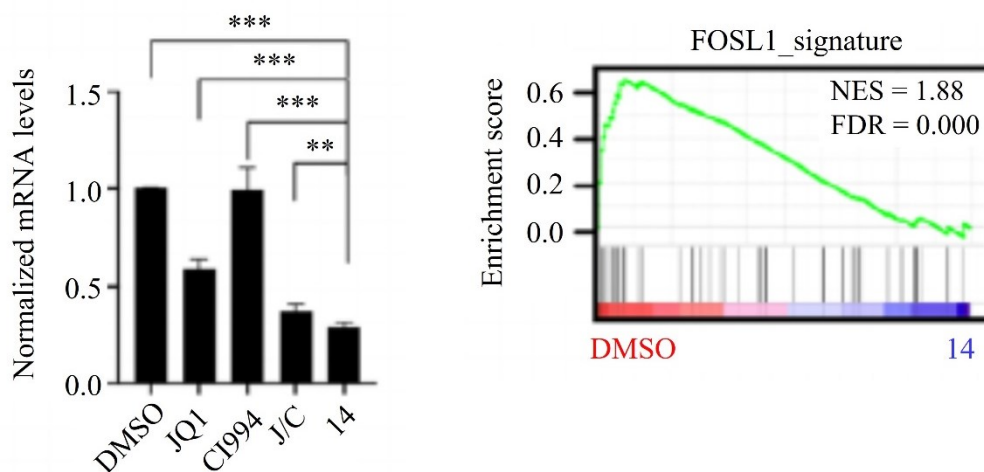


Figure 53: Quantitative RT-PCR analysis of FOSL1 gene in PANC-1 cells. Cells were treated with 1  $\mu$ M indicated inhibitors for 24 hours. Mean  $\pm$  SEM from six independent experiments, \*\*\* $P \leq 0.001$ , \*\* $P \leq 0.01$ , \* $P \leq 0.05$ . mRNA level of FOSL1 is significantly downregulated by **14** compared to JQ1, CI994 and combined treatment. The GSEA plot compares the enrichment of FOSL1 signature. FOSL1 targets are significantly downregulated by **14**.

Looking around the FOSL1 gene locus in PANC-1 cells it is not surprising that SEs can be found here, since the level of FOSL1 in PDAC is elevated. Interestingly there are none in healthy pancreatic cells which supports the idea that cancer cells establish SEs at oncogenes during tumor pathogenesis (Figure 54).<sup>[104]</sup>



Figure 54: H3K27ac occupancy profiles at the FOSL1 gene in healthy pancreas compared to PANC-1 cells. Obviously, there are only SEs around the FOSL1 gene locus in PANC-1 cells.

#### 4.1.10. NUT midline carcinoma cells treated with **14**

In addition to PDAC cells, nuclear protein in testis (NUT) midline carcinoma (NMC) cells were treated with **14** as well. NMC is an extremely aggressive subtype of poorly differentiated squamous cell carcinoma with a median survival time of only 6.7 months.<sup>[107][108]</sup> Defined by chromosomal rearrangements the *NUT* gene is most often fused with *BRD4*<sup>[107]</sup> and therefore potentially prone to BET inhibitors. Indeed, a previous study<sup>[40]</sup> already showed that JQ1 was able to induce squamous differentiation by inhibiting BRD4-NUT. Again, it is logical to test if **14** could induce differentiation in HCC2429, a NMC cell line, as well may be even in an enhanced way.<sup>[109]</sup> Quite similar to JQ1, **14** provoked a differentiation phenotype in these cancer cells, including cell flattening, spreading and striking spindle morphology. Additionally,

immunoblot showed **14** induced gene expression of a specific marker for squamous differentiation called Involucrin.<sup>[110]</sup>

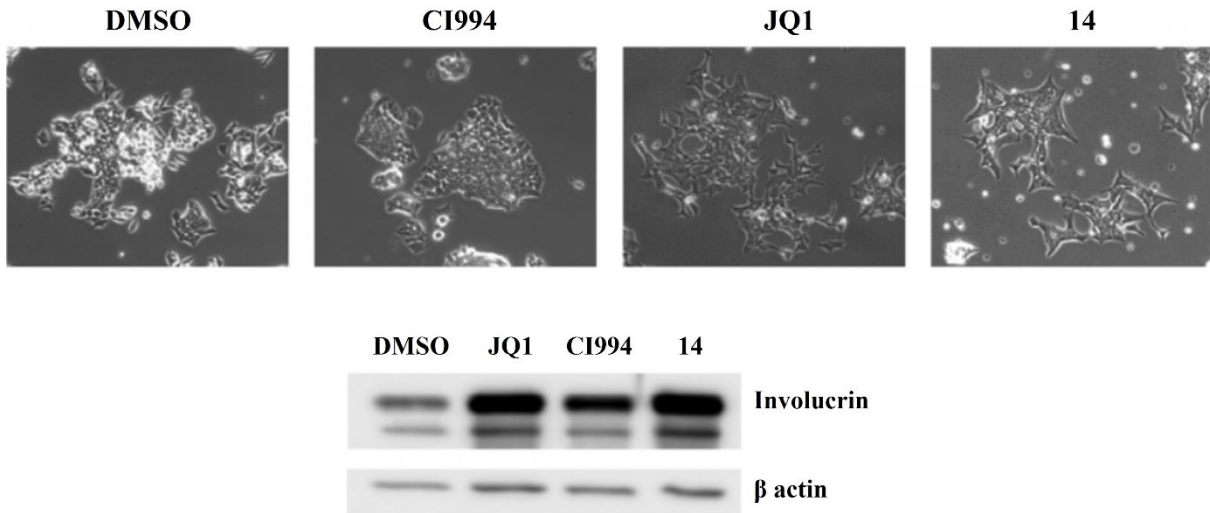


Figure 55: Morphological changes of HCC2429 cells after treatment with 500 nM of indicated inhibitors for 48 h. **14** and JQ1 provoke a differentiation phenotype in these cells and immunoblot analysis of the differentiation marker Involucrin. HCC2429 cells were treated with 500 nM of indicated inhibitors for 72 hours.

Furthermore, RT-PCR was used to investigate the expression level of *KRT14*, *KRT10* and *TGM1*, three typical squamous tissue genes. While the results showed a modest induction of the genes *KRT10* and *TGM1* upon treatment with **14**, induction of *KRT14* was increased 700-fold. Remarkably, **14** was able to induce the expression of all three genes more efficiently than JQ1 or let alone CI994.

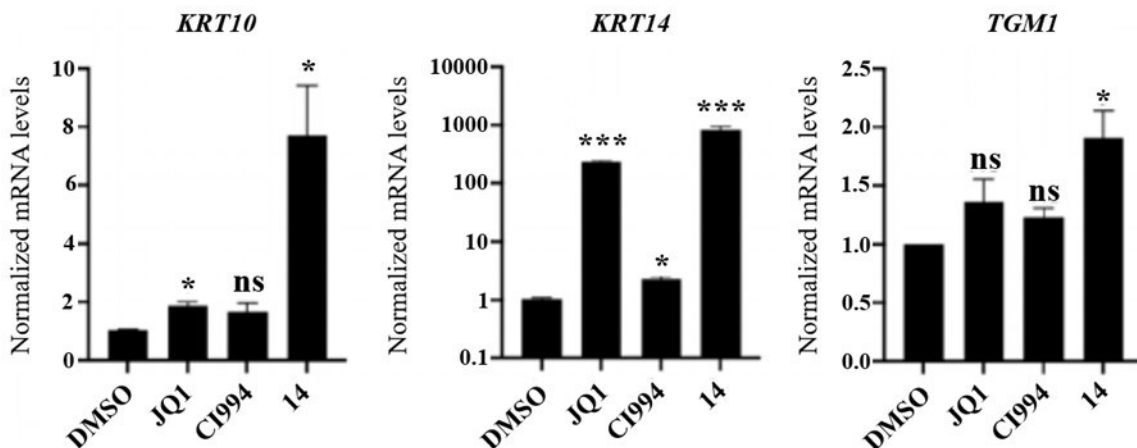


Figure 56: Quantitative RT-PCR analysis of three typical squamous tissue genes (*KRT10*, *KRT14* and *TGM1*). HCC2429 cells were treated with 500 nM of indicated inhibitors for 72 h. Mean  $\pm$  SEM from three independent experiments, \*\*\* $P \leq 0.001$ , \*\* $P \leq 0.01$ , \* $P \leq 0.05$ ; n.s., not significant.

## 4.2. Dual BET/HDAC inhibitors of the second generation

In total five potential dual BET/HDAC inhibitors are members of the second generation (Figure 57) and all of them are derived from the selective CBP/p300 inhibitor **17** (Figure 18). In order to introduce the HDACi activity while hoping to enhance the still remaining BETi activity the morpholine moiety (Figure 18, black) was replaced. As substitutes the side chain of panobinostat and a selection of CI994 derivatives were chosen. To further increase the chance of BETi activity, the chlorine atom and methoxy group of one compound were additionally replaced by a hydrogen atom and a methyl group, respectively.

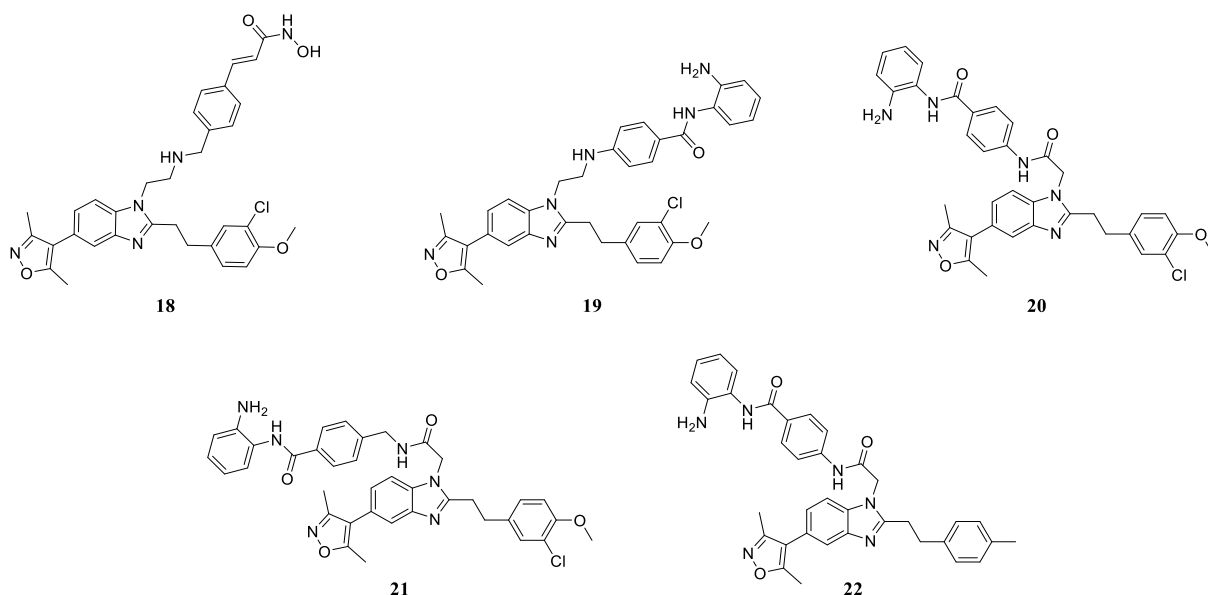


Figure 57: Dual BET/HDAC inhibitors of the second generation.

## 4.2.1. DSF results

As before the interaction of the synthesized compounds with BRD4 were evaluated by DSF. Additionally, since all of them were derived from a selective CBP/p300 inhibitor those bromodomain containing proteins were included in this assay as well together with the inhibitor itself (**17**). The compounds were tested twice in duplicates (Table 9).

Table 9: DSF assay results of the second generation.  $\Delta T_m$  in  $^{\circ}\text{C}$ .

Nr.	BRD4 1		BRD4 2		EP300		CBP	
	Run 1	Run 2	Run 1	Run 2	Run1	Run2	Run1	Run2
<b>17</b>	1.0 $\pm$ 0.3	1.0 $\pm$ 0.2	0.3 $\pm$ 0.3	0.2 $\pm$ 0.2	7.1 $\pm$ 0.0	5.8 $\pm$ 0.2	5.6 $\pm$ 0.1	4.4 $\pm$ 0.3
<b>18</b>	1.7 $\pm$ 0.5	0.8 $\pm$ 0.1	1.2 $\pm$ 0.3	1.3 $\pm$ 0.1	2.6 $\pm$ 0.1	2.7 $\pm$ 0.3	2.6 $\pm$ 0.3	2.4 $\pm$ 0.2
<b>19</b>	0.8 $\pm$ 0.3	0.3 $\pm$ 0.3	1.0 $\pm$ 0.2	1.3 $\pm$ 0.1	0.6 $\pm$ 0.4	0.3 $\pm$ 0.2	0.9 $\pm$ 0.2	0.7 $\pm$ 0.1
<b>20</b>	1.1 $\pm$ 0.1	0.9 $\pm$ 0.1	7.7 $\pm$ 3.7	-4.8 $\pm$ 4.5	2.1 $\pm$ 0.3	1.1 $\pm$ 0.2	1.7 $\pm$ 0.3	2.1 $\pm$ 0.4
<b>21</b>	1.0 $\pm$ 0.1	0.3 $\pm$ 0.1	1.8 $\pm$ 0.6	0.9 $\pm$ 0.4	1.3 $\pm$ 0.2	2.0 $\pm$ 0.6	1.9 $\pm$ 0.2	1.1 $\pm$ 0.5
<b>22</b>	1.6 $\pm$ 0.1	1.7 $\pm$ 0.3	2.2 $\pm$ 0.0	6.6 $\pm$ 3.6	1.3 $\pm$ 0.7	1.3 $\pm$ 0.3	2.0 $\pm$ 0.5	2.4 $\pm$ 0.2

Fields are colored according to the measured thermal shift  $\Delta T_m$  whereas green indicates a low, yellow a mediocre and red a strong shift (relative).

As the results show **17** is indeed a selective inhibitor for CBP and EP300 although the shifts on those targets should be around 9  $^{\circ}\text{C}$ .<sup>[81]</sup> Nevertheless it is obvious that by replacing the morpholine moiety the affinity to EP300 and CBP significantly dropped. Unfortunately, it looks like the absence of this moiety does not affect its affinity towards BRD4 with maybe two exceptions. Compounds **20** and **22** are the only ones that seem to influence the second bromodomain of BRD4 exclusively but only in one of the two runs. Additionally, in these cases the standard deviation is comparatively high, so those two compounds were tested again twice in duplicates on every BET protein.

Table 10: Repetition of the DSF assay for compounds **20** and **22**.  $\Delta T_m$  in  $^{\circ}\text{C}$ .

Nr.	BRD2 1		BRD2 2		BRD3 1		BRD3 2	
	Run 1	Run 2	Run 1	Run 2	Run 1	Run 2	Run 1	Run 2
<b>20</b>	-5,5 $\pm$ 2,0	-1,8 $\pm$ 3,0	24,7 $\pm$ 0,1	-21,6 $\pm$ 0,4	10,3 $\pm$ 0,0	13,2 $\pm$ 13,1	27,3 $\pm$ 0,3	-10,6 $\pm$ 0,8
<b>22</b>	-1,4 $\pm$ 11,2	-1,9 $\pm$ 1,4	23,2 $\pm$ 0,0	0,5 $\pm$ 0,2	3,6 $\pm$ 3,7	-3,3 $\pm$ 3,7	0,8 $\pm$ 12,5	-0,5 $\pm$ 0,8
	BRD4 1		BRD4 2		BRDT 1		BRDT 2	
	Run 1	Run 2	Run 1	Run 2	Run 1	Run 2	Run 1	Run 2
<b>20</b>	0,6 $\pm$ 0,3	-0,7 $\pm$ 0,5	30,8 $\pm$ 0,4	-11,4 $\pm$ 3,5	0,2 $\pm$ 0,2	-2,5 $\pm$ 1,1	-1,2 $\pm$ 0,5	-0,1 $\pm$ 0,0
<b>22</b>	1,0 $\pm$ 0,0	-0,7 $\pm$ 0,4	4,3 $\pm$ 11,8	17,2 $\pm$ 13,7	5,4 $\pm$ 4,5	0,5 $\pm$ 0,0	-3,6 $\pm$ 0,2	0,6 $\pm$ 0,0

Fields are colored according to the measured thermal shift  $\Delta T_m$  whereas green indicates a low, yellow a mediocre and red a strong shift (relative).



Again, the results are very ambiguous, especially with respect to the second binding domain of the BETs excluding BRDT. While the  $\Delta T_m$  shift of **20** is very high (24 °C or higher) on those domains in the first run, it is in the negative range all at once in the second run of the assay. At first glance, there seems to be only one confirmation in the second run, apart from the low  $\Delta T_m$  shifts, of course. Unfortunately, the standard deviation in the second run of BRD3 1 is too high, so that this value cannot be trusted either. The other compound tested is quite similar with the distinction that on BRD4 2 it is the second run which shows the higher shift in combination with a high standard deviation. Compound **22** should have had the higher affinity for BRD4 due to the modification<sup>[81]</sup> compared to compound **20**, but this is obviously not the case. Lamentably the repetition of the assay did not yield any new findings regarding BRD4 2 and the new results even showed the exact same pattern as before. Although negative  $\Delta T_m$  shifts seem to be counterintuitive considering that a non-binding compound should show a  $\Delta T_m$  of 0 °C there are explanations aside from faulty performance or poor protein activity. Some ligands for example bind primarily to the unfolded state of a protein and are therefore destabilizing it.<sup>[111]</sup> Whatever the actual reason for the negative  $\Delta T_m$  shift is, it could mean that the compounds in fact do interact with the proteins, but not necessarily in the desired way, which is why they tend not to be dual inhibitors.

#### 4.2.2. Fluorogenic HDAC and nanoBRET assay results

This time the fluorogenic HDAC assay was performed on HDACs 1-3. Unfortunately, HDAC 1 had poor activity and HDAC2 was not active at all. For that reason, no HDAC2 data is available and HDAC1 data is only reliable to some extent. HDAC3 on the other hand worked and the assay itself as well, which was confirmed by the TSA control. Additionally, nanoBRET assay on HDAC1 was performed as well.

Table 11: IC<sub>50</sub> values (in  $\mu\text{M}$ ) obtained from cell-free fluorogenic HDAC assay and nanoBRET, respectively.

	Fluorogenic HDAC assay		nanoBRET
	HDAC1	HDAC3	HDAC1
<b>18</b>	1,9	0,09	28,8
<b>19</b>	-	56,4	1,43
<b>20</b>	5,1	21,3	0,31
<b>21</b>	6,9	19,2	1,25
<b>22</b>	11,2	43,2	-

Fields are colored according to the measured IC<sub>50</sub> whereas red indicates a low, yellow a mediocre and green a high IC<sub>50</sub> (relative). - = no data.

Considering only the results of the cell-free assay, compound **18** appears to inhibit HDACs most strongly. Since **18** shows the highest similarity to panobinostat of the tested compounds this result was not unexpected. The results of the other compounds however are pretty much unexpected and their  $IC_{50}$  is significantly higher. These differ from **18** in the use of CI994-like structure as the zinc-binding moiety and from each other by different linkage to the rest of the compound. The results seem to indicate that the linkage via an amide as present in compound **20** is most suitable. As previously mentioned, compound **22** was synthesized to enhance the BET activity, assuming that this change would have little or no effect on HDAC activity. Since this is obviously not the case and the  $IC_{50}$  doubled, **22** was therefore not included in the nanoBRET assay. Surprisingly, the results of the nanoBRET assay showed a completely different affinity profile. In cells the affinity of **18** dropped to 28  $\mu$ M which is two orders of magnitude lower than the  $IC_{50}$  of compound **20** and panobinostat ( $IC_{50} = 0,19 \mu$ M, Table 8), respectively. Due to the structural similarities of the three compounds, it is not possible to determine whether a specific part of the structure of **18** is responsible for the loss of affinity. Presumably, the cause is more likely to be found in this very particular combination of these parts.

Although none of the synthesized compounds are suitable dual inhibitors some conclusions can be drawn. In terms of HDAC inhibition, benzamines appear to be superior to hydroxamic acid in dual inhibitors, whereas it seems to be the other way around for pure HDACi. Additionally, the results indicate, that the amide in form of an anilide present in **20** is important for a good activity, which has already been suggested by compounds **14** and **62**. Regarding the DSF assay it is difficult to say, what the cause of the large fluctuations is. Nevertheless compound **20** has some affinity to the BET especially to their second BD. Together with its effect on HDAC, it could be a candidate for further optimization to turn it into a promising dual inhibitor. Alternatively, there may be an opportunity to develop a BD2-specific inhibitor, should one be interested.

### 4.3. Dual BET/HDAC inhibitors of the third generation

In total ten potential dual BET/HDAC inhibitors are members of the second generation and the majority of them are derived from the rather small BETi **23** (Figure 20). The exception is compound **37** which origin is PLX51107 (Figure 22, **36**), a BET inhibitor in the single digit nanomolar range. In order to introduce the HDACi activity the focus was on benzamides although some hydroxamic acids were included as well.

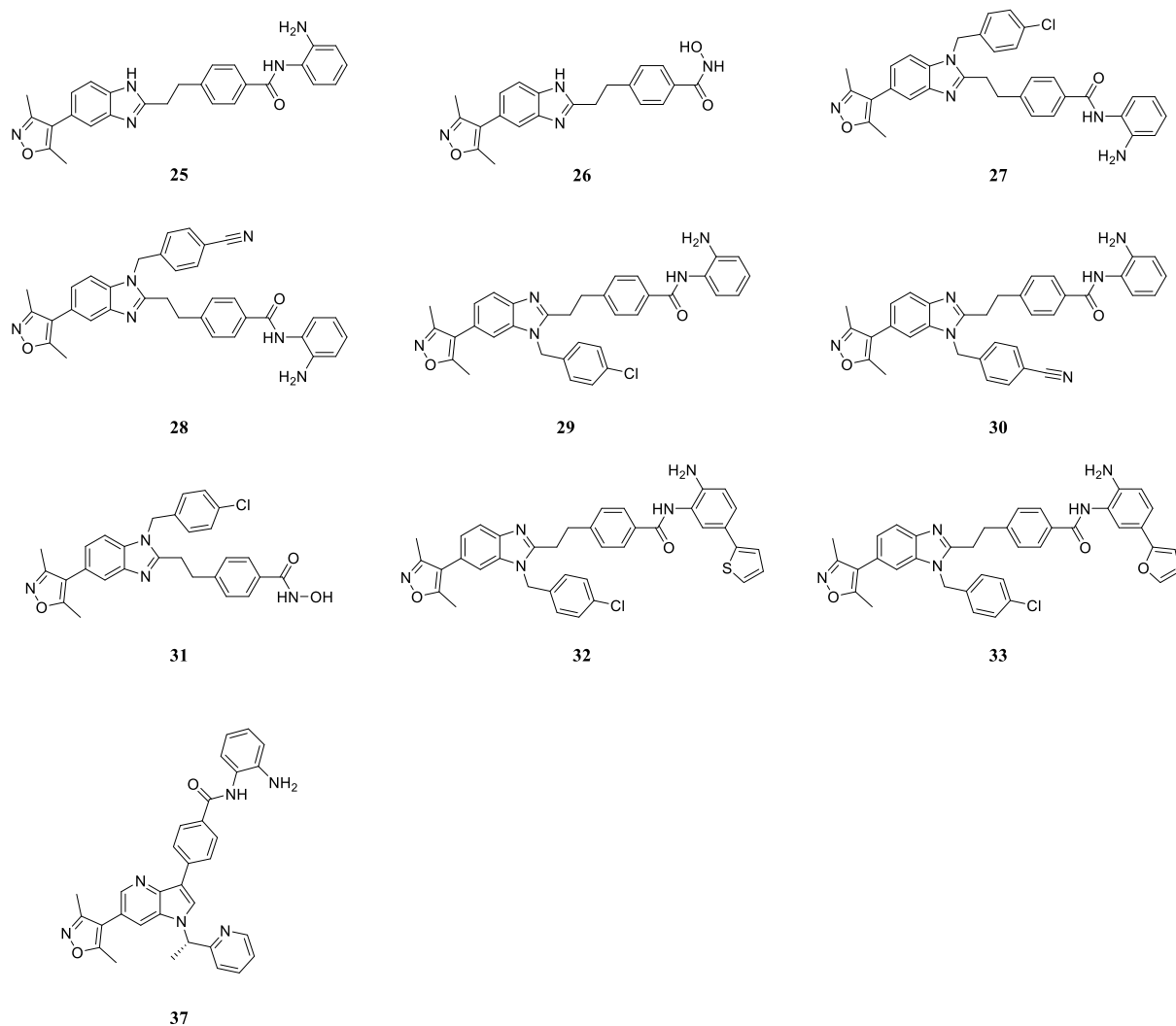


Figure 58: Dual BET/HDAC inhibitors of the third generation.

## 4.3.1. DSF results

Again, the interaction of the synthesized compounds with the BET proteins was evaluated by DSF. The compounds were tested twice in duplicates (Table 12).

Table 12: DSF assay results of the third generation.  $\Delta T_m$  in °C.

Nr.	BRD2 1		BRD2 2		BRD3 1		BRD3 2	
	Run 1	Run 2	Run 1	Run 2	Run 1	Run 2	Run 1	Run 2
25	2.8 ± 0.2	3.9 ± 0.1	2.7 ± 0.1	3.7 ± 0.0	3.3 ± 0.1	4.0 ± 0.0	3.8 ± 0.3	3.9 ± 0.1
26	2.3 ± 0.1	3.6 ± 0.1	2.5 ± 0.1	3.3 ± 0.0	1.8 ± 0.1	3.0 ± 0.0	3.5 ± 0.0	3.0 ± 0.1
27	3.4 ± 0.1	6.9 ± 4.9	9.1 ± 0.6	-5.5 ± 4.9	7.8 ± 0.7	5.1 ± 2.5	12.6 ± 0.7	0.6 ± 0.0
28	1.9 ± 0.3	4.9 ± 1.2	4.0 ± 0.0	7.9 ± 0.3	3.1 ± 1.4	7.4 ± 0.3	5.0 ± 0.3	0.7 ± 0.0
29	1.0 ± 0.1	4.8 ± 2.6	6.3 ± 0.4	1.6 ± 4.7	7.9 ± 0.6	5.4 ± 3.3	10.1 ± 1.6	1.6 ± 0.3
30	2.8 ± 13.7	3.3 ± 1.8	4.0 ± 0.3	4.0 ± 3.7	3.0 ± 0.2	6.1 ± 1.5	5.6 ± 0.1	5.6 ± 4.1
31	2.9 ± 0.4	2.4 ± 0.2	10.4 ± 0.1	2.5 ± 0.4	2.9 ± 0.0	2.2 ± 0.1	4.5 ± 0.0	2.3 ± 0.0
32	-0.5 ± 0.1	-0.2 ± 0.4	-1.1 ± 0.4	-3.1 ± 0.3	-2.2 ± 0.3	-0.9 ± 0.4	0.4 ± 0.3	-1.4 ± 0.5
33	-0.6 ± 0.1	1.0 ± 0.2	20.8 ± 21.9	0.8 ± 0.2	-1.4 ± 1.0	0.2 ± 0.4	0.9 ± 0.3	0.5 ± 0.3
37	8.4 ± 0.1	9.1 ± 0.0	7.0 ± 16.5	4.1 ± 1.2	8.2 ± 0.0	9.2 ± 0.2	9.6 ± 0.0	9.1 ± 2.9
	BRD4 1		BRD4 2		BRDT 1		BRDT 2	
	Run 1	Run 2	Run 1	Run 2	Run 1	Run 2	Run 1	Run 2
25	2.4 ± 0.1	4.5 ± 0.0	6.5 ± 0.2	7.3 ± 0.1	1.4 ± 0.0	2.5 ± 0.2	0.8 ± 0.4	2.2 ± 0.3
26	2.9 ± 0.1	3.8 ± 0.0	5.7 ± 1.0	5.0 ± 0.1	1.3 ± 0.1	2.2 ± 0.1	-2.6 ± 0.3	0.7 ± 0.3
27	9.4 ± 0.2	14.7 ± 0.2	15.6 ± 1.5	13.1 ± 4.9	9.7 ± 1.2	2.6 ± 1.7	4.7 ± 5.9	3.4 ± 2.8
28	0.7 ± 0.2	8.1 ± 1.2	9.2 ± 4.2	10.9 ± 0.1	3.3 ± 0.2	8.2 ± 2.9	-2.1 ± 0.7	2.8 ± 0.0
29	1.1 ± 0.2	8.5 ± 2.8	9.2 ± 3.4	11.3 ± 3.7	5.4 ± 1.5	6.4 ± 1.7	1.2 ± 2.7	0.3 ± 0.3
30	4.3 ± 0.1	6.8 ± 3.0	8.9 ± 1.6	8.9 ± 1.2	3.6 ± 0.5	0.4 ± 2.3	-2.4 ± 0.6	2.9 ± 0.8
31	3.1 ± 0.7	3.4 ± 0.2	10.7 ± 3.6	5.5 ± 0.0	2.6 ± 1.2	2.1 ± 0.3	-2.5 ± 0.1	2.8 ± 0.7
32	-0.8 ± 0.2	-1.5 ± 0.3	3.3 ± 0.5	1.6 ± 0.1	-0.4 ± 0.1	0.4 ± 0.1	-2.2 ± 0.3	0.6 ± 0.2
33	-1.0 ± 0.0	0.7 ± 0.2	3.6 ± 0.0	4.0 ± 0.5	0.1 ± 0.1	0.4 ± 0.4	-3.0 ± 0.1	0.0 ± 0.3
37	10.7 ± 0.2	12.3 ± 0.6	11.2 ± 0.7	12.0 ± 0.5	7.4 ± 0.1	8.3 ± 0.9	-1.0 ± 0.3	4.3 ± 0.2

Fields are colored according to the measured thermal shift  $\Delta T_m$  whereas green indicates a low, yellow a mediocre and red a strong shift (relative). The blue colored fields contain a clear outlier and was not taken into account when comparing the values.

Just as with the compounds of the second generation, there are some ambiguous results here as well, but not as many. Those results mainly occurred with the compounds **27**, **28** and **29** on all tested proteins except for BRDT 2 and BRD4 2. But starting at the beginning with **25** and **26** the results show that these compounds already have a low affinity to the BET proteins with the highest on BRD4 2. This affinity can be enhanced by introducing benzyl derivatives on either side. Literature suggested that a nitrile substituted benzyl derivative on the same side as the isoxazole group should be the best option.<sup>[112]</sup> But together with the HDAC inhibiting part it seems to be the exact opposite.

This becomes clear when compound **27** is compared to **28** and **29**. Both the exchange of the chlorine atom with a nitrile group and the side change of the benzyl derivative resulted in a lower shift. This is also true for the replacement of the benzamine with a hydroxamic acid, as seen in compounds **27**, **25**, **26** and **31**.

The compounds **32** and **33** are comparable to **29** and have an additional thiophen and furan residue on the benzamine, respectively. As previously described this group should rise the HDAC activity by reaching in the foot pocket next to the catalytic side. Unfortunately, this measure has an unanticipated negative impact on BET activity and the compounds lose much of their affinity to the BET proteins. Additionally, they do not seem to reach the foot pocket as there HDAC affinity is reduced as well. Finally, compound **37** still shows a relatively high shift on almost every BET protein, indicating that compared to its parental molecule PLX51107 (**36**, not included in DSF assay), BET activity was not compromised or compromised only to a minor extent.

#### 4.3.2. Fluorogenic HDAC assay results

Since the third generation and second-generation compounds were tested at the same time, the same applies here as before. However, one distinction has to be made here regarding the HDAC1 results. The colored results of HDAC1 are again only reliable to some extent, while the grey colored numbers are not reliable at all. In addition, PLX51107 was measured here to see whether this compound already influences HDAC activity.

Table 13: IC<sub>50</sub> values (in  $\mu\text{M}$ ) obtained from cell-free fluorogenic HDAC assay.

Nr.	HDAC1	HDAC3
<b>25</b>	-	1.8
<b>26</b>	1.9	0.2
<b>27</b>	17.2	31.1
<b>28</b>	6.3	7.5
<b>29</b>	79.4	31.6
<b>30</b>	5.6	6.4
<b>31</b>	5.6	1.6
<b>32</b>	13.1	1613
<b>33</b>	47.3	463.1
<b>37</b>	41.0	12.6
<b>36</b>	4.8	413.1

Fields are colored according to the measured IC<sub>50</sub> whereas red indicates a low, yellow a mediocre and green a high IC<sub>50</sub> (relative). - = no data. Grey numbers are not reliable.

As seen before in the second generation, again the hydroxamic acid appears to be superior to the benzamine in the cell-free assay, although the difference is not as significant. By introducing the benzyl derivatives necessary to enhance BET affinity, the HDAC activity is significantly reduced. While it does not seem to matter for the HDAC activity on which side the benzyl derivative is inserted, the substituent on the latter has a major impact. By replacing the chlorine (**27** and **29**) with a nitrile group (**28** and **30**) the affinity increases by a factor of 4.5. Very surprising, however, is compound **31** ( $IC_{50} = 1.6 \mu M$ ). Compared to **27** ( $IC_{50} = 31.1 \mu M$ ) this increase in affinity is again achieved by using hydroxamic acid as the zinc-binding group. To avoid the use of hydroxamic acids, an attempt was made to increase the affinity of benzamides by introducing an additional thiophen group. As previously described, this worked exceptionally well in the case of CI994 (Figure 12, right)<sup>[57]</sup>, increasing the activity by a factor of 900.<sup>[64,65]</sup> Unfortunately, just the opposite was true and this rather small structural change designed to increase the activity resulted in a high loss of that very same (**32**,  $IC_{50} = 1613 \mu M$ ). Although the activity increased significantly again due to the replacement of thiophene by furan (**33**,  $IC_{50} = 463 \mu M$ ), it was still lower than that of PLX51107 (**36**,  $IC_{50} = 413 \mu M$ ), a BET inhibitor without a proper zinc-binding domain. By simply adding the zinc-binding domain the activity could be increased 30-fold (**37**,  $IC_{50} = 12.6 \mu M$ ), resulting in a promising starting point for further optimization.

Compared to the compounds of the previous generation (see chapter 4.2.), these seem to be much more promising. Not only do they have a lower molecular mass and offer room for optimization, but they already have a decent impact on both targets as well, especially compounds **30**, **31** and **37**. Unfortunately, one rather simple way to enhance HDAC activity does not seem to work in this combination neither on HDAC nor on BET. The reason for the loss in HDAC activity could be, for example, a too short reach into the binding pocket whereby the thiophene cannot enter the foot pocket next to the catalytic side. However, the loss of BET activity is difficult to explain since this substructure should be solvent exposed and therefore not contribute to BET activity in any way. Here, presumably only a crystal structure analysis could clarify the reason behind this behavior. Furthermore, it would be interesting to see if compound **14** behaves similarly when a thiophene is inserted at the corresponding position.

## 5. Summary

The term "epigenetics" has been known since 1942 and was introduced by Conrad Waddington and defined as the interactions between genes and the proteins encoded in them that are responsible for phenotype development.<sup>[13]</sup> With this definition, Waddington included all molecular pathways that regulate the expression of a genotype into a specific phenotype.<sup>[14]</sup> Over the years, as research progressed and knowledge grew, this definition was adapted repeatedly. Today, epigenetics refers to the study of meiotic and mitotic heritable changes in the function of a gene without altering the DNA sequence.<sup>[15]</sup> These changes are DNA modifications, primarily in the form of methylation of cytosine<sup>[16]</sup> and histone modifications. While DNA modifications are limited to methylations, histone modifications include many other modifications besides methylation, including acetylation of lysines at the histone end.<sup>[17]</sup> The proteins involved in the addition of modifications are called writers, while readers recognize these epigenetic marks and erasers remove them.<sup>[22]</sup> Acetylations occurring at the lysines of histone ends,<sup>[14]</sup> for example, are set by histone acetyltransferases (HATs), while proteins with bromodomains (BRDs) recognize this modification and histone deacetylases (HDACs) remove them.<sup>[22]</sup> In transcription, acetylations play an important role by neutralizing the positive charge of lysines and weakening their electrostatic interaction with the negatively charged backbone of DNA,<sup>[23]</sup> thus opening the chromatin structure and allowing transcription factors to access the promoters of targeted genes. Since BET proteins play a critical role in cell proliferation and differentiation, the targeted genes are mainly growth-promoting genes such as the oncogene MYC.<sup>[33,34]</sup> Dysregulation of this process leads to abnormal gene expression as seen in many diseases, including cancer. Similarly, HDACs, although generally more associated with gene deactivation and therefore considered transcriptional repressors,<sup>[58]</sup> are also capable of deacetylating non-histone proteins, such as the tumor suppressor protein p53, which is then susceptible to ubiquitination and subsequent degradation.<sup>[59]</sup> These results contributed to the idea of developing both BET and HDAC inhibitors for cancer therapy, and indeed both types of inhibitors had an inhibitory effect on cancer cell growth. Regarding drug discovery, for a very long time the paradigm was "one gene, one drug, one disease." This is slowly changing due to functional redundancies and alternative compensatory cell signaling, which are particular prevalent in cancer.<sup>[113]</sup> Therefore, the logical consequence can only be to consider multi-target strategies over single-target approaches. Since it is difficult to achieve consistency in biodistribution and pharmacokinetics with a combination of two individual drugs, single molecules displaying multiple inhibitory activities were sought.

This was initially accomplished by conjugating two distinct pharmacophores, in this thesis BET and HDAC inhibitors. In total four different ligands of this type were first synthesized and one of them, compound **14**, showed very promising results. **14** contains JQ1 and CI994 moieties and has inhibitory effect against BRD4 and HDAC proteins, as shown by DSF and nanoBRET assay. Moreover *in vitro* assays in PDAC cells showed that **14** is an even more potent dual BET/HDAC inhibitor than the combination of JQ1 and CI994. While the effects of **14** on BETi response gene *MYC* are pretty similar to JQ1, it is notably the HDAC inhibitory effects which are more sustained and enhanced, probably due to a longer residence time of **14** on HDAC than CI994, visible in the high level of acetylated lysins of histone H3. This change in expression behavior had a major impact on cell growth and cell survival in all PDAC cell lines tested. Here, the superiority of **14** over simultaneous treatment of the cells with JQ1 and CI994 became properly evident as both the survival and growth of PDAC cells could be reduced more significantly by **14** than with the parental molecules combined. In fact, the genes mentioned above are not the only ones that are influenced by **14**. By determining the transcriptome, it could be shown that **14** only influences 605 genes (70%) of the genes regulated by JQ1, but additionally 551 other genes. Interestingly, the majority of these genes are mainly related to the organization of cellular components as well as metabolic and cell cycle-related processes. Previous studies<sup>[104]</sup> suggested that in cancer cells, transcription factors controlling the cell cycle are driven by so-called super-enhancers. PANC-1 tumor cells were found to have super-enhancers at the *FOSL1* transcription factor gene and *FOSL1* is selectively downregulated by **14**. In addition, it was shown by GSEA that the *FOSL1* targets are downregulated as well, suggesting that **14** impairs the whole transcriptional program of *FOSL1*.

Chemotherapy is still the standard treatment for cancer despite many side effects. For this reason, **14** was combined with gemcitabine a well-tolerated chemotherapeutic agent that alone only has a limited activity on PDAC. It turned out that the order in which the drugs were administered had a major impact on efficacy. Cell-cycle arrest induced by **14** interferes with the incorporation of gemcitabine in DNA, when **14** is administered prior to or simultaneously with gemcitabine. However, if treatment with **14** follows gemcitabine administration the induced S-phase arrest and replication stress is sustained, and cell growth is significantly reduced.

Compared to most of the previous studies, which focused on dual BET/HDAC inhibitors<sup>[76,77,114]</sup> this is a major improvement as there was previously no significant difference between the use of a dual BET/HDAC inhibitor and the combination of two single inhibitors.



Only the most recent study<sup>[115]</sup> reported a dual BET/HDAC inhibitor (compound 13a) that has a very similar structure and properties to compound **14**. Compound 13a utilizes an hydroxamic acid instead of the *ortho*-aminoanilide which is used in **14** making 13a an extremely potent pan-HDAC inhibitor. Since **14** is class I selective, both compounds complement each other and are therefore valuable tools in cellular context-dependent studies. However, as **14** is a compound with a comparably high molecular weight, its uses are limited but serving as a proof of concept the data supports further efforts to develop additional dual BET/HDAC inhibitors. Therefore, a next generation of potential dual BET/HDAC inhibitors were developed based on a selective inhibitor of CBP and EP300 called SGC-CBP30 (**17**). Although the affinity for CBP and EP300 could be reduced as planned, the affinity for BET proteins was not consistent. While most compounds had no effect on thermal stability and thus presumably no inhibitory effect, there are two exceptions. Compounds **20** and **22** seem to influence primarily the second bromodomain of several BET proteins, in both a stabilizing and destabilizing manner. Albeit a destabilizing manner seems to be counterintuitive considering that a non-binding compound should have neither, there are explanations aside from faulty performance or poor protein activity. Some ligands for example bind primarily to the unfolded state of a protein, thereby destabilizing it.<sup>[111]</sup> This could mean that these compounds probably interact with the proteins, but not necessarily in the desired way. Additionally, the compounds still had a high molecular mass, which overall led to the decision to change part of the basic structure. While the benzimidazole motif was retained, the position of the HDAC inhibitory moiety was swapped with the BET inhibitory part (Figure 59).

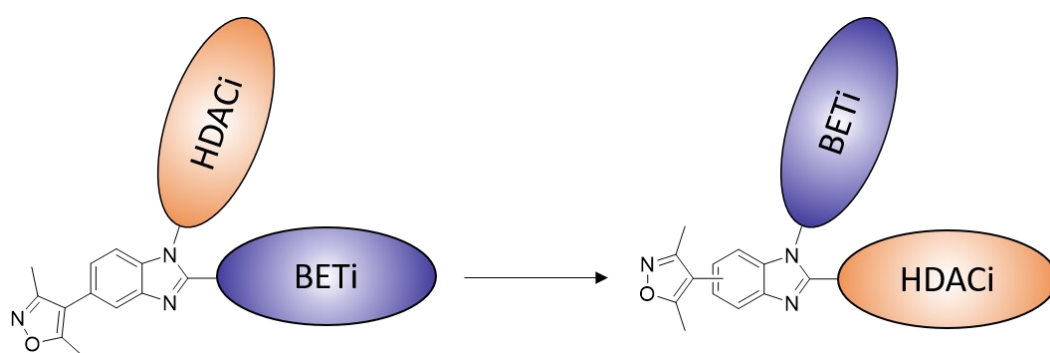


Figure 59: Transformation of the basic structure of the second-generation inhibitors (left) to third generation (right). Position of HDAC inhibitory moiety and BET inhibitory moiety were swapped.

This measure was chosen because the results showed that altering the HDAC inhibitory moiety also affected BET activity in some cases. However, when the putative BET inhibiting substructure was altered, it had no detectable effect on BET activity in the DSF assay, contrary to expectations of increasing it.

As a result, the measure of exchanging the position of the two substructures for each other not only reduced the molecular weight of the compounds but also significantly increased their affinity to the BET proteins, as other BET-inhibiting substructures could be used now. In addition, an attempt was made to modify the HDAC-inhibiting structure by adding a thiophene or furan residue, respectively, as this significantly increased HDAC affinity in the case of CI994 (**12**). However, contrary to expectations, this measure led to a decrease in affinity for HDAC, possibly because the pocket intended for this purpose could not be reached. Much more surprising is the decrease in BET affinity. This fact is difficult to explain since this part of the structure should be solvent-exposed and thus have no effect on BET activity. It would be interesting to see if compound **14** behaves similarly after this modification, since here this part of the structure is undoubtedly solvent-exposed as seen in the crystal structure. Nevertheless, there are still further possibilities for optimizations, especially if compound **37** is considered. This compound is derived from a very potent BET inhibitor and by two simple reactions a moderate HDAC activity could be added. The combination of **37** and the rest of the third-generation compounds gives rise to further derivatives that could be worth synthesizing and investigate (Figure 60).

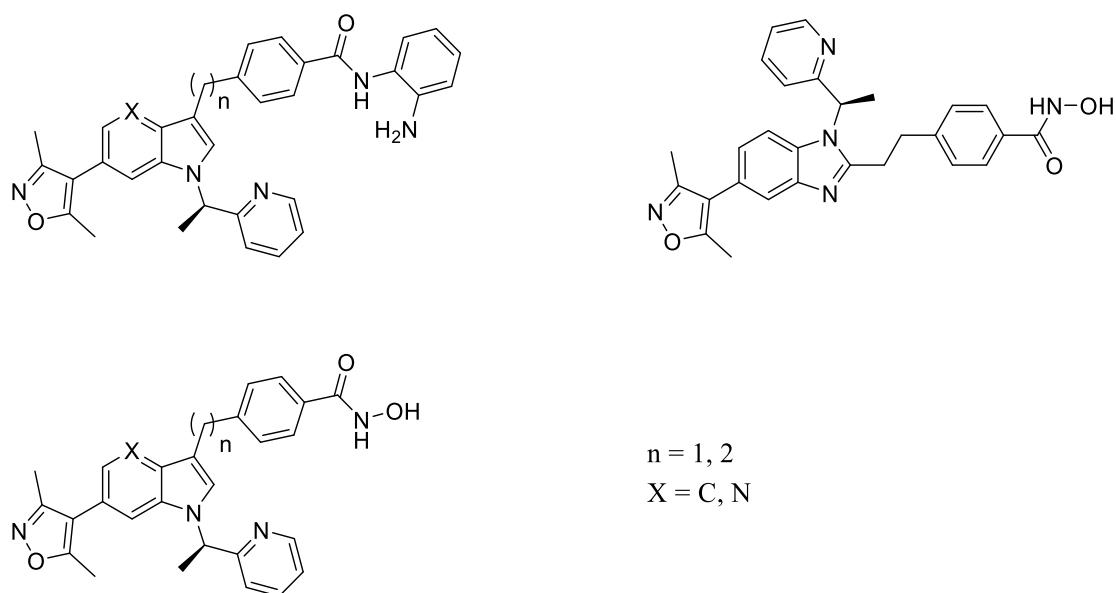


Figure 60: Additional derivatives that could be interesting to synthesize and investigate.

In general, it can be said that the idea of dual BET/HDAC inhibitors is extremely promising and worth pursuing further. This is mainly due to the good test results obtained with compound **14**. With the help of this type of inhibitors it might be possible to increase the survival rate of PDAC patients, if not as a sole drug possibly as an add-on to chemotherapy.

In addition, the use of dual BET/HDAC inhibitors do not seem to be limited to the treatment of PDAC alone and can be applied to other types of cancer as well. NMC for example is a rare as well as deadly subtype of poorly differentiated squamous cell carcinoma and characterized by fusion of the *NUT* gene with *BRD4* making it potentially susceptible to BET inhibition. In fact, **14** had a higher positive effect on the tested NMC cells than JQ1 or CI994, causing the cells to differentiate, among other effects. These results also attest to the potential of dual BET/HDAC inhibitors. If a compound is found that successfully passes the preclinical tests, the three phases of clinical testing will follow. Only after passing the third phase a dual inhibitor of BET and HDAC would be found and could in the future increase the survival time and chances of patients with pancreatic cancer as well as possibly those with other types of cancer. However, this is still years away, only the start has been made here.

## 6. Zusammenfassung

Der Begriff "Epigenetik" ist seit 1942 bekannt und wurde von Conrad Waddington eingeführt und definiert als die Wechselwirkungen zwischen Genen und den darin kodierten Proteinen, die für die Entwicklung des Phänotyps verantwortlich sind.<sup>[13]</sup> Mit dieser Definition schloss Waddington alle molekularen Wege ein, die die Ausprägung eines Genotyps in einen bestimmten Phänotyp regulieren.<sup>[14]</sup> Im Laufe der Jahre, als die Forschung voran kam und das Wissen wuchs, wurde diese Definition immer wieder angepasst. Heute bezieht sich die Epigenetik auf die Untersuchung der meiotisch und mitotisch vererbaren Veränderungen der Funktion eines Gens, ohne dass die DNA-Sequenz verändert wird.<sup>[15]</sup> Diese Veränderungen sind DNA-Modifikationen, vor allem in Form von Methylierung von Cytosin<sup>[16]</sup> und Histonmodifikationen. Während sich die DNA-Modifikationen auf die Methylierungen beschränken, umfassen die Histonmodifikationen neben der Methylierung viele weitere Modifikationen, unter anderem die Acetylierung von Lysinen am Histonende<sup>[17]</sup>. Die Proteine, die an der Hinzufügung von Modifikationen beteiligt sind, werden als "Schreiber" (engl. *writers*) bezeichnet, während die "Leser" (engl. *reader*) diese epigenetischen Markierungen erkennen und die "Radierer" (engl. *erasers*) sie wieder entfernen.<sup>[22]</sup> Acetylierungen, die an den Lysinen der Histonenden auftreten,<sup>[14]</sup> werden beispielsweise von Histonacetyltransferasen (HATs) gesetzt, während Proteine mit Bromodomänen (BRD) diese Modifikation erkennen und Histondeacetylasen (HDACs) sie wieder entfernen.<sup>[22]</sup> Bei der Transkription spielen Acetylierungen eine wichtige Rolle, da sie die positive Ladung der Lysine neutralisieren und ihre elektrostatische Wechselwirkung mit dem negativ geladenen Rückgrat der DNA schwächen,<sup>[23]</sup> wodurch sich die Chromatinstruktur öffnet und Transkriptionsfaktoren Zugang zu den Promotoren der angesteuerten Gene erhalten. Da die BET-Proteine eine entscheidende Rolle bei der Zellproliferation und -differenzierung spielen, handelt es sich bei den angesteuerten Genen hauptsächlich um wachstumsfördernde Gene wie zum Beispiel dem Onkogen *MYC*.<sup>[33,34]</sup> Eine Dysregulation dieses Prozesses führt zu einer abnormen Genexpression, die bei vielen Krankheiten, unter anderem auch bei Krebs, zu beobachten ist. Ähnliches gilt für HDACs, obwohl sie im Allgemeinen eher mit der Deaktivierung von Genen in Verbindung gebracht und daher als Transkriptionsrepressoren betrachtet werden.<sup>[58]</sup> Allerdings sind HDACs auch in der Lage Proteine zu deacetylieren bei denen es sich nicht um Histone handelt, wie zum Beispiel das Tumorsuppressorprotein p53, das dann für die Ubiquitinierung und den anschließenden Abbau zugänglich ist.<sup>[59]</sup> Diese Ergebnisse trugen zu der Idee bei, sowohl BET- als auch HDAC Inhibitoren zur Krebstherapie zu entwickeln und tatsächlich hatten beide Arten von Inhibitoren einen hemmenden Effekt auf das Wachstum von

Krebszellen. Bezüglich der Arzneimittelforschung galt für sehr lange Zeit das Paradigma "ein Gen, ein Medikament, eine Krankheit". In jüngerer Zeit ändert sich dieses Paradigma jedoch auf Grund von redundanten Funktionen und alternativen sich kompensierenden Signalmustern, die insbesondere bei Krebserkrankungen vorherrschend sind. Daher kann die logische Konsequenz nur sein, Multi-Target-Strategien gegenüber Single-Target-Ansätzen in Betracht zu ziehen. Auf Grund der Schwierigkeit, mit einer Kombination von zwei Einzelwirkstoffen, in diesem Fall BET- und HDAC-Inhibitoren eine konsistente Biodistribution und Pharmakokinetik zu erreichen, wurde nach Einzelmolekülen gesucht, die mehrere inhibitorische Aktivitäten aufweisen. Dies wurde in dieser Arbeit zunächst durch die einfache Konjugation von zwei unterschiedlichen Pharmakophoren erreicht. Insgesamt wurden vier verschiedene Liganden dieses Typs synthetisiert und einer von ihnen, Verbindung **14**, zeigte sehr vielversprechende Ergebnisse. **14** vereint den BET Inhibitor JQ1- mit dem HDAC Inhibitor CI994 und hat eine hemmende Wirkung sowohl gegen BRD4- als auch HDAC-Proteine wie durch DSF- und nanoBRET-Assay gezeigt werden konnte. Außerdem zeigten *in vitro* Assays in PDAC-Zellen, dass **14** ein noch potenterer dualer BET/HDAC-Inhibitor ist als die Kombination aus JQ1 und CI994. Während die Effekte von **14** auf das BETi-Antwortgen *MYC* denen von JQ1 ziemlich ähnlich waren, sind insbesondere die HDAC-inhibitorischen Effekte nachhaltiger und verstärkt, wahrscheinlich aufgrund einer längeren Verweildauer von **14** auf HDAC als dies bei CI994 der Fall ist. Dies ist durch das hohe Niveau der acetylierten Lysine von Histon H3 im Western Blot erkennbar. Dieses veränderte Expressionsverhalten hatte einen großen Einfluss auf das Zellwachstum und -überleben in allen getesteten PDAC-Zelllinien. Hier wurde die Überlegenheit von **14** gegenüber der gleichzeitigen Behandlung der Zellen mit JQ1 und CI994 sehr deutlich. Wurden PDAC-Zellen mit dem dualen Inhibitor **14** behandelt, hatte dies ein geringeres Wachstum und Überleben der Krebszellen zur Folge als mit beiden ursprünglichen Molekülen, unabhängig davon, ob diese einzeln oder simultan verabreicht wurden. Tatsächlich sind die zuvor genannten Gene nicht die einzigen, die durch **14** beeinflusst werden. Durch Bestimmung des Transkriptomts konnte gezeigt werden, dass **14** zwar nur 605 (70 %) der Gene beeinflusst, die durch JQ1 reguliert werden, dafür allerdings noch 551 weitere Gene. Interessanterweise steht die Mehrheit dieser Gene hauptsächlich in Verbindung mit der Organisation zellulärer Komponenten sowie metabolischen und zellzyklusbezogenen Prozessen. Frühere Studien<sup>[104]</sup> deuten darauf hin, dass in Krebszellen Transkriptionsfaktoren, die den Zellzyklus kontrollieren, von sogenannten *super-enhancern* angetrieben werden. Es stellte sich heraus, dass PANC-1-Tumorzellen *super-enhancer* am Gen des Transkriptionsfaktor FOSL1 aufweisen und FOSL1 selektiv von **14** herunterreguliert wird.

Darüber hinaus konnte durch GSEA gezeigt werden, dass die FOSL1-Targents ebenfalls herunterreguliert werden, was nahelegt, dass durch **14** das Transkriptionsprogramm von FOSL1 deutlich beeinträchtigt wird.

Bei der Chemotherapie handelt es sich trotz vieler Nebenwirkungen noch immer um die Standardbehandlung bei Krebs. Aus diesem Grund wurde **14** mit Gemcitabin, einem gut verträglichen Chemotherapeutikum, kombiniert, das bei PDAC allein nur eine begrenzte Aktivität aufweist. Es stellte sich heraus, dass die Reihenfolge, in der die Medikamente verabreicht werden, einen großen Einfluss auf die Effektivität hatte. Der durch **14** induzierte Stopp des Zellzyklus verhindert den Einbau von Gemcitabin in die DNA, wenn **14** vor oder gleichzeitig mit Gemcitabin verabreicht wird. Wenn jedoch die Behandlung mit **14** nach der Verabreichung von Gemcitabin folgt, wird der durch Gemcitabin induzierte S-Phasen-Arrest und Replikationsstress aufrechterhalten und das Zellwachstum stark reduziert.

Im Vergleich zu den meisten früheren Studien,<sup>[76,77,114]</sup> die sich mit dualen BET/HDAC-Inhibitoren beschäftigten, ist dies eine große Verbesserung, da es bisher keinen signifikanten Unterschied zwischen der Verwendung eines dualen BET/HDAC-Inhibitors und der Kombination von zwei Einzelinhibitoren gab. Erst die jüngste Studie<sup>[115]</sup> berichtete über einen dualen BET/HDAC-Inhibitor (Verbindung 13a), der eine sehr ähnliche Struktur und Eigenschaften wie **14** aufweist. In Verbindung 13a wird eine Hydroxamsäure anstelle des in **14** genutzten *ortho*-Aminoanilids verwendet, weswegen 13a ein extrem potenter pan-HDAC-Inhibitor ist. Da **14** selektiv für die Klasse I ist, ergänzen sich beide Verbindungen und sind daher wertvolle Werkzeuge für zelluläre, kontextabhängige Studien. Da es sich bei **14** jedoch um eine Verbindung mit einem relativ hohen Molekulargewicht handelt, sind seine Einsatzmöglichkeiten begrenzt. Als *Proof of Concept* unterstützten die Daten allerdings weitere Bemühungen zur Entwicklung zusätzlicher dualer BET/HDAC-Inhibitoren. Daher wurde eine nächste Generation entwickelt, die auf einem selektiven Inhibitor von CBP und EP300 namens SGC-CBP30 (**17**) basiert. Hier ergab sich, dass zwar die Affinität zu CBP und EP300 wie geplant reduziert werden konnte, die Affinität für BET-Proteine aber kaum gegeben war. Während die meisten Verbindungen keinen Einfluss auf die thermische Stabilität und damit vermutlich auch keine hemmende Wirkung haben, gibt es zwei Ausnahmen. Die Verbindungen **20** und **22** scheinen selektiv die zweite Bromodomäne mehrerer BET-Proteine zu beeinflussen, sowohl auf stabilisierende als auch auf destabilisierende Weise. Vergleicht man die Strukturen aller Inhibitoren dieser Generation, sollte der strukturelle Grund für dieses Verhalten auf die Amidbindung der beiden Verbindungen zurückzuführen sein. Zwar hat auch Verbindung **21** eine Amidbindung jedoch handelte es sich hier beim Edukt um ein Benzylamin und nicht um

ein Anilin. Dass diese vergleichsweise kleinen Veränderungen der Struktur eine teilweise destabilisierende Wirkung auf die BET-Proteine haben, scheint kontraintuitiv zu sein, wenn man bedenkt, dass eine nicht-bindende Verbindung weder das eine noch das andere aufweisen sollte. Es gibt jedoch Erklärungen für dieses Verhalten, abgesehen von fehlerhafter Durchführung oder schlechter Proteinaktivität. Es gibt Liganden, die binden zum Beispiel primär an den ungefalteten Zustand eines Proteins und destabilisieren es dadurch.<sup>[111]</sup> Auf die hier vorliegenden Ergebnisse bezogen, könnte das bedeuten, dass diese Verbindungen eventuell auf mehr als nur eine Art und Weise mit den BET-Proteinen interagieren, und nicht unbedingt auf die gewünschte. Zusätzlich handelt es sich bei diesen Verbindungen immer noch um Exemplare mit einer sehr hohen Molekülmasse, was insgesamt zu der Entscheidung führte, einen Teil der Grundstruktur zu verändern. Während das Benzimidazol-Motiv beibehalten wurde, wurde die Position des HDAC-hemmenden Teils mit dem BET-hemmenden Teil vertauscht (Figure 59). Diese Maßnahme wurde gewählt, weil die Ergebnisse zeigten, dass die Veränderung der HDAC-inhibitorischen Einheit wie zuvor beschrieben in einigen Fällen auch die BET-Aktivität beeinflusste. Wenn jedoch die vermeintlich BET-inhibierende Substruktur verändert wurde, hatte dies entgegen der Erwartung einer Erhöhung der Affinität keinen nachweisbaren Effekt auf die BET-Aktivität im DSF-Assay. Die Maßnahme, die Position der beiden Substrukturen gegeneinander auszutauschen, reduzierte nicht nur das Molekulargewicht der Verbindungen, sondern erhöhte auch deren Affinität zu den BET-Proteinen deutlich, da nun andere BET-hemmende Substrukturen eingesetzt werden konnten. Die hier zu Grunde liegende Literatur<sup>[112]</sup> suggerierte, dass ein nitrilsubstituiertes Benzylderivat, das sich auf der gleichen Seite wie die Isoxazolgruppe befindet (vergleiche Verbindung **23**), die vielversprechendste Option für die dualen Inhibitoren sein sollte. Zusammen mit dem HDAC-inhibierenden Teil jedoch scheint das genaue Gegenteil eingetroffen zu sein. Dies wird deutlich, wenn die Verbindungen **28** und **29** mit **27** verglichen werden. Sowohl der Austausch des Chloratoms (**27**) durch eine Nitrilgruppe (**28**) als auch der Seitenwechsel des Benzylderivats (**29**) führten zu einem verringertem Shift im DSF-Assay. Darüber hinaus wurde außerdem versucht, die HDAC-hemmende Struktur durch Hinzufügen eines Thiophen- beziehungsweise Furan-Restes zu modifizieren, da dadurch zumindest im Falle von CI994 (**12**) die HDAC-Affinität deutlich gesteigert werden konnte. Wider Erwarten führte diese Maßnahme jedoch zu einer Abnahme der Affinität für HDAC, möglicherweise weil die dafür vorgesehene Tasche nicht erreicht werden konnte. Deutlich überraschender ist die Abnahme der BET-Affinität. Diese Tatsache ist schwierig zu erklären, da dieser Teil der Struktur lösungsmittel exponiert sein und somit keinen Einfluss auf die BET-Aktivität haben sollte.

Es wäre interessant zu sehen, ob sich **14** nach dieser Modifikation ähnlich verhält, da hier dieser Teil der Struktur wie in der Kristallstruktur zu sehen ohne Zweifel dem Lösungsmittel ausgesetzt ist.

Bezüglich der Optimierung der Verbindungen der dritten Generation gibt es einige Möglichkeiten, insbesondere wenn Verbindung **37** berücksichtigt wird. Diese Verbindung war von einem sehr potenten BET-Inhibitor abgeleitet und durch zwei einfache Reaktionen konnte eine moderate HDAC-Aktivität hinzugefügt werden. Aus der Kombination von **37** und den übrigen Verbindungen der dritten Generation ergeben sich weitere Derivate, die es wert sein könnten, synthetisiert und untersucht zu werden (Figure 60). Wie hier in nahezu allen Verbindungen zu sehen ist, sind die HDAC Inhibitoren größtenteils relativ einfach aufgebaut. So lange die wichtige zinkbindende Gruppe vorhanden ist, scheint der Linker sowie die Capping-Gruppe zweitrangig für eine gute Aktivität zu sein. Die größere Herausforderung wird vermutlich die Suche nach dem passenden BET Inhibitor sein und die Wahlmöglichkeiten sind schon jetzt vielfältig.<sup>[27]</sup> Es ist nicht unwahrscheinlich, dass, sollte es in Zukunft einen zugelassenen dualen BET/HDAC Inhibitor geben, dieser keine der hier verwendeten BETi verwendet werden, aber noch immer vergleichbare HDAC inhibierende Strukturen.

Generell lässt sich sagen, dass die Idee der dualen BET/HDAC-Inhibitoren äußerst vielversprechend und es wert ist, weiter verfolgt zu werden. Dies liegt vor allem an den guten Testergebnissen, die mit Verbindung **14** erzielt wurden. Mit Hilfe dieser Art von Inhibitoren könnte es in Zukunft möglich sein, die Überlebensrate von PDAC-Patienten zu erhöhen, wenn nicht als alleiniges Medikament, so vielleicht als Zusatz zur Chemotherapie. Darüber hinaus scheint der Einsatz von dualen BET/HDAC-Inhibitoren nicht nur auf die Behandlung von PDAC beschränkt zu sein und kann auch bei anderen Krebsarten angewendet werden. NMC zum Beispiel ist ein ebenso seltener wie tödlicher Subtyp des schlecht differenzierten Plattenepithelkarzinoms und zeichnet sich durch eine Fusion des *NUT*-Gens mit *BRD4* aus, wodurch es potenziell anfällig für eine BET-Inhibition ist. Tatsächlich zeigte **14** auch hier einen größeren positiven Effekt auf die getesteten NMC-Zellen als JQ1 oder CI994 und veranlasste die Zellen unter anderem zur Differenzierung. Diese Ergebnisse belegen das Potenzial von dualen BET/HDAC-Inhibitoren und sollte in Zukunft ein Wirkstoff gefunden werden, der die präklinischen Tests erfolgreich besteht, würden anschließend die drei Phasen der klinischen Prüfung folgen. Erst nach Bestehen der dritten Phase wäre ein dualer Inhibitor von BET und HDAC gefunden und könnte die Überlebenszeit und -chancen von Patienten mit Bauchspeicheldrüsenkrebs und möglicherweise auch die von Patienten mit anderen Krebsarten, erhöhen. Davon ist man aber noch Jahre entfernt, hier wurde nur der Anfang gemacht.



## 7. Experimental section

### 7.1. General procedures

All solvents and reagents were obtained either from *Merck*, *Alfa Aesar*, *TCI*, *Apollo Scientific*, *Enamine* or *MedChemExpress* and used without further purification. Unless otherwise indicated, the syntheses were performed under argon gas with anhydrous solvents. Their progress was monitored and the  $R_f$  values were determined by thin layer chromatography (TLC). The therefore silica gel coated (particle size 60  $\mu\text{m}$ ) aluminum plates were purchased from Merck.

#### **Microwave**

The microwave used is a Discover SP microwave synthesizer from *CEM*.

#### **Flash column chromatography**

A PURIFLASH XS 420 system with puriFlash cartridges (15  $\mu\text{m}$ , 30  $\mu\text{m}$  or 50  $\mu\text{m}$ ) from *Interchim* and technical grade solvents were used to purify compounds. UV absorption was detected at 254 nm.

#### **ESI and HRMS**

To characterize the synthesized products by electrospray ionization (ESI), a *ThermoFischer* Surveyor MSQ was used to record mass spectra. TLC-MS was measured with a TLC-MS interface 2 of the company *Camag*. The determination of precision masses was performed with an LTQ Orbitrap XL from Thermo Scientific. The method used is matrix-assisted laser desorption/ionization (MALDI) with the standard matrix  $\alpha$ -cyano-4-hydroxycinnamic acid (HCCA).

#### **NMR**

A DPX-250, an AV-500 or a DRX-600 from Bruker were used to record the  $^1\text{H}$  and  $^{13}\text{C}$ -NMR spectra, respectively. The NMR spectra were evaluated by means of the software MestReNova. The chemical shift  $\delta$  is given in the unit parts per million (ppm) and is based on the internal standard of tetramethylsilane ( $\delta = 0$ ). For the fine structure of the signals the abbreviations "s" for singlet, "d" for doublet, "dd" for doublet of doublet, "t" for triplet, "q" for quartet and "m" for multiplet etc. are used.

**HPLC**

Purity of final compounds was determined on an Agilent system with a 1260 Infinity II MWD and an Eclipse XDB-C18 (5  $\mu$ m, 4.6x250 mm) column. H<sub>2</sub>O and ACN were used as solvents, both contain an additional 0.1 % TFA. UV absorption was detected at 254.4 nm and 280.0 nm.

**7.2. Syntheses****General procedure A**

The appropriate amine (1.5 eq) was added to a solution of compound **63** or **94** (1 eq) and DIPEA (1.5 eq) in THF. The resulting solution was stirred at RT overnight and then partitioned between EtOAc and HCl solution (10 %). Aqueous phase was extracted with EtOAc twice and combined organic phases were washed with brine and dried over MgSO<sub>4</sub>.

**General procedure B1**

Reduction of the nitro group was performed in a mixture of EtOH and EtOAc (1:2). After addition of 10 % Pd/C (0.1 eq) without stirring, the flask is flooded with argon 3 times. Subsequently the flask is flooded H<sub>2</sub> and stirred at RT until TLC indicates completion of the reaction. The mixture is filtered through celite, washed with EtOH and EtOAc until the filtrate is clear. The solvent is removed under reduced pressure.

**General procedure B2**

Reduction of the nitro group was performed in EtOH. While stirring at 0 °C SnCl<sub>2</sub>\*H<sub>2</sub>O (4 eq) was added. The resulting solution was stirred at RT for 10 minutes and then refluxed until TLC indicated the end of reaction (approximately 4 h). Then ice cold water and 1 M NaOH was added, and product was extracted with EtOAc. Organic layer was washed with brine and dried over MgSO<sub>4</sub>.

**General procedure C**

HATU (1.2 eq) was added to a solution of the corresponding carboxylic acid (1 eq) with DIPEA (1.2 eq) in DMF. The mixture was stirred for one hour, then the corresponding amine (1.2 eq) was added and stirred overnight. The solvent was removed under reduced pressure and partitioned between EtOAc and water. The aqueous phase was extracted three times with EtOAc, and the combined organic fractions were washed with brine and dried over MgSO<sub>4</sub>.

**General procedure D**

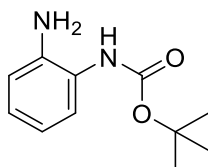
Ring closure and cleavage of the Boc-group and/or ester group respectively was performed in hydrogen chloride solution (4 M in dioxane). Corresponding educt was dissolved in an appropriate amount of hydrogen chloride solution and was stirred under reflux for several hours.

**General procedure E**

The Boc-protected compound (1 eq) was dissolved in DCM and TFA (20 % of total volume) was added at 0 °C. The reaction was stirred at RT and monitored via TLC. After completion the solvent was removed under reduced pressure, the residue was purified via flash chromatography.

**General procedure F**

To a solution of methylcarboxylester (1 eq) with hydroxylamine hydrochloride (15 eq) in MeOH, sodium methoxide (25 %(w/v) in methanol, 25 eq) was added slowly at -78°C. The resulting mixture was stirred at -20°C for 1 h before it was warmed up to RT. After 2 more hours the reaction (monitored via TLC) was complete. The solvent was removed under reduced pressure, and the remaining residue was partitioned between EtOAc and water. The aqueous phase was extracted three times with EtOAc, and the combined organic fractions were washed with brine and dried over MgSO<sub>4</sub>. The residue was purified via flash chromatography.

***tert*-butyl (2-aminophenyl)carbamate (**39**)**

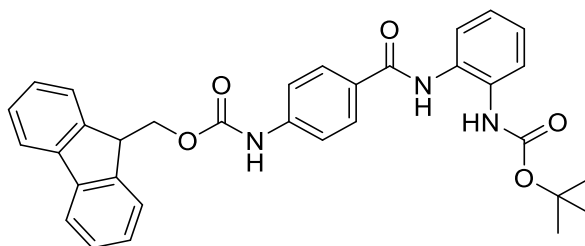
A solution of di-*tert*-butyl dicarbonate (2.02 g, 9.25 mmol, 1 eq) in CH<sub>2</sub>Cl<sub>2</sub> (25 mL) was added dropwise at 0°C to a solution of *o*-phenylenediamine **38** (1 g, 9.25 mmol, 1 eq) in DCM (20 mL). The reaction mixture was stirred overnight at RT. The solvent was removed under reduced pressure. The residue was purified by flash chromatography with hexane/EtOAc (70:30), yielding compound **39** as a white solid (1.48 g, 77 %). Reaction was carried out several times. If expected yield was higher than 3 g, purification was performed by recrystallization from hexane and EtOAc.

$R_f(\text{hexane}/\text{EtOAc} = 60:40) = 0.58$

$^1\text{H-NMR}$  (250 MHz,  $\text{DMSO-}d_6$ ):  $\delta = 8.26$  (s, 1H, NH), 7.22 - 7.12 (m, 1H,  $\text{CH}_{\text{ar}}$ ), 6.83 (td,  $J = 7.9, 1.5$  Hz, 1H,  $\text{CH}_{\text{ar}}$ ), 6.67 (dd,  $J = 8.0, 1.5$  Hz, 1H,  $\text{CH}_{\text{ar}}$ ), 6.52 (td,  $J = 7.8, 1.5$  Hz, 1H,  $\text{CH}_{\text{ar}}$ ), 4.80 (s, 2H,  $\text{NH}_2$ ), 1.45 (s, 9H,  $\text{C}(\text{CH}_3)_3$ ) ppm.

MS (ESI-):  $m/z$  231.12 ( $[\text{M-H}]$ , 100)

**(9H-fluoren-9-yl)methyl (4-((2-((*tert*-butoxycarbonyl) amino) phenyl)carbamoyl)phenyl) carbamate (41)**



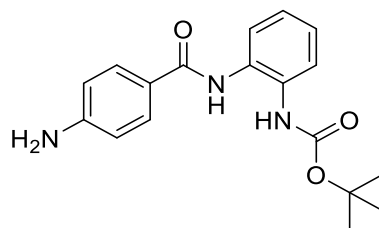
The reaction was performed by following the general procedure C with 4-(Fmoc-amino)benzoic acid **40** (400 mg, 1.1 mmol, 1 eq) and **39** (231.8 mg, 1.1 mmol, 1 eq). Crude product was purified via flash chromatography with hexane:EtOAc (80:20) as mobile phase to obtain **41** as a colorless solid (370 mg, 61 %).

$R_f(\text{hexane}/\text{EtOAc} = 60:40) = 0.43$ .

$^1\text{H-NMR}$  (250 MHz,  $\text{DMSO-}d_6$ ):  $\delta = 10.05$  (s, 1H, NH), 9.73 (s, 1H, NH), 8.66 (s, 1H, NH), 7.90 (t,  $J = 7.8$  Hz, 4H,  $\text{CH}_{\text{ar}}$ ), 7.77 (d,  $J = 7.3$  Hz, 2H,  $\text{CH}_{\text{ar}}$ ), 7.54 (ddd,  $J = 9.9, J - = 7.5, J = 5.6$  Hz, 4H,  $\text{CH}_{\text{ar}}$ ), 7.48 - 7.32 (m, 4H,  $\text{CH}_{\text{ar}}$ ), 7.17 (ddd,  $J = 7.7$  Hz, 5.4 Hz,  $-^4J_{\text{HH}} = 1.9$  Hz, 2H,  $\text{CH}_{\text{ar}}$ ), 4.54 (d,  $J = 6.5$  Hz, 2H,  $\text{CH}_2$ ), 4.34 (t,  $J = 6.4$  Hz, 1H, CH), 1.45 (s, 9H,  $\text{C}(\text{CH}_3)_3$ ) ppm.

MS (ESI-):  $m/z$  572.13 ( $[\text{M-H}]$ , 100).

***tert*-butyl (2-(4-aminobenzamido)phenyl)carbamate (42)**



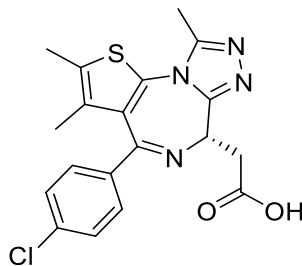
To a solution of compound **41** (370 mg, 0.067 mmol, 1 eq) in DCM morpholine (20 % of total volume of 25 mL) was added. Reaction was monitored via TLC and after 45 minutes reaction was complete. Solvent was removed under reduced pressure and remaining residue was partitioned between EtOAc and HCl solution (10 %). The aqueous phase was extracted three times with EtOAc, and the combined organic fractions were washed with brine and dried over MgSO<sub>4</sub>. Crude product was purified via flash chromatography with a gradient of DCM/MeOH (after 2 CVs increased linear from 100:0 to 95:5 over 10 CV) to obtain **42** as a colorless solid (150 mg, 68 %).

R<sub>f</sub>(hexane/EtOAc = 40:60) = 0.54.

<sup>1</sup>H-NMR (250 MHz, DMSO-*d*<sub>6</sub>): δ = 9.59 (s, 1H, NH), 8.67 (s, 1H, NH), 7.76 (d, J = 8.6 Hz, 2H, CH<sub>ar</sub>), 7.59 - 7.44 (m, 2H, CH<sub>ar</sub>), 7.20 - 7.07 (m, 2H, CH<sub>ar</sub>), 6.80 (d, J = 7.9 Hz, 2H, CH<sub>ar</sub>), 1.45 (s, 9H, C(CH<sub>3</sub>)<sub>3</sub>) ppm.

MS (ESI<sup>+</sup>): m/z 350.09 ([M+Na], 100)

**(*S*)-2-(4-(4-chlorophenyl)-2,3,9-trimethyl-6*H*-thieno[3,2-*f*][1,2,4]triazolo[4,3-*a*][1,4]diazepin-6-yl) acetic acid (43)**



To a solution of (+)-JQ1 **3** (350 mg, 0.77 mmol, 1 eq) in THF/MeOH/H<sub>2</sub>O (3:2:1), LiOH (321 mg, 7.7 mmol, 10 eq) was added. The reaction was stirred overnight at RT. After removing the solvents under reduced pressure, the residue was dissolved in water, acidified, and extracted with EtOAc. The organic layer was washed with brine and dried over MgSO<sub>4</sub>. The solvent was

removed under reduced pressure, and the residue was purified via flash chromatography with DCM/MeOH (90:10) as mobile phase to obtain compound **43** (286 mg, 93 %) as a colorless solid.

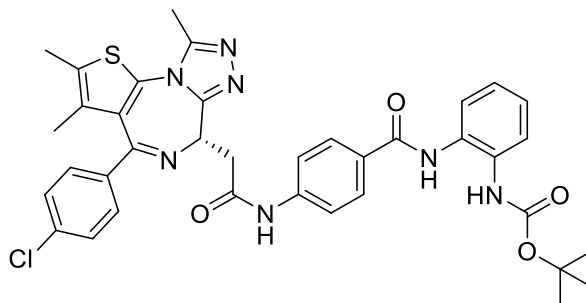
$R_f$ (EtOAc/AcOH = 98:2) = 0.30.

$^1\text{H-NMR}$  (250 MHz, DMSO- $d_6$ ):  $\delta$  = 12.22 (s, 1H, OH), 7.54 - 7.40 (m, 4H, CH<sub>ar</sub>), 4.45 (t, J = 7.1 Hz, 1H, CH), 3.52 - 3.23 (m, 2H, CH), 2.60 (s, 3H, CH<sub>3</sub>), 2.41 (s, 3H, CH<sub>3</sub>), 1.63 (s, 3H, CH<sub>3</sub>) ppm.

$^{13}\text{C-NMR}$  (126 MHz, DMSO- $d_6$ ):  $\delta$  = 172.04, 163.12, 154.85, 149.89, 136.67, 135.27, 132.25, 130.75, 130.16, 129.86, 129.52, 128.52, 128.51, 53.60, 14.06, 12.69, 11.29 ppm.

MS (ESI-):  $m/z$  399.01 ([M-H], 100)

***tert*-butyl (S)-(2-(4-(2-(4-(4-chlorophenyl)-2,3,9-trimethyl-6H-thieno[3,2-f][1,2,4]triazolo[4,3-a][1,4]diazepin-6-yl)acetamido)benzamido)phenyl)carbamate (44)**



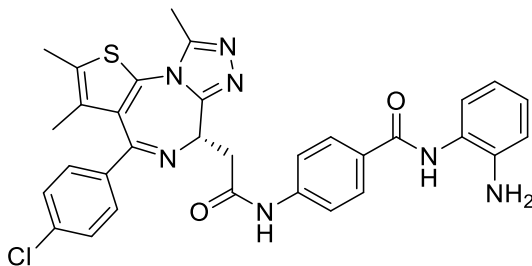
Reaction performed by following the general procedure C with **43** (124.9 mg, 0.31 mmol, 1 eq) and **42** (102 mg, 0.31 mmol, 1 eq). Crude product was purified via flash chromatography with a gradient of DCM/MeOH (after 3 CVs increased linear from 100:0 to 90:10 over 10 CVs) to obtain **44** as a light yellow solid (85 mg, 38.4 %).

$R_f$ (DCM/MeOH = 90:10) = 0.6.

$^1\text{H-NMR}$  (250 MHz, DMSO- $d_6$ ):  $\delta$  = 10.62 (s, 1H, NH), 9.76 (s, 1H, NH), 8.67 (s, 1H, NH), 7.94 (d, J = 8.8 Hz, 2H, CH<sub>ar</sub>), 7.79 (d, J = 8.8 Hz, 2H, CH<sub>ar</sub>), 7.58 - 7.35 (m, 6H, CH<sub>ar</sub>), 7.24 - 7.08 (m, 2H, CH<sub>ar</sub>), 4.63 (t, J = 7.1 Hz, 1H, CH), 3.57 (d, J = 7.1 Hz, 2H, CH<sub>2</sub>), 2.60 (d, J = 4.6 Hz, 3H, CH<sub>3</sub>), 2.43 (s, 3H, CH<sub>3</sub>), 1.64 (s, 3H, CH<sub>3</sub>), 1.45 (s, 9H, C(CH<sub>3</sub>)<sub>3</sub>) ppm.

MS (ESI-):  $m/z$  732.30 ([M-H], 100).

**(S)-N-(2-aminophenyl)-4-(2-(4-(4-chlorophenyl)-2,3,9-trimethyl-6H-thieno[3,2-f][1,2,4]triazolo[4,3-a][1,4]diazepin-6-yl)acetamido)benzamide (14)**



Reaction performed by following the general procedure E with **44** (85 mg, 0.12 mmol). Crude product was purified via reversed flash chromatography with a gradient of ACN/H<sub>2</sub>O (after 2 CVs increased linear from 10:90 to 100:0 over 10 CVs) to obtain **14** as a light yellow solid (47 mg, 64 %).

R<sub>f</sub>(DCM/MeOH = 90:10) = 0.42.

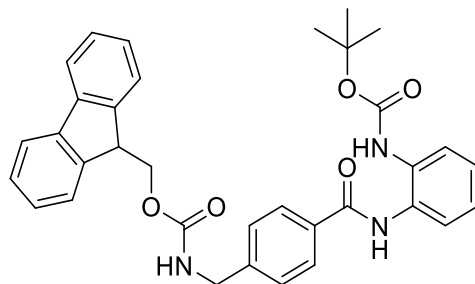
<sup>1</sup>H-NMR (500 MHz, DMSO-*d*<sub>6</sub>): δ = 10.59 (s, 1H, NH), 9.58 (s, 1H, NH), 7.97 (d, J = 8.6 Hz, 2H, CH<sub>ar</sub>), 7.76 (d, J = 8.7 Hz, 2H, CH<sub>ar</sub>), 7.49 (d, J = 8.8 Hz, 2H, CH<sub>ar</sub>), 7.43 (d, J = 8.5 Hz, 2H, CH<sub>ar</sub>), 7.16 (d, J = 7.4 Hz, 1H, CH<sub>ar</sub>), 6.98 - 6.95 (m, 1H, CH<sub>ar</sub>), 6.78 (dd, J = 8.0 Hz, J = 1.2 Hz, 1H, CH<sub>ar</sub>), 6.62 - 6.58 (m, 1H, CH<sub>ar</sub>), 4.89 (s, 2H, NH<sub>2</sub>), 4.62 (t, J = 7.1 Hz, 1H, CH), 3.56 (d, J = 7.1 Hz, 2H, CH<sub>2</sub>), 2.61 (s, 3H, CH<sub>3</sub>), 2.43 (s, 3H, CH<sub>3</sub>), 1.64 (s, 3H, CH<sub>3</sub>) ppm.

<sup>13</sup>C-NMR (126 MHz, DMSO-*d*<sub>6</sub>): δ = 169.13, 164.72, 163.31, 155.01, 149.98, 143.17, 141.96, 136.74, 135.29, 130.79, 130.16, 129.90, 129.56, 128.77, 128.54, 126.69, 123.39, 123.48, 118.18, 116.29, 116.15, 53.69, 14.10, 12.72, 11.34 ppm.

MS (ESI<sup>-</sup>): m/z 608.26 ([M-H], 100).

HRMS (MALDI) m/z calculated 610.17865 for C<sub>32</sub>H<sub>29</sub>ClN<sub>7</sub>O<sub>2</sub>, found 610.17855.

HPLC: purity > 95 %

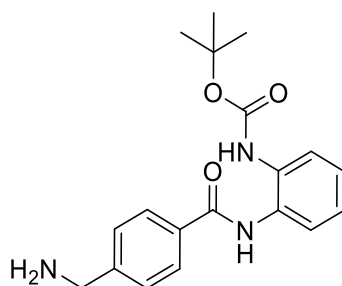
**(9H-fluoren-9-yl)methyl (4-((2-((tert-butoxycarbonyl)amino)phenyl)carbamoyl)benzyl)carbamate (59)**

The reaction was performed by following the general procedure C with 4-((((9H-fluoren-9-yl)methoxy)carbonyl)amino)methyl)benzoic acid **58** (200 mg, 0.54 mmol, 1 eq) and **39** (231 mg, 1.1 mmol, 1.2 eq). Crude product was purified via flash chromatography with hexane:EtOAc (50:50) as mobile phase to obtain **59** as a colorless solid (226 mg, 75 %).

$R_f$ (hexane/EtOAc = 50:50) = 0.58

$^1\text{H-NMR}$  (250 MHz,  $\text{DMSO-}d_6$ ):  $\delta$  = 9.80 (s, 1H, NH), 8.67 (s, 1H, NH), 7.99 - 7.83 (m, 7H,  $\text{CH}_{\text{ar}}$  + NH), 7.71 (d,  $J$  = 7.3 Hz, 2H,  $\text{CH}_{\text{ar}}$ ), 7.58 - 7.50 (m, 2H,  $\text{CH}_{\text{ar}}$ ), 7.45 - 7.30 (m, 6H,  $\text{CH}_{\text{ar}}$ ), 4.38 (d,  $J$  = 6.7 Hz, 2H,  $\text{CH}_2$ ), 4.31 - 4.18 (m, 3H, CH +  $\text{CH}_2$ ), 1.43 (s, 9H,  $\text{C}(\text{CH}_3)_3$ ) ppm.

MS(ESI<sup>+</sup>):  $m/z$  586.25 ( $[\text{M}+\text{Na}]$ , 100)

**tert-butyl (2-(4-(aminomethyl)benzamido)phenyl)carbamate (60)**

To a solution of compound **59** (226 mg, 0.4 mmol, 1 eq) in DCM morpholine (20 % of total volume of 20 mL) was added. Reaction was monitored via TLC and after 45 minutes reaction was complete. Solvent was removed under reduced pressure and remaining residue was partitioned between EtOAc and HCl solution (10 %). The aqueous phase was extracted three times with EtOAc, and the combined organic fractions were washed with brine and dried over  $\text{MgSO}_4$ . Crude product was purified via flash chromatography with a gradient of DCM/MeOH (after 2 CVs increased linear from 99:1 to 90:10 over 9 CV and held for 4 CVs) to obtain **60** as a colorless solid (136 mg, > 95 %).

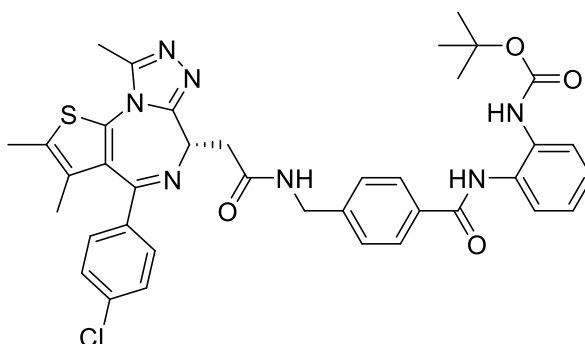


$R_f(\text{DCM}/\text{MeOH} = 90:10) = 0.41$

$^1\text{H-NMR}$  (250 MHz,  $\text{DMSO-}d_6$ ):  $\delta = 9.80$  (s, 1H, NH), 8.69 (s, 1H, NH), 7.91 (d,  $J = 8.3$  Hz, 2H,  $\text{CH}_{\text{ar}}$ ), 7.60 - 7.46 (m, 4H,  $\text{CH}_{\text{ar}}$ ), 7.25 - 7.11 (m, 2H,  $\text{CH}_{\text{ar}}$ ), 3.83 (s, 2H,  $\text{CH}_2$ ), 1.45 (s, 9H,  $\text{C}(\text{CH}_3)_3$ ) ppm.

$\text{MS}(\text{ESI}^+)$ :  $m/z$  364.21 ( $[\text{M}+\text{Na}]$ , 30)

***tert*-butyl (S)-(2-(4-((2-(4-(4-chlorophenyl)-2,3,9-trimethyl-6H-thieno[3,2-f][1,2,4]triazolo[4,3-a][1,4]diazepin-6-yl)acetamido)methyl)benzamido)phenyl)carbamate (61)**



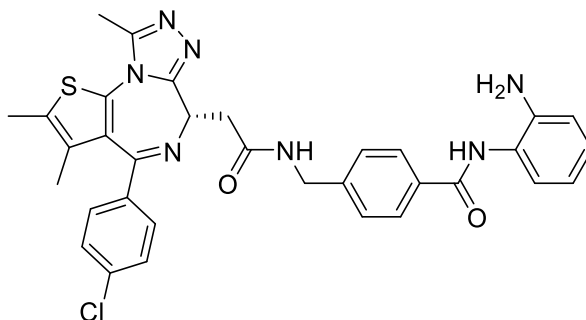
Reaction performed by following the general procedure C with **43** (100 mg, 0.25 mmol, 1 eq) and **60** (85 mg, 0.25 mmol, 1 eq). Crude product was purified via flash chromatography with a gradient of DCM/MeOH (after 3 CVs increased linear from 100:0 to 90:10 over 10 CVs) to obtain **61** as a colorless solid (150 mg, 84 %).

$R_f(\text{DCM}/\text{MeOH} = 90:10) = 0.52$

$^1\text{H-NMR}$  (250 MHz,  $\text{DMSO-}d_6$ ):  $\delta = 9.85$  (s, 1H, NH), 8.87 (s, 1H, NH), 8.68 (s, 1H, NH), 7.93 (d,  $J = 8.4$  Hz, 2H,  $\text{CH}_{\text{ar}}$ ), 7.59 - 7.43 (m, 6H,  $\text{CH}_{\text{ar}}$ ), 7.37 (d,  $J = 8.6$  Hz, 2H,  $\text{CH}_{\text{ar}}$ ), 7.26 - 7.09 (m, 2H,  $\text{CH}_{\text{ar}}$ ), 4.56 (t,  $J = 7.2$  Hz, 1H, CH), 4.48 - 4.39 (m, 2H,  $\text{CH}_2$ ), 2.61 (s, 3H,  $\text{CH}_3$ ), 2.41 (s, 3H,  $\text{CH}_3$ ), 1.62 (s, 3H,  $\text{CH}_3$ ), 1.43 (s, 9H,  $\text{C}(\text{CH}_3)_3$ ), 1.28 - 1.22 (m, 2H,  $\text{CH}_2$ ) ppm.

$\text{MS}(\text{ESI})$

**(S)-N-(2-aminophenyl)-4-((2-(4-(4-chlorophenyl)-2,3,9-trimethyl-6H-thieno[3,2-f][1,2,4]triazolo[4,3-a][1,4]diazepin-6-yl)acetamido)methyl)benzamide (62)**



Reaction performed by following the general procedure E with **61** (130 mg, 0.18 mmol). Crude product was purified via reversed flash chromatography with a gradient of ACN/H<sub>2</sub>O (after 2 CVs increased linear from 10:90 to 100:0 over 10 CVs) to obtain **62** as a light beige solid (90 mg, 81 %).

R<sub>f</sub>(DCM/MeOH = 90:10) = 0.25

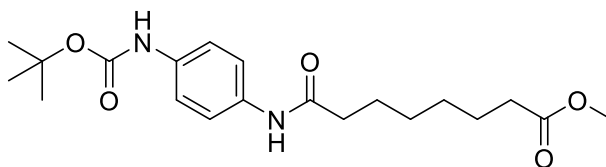
<sup>1</sup>H-NMR (400 MHz, DMSO-*d*<sub>6</sub>): δ = 9.66 (s, 1H), 8.84 (t, J = 6.1 Hz, 1H), 7.96 (d, J = 7.9 Hz, 2H), 7.46 (t, J = 8.2 Hz, 4H), 7.37 (d, J = 8.6 Hz, 2H), 7.18 (d, J = 7.7 Hz, 1H), 6.98 (td, J = 7.4, 1.4 Hz, 1H), 6.79 (dd, J = 8.0, 1.4 Hz, 1H), 6.61 (td, J = 7.5, 1.4 Hz, 1H) ppm.

<sup>13</sup>C-NMR (126 MHz, DMSO-*d*<sub>6</sub>): δ = 169.78, 165.08, 163.18, 155.08, 149.88, 143.27, 143.21, 136.76, 135.27, 133.04, 132.31, 130.72, 130.14, 129.85, 129.58, 128.47, 127.79, 126.96, 126.76, 126.51, 123.34, 116.28, 116.16, 53.97, 41.75, 37.66, 14.09, 12.70, 11.34 ppm.

MS (ESI<sup>-</sup>): m/z 624.17 ([M+H], 100).

HRMS (MALDI) m/z calculated 624.19430 for C<sub>33</sub>H<sub>31</sub>ClN<sub>7</sub>O<sub>2</sub>S, found 624.19396.

HPLC: purity > 95 %

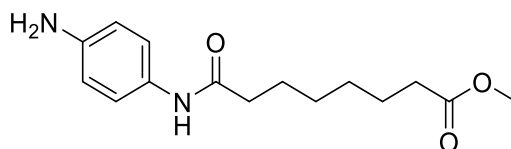
**Methyl 8-((4-((*tert*-butoxycarbonyl)amino)phenyl)amino)-8-oxooctanoate (47)**

Reaction performed by following the general procedure C with *tert*-butyl (4-aminophenyl) carbamate (500 mg, 2.4 mmol, 1 eq) and 8-methoxy-8-oxooctanoic acid (0.4 mL, 2.4 mmol, 1 eq). Crude product was purified via flash chromatography with hexane/EtOAc (50:50) to obtain **47** as a colorless solid (800 mg, 88 %).

$R_f(\text{hexane/EtOAc} = 50:50) = 0.5$

$^1\text{H-NMR}$  (250 MHz,  $\text{DMSO-}d_6$ ):  $\delta = 9.70$  (s, 1H, NH), 9.19 (s, 1H, NH), 7.44 (d,  $J = 9.0$  Hz, 2H,  $\text{CH}_{\text{ar}}$ ), 7.33 (d,  $J = 9.0$  Hz, 2H,  $\text{CH}_{\text{ar}}$ ), 3.57 (s, 3H,  $\text{CH}_3$ ), 2.27 (dt,  $J = 11.3, 7.4$  Hz, 4H,  $2 \times \text{CH}_2$ ), 1.63 - 1.49 (m, 4H,  $2 \times \text{CH}_2$ ), 1.46 (s, 9H,  $\text{C}(\text{CH}_3)_3$ ), 1.32 - 1.23 (m, 4H,  $2 \times \text{CH}_2$ ) ppm.

MS (ESI-):  $m/z$  377.14 ( $[\text{M-H}]$ , 100).

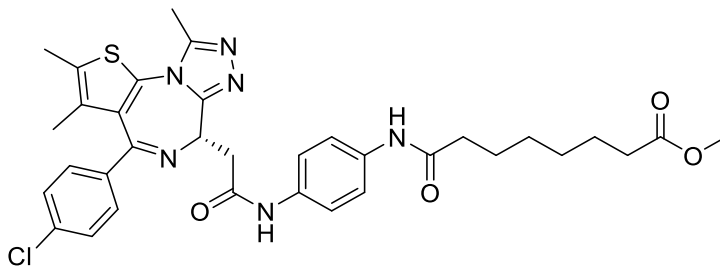
**Methyl 8-((4-aminophenyl)amino)-8-oxooctanoate (48)**

Reaction performed by following the general procedure E with **47** (508 mg, 1.34 mmol). Crude product was purified via flash chromatography with DCM/MeOH (95:5) to obtain) as a colorless solid **48** (194 mg, 52 %).

$R_f(\text{CH}_2\text{Cl}_2/\text{MeOH} = 95:5) = 0.24$ .

$^1\text{H-NMR}$  (250 MHz,  $\text{DMSO-}d_6$ ):  $\delta = 9.86$  (s, 1H, NH), 7.55 (d,  $J = 8.8$  Hz, 2H,  $\text{CH}_{\text{ar}}$ ), 7.05 (d,  $J = 8.7$  Hz, 2H,  $\text{CH}_{\text{ar}}$ ), 3.57 (s, 3H,  $\text{CH}_3$ ), 2.33 - 2.23 (m, 4H,  $2 \times \text{CH}_2$ ), 1.54 (d,  $J = 7.1$  Hz, 4H,  $2 \times \text{CH}_2$ ), 1.28 (q,  $J = 5.4, 3.8$  Hz, 4H,  $2 \times \text{CH}_2$ ) ppm.

MS (ESI-):  $m/z$  277.09 ( $[\text{M-H}]$ , 75)

**Methyl (S)-8-((4-(2-(4-(4-chlorophenyl)-2,3,9-trimethyl-6H-thieno[3,2-f][1,2,4]triazolo[4,3-a][1,4]diazepin-6-yl)acetamido)phenyl)amino)-8-oxooctanoate (49)**

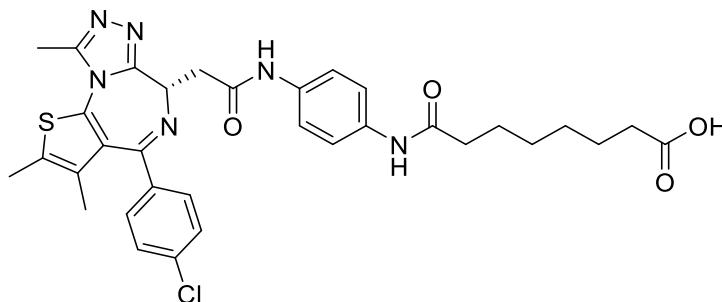
Reaction performed by following the general procedure C with **43** (120 mg, 0.30 mmol, 1 eq) and **48** (140 mg, 0.50 mmol, 1.7 eq). Crude product was purified via flash chromatography with DCM /MeOH (after 2 CV increased linear from 100:0 to 95:5 over 8 CV and held for 2 CV) to obtain **49** as a light purple solid (85 mg, 45 %).

$R_f(\text{CH}_2\text{Cl}_2/\text{MeOH} = 95:5) = 0.15$ .

$^1\text{H-NMR}$  (500 MHz,  $\text{DMSO-}d_6$ ):  $\delta = 10.23$  (s, 1H, NH), 9.79 (s, 1H, NH), 7.54 - 7.46 (m, 6H,  $\text{CH}_{\text{ar}}$ ), 7.42 (d,  $J = 8.5$  Hz, 2H,  $\text{CH}_{\text{ar}}$ ), 4.59 (t,  $J = 7.1$  Hz, 1H, CH), 3.58 (s, 3H,  $\text{CH}_3$ ), 3.48 (d,  $J = 6.1$  Hz, 2H,  $\text{CH}_2$ ), 2.60 (s, 3H,  $\text{CH}_3$ ), 2.42 (s, 3H,  $\text{CH}_3$ ), 2.31 - 2.25 (m, 4H,  $2 \times \text{CH}_2$ ), 1.63 (s, 3H,  $\text{CH}_3$ ), 1.58 - 1.50 (m, 4H,  $2 \times \text{CH}_2$ ), 1.32 - 1.26 (m, 4H,  $2 \times \text{CH}_2$ ) ppm.

$^{13}\text{C-NMR}$  (126 MHz,  $\text{DMSO-}d_6$ ):  $\delta = 173.82, 171.35, 168.73, 163.67, 162.78, 155.53, 150.37, 137.20, 135.72, 135.24, 134.92, 132.77, 131.22, 130.61, 130.34, 130.04, 128.99, 119.94, 119.89, 54.25, 51.65, 36.71, 33.71, 28.80, 28.70, 25.45, 24.80, 14.55, 13.17, 11.79$  ppm.

MS (ESI<sup>+</sup>):  $m/z$  683.30 ( $[\text{M}+\text{Na}]$ , 100)

**(S)-8-((4-(2-(4-(4-chlorophenyl)-2,3,9-trimethyl-6H-thieno[3,2-f][1,2,4]triazolo[4,3-a][1,4]diazepin-6-yl)acetamido)phenyl)amino)-8-oxooctanoic acid (50)**

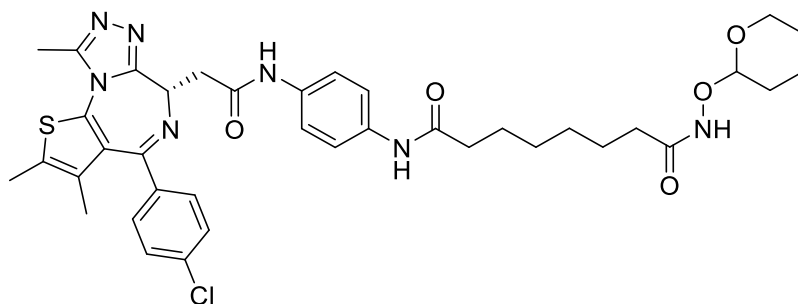
To a solution of **49** (88 mg, 0.13 mmol, 1 eq) in THF/MeOH/H<sub>2</sub>O (3:2:1), LiOH (31 mg, 1.3 mol, 10 eq) was added. The reaction was stirred at RT for 3 days. After removing the solvents under reduced pressure, the residue was dissolved in water, acidified, and extracted with EtOAc. The organic layer was washed with brine and dried over MgSO<sub>4</sub>. The solvent was removed under reduced pressure, and the residue was purified via flash chromatography with DCM/MeOH (90:10) as mobile phase to obtain compound **50** (66 mg, 77 %) as a colorless solid.

R<sub>f</sub>(DCM/MeOH/AcOH = 95:5:1) = 0.51

<sup>1</sup>H-NMR (250 MHz, DMSO-*d*<sub>6</sub>): δ = 11.94 (s, 1H, OH), 10.22 (s, 1H, NH), 9.78 (s, 1H, NH), 7.60 - 7.35 (m, 8H, CH<sub>ar</sub>), 4.59 (t, J = 7.1 Hz, 1H, CH), 3.48 (d, J = 7.2 Hz, 2H, CH<sub>2</sub>), 2.60 (s, 3H, CH<sub>3</sub>), 2.42 (s, 3H, CH<sub>3</sub>), 2.29 - 2.15 (m, 4H, 2xCH<sub>2</sub>), 1.63 (s, 3H, CH<sub>3</sub>), 1.59 - 1.44 (m, 4H, 2xCH<sub>2</sub>), 1.29 - 1.23 (m, 4H, 2xCH<sub>2</sub>) ppm.

MS(ESI<sup>-</sup>): m/z 645.16 ([M-H], 100)

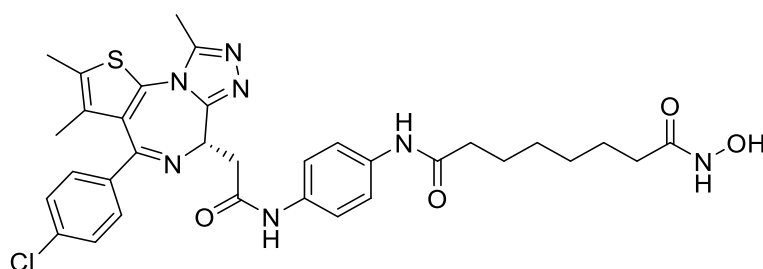
*N*<sup>1</sup>-(4-(2-((*S*)-4-(4-chlorophenyl)-2,3,9-trimethyl-6*H*-thieno[3,2-*f*][1,2,4]triazolo[4,3-*a*][1,4]diazepin-6-yl)acetamido)phenyl)-*N*<sup>8</sup>-((tetrahydro-2*H*-pyran-2-yl)oxy)octanediamide (**51**)



Reaction performed by following the general procedure C with **50** (66 mg, 0.10 mmol, 1 eq), *O*-(tetrahydro-2*H*-pyran-2-yl)hydroxylamine (24 mg, 0.20 mmol, 2 eq), HATU (76 mg, 0.20 mmol, 2 eq) and DIPEA (0.039 mL, 0.22 mmol, 2.2 eq). Crude product **51** was filtered through silica and used without further purification or analytic (50 mg, 0.06 mmol, 66 %).

MS(ESI<sup>+</sup>): *m/z* 768.40 ([*M*+Na], 100)

(*S*)-*N*<sup>1</sup>-(4-(2-(4-(4-chlorophenyl)-2,3,9-trimethyl-6*H*-thieno[3,2-*f*][1,2,4]triazolo[4,3-*a*][1,4]diazepin-6-yl)acetamido)phenyl)-*N*<sup>8</sup>-hydroxyoctanediamide (**15**)



### First reaction path

Crude **51** (50 mg, 0.06 mmol, 1 eq) was dissolved in MeOH (5 mL) and TFA (0.5 mL, 0.06 mmol, 1 eq) and stirred at RT for 90 minutes. Crude product was purified via reverse flash chromatography with a gradient of ACN/H<sub>2</sub>O (after 2 CVs increased linear from 10:90 to 100:0 over 10 CVs) to obtain **15** as a light purple solid (16 mg, 36 %).

### Second reaction path

Reaction performed by following the general procedure F with **49** (120 mg, 0.18 mmol). Crude product was purified via reverse flash chromatography with a gradient of ACN/H<sub>2</sub>O (after

2 CVs increased linear from 10:90 to 100:0 over 10 CVs) to obtain **15** as a light purple solid (31 mg, 26 %).

$R_f(\text{CH}_2\text{Cl}_2/\text{MeOH} = 9:1) = 0.24$ .

$^1\text{H-NMR}$  (500 MHz,  $\text{DMSO-}d_6$ ):  $\delta = 10.33$  (s, 1H, NH), 10.24 (s, 1H, NH), 9.80 (s, 1H, NH), 8.65 (s, br, 1H, OH), 7.55 - 7.46 (m, 6H,  $\text{CH}_{\text{ar}}$ ), 7.42 (d,  $J = 8.6$  Hz, 2H,  $\text{CH}_{\text{ar}}$ ), 4.59 (t,  $J = 7.1$  Hz, 1H, CH), 3.47 (d,  $J = 7.1$  Hz, 2H,  $\text{CH}_2$ ), 2.60 (s, 3H,  $\text{CH}_3$ ), 2.42 (s, 3H,  $\text{CH}_3$ ), 2.26 (t,  $J = 7.4$  Hz, 2H,  $\text{CH}_2$ ), 1.93 (t,  $J = 7.4$  Hz, 2H,  $\text{CH}_2$ ), 1.63 (s, 3H,  $\text{CH}_3$ ), 1.56 (p,  $J = 7.4$  Hz, 2H,  $\text{CH}_2$ ), 1.48 (p,  $J = 7.3$  Hz, 2H,  $\text{CH}_2$ ), 1.31 - 1.22 (m, 4H,  $2 \times \text{CH}_2$ ) ppm.

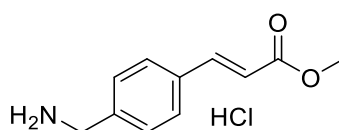
$^{13}\text{C-NMR}$  (126 MHz,  $\text{DMSO-}d_6$ ):  $\delta = 170.90, 169.09, 168.26, 163.22, 155.07, 149.93, 136.73, 135.26, 134.78, 134.45, 132.31, 130.77, 130.15, 129.88, 129.57, 128.53, 119.48, 119.42, 54.25, 38.50, 36.20, 32.25, 28.45, 28.42, 25.08, 25.05, 14.09, 12.72, 11.33$  ppm.

MS (ESI<sup>+</sup>):  $m/z$  662.41 ( $[\text{M}+\text{H}]$ , 100).

HRMS (MALDI)  $m/z$  calculated 662.23108 for  $\text{C}_{33}\text{H}_{37}\text{ClN}_7\text{O}_4\text{S}$ , found 662.23109.

HPLC: purity > 95 %

#### Methyl (E)-3-(4-(aminomethyl)phenyl)acrylate hydrochloride (**54**)

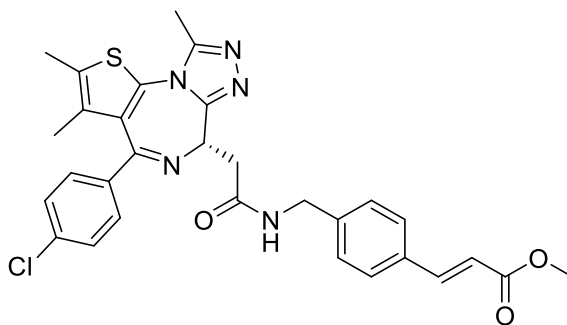


To a solution of methyl (E)-3-(4-(bromomethyl)phenyl)acrylate **52** (1 g, 3.92 mmol, 1 eq) in DMF (12 mL),  $\text{NaN}_3$  (305.8 mg, 4.7 mmol, 1.2 eq) was added. The reaction was stirred at 80 °C for 2 hours. After the mixture was cooled down, brine was added, and the reaction was extracted with  $\text{Et}_2\text{O}$ /hexane (1:1). The combined organic layers were washed with water, dried over  $\text{MgSO}_4$ , and concentrated under reduced pressure. The residue was dissolved in THF (18 mL) and  $\text{H}_2\text{O}$  (3 mL), then  $\text{PPh}_3$  (1.13 g, 4.3 mmol, 1.1 eq) was added. The reaction was stirred overnight at RT. The solvents were removed under reduced pressure. Salt **54** was obtained after resolving remaining residue in DCM and precipitating with HCl (1.0 M in diethyl ether) as a colorless solid (0.74 mg 87 %).

<sup>1</sup>H-NMR (250 MHz, DMSO-*d*<sub>6</sub>): δ = 8.58 (s, 3H, NH<sub>3</sub><sup>+</sup>), 7.76 (d, J = 8.0 Hz, 2H, CH<sub>ar</sub>), 7.67 (d, J = 16.1 Hz, 1H, CH), 7.55 (d, J = 8.1 Hz, 2H, CH<sub>ar</sub>), 6.69 (d, J = 16.1 Hz, 1H, CH), 4.03 (s, 2H, CH<sub>2</sub>), 3.73 (s, 3H, CH<sub>3</sub>) ppm.

MS (ESI<sup>+</sup>): m/z 192.11 ([M-Cl], 10).

**Methyl (*S,E*)-3-(4-((2-(4-(4-chlorophenyl)-2,3,9-trimethyl-6*H*-thieno[3,2-*f*][1,2,4]triazolo[4,3-*a*][1,4] diazepin-6-yl)acetamido)methyl)phenyl)acrylate (**55**)**



Reaction performed by following the general procedure C with **43** (100 mg, 0.25 mmol) and **54** (73.8 mg, 0.32 mmol). Crude product was purified via flash chromatography with DCM /MeOH (95:5) to obtain **55** as a colorless solid (105 mg, 73 %).

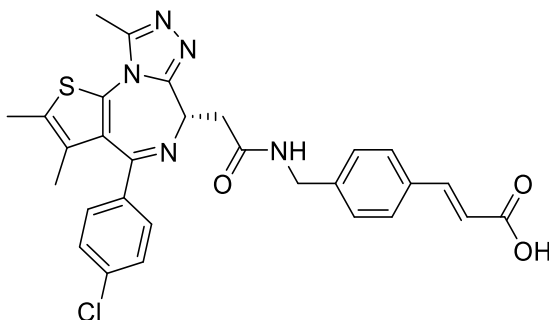
R<sub>f</sub>(CH<sub>2</sub>Cl<sub>2</sub>/MeOH = 95:5) = 0.27.

<sup>1</sup>H-NMR (250 MHz, DMSO-*d*<sub>6</sub>): δ = 8.77 (t, J = 6.0 Hz, 1H, NH), 7.73 - 7.62 (m, 3H, CH<sub>ar</sub> + CH), 7.49 - 7.41 (m, 2H, CH<sub>ar</sub>), 7.41 - 7.30 (m, 4H, CH<sub>ar</sub>), 6.62 (d, J = 16.1 Hz, 1H, CH), 4.59 - 4.25 (m, 3H, CH + CH<sub>2</sub>), 3.73 (s, 3H, CH<sub>3</sub>), 3.42 - 3.20 (u, 2H, CH<sub>2</sub>, behind H<sub>2</sub>O-signal), 2.60 (s, 3H, CH<sub>3</sub>), 2.41 (s, 3H, CH<sub>3</sub>), 1.61 (s, 3H, CH<sub>3</sub>) ppm.

MS (ESI<sup>-</sup>): m/z 572.24 ([M-H], 70).



**(*S,E*)-3-(4-((2-(4-(4-chlorophenyl)-2,3,9-trimethyl-6*H*-thieno[3,2-*f*][1,2,4]triazolo[4,3-*a*][1,4] diazepin-6-yl)acetamido)methyl)phenyl)acrylic acid (**56**)**



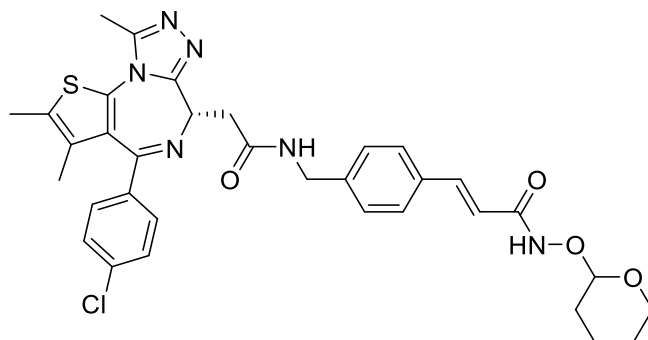
To a solution of **55** (100 mg, 0.17 mmol, 1 eq) in THF/MeOH/H<sub>2</sub>O (3:2:1), LiOH (73 mg, 1.7 mol, 10 eq) was added. The reaction was stirred at RT for 3 days. After removing the solvents under reduced pressure, the residue was dissolved in water, acidified, and extracted with EtOAc. The organic layer was washed with brine and dried over MgSO<sub>4</sub>. The solvent was removed under reduced pressure, and the residue was purified via flash chromatography with DCM/MeOH (90:10) as mobile phase to obtain compound **56** as a colorless solid (68 mg, 70 %).

R<sub>f</sub>(DCM/MeOH/TEA = 90:10:2) = 0.33.

<sup>1</sup>H-NMR (250 MHz, DMSO-*d*<sub>6</sub>): δ = 8.77 (t, J = 5.8 Hz, 1H, NH), 7.69 - 7.54 (m, 3H, CH<sub>ar</sub> + CH), 7.49 - 7.41 (m, 2H, CH<sub>ar</sub>), 7.39 - 7.31 (m, 4H, CH<sub>ar</sub>), 6.50 (d, J = 16.0 Hz, 1H, CH), 4.54 (dd, J = 8.3, 5.8 Hz, 1H, CH), 4.36 (dd, J = 16.2, 5.9 Hz, 2H, CH<sub>2</sub>), 2.60 (s, 3H, CH<sub>3</sub>), 2.41 (s, 3H, CH<sub>3</sub>), 1.61 (s, 3H, CH<sub>3</sub>) ppm.

MS(ESI+) - m/z 559.90 ([M+H], 100)

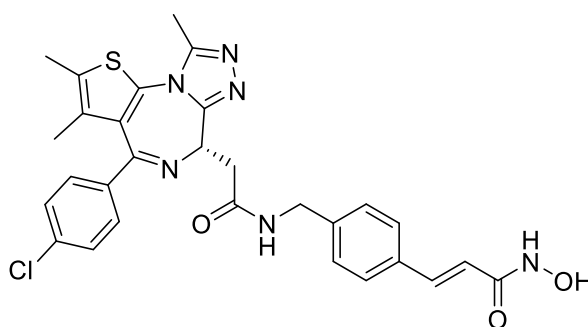
**(*E*)-3-(4-((2-((*S*)-4-(4-chlorophenyl)-2,3,9-trimethyl-6*H*-thieno[3,2-*f*][1,2,4]triazolo[4,3-*a*][1,4]diazepin-6-yl)acetamido)methyl)phenyl)-*N*-((tetrahydro-2*H*-pyran-2-yl)oxy)acrylamide (**57**)**



Reaction performed by following the general procedure C with **56** (63 mg, 0.11 mmol, 1 eq), *O*-(tetrahydro-2*H*-pyran-2-yl)hydroxylamine (26 mg, 0.22 mmol, 2 eq), HATU (64 mg, 0.17 mmol, 1.5 eq) and DIPEA (0.023 mL, 0.13 mmol, 1.2 eq). Crude product **57** was filtered through silica and used without further purification and analytic (125 mg, 0.06 mmol, 186 %).

MS(ESI-):  $m/z$  657.31 ([*M*-H], 100)

**(*S,E*)-3-(4-((2-(4-(4-chlorophenyl)-2,3,9-trimethyl-6*H*-thieno[3,2-*f*][1,2,4]triazolo[4,3-*a*][1,4]diazepin-6-yl)acetamido)methyl)phenyl)-*N*-hydroxyacrylamide**



#### First reaction path

Crude **57** (125 mg, 0.19 mmol, 1 eq) was dissolved in MeOH (5 mL) and TFA (0.5 mL, 0.06 mmol, 1 eq) and stirred at RT for 90 minutes. Crude product was purified via reverse flash chromatography with a gradient of ACN/H<sub>2</sub>O (after 2 CVs increased linear from 10:90 to 100:0 over 10 CVs) to obtain **16** as colorless solid (50 mg, 46 %).

**Second reaction path**

Reaction performed by following the general procedure F with **55** (105 mg, 0.18 mmol). Crude product was purified via reversed flash chromatography with a gradient of ACN/H<sub>2</sub>O (after 2 CVs increased linear from 10:90 to 100:0 over 10 CVs) to obtain **16** as a colorless solid (31 mg, 29 %).

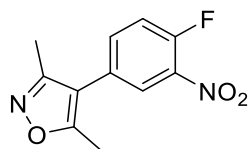
<sup>1</sup>H-NMR (500 MHz, DMSO-*d*<sub>6</sub>): δ = 10.74 (s, 1H, OH), 9.04 (s, 1H, NH), 8.78 (t, J = 6.0 Hz, 1H, NH), 7.52 (d, J = 8.1 Hz, 2H, CH<sub>ar</sub>), 7.49 - 7.42 (m, 3H, CH<sub>ar</sub> + CH), 7.40 - 7.31 (m, 4H, CH<sub>ar</sub>), 6.45 (d, J = 15.8 Hz, 1H, CH), 4.54 (dd, J = 8.4, 5.9 Hz, 1H, CH), 4.36 (dd, J = 27.3, 5.9 Hz, 2H, CH<sub>2</sub>), 3.37 - 3.31 (u, 2H, CH<sub>2</sub>, behind H<sub>2</sub>O-signal), 2.60 (s, 3H, CH<sub>3</sub>), 2.41 (s, 3H, CH<sub>3</sub>), 1.61 (s, 3H, CH<sub>3</sub>) ppm.

<sup>13</sup>C-NMR (126 MHz, DMSO-*d*<sub>6</sub>): δ = 169.71, 163.14, 162.81, 155.08, 149.88, 141.19, 138.13, 136.74, 135.26, 133.40, 132.30, 130.73, 130.14, 129.85, 129.58, 128.47, 127.78, 127.46, 118.63, 53.95, 41.91, 37.64, 14.09, 12.72, 11.35 ppm.

MS (ESI<sup>+</sup>): m/z 574.92 ([M+H], 100).

HRMS (MALDI) m/z calculated 575.16266 for C<sub>29</sub>H<sub>28</sub>ClN<sub>6</sub>O<sub>3</sub>S, found 575.16165.

HPLC: purity > 95 %.

**4-(4-fluoro-3-nitrophenyl)-3,5-dimethylisoxazole (64)**

XPhos Palladacycle Gen. 3 (20 mg, 0.02 mmol, 0.01 eq) was added to a solution of 4-bromo-1-fluoro-2-nitrobenzene **63** (500 mg, 2.3 mmol, 1 eq) and 3,5-dimethylisoxazole-4-boronic acid pinacol ester **77** (608 mg, 2.7 mmol, 1.2 eq) in DME (10 mL). The mixture was stirred and saturated NaHCO<sub>3</sub> solution (10 mL) was added. The mixture was degassed by placing it in an ultrasonic bath and argon was bubbled into the reaction for 20 minutes. Then the mixture was heated at 80 °C for 3 h. The reaction was allowed to cool then partitioned between EtOAc (10 mL) and water (10 mL). The phases were separated, and the organic phase was washed with brine and dried over MgSO<sub>4</sub>. Crude product was purified via flash chromatography with hexane:EtOAc (70:30) as mobile phase to obtain **64** as a beige solid. (446 mg, 83 %).

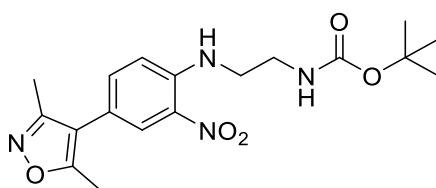
In a higher scale (5 g of **63**) product could be purified by recrystallizing from hexane (5.4 g, 57 %)

$R_f(\text{hexane/EtOAc} = 70:30) = 0.52$ .

$^1\text{H-NMR}$  (250 MHz,  $\text{DMSO-}d_6$ ):  $\delta = 8.14$  (dd, 1H,  $\text{CH}_{\text{ar}}$ ), 7.90 - 7.82 (m, 1H,  $\text{CH}_{\text{ar}}$ ), 7.76 - 7.65 (m, 1H,  $\text{CH}_{\text{ar}}$ ), 2.43 (s, 3H,  $\text{CH}_3$ ), 2.24 (s, 3H,  $\text{CH}_3$ ) ppm.

MS(ESI<sup>+</sup>): not measurable

***tert*-butyl (2-((4-(3,5-dimethylisoxazol-4-yl)-2-nitrophenyl)amino)ethyl)carbamate (**66**)**

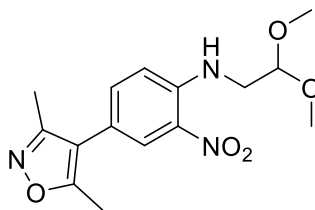


Compound **64** (100 mg, 0.42 mmol, 1 eq) was reacted with N-Boc-ethylenediamine (0.1 mL, 0.64 mmol, 1.5 eq) according to general procedure A. Crude product was purified via flash chromatography with hexane/EtOAc (60:40) as mobile phase to obtain **66** as an orange solid (153 mg, 96 %).

$R_f(\text{hexane/EtOAc} = 50:50) = 0.52$ .

$^1\text{H-NMR}$  (250 MHz,  $\text{DMSO-}d_6$ ):  $\delta = 8.28$  (t,  $J = 5.8$  Hz, 1H, NH), 7.99 (d,  $J = 2.2$  Hz, 1H,  $\text{CH}_{\text{ar}}$ ), 7.56 (dd,  $J = 8.9, 2.2$  Hz, 1H,  $\text{CH}_{\text{ar}}$ ), 7.20 (d,  $J = 9.0$  Hz, 1H,  $\text{CH}_{\text{ar}}$ ), 7.05 (t,  $J = 5.7$  Hz, 1H, NH), 3.46 (q,  $J = 6.0$  Hz, 2H,  $\text{CH}_2$ ), 3.21 (q,  $J = 6.0$  Hz, 2H,  $\text{CH}_2$ ), 2.39 (s, 3H,  $\text{CH}_3$ ), 2.21 (s, 3H,  $\text{CH}_3$ ), 1.37 (s, 9H,  $\text{C}(\text{CH}_3)_3$ ) ppm.

MS(ESI<sup>+</sup>):  $m/z$  377 ( $[\text{M}+\text{H}]$ , 40)

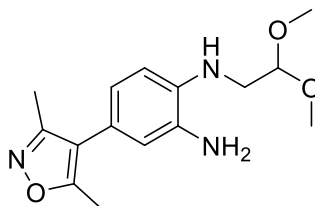
***N*-(2,2-dimethoxyethyl)-4-(3,5-dimethylisoxazol-4-yl)-2-nitroaniline (65)**

Compound **64** (100 mg, 0.42 mmol, 1 eq) was reacted with 2,2-dimethoxyethanamine according to general procedure A. Crude product was purified via flash chromatography with a gradient of hexane:EtOAc (increased linear from 70:30 to 60:40 over 10 CVs) as mobile phase to obtain **65** as a red solid (1.1 g, 89 %).

$R_f(\text{hexane}/\text{EtOAc} = 80:20) = 0.58$ .

$^1\text{H-NMR}$  (250 MHz, DMSO):  $\delta = 8.15$  (t,  $J = 5.5$  Hz, 1H, NH), 8.01 (d,  $J = 2.2$  Hz, 1H,  $\text{CH}_{\text{ar}}$ ), 7.58 (dd,  $J = 8.9, 2.1$  Hz, 1H,  $\text{CH}_{\text{ar}}$ ), 7.21 (d,  $J = 9.0$  Hz, 1H,  $\text{CH}_{\text{ar}}$ ), 4.67 (t,  $J = 5.2$  Hz, 1H, CH), 3.53 (t,  $J = 5.4$  Hz, 2H,  $\text{CH}_2$ ), 3.36 (s, 6H,  $2 \times \text{CH}_3$ ), 2.39 (s, 3H,  $\text{CH}_3$ ), 2.21 (s, 3H,  $\text{CH}_3$ ) ppm.

MS(ESI+):  $m/z$  344.14 ( $[\text{M}+\text{H}]$ , 100)

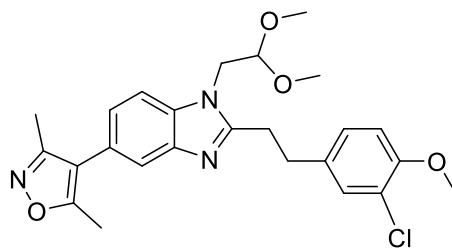
***N*<sup>1</sup>-(2,2-dimethoxyethyl)-4-(3,5-dimethylisoxazol-4-yl)benzene-1,2-diamine (68)**

Compound **65** (309 mg, 0.96 mmol) was reduced according to general procedure B1. Product was purified via flash chromatography with a gradient of DCM/MeOH (increased linear from 100:0 to 90:10 over 10 CVs) as mobile phase to obtain **68** as a light brown gum (267 mg, 95 %).

$R_f(\text{hexane}/\text{EtOAc} = 25:75) = 0.55$ .

$^1\text{H-NMR}$  (250 MHz, DMSO):  $\delta = 6.57 - 6.45$  (m, 3H,  $\text{CH}_{\text{ar}}$ ), 4.64 (s, 2H,  $\text{NH}_2$ ), 4.56 (t,  $J = 5.3$  Hz, 1H, NH or CH), 4.50 (t,  $J = 5.8$  Hz, 1H, NH or CH), 3.33 (s, 6H,  $2 \times \text{CH}_3$ ), 3.18 (t,  $J = 5.6$  Hz, 2H,  $\text{CH}_2$ ), 2.34 (s, 3H,  $\text{CH}_3$ ), 2.17 (s, 3H,  $\text{CH}_3$ ) ppm.

MS(ESI+): not measurable

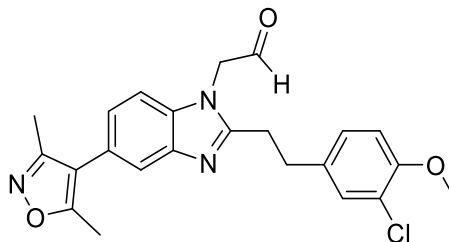
**4-(2-(3-chloro-4-methoxyphenethyl)-1-(2,2-dimethoxyethyl)-1*H*-benzo[d]imidazol-5-yl)-3,5-dimethylisoxazole (71)**

Compound **68** (50 mg, 0.17 mmol, 1 eq) was reacted with 3-(3-chloro-4-methoxyphenyl)propanoic acid (41 mg, 0.19 mmol, 1 eq) according to general procedure C. Product was purified via flash chromatography with a gradient of hexane/EtOAc (increased linear from 60:40 to 20:80 over 4 CVs) as mobile phase to obtain **71** as a colorless solid (68 mg, 84 %).

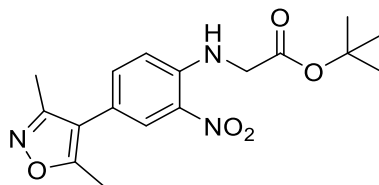
$R_f(\text{hexane/EtOAc} = 25:75) = 0.65$ .

$^1\text{H-NMR}$  (600 MHz, DMSO):  $\delta = 7.59$  (d,  $J = 8.3$  Hz, 1H,  $\text{CH}_{\text{ar}}$ ), 7.56 (s, 1H,  $\text{CH}_{\text{ar}}$ ), 7.41 (s, 1H,  $\text{CH}_{\text{ar}}$ ), 7.25 (d,  $J = 8.4$  Hz, 1H,  $\text{CH}_{\text{ar}}$ ), 7.17 (d,  $J = 8.2$  Hz, 1H,  $\text{CH}_{\text{ar}}$ ), 7.07 (d,  $J = 8.5$  Hz, 1H,  $\text{CH}_{\text{ar}}$ ), 4.58 (t,  $J = 5.0$  Hz, 1H, CH), 4.32 (d,  $J = 4.9$  Hz, 2H,  $\text{CH}_2$ ), 3.81 (s, 3H,  $\text{CH}_3$ ), 3.30 (s, 6H, 2x $\text{CH}_3$ ), 3.15 (dt,  $J = 38.2, 7.0$  Hz, 4H, 2x $\text{CH}_2$ ), 2.40 (s, 3H,  $\text{CH}_3$ ), 2.23 (s, 3H,  $\text{CH}_3$ ) ppm.

MS(ESI<sup>+</sup>):  $m/z$  469.92 ( $[\text{M}+\text{H}]$ , 100)

**2-(2-(3-chloro-4-methoxyphenethyl)-5-(3,5-dimethylisoxazol-4-yl)-1H-benzo[d]imidazol-1-yl)acetaldehyde (72)**

A mixture of compound 71 (100 mg, 0.21 mmol), water (3 mL), TFA (3 mL) and EtCl<sub>2</sub> (5 mL). After 2 hours reflux the solvent was reduced under reduced pressure and EE was added. Solution was neutralized by adding sat. K<sub>2</sub>CO<sub>3(aq)</sub>. Phases were separated, and aqueous phase was extracted with EtOAc twice. Combined organic phases were washed with brine and dried over MgSO<sub>4</sub>. Although TLC indicated a successful reaction the product could not be isolated.

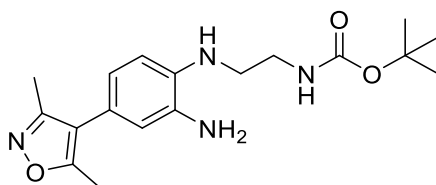
***tert*-butyl (4-(3,5-dimethylisoxazol-4-yl)-2-nitrophenyl)glycinate (67)**

Compound **64** (500 mg, 2.12 mmol, 1 eq) was reacted with glycine *tert*-butyl ester hydrochloride according to general procedure A with an additional equivalent of DIPEA. Crude product was purified via flash chromatography with hexane:EtOAc (60:40) as mobile phase and recrystallized from EtOAc and hexane to obtain **67** as an orange solid (440 mg, 60 %).

R<sub>f</sub>(hexane/EtOAc = 70:30) = 0.58.

<sup>1</sup>H-NMR (250 MHz, DMSO-*d*<sub>6</sub>): δ = 8.41 (t, J = 5.6 Hz, 1H, NH), 8.03 (d, J = 2.1 Hz, 1H, CH<sub>ar</sub>), 7.58 (dd, J = 8.8, 2.2 Hz, 1H, CH<sub>ar</sub>), 6.99 (d, J = 8.9 Hz, 1H, CH<sub>ar</sub>), 4.20 (d, J = 5.7 Hz, 2H, CH<sub>2</sub>), 2.39 (s, 3H, CH<sub>3</sub>), 2.21 (s, 3H, CH<sub>3</sub>), 1.46 (s, 9H, C(CH<sub>3</sub>)<sub>3</sub>) ppm.

MS(ESI<sup>+</sup>): m/z 348.04 ([M+H], 100)

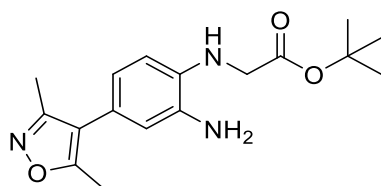
**tert-butyl (2-((2-amino-4-(3,5-dimethylisoxazol-4-yl)phenyl)amino)ethyl)carbamate (69)**

Compound **66** (1.36 g, 3.6 mmol) was reduced according to General procedure B1. Product was purified via flash chromatography with a gradient of DCM/MeOH (increased linear from 100:0 to 90:10 over 10 CVs) as mobile phase to obtain **69** as a light brown solid (1.1 g, 89 %).

$R_f$ (DCM/MeOH = 90:10) = 0.54.

$^1\text{H-NMR}$  (250 MHz,  $\text{DMSO-}d_6$ ):  $\delta$  = 6.92 (s, 1H, NH), 6.56 - 6.47 (m, 3H,  $\text{CH}_{\text{ar}}$ ), 4.62 (s, 1H, NH), 4.57 (s, 2H,  $\text{NH}_2$ ), 3.19 - 3.07 (m, 4H,  $2 \times \text{CH}_2$ ), 2.33 (s, 3H,  $\text{CH}_3$ ), 2.17 (s, 3H,  $\text{CH}_3$ ), 1.39 (s, 9H,  $\text{C}(\text{CH}_3)_3$ ) ppm.

MS(ESI<sup>+</sup>):  $m/z$  347.14 ( $[\text{M}+\text{H}]$ , 100)

**tert-butyl (2-amino-4-(3,5-dimethylisoxazol-4-yl)phenyl)glycinate (70)**

Compound **67** (300 mg) was reduced according to general procedure B1. Product was purified via flash chromatography with a gradient of hexane/EtOAc (increased linear from 60:40 to 40:60 over 4 CVs) as mobile phase to obtain **70** as a brown oil (190 mg, 70 %).

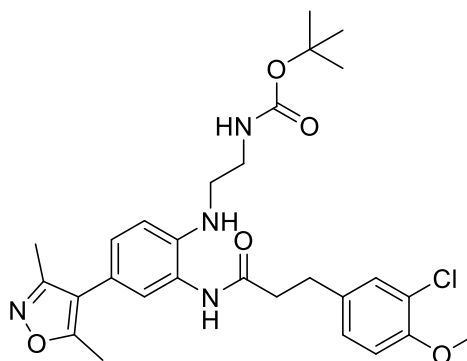
$R_f$ (hexane/EtOAc = 66:33) = 0.24.

$^1\text{H-NMR}$  (250 MHz,  $\text{DMSO-}d_6$ ):  $\delta$  = 6.57 (d,  $J$  = 2.0 Hz, 1H,  $\text{CH}_{\text{ar}}$ ), 6.46 (dd,  $J$  = 8.0, 2.0 Hz, 1H,  $\text{CH}_{\text{ar}}$ ), 6.32 (d,  $J$  = 8.0 Hz, 1H,  $\text{CH}_{\text{ar}}$ ), 5.04 (t,  $J$  = 6.3 Hz, 1H, NH), 4.64 (s, 2H, NH), 3.81 (d,  $J$  = 6.2 Hz, 2H,  $\text{CH}_2$ ), 2.33 (s, 3H,  $\text{CH}_3$ ), 2.17 (s, 3H,  $\text{CH}_3$ ), 1.43 (s, 9H,  $\text{C}(\text{CH}_3)_3$ ) ppm.

MS(ESI<sup>+</sup>):  $m/z$  340.17 ( $[\text{M}+\text{Na}]$ , 70)



***tert*-butyl (2-((2-(3-(3-chloro-4-methoxyphenyl)propanamido)-4-(3,5-dimethylisoxazol-4-yl)phenyl)amino)ethyl)carbamate (73)**

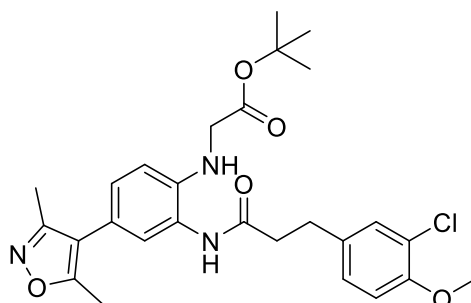


Compound **69** (628 mg, 1.81 mmol, 1 eq) was reacted with 3-(3-chloro-4-methoxyphenyl)propanoic acid (389 mg, 1.81 mmol, 1 eq) according to general procedure C. Product was purified via flash chromatography with a gradient of hexane/EtOAc (increased linear from 60:40 to 20:80 over 4 CVs) as mobile phase to obtain **73** as a yellow orange solid (619 mg, 63 %).

$R_f(\text{hexane/EtOAc} = 1:3) = 0.5$ .

$^1\text{H-NMR}$  (250 MHz,  $\text{DMSO-}d_6$ ):  $\delta = 9.07$  (s, 1H, NH), 7.32 (d,  $J = 2.1$  Hz, 1H,  $\text{CH}_{\text{ar}}$ ), 7.19 (dd,  $J = 8.5, 2.1$  Hz, 1H,  $\text{CH}_{\text{ar}}$ ), 7.09 - 6.99 (m, 3H,  $\text{CH}_{\text{ar}}$ ), 6.92 (bs, 1H, NH), 6.74 (d,  $J = 8.3$  Hz, 1H,  $\text{CH}_{\text{ar}}$ ), 5.07 (bs, 1H, NH), 3.81 (s, 3H,  $\text{OCH}_3$ ), 3.13 (s, 4H,  $2 \times \text{CH}_2$ ), 2.87 (t,  $J = 7.4$  Hz, 2H,  $\text{CH}_2$ ), 2.63 (t,  $J = 7.5$  Hz, 2H,  $\text{CH}_2$ ), 2.35 (s, 3H,  $\text{CH}_3$ ), 2.18 (s, 3H,  $\text{CH}_3$ ), 1.39 (s, 9H,  $\text{C}(\text{CH}_3)_3$ ) ppm.

$\text{MS}(\text{ESI}^+)$ :  $m/z$  543.23 ( $[\text{M}+\text{H}]$ , 95)

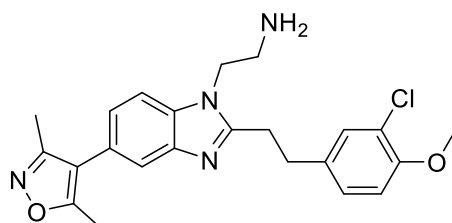
***tert*-butyl (2-(3-(3-chloro-4-methoxyphenyl)propanamido)-4-(3,5-dimethylisoxazol-4-yl)phenyl)glycinate (74)**

Compound **70** (190 mg, 0.6 mmol, 1 eq) was reacted with 3-(3-chloro-4-methoxyphenyl) propanoic acid (128 mg, 0.6 mmol, 1 eq) according to general procedure C. Product was purified via flash chromatography with a gradient of hexane/EtOAc (increased linear from 60:40 to 20:80 over 4 CVs) as mobile phase to obtain **74** as a colorless solid (254 mg, 83 %).

$R_f$ (hexane/EtOAc = 50:50) = 0.4.

$^1\text{H-NMR}$  (250 MHz,  $\text{DMSO-}d_6$ ):  $\delta$  = 9.23 (s, 1H, NH), 7.33 (d,  $J$  = 2.1 Hz, 1H,  $\text{CH}_{\text{ar}}$ ), 7.20 (dd,  $J$  = 8.4, 2.1 Hz, 1H,  $\text{CH}_{\text{ar}}$ ), 7.13 - 6.96 (m, 3H,  $\text{CH}_{\text{ar}}$ ), 6.55 (d,  $J$  = 8.4 Hz, 1H,  $\text{CH}_{\text{ar}}$ ), 3.85 (d,  $J$  = 5.9 Hz, 2H,  $\text{CH}_2$ ), 3.80 (s, 3H,  $\text{OCH}_3$ ), 2.87 (t,  $J$  = 7.4 Hz, 2H,  $\text{CH}_2$ ), 2.64 (t,  $J$  = 7.4 Hz, 2H,  $\text{CH}_2$ ), 2.35 (s, 3H,  $\text{CH}_3$ ), 2.18 (s, 3H,  $\text{CH}_3$ ), 1.44 (s, 9H,  $\text{C}(\text{CH}_3)_3$ ) ppm.

MS(ESI-):  $m/z$  512.31 ( $[\text{M-H}]$ , 80)

**2-(2-(3-chloro-4-methoxyphenethyl)-5-(3,5-dimethylisoxazol-4-yl)-1H-benzo[d]imidazol-1-yl)ethan-1-amine (75)**

Compound **73** (100 mg, 0.18 mmol) was converted according to general procedure D for 15 h. Solvent was removed under reduced pressure and remaining residue was resolved in NaOH (1 M) and EtOAc. Phases were separated and aqueous phase was extracted with EtOAc twice. Combined organic phases were washed with brine and dried over  $\text{MgSO}_4$ . Product was purified

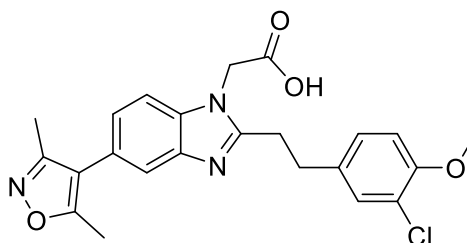
via reversed flash chromatography with a gradient of ACN/H<sub>2</sub>O (after 2 CVs increased linear from 10:90 to 100:0 over 10 CVs) to obtain **75** as light yellow solid (75 mg, 95 %).

R<sub>f</sub>(DCM/MeOH = 9:1) = 0.43.

<sup>1</sup>H-NMR (250 MHz, DMSO-*d*<sub>6</sub>): δ = 7.60 (d, J = 8.3 Hz, 1H, CH<sub>ar</sub>), 7.55 (d, J = 1.5 Hz, 1H, CH<sub>ar</sub>), 7.43 (d, J = 2.1 Hz, 1H, CH<sub>ar</sub>), 7.26 (dd, J = 8.4, 2.2 Hz, 1H, CH<sub>ar</sub>), 7.16 (dd, J = 8.3, 1.6 Hz, 1H, CH<sub>ar</sub>), 7.06 (d, J = 8.5 Hz, 1H, CH<sub>ar</sub>), 4.16 (t, J = 6.5 Hz, 2H, CH<sub>2</sub>), 3.82 (s, 3H, OCH<sub>3</sub>), 3.26 - 3.03 (m, 4H, 2xCH<sub>2</sub>), 2.85 (t, J = 6.4 Hz, 2H, CH<sub>2</sub>), 2.40 (s, 3H, CH<sub>3</sub>), 2.23 (s, 3H, CH<sub>3</sub>) ppm.

MS(ESI<sup>+</sup>): m/z 425.06 ([M+H], 100)

**2-(2-(3-chloro-4-methoxyphenethyl)-5-(3,5-dimethylisoxazol-4-yl)-1H-benzo[d]imidazol-1-yl)acetic acid (76)**

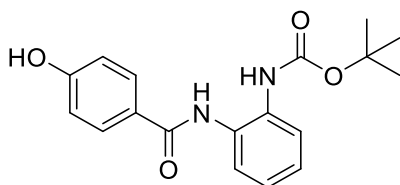


Compound **74** (332 mg, 0.65 mmol) was converted according to general procedure D for 15 h. Solvent was removed under reduced pressure and remaining residue was resolved in HCl (1 M) and EtOAc. Phases were separated and aqueous phase was extracted with EtOAc twice. Combined organic phases were washed with brine and dried over MgSO<sub>4</sub>. Product was purified via flash chromatography with a gradient of DCM (containing 1 % AcOH)/MeOH (increased linear from 100:0 to 90:10 over 10 CVs) to obtain **76** as a beige solid (231 mg, 81 %).

R<sub>f</sub>(DCM/MeOH/AcOH= 90:10:1) = 0.54.

<sup>1</sup>H-NMR (250 MHz, DMSO-*d*<sub>6</sub>): δ = 7.61 - 7.52 (m, 2H, CH<sub>ar</sub>), 7.41 (d, J = 2.1 Hz, 1H, CH<sub>ar</sub>), 7.21 (ddd, J = 18.2, 8.4, 1.9 Hz, 2H, CH<sub>ar</sub>), 7.06 (d, J = 8.4 Hz, 1H, CH<sub>ar</sub>), 5.13 (s, 2H, CH<sub>2</sub>), 3.82 (s, 3H, OCH<sub>3</sub>), 3.08 (s, 4H, 2xCH<sub>2</sub>), 2.40 (s, 3H, CH<sub>3</sub>), 2.23 (s, 3H, CH<sub>3</sub>) ppm.

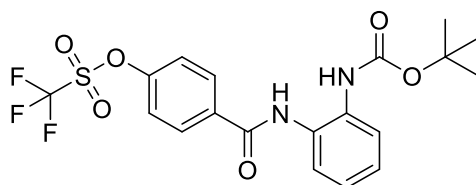
MS(ESI<sup>+</sup>): m/z 440.18 ([M+H], 100)

***tert*-butyl (2-(4-hydroxybenzamido)phenyl)carbamate (**88**)**

To a solution of 4-hydroxybenzoic acid **87** (600 mg, 4.34 mmol, 1 eq), **39** (995 mg, 4.78 mmol, 1.1 eq), HOBt hydrate (20 % H<sub>2</sub>O, 411 mg, 3.04 mmol, 0.7 eq) and HATU (1.65 g, 4.34 mmol, 1 eq) in DCM/DMF (2:1), DIPEA (0.98 mL, 5.7 mmol, 1.3 eq) was added dropwise and the resulting mixture was stirred at RT overnight. The solvent was removed under reduced pressure and partitioned between EtOAc and water. The aqueous phase was extracted three times with EtOAc, and the combined organic fractions were washed with brine and dried over MgSO<sub>4</sub>. The residue was purified via flash chromatography with a gradient of hexane/ethyl acetate (increased linear from 90:10 to 40:60 over 10 CVs) to obtain **88** as a colorless solid (834 mg, 58 %).

<sup>1</sup>H-NMR (400 MHz, DMSO-*d*<sub>6</sub>): δ = 10.14 (s, 1H, NH), 9.64 (s, 1H, OH), 8.64 (s, 1H, NH), 7.83 (d, J = 8.7, 2H, CH<sub>ar</sub>), 7.51 (ddd, J = 8.0, 6.1, 1.9 Hz, 2H, CH<sub>ar</sub>), 7.20 - 7.11 (m, 2H, CH<sub>ar</sub>), 6.87 (d, J = 8.7 Hz, 2H, CH<sub>ar</sub>), 1.45 (s, 9H, C(CH<sub>3</sub>)<sub>3</sub>) ppm.

MS(ESI<sup>+</sup>): m/z 351.17 ([M+Na], 100)

**4-((2-((*tert*-butoxycarbonyl)amino)phenyl)carbamoyl)phenyl trifluoromethanesulfonate (**89**)**

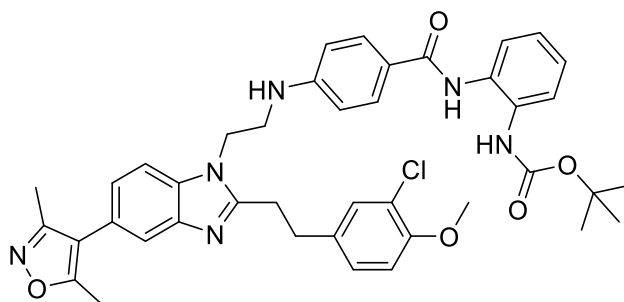
Compound **88** (500 mg, 1.52 mmol, 1 eq), DMAP (186 mg, 1.52 mmol, 1 eq) and pyridine (1.2 mL, 15.23 mmol, 10 eq) were solved in DCM (25 mL) and cooled to -17 °C. Then Tf<sub>2</sub>O (1 M in DCM, 2.1 mL, 2.13 mmol, 1.4 eq) was added dropwise and reaction was stirred and reached RT overnight. Reaction mixture was washed with 5 % HCl solution and saturated NaHCO<sub>3</sub> solution. Aqueous phases were extracted with DCM and combined organic phases were dried over MgSO<sub>4</sub>. Product was purified via flash chromatography with hexane/EtOAc (66:33) as a mobile phase to obtain **89** as a yellow solid (337 mg, 48 %).

$R_f(\text{hexane/EtOAc} = 66:33) = 0.61$ .

$^1\text{H-NMR}$  (250 MHz,  $\text{DMSO-}d_6$ ):  $\delta = 9.93$  (s, 1H, NH), 8.68 (s, 1H, NH), 8.13 (d,  $J = 8.8$  Hz, 2H,  $\text{CH}_{\text{ar}}$ ), 7.71 (d,  $J = 8.8$  Hz, 2H,  $\text{CH}_{\text{ar}}$ ), 7.60 (dd,  $J = 8.0, 1.6$  Hz, 1H,  $\text{CH}_{\text{ar}}$ ), 7.48 (dd,  $J = 7.7, 1.7$  Hz, 1H,  $\text{CH}_{\text{ar}}$ ), 7.26 - 7.09 (m, 2H,  $\text{CH}_{\text{ar}}$ ), 1.43 (s, 9H,  $\text{C}(\text{CH}_3)_3$ ) ppm.

$\text{MS}(\text{ESI}^+)$ :  $m/z$  483.12 ( $[\text{M}+\text{Na}]$ , 100)

***tert*-butyl (2-(4-((2-(2-(3-chloro-4-methoxyphenethyl)-5-(3,5-dimethylisoxazol-4-yl)-1H-benzo[d]imidazol-1-yl)ethyl)amino)benzamido)phenyl)carbamate (90)**



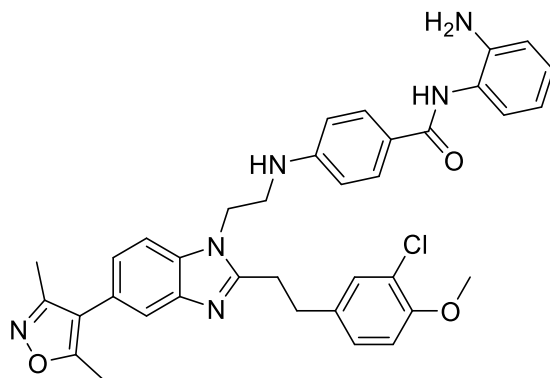
Compound **89** (160 mg, 0.35 mmol, 1 eq) and **75** (177 mg, 0.42 mmol, 1.2 eq), XPhos Palladacycle Gen. 3 (29 mg, 0.03 mmol, 0.1 eq) and  $\text{Cs}_2\text{CO}_3$  (94 mg, 0.29 mmol, 0.85 eq) were dissolved in toluene (10 mL) and degassed by placing it in an ultrasonic bath and argon was bubbled into the reaction for 30 minutes. Then the mixture was heated at 80 °C overnight. Solvent was removed under reduced pressure and the remaining residue was partitioned between EtOAc and  $\text{H}_2\text{O}$ . Aqueous phase was extracted with EtOAc twice and combined organic phases were washed with brine and dried over  $\text{MgSO}_4$ . Product was purified via flash chromatography with a gradient of DCM/MeOH (increased linear from 100:0 to 90:10 over 10 CVs) as mobile phase to obtain **90** as a colorless solid (50 mg, 31 %).

$R_f(\text{DCM/MeOH} = 95:5) = 0.69$ .

$^1\text{H-NMR}$  (250 MHz,  $\text{DMSO-}d_6$ ):  $\delta = 9.64$  (s, 1H, NH), 9.55 (s, 1H, NH), 8.64 (s, 1H, NH), 7.87 - 7.79 (m, 2H,  $\text{CH}_{\text{ar}}$ ), 7.79 - 7.73 (m, 1H,  $\text{CH}_{\text{ar}}$ ), 7.54 - 7.45 (m, 4H,  $\text{CH}_{\text{ar}}$ ), 6.98 - 6.83 (m, 4H,  $\text{CH}_{\text{ar}}$ ), 6.69 - 6.61 (m, 1H,  $\text{CH}_{\text{ar}}$ ), 6.58 (s, 1H,  $\text{CH}_{\text{ar}}$ ), 4.38 (s, 2H), 3.74 (s, 3H), 3.57 (s, 2H), 3.00 (s, 4H), 2.40 (s, 3H), 2.23 (s, 3H), 1.45 (s, 9H) ppm.

$\text{MS}(\text{ESI}^+)$ :  $m/z$  735.45 ( $[\text{M}+\text{H}]$ , 100)

***N*-(2-aminophenyl)-4-((2-(2-(3-chloro-4-methoxyphenethyl)-5-(3,5-dimethylisoxazol-4-yl)-1*H*-benzo[*d*]imidazol-1-yl)ethyl)amino)benzamide (19)**



Reaction was performed according to general procedure E with compound **90** (50 mg, 0.06 mmol). Product was purified via reversed flash chromatography with a gradient of ACN/H<sub>2</sub>O (after 2 CVs increased linear from 10:90 to 100:0 over 10 CVs) to obtain **19** as a colorless solid (38 mg, 88 %).

$R_f(\text{DCM/MeOH/TEA} = 95:5:1) = 0.46$ .

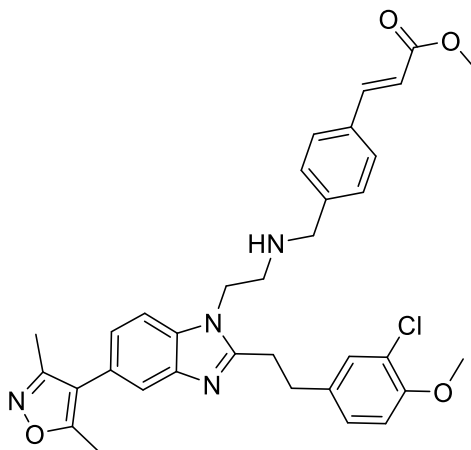
<sup>1</sup>H-NMR (500 MHz, DMSO-*d*<sub>6</sub>):  $\delta = 9.72$  (s, 1H, NH), 7.96 (d,  $J = 8.5$  Hz, 1H, CH<sub>ar</sub>), 7.83 (d,  $J = 8.7$  Hz, 2H, CH<sub>ar</sub>), 7.79 (s, 1H, CH<sub>ar</sub>), 7.51 (d,  $J = 9.3$  Hz, 1H, CH<sub>ar</sub>), 7.26 (d,  $J = 7.8$  Hz, 1H, CH<sub>ar</sub>), 7.18 (s, 1H, CH<sub>ar</sub>), 7.13 (t,  $J = 7.6$  Hz, 1H, CH<sub>ar</sub>), 7.06 (d,  $J = 8.9$  Hz, 1H, CH<sub>ar</sub>), 7.00 (s, 2H, CH<sub>ar</sub>), 7.00 - 6.94 (m, 1H, CH<sub>ar</sub>), 6.65 (d,  $J = 8.7$  Hz, 2H, CH<sub>ar</sub>), 4.66 - 4.53 (m, 3H, CH<sub>2</sub> + NH), 3.77 (s, 3H, OCH<sub>3</sub>), 3.69 - 3.64 (m, 2H, CH<sub>2</sub>), 3.22 - 3.16 (m, 2H, CH<sub>2</sub>), 3.05 - 2.99 (m, 2H, CH<sub>2</sub>), 2.43 (s, 3H, CH<sub>3</sub>), 2.25 (s, 3H, CH<sub>3</sub>) ppm.

<sup>13</sup>C-NMR (126 MHz, DMSO-*d*<sub>6</sub>):  $\delta = 165.91, 165.61, 158.86, 158.72, 158.56, 154.88, 153.62, 151.29, 150.12, 133.04, 130.29, 130.02, 129.67, 128.47, 126.95, 126.72, 126.19, 121.55, 121.34, 117.97, 116.17, 115.92, 115.63, 113.72, 113.26, 113.17, 111.36, 56.45, 44.45, 41.58, 31.31, 27.59, 11.77, 10.91$  ppm.

MS(ESI<sup>+</sup>):  $m/z$  633.06 ([M-H], 100).

HRMS (MALDI):  $m/z$  calculated 635.25319 for C<sub>36</sub>H<sub>36</sub>ClN<sub>6</sub>O<sub>3</sub>, found 635.25244.

HPLC: purity > 95 %

**Methyl (*E*)-3-(4-(((2-(2-(3-chloro-4-methoxyphenethyl)-5-(3,5-dimethylisoxazol-4-yl)-1*H*-benzo[d]imidazol-1-yl)ethyl)amino)methyl)phenyl)acrylate (**84**)**

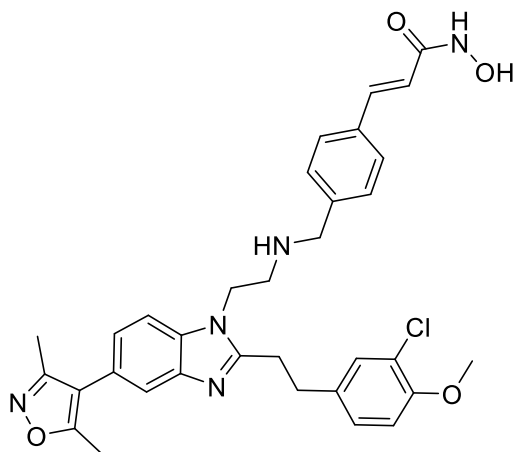
Compound **75** (420 mg, 0.99, 1 eq) and methyl (*E*)-3-(4-formylphenyl)acrylate **83** (226 mg, 1.2 mmol, 1.2 eq) were dissolved in DMF and stirred at RT for 1 hour. Then NaBH<sub>4</sub> (19 mg, 0.5 mmol, 0.5 eq) was added portion wise at 0 °C. The mixture was stirred for 2 hours and warmed to RT. Reaction was quenched with H<sub>2</sub>O and extracted with EtOAc three times. Combined organic phases were washed with brine and dried over MgSO<sub>4</sub>. Product was purified via reversed flash chromatography with a gradient of ACN/H<sub>2</sub>O (increased linear from 10:90 to 100:0 over 10 CVs) to obtain **84** as a colorless solid (168 mg, 28 %).

R<sub>f</sub>(DCM/MeOH/TEA = 99:1:1) = 0.55.

<sup>1</sup>H-NMR (250 MHz, DMSO-*d*<sub>6</sub>): δ = 7.67 - 7.50 (m, 5H, CH<sub>ar</sub>+ CH), 7.38 (d, J = 2.1 Hz, 1H, CH<sub>ar</sub>), 7.27 - 7.10 (m, 4H, CH<sub>ar</sub>), 7.03 (d, J = 8.5 Hz, 1H, CH<sub>ar</sub>), 6.56 (d, J = 16.1 Hz, 1H, CH), 4.27 (t, J = 5.7 Hz, 2H, CH<sub>2</sub>), 3.81 (s, 3H, OCH<sub>3</sub>), 3.71 (s, 3H, OCH<sub>3</sub>), 3.69 (s, 2H, CH<sub>2</sub>), 3.22 - 3.06 (m, 4H, 2xCH<sub>2</sub>), 2.85 - 2.74 (m, 2H, CH<sub>2</sub>), 2.40 (s, 3H, CH<sub>3</sub>), 2.22 (s, 3H, CH<sub>3</sub>) ppm.

MS(ESI<sup>+</sup>): m/z 599.30 ([M+H], 100)

**(E)-3-(4-(((2-(2-(3-chloro-4-methoxyphenethyl)-5-(3,5-dimethylisoxazol-4-yl)-1H-benzo[d]imidazole-1-yl)ethyl)amino)methyl)phenyl)-N-hydroxyacrylamide (18)**



Compound **84** (100 mg, 0.17 mmol, 1 eq) was reacted according to general procedure F. Crude product was purified via reversed flash chromatography with a gradient of ACN/H<sub>2</sub>O (after 2 CVs increased linear from 10:90 to 100:0 over 10 CVs) to obtain **18** as a colorless solid (35 mg, 35 %).

$R_f(\text{DCM/MeOH/AcOH} = 95:5:1) = 0.10$ .

<sup>1</sup>H-NMR (500 MHz, DMSO-*d*<sub>6</sub>):  $\delta = 10.73$  (s, 1H, OH), 9.04 (s, 1H, NH), 7.59 - 7.54 (m, 2H, CH<sub>ar</sub>), 7.47 - 7.37 (m, 4H, CH<sub>ar</sub> + CH), 7.26 (d,  $J = 7.0$  Hz, 2H, CH<sub>ar</sub>), 7.20 (dd,  $J = 8.4, 1.9$  Hz, 1H, CH<sub>ar</sub>), 7.15 (d,  $J = 8.5$  Hz, 1H, CH<sub>ar</sub>), 7.03 (d,  $J = 8.5$  Hz, 1H, CH<sub>ar</sub>), 6.41 (d,  $J = 15.8$  Hz, 1H, CH), 4.29 (s, 2H, CH<sub>2</sub>), 3.81 (s, 3H, OCH<sub>3</sub>), 3.72 (bs, 2H, CH<sub>2</sub>), 3.21 - 3.14 (m, 2H, CH<sub>2</sub>), 3.14 - 3.07 (m, 2H, CH<sub>2</sub>), 2.85 (bs, 2H, CH<sub>2</sub>), 2.40 (s, 3H, CH<sub>3</sub>), 2.23 (s, 3H, CH<sub>3</sub>) ppm.

<sup>13</sup>C-NMR (126 MHz, DMSO-*d*<sub>6</sub>):  $\delta = 164.52, 162.76, 158.39, 155.44, 152.84, 142.63, 142.30, 138.15, 134.65, 134.49, 133.15, 129.73, 128.22, 128.17, 127.28, 122.65, 122.57, 120.70, 118.85, 118.36, 116.75, 112.64, 110.39, 56.02, 52.30, 47.85, 43.37, 31.45, 28.37, 11.29, 10.53$  ppm.

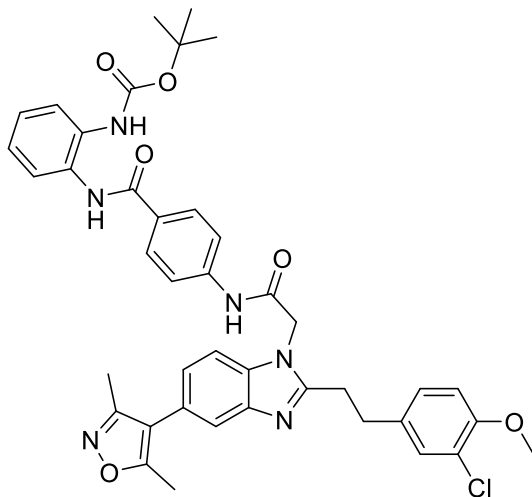
MS(ESI<sup>+</sup>):  $m/z$  600.10 ([M+H], 100).

HRMS (MALDI):  $m/z$  calculated 600.23721 for C<sub>33</sub>H<sub>35</sub>ClN<sub>5</sub>O<sub>4</sub>, found 600.23647.

HPLC: purity > 95 %



***tert*-Butyl (2-(4-(2-(2-(3-chloro-4-methoxyphenethyl)-5-(3,5-dimethylisoxazol-4-yl)-1H-benzo[d]imidazol-1-yl)acetamido)benzamido)phenyl)carbamate (91)**



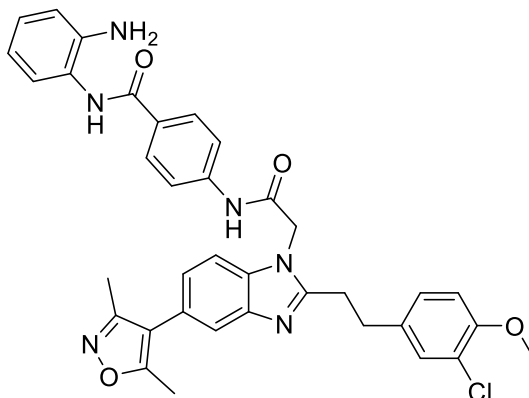
Reaction was performed according to general procedure C with compound **76** (150 mg, 0.34 mmol, 1 eq) and **42** (134 mg, 0.41 mmol, 1.2 eq). Product was purified via reversed flash chromatography with a gradient of ACN/H<sub>2</sub>O (increased linear from 10:90 to 100:0 over 10 CVs) to obtain **91** as a colorless solid (126 mg, 49 %).

R<sub>f</sub>(DCM/MeOH = 95:5) = 0.56.

<sup>1</sup>H-NMR (250 MHz, DMSO-*d*<sub>6</sub>): δ = 10.82 (s, 1H, NH), 9.76 (s, 1H, NH), 8.68 (s, 1H, NH), 7.95 (d, J = 8.7 Hz, 2H, CH<sub>ar</sub>), 7.75 (d, J = 8.7 Hz, 2H, CH<sub>ar</sub>), 7.54 (dd, J = 18.8, 9.1 Hz, 4H, CH<sub>ar</sub>), 7.41 (d, J = 2.0 Hz, 1H, CH<sub>ar</sub>), 7.29 - 7.11 (m, 4H, CH<sub>ar</sub>), 7.05 (d, J = 8.5 Hz, 1H, CH<sub>ar</sub>), 5.22 (s, 2H, CH<sub>2</sub>), 3.81 (s, 3H, CH<sub>3</sub>), 3.13 (s, 4H, 2xCH<sub>2</sub>), 2.41 (s, 3H, CH<sub>3</sub>), 2.24 (s, 3H, CH<sub>3</sub>), 1.44 (s, 9H, C(CH<sub>3</sub>)<sub>3</sub>) ppm.

MS(ESI<sup>+</sup>): m/z 749.54 ([M+H], 100)

***N*-(2-aminophenyl)-4-(2-(2-(3-chloro-4-methoxyphenethyl)-5-(3,5-dimethylisoxazol-4-yl)-1H-benzo[d]imidazol-1-yl)acetamido)benzamide (20)**



Reaction was performed according to general procedure E with compound **91** (120 mg, 0.15 mmol, 1 eq) in DCM (10 mL). Crude product was purified via reversed flash chromatography with a gradient of ACN/H<sub>2</sub>O (after 2 CVs increased linear from 10:90 to 100:0 over 10 CVs) to obtain **20** as a colorless solid (79 mg, 76 %).

R<sub>f</sub>(DCM/MeOH = 95:5) = 0.56.

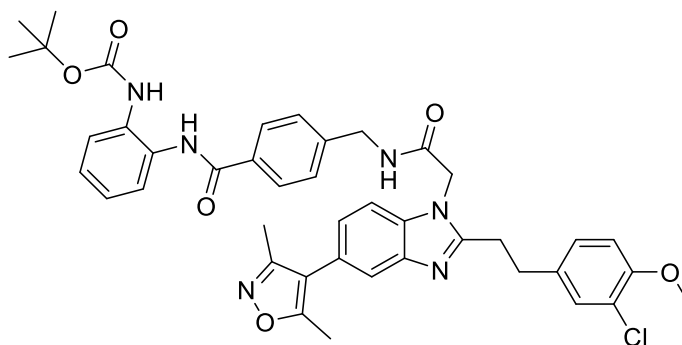
<sup>1</sup>H-NMR (500 MHz, DMSO-*d*<sub>6</sub>): δ = 10.79 (s, 1H, NH), 9.60 (s, 1H, NH), 7.98 (d, J = 8.6 Hz, 2H, CH<sub>ar</sub>), 7.72 (d, J = 8.7 Hz, 2H, CH<sub>ar</sub>), 7.61 (d, J = 1.1 Hz, 1H, CH<sub>ar</sub>), 7.58 (d, J = 8.3 Hz, 1H, CH<sub>ar</sub>), 7.41 (d, J = 2.1 Hz, 1H, CH<sub>ar</sub>), 7.25 (dd, J = 8.5, 2.1 Hz, 1H, CH<sub>ar</sub>), 7.20 (dd, J = 8.3, 1.5 Hz, 1H, CH<sub>ar</sub>), 7.15 (d, J = 7.6 Hz, 1H, CH<sub>ar</sub>), 7.05 (d, J = 8.5 Hz, 1H, CH<sub>ar</sub>), 7.00 - 6.93 (m, 1H, CH<sub>ar</sub>), 6.78 (dd, J = 8.0, 1.2 Hz, 1H, CH<sub>ar</sub>), 6.62 - 6.57 (m, 1H, CH<sub>ar</sub>), 5.21 (s, 2H, CH<sub>2</sub>), 4.88 (s, 2H, NH<sub>2</sub>), 3.81 (s, 3H, OCH<sub>3</sub>), 3.17 - 3.09 (m, 4H, 2xCH<sub>2</sub>), 2.41 (s, 3H, CH<sub>3</sub>), 2.24 (s, 3H, CH<sub>3</sub>) ppm.

<sup>13</sup>C-NMR (126 MHz, DMSO-*d*<sub>6</sub>): δ = 165.99, 164.61, 158.41, 155.82, 152.87, 143.17, 142.53, 141.25, 135.20, 134.34, 129.71, 129.50, 128.87, 128.20, 126.70, 126.43, 123.40, 123.04, 123.00, 120.71, 119.01, 118.43, 116.69, 116.28, 116.15, 112.69, 110.13, 56.02, 46.22, 31.28, 28.35, 11.30, 10.53 ppm.

MS(ESI<sup>+</sup>): m/z 649.11 ([M+H], 100).

HRMS (MALDI): m/z calculated 649.23246 for C<sub>36</sub>H<sub>34</sub>N<sub>6</sub>O<sub>4</sub>, found 649.23209.

***tert*-butyl (2-(4-((2-(2-(3-chloro-4-methoxyphenethyl)-5-(3,5-dimethylisoxazol-4-yl)-1H-benzo[d]imidazol-1-yl)acetamido)methyl)benzamido)phenyl)carbamate (92)**



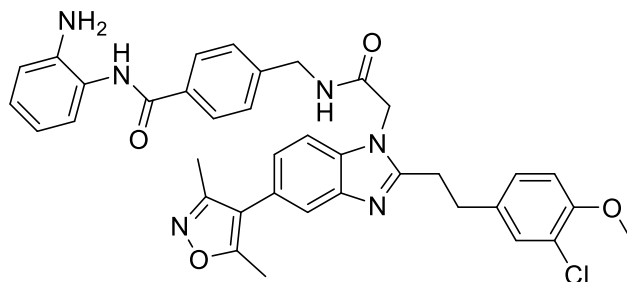
Reaction was performed according to general procedure C with compound **76** (120 mg, 0.34 mmol, 1 eq) and **60** (134 mg, 0.41 mmol, 1.2 eq). Product was purified via reversed flash chromatography with a gradient of ACN/H<sub>2</sub>O (after 2 CVs increased linear from 10:90 to 100:0 over 10 CVs) to obtain **92** as a colorless solid (121 mg, 48 %).

$R_f(\text{DCM/MeOH} = 95:5) = 0.49$ .

<sup>1</sup>H-NMR (250 MHz, DMSO-*d*<sub>6</sub>):  $\delta$  = 9.80 (s, 1H, NH), 8.96 (t,  $J = 5.7$  Hz, 1H, NH), 8.66 (s, 1H, NH), 7.89 (d,  $J = 8.2$  Hz, 2H, CH<sub>ar</sub>), 7.62 - 7.49 (m, 4H, CH<sub>ar</sub>), 7.47 - 7.37 (m, 3H, CH<sub>ar</sub>), 7.25 - 7.13 (m, 4H, CH<sub>ar</sub>), 7.05 (d,  $J = 8.5$  Hz, 1H, CH<sub>ar</sub>), 5.04 (s, 2H, CH<sub>2</sub>), 4.42 (d,  $J = 5.8$  Hz, 2H, CH<sub>2</sub>), 3.80 (s, 3H, CH<sub>3</sub>), 3.10 (s, 4H, 2xCH<sub>2</sub>), 2.40 (s, 3H, CH<sub>3</sub>), 2.23 (s, 3H, CH<sub>3</sub>), 1.43 (s, 9H, C(CH<sub>3</sub>)<sub>3</sub>) ppm.

MS(ESI<sup>+</sup>):  $m/z$  763.56([M+H], 80).

***N*-(2-aminophenyl)-4-((2-(2-(3-chloro-4-methoxyphenethyl)-5-(3,5-dimethylisoxazol-4-yl)-1H-benzo[d]imidazol-1-yl)acetamido)methyl)benzamide (21)**



Reaction was performed according to general procedure E with compound **92** (113 mg, 0.15 mmol, 1 eq) in DCM (10 mL). Product was purified via reversed flash chromatography with a gradient of ACN/H<sub>2</sub>O (after 2 CVs increased linear from 10:90 to 100:0 over 10 CVs) to obtain **21** as a colorless solid (60 mg, 61 %).

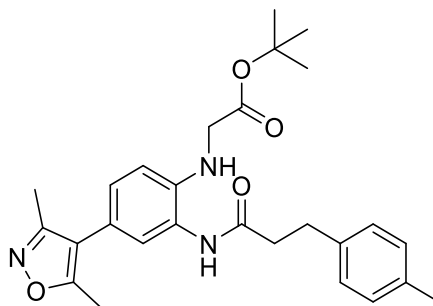
$R_f(\text{DCM/MeOH} = 95:5) = 0.43$ .

<sup>1</sup>H-NMR (500 MHz, DMSO-*d*<sub>6</sub>):  $\delta = 9.70$  (s, 1H, NH), 9.04 (t,  $J = 5.9$  Hz, 1H, NH), 7.94 (d,  $J = 8.0$  Hz, 2H, CH<sub>ar</sub>), 7.67 - 7.63 (m, 2H, CH<sub>ar</sub>), 7.44 - 7.39 (m, 3H, CH<sub>ar</sub>), 7.30 (d,  $J = 8.6$  Hz, 1H, CH<sub>ar</sub>), 7.23 - 7.16 (m, 2H, CH<sub>ar</sub>), 7.06 (d,  $J = 8.5$  Hz, 1H, CH<sub>ar</sub>), 7.03 - 6.98 (m, 1H, CH<sub>ar</sub>), 6.87 - 6.80 (m, 1H, CH<sub>ar</sub>), 6.66 (t,  $J = 7.4$  Hz, 1H, CH<sub>ar</sub>), 5.14 (s, 2H, CH<sub>2</sub>), 4.43 (d,  $J = 5.8$  Hz, 2H, CH<sub>2</sub>), 3.81 (s, 3H, CH<sub>3</sub>), 3.22 - 3.17 (m, 2H, CH<sub>2</sub>), 3.11 - 3.06 (m, 2H, CH<sub>2</sub>), 2.41 (s, 3H, CH<sub>3</sub>), 2.24 (s, 3H, CH<sub>3</sub>) ppm.

<sup>13</sup>C-NMR (126 MHz, DMSO-*d*<sub>6</sub>):  $\delta = 166.49, 165.08, 164.89, 158.38, 155.51, 152.99, 142.46, 142.09, 142.06, 134.31, 133.81, 133.23, 129.71, 128.18, 127.92, 127.05, 126.72, 126.56, 124.23, 123.91, 123.85, 120.78, 117.87, 117.12, 116.71, 116.36, 112.74, 110.88, 56.04, 45.95, 42.29, 31.12, 28.04, 11.31, 10.51$  ppm.

HRMS (MALDI):  $m/z$  calculated 663.24811 for C<sub>37</sub>H<sub>36</sub>ClN<sub>6</sub>O<sub>4</sub>, found 663.24788.

***tert*-butyl (4-(3,5-dimethylisoxazol-4-yl)-2-(3-(*p*-tolyl)propanamido)phenyl)glycinate (92)**



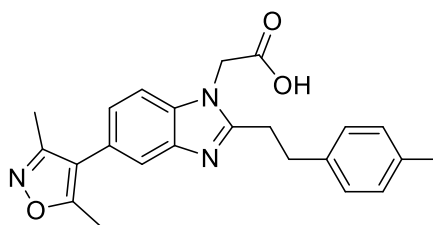
Compound **70** (200 mg, 0.63 mmol, 1 eq) was reacted with 3-(*p*-Tolyl)propionic acid **91** (124 mg, 0.76 mmol, 1.2 eq) according to general procedure C. Product was purified via flash chromatography with hexane/EtOAc (1:1) as mobile phase to obtain **92** as light yellow oil (290 mg, > 95 %).

$R_f$ (hexane/EtOAc = 1:1) = 0.32.

$^1\text{H-NMR}$  (250 MHz, DMSO- $d_6$ ):  $\delta$  = 9.22 (s, 1H, NH), 7.14 - 7.06 (m, 5H,  $\text{CH}_{\text{ar}}$ ), 7.04 - 6.98 (m, 1H,  $\text{CH}_{\text{ar}}$ ), 6.54 (d,  $J$  = 8.4 Hz, 1H,  $\text{CH}_{\text{ar}}$ ), 5.34 (t,  $J$  = 6.0 Hz, 1H, NH), 3.84 (d,  $J$  = 6.0 Hz, 2H,  $\text{CH}_2$ ), 2.89 (t,  $J$  = 7.5 Hz, 2H,  $\text{CH}_2$ ), 2.63 (t,  $J$  = 7.6 Hz, 2H,  $\text{CH}_2$ ), 2.35 (s, 3H,  $\text{CH}_3$ ), 2.25 (s, 3H,  $\text{CH}_3$ ), 2.18 (s, 3H,  $\text{CH}_3$ ), 1.44 (s, 9H,  $\text{C}(\text{CH}_3)_3$ ) ppm.

MS(ESI $^+$ ):  $m/z$  = 486.15 ( $[\text{M}+\text{Na}]$ , 100).

**2-(5-(3,5-dimethylisoxazol-4-yl)-2-(4-methylphenethyl)-1H-benzo[d]imidazol-1-yl) acetic acid (93)**



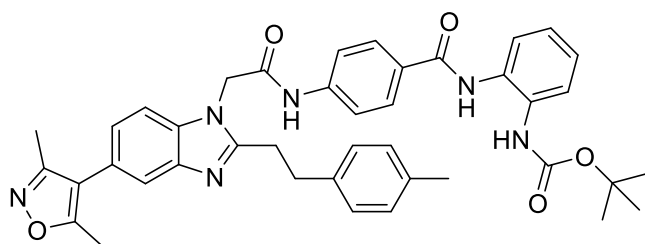
Compound **92** (290 mg, 0.63 mmol, 1 eq) was converted according to general procedure D for 4 h. Solvents were removed under reduced pressure and crude product was purified via flash chromatography with a gradient of DCM/MeOH with 1 % AcOH (increased linear from 100:0 to 90:10 over 8 CVs and held for 15 CVs) as a mobile phase to obtain **93** as a light yellow solid (180 mg, 71 %).

$R_f$ (DCM/MeOH/AcOH = 90:10:1) = 0.43.

<sup>1</sup>H-NMR (250 MHz, DMSO-*d*<sub>6</sub>): δ = 7.82 (d, J = 8.4 Hz, 1H, CH<sub>ar</sub>), 7.70 (d, J = 1.5 Hz, 1H, CH<sub>ar</sub>), 7.40 (dd, J = 8.5, 1.5 Hz, 1H, CH<sub>ar</sub>), 7.20 (d, J = 8.0 Hz, 2H, CH<sub>ar</sub>), 7.12 (d, J = 7.9 Hz, 2H, CH<sub>ar</sub>), 5.32 (s, 2H, CH<sub>2</sub>), 3.33 - 3.24 (m, 2H, CH<sub>2</sub>), 3.13 - 3.05 (m, 2H, CH<sub>2</sub>), 2.42 (s, 3H, CH<sub>3</sub>), 2.27 (s, 3H, CH<sub>3</sub>), 2.24 (s, 3H, CH<sub>3</sub>) ppm.

MS(ESI<sup>+</sup>): m/z = 390.10 ([M+H], 100).

***tert*-butyl (2-(4-(2-(5-(3,5-dimethylisoxazol-4-yl)-2-(4-methylphenethyl)-1H-benzo [d]imidazo-1-yl)acetamido)benzamido)phenyl)carbamate (**94**)**

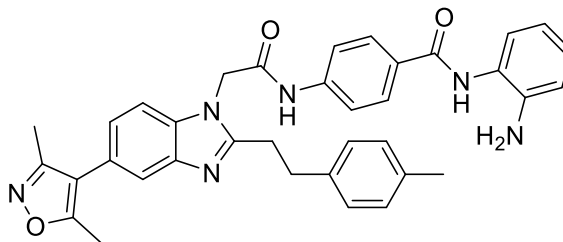


Reaction was performed according to general procedure C with **93** (180 mg, 0.46 mmol, 1 eq) and **42** (182 mg, 0.55 mmol, 1.2 eq). Crude product was purified via reverse flash chromatography with a gradient of ACN/H<sub>2</sub>O (after 2 CVs increased linear from 10:90 to 100:0 over 10 CVs) as a mobile phase to obtain **94** as a colorless solid (98 mg, 30 %).

R<sub>f</sub>(DCM/MeOH = 95:5) = 0.52.

<sup>1</sup>H-NMR (250 MHz, DMSO-*d*<sub>6</sub>): δ = 10.81 (s, 1H, NH), 9.76 (s, 1H, NH), 8.67 (s, 1H, NH), 7.95 (d, J = 8.4 Hz, 2H, CH<sub>ar</sub>), 7.74 (d, J = 8.5 Hz, 2H, CH<sub>ar</sub>), 7.62 - 7.46 (m, 4H, CH<sub>ar</sub>), 7.24 - 7.15 (m, 5H, CH<sub>ar</sub>), 7.09 (d, J = 7.9 Hz, 2H, CH<sub>ar</sub>), 5.20 (s, 2H, CH<sub>2</sub>), 3.13 (s, 4H, 2xCH<sub>2</sub>), 2.41 (s, 3H, CH<sub>3</sub>), 2.25 (s, 3H, CH<sub>3</sub>), 2.24 (s, 3H, CH<sub>3</sub>), 1.43 (s, 9H, C(CH<sub>3</sub>)<sub>3</sub>) ppm.

MS(ESI<sup>+</sup>): m/z = 699.37 ([M+H], 100).

***N*-(2-aminophenyl)-4-(2-(5-(3,5-dimethylisoxazol-4-yl)-2-(4-methylphenethyl)-1H-benzo [d] imidazole-1-yl)acetamido)benzamide (22)**

Reaction was performed according to general procedure E with **94** (98 mg, 0.14 mmol, 1 eq) DCM and TFA (20 % of total volume of 12.5 mL). Crude product was purified via reverse flash chromatography with a gradient of ACN/H<sub>2</sub>O (after 2 CVs increased linear from 10:90 to 100:0 over 10 CVs) as a mobile phase to obtain **22** as a colorless solid (64 mg, 76 %).

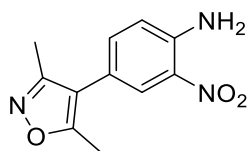
$R_f(\text{DCM/MeOH} = 95:5) = 0.81$

<sup>1</sup>H-NMR (500 MHz, DMSO-*d*<sub>6</sub>):  $\delta = 10.78$  (s, 1H, NH), 9.59 (s, 1H, NH), 7.98 (d,  $J = 8.5$  Hz, 2H, CH<sub>ar</sub>), 7.72 (d,  $J = 8.8$  Hz, 2H, CH<sub>ar</sub>), 7.62 - 7.56 (m, 2H, CH<sub>ar</sub>), 7.22 - 7.18 (m, 3H, CH<sub>ar</sub>), 7.15 (d,  $J = 7.9$  Hz, 1H, CH<sub>ar</sub>), 7.09 (d,  $J = 7.8$  Hz, 2H, CH<sub>ar</sub>), 6.96 (td,  $J = 7.6, 1.6$  Hz, 1H, CH<sub>ar</sub>), 6.78 (dd,  $J = 8.0, 1.5$  Hz, 1H, CH<sub>ar</sub>), 6.59 (td,  $J = 7.6, 1.5$  Hz, 1H, CH<sub>ar</sub>), 5.20 (s, 2H, CH<sub>2</sub>), 4.88 (s, 2H, NH<sub>2</sub>), 3.13 (d,  $J = 1.9$  Hz, 4H, 2xCH<sub>2</sub>), 2.41 (s, 3H, CH<sub>3</sub>), 2.26 (s, 3H, CH<sub>3</sub>), 2.24 (s, 3H, CH<sub>3</sub>) ppm.

<sup>13</sup>C-NMR (126 MHz, DMSO-*d*):  $\delta = 165.99, 164.60, 158.41, 156.00, 143.16, 142.53, 141.24, 137.98, 135.21, 134.99, 129.51, 128.92, 128.86, 128.24, 126.69, 126.43, 123.41, 123.02, 122.96, 118.99, 118.43, 116.70, 116.28, 116.15, 110.14, 46.21, 32.21, 28.54, 20.65, 11.30, 10.54$  ppm.

MS(ESI<sup>+</sup>):  $m/z = 599.37$  ([M+H], 100).

HRMS (MALDI):  $m/z$  calculated 599.27652 for C<sub>36</sub>H<sub>35</sub>N<sub>6</sub>O<sub>3</sub>, found 599.272650.

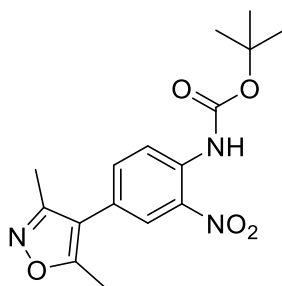
**4-(3,5-dimethylisoxazol-4-yl)-2-nitroaniline (96)**

Compound **64** (300 mg, 1.3 mmol, 1 eq) was dissolved in EtOH (15 mL) and ammonia solution (25 % in H<sub>2</sub>O, 15 mL) and stirred at 75 °C overnight. Solvent was removed under reduced pressure and crude product was purified via flash chromatography with a gradient of hexane/EtOAc (after 3 CVs increased linear from 70:30 to 40:60 over 7 CVs and held for 2 CVs) as a mobile phase to obtain **96** as an orange solid (289 mg, > 95 %).

R<sub>f</sub>(hexane/EtOAc = 7:3) = 0.24.

<sup>1</sup>H-NMR (250 MHz, DMSO-*d*<sub>6</sub>): δ = 7.89 (d, J = 2.1 Hz, 1H, CH<sub>ar</sub>), 7.53 (s, 2H, NH<sub>2</sub>), 7.44 (dd, J = 8.8, 2.1 Hz, 1H, CH<sub>ar</sub>), 7.11 (d, J = 8.8 Hz, 1H, CH<sub>ar</sub>), 2.38 (s, 3H, CH<sub>3</sub>), 2.20 (s, 3H, CH<sub>3</sub>) ppm.

MS(ESI<sup>+</sup>): m/z 234 ([M+H])

***tert*-butyl (4-(3,5-dimethylisoxazol-4-yl)-2-nitrophenyl)carbamate (97)****First reaction path**

Compound **96** (357 mg, 1.5 mmol, 1 eq) was dissolved in DCM (15 mL) and Boc<sub>2</sub>O (668 mg, 3.1 mmol, 2 eq), DIPEA (0.42 mL, 3.1 mmol, 2 eq) and a small crystal of DMAP (20 mg, 0.15 mmol, 0.1 eq) were added. Mixture was stirred under reflux overnight and then was allowed to cool, partitioned between EtOAc and HCl solution (10 %). The phases were separated, and the organic phase was washed with brine and dried over MgSO<sub>4</sub>. Crude product was purified via flash chromatography with a gradient of hexane/EtOAc (after 2 CVs increased linear from 100:0 to 50:50 over 12 CVs and held for 3 CVs) as a mobile phase to obtain **97** as



an orange solid (130 mg, 25 %). Main product was the double protected form **119** (507 mg, 76 %).

### Second reaction path

Compound **96** (291 mg, 1.2 mmol, 1 eq) was dissolved in DCM (15 mL) and Boc<sub>2</sub>O (354 mg, 1.6 mmol, 1.3 eq), DIPEA (0.24 mL, 1.5 mmol, 1.2 eq) and a small crystal of DMAP (15 mg, 0.12 mmol, 0.1 eq) were added. Mixture was stirred under reflux overnight and then was allowed to cool, partitioned between EtOAc and HCl solution (10 %). The phases were separated, and the organic phase was washed with brine and dried over MgSO<sub>4</sub>. Crude product was purified via flash chromatography with a gradient of hexane/EtOAc (after 2 CVs increased linear from 100:0 to 50:50 over 12 CVs and held for 3 CVs) as a mobile phase to obtain **97** as an orange solid (190 mg, 45 %). Side product was the double protected form **119** (150 mg, 28 %). Starting material in form of **96** could also be regained (40 mg, 14 %)

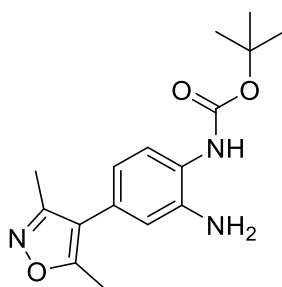
### Third reaction path

A solution of NaH (60 % in mineral oil, 188 mg, 4.9 mmol, 2.2 eq) in THF (20 mL) at 0 °C was slowly treated with a solution of **96** (521 mg, 2.2 mmol, 1 eq) in THF (20 mL). The solution was stirred at 0 °C for 10 minutes followed by 30 minutes at RT. A solution of Boc<sub>2</sub>O (585 mg, 2.7 mmol, 1.2) in THF (5 mL) was added and mixture was stirred for 1 h. Ice-cold water (35 mL) was slowly added, and reaction mixture was extracted with EtOAc. Organic phase was washed with brine and dried over MgSO<sub>4</sub>. Crude product was purified via flash chromatography with hexane/EtOAc (85:15 over 10 CVs) as a mobile phase to obtain **97** as an orange solid (586 mg, 79 %).

$R_f(\text{hexane/MeOH} = 75:15) = 0.38$

<sup>1</sup>H-NMR (250 MHz, DMSO-*d*<sub>6</sub>): δ = 9.68 (s, 1H, NH), 7.92 (d, J = 1.7 Hz, 1H, CH<sub>ar</sub>), 7.78 - 7.63 (m, 2H, CH<sub>ar</sub>), 2.42 (s, 3H, CH<sub>3</sub>), 2.24 (s, 3H, CH<sub>3</sub>), 1.46 (s, 9H, C(CH<sub>3</sub>)<sub>3</sub>) ppm.

MS(ESI-): m/z 332.18 ([M-H], 100)

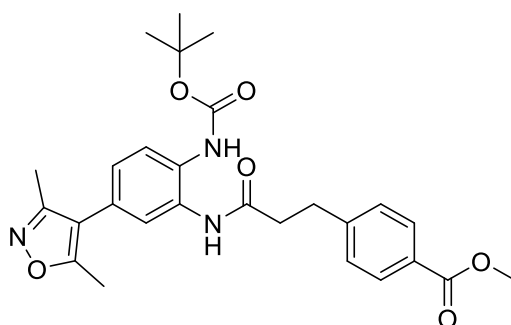
***tert*-butyl (2-amino-4-(3,5-dimethylisoxazol-4-yl)phenyl)carbamate (**98**)**

Compound **97** (566 mg, 1.7 mmol, 1 eq) was reduced according to General procedure B1. Product was purified via flash chromatography with a gradient of hexane/EtOAc (after 4.5 CV increased linear from 60:40 to 30:70 over 7 CVs and held for 5 CVs) as mobile phase to obtain **98** as a colorless solid (410 mg, 80 %).

$R_f$ (hexane/EtOAc = 50:50) = 0.52

$^1\text{H-NMR}$  (250 MHz,  $\text{DMSO-}d_6$ ):  $\delta$  = 8.35 (s, 1H, NH), 7.28 (d,  $J$  = 8.1 Hz, 1H,  $\text{CH}_{\text{ar}}$ ), 6.68 (d,  $J$  = 2.0 Hz, 1H,  $\text{CH}_{\text{ar}}$ ), 6.51 (dd,  $J$  = 8.1, 2.0 Hz, 1H,  $\text{CH}_{\text{ar}}$ ), 4.96 (s, 2H,  $\text{NH}_2$ ), 2.37 (s, 3H,  $\text{CH}_3$ ), 2.19 (s, 3H,  $\text{CH}_3$ ), 1.47 (s, 9H,  $\text{C}(\text{CH}_3)_3$ ) ppm.

MS(ESI<sup>+</sup>): not measurable

**Methyl 4-(3-((2-((*tert*-butoxycarbonyl)amino)-5-(3,5-dimethylisoxazol-4-yl)phenyl)amino)-3-oxopropyl)benzoate (**99**)**

Compound **98** (158 mg, 0.52 mmol, 1 eq) was reacted with 3-(4-methoxycarbonylphenyl) propanoic acid **120** (130 mg, 0.63 mmol, 1.2 eq) according to general procedure C. Crude product was purified via flash chromatography with a gradient of hexane/EtOAc (after 3 CVs increased linear from 60:40 to 40:60 over 5 CVs and held for 7 CVs) to obtain **99** as a colorless solid (207 mg, 81 %).

$R_f$ (hexane/EtOAc = 50:50) = 0.41

<sup>1</sup>H-NMR (250 MHz, DMSO-*d*<sub>6</sub>): δ = 9.49 (s, 1H, NH), 8.44 (s, 1H, NH), 7.89 (d, J = 8.2 Hz, 2H, CH<sub>ar</sub>), 7.65 (d, J = 8.4 Hz, 1H, CH<sub>ar</sub>), 7.46 - 7.34 (m, 3H, CH<sub>ar</sub>), 7.14 (dd, J = 8.4, 2.1 Hz, 1H, CH<sub>ar</sub>), 3.83 (s, 3H, CH<sub>3</sub>), 3.02 (t, J = 7.3 Hz, 2H, CH<sub>2</sub>), 2.78 - 2.68 (m, 2H, CH<sub>2</sub>), 2.38 (s, 3H, CH<sub>3</sub>), 2.20 (s, 3H, CH<sub>3</sub>), 1.47 (s, 9H, C(CH<sub>3</sub>)<sub>3</sub>) ppm.

MS(ESI<sup>+</sup>): m/z 516.19 ([M+Na], 100)

**4-(2-(5-(3,5-dimethylisoxazol-4-yl)-1H-benzo[d]imidazol-2-yl)ethyl)benzoic acid (100) and methyl 4-(2-(5-(3,5-dimethylisoxazol-4-yl)-1H-benzo[d]imidazol-2-yl)ethyl)benzoate (101)**



Compound **99** (600 mg, 1.22 mmol, 1 eq) was converted according to general procedure D for 30 minutes. Solvents were removed under reduced pressure and remaining residue was resolved in water, neutralized with sat. NaHCO<sub>3</sub> solution and extracted with EtOAc. The organic phase was washed with brine and dried over MgSO<sub>4</sub>. Crude product was purified via reversed flash chromatography with a gradient of ACN/H<sub>2</sub>O (after 2 CVs increased linear from 10:90 to 100:0 over 10 CVs) as a mobile phase to obtain **100** (188 mg, 42 %) and **101** (65 mg, 14 %) as colorless solids.

R<sub>f</sub>(DCM/MeOH = 95:5) = 0.23

<sup>1</sup>H-NMR (250 MHz, DMSO-*d*<sub>6</sub>): δ = 12.80 (s, 1H, COOH), 12.35 (s, 1H, NH), 7.86 (d, J = 8.2 Hz, 2H, CH<sub>ar</sub>), 7.55 (d, J = 8.0 Hz, 1H, CH<sub>ar</sub>), 7.47 - 7.31 (m, 3H, CH<sub>ar</sub>), 7.10 (dd, J = 8.2, 1.6 Hz, 1H, CH<sub>ar</sub>), 3.19 (bs, 4H, 2xCH<sub>2</sub>), 2.39 (s, 3H, CH<sub>3</sub>), 2.22 (s, 3H, CH<sub>3</sub>) ppm.

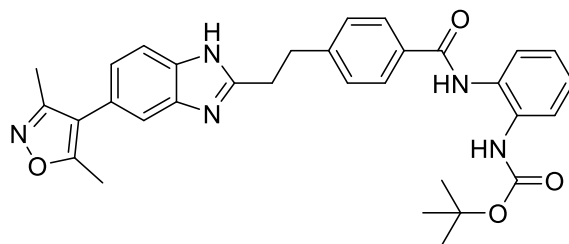
MS(ESI<sup>+</sup>): m/z 362.07 ([M+H], 100)

R<sub>f</sub>(DCM/MeOH = 95:5) = 0.46

<sup>1</sup>H-NMR (250 MHz, DMSO-*d*<sub>6</sub>): δ = 12.33 (s, 1H, NH), 7.88 (d, J = 8.1 Hz, 2H, CH<sub>ar</sub>), 7.65 - 7.36 (m, 4H, CH<sub>ar</sub>), 7.09 (ddd, J = 8.2, 5.3, 1.4 Hz, 1H, CH<sub>ar</sub>), 3.83 (s, 3H, OCH<sub>3</sub>), 3.28 - 3.11 (m, 4H, 2xCH<sub>2</sub>), 2.39 (s, 3H, CH<sub>3</sub>), 2.22 (s, 3H, CH<sub>3</sub>) ppm.

MS(ESI<sup>+</sup>): m/z 376.17 ([M+H], 100)

***tert*-butyl (2-(4-(2-(5-(3,5-dimethylisoxazol-4-yl)-1H-benzo[d]imidazol-2-yl)ethyl)benzamido)phenyl)carbamate (121)**



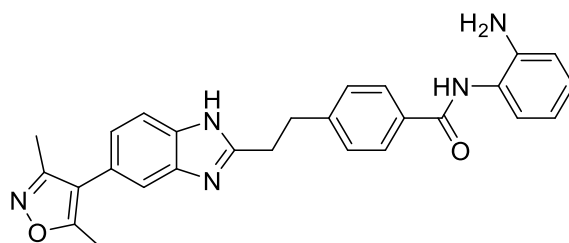
Compound **100** (181 mg, 0.5 mmol, 1 eq) was reacted with **39** (114 mg, 0.55 mmol, 1.1 eq) according to general procedure C. Product was purified via flash chromatography with a gradient of DCM/MeOH (after 3 CVs increased linear from 100:0 to 95:5 over 8 CVs and held for 5 CVs) as mobile phase to obtain **121** as a colorless solid (230 mg, 83 %).

$R_f(\text{DCM/MeOH} = 95:5) = 0.46$

$^1\text{H-NMR}$  (250 MHz,  $\text{DMSO-}d_6$ ):  $\delta = 12.36$  (s, 1H, NH), 9.75 (s, 1H, NH), 8.65 (s, 1H, NH), 7.92 - 7.80 (m, 2H,  $\text{CH}_{\text{ar}}$ ), 7.60 - 7.38 (m, 6H,  $\text{CH}_{\text{ar}}$ ), 7.25 - 7.02 (m, 3H,  $\text{CH}_{\text{ar}}$ ), 3.22 (s, 4H,  $2 \times \text{CH}_2$ ), 2.40 (s, 3H,  $\text{CH}_3$ ), 2.23 (s, 3H,  $\text{CH}_3$ ), 1.43 (s, 9H,  $\text{C}(\text{CH}_3)_3$ ) ppm.

MS(ESI<sup>+</sup>):  $m/z$  552.22 ( $[\text{M}+\text{H}]$ , 35)

***N*-(2-aminophenyl)-4-(2-(5-(3,5-dimethylisoxazol-4-yl)-1H-benzo[d]imidazol-2-yl) ethyl) benzamide (25)**



Reaction was performed according to general procedure E with **121** (20 mg, 0.04 mmol, 1 eq) DCM and TFA (20 % of total volume of 3.6 mL). Crude product was purified via reverse flash chromatography with a gradient of ACN/ $\text{H}_2\text{O}$  (after 2 CVs increased linear from 10:90 to 100:0 over 10 CVs) as a mobile phase to obtain **25** as a colorless solid (16 mg, > 95 %).

$R_f(\text{DCM/MeOH}) = 0.10$

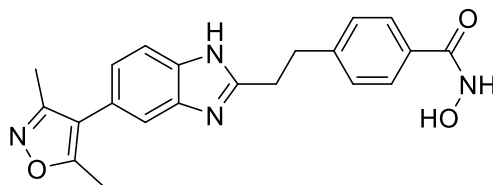
<sup>1</sup>H-NMR (500 MHz, DMSO-*d*<sub>6</sub>): δ = 10.22 (s, 1H, NH), 8.03 (d, J = 8.0 Hz, 2H, CH<sub>ar</sub>), 7.86 (d, J = 8.4 Hz, 1H, CH<sub>ar</sub>), 7.75 (s, 1H, CH<sub>ar</sub>), 7.49 (m, 3H, CH<sub>ar</sub>), 7.42 (d, J = 7.5 Hz, 1H, CH<sub>ar</sub>), 7.26 - 7.17 (m, 2H, CH<sub>ar</sub>), 7.11 (t, J = 6.8 Hz, 1H, CH<sub>ar</sub>), 3.55 (t, J = 7.6 Hz, 2H, CH<sub>2</sub>), 3.38 (t, J = 7.5 Hz, 2H, CH<sub>2</sub>), 2.42 (s, 3H, CH<sub>3</sub>), 2.24 (s, 3H, CH<sub>3</sub>) ppm.

<sup>13</sup>C-NMR (126 MHz, DMSO-*d*<sub>6</sub>): δ = 165.55, 165.24, 158.18, 154.10, 143.30, 132.29, 131.47, 130.40, 128.35, 128.21, 127.20, 127.05, 126.59, 126.50, 115.50, 114.22, 113.97, 31.75, 27.65, 11.29, 10.40 ppm.

MS(ESI<sup>+</sup>): m/z = 452.26 ([M+H], 65).

HRMS (MALDI): m/z calculated 452.20810 for C<sub>27</sub>H<sub>26</sub>N<sub>5</sub>O<sub>3</sub>, found 452.20782.

**4-(2-(5-(3,5-dimethylisoxazol-4-yl)-1H-benzo[d]imidazol-2-yl)ethyl)-N-hydroxybenzamide (26)**



Compound **101** (65 mg, 0.173 mmol, 1 eq) was reacted according to general procedure F. Crude product was purified via reversed flash chromatography with a gradient of ACN/H<sub>2</sub>O (after 2 CVs increased linear from 10:90 to 100:0 over 10 CVs) to obtain **26** as a light grey solid (20 mg, 31 %).

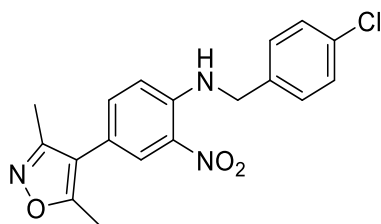
R<sub>f</sub>(DCM/MeOH = 95:5) = 0.14

<sup>1</sup>H-NMR (500 MHz, DMSO-*d*<sub>6</sub>): δ = 12.34 (double s, 1H, NH), 11.13 (s, 1H, OH), 8.97 (s, 1H, NH), 7.67 (d, J = 8.2 Hz, 2H, CH<sub>ar</sub>), 7.62 - 7.37 (m, 2H, CH<sub>ar</sub>), 7.35 (d, J = 8.3 Hz, 2H, CH<sub>ar</sub>), 7.09 (t, J = 8.2 Hz, 1H, CH<sub>ar</sub>), 3.21 - 3.13 (m, 4H, 2xCH<sub>2</sub>), 2.39 (s, 3H, CH<sub>3</sub>), 2.22 (s, 3H, CH<sub>3</sub>) ppm.

<sup>13</sup>C-NMR (126 MHz, DMSO-*d*<sub>6</sub>): δ = 164.14, 158.33, 155.06, 144.30, 130.66, 128.24, 126.97, 122.70, 122.19, 118.65, 118.36, 116.78, 116.71, 111.22, 111.06, 32.94, 29.88, 11.28, 10.51 ppm.

MS(ESI<sup>+</sup>): m/z 377.16 ([M+H], 100)

HRMS (MALDI): m/z calculated 377.16082 for C<sub>21</sub>H<sub>21</sub>N<sub>4</sub>O<sub>3</sub>, found 377.16102.

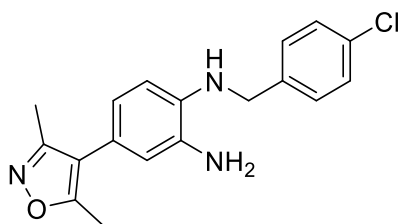
***N*-(4-chlorobenzyl)-4-(3,5-dimethylisoxazol-4-yl)-2-nitroaniline (102)**

Compound **63** (1036 mg, 4.3 mmol, 1 eq) was reacted with (4-chlorophenyl)methanamine **122** (1.1 mL, 8.7 mmol, 2 eq) according to general procedure A. For purification product was recrystallized from hexane/EtOAc to obtain product as a bright orange solid (1034 mg, 66 %).

$R_f$ (hexane/EtOAc = 70:30) = 0.52.

$^1\text{H}$ -NMR (250 MHz, DMSO- $d_6$ ):  $\delta$  = 8.77 (t,  $J$  = 6.2 Hz, 1H, NH), 8.02 (d,  $J$  = 2.1 Hz, 1H, CH<sub>ar</sub>), 7.49 (dd,  $J$  = 8.9, 2.2 Hz, 1H, CH<sub>ar</sub>), 7.42 (s, 4H, CH<sub>ar</sub>), 6.96 (d,  $J$  = 9.0 Hz, 1H, CH<sub>ar</sub>), 4.66 (d,  $J$  = 6.2 Hz, 2H, CH<sub>2</sub>), 2.36 (s, 3H, CH<sub>3</sub>), 2.18 (s, 3H, CH<sub>3</sub>) ppm.

MS(ESI+) =  $m/z$  358.04 ([M+H], 40)

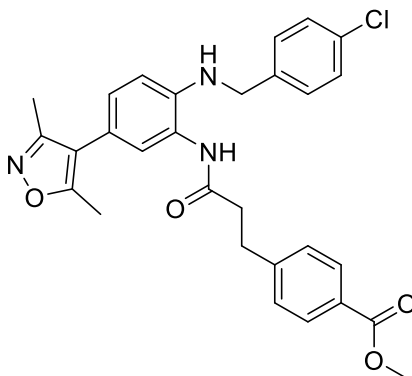
***N*<sup>1</sup>-(4-chlorobenzyl)-4-(3,5-dimethylisoxazol-4-yl)benzene-1,2-diamine (106)**

Compound **102** (632 mg, 1.77 mmol, 1 eq) was reacted with SnCl<sub>2</sub>·H<sub>2</sub>O (1.59 g, 7.07 mmol, 4 eq) according to general procedure B2. Crude product was purified via flash chromatography with a gradient of hexane/EtOAc (after 3 CVs increased linear from 75:25 to 40:60 over 5 CVs and held for 3 CVs) to obtain **106** as a light yellow solid (540 mg, 93 %).

$R_f$ (hexane/EtOAc) = 0.42

$^1\text{H}$ -NMR (250 MHz, DMSO- $d_6$ ):  $\delta$  = 7.40 (s, 4H, CH<sub>ar</sub>), 6.56 (d,  $J$  = 1.8 Hz, 1H, CH<sub>ar</sub>), 6.42 - 6.31 (m, 2H, CH<sub>ar</sub>), 5.34 (t,  $J$  = 5.8 Hz, 1H, NH), 4.70 (s, 2H, NH<sub>2</sub>), 4.32 (d,  $J$  = 5.8 Hz, 2H, CH<sub>2</sub>), 2.31 (s, 3H, CH<sub>3</sub>), 2.15 (s, 3H, CH<sub>3</sub>) ppm.

MS(ESI+) =  $m/z$  358.07 ([M+H], 100)

**Methyl 4-(3-((2-((4-chlorobenzyl)amino)-5-(3,5-dimethylisoxazol-4-yl)phenyl)amino)-3-oxopropyl)benzoate (110)**

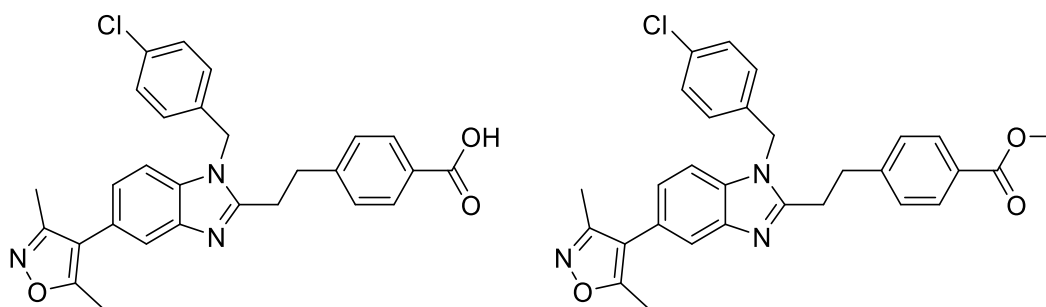
Compound **106** (131 mg, 0.4 mmol, 1 eq) was reacted with 3-(4-(methoxycarbonyl)phenyl)propanoic acid **120** (100 mg, 0.48 mmol, 1.2 eq) according to general procedure C. Crude product was purified via flash chromatography with a gradient of hexane/EtOAc (after 2 CVs increased linear from 60:40 to 30:70 over 6 CVs and held for 5 CVs) as mobile phase to obtain **110** as a colorless solid (144 mg, 70 %).

$R_f(\text{hexane/EtOAc} = 40:60) = 0.42$

$^1\text{H-NMR}$  (250 MHz,  $\text{DMSO-}d_6$ ):  $\delta = 9.24$  (s, 1H, NH), 7.88 (d,  $J = 8.3$  Hz, 2H,  $\text{CH}_{\text{ar}}$ ), 7.43 (d,  $J = 8.3$  Hz, 2H,  $\text{CH}_{\text{ar}}$ ), 7.38 (s, 4H,  $\text{CH}_{\text{ar}}$ ), 7.05 (d,  $J = 2.0$  Hz, 1H,  $\text{CH}_{\text{ar}}$ ), 6.93 (dd,  $J = 8.4, 2.1$  Hz, 1H,  $\text{CH}_{\text{ar}}$ ), 6.50 (d,  $J = 8.4$  Hz, 1H,  $\text{CH}_{\text{ar}}$ ), 5.65 (t,  $J = 5.9$  Hz, 1H, NH), 4.33 (d,  $J = 5.9$  Hz, 2H,  $\text{CH}_2$ ), 3.82 (s, 3H,  $\text{OOCH}_3$ ), 3.02 (t,  $J = 7.5$  Hz, 2H,  $\text{CH}_2$ ), 2.73 (t,  $J = 7.5$  Hz, 2H,  $\text{CH}_2$ ), 2.32 (s, 3H,  $\text{CH}_3$ ), 2.15 (s, 3H,  $\text{CH}_3$ ) ppm.

$\text{MS}(\text{ESI}^+) = m/z 540.25$  ( $[\text{M}+\text{Na}]$ , 100)

**4-(2-(1-(4-chlorobenzyl)-5-(3,5-dimethylisoxazol-4-yl)-1H-benzo[d]imidazol-2-yl)ethyl)-benzoic acid (114) and methyl 4-(2-(1-(4-chlorobenzyl)-5-(3,5-dimethylisoxazol-4-yl)-1H-benzo[d]imidazol-2-yl)ethyl)benzoate (118)**



Compound **110** (250 mg, 0.482 mmol, 1 eq) was converted according to general procedure D for 1 hour. Crude product was purified via reversed flash chromatography with a gradient of DCM/MeOH (after 2 CVs increased linear from 99:1 to 90:10 over 8 CVs and held for 3 CVs) as a mobile phase to obtain **114** (135 mg, 58 %) and **118** (100 mg, 41 %) as colorless solids.

$R_f(\text{DCM/MeOH} = 90:10) = 0.40$

$^1\text{H-NMR}$  (500 MHz,  $\text{DMSO-}d_6$ ):  $\delta = 12.78$  (s, 1H, OH), 7.84 (d,  $J = 8.3$  Hz, 2H,  $\text{CH}_{\text{ar}}$ ), 7.62 - 7.61 (m, 1H,  $\text{CH}_{\text{ar}}$ ), 7.54 (d,  $J = 8.1$  Hz, 1H,  $\text{CH}_{\text{ar}}$ ), 7.40 - 7.35 (m, 4H,  $\text{CH}_{\text{ar}}$ ), 7.16 (dd,  $J = 8.3$ , 1.6 Hz, 1H,  $\text{CH}_{\text{ar}}$ ), 7.13 (d,  $J = 8.6$  Hz, 2H,  $\text{CH}_{\text{ar}}$ ), 5.52 (s, 2H,  $\text{CH}_2$ ), 3.20 (s, 4H,  $2 \times \text{CH}_2$ ), 2.40 (s, 3H,  $\text{CH}_3$ ), 2.23 (s, 3H,  $\text{CH}_3$ ) ppm.

MS(ESI<sup>+</sup>):  $m/z$  486.23 ( $[\text{M}+\text{H}]$ , 100)

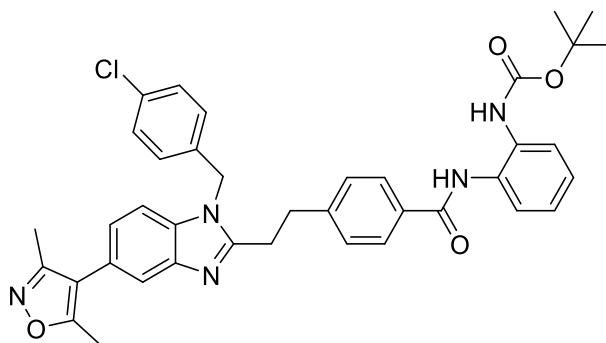
$R_f(\text{DCM/MeOH} = 95:5) = 0.73$

$^1\text{H-NMR}$  (500 MHz,  $\text{DMSO-}d_6$ ):  $\delta = 7.85$  (d,  $J = 8.4$  Hz, 2H,  $\text{CH}_{\text{ar}}$ ), 7.62 - 7.60 (m, 1H,  $\text{CH}_{\text{ar}}$ ), 7.54 (d,  $J = 8.3$  Hz, 1H,  $\text{CH}_{\text{ar}}$ ), 7.40 (d,  $J = 8.4$  Hz, 2H,  $\text{CH}_{\text{ar}}$ ), 7.37 (d,  $J = 8.5$  Hz, 2H,  $\text{CH}_{\text{ar}}$ ), 7.16 (dd,  $J = 8.3$ , 1.6 Hz, 1H,  $\text{CH}_{\text{ar}}$ ), 7.12 (d,  $J = 8.6$  Hz, 2H,  $\text{CH}_{\text{ar}}$ ), 5.52 (s, 2H,  $\text{CH}_2$ ), 3.83 (s, 3H,  $\text{OOCCH}_3$ ), 3.21 (s, 4H,  $2 \times \text{CH}_2$ ), 2.40 (s, 3H,  $\text{CH}_3$ ), 2.23 (s, 3H,  $\text{CH}_3$ ) ppm.

MS(ESI<sup>+</sup>) =  $m/z$  500.25 ( $[\text{M}+\text{H}]$ , 100)



***tert*-butyl (2-(4-(2-(1-(4-chlorobenzyl)-5-(3,5-dimethylisoxazol-4-yl)-1H-benzo[d]imidazole-2-yl)ethyl)benzamido)phenyl)carbamate (**124**)**



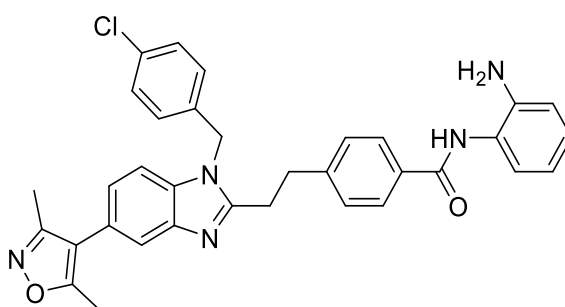
Compound **114** (61 mg, 0.125 mmol, 1 eq) was reacted with **39** (31 mg, 0.15 mmol, 1.2 eq) according to general procedure C. Product was purified via reverse flash chromatography with a gradient of ACN/H<sub>2</sub>O (after 2 CVs increased linear from 10:90 to 100:0 over 10 CVs) to obtain **124** as a colorless solid (40 mg, 47 %).

R<sub>f</sub>(DCM/MeOH = 99:1) = 0.66

<sup>1</sup>H-NMR (250 MHz, DMSO-*d*<sub>6</sub>): δ = 9.76 (s, 1H, NH), 8.66 (s, 1H, NH), 7.85 (d, J = 8.1 Hz, 2H, CH<sub>ar</sub>), 7.63 (s, 1H, CH<sub>ar</sub>), 7.55 (d, J = 8.1 Hz, 3H, CH<sub>ar</sub>), 7.40 (t, J = 8.2 Hz, 4H, CH<sub>ar</sub>), 7.21 - 7.10 (m, 5H, CH<sub>ar</sub>), 5.53 (s, 2H, CH<sub>2</sub>), 3.22 (s, 4H, 2xCH<sub>2</sub>), 2.40 (s, 3H, CH<sub>3</sub>), 2.23 (s, 3H, CH<sub>3</sub>), 1.42 (s, 9H, C(CH<sub>3</sub>)<sub>3</sub>) ppm.

MS(ESI+) = 676.38 ([M+H], 100)

***N*-(2-aminophenyl)-4-(2-(1-(4-chlorobenzyl)-5-(3,5-dimethylisoxazol-4-yl)-1H-benzo[d]imidazol-2-yl)ethyl)benzamide (**27**)**



Reaction was performed according to general procedure E with **124** (37 mg, 0.054 mmol, 1 eq) DCM and TFA (20 % of total volume of 3.6 mL). Crude product was purified via reverse flash

chromatography with a gradient of ACN/H<sub>2</sub>O (after 2 CVs increased linear from 10:90 to 100:0 over 10 CVs) as a mobile phase to obtain **27** as a colorless solid (25 mg, 79 %).

$R_f(\text{DCM/MeOH} = 95:5) = 0.47$

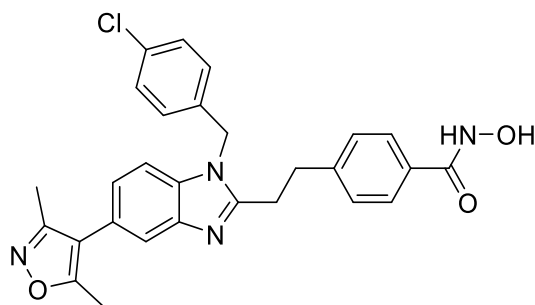
<sup>1</sup>H-NMR (500 MHz, DMSO-*d*<sub>6</sub>):  $\delta = 9.60$  (s, 1H, NH), 7.89 (d,  $J = 7.9$  Hz, 2H, CH<sub>ar</sub>), 7.63 (d,  $J = 1.5$  Hz, 1H), 7.54 (d,  $J = 8.3$  Hz, 1H, CH<sub>ar</sub>), 7.42 - 7.36 (m, 4H, CH<sub>ar</sub>), 7.19 - 7.11 (m, 4H, CH<sub>ar</sub>), 6.97 (td,  $J = 7.6, 1.5$  Hz, 1H, CH<sub>ar</sub>), 6.78 (dd,  $J = 8.1, 1.4$  Hz, 1H, CH<sub>ar</sub>), 6.60 (td,  $J = 7.5, 1.4$  Hz, 1H, CH<sub>ar</sub>), 5.53 (s, 2H, CH<sub>2</sub>), 4.91 (s, 2H, NH<sub>2</sub>), 3.21 (s, 4H, 2xCH<sub>2</sub>), 2.40 (s, 3H, CH<sub>3</sub>), 2.23 (s, 3H, CH<sub>3</sub>) ppm.

<sup>13</sup>C-NMR (126 MHz, DMSO-*d*<sub>6</sub>):  $\delta = 165.10, 164.61, 158.34, 155.07, 144.59, 143.08, 142.59, 135.99, 134.63, 132.48, 132.15, 128.77, 128.59, 128.29, 127.83, 126.66, 126.42, 123.39, 123.20, 123.07, 119.02, 116.54, 116.27, 116.13, 110.51, 45.44, 32.36, 28.02, 11.31, 10.53$  ppm.

MS(ESI<sup>+</sup>):  $m/z$  576.29 ([M+H], 100)

HRMS (MALDI):  $m/z$  calculated 576.21608 for C<sub>34</sub>H<sub>31</sub>ClN<sub>5</sub>O<sub>2</sub>, found 576.21539.

**4-(2-(1-(4-chlorobenzyl)-5-(3,5-dimethylisoxazol-4-yl)-1H-benzo[d]imidazol-2-yl)ethyl)-*N*-hydroxybenzamide (31)**



Compound **118** (100 mg, 0.2 mmol, 1 eq) was reacted according to general procedure F. Crude product was purified via reversed flash chromatography with a gradient of ACN/H<sub>2</sub>O (after 2 CVs increased linear from 10:90 to 100:0 over 10 CVs) to obtain **31** as a colorless solid (75 mg, 75 %).

$R_f(\text{DCM/MeOH} = 95:5) = 0.38$

<sup>1</sup>H-NMR (500 MHz, DMSO-*d*<sub>6</sub>):  $\delta = 7.66$  (d,  $J = 8.2$  Hz, 2H, CH<sub>ar</sub>), 7.61 (d,  $J = 1.2$  Hz, 1H, CH<sub>ar</sub>), 7.53 (d,  $J = 8.3$  Hz, 1H, CH<sub>ar</sub>), 7.38 (d,  $J = 8.5$  Hz, 2H, CH<sub>ar</sub>), 7.34 (d,  $J = 8.2$  Hz, 2H,

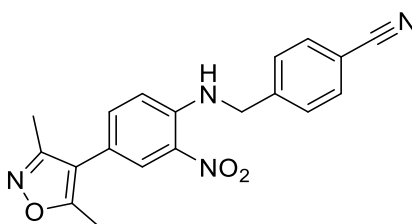
$^1\text{H-NMR}$  (400 MHz,  $\text{DMSO-}d_6$ ):  $\delta$  = 7.16 (dd,  $J$  = 8.3, 1.5 Hz, 1H,  $\text{CH}_{\text{ar}}$ ), 7.13 (d,  $J$  = 8.5 Hz, 2H,  $\text{CH}_{\text{ar}}$ ), 5.52 (s, 2H,  $\text{CH}_2$ ), 3.18 (s, 4H,  $2 \times \text{CH}_2$ ), 2.40 (s, 3H,  $\text{CH}_3$ ), 2.23 (s, 3H,  $\text{CH}_3$ ) ppm.

$^{13}\text{C-NMR}$  (126 MHz,  $\text{DMSO-}d_6$ ):  $\delta$  = 165.08, 164.53, 158.82, 155.57, 144.76, 143.11, 136.48, 135.11, 132.63, 131.14, 129.24, 129.07, 128.85, 127.38, 123.65, 123.54, 119.52, 117.03, 110.96, 45.89, 32.79, 28.44, 11.79, 11.00 ppm.

MS(ESI<sup>+</sup>):  $m/z$  501.23 ( $[\text{M}+\text{H}]$ , 100)

HRMS (MALDI):  $m/z$  calculated 501.16879 for  $\text{C}_{28}\text{H}_{26}\text{ClN}_4\text{O}_3$ , found 501.16828.

#### 4-(((4-(3,5-dimethylisoxazol-4-yl)-2-nitrophenyl)amino)methyl)benzonitrile (**104**)

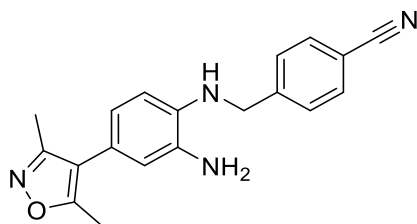


Compound **64** (500 mg, 2.12 mmol, 1 eq) was reacted with 4-(aminomethyl)benzonitrile hydrochloride (428 mg, 2.54 mmol, 1.2 eq) and DIPEA (0.86 mL, 5.08 mmol, 2.4 eq) according to general procedure A for 24 h. Crude product was purified via flash chromatography with a gradient of hexane/EtOAc (after 3 CVs increased linear from 70:30 to 40:60 over 5 CV and held for 2 CVs) to obtain **104** as a red solid (319 mg, 43 %).

$R_f$ (hexane/EtOAc = 40:60) = 0.31

$^1\text{H-NMR}$  (250 MHz,  $\text{DMSO-}d_6$ ):  $\delta$  = 8.83 (t,  $J$  = 6.3 Hz, 1H), 8.03 (d,  $J$  = 2.2 Hz, 1H,  $\text{CH}_{\text{ar}}$ ), 7.82 (d,  $J$  = 8.1 Hz, 2H,  $\text{CH}_{\text{ar}}$ ), 7.59 (d,  $J$  = 8.2 Hz, 2H,  $\text{CH}_{\text{ar}}$ ), 7.48 (dd,  $J$  = 8.9, 2.1 Hz, 1H,  $\text{CH}_{\text{ar}}$ ), 6.91 (d,  $J$  = 8.9 Hz, 1H,  $\text{CH}_{\text{ar}}$ ), 4.77 (d,  $J$  = 6.3 Hz, 2H,  $\text{CH}_2$ ), 2.36 (s, 3H,  $\text{CH}_3$ ), 2.18 (s, 3H,  $\text{CH}_3$ ) ppm.

MS(ESI<sup>+</sup>):  $m/z$  371.17 ( $[\text{M}+\text{Na}]$ , 50)

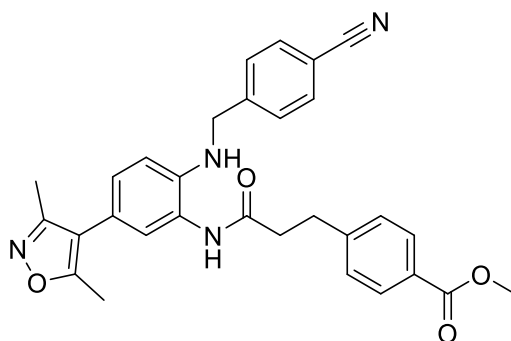
**4-(((2-amino-4-(3,5-dimethylisoxazol-4-yl)phenyl)amino)methyl)benzonitrile (108)**

Compound **104** (319 mg, 0.91 mmol, 1 eq) was reacted with  $\text{SnCl}_2 \cdot \text{H}_2\text{O}$  (1.03 g, 4.58 mmol, 5 eq) according to general procedure B2. Crude product was purified via flash chromatography with a gradient of hexane/EtOAc (after 3 CVs increased linear from 70:30 to 40:60 over 5 CV and held for 2 CVs) to obtain **108** as a colorless solid (238 mg, 81 %).

$R_f(\text{hexane/EtOAc} = 50:50) = 0.25$

$^1\text{H-NMR}$  (250 MHz,  $\text{DMSO-}d_6$ ):  $\delta = 7.80$  (d,  $J = 8.0$  Hz, 2H,  $\text{CH}_{\text{ar}}$ ),  $7.58$  (d,  $J = 8.1$  Hz, 2H,  $\text{CH}_{\text{ar}}$ ),  $6.57$  (d,  $J = 1.8$  Hz, 1H,  $\text{CH}_{\text{ar}}$ ),  $6.38$  (dd,  $J = 8.0, 1.8$  Hz, 1H,  $\text{CH}_{\text{ar}}$ ),  $6.30$  (d,  $J = 8.1$  Hz, 1H,  $\text{CH}_{\text{ar}}$ ),  $5.47$  (t,  $J = 5.8$  Hz, 1H, NH),  $4.71$  (s, 2H,  $\text{NH}_2$ ),  $4.43$  (d,  $J = 5.8$  Hz, 2H,  $\text{CH}_2$ ),  $2.31$  (s, 3H,  $\text{CH}_3$ ),  $2.14$  (s, 3H,  $\text{CH}_3$ ) ppm.

MS(ESI+):  $m/z$  315.07 ( $[\text{M}+\text{Na}-\text{CN}]$ , 100)

**Methyl 4-(3-((2-((4-cyanobenzyl)amino)-5-(3,5-dimethylisoxazol-4-yl)phenyl)amino)-3-oxopropyl)benzoate (112)**

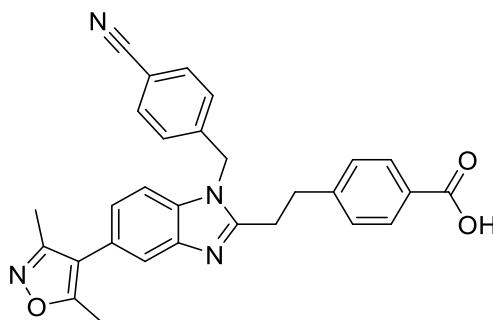
Compound **108** (238 mg, 0.74 mmol, 1 eq) was reacted with 3-(4-methoxycarbonylphenyl) propanoic acid **120** (186 mg, 0.9 mmol, 1.2 eq) according to general procedure C. Crude product was purified via flash chromatography with a gradient of DCM/MeOH (after 3 CVs increased linear from 99:1 to 95:5 over 5 CVs and held for 4 CVs) to obtain **112** as a colorless solid (220 mg, 58 %).

$R_f(\text{DCM}/\text{MeOH} = 95:5) = 0.71$

$^1\text{H-NMR}$  (250 MHz,  $\text{DMSO-}d_6$ ):  $\delta = 9.27$  (s, 1H, NH), 7.88 (d,  $J = 8.1$  Hz, 2H,  $\text{CH}_{\text{ar}}$ ), 7.79 (d,  $J = 8.1$  Hz, 2H,  $\text{CH}_{\text{ar}}$ ), 7.55 (d,  $J = 8.1$  Hz, 2H,  $\text{CH}_{\text{ar}}$ ), 7.43 (d,  $J = 8.1$  Hz, 2H,  $\text{CH}_{\text{ar}}$ ), 7.03 (d,  $J = 1.8$  Hz, 1H,  $\text{CH}_{\text{ar}}$ ), 6.92 (dd,  $J = 8.4, 1.9$  Hz, 1H,  $\text{CH}_{\text{ar}}$ ), 6.45 (d,  $J = 8.5$  Hz, 1H,  $\text{CH}_{\text{ar}}$ ), 5.74 (t,  $J = 6.0$  Hz, 1H, NH), 4.44 (d,  $J = 5.9$  Hz, 2H,  $\text{CH}_2$ ), 3.82 (s, 3H,  $\text{OOCCH}_3$ ), 3.03 (t,  $J = 7.4$  Hz, 2H,  $\text{CH}_2$ ), 2.74 (t,  $J = 7.4$  Hz, 2H,  $\text{CH}_2$ ), 2.32 (s, 3H,  $\text{CH}_3$ ), 2.14 (s, 3H,  $\text{CH}_3$ ) ppm.

$\text{MS}(\text{ESI}^+)$ :  $m/z$  531.26 ( $[\text{M}+\text{Na}]$ , 100)

**4-(2-(1-(4-cyanobenzyl)-5-(3,5-dimethylisoxazol-4-yl)-1H-benzo[d]imidazol-2-yl)ethyl)benzoic acid (116)**



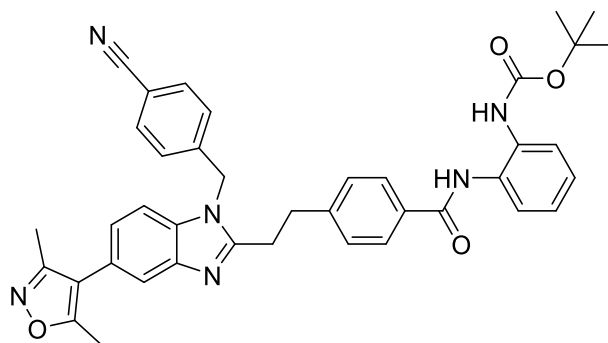
Compound **112** (220 mg, 0.43 mmol, 1 eq) was converted according to general procedure D for 2 h. Solvents were removed under reduced pressure and crude product was purified via reversed flash chromatography with a gradient of  $\text{ACN}/\text{H}_2\text{O}$  (after 2 CVs increased linear from 10:90 to 100:0 over 10 CVs) as a mobile phase to obtain **116** (144 mg, 70 %) as a colorless solid.

$R_f(\text{DCM}/\text{MeOH} = 95:5) = 0.52$

$^1\text{H-NMR}$  (250 MHz,  $\text{DMSO-}d_6$ ):  $\delta = 12.72$  (s, 1H, OH), 7.81 (dd,  $J = 11.9, 8.0$  Hz, 4H,  $\text{CH}_{\text{ar}}$ ), 7.63 (s, 1H,  $\text{CH}_{\text{ar}}$ ), 7.51 (d,  $J = 8.3$  Hz, 1H,  $\text{CH}_{\text{ar}}$ ), 7.37 (d,  $J = 8.0$  Hz, 2H,  $\text{CH}_{\text{ar}}$ ), 7.25 (d,  $J = 8.0$  Hz, 2H,  $\text{CH}_{\text{ar}}$ ), 7.16 (d,  $J = 8.4$  Hz, 1H,  $\text{CH}_{\text{ar}}$ ), 5.64 (s, 2H,  $\text{CH}_2$ ), 3.19 (s, 4H,  $2 \times \text{CH}_2$ ), 2.40 (s, 3H,  $\text{CH}_3$ ), 2.23 (s, 3H,  $\text{CH}_3$ ) ppm.

$\text{MS}(\text{ESI}^+)$ :  $m/z$  477.21 ( $[\text{M}+\text{H}]$ , 100)

***tert*-butyl (2-(4-(2-(1-(4-cyanobenzyl)-5-(3,5-dimethylisoxazol-4-yl)-1*H*-benzo[*d*]imidazol-2-yl)ethyl)benzamido)phenyl)carbamate (125)**



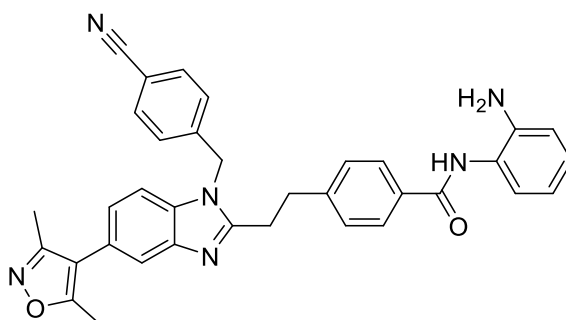
Compound **116** (140 mg, 0.294 mmol, 1 eq) was reacted with **39** (73 mg, 0.353 mmol, 1.2 eq) according to general procedure C. Product was purified via reverse flash chromatography with a gradient of ACN/H<sub>2</sub>O (after 2 CVs increased linear from 10:90 to 100:0 over 10 CVs) to obtain **125** as a colorless solid (132 mg, 67 %).

R<sub>f</sub>(DCM/MeOH = 95:5) = 0.54

<sup>1</sup>H-NMR (250 MHz, DMSO-*d*<sub>6</sub>): δ = 9.76 (s, 1H, NH), 8.65 (s, 1H, NH), 7.88 - 7.77 (m, 4H, CH<sub>ar</sub>), 7.64 (s, 1H, CH<sub>ar</sub>), 7.57 - 7.49 (m, 3H, CH<sub>ar</sub>), 7.42 (d, J = 8.2 Hz, 2H, CH<sub>ar</sub>), 7.26 (d, J = 8.2 Hz, 2H, CH<sub>ar</sub>), 7.21 - 7.11 (m, 3H, CH<sub>ar</sub>), 5.66 (s, 2H, CH<sub>2</sub>), 3.21 (s, 4H, 2xCH<sub>2</sub>), 2.40 (s, 3H, CH<sub>3</sub>), 2.23 (s, 3H, CH<sub>3</sub>), 1.42 (s, 9H, C(CH<sub>3</sub>)<sub>3</sub>) ppm.

MS(ESI<sup>+</sup>): m/z 567.30 ([M-Boc+H], 100); 667.39 ([M+H], 15)

***N*-(2-aminophenyl)-4-(2-(1-(4-cyanobenzyl)-5-(3,5-dimethylisoxazol-4-yl)-1*H*-benzo[*d*]imidazol-2-yl)ethyl)benzamide (28)**



Reaction was performed according to general procedure E with **125** (130 mg, 0.195 mmol, 1 eq) DCM and TFA (20 % of total volume of 6 mL). Crude product was purified via reverse flash

chromatography with a gradient of ACN/H<sub>2</sub>O (after 2 CVs increased linear from 10:90 to 100:0 over 10 CVs) as a mobile phase to obtain **28** as a colorless solid (80 mg, 72 %).

$R_f(\text{DCM/MeOH} = 95:5) = 0.53$

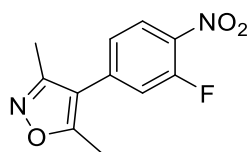
<sup>1</sup>H-NMR (500 MHz, DMSO-*d*<sub>6</sub>):  $\delta = 9.59$  (s, 1H, NH), 7.89 (d,  $J = 8.1$  Hz, 2H, CH<sub>ar</sub>), 7.80 (d,  $J = 8.3$  Hz, 2H, CH<sub>ar</sub>), 7.65 (d,  $J = 1.2$  Hz, 1H, CH<sub>ar</sub>), 7.53 (d,  $J = 8.3$  Hz, 1H, CH<sub>ar</sub>), 7.39 (d,  $J = 8.2$  Hz, 2H, CH<sub>ar</sub>), 7.27 (d,  $J = 8.3$  Hz, 2H, CH<sub>ar</sub>), 7.20 - 7.14 (m, 2H, CH<sub>ar</sub>), 6.97 (td,  $J = 8.1, 1.5$  Hz, 1H, CH<sub>ar</sub>), 6.78 (dd,  $J = 8.0, 1.3$  Hz, 1H, CH<sub>ar</sub>), 6.60 (td,  $J = 7.7, 1.2$  Hz, 1H, CH<sub>ar</sub>), 5.66 (s, 2H, CH<sub>2</sub>), 4.98 (s, 2H, NH<sub>2</sub>), 3.21 (s, 4H, 2xCH<sub>2</sub>), 2.41 (s, 3H, CH<sub>3</sub>), 2.23 (s, 3H, CH<sub>3</sub>) ppm.

<sup>13</sup>C-NMR (126 MHz, DMSO-*d*<sub>6</sub>):  $\delta = 165.10, 164.64, 158.34, 155.15, 144.53, 143.00, 142.66, 142.52, 134.58, 132.76, 132.49, 128.28, 127.82, 127.52, 126.69, 126.43, 123.43, 123.37, 123.21, 119.06, 118.57, 116.50, 116.34, 116.18, 110.47, 110.37, 45.76, 32.31, 27.92, 11.32, 10.53$  ppm.

MS(ESI<sup>+</sup>):  $m/z$  567.30 ([M+H], 100)

HRMS (MALDI):  $m/z$  calculated 567.25030 for C<sub>35</sub>H<sub>31</sub>N<sub>6</sub>O<sub>2</sub>, found 567.25028.

#### 4-(3-fluoro-4-nitrophenyl)-3,5-dimethylisoxazole (**95**)



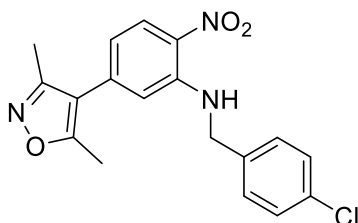
XPhos Palladacycle Gen. 3 (192 mg, 0.227 mmol, 0.01 eq) was added to a solution of 4-bromo-2-fluoro-1-nitrobenzene **94** (5 g, 22.7 mmol, 1 eq) and 3,5-dimethylisoxazole-4-boronic acid pinacol ester **77** (6 g, 27.2 mmol, 1.2 eq) in DME (20 mL). The mixture was stirred and saturated NaHCO<sub>3</sub> solution (20 mL) was added. The mixture was degassed by placing it in an ultrasonic bath and argon was bubbled into the reaction for 20 minutes. Then the mixture was heated at 80 °C for 3 h. The reaction was allowed to cool then partitioned between EtOAc (10 mL) and water (10 mL). The phases were separated, and the organic phase was washed with brine and dried over MgSO<sub>4</sub>. Solvents were removed under reduced pressure and residue was washed with hexane to obtain **95** as a beige solid (2.43 g, 45 %)

$R_f(\text{hexane/EtOAc} = 80:20) = 0.35$

$^1\text{H-NMR}$  (250 MHz,  $\text{DMSO-}d_6$ ):  $\delta$  = 8.24 (t,  $J$  = 8.4 Hz, 1H,  $\text{CH}_{\text{ar}}$ ), 7.71 (dd,  $J$  = 12.5, 1.8 Hz, 1H,  $\text{CH}_{\text{ar}}$ ), 7.56 - 7.44 (m, 1H,  $\text{CH}_{\text{ar}}$ ), 2.48 (s, 3H,  $\text{CH}_3$ ), 2.29 (s, 3H,  $\text{CH}_3$ ) ppm.

MS(ESI+): not measurable

***N*-(4-chlorobenzyl)-5-(3,5-dimethylisoxazol-4-yl)-2-nitroaniline (103)**



Compound **95** (300 mg, 1.27 mmol, 1 eq) was reacted with (4-chlorophenyl)methanamine **122** (0.23 mL, 1.91 mmol, 1.5 eq) according to general procedure A. **103** was neither purifiable by flash chromatography nor by recrystallization (300 mg with approximately 100 mg desired **103** and 200 mg **95** according to NMR, 22 %).

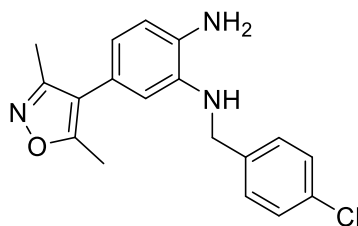
Reaction was repeated with higher equivalents of (4-chlorophenyl)methanamine **122** (0.31 mL, 2.54 mmol, 2 eq). Again, product is contaminated with **95** (300 mg with approximately 180 mg of desired **103** and 120 mg **95** according to NMR, 40 %).

$R_f$ (hexane/EtOAc = 80:20) = 0.35

$^1\text{H-NMR}$  (250 MHz,  $\text{DMSO-}d_6$ ):  $\delta$  = 8.81 (t,  $J$  = 6.1 Hz, 1H, NH), 8.15 (d,  $J$  = 9.2 Hz, 1H,  $\text{CH}_{\text{ar}}$ ), 7.41 (s, 4H,  $\text{CH}_{\text{ar}}$ ), 6.74 - 6.67 (m, 2H,  $\text{CH}_{\text{ar}}$ ), 4.67 (d,  $J$  = 6.2 Hz, 2H,  $\text{CH}_2$ ), 2.19 (s, 3H,  $\text{CH}_3$ ), 2.01 (s, 3H,  $\text{CH}_3$ ) ppm.

MS(ESI+):  $m/z$  358.07 ( $[\text{M}+\text{H}]$ , 100)



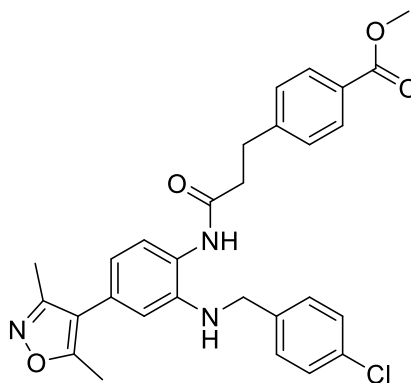
***N*<sup>1</sup>-(4-chlorobenzyl)-5-(3,5-dimethylisoxazol-4-yl)benzene-1,2-diamine (107)**

Unpurified compound **103** (420 mg, 1.17 mmol, 1 eq) was reacted according to general procedure B2. Crude product was purified via flash chromatography with a gradient of hexane/EtOAc (after 2 CVs increased linear from 70:30 to 30:70 over 7 CVs and held for 2 CVs) to obtain **107** as a light yellow solid (244 mg, 63 %).

$R_f(\text{hexane/EtOAc} = 50:50) = 0.40$

<sup>1</sup>H-NMR (250 MHz, DMSO-*d*<sub>6</sub>):  $\delta = 7.38$  (s, 4H, CH<sub>ar</sub>), 6.63 (d, *J* = 7.8 Hz, 1H, CH<sub>ar</sub>), 6.38 (dd, *J* = 7.8, 1.8 Hz, 1H, CH<sub>ar</sub>), 6.14 (d, *J* = 1.8 Hz, 1H, CH<sub>ar</sub>), 5.41 (t, *J* = 5.4 Hz, 1H, NH), 4.75 (s, 2H, NH<sub>2</sub>), 4.33 (d, *J* = 5.3 Hz, 2H, CH<sub>2</sub>), 2.13 (s, 3H, CH<sub>3</sub>), 1.97 (s, 3H, CH<sub>3</sub>) ppm.

MS(ESI<sup>+</sup>): *m/z* 328.11 ([M+H], 95)

**Methyl 4-(3-((2-((4-chlorobenzyl)amino)-4-(3,5-dimethylisoxazol-4-yl)phenyl)amino)-3-oxopropyl)benzoate (113)**

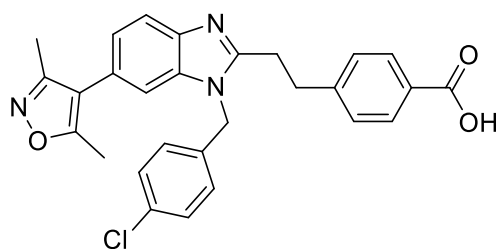
Compound **107** (340 mg, 0.74 mmol, 1 eq) was reacted with 3-(4-methoxycarbonylphenyl) propanoic acid **120** (238 mg, 1.14 mmol, 1.2 eq) according to general procedure C. Crude product was purified via flash chromatography with a gradient of DCM/MeOH (after 2 CVs increased linear from 100:0 to 95:5 over 7 CVs and held for 4 CVs) to obtain **113** as a colorless solid (502 mg, 93 %).

$R_f(\text{DCM/MeOH} = 95:5) = 0.55$

<sup>1</sup>H-NMR (250 MHz, DMSO-*d*<sub>6</sub>): δ = 9.25 (s, 1H, NH), 7.90 (d, J = 8.2 Hz, 2H, CH<sub>ar</sub>), 7.44 (d, J = 8.2 Hz, 2H, CH<sub>ar</sub>), 7.37 (s, 4H, CH<sub>ar</sub>), 7.15 (d, J = 8.0 Hz, 1H, CH<sub>ar</sub>), 6.52 (dd, J = 8.0, 1.6 Hz, 1H, CH<sub>ar</sub>), 6.27 (d, J = 1.5 Hz, 1H, CH<sub>ar</sub>), 5.67 (t, J = 5.8 Hz, 1H, NH), 4.34 (d, J = 5.6 Hz, 2H, CH<sub>2</sub>), 3.82 (s, 3H, OCH<sub>3</sub>), 3.04 (t, J = 7.4 Hz, 2H, CH<sub>2</sub>), 2.74 (t, J = 7.4 Hz, 2H, CH<sub>2</sub>), 2.14 (s, 3H, CH<sub>3</sub>), 1.97 (s, 3H, CH<sub>3</sub>) ppm.

MS(ESI<sup>+</sup>): m/z 540.23 ([M+Na], 100)

**4-(2-(1-(4-chlorobenzyl)-6-(3,5-dimethylisoxazol-4-yl)-1H-benzo[d]imidazol-2-yl)ethyl)benzoic acid (117)**



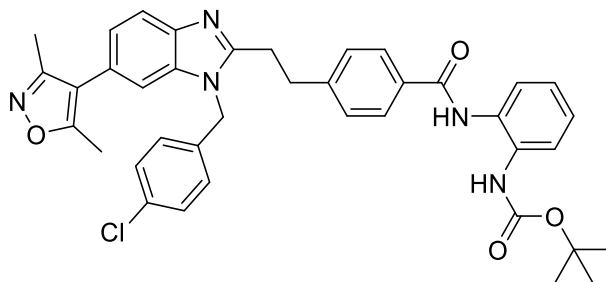
Compound **113** (502 mg, 0.97 mmol, 1 eq) was converted according to general procedure D for 2 h. Solvents were removed under reduced pressure and crude product was purified via reversed flash chromatography with a gradient of ACN/H<sub>2</sub>O (after 2 CVs increased linear from 10:90 to 100:0 over 10 CVs) as a mobile phase to obtain **117** as a light beige solid (215 mg, 46 %).

R<sub>f</sub>(DCM/MeOH = 95:5) = 0.41

<sup>1</sup>H-NMR (500 MHz, DMSO-*d*<sub>6</sub>): δ = 12.81 (s, 1H, OH), 7.83 (d, J = 8.4 Hz, 2H, CH<sub>ar</sub>), 7.68 (dd, J = 8.3, 0.5 Hz, 1H, CH<sub>ar</sub>), 7.45 (d, J = 1.1 Hz, 1H, CH<sub>ar</sub>), 7.39 - 7.34 (m, 4H, CH<sub>ar</sub>), 7.16 (dd, J = 8.3, 1.6 Hz, 1H, CH<sub>ar</sub>), 7.12 (d, J = 8.6 Hz, 2H, CH<sub>ar</sub>), 5.52 (s, 2H, CH<sub>2</sub>), 3.21 (m, 4H, 2xCH<sub>2</sub>), 2.35 (s, 3H, CH<sub>3</sub>), 2.18 (s, 3H, CH<sub>3</sub>) ppm.

MS(ESI<sup>+</sup>): m/z 486.23 ([M+H], 100)

***tert*-butyl (2-(4-(2-(1-(4-chlorobenzyl)-6-(3,5-dimethylisoxazol-4-yl)-1*H*-benzo[d]imidazol-2-yl)ethyl)benzamido)phenyl)carbamate (126)**



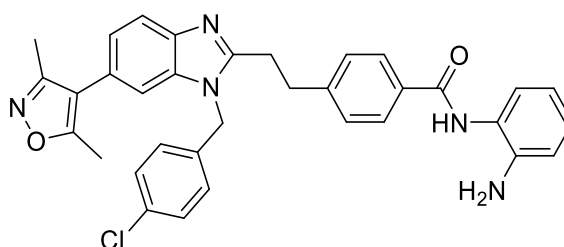
Compound **117** (100 mg, 0.20 mmol, 1 eq) was reacted with **39** (51 mg, 0.25 mmol, 1.2 eq) according to general procedure C. Product was purified via flash chromatography with a gradient of DCM/MeOH (after 2 CVs increased linear from 99:1 to 95:5 over 5 CVs and held for 3 CV) as mobile phase to obtain **126** as a colorless solid (100 mg, 72 %).

$R_f(\text{DCM/MeOH} = 95:5) = 0.52$

$^1\text{H-NMR}$  (500 MHz,  $\text{DMSO-}d_6$ ):  $\delta = 9.76$  (s, 1H, NH), 8.66 (s, 1H, NH), 7.84 (d,  $J = 8.3$  Hz, 2H,  $\text{CH}_{\text{ar}}$ ), 7.69 (dd,  $J = 8.3, 0.5$  Hz, 1H,  $\text{CH}_{\text{ar}}$ ), 7.53 (ddd,  $J = 11.0, 7.9, 1.7$  Hz, 2H,  $\text{CH}_{\text{ar}}$ ), 7.46 (d,  $J = 1.1$  Hz, 1H,  $\text{CH}_{\text{ar}}$ ), 7.41 (d,  $J = 8.4$  Hz, 2H,  $\text{CH}_{\text{ar}}$ ), 7.36 (d,  $J = 8.6$  Hz, 2H,  $\text{CH}_{\text{ar}}$ ), 7.20 - 7.14 (m, 3H,  $\text{CH}_{\text{ar}}$ ), 7.12 (d,  $J = 8.7$  Hz, 2H,  $\text{CH}_{\text{ar}}$ ), 5.54 (s, 2H,  $\text{CH}_2$ ), 3.22 (s, 4H,  $2 \times \text{CH}_2$ ), 2.35 (s, 3H,  $\text{CH}_3$ ), 2.18 (s, 3H,  $\text{CH}_3$ ), 1.42 (s, 9H,  $\text{C}(\text{CH}_3)_3$ ) ppm.

MS(ESI+):  $m/z$  676.41 ( $[\text{M}+\text{H}]$ , 100)

***N*-(2-aminophenyl)-4-(2-(1-(4-chlorobenzyl)-6-(3,5-dimethylisoxazol-4-yl)-1*H*-benzo[d]imidazol-2-yl)ethyl)benzamide (29)**



Reaction was performed according to general procedure E with **126** (50 mg, 0.74 mmol, 1 eq) DCM and TFA (20 % of total volume of 3.6 mL). Crude product was purified via reverse flash chromatography with a gradient of ACN/ $\text{H}_2\text{O}$  (after 2 CVs increased linear from 10:90 to 100:0 over 10 CVs) as a mobile phase to obtain **29** as a colorless solid (41 mg, >95 %).

$R_f(\text{DCM}/\text{MeOH} = 95:5) = 0.44$

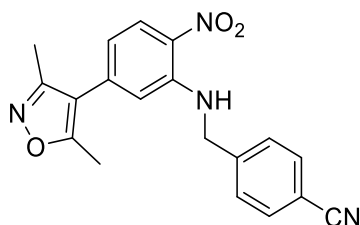
$^1\text{H-NMR}$  (500 MHz,  $\text{DMSO-}d_6$ ):  $\delta = 9.60$  (s, 1H, NH), 7.89 (d,  $J = 8.1$  Hz, 2H,  $\text{CH}_{\text{ar}}$ ), 7.69 (d,  $J = 8.3$  Hz, 1H,  $\text{CH}_{\text{ar}}$ ), 7.47 - 7.45 (m, 1H,  $\text{CH}_{\text{ar}}$ ), 7.38 (m, 4H,  $\text{CH}_{\text{ar}}$ ), 7.19 - 7.15 (m, 2H,  $\text{CH}_{\text{ar}}$ ), 7.13 (d,  $J = 8.5$  Hz, 2H,  $\text{CH}_{\text{ar}}$ ), 6.97 (td,  $J = 8.0, 1.5$  Hz, 1H,  $\text{CH}_{\text{ar}}$ ), 6.78 (dd,  $J = 8.0, 1.3$  Hz, 1H,  $\text{CH}_{\text{ar}}$ ), 6.60 (td,  $J = 7.7, 1.2$  Hz, 1H,  $\text{CH}_{\text{ar}}$ ), 5.54 (s, 2H,  $\text{CH}_2$ ), 3.26 - 3.18 (m, 4H,  $2 \times \text{CH}_2$ ), 2.35 (s, 3H,  $\text{CH}_3$ ), 2.18 (s, 3H,  $\text{CH}_3$ ) ppm.

$^{13}\text{C-NMR}$  (126 MHz,  $\text{DMSO-}d_6$ ):  $\delta = 165.21, 158.72, 155.48, 145.02, 143.45, 136.46, 135.94, 132.96, 132.64, 129.22, 129.19, 128.81, 128.30, 127.14, 126.91, 123.99, 123.93, 123.23, 119.22, 116.95, 116.84, 116.68, 111.29, 45.95, 32.88, 28.49, 11.72, 10.89$  ppm.

MS(ESI<sup>+</sup>):  $m/z$  576.29 ( $[\text{M}+\text{H}]$ , 100)

HRMS (MALDI):  $m/z$  calculated 576.21608 for  $\text{C}_{34}\text{H}_{31}\text{ClN}_5\text{O}_2$ , found 576.21558.

#### 4-(((5-(3,5-dimethylisoxazol-4-yl)-2-nitrophenyl)amino)methyl)benzonitrile (**105**)



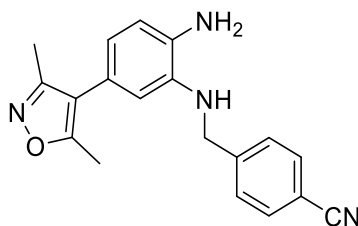
Compound **95** (400 mg, 1.69 mmol, 1 eq) was reacted with 4-(aminomethyl)benzonitrile hydrochloride (0.23 mL, 1.91 mmol, 1.5 eq) and DIPEA (0.86 mL, 5.08 mmol, 2.8 eq) according to general procedure A for 24 h. Crude product was purified via flash chromatography with a gradient of hexane/EtOAc (after 4 CVs increased linear from 70:30 to 50:50 over 4 CV and held for 4 CVs) to obtain **105** as an orange solid (226 mg, 38 %).

$R_f(\text{hexane}/\text{EtOH} = 60:40) = 0.62$

$^1\text{H-NMR}$  (250 MHz,  $\text{DMSO-}d_6$ ):  $\delta = 8.86$  (t,  $J = 6.2$  Hz, 1H, NH), 8.16 (d,  $J = 8.8$  Hz, 1H,  $\text{CH}_{\text{ar}}$ ), 7.81 (d,  $J = 8.1$  Hz, 2H,  $\text{CH}_{\text{ar}}$ ), 7.57 (d,  $J = 8.1$  Hz, 2H,  $\text{CH}_{\text{ar}}$ ), 6.75 - 6.64 (m, 2H,  $\text{CH}_{\text{ar}}$ ), 4.78 (d,  $J = 6.3$  Hz, 2H,  $\text{CH}_2$ ), 2.14 (s, 3H,  $\text{CH}_3$ ), 1.97 (s, 3H,  $\text{CH}_3$ ) ppm.

MS(ESI<sup>+</sup>):  $m/z$  371.17 ( $[\text{M}+\text{Na}]$ , 10)

**4-(((2-amino-5-(3,5-dimethylisoxazol-4-yl)phenyl)amino)methyl)benzonitrile (109)**



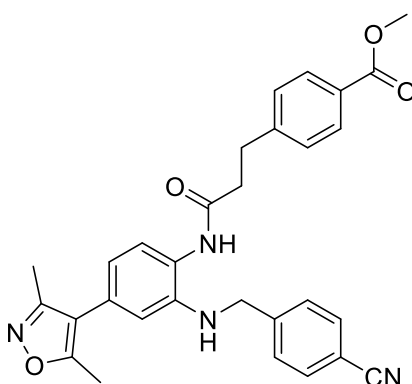
Compound **105** (226 mg, 0.649 mmol, 1 eq) was reacted with  $\text{SnCl}_2 \cdot \text{H}_2\text{O}$  (585 mg, 2.6 mmol, 4 eq) according to general procedure B2. Crude product was purified via flash chromatography with a gradient of hexane/EtOAc (after 2 CVs increased linear from 60:40 to 30:70 over 5 CV and held for 3 CVs) to obtain **109** as a red orange solid (131 mg, 63 %).

$R_f(\text{hexane/EtOAc} = 50:50) = 0.71$

$^1\text{H-NMR}$  (250 MHz,  $\text{DMSO-}d_6$ ):  $\delta = 7.79$  (d,  $J = 8.0$  Hz, 2H,  $\text{CH}_{\text{ar}}$ ),  $7.56$  (d,  $J = 8.1$  Hz, 2H,  $\text{CH}_{\text{ar}}$ ),  $6.63$  (d,  $J = 7.9$  Hz, 1H,  $\text{CH}_{\text{ar}}$ ),  $6.38$  (dd,  $J = 7.8, 1.5$  Hz, 1H,  $\text{CH}_{\text{ar}}$ ),  $6.07$  (d,  $J = 1.6$  Hz, 1H,  $\text{CH}_{\text{ar}}$ ),  $5.52$  (t,  $J = 5.8$  Hz, 1H, NH),  $4.76$  (s, 2H,  $\text{NH}_2$ ),  $4.44$  (d,  $J = 5.7$  Hz, 2H,  $\text{CH}_2$ ),  $2.09$  (s, 3H,  $\text{CH}_3$ ),  $1.92$  (s, 3H,  $\text{CH}_3$ ) ppm.

MS(ESI+):  $m/z$  315.07 ( $[\text{M}+\text{Na}-\text{CN}]$ , 100)

**Methyl 4-(3-(((2-amino-5-(3,5-dimethylisoxazol-4-yl)phenyl)amino)methyl)benzoate (113)**



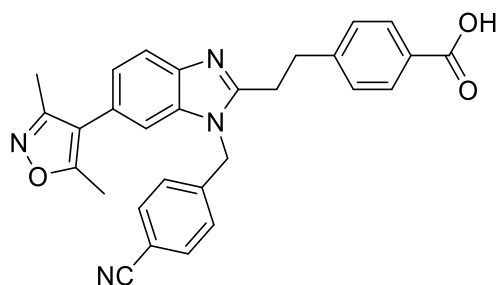
Compound **109** (131 mg, 0.411 mmol, 1 eq) was reacted with 3-(4-methoxycarbonylphenyl) propanoic acid **120** (94 mg, 0.453 mmol, 1.1 eq) according to general procedure C. Crude product was purified via flash chromatography with a gradient of DCM/MeOH (after 4 CVs increased linear from 100:0 to 95:5 over 8 CVs and held for 2 CVs) to obtain **113** as light yellow solid (185 mg, 88 %).

$R_f(\text{DCM}/\text{MeOH} = 95:5) = 0.66$

$^1\text{H-NMR}$  (250 MHz,  $\text{DMSO-}d_6$ ):  $\delta = 9.28$  (s, 1H, NH), 7.90 (d,  $J = 8.2$  Hz, 2H,  $\text{CH}_{\text{ar}}$ ), 7.79 (d,  $J = 8.3$  Hz, 2H,  $\text{CH}_{\text{ar}}$ ), 7.55 (d,  $J = 8.3$  Hz, 2H,  $\text{CH}_{\text{ar}}$ ), 7.45 (d,  $J = 8.3$  Hz, 2H,  $\text{CH}_{\text{ar}}$ ), 7.14 (d,  $J = 8.0$  Hz, 1H,  $\text{CH}_{\text{ar}}$ ), 6.53 (dd,  $J = 7.9, 1.7$  Hz, 1H,  $\text{CH}_{\text{ar}}$ ), 6.22 (d,  $J = 1.7$  Hz, 1H,  $\text{CH}_{\text{ar}}$ ), 5.76 (t,  $J = 6.1$  Hz, 1H, NH), 4.46 (d,  $J = 5.9$  Hz, 2H,  $\text{CH}_2$ ), 3.82 (s, 3H,  $\text{OOCCH}_3$ ), 3.05 (t,  $J = 7.5$  Hz, 2H,  $\text{CH}_2$ ), 2.74 (t,  $J = 7.6$  Hz, 2H,  $\text{CH}_2$ ), 2.11 (s, 3H,  $\text{CH}_3$ ), 1.93 (s, 3H,  $\text{CH}_3$ ) ppm.

MS(ESI<sup>+</sup>):  $m/z$  531.17 ( $[\text{M}+\text{Na}]$ , 100)

**4-(2-(1-(4-cyanobenzyl)-6-(3,5-dimethylisoxazol-4-yl)-1H-benzo[d]imidazol-2-yl)ethyl)benzoic acid (117)**



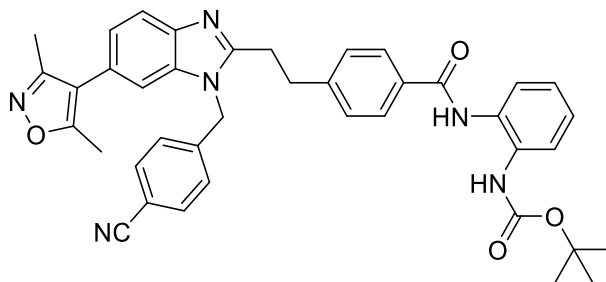
Compound **113** (185 mg, 0.364 mmol, 1 eq) was converted according to general procedure D for 2 h. Solvents were removed under reduced pressure and crude product was purified via reversed flash chromatography with a gradient of ACN/ $\text{H}_2\text{O}$  (after 2 CVs increased linear from 10:90 to 100:0 over 10 CVs) as a mobile phase to obtain **117** as a colorless solid (144 mg, 70 %).

$R_f(\text{DCM}/\text{MeOH} = 95:5) = 0.30$

$^1\text{H-NMR}$  (250 MHz,  $\text{DMSO-}d_6$ ):  $\delta = 12.81$  (s, 1H, OH), 7.86 - 7.67 (m, 5H,  $\text{CH}_{\text{ar}}$ ), 7.42 (s, 1H,  $\text{CH}_{\text{ar}}$ ), 7.37 (d,  $J = 8.2$  Hz, 2H,  $\text{CH}_{\text{ar}}$ ), 7.24 (d,  $J = 8.2$  Hz, 2H,  $\text{CH}_{\text{ar}}$ ), 7.17 (dd,  $J = 8.2, 1.2$  Hz, 1H,  $\text{CH}_{\text{ar}}$ ), 5.64 (s, 2H,  $\text{CH}_2$ ), 3.20 (s, 4H,  $2 \times \text{CH}_2$ ), 2.33 (s, 3H,  $\text{CH}_3$ ), 2.16 (s, 3H,  $\text{CH}_3$ ) ppm.

MS(ESI<sup>+</sup>):  $m/z$  477.25 ( $[\text{M}+\text{H}]$ , 100)

***tert*-butyl (2-(4-(2-(1-(4-cyanobenzyl)-6-(3,5-dimethylisoxazol-4-yl)-1*H*-benzo[d]imidazol-2-yl)ethyl)benzamido)phenyl)carbamate (127)**



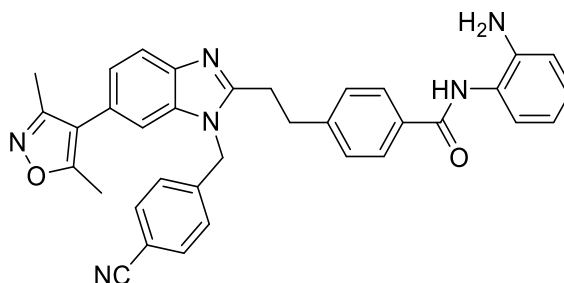
Compound **117** (91 mg, 0.191 mmol, 1 eq) was reacted with **39** (43 mg, 0.21 mmol, 1.1 eq) according to general procedure C. Product was purified via reverse flash chromatography with a gradient of DCM/MeOH (after 3 CVs increased linear from 100:0 to 95:5 over 7 CVs and held for 2 CVs) to obtain **127** as a colorless solid (104 mg, 82 %).

$R_f(\text{DCM/MeOH} = 95:5) = 0.77$

$^1\text{H-NMR}$  (250 MHz,  $\text{DMSO-}d_6$ ):  $\delta = 9.76$  (s, 1H, NH), 8.66 (s, 1H, NH), 7.82 (m, 4H,  $\text{CH}_{\text{ar}}$ ), 7.71 (d,  $J = 8.3$  Hz, 1H,  $\text{CH}_{\text{ar}}$ ), 7.54 (td,  $J = 7.0, 2.1$  Hz, 2H,  $\text{CH}_{\text{ar}}$ ), 7.47 - 7.39 (m, 3H,  $\text{CH}_{\text{ar}}$ ), 7.29 - 7.13 (m, 5H,  $\text{CH}_{\text{ar}}$ ), 5.67 (s, 2H,  $\text{CH}_2$ ), 3.22 (s, 4H,  $2 \times \text{CH}_2$ ), 2.35 (s, 3H,  $\text{CH}_3$ ), 2.17 (s, 3H,  $\text{CH}_3$ ), 1.43 (s, 9H,  $\text{C}(\text{CH}_3)_3$ ) ppm.

$\text{MS}(\text{ESI}^+)$ :  $m/z$  667.41 ( $[\text{M}+\text{H}]$ , 40)

***N*-(2-aminophenyl)-4-(2-(1-(4-cyanobenzyl)-6-(3,5-dimethylisoxazol-4-yl)-1*H*-benzo[d]imidazol-2-yl)ethyl)benzamide (30)**



Reaction was performed according to general procedure E with **127** (104 mg, 0.156 mmol, 1 eq) DCM and TFA (20 % of total volume of 4.8 mL). Crude product was purified via reverse flash chromatography with a gradient of ACN/ $\text{H}_2\text{O}$  (after 2 CVs increased linear from 10:90 to 100:0 over 10 CVs) as a mobile phase to obtain **30** as a colorless solid (30 mg, 34 %).

$R_f(\text{DCM}/\text{MeOH} = 95:5) = 0.33$

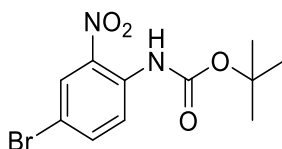
$^1\text{H-NMR}$  (500 MHz,  $\text{DMSO-}d_6$ ):  $\delta = 9.59$  (s, 1H, NH), 7.88 (d,  $J = 8.0$  Hz, 2H,  $\text{CH}_{\text{ar}}$ ), 7.79 (d,  $J = 8.3$  Hz, 2H,  $\text{CH}_{\text{ar}}$ ), 7.71 (d,  $J = 8.3$  Hz, 1H,  $\text{CH}_{\text{ar}}$ ), 7.45 - 7.42 (m, 1H,  $\text{CH}_{\text{ar}}$ ), 7.39 (d,  $J = 8.2$  Hz, 2H,  $\text{CH}_{\text{ar}}$ ), 7.26 (d,  $J = 8.3$  Hz, 2H,  $\text{CH}_{\text{ar}}$ ), 7.21 - 7.14 (m, 2H,  $\text{CH}_{\text{ar}}$ ), 6.97 (dd,  $J = 15.2, 1.4$  Hz, 1H,  $\text{CH}_{\text{ar}}$ ), 6.78 (dd,  $J = 8.0, 1.2$  Hz, 1H,  $\text{CH}_{\text{ar}}$ ), 6.60 (td,  $J = 7.5, 0.9$  Hz, 1H,  $\text{CH}_3$ ), 5.66 (s, 2H,  $\text{CH}_2$ ), 3.21 (s, 4H,  $2\times\text{CH}_2$ ), 2.34 (s, 3H,  $\text{CH}_3$ ), 2.16 (s, 3H,  $\text{CH}_3$ ) ppm.

$^{13}\text{C-NMR}$  (126 MHz,  $\text{DMSO-}d_6$ ):  $\delta = 165.21, 158.71, 155.55, 144.97, 143.15, 135.95, 133.17, 132.96, 128.79, 128.29, 128.12, 127.16, 126.91, 124.09, 123.33, 119.34, 119.03, 116.90, 116.84, 116.67, 111.18, 110.80, 46.24, 32.84, 28.40, 11.72, 10.88$  ppm.

MS(ESI+):  $m/z$  567.32 ( $[\text{M}+\text{H}]$ , 100)

HRMS (MALDI):  $m/z$  calculated 567.25030 for  $\text{C}_{35}\text{H}_{31}\text{N}_6\text{O}_2$ , found 567.24951.

#### *tert*-butyl (4-bromo-2-nitrophenyl)carbamate



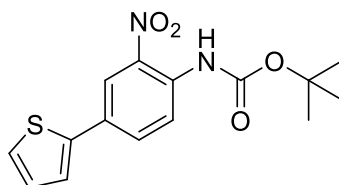
A solution of NaH (60 % in mineral oil, 405 mg, 10.1 mmol, 2.2 eq) in THF (30 mL) at 0 °C was slowly treated with a solution of 4-bromo-2-nitroaniline **128** (1 g, 4.6 mmol, 1 eq) in THF (30 mL). The solution was stirred at 0 °C for 10 minutes followed by 30 minutes at RT. A solution of  $\text{Boc}_2\text{O}$  (1.11 g, 5.1 mmol, 1.1) in THF (20 mL) was added and mixture was stirred for 1 h. Ice-cold water (50 mL) was slowly added, and reaction mixture was extracted with EtOAc. Organic phase was washed with brine and dried over  $\text{MgSO}_4$ . Crude product was purified via flash chromatography with a gradient of hexane/EtOAc (after 3 CVs increased linear from 100:0 to 90:10 over 3 CVs and held for 3 CVs) as a mobile phase to obtain **129** as a yellow solid (1.43 g, > 95 %).

$R_f(\text{hexane}/\text{EtOAc} = 60:40) = 0.89$

$^1\text{H-NMR}$  (250 MHz,  $\text{DMSO-}d_6$ ):  $\delta = 9.66$  (s, 1H, NH), 8.12 (d,  $J = 2.3$  Hz, 1H,  $\text{CH}_{\text{ar}}$ ), 7.86 (dd,  $J = 8.8, 2.4$  Hz, 1H,  $\text{CH}_{\text{ar}}$ ), 7.60 (d,  $J = 8.8$  Hz, 1H,  $\text{CH}_{\text{ar}}$ ), 1.44 (s, 9H,  $\text{C}(\text{CH}_3)_3$ ) ppm.

MS(ESI+):  $m/z$  338.94 ( $[\text{M}+\text{Na}]$ , 100)



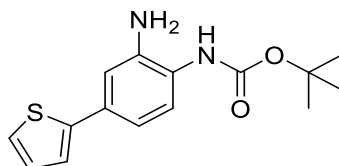
***tert*-butyl (2-nitro-4-(thiophen-2-yl)phenyl)carbamate (132)**

XPhos Palladacycle Gen. 3 (56 mg, 0.066 mmol, 0.07 eq) was added to a solution of **129** (300 mg, 0.94 mmol, 1 eq) and thiophen-2-ylboronic acid **130** (145 mg, 1.14 mmol, 1.2 eq) in DME (10 mL). The mixture was stirred and  $K_2CO_3$  (522 mg, 3.78 mmol, 4 eq) and saturated  $NaHCO_3$  solution (10 mL) was added. The mixture was degassed by placing it in an ultrasonic bath and argon was bubbled into the reaction for 30 minutes. Then the mixture was heated at 80 °C for 3 h. The reaction was allowed to cool then partitioned between EtOAc (10 mL) and water (10 mL). The phases were separated, and the organic phase was washed with brine and dried over  $MgSO_4$ . Crude product was purified via flash chromatography with hexane as mobile phase to obtain **132** as a yellow solid (183 mg, 60 %).

$R_f(\text{hexane}/\text{EtOAc} = 90:10) = 0.71$

$^1H$ -NMR (250 MHz,  $DMSO-d_6$ ):  $\delta = 9.63$  (s, 1H, NH), 8.15 (d,  $J = 2.2$  Hz, 1H,  $CH_{ar}$ ), 7.94 (dd,  $J = 8.6, 2.2$  Hz, 1H,  $CH_{ar}$ ), 7.70 (d,  $J = 8.6$  Hz, 1H,  $CH_{ar}$ ), 7.64 - 7.60 (m, 2H,  $CH_{ar}$ ), 7.17 (dd,  $J = 5.0, 3.7$  Hz, 1H,  $CH_{ar}$ ), 1.45 (s, 9H,  $C(CH_3)_3$ ) ppm.

MS(ESI+):  $m/z$  342.94 ( $[M+Na]$ , 100)

***tert*-butyl (2-amino-4-(thiophen-2-yl)phenyl)carbamate (134)**

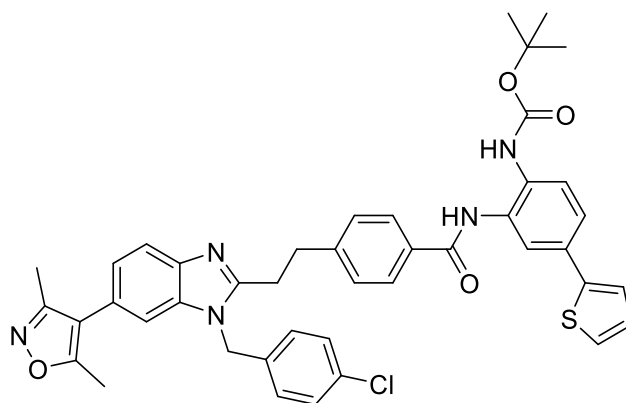
Compound **132** (220 mg, 0.69 mmol, 1 eq) was reacted according to general procedure B2. Crude product was purified via flash chromatography with hexane/EtOAc (50:50 over 10 CVs) to obtain **134** as a grey, brown solid (150 mg, 75 %).

$R_f(\text{hexane}/\text{EtOAc} = 8:2) = 0.15$

<sup>1</sup>H-NMR (250 MHz, DMSO-*d*<sub>6</sub>): δ = 8.33 (s, 1H, NH), 7.44 (dd, J = 5.1, 1.1 Hz, 1H, CH<sub>ar</sub>), 7.32 - 7.24 (m, 2H, CH<sub>ar</sub>), 7.08 (dd, J = 5.0, 3.6 Hz, 1H, CH<sub>ar</sub>), 6.98 (d, J = 2.1 Hz, 1H, CH<sub>ar</sub>), 6.84 (dd, J = 8.2, 2.1 Hz, 1H, CH<sub>ar</sub>), 5.00 (s, 2H, NH<sub>2</sub>), 1.47 (s, 9H, C(CH<sub>3</sub>)<sub>3</sub>) ppm.

MS(ESI<sup>+</sup>): m/z 313.00 ([M+Na], 20)

***tert*-butyl (2-(4-(2-(1-(4-chlorobenzyl)-6-(3,5-dimethylisoxazol-4-yl)-1H-benzo[d]imidazol-2-yl)ethyl)benzamido)-4-(thiophen-2-yl)phenyl)carbamate (136)**



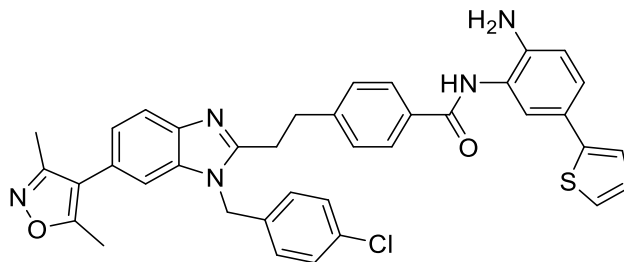
Compound **115** (82 mg, 0.17 mmol, 1 eq) was reacted with **134** (59 mg, 0.20 mmol, 1.2 eq) according to general procedure C. Product was purified via flash chromatography with a gradient of ACN/H<sub>2</sub>O (after 2 CVs increased linear from 10:90 to 100:0 over 10 CVs) as mobile phase to obtain **136** as a colorless solid (40 mg, 31 %).

R<sub>f</sub>(DCM/MeOH = 95:5) = 0.62

<sup>1</sup>H-NMR (250 MHz, DMSO-*d*<sub>6</sub>): δ = 9.84 (s, 1H, NH), 8.71 (s, 1H, NH), 7.92 - 7.80 (m, 3H, CH<sub>ar</sub>), 7.69 (d, J = 8.2 Hz, 1H, CH<sub>ar</sub>), 7.60 (d, J = 8.5 Hz, 1H, CH<sub>ar</sub>), 7.55 - 7.48 (m, 2H, CH<sub>ar</sub>), 7.46 - 7.33 (m, 6H, CH<sub>ar</sub>), 7.20 - 7.08 (m, 4H, CH<sub>ar</sub>), 5.54 (s, 2H, CH<sub>2</sub>), 3.23 (s, 4H, 2xCH<sub>2</sub>), 2.35 (s, 3H, CH<sub>3</sub>), 2.18 (s, 3H, CH<sub>3</sub>), 1.43 (s, 9H, C(CH<sub>3</sub>)<sub>3</sub>) ppm.

MS(ESI<sup>+</sup>): m/z 757.90 ([M+H], 100)

***N*-(2-amino-5-(thiophen-2-yl)phenyl)-4-(2-(1-(4-chlorobenzyl)-6-(3,5-dimethylisoxazol-4-yl)-1*H*-benzo[d]imidazol-2-yl)ethyl)benzamide (32)**



Reaction was performed according to general procedure E with **136** (58 mg, 0.076 mmol, 1 eq) DCM and TFA (20 % of total volume of 6 mL). Crude product was purified via reverse flash chromatography with a gradient of ACN/H<sub>2</sub>O (after 2 CVs increased linear from 10:90 to 100:0 over 10 CVs) as a mobile phase to obtain **32** as a colorless solid (50 mg, > 95 %).

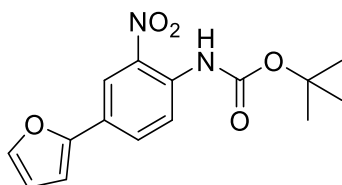
R<sub>f</sub>(DCM/MeOH = 95:5) = 0.5

<sup>1</sup>H-NMR (500 MHz, DMSO-*d*<sub>6</sub>): δ = 9.69 (s, 1H, NH), 7.92 (d, J = 8.2 Hz, 2H, CH<sub>ar</sub>), 7.72 (d, J = 8.3 Hz, 1H, CH<sub>ar</sub>), 7.48 (d, J = 2.5 Hz, 2H, CH<sub>ar</sub>), 7.41 (d, J = 8.3 Hz, 2H, CH<sub>ar</sub>), 7.38 (d, J = 8.5 Hz, 2H, CH<sub>ar</sub>), 7.35 (dd, J = 5.1, 1.1 Hz, 1H, CH<sub>ar</sub>), 7.30 (dd, J = 8.3, 2.2 Hz, 1H, CH<sub>ar</sub>), 7.24 (dd, J = 3.6, 1.1 Hz, 1H, CH<sub>ar</sub>), 7.20 (dd, J = 8.3, 1.5 Hz, 1H, CH<sub>ar</sub>), 7.14 (d, J = 8.5 Hz, 2H, CH<sub>ar</sub>), 7.05 (dd, J = 5.1, 3.6 Hz, 1H, CH<sub>ar</sub>), 6.82 (d, J = 8.3 Hz, 1H, CH<sub>ar</sub>), 5.57 (s, 2H, CH<sub>2</sub>), 3.30 - 3.19 (m, 4H, 2xCH<sub>2</sub>), 2.35 (s, 3H, CH<sub>3</sub>), 2.18 (s, 3H, CH<sub>3</sub>) ppm.

<sup>13</sup>C-NMR (126 MHz, DMSO-*d*<sub>6</sub>): δ = 165.76, 165.27, 158.72, 155.44, 145.00, 144.68, 143.32, 136.29, 135.73, 132.86, 132.70, 129.25, 129.20, 128.83, 128.68, 128.40, 124.40, 124.26, 124.01, 123.73, 123.52, 122.85, 121.51, 118.98, 116.94, 116.87, 111.46, 46.06, 32.84, 28.40, 11.72, 10.88 ppm.

MS(ESI<sup>+</sup>): m/z 658.15 ([M+H], 100)

HRMS (MALDI): m/z calculated 658.20380 for C<sub>38</sub>H<sub>33</sub>ClN<sub>5</sub>O<sub>2</sub>S, found 658.20260.

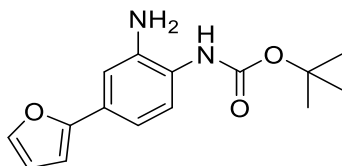
***tert*-butyl (4-(furan-2-yl)-2-nitrophenyl)carbamate (133)**

XPhos Palladacycle Gen. 3 (66 mg, 0.079 mmol, 0.1 eq) was added to a solution of **129** (250 mg, 0.79 mmol, 1 eq) and furan-2-ylboronic acid **131** (97 mg, 0. mmol, 1.2 eq) in DME (15 mL). The mixture was stirred and K<sub>2</sub>CO<sub>3</sub> (436 mg, 3.15 mmol, 4 eq) and saturated NaHCO<sub>3</sub> solution (15 mL) was added. The mixture was degassed by placing it in an ultrasonic bath and argon was bubbled into the reaction for 30 minutes. Then the mixture was heated at 80 °C for 3 h. The reaction was allowed to cool then partitioned between EtOAc (10 mL) and water (10 mL). The phases were separated, and the organic phase was washed with brine and dried over MgSO<sub>4</sub>. Crude product was purified via flash chromatography with a gradient of hexane/EtOAc (after 2 CVs increased linear from 100:0 to 90:10 over 4 CVs and held for 3 CV) as a mobile phase to obtain **133** as a red solid (120 mg, 50 %).

R<sub>f</sub>(hexane/EtOAc = 90:10) = 0.6

<sup>1</sup>H-NMR (250 MHz, DMSO-*d*<sub>6</sub>): δ = 9.63 (s, 1H, NH), 8.19 (d, J = 2.1 Hz, 1H, CH<sub>ar</sub>), 7.97 (dd, J = 8.6, 2.1 Hz, 1H, CH<sub>ar</sub>), 7.82 - 7.78 (m, 1H, CH<sub>ar</sub>), 7.72 (d, J = 8.7 Hz, 1H, CH<sub>ar</sub>), 7.15 - 7.06 (m, 1H, CH<sub>ar</sub>), 6.63 (dd, J = 3.4, 1.8 Hz, 1H, CH<sub>ar</sub>), 1.45 (s, 9H, C(CH<sub>3</sub>)<sub>3</sub>) ppm.

MS(ESI<sup>+</sup>): m/z 327.08 ([M+Na], 100)

***tert*-butyl (2-amino-4-(furan-2-yl)phenyl)carbamate (135)**

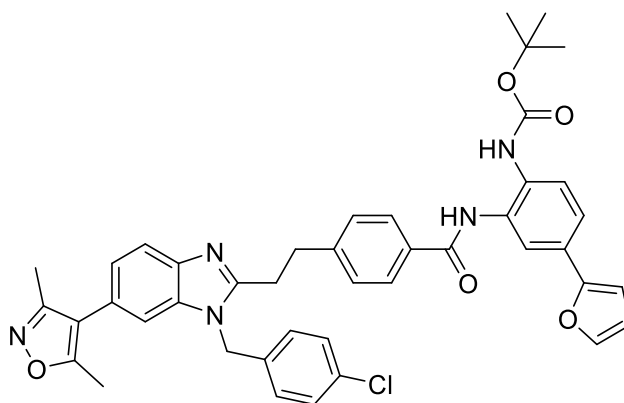
Compound **133** (120 mg, 0.39 mmol, 1 eq) was reacted according to general procedure B2. Crude product was purified via flash chromatography with hexane/EtOAc (50:50 over 10 CVs) to obtain **135** as a brown solid (75 mg, 69 %).

R<sub>f</sub>(hexane/EtOAc = 50:50) = 0.64

$^1\text{H-NMR}$  (250 MHz,  $\text{DMSO-}d_6$ ):  $\delta$  = 8.32 (s, 1H, NH), 7.28 (d,  $J$  = 8.3 Hz, 1H,  $\text{CH}_{\text{ar}}$ ), 7.04 (d,  $J$  = 2.0 Hz, 1H,  $\text{CH}_{\text{ar}}$ ), 6.88 (dd,  $J$  = 8.2, 2.0 Hz, 1H,  $\text{CH}_{\text{ar}}$ ), 6.68 (dd,  $J$  = 3.3, 0.6 Hz, 1H,  $\text{CH}_{\text{ar}}$ ), 6.53 (dd,  $J$  = 3.4, 1.8 Hz, 1H,  $\text{CH}_{\text{ar}}$ ), 4.98 (s, 2H,  $\text{NH}_2$ ), 1.46 (s, 9H,  $\text{C}(\text{CH}_3)_3$ ) ppm.

MS(ESI+):  $m/z$  297.12 ( $[\text{M}+\text{Na}]$ , 100)

***tert*-butyl (2-(4-(2-(1-(4-chlorobenzyl)-6-(3,5-dimethylisoxazol-4-yl)-1*H*-benzo [d]imidazol-2-yl)ethyl)benzamido)-4-(furan-2-yl)phenyl)carbamate (137)**



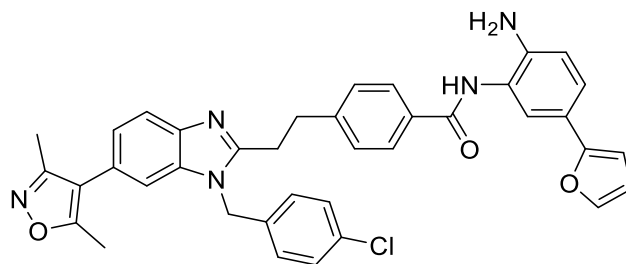
Compound **115** (60 mg, 0.12 mmol, 1 eq) was reacted with **135** (37 mg, 0.14 mmol, 1.2 eq) according to general procedure C. Product was purified via flash chromatography with a gradient of ACN/ $\text{H}_2\text{O}$  (after 2 CVs increased linear from 10:90 to 100:0 over 10 CVs) as mobile phase to obtain **137** as a red solid (48 mg, 52 %).

$R_f(\text{DCM}/\text{MeOH} = 95:5) = 0.53$

$^1\text{H-NMR}$  (250 MHz,  $\text{DMSO-}d_6$ ):  $\delta$  = 9.82 (s, 1H, NH), 8.73 (s, 1H, NH), 7.92 - 7.82 (m, 3H,  $\text{CH}_{\text{ar}}$ ), 7.74 - 7.67 (m, 2H,  $\text{CH}_{\text{ar}}$ ), 7.64 - 7.50 (m, 2H,  $\text{CH}_{\text{ar}}$ ), 7.48 - 7.34 (m, 5H,  $\text{CH}_{\text{ar}}$ ), 7.19 - 7.07 (m, 3H,  $\text{CH}_{\text{ar}}$ ), 6.87 (d,  $J$  = 3.3 Hz, 1H,  $\text{CH}_{\text{ar}}$ ), 6.59 (dd,  $J$  = 3.4, 1.8 Hz, 1H,  $\text{CH}_{\text{ar}}$ ), 5.54 (s, 2H), 3.23 (s, 4H), 2.35 (s, 3H), 2.18 (s, 3H), 1.43 (s, 9H) ppm.

MS(ESI+):  $m/z$  742.52

***N*-(2-amino-5-(furan-2-yl)phenyl)-4-(2-(1-(4-chlorobenzyl)-6-(3,5-dimethylisoxazol-4-yl)-1*H*-benzo[*d*]imidazol-2-yl)ethyl)benzamide (33)**



Reaction was performed according to general procedure E with **137** (48 mg, 0.064 mmol, 1 eq) DCM and TFA (20 % of total volume of 6 mL). Crude product was purified via reverse flash chromatography with a gradient of ACN/H<sub>2</sub>O (after 2 CVs increased linear from 10:90 to 100:0 over 10 CVs) as a mobile phase to obtain **33** as a yellow solid (23 mg, 55 %).

R<sub>f</sub>(hexane/EtOAc = 50:50) = 0.45

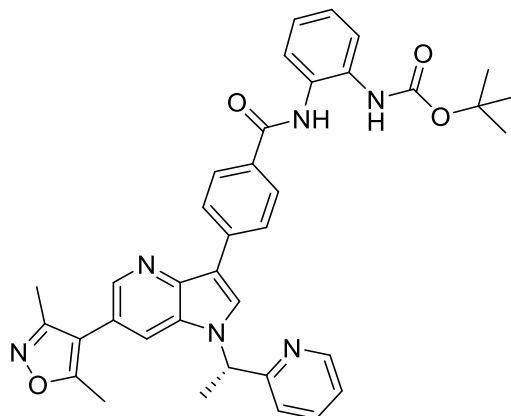
<sup>1</sup>H-NMR (500 MHz, DMSO-*d*<sub>6</sub>): δ = 9.66 (s, 1H, NH), 7.91 (d, J = 6.3 Hz, 2H, CH<sub>ar</sub>), 7.71 (d, J = 7.4 Hz, 1H, CH<sub>ar</sub>), 7.63 - 7.29 (m, 8H, CH<sub>ar</sub>), 7.23 - 7.09 (m, 3H, CH<sub>ar</sub>), 6.82 (d, J = 7.7 Hz, 1H, CH<sub>ar</sub>), 6.55 (d, J = 46.4 Hz, 2H, CH<sub>ar</sub>), 5.56 (s, 2H, CH<sub>2</sub>), 3.28 - 3.19 (m, 4H, 2xCH<sub>2</sub>), 2.35 (s, 3H, CH<sub>3</sub>), 2.18 (s, 3H, CH<sub>3</sub>) ppm.

<sup>13</sup>C-NMR (126 MHz, DMSO-*d*<sub>6</sub>): δ = 165.29, 164.75, 158.24, 154.98, 153.78, 144.55, 142.84, 141.22, 135.90, 135.36, 132.40, 132.18, 128.76, 128.71, 128.33, 127.88, 123.63, 123.33, 122.88, 122.29, 122.24, 119.25, 118.63, 116.43, 116.23, 111.78, 110.88, 102.40, 45.51, 32.38, 27.95, 11.24, 10.41 ppm.

MS(ESI<sup>+</sup>): m/z 642.19 ([M+H], 100)

HRMS (MALDI): m/z calculated 642.22664 for C<sub>38</sub>H<sub>33</sub>ClN<sub>5</sub>O<sub>3</sub>, found 642.22653.

***tert*-butyl (S)-(2-(4-(6-(3,5-dimethylisoxazol-4-yl)-1-(1-(pyridin-2-yl)ethyl)-1*H*-pyrrolo[3,2-*b*] pyridin-3-yl)benzamido)phenyl)carbamate (142)**



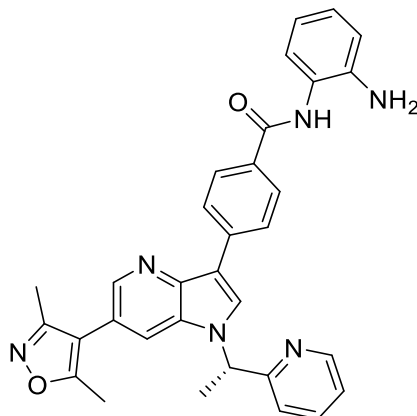
PLX51107 **36** (48 mg, 0.109 mmol, 1 eq) was reacted with **39** (27 mg, 0.131 mmol, 1.2 eq) according to general procedure C. Product was purified via flash chromatography with a gradient of ACN/H<sub>2</sub>O (after 2 CVs increased linear from 10:90 to 100:0 over 10 CVs) as mobile phase to obtain **142** as a colorless solid (48 mg, 70 %).

R<sub>f</sub>(DCM/MeOH = 95:5) = 0.71

<sup>1</sup>H-NMR (250 MHz, DMSO-*d*<sub>6</sub>): δ = 9.85 (s, 1H, NH), 8.74 (s, 1H, CH<sub>ar</sub>), 8.67 (s, 1H, NH), 8.58 - 8.47 (m, 4H, CH<sub>ar</sub>), 8.07 - 7.97 (m, 3H, CH<sub>ar</sub>), 7.79 (td, J = 7.7, 1.8 Hz, 1H, CH<sub>ar</sub>), 7.60 - 7.52 (m, 2H, CH<sub>ar</sub>), 7.43 (d, J = 7.9 Hz, 1H, CH<sub>ar</sub>), 7.30 (dd, J = 7.1, 5.3 Hz, 1H, CH<sub>ar</sub>), 7.19 (ddd, J = 7.2, 4.9, 2.0 Hz, 2H, CH<sub>ar</sub>), 6.09 (q, J = 7.1 Hz, 1H, CH), 2.41 (s, 3H, CH<sub>3</sub>), 2.22 (s, 3H, CH<sub>3</sub>), 2.04 (d, J = 7.0 Hz, 3H, CH<sub>3</sub>), 1.46 (s, 9H, C(CH<sub>3</sub>)<sub>3</sub>) ppm.

MS(ESI<sup>-</sup>): m/z 629.34 ([M+H], 100)

**(S)-N-(2-aminophenyl)-4-(6-(3,5-dimethylisoxazol-4-yl)-1-(1-(pyridin-2-yl)ethyl)-1H-pyrrolo[3,2-b]pyridin-3-yl)benzamide (37)**



Reaction was performed according to general procedure E with **142** (48 mg, 0.076 mmol, 1 eq) DCM and TFA (20 % of total volume of 6 mL). Crude product was purified via reverse flash chromatography with a gradient of ACN/H<sub>2</sub>O (after 2 CVs increased linear from 10:90 to 100:0 over 10 CVs) as a mobile phase to obtain **37** as a colorless solid (40 mg, > 95 %).

R<sub>f</sub>(DCM/MeOH = 95:5) = 0.49

<sup>1</sup>H-NMR (500 MHz, DMSO-*d*<sub>6</sub>): δ = 9.67 (s, 1H, NH), 8.72 (s, 1H, CH<sub>ar</sub>), 8.55 (d, J = 4.8 Hz, 1H, CH<sub>ar</sub>), 8.51 (d, J = 7.8 Hz, 3H, CH<sub>ar</sub>), 8.06 (d, J = 8.2 Hz, 2H, CH<sub>ar</sub>), 8.01 - 7.97 (m, 1H, CH<sub>ar</sub>), 7.78 (t, J = 7.7 Hz, 1H, CH<sub>ar</sub>), 7.42 (d, J = 7.8 Hz, 1H, CH<sub>ar</sub>), 7.30 (dd, J = 7.4, 4.9 Hz, 1H, CH<sub>ar</sub>), 7.20 (d, J = 7.7 Hz, 1H, CH<sub>ar</sub>), 6.98 (t, J = 7.6 Hz, 1H, CH<sub>ar</sub>), 6.81 (d, J = 8.0 Hz, 1H, CH<sub>ar</sub>), 6.62 (t, J = 7.5 Hz, 1H, CH<sub>ar</sub>), 6.08 (q, J = 7.0 Hz, 1H, CH), 4.91 (s, 2H, NH<sub>2</sub>), 2.40 (s, 3H, CH<sub>3</sub>), 2.22 (s, 3H, CH<sub>3</sub>), 2.04 (d, J = 7.0 Hz, 3H, CH<sub>3</sub>) ppm.

<sup>13</sup>C-NMR (126 MHz, DMSO-*d*<sub>6</sub>): δ = 165.58, 165.14, 159.73, 158.49, 149.33, 143.60, 143.22, 142.93, 137.35, 137.30, 131.13, 129.61, 129.05, 128.02, 126.73, 126.42, 125.24, 123.56, 123.03, 121.16, 118.80, 118.38, 116.32, 116.19, 113.94, 113.40, 56.21, 19.48, 11.27, 10.35 ppm.

MS(ESI-): m/z 527.17 ([M-H], 100)

HRMS (MALDI): m/z calculated 529.23465 for C<sub>32</sub>H<sub>29</sub>N<sub>6</sub>O<sub>2</sub>, found 529.23379.



## 8. References

- [1] World Health Organization. Global Health Observatory. Geneva: World Health Organization, *gco.iarc.fr* **2018**.
- [2] F. Bray, J. Ferlay, I. Soerjomataram, R. L. Siegel, L. A. Torre, A. Jemal, *CA: a cancer journal for clinicians* **2018**, 68, 394.
- [3] C. Allemani, H. K. Weir, H. Carreira, R. Harewood, D. Spika, X.-S. Wang, F. Bannon, J. V. Ahn, C. J. Johnson, A. Bonaventure et al., *The Lancet* **2015**, 385, 977.
- [4] a) M. Hidalgo, *The New England journal of medicine* **2010**, 362, 1605; b) M. J. Pishvaian, J. R. Brody, *Oncology (Williston Park, N.Y.)* **2017**, 31, 159.
- [5] Ferlay J, Ervik M, Lam F, Colombet M, Mery L, Piñeros M, Znaor A, Soerjomataram I, Bray F (2018). Global Cancer Observatory: Cancer Today. Lyon, France: International Agency for Research on Cancer. Available from: <https://gco.iarc.fr/today>, accessed 17.07.2020.
- [6] A. F. Hezel, A. C. Kimmelman, B. Z. Stanger, N. Bardeesy, R. A. Depinho, *Genes & development* **2006**, 20, 1218.
- [7] W. Plunkett, P. Huang, Y. Z. Xu, V. Heinemann, R. Grunewald, V. Gandhi, *Seminars in oncology* **1995**, 22, 3.
- [8] J. Zhao, *Pharmacology & therapeutics* **2016**, 160, 145.
- [9] L. Kumar, V. Kochupillai, *Acta oncologica (Stockholm, Sweden)* **1990**, 29, 471.
- [10] R. Paus, I. S. Haslam, A. A. Sharov, V. A. Botchkarev, *The Lancet Oncology* **2013**, 14, e50-e59.
- [11] A. Adamska, A. Domenichini, M. Falasca, *International journal of molecular sciences* **2017**, 18.
- [12] P. A. Jones, S. B. Baylin, *Nature reviews. Genetics* **2002**, 3, 415.
- [13] C. H. Waddington, *International journal of epidemiology* **2012**, 41, 10.
- [14] C. Dupont, D. R. Armant, C. A. Brenner, *Seminars in reproductive medicine* **2009**, 27, 351.
- [15] C. Wu, J. R. Morris, *Science (New York, N.Y.)* **2001**, 293, 1103.
- [16] R. L. SINSHEIMER, *The Journal of biological chemistry* **1955**, 215, 579.
- [17] V. G. ALLFREY, R. FAULKNER, A. E. MIRSKY, *Proceedings of the National Academy of Sciences of the United States of America* **1964**, 51, 786.
- [18] A. J. Bannister, T. Kouzarides, *Cell research* **2011**, 21, 381.
- [19] P. O. Hassa, S. S. Haenni, M. Elser, M. O. Hottiger, *Microbiology and molecular biology reviews : MMBR* **2006**, 70, 789.

- [20] M. A. Osley, *Briefings in functional genomics & proteomics* **2006**, *5*, 179.
- [21] J.-S. Seeler, A. Dejean, *Nature reviews. Molecular cell biology* **2003**, *4*, 690.
- [22] T. G. Gillette, J. A. Hill, *Circulation research* **2015**, *116*, 1245.
- [23] R. J. Gibbons, *Human molecular genetics* **2005**, *14 Spec No 1*, 92.
- [24] C. A. Iacobuzio-Donahue, *Annual review of pathology* **2009**, *4*, 229.
- [25] J. W. Tamkun, R. Deuring, M. P. Scott, M. Kissinger, A. M. Pattatucci, T. C. Kaufman, J. A. Kennison, *Cell* **1992**, *68*, 561.
- [26] P. Filippakopoulos, S. Picaud, M. Mangos, T. Keates, J.-P. Lambert, D. Barsyte-Lovejoy, I. Felletar, R. Volkmer, S. Müller, T. Pawson et al., *Cell* **2012**, *149*, 214.
- [27] E. Ferri, C. Petosa, C. E. McKenna, *Biochemical pharmacology* **2016**, *106*, 1.
- [28] Z. Nagy, L. Tora, *Oncogene* **2007**, *26*, 5341.
- [29] G. D. Gregory, C. R. Vakoc, T. Rozovskaia, X. Zheng, S. Patel, T. Nakamura, E. Canaani, G. A. Blobel, *Molecular and cellular biology* **2007**, *27*, 8466.
- [30] R. H. Jacobson, A. G. Ladurner, D. S. King, R. Tjian, *Science (New York, N.Y.)* **2000**, *288*, 1422.
- [31] J. L. Morgado-Pascual, S. Rayego-Mateos, L. Tejedor, B. Suarez-Alvarez, M. Ruiz-Ortega, *Frontiers in pharmacology* **2019**, *10*, 1315.
- [32] C. Dhalluin, J. E. Carlson, L. Zeng, C. He, A. K. Aggarwal, M. M. Zhou, *Nature* **1999**, *399*, 491.
- [33] Y. Taniguchi, *International journal of molecular sciences* **2016**, *17*.
- [34] J. E. Delmore, G. C. Issa, M. E. Lemieux, P. B. Rahl, J. Shi, H. M. Jacobs, E. Kastritis, T. Gilpatrick, R. M. Paranal, J. Qi et al., *Cell* **2011**, *146*, 904.
- [35] A. Alqahtani, K. Choucair, M. Ashraf, D. M. Hammouda, A. Alloghbi, T. Khan, N. Senzer, J. Nemunaitis, *Future science OA* **2019**, *5*, FSO372.
- [36] R. Beroukhim, C. H. Mermel, D. Porter, G. Wei, S. Raychaudhuri, J. Donovan, J. Barretina, J. S. Boehm, J. Dobson, M. Urashima et al., *Nature* **2010**, *463*, 899.
- [37] a) M. Vita, M. Henriksson, *Seminars in cancer biology* **2006**, *16*, 318; b) M. Buchholz, A. Schatz, M. Wagner, P. Michl, T. Linhart, G. Adler, T. M. Gress, V. Ellenrieder, *The EMBO journal* **2006**, *25*, 3714.
- [38] a) D. W. Felsher, *Genes & cancer* **2010**, *1*, 597; b) L. Soucek, M. Helmer-Citterich, A. Sacco, R. Jucker, G. Cesareni, S. Nasi, *Oncogene* **1998**, *17*, 2463; c) L. Soucek, R. Jucker, L. Panacchia, R. Ricordy, F. Tatò, S. Nasi, *Cancer research* **2002**, *62*, 3507.
- [39] Sachchidanand, L. Resnick-Silverman, S. Yan, S. Mutjaba, W.-J. Liu, L. Zeng, J. J. Manfredi, M.-M. Zhou, *Chemistry & biology* **2006**, *13*, 81.

- [40] P. Filippakopoulos, J. Qi, S. Picaud, Y. Shen, W. B. Smith, O. Fedorov, E. M. Morse, T. Keates, T. T. Hickman, I. Felletar et al., *Nature* **2010**, *468*, 1067.
- [41] D. S. Hewings, M. Wang, M. Philpott, O. Fedorov, S. Uttarkar, P. Filippakopoulos, S. Picaud, C. Vuppusetty, B. Marsden, S. Knapp et al., *Journal of medicinal chemistry* **2011**, *54*, 6761.
- [42] S. Sengupta, M. C. Biarnes, R. Clarke, V. C. Jordan, *Breast cancer research and treatment* **2015**, *150*, 265.
- [43] P. L. Garcia, A. L. Miller, K. M. Kreitzburg, L. N. Council, T. L. Gamblin, J. D. Christein, M. J. Heslin, J. P. Arnoletti, J. H. Richardson, D. Chen et al., *Oncogene* **2016**, *35*, 833.
- [44] a) D. B. Doroshow, J. P. Eder, P. M. LoRusso, *Annals of oncology : official journal of the European Society for Medical Oncology* **2017**, *28*, 1776; b) M. W. Moyer, *Nature medicine* **2011**, *17*, 1325.
- [45] A. Henssen, T. Thor, A. Odersky, L. Heukamp, N. El-Hindy, A. Beckers, F. Speleman, K. Althoff, S. Schäfers, A. Schramm et al., *Oncotarget* **2013**, *4*, 2080.
- [46] a) S. Postel-Vinay, K. Herbschleb, C. Massard, V. Woodcock, J.-C. Soria, A. O. Walter, F. Ewerton, M. Poelman, N. Benson, M. Ocker et al., *European journal of cancer (Oxford, England : 1990)* **2019**, *109*, 103; b) J. Lewin, J.-C. Soria, A. Stathis, J.-P. Delord, S. Peters, A. Awada, P. G. Aftimos, M. Bekradda, K. Rezai, Z. Zeng et al., *Journal of clinical oncology : official journal of the American Society of Clinical Oncology* **2018**, *36*, 3007.
- [47] A. Inoue, D. Fujimoto, *Biochemical and Biophysical Research Communications* **1969**, *36*, 146.
- [48] C. H. Arrowsmith, C. Bountra, P. V. Fish, K. Lee, M. Schapira, *Nature reviews. Drug discovery* **2012**, *11*, 384.
- [49] a) R. L. Montgomery, C. A. Davis, M. J. Potthoff, M. Haberland, J. Fielitz, X. Qi, J. A. Hill, J. A. Richardson, E. N. Olson, *Genes & development* **2007**, *21*, 1790; b) G. Lager, D. O'Carroll, M. Rembold, H. Khier, J. Tischler, G. Weitzer, B. Schuettengruber, C. Hauser, R. Brunmeir, T. Jenuwein et al., *The EMBO journal* **2002**, *21*, 2672.
- [50] a) C. L. Zhang, T. A. McKinsey, S. Chang, C. L. Antos, J. A. Hill, E. N. Olson, *Cell* **2002**, *110*, 479; b) R. B. Vega, K. Matsuda, J. Oh, A. C. Barbosa, X. Yang, E. Meadows, J. McAnally, C. Pomajzl, J. M. Shelton, J. A. Richardson et al., *Cell* **2004**, *119*, 555.

- [51] E. Seto, M. Yoshida, *Cold Spring Harbor perspectives in biology* **2014**, *6*, a018713.
- [52] A. Villar-Garea, M. Esteller, *International journal of cancer* **2004**, *112*, 171.
- [53] M. Haberland, R. L. Montgomery, E. N. Olson, *Nature reviews. Genetics* **2009**, *10*, 32.
- [54] de Ruijter, Annemieke J M, A. H. van Gennip, H. N. Caron, S. Kemp, van Kuilenburg, André B P, *The Biochemical journal* **2003**, *370*, 737.
- [55] A. A. Sauve, *Biochimica et biophysica acta* **2010**, *1804*, 1591.
- [56] M. S. Finnin, J. R. Donigian, A. Cohen, V. M. Richon, R. A. Rifkind, P. A. Marks, R. Breslow, N. P. Pavletich, *Nature* **1999**, *401*, 188.
- [57] A. R. Maolanon, A. S. Madsen, C. A. Olsen, *Cell chemical biology* **2016**, *23*, 759.
- [58] I. Nusinzon, C. M. Horvath, *Science's STKE : signal transduction knowledge environment* **2005**, *2005*, re11.
- [59] J. Luo, F. Su, D. Chen, A. Shiloh, W. Gu, *Nature* **2000**, *408*, 377.
- [60] V. Sandor, A. Senderowicz, S. Mertins, D. Sackett, E. Sausville, M. V. Blagosklonny, S. E. Bates, *British journal of cancer* **2000**, *83*, 817.
- [61] T. Eckschlager, J. Plch, M. Stiborova, J. Hrabeta, *International journal of molecular sciences* **2017**, *18*.
- [62] A. Fabre, F. Dequiedt, A. Restouin, R. Castellano, S. Garbit, P. Roche, X. Morelli, J. M. Brunel, Y. Collette, *Journal of medicinal chemistry* **2010**, *53*, 3038.
- [63] S. Di Micco, M. G. Chini, S. Terracciano, I. Bruno, R. Riccio, G. Bifulco, *Bioorganic & medicinal chemistry* **2013**, *21*, 3795.
- [64] O. M. Moradei, T. C. Mallais, S. Frechette, I. Paquin, P. E. Tessier, S. M. Leit, M. Fournel, C. Bonfils, M.-C. Trachy-Bourget, J. Liu et al., *Journal of medicinal chemistry* **2007**, *50*, 5543.
- [65] F. A. Schroeder, M. C. Lewis, D. M. Fass, F. F. Wagner, Y.-L. Zhang, K. M. Hennig, J. Gale, W.-N. Zhao, S. Reis, D. D. Barker et al., *PloS one* **2013**, *8*, e71323.
- [66] X. Zhang, T. Zegar, T. Weiser, F. H. Hamdan, B.-T. Berger, R. Lucas, D.-I. Balourdas, S. Ladigan, P. F. Cheung, S.-T. Liffers et al., *International journal of cancer* **2020**.
- [67] G. Montalban-Bravo, X. Huang, K. Naqvi, E. Jabbour, G. Borthakur, C. D. DiNardo, N. Pemmaraju, J. Cortes, S. Verstovsek, T. Kadia et al., *Leukemia* **2017**, *31*, 318.
- [68] M. Dimopoulos, D. S. Siegel, S. Lonial, J. Qi, R. Hajek, T. Facon, L. Rosinol, C. Williams, H. Blacklock, H. Goldschmidt et al., *The Lancet Oncology* **2013**, *14*, 1129.
- [69] D. A. Richards, K. A. Boehm, D. M. Waterhouse, D. J. Wagener, S. S. Krishnamurthi, A. Rosemurgy, W. Grove, K. Macdonald, S. Gulyas, M. Clark et al., *Annals of oncology : official journal of the European Society for Medical Oncology* **2006**, *17*, 1096.

- [70] D. H. Lee, J. Qi, J. E. Bradner, J. W. Said, N. B. Doan, C. Forscher, H. Yang, H. P. Koeffler, *International journal of cancer* **2015**, *136*, 2055.
- [71] U. Tontsch-Grunt, F. Savarese, A. Baum, D. Scharn, D. Gerlach, M. H. Hofmann, J. Popow, N. Schweifer, H. Engelhardt, H. Musa et al., *European Journal of Cancer* **2016**, *69*, S89.
- [72] S. V. Muralidharan, J. Bhadury, L. M. Nilsson, L. C. Green, K. G. McLure, J. A. Nilsson, *Oncogene* **2016**, *35*, 4689.
- [73] W. Fiskus, S. Sharma, J. Qi, J. A. Valenta, L. J. Schaub, B. Shah, K. Peth, B. P. Portier, M. Rodriguez, S. G. T. Devaraj et al., *Molecular cancer therapeutics* **2014**, *13*, 1142.
- [74] P. K. Mazur, A. Herner, S. S. Mello, M. Wirth, S. Hausmann, F. J. Sánchez-Rivera, S. M. Lofgren, T. Kuschma, S. A. Hahn, D. Vangala et al., *Nature medicine* **2015**, *21*, 1163.
- [75] J. Schmidt, M. Rotter, T. Weiser, S. Wittmann, L. Weizel, A. Kaiser, J. Heering, T. Goebel, C. Angioni, M. Wurglics et al., *Journal of medicinal chemistry* **2017**, *60*, 7703.
- [76] S. J. Atkinson, P. E. Soden, D. C. Angell, M. Bantscheff, C.-w. Chung, K. A. Giblin, N. Smithers, R. C. Furze, L. Gordon, G. Drewes et al., *Med. Chem. Commun.* **2014**, *5*, 342.
- [77] S. Amemiya, T. Yamaguchi, Y. Hashimoto, T. Noguchi-Yachide, *Bioorganic & medicinal chemistry* **2017**, *25*, 3677.
- [78] R. Morphy, C. Kay, Z. Rankovic, *Drug Discovery Today* **2004**, *9*, 641.
- [79] R. Morphy, Z. Rankovic, *Journal of medicinal chemistry* **2005**, *48*, 6523.
- [80] T. Noguchi-Yachide, T. Sakai, Y. Hashimoto, T. Yamaguchi, *Bioorganic & medicinal chemistry* **2015**, *23*, 953.
- [81] D. A. Hay, O. Fedorov, S. Martin, D. C. Singleton, C. Tallant, C. Wells, S. Picaud, M. Philpott, O. P. Monteiro, C. M. Rogers et al., *Journal of the American Chemical Society* **2014**, *136*, 9308.
- [82] A. El-Faham, F. Albericio, *Chemical reviews* **2011**, *111*, 6557.
- [83] H. Staudinger, J. Meyer, *HCA* **1919**, *2*, 635.
- [84] N. C. Bruno, M. T. Tudge, S. L. Buchwald, *Chemical science* **2013**, *4*, 916.
- [85] A. Bruneau, M. Roche, M. Alami, S. Messaoudi, *ACS Catal.* **2015**, *5*, 1386.
- [86] R. Martin, S. L. Buchwald, *Accounts of chemical research* **2008**, *41*, 1461.
- [87] W. Eschweiler, *Ber. Dtsch. Chem. Ges.* **1905**, *38*, 880.
- [88] F. H. Niesen, H. Berglund, M. Vedadi, *Nature protocols* **2007**, *2*, 2212.
- [89] a) *Anal. Chem.* **2012**, *62*, 950; b) I. Jelesarov, H. R. Bosshard, *J. Mol. Recognit.* **1999**, *12*, 3.

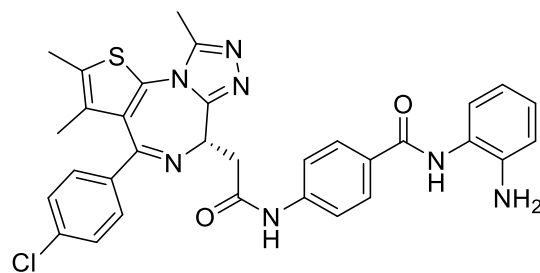
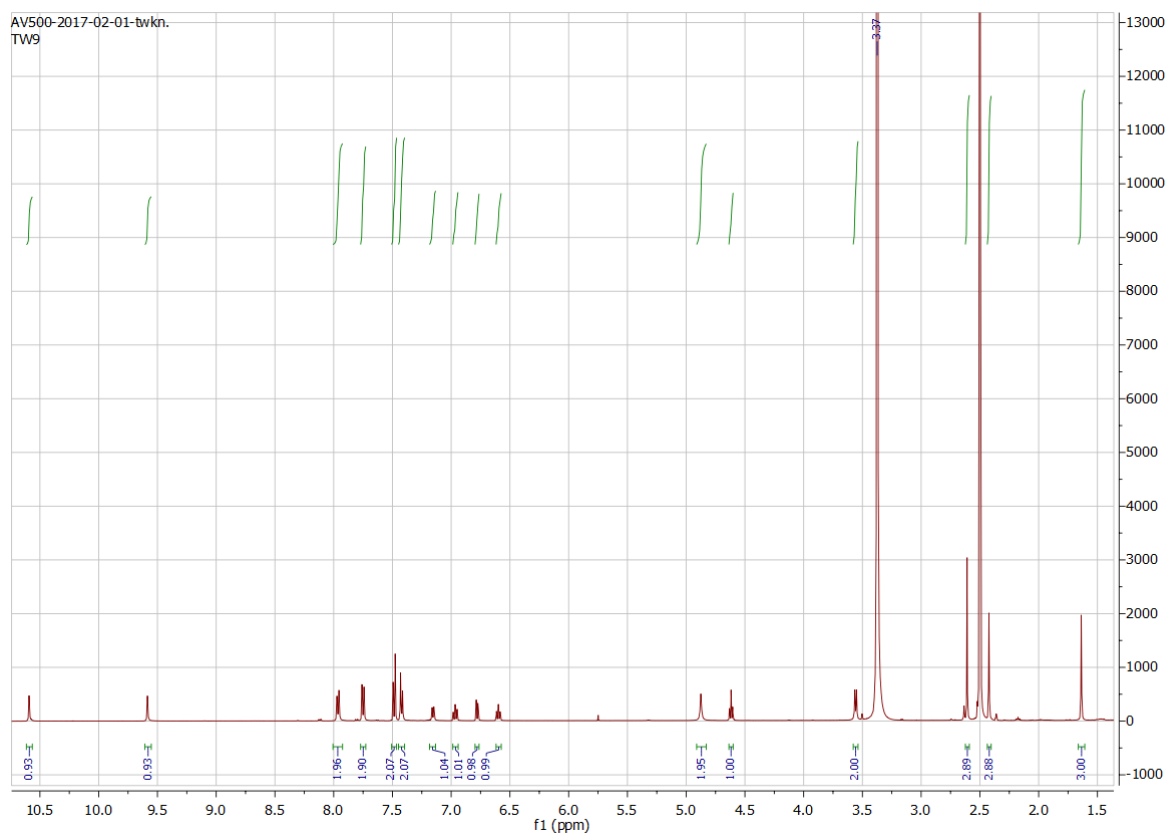
- [90] C. Song, S. Zhang, H. Huang, *Frontiers in microbiology* **2015**, *6*, 1049.
- [91] J. D. Vasta, C. R. Corona, J. Wilkinson, C. A. Zimprich, J. R. Hartnett, M. R. Ingold, K. Zimmerman, T. Machleidt, T. A. Kirkland, K. G. Huwiler et al., *Cell chemical biology* **2018**, *25*, 206.
- [92] T. Machleidt, C. C. Woodrooffe, M. K. Schwinn, J. Méndez, M. B. Robers, K. Zimmerman, P. Otto, D. L. Daniels, T. A. Kirkland, K. V. Wood, *ACS chemical biology* **2015**, *10*, 1797.
- [93] A. McPherson, J. A. Gavira, *Acta crystallographica. Section F, Structural biology communications* **2014**, *70*, 2.
- [94] A. M. Hassell, G. An, R. K. Bledsoe, J. M. Bynum, H. L. Carter, S.-J. J. Deng, R. T. Gampe, T. E. Grisard, K. P. Madauss, R. T. Nolte et al., *Acta crystallographica. Section D, Biological crystallography* **2007**, *63*, 72.
- [95] A. Subramanian, P. Tamayo, V. K. Mootha, S. Mukherjee, B. L. Ebert, M. A. Gillette, A. Paulovich, S. L. Pomeroy, T. R. Golub, E. S. Lander et al., *Proceedings of the National Academy of Sciences of the United States of America* **2005**, *102*, 15545.
- [96] S. Picaud, C. Wells, I. Felletar, D. Brotherton, S. Martin, P. Savitsky, B. Diez-Dacal, M. Philpott, C. Bountra, H. Lingard et al., *Proceedings of the National Academy of Sciences of the United States of America* **2013**, *110*, 19754.
- [97] X. Lin, X. Huang, T. Uziel, P. Hessler, D. H. Albert, L. A. Roberts-Rapp, K. F. McDaniel, W. M. Kati, Y. Shen, *Molecular cancer therapeutics* **2017**, *16*, 388.
- [98] P. Vlachos, U. Nyman, N. Hajji, B. Joseph, *Cell death and differentiation* **2007**, *14*, 1497.
- [99] J. Walters, C. Pop, F. L. Scott, M. Drag, P. Swartz, C. Mattos, G. S. Salvesen, A. C. Clark, *The Biochemical journal* **2009**, *424*, 335.
- [100] A. Ianevski, L. He, T. Aittokallio, J. Tang, *Bioinformatics (Oxford, England)* **2017**, *33*, 2413.
- [101] P. Cappella, D. Tomasoni, M. Faretta, M. Lupi, F. Montalenti, F. Viale, F. Banzato, M. D'Incalci, P. Ubezio, *International journal of cancer* **2001**, *93*, 401.
- [102] J. Wang, Y. Wang, H. Mei, Z. Yin, Y. Geng, T. Zhang, G. Wu, Z. Lin, *Cancer letters* **2017**, *391*, 141.
- [103] A. L. Gartel, M. S. Serfas, A. L. Tyner, *Proceedings of the Society for Experimental Biology and Medicine. Society for Experimental Biology and Medicine (New York, N.Y.)* **1996**, *213*, 138.

- [104] D. Hnisz, B. J. Abraham, T. I. Lee, A. Lau, V. Saint-André, A. A. Sigova, H. A. Hoke, R. A. Young, *Cell* **2013**, *155*, 934.
- [105] A. Vallejo, N. Perurena, E. Guruceaga, P. K. Mazur, S. Martinez-Canarias, C. Zanduetta, K. Valencia, A. Arricibita, D. Gwinn, L. C. Sayles et al., *Nature communications* **2017**, *8*, 14294.
- [106] M. Uhlen, C. Zhang, S. Lee, E. Sjöstedt, L. Fagerberg, G. Bidkhorji, R. Benfeitas, M. Arif, Z. Liu, F. Edfors et al., *Science (New York, N.Y.)* **2017**, *357*.
- [107] C. A. French, C. L. Ramirez, J. Kolmakova, T. T. Hickman, M. J. Cameron, M. E. Thyne, J. L. Kutok, J. A. Toretsky, A. K. Tadavarthy, U. R. Kees et al., *Oncogene* **2008**, *27*, 2237.
- [108] D. E. Bauer, C. M. Mitchell, K. M. Strait, C. S. Lathan, E. B. Stelow, S. C. Lüer, S. Muhammed, A. G. Evans, L. M. Sholl, J. Rosai et al., *Clinical cancer research : an official journal of the American Association for Cancer Research* **2012**, *18*, 5773.
- [109] A. E. Walts, J. W. Said, M. B. Siegel, S. Banks-Schlegel, *The Journal of pathology* **1985**, *145*, 329.
- [110] J. W. Said, G. Nash, A. F. Sassoon, I. P. Shintaku, S. Banks-Schlegel, *Laboratory investigation; a journal of technical methods and pathology* **1983**, *49*, 563.
- [111] P. Cimperman, L. Baranauskiene, S. Jachimoviciūte, J. Jachno, J. Torresan, V. Michailoviene, J. Matuliene, J. Sereikaite, V. Bumelis, D. Matulis, *Biophysical journal* **2008**, *95*, 3222.
- [112] D. Hay, O. Fedorov, P. Filippakopoulos, S. Martin, M. Philpott, S. Picaud, D. S. Hewings, S. Uttakar, T. D. Heightman, S. J. Conway et al., *Med. Chem. Commun.* **2013**, *4*, 140.
- [113] V. von Manstein, C. M. Yang, D. Richter, N. Delis, V. Vafaizadeh, B. Groner, *Current signal transduction therapy* **2013**, *8*, 193.
- [114] Z. Zhang, S. Hou, H. Chen, T. Ran, F. Jiang, Y. Bian, D. Zhang, Y. Zhi, L. Wang, L. Zhang et al., *Bioorganic & medicinal chemistry letters* **2016**, *26*, 2931.
- [115] S. He, G. Dong, Y. Li, S. Wu, W. Wang, C. Sheng, *Angewandte Chemie (International ed. in English)* **2020**, *59*, 3028.

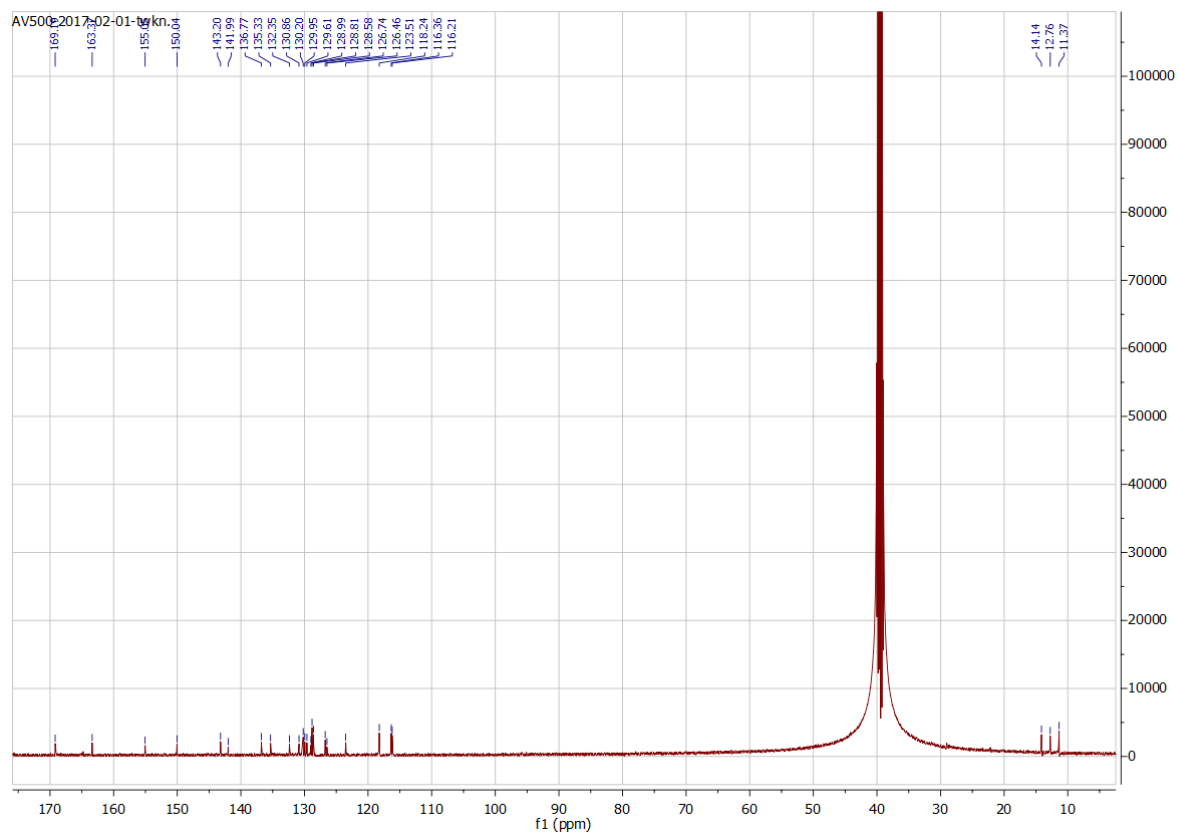
## 9. Supplementary Information

## 9.1. Analytical data

## 9.1.1. Compound 14

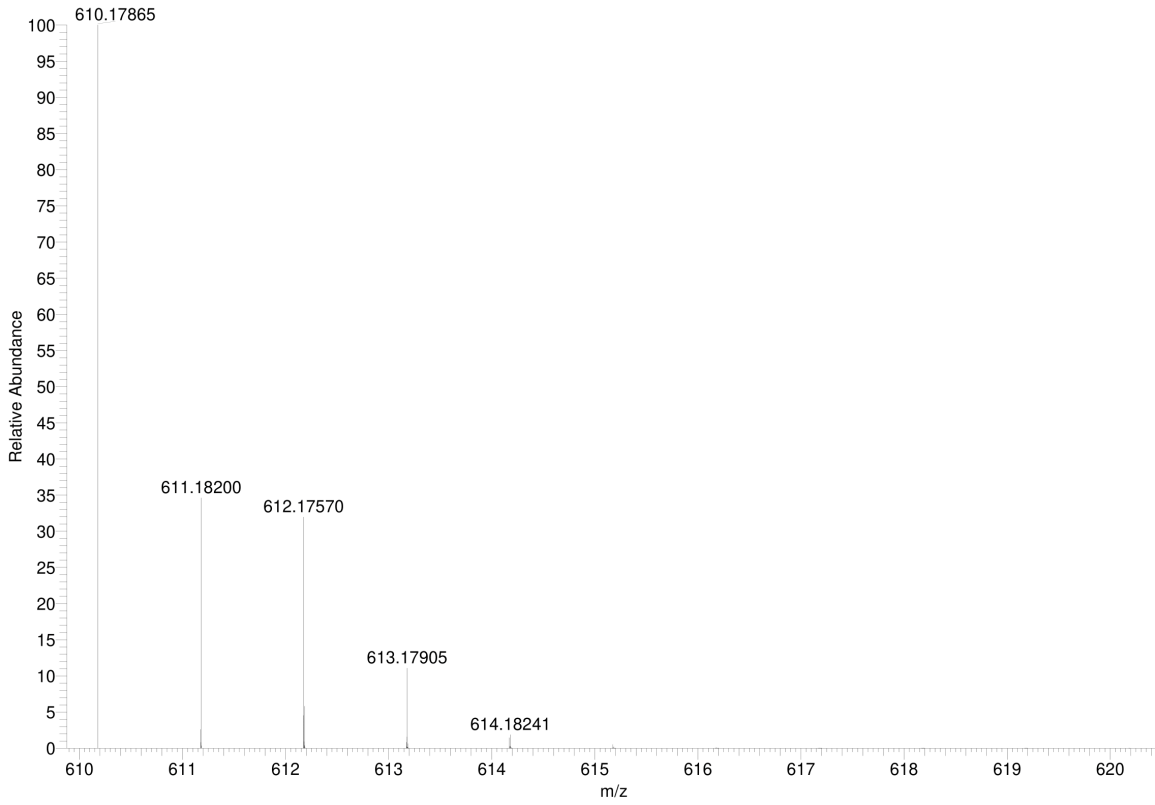
<sup>1</sup>H NMR



$^{13}\text{C}$  NMR

### Simulated HRMS

C<sub>32</sub>H<sub>28</sub>Cl<sub>1</sub>N<sub>7</sub>O<sub>2</sub>S<sub>1</sub> +H: C<sub>32</sub> H<sub>29</sub> Cl<sub>1</sub> N<sub>7</sub> O<sub>2</sub> S<sub>1</sub> pa Chrg 1



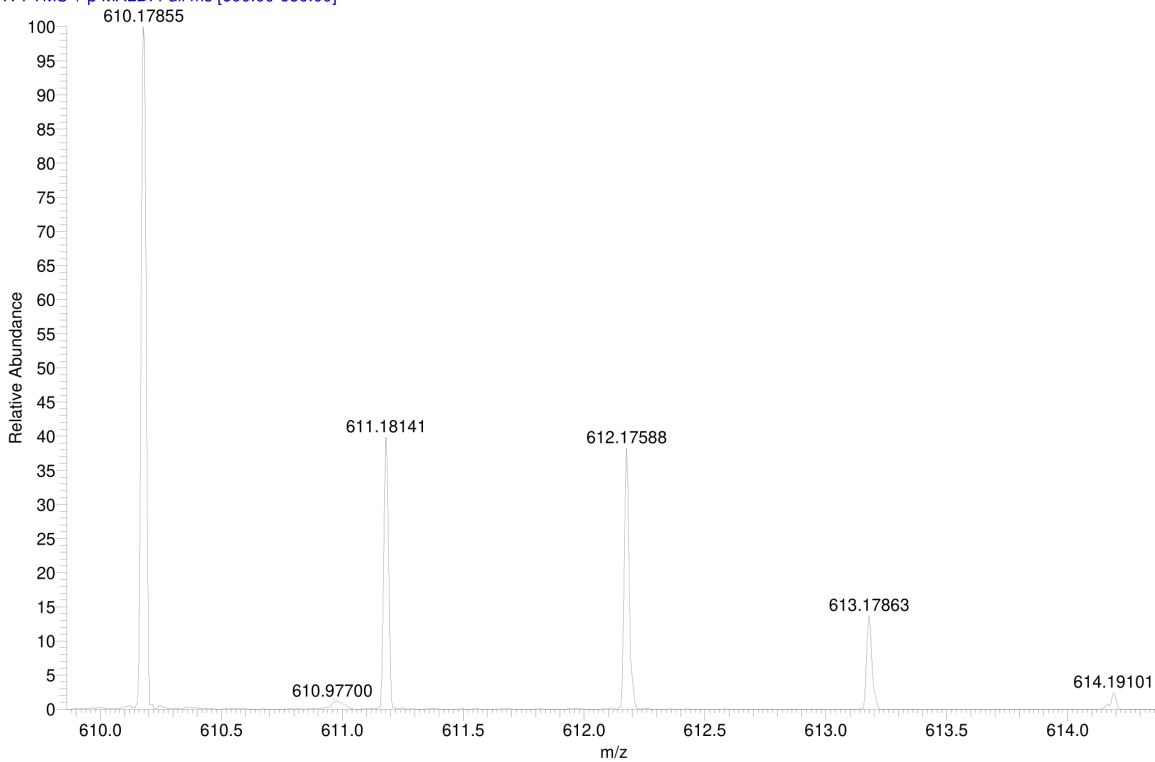
### MALDI HRMS

C:\User\...\Knapp\2017\170201\TW9\_B12

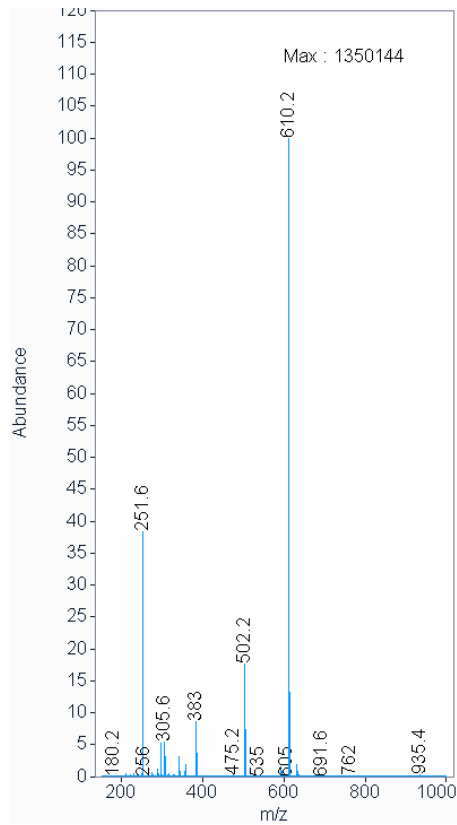
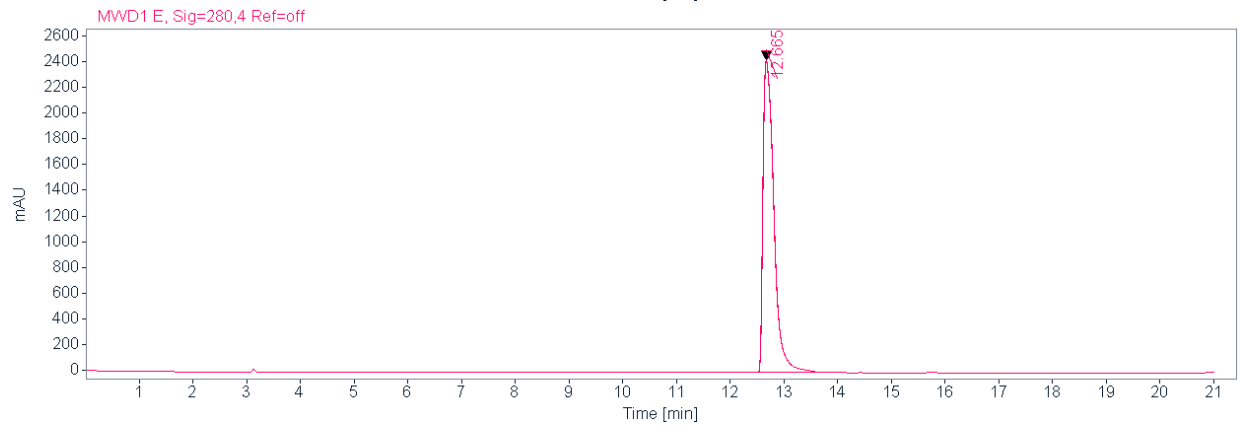
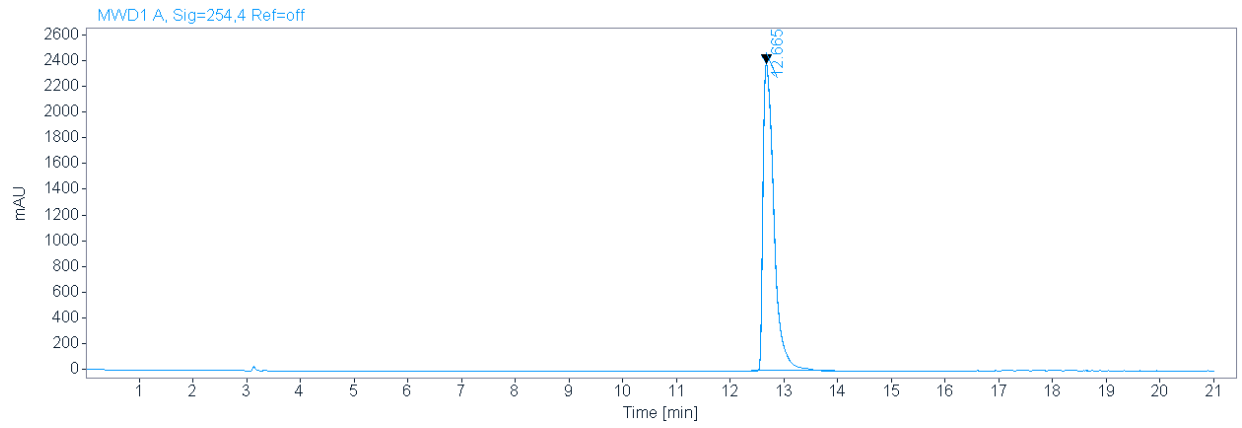
2/1/2017 12:43:01 PM

TW9 mit HCCA gemessen.

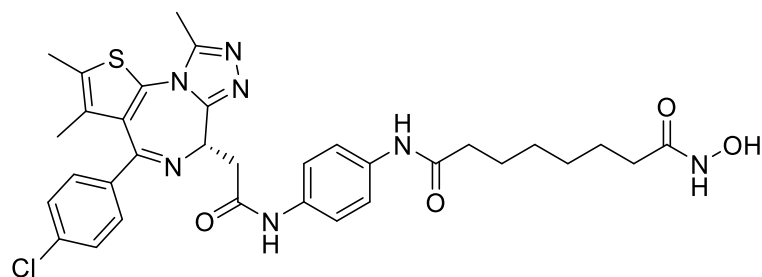
TW9\_B12 #1-13 RT: 0.00-1.40 AV: 13 NL: 4.48E5  
T: FTMS + p MALDI Full ms [600.00-650.00]

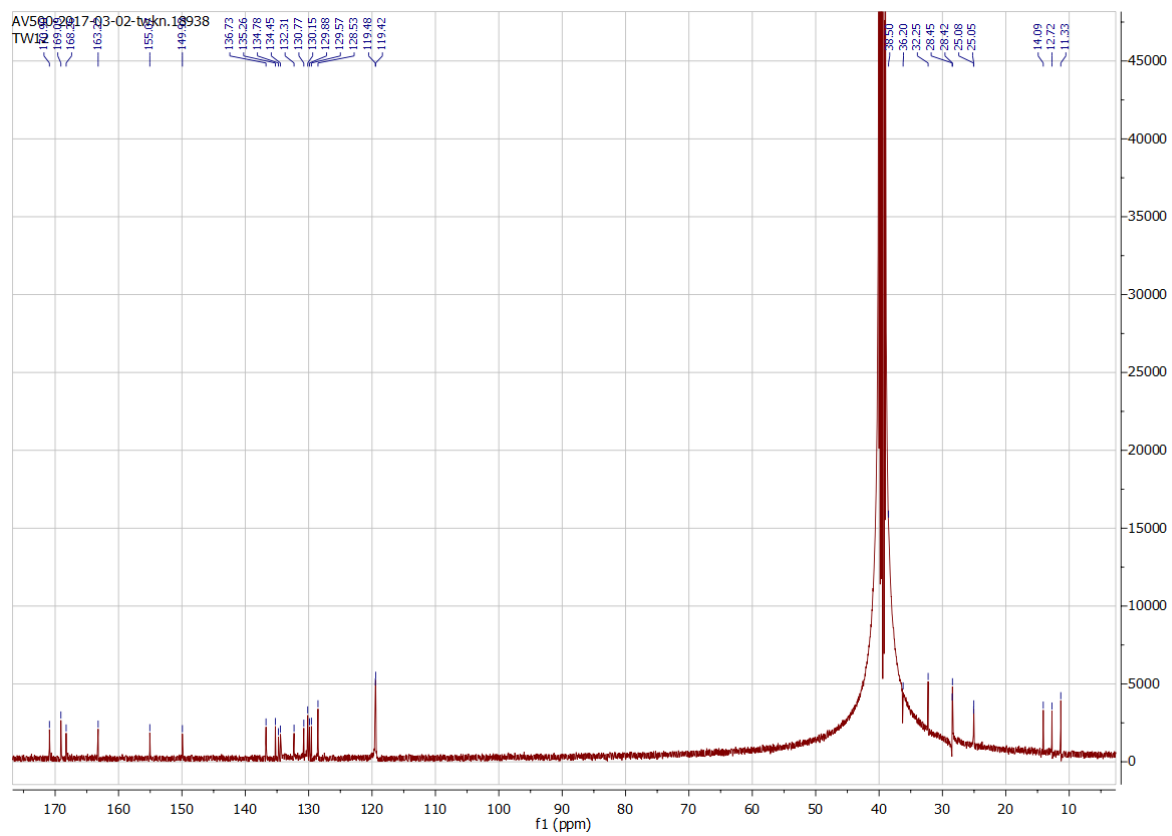


HPLC



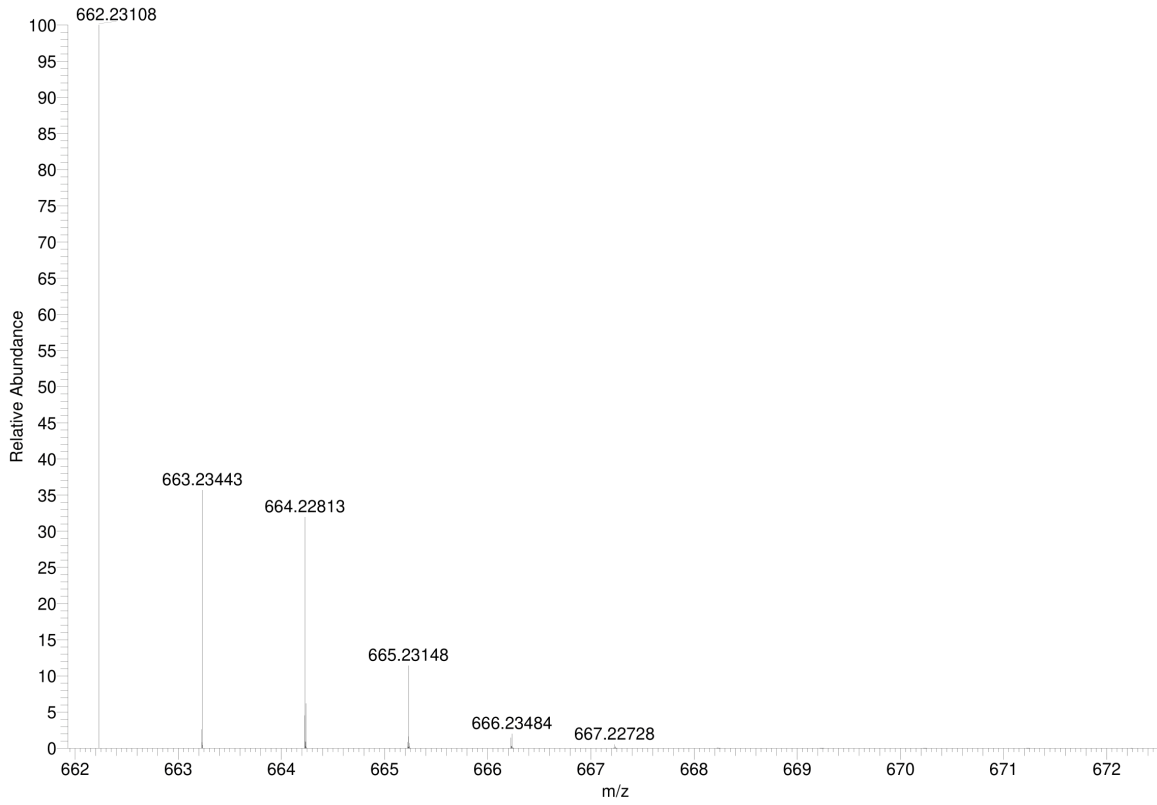
## 9.1.2. Compound 15

<sup>1</sup>H NMR

$^{13}\text{C}$  NMR

### Simulated HRMS

C33H36Cl1N7O4S1 +H: C33 H37 Cl1 N7 O4 S1 pa Chrg 1



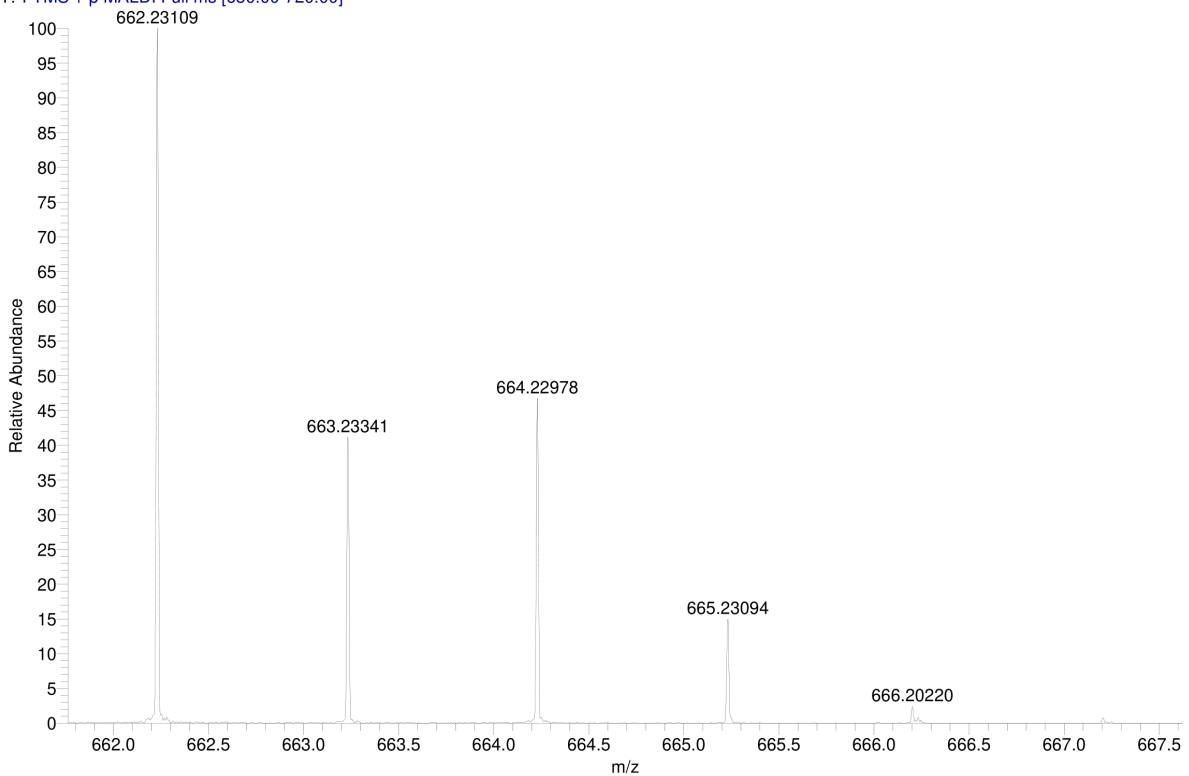
### MALDI HRMS

C:\User\...\Knapp\2017\170301\TW12\_H9

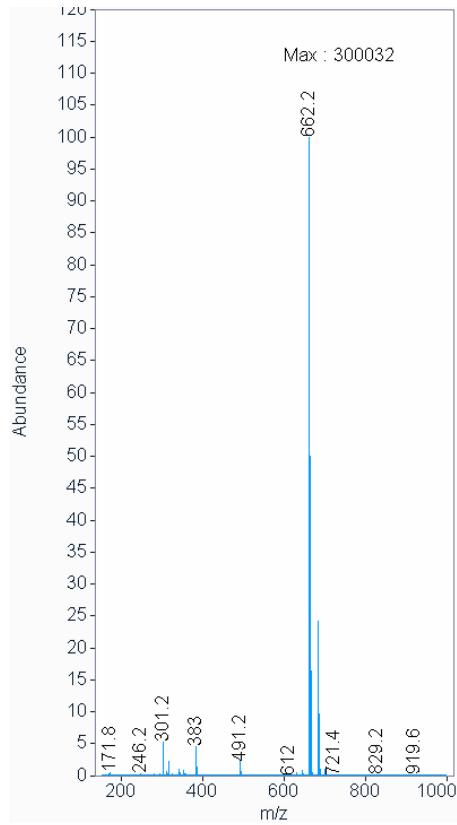
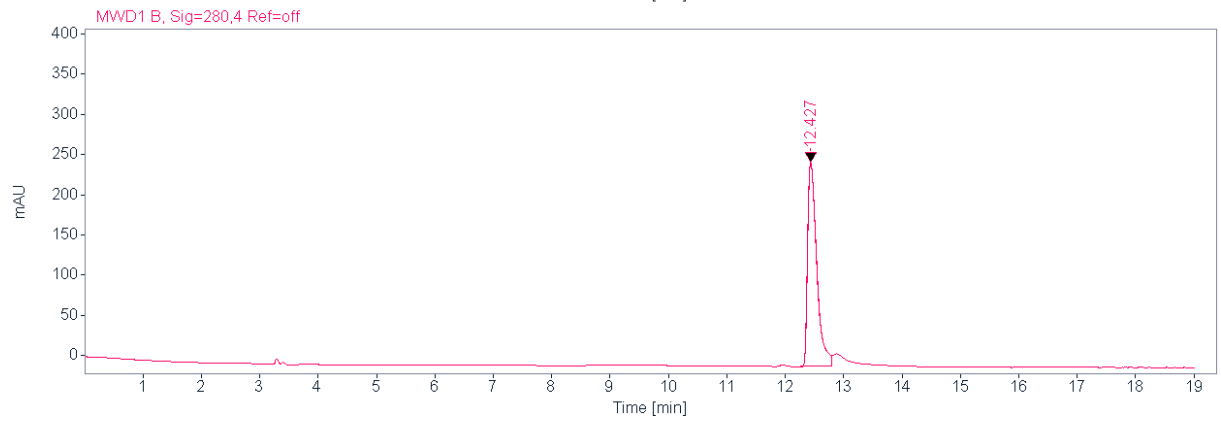
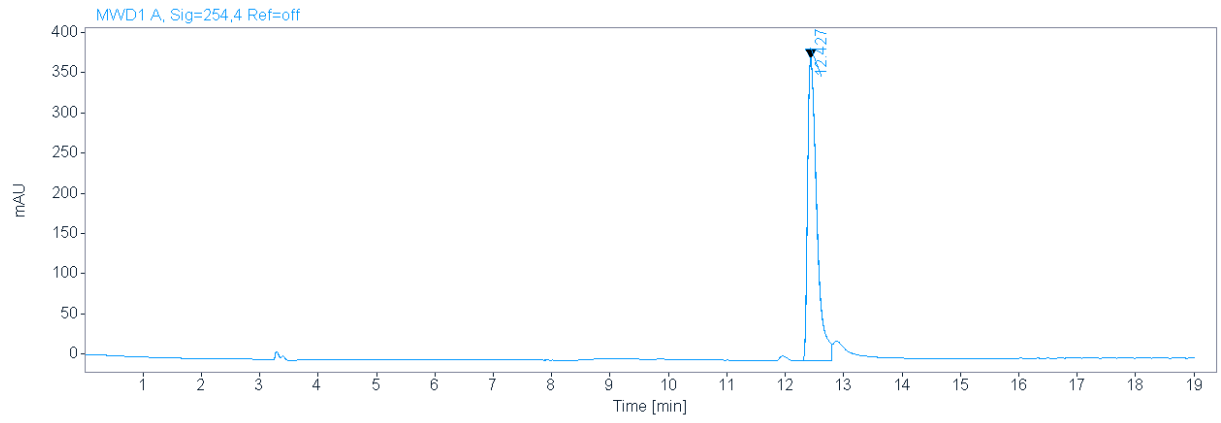
3/1/2017 1:31:05 PM

TW12 mit HCCA gemessen.

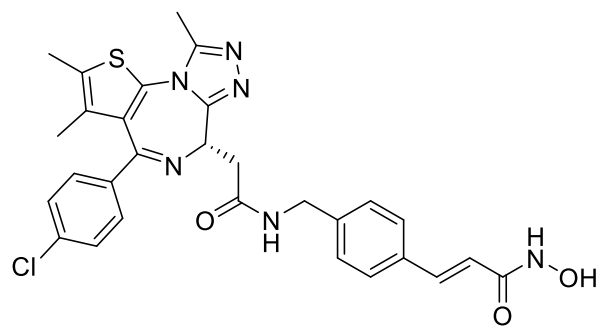
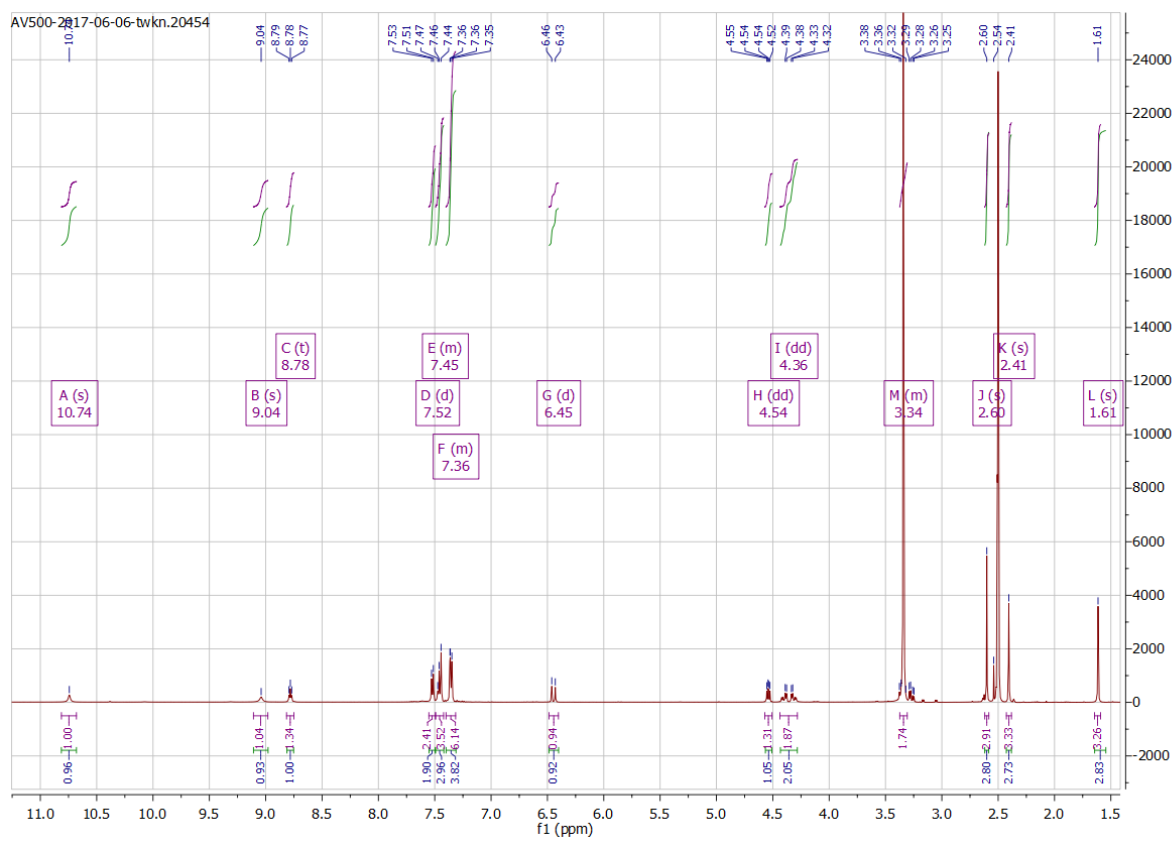
TW12\_H9 #1-2 RT: 0.00-0.05 AV: 2 NL: 1.27E7  
T: FTMS + p MALDI Full ms [650.00-720.00]



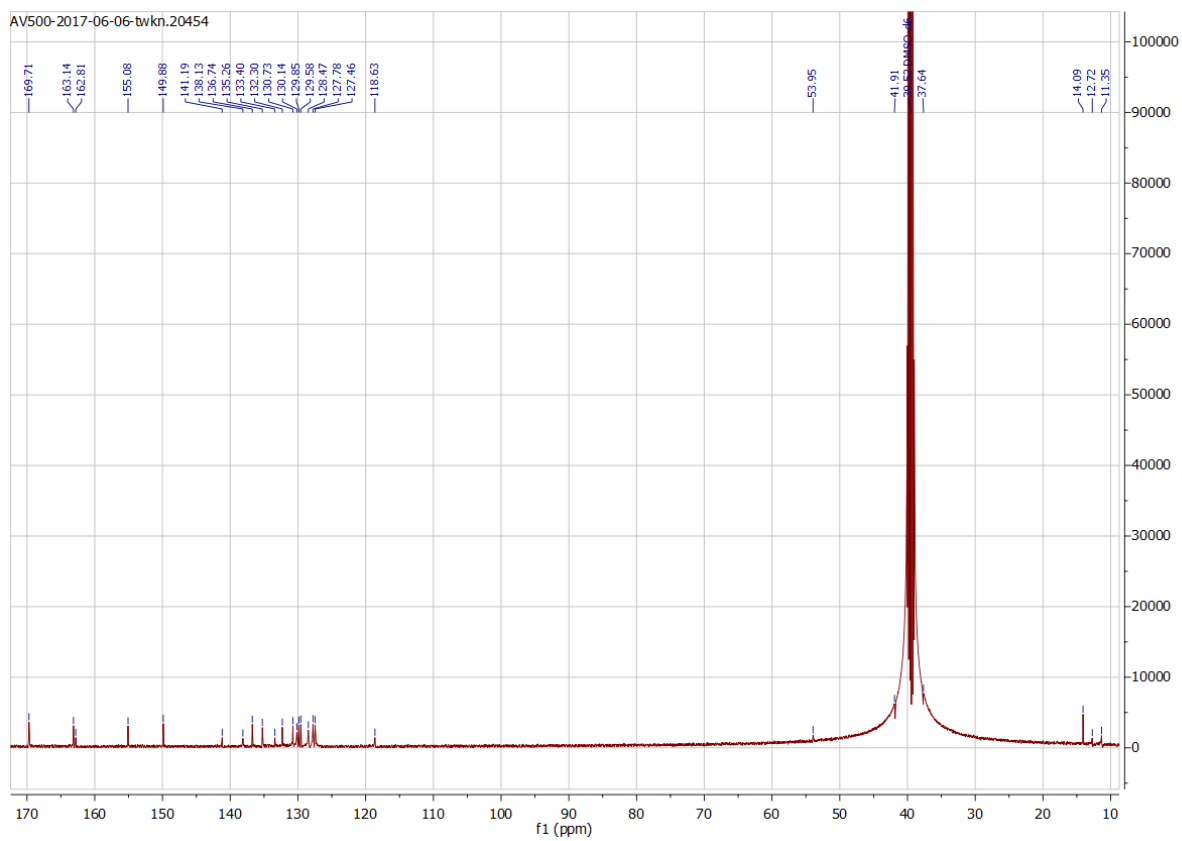
HPLC



## 9.1.3. Compound 16

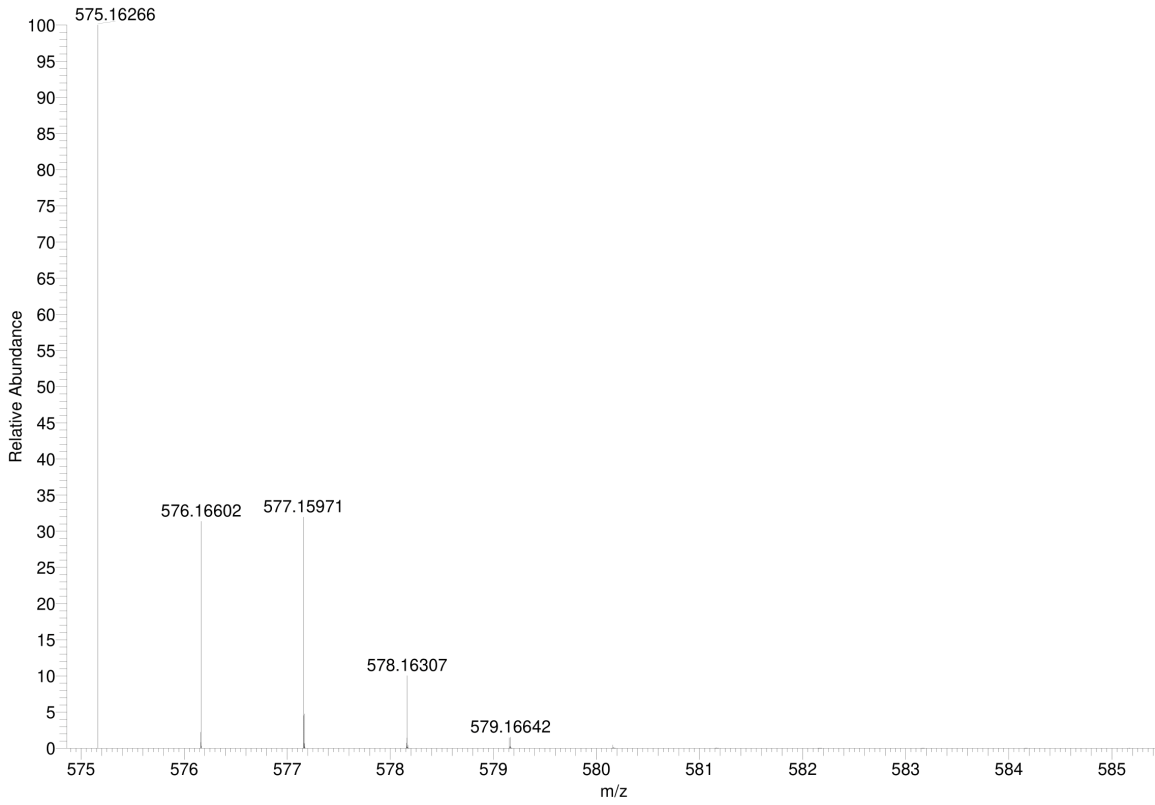
 $^1\text{H NMR}$ 



$^{13}\text{C}$  NMR

### Simulated HRMS

C<sub>29</sub>H<sub>27</sub>Cl<sub>1</sub>N<sub>6</sub>O<sub>3</sub>S<sub>1</sub> +H: C<sub>29</sub> H<sub>28</sub> Cl<sub>1</sub> N<sub>6</sub> O<sub>3</sub> S<sub>1</sub> pa Chrg 1



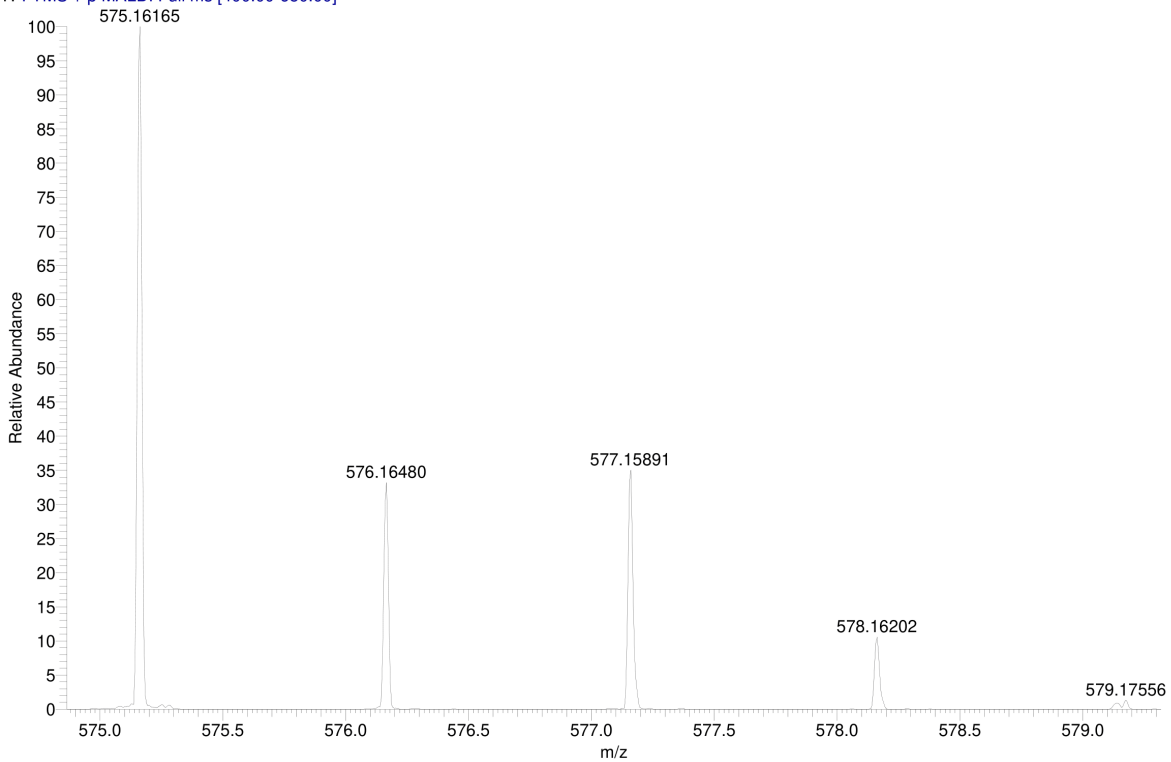
### MALDI HRMS

C:\User\...\Knapp\2017\170628\TW22\_H3

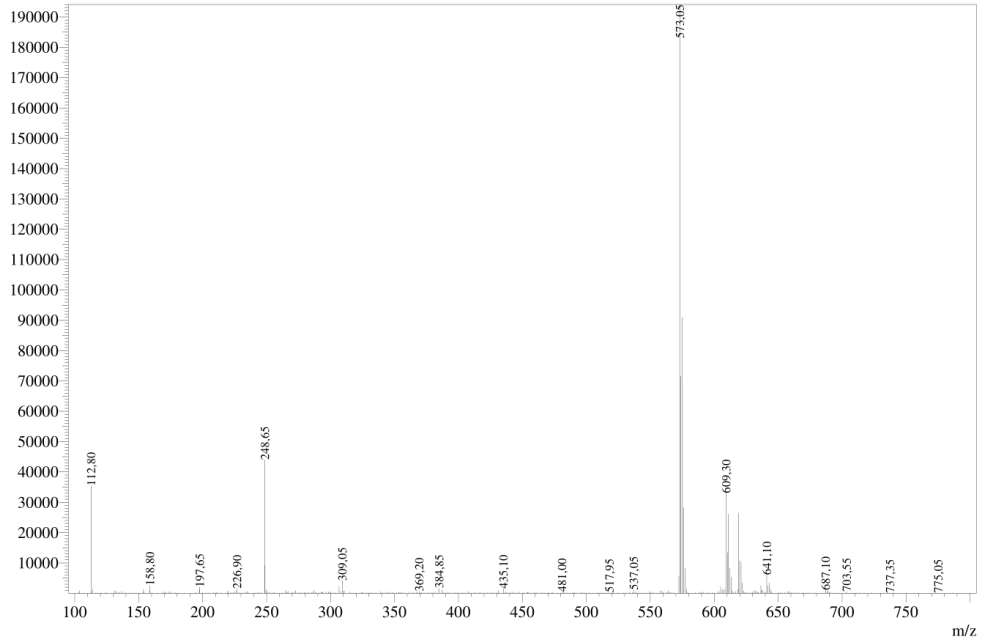
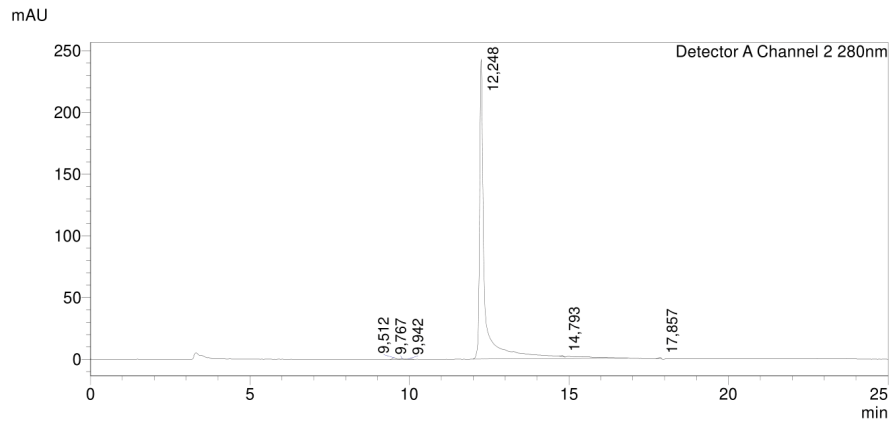
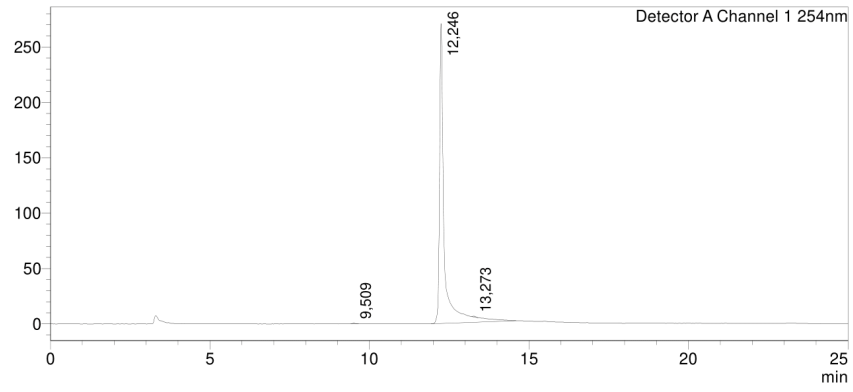
6/28/2017 10:14:14 AM

TW22 mit HCCA gemessen.

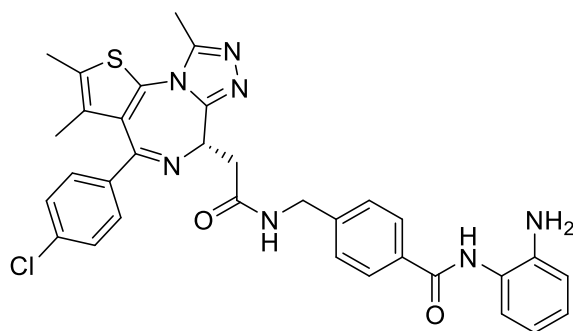
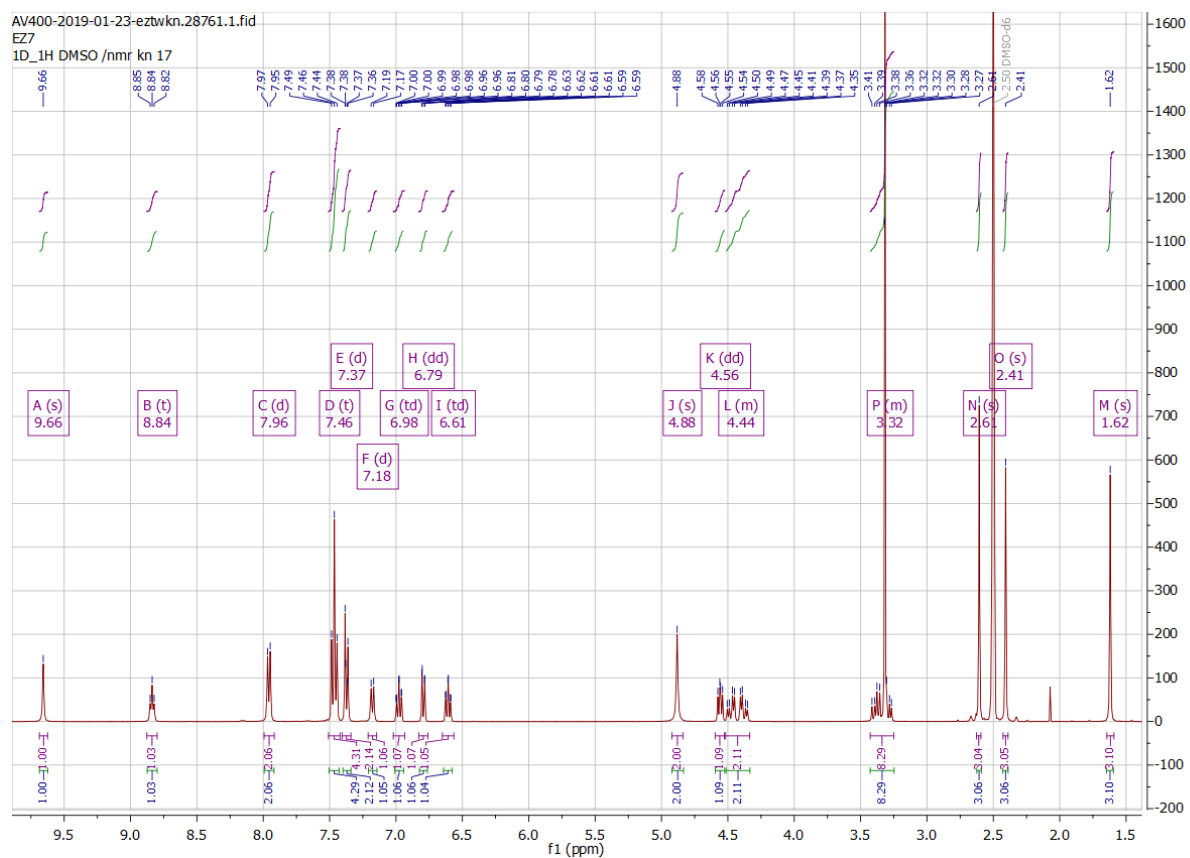
TW22\_H3 #1-9 RT: 0.00-0.91 AV: 9 NL: 8.83E5  
T: FTMS + p MALDI Full ms [400.00-650.00]

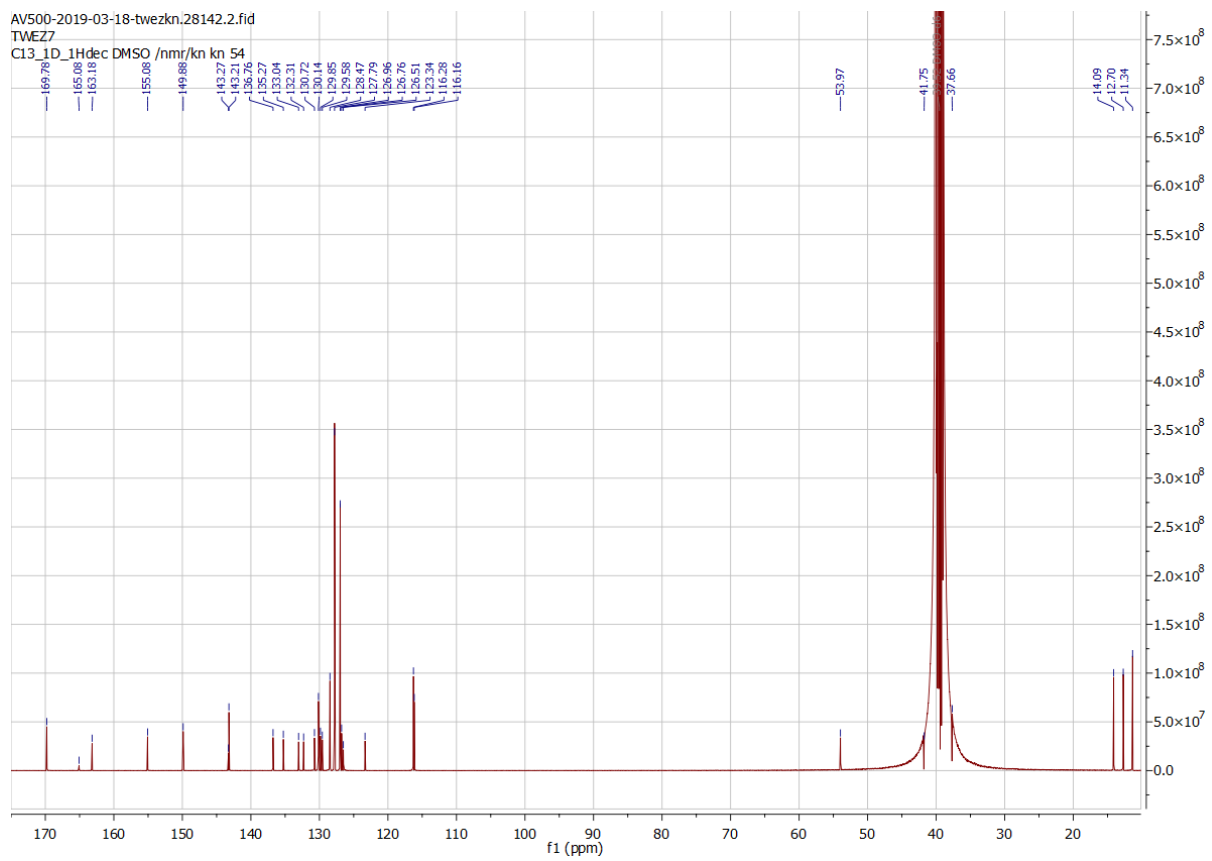


HPLC



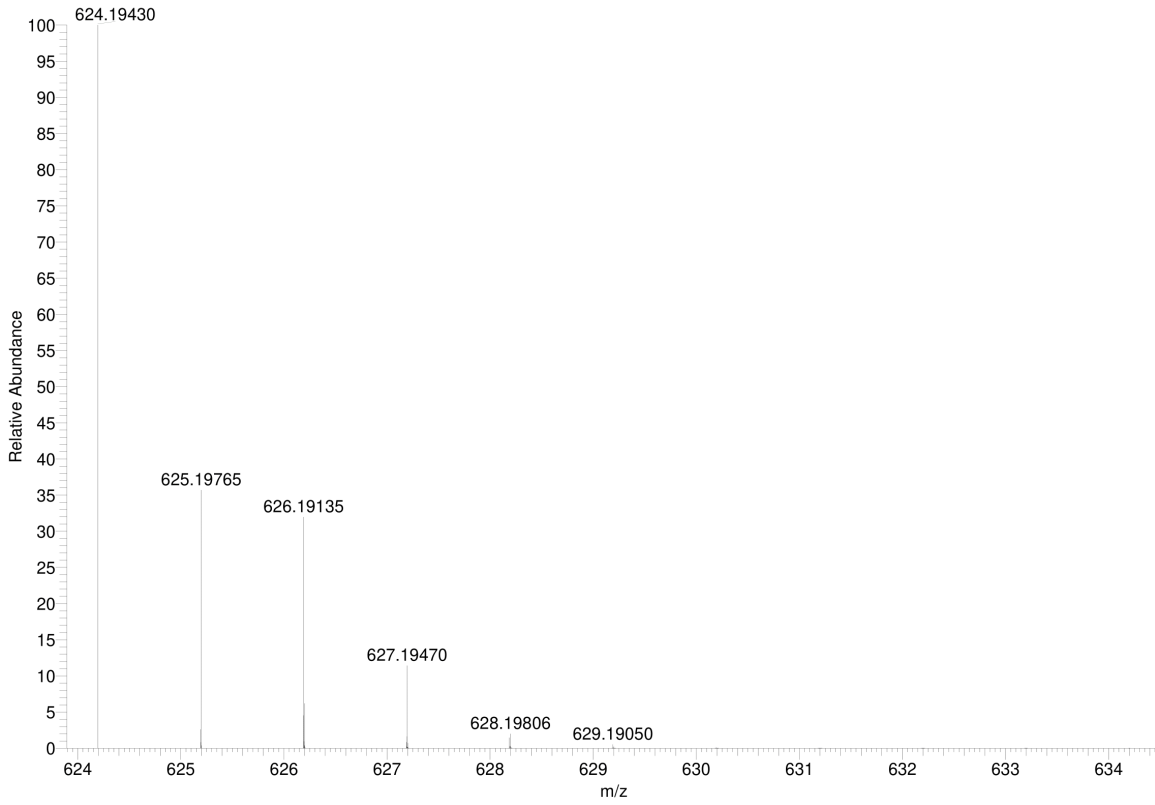
## 9.1.4. Compound 62

<sup>1</sup>H NMR

$^{13}\text{C}$  NMR

### Simulated HRMS

C<sub>33</sub>H<sub>30</sub>Cl<sub>1</sub>N<sub>7</sub>O<sub>2</sub>S<sub>1</sub> +H: C<sub>33</sub> H<sub>31</sub> Cl<sub>1</sub> N<sub>7</sub> O<sub>2</sub> S<sub>1</sub> pa Chrg 1



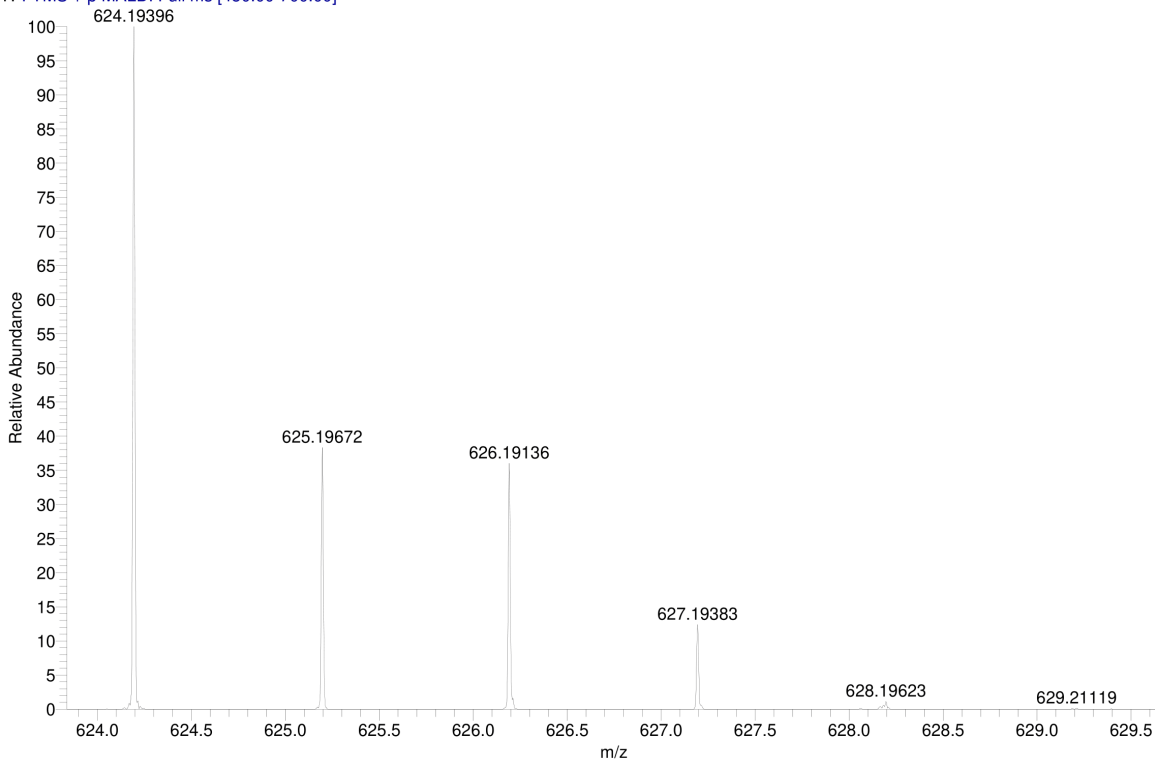
### MALDI HRMS

C:\User\...\2020\16.07.2020\TWEt 7\_D11

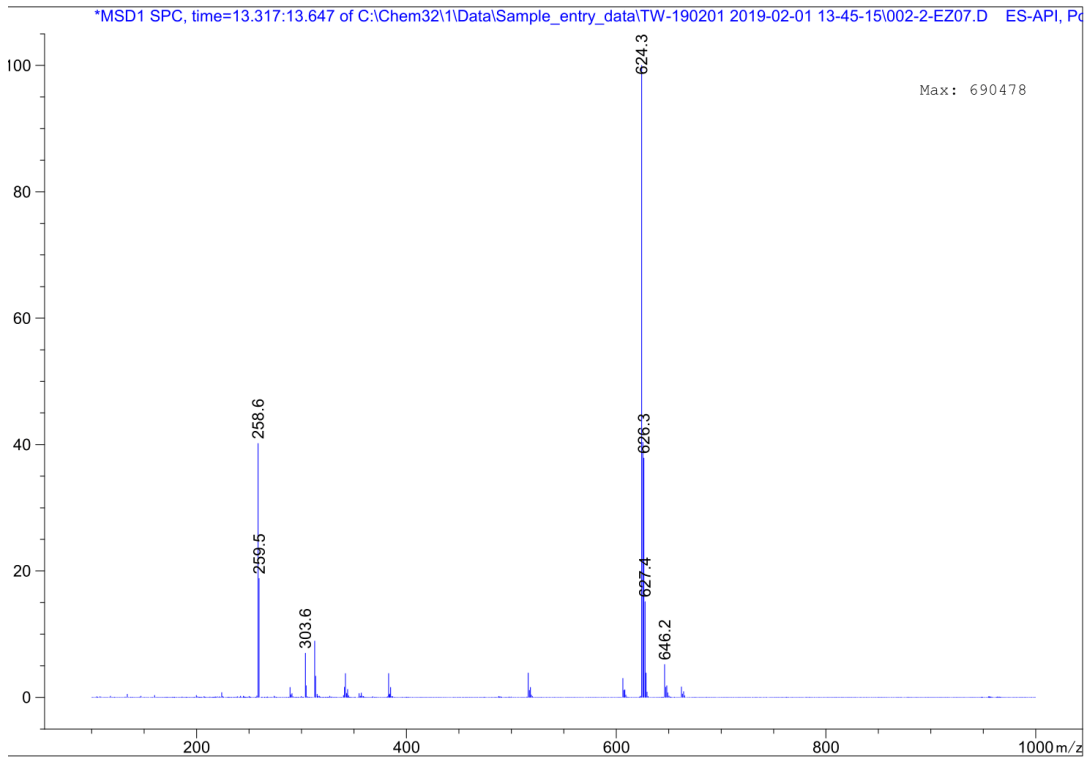
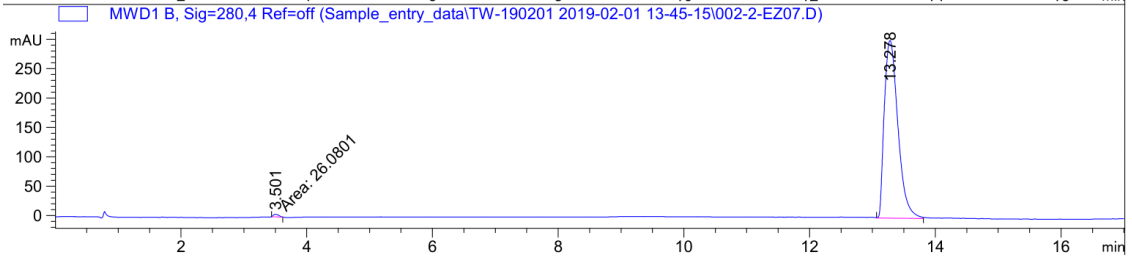
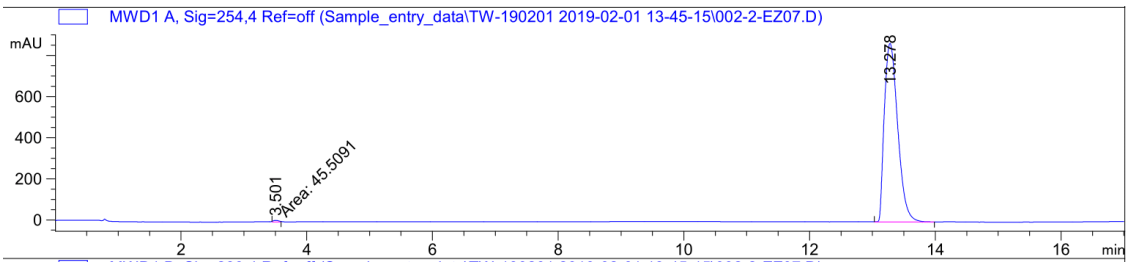
7/16/2020 6:26:26 PM

TWEt 7 mit HCCA gemessen.

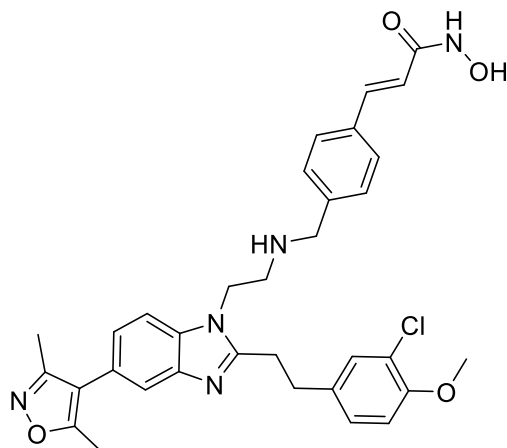
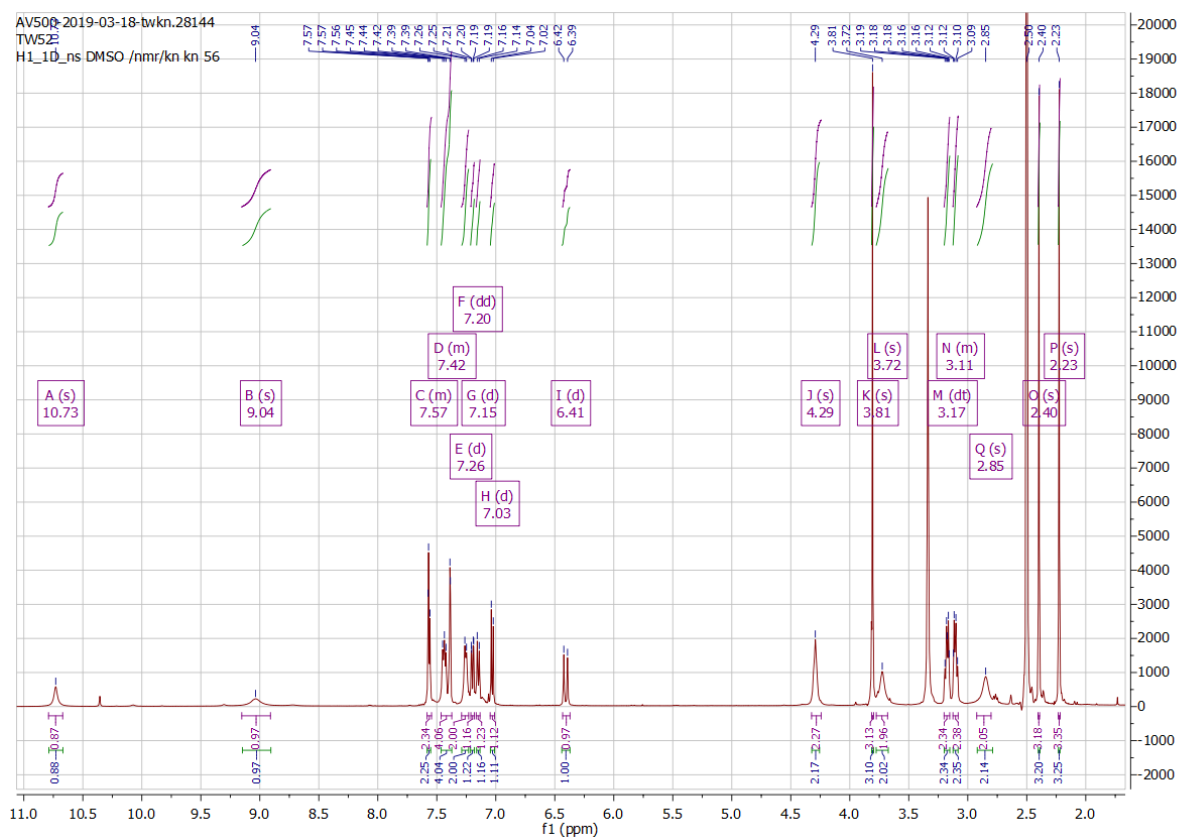
TWEt 7\_D11 #1-5 RT: 0.00-0.44 AV: 5 NL: 6.03E5  
T: FTMS + p MALDI Full ms [450.00-700.00]



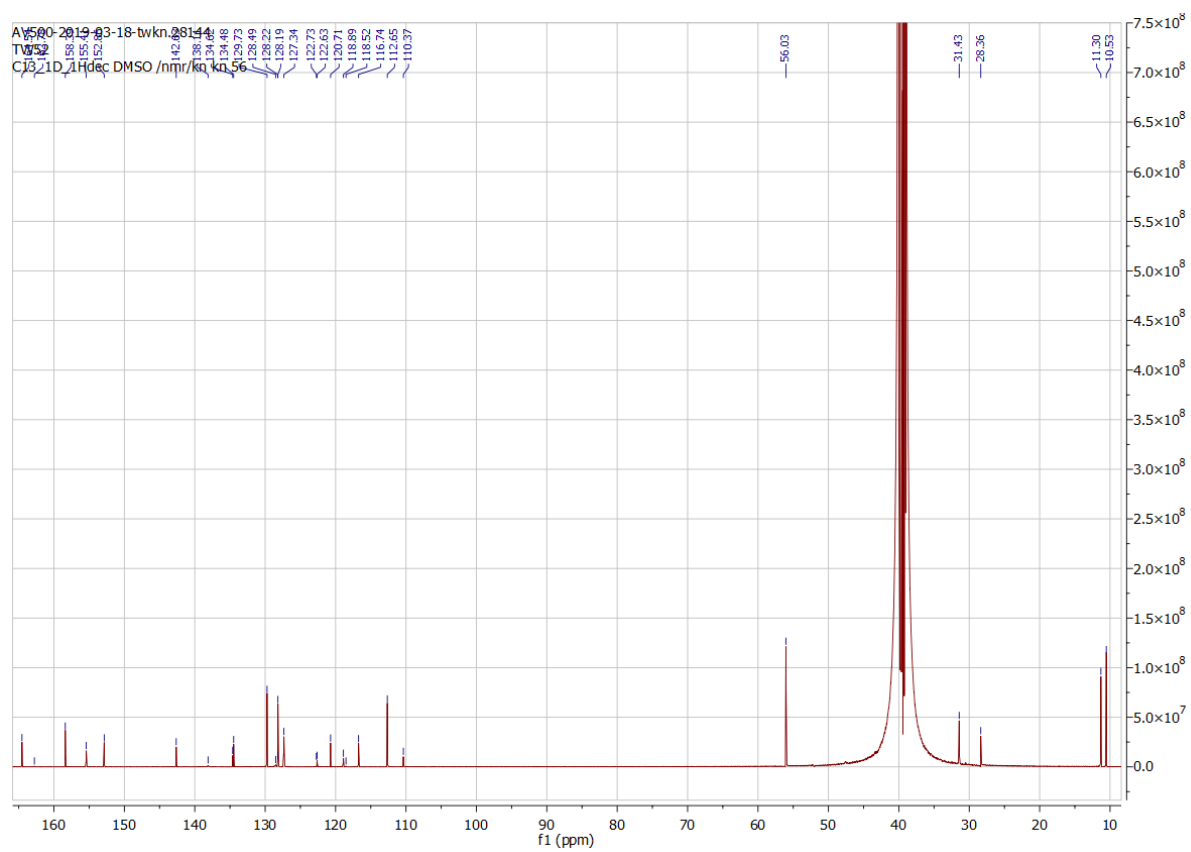
HPLC



## 9.1.5. Compound 18

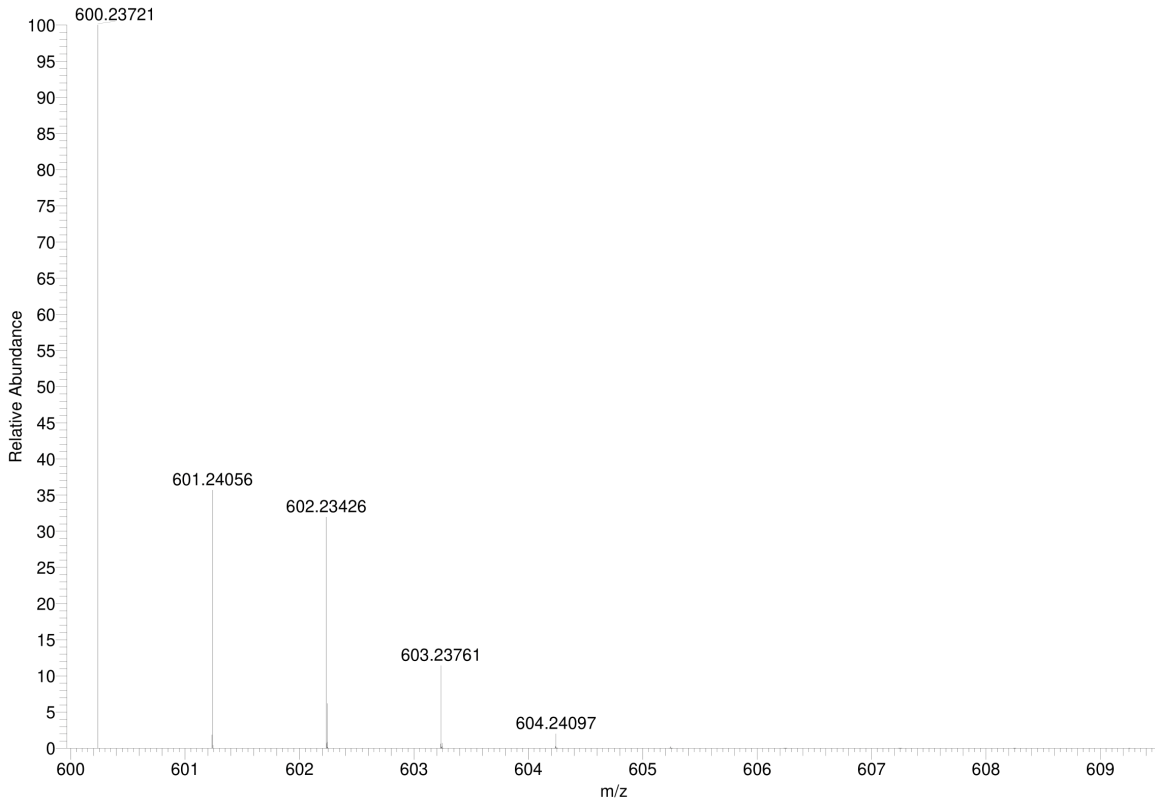
<sup>1</sup>H NMR



$^{13}\text{C}$  NMR

### Simulated HRMS

C<sub>33</sub>H<sub>34</sub>Cl<sub>1</sub>N<sub>5</sub>O<sub>4</sub> +H: C<sub>33</sub> H<sub>35</sub> Cl<sub>1</sub> N<sub>5</sub> O<sub>4</sub> pa Chrg 1



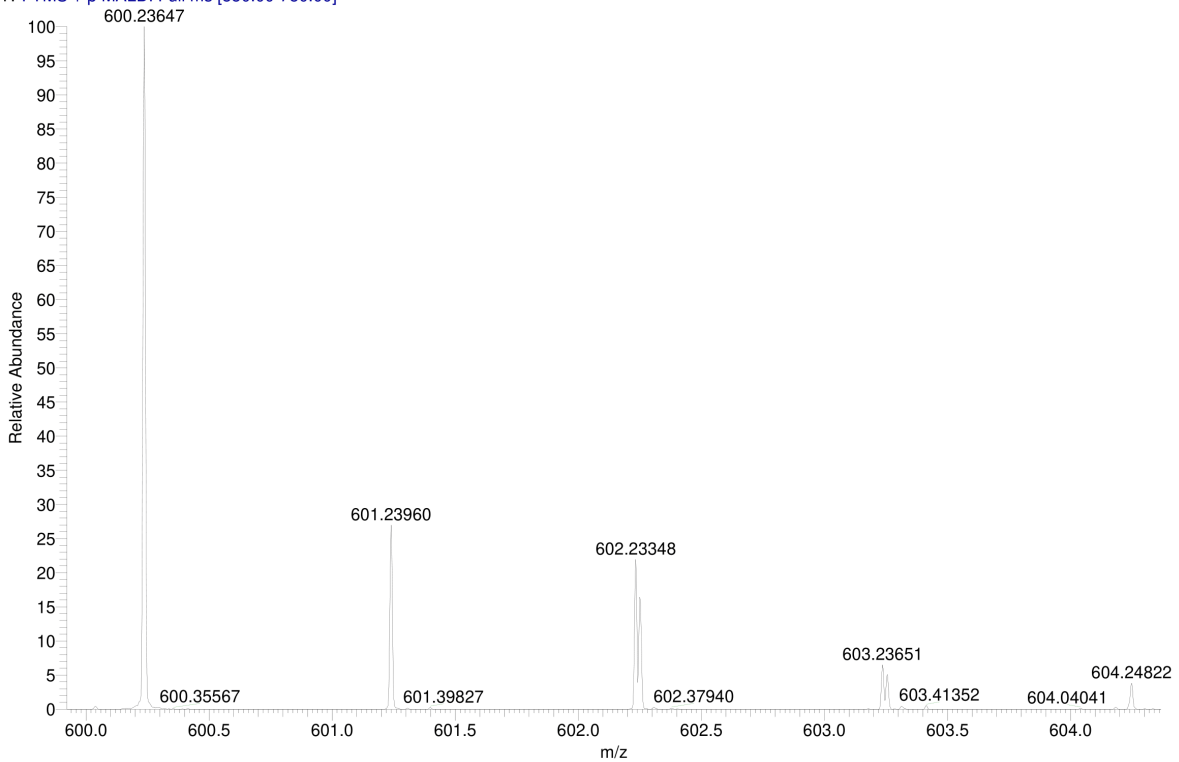
### MALDI HRMS

C:\User\...\Knapp\2019\190821\TW52\_B1

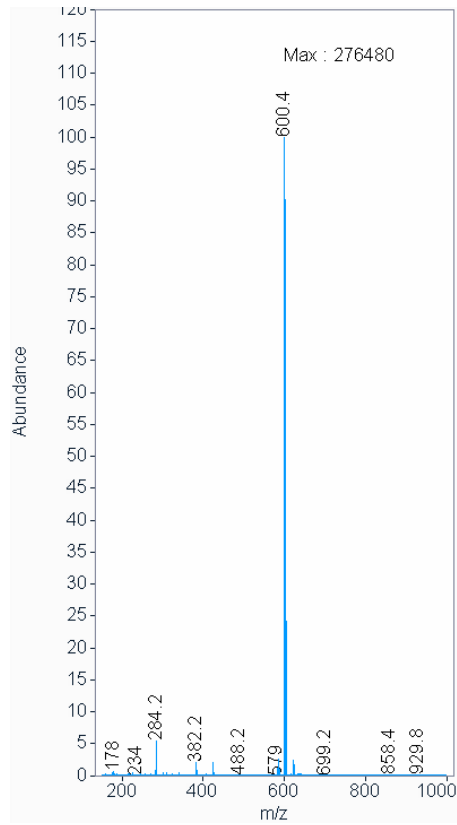
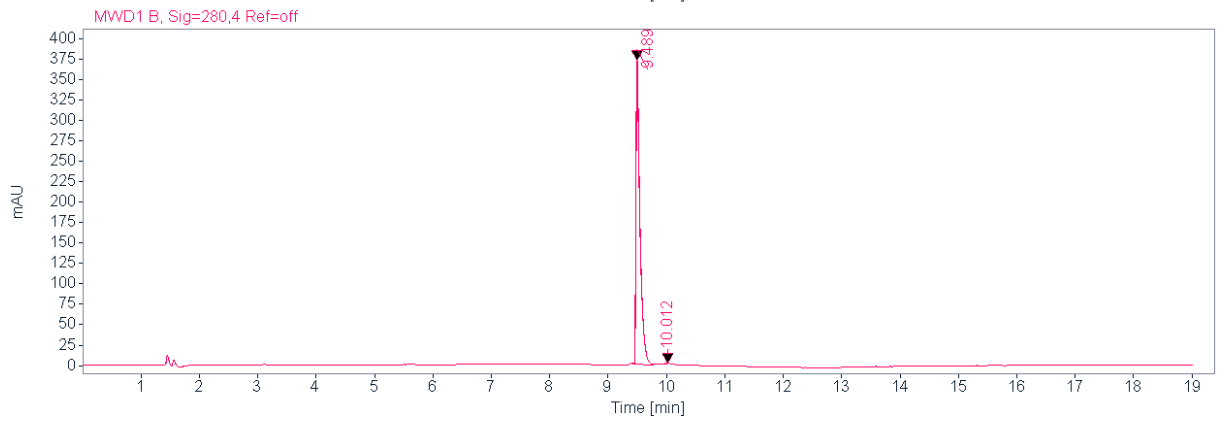
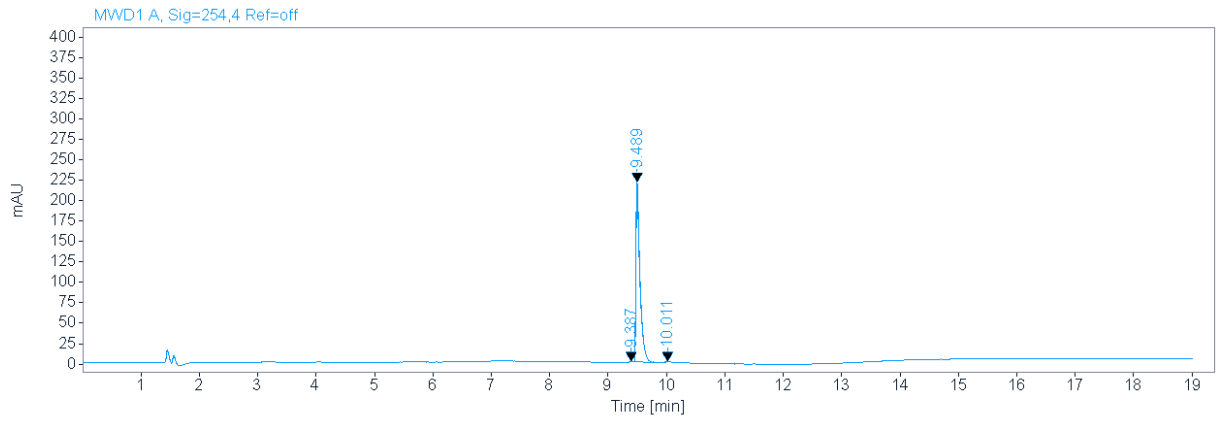
8/21/2019 4:09:43 PM

TW52 mit HCCA gemessen.

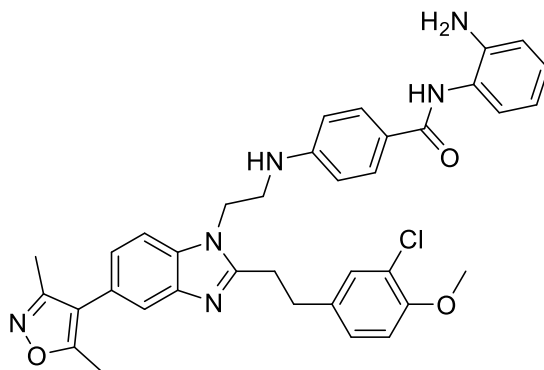
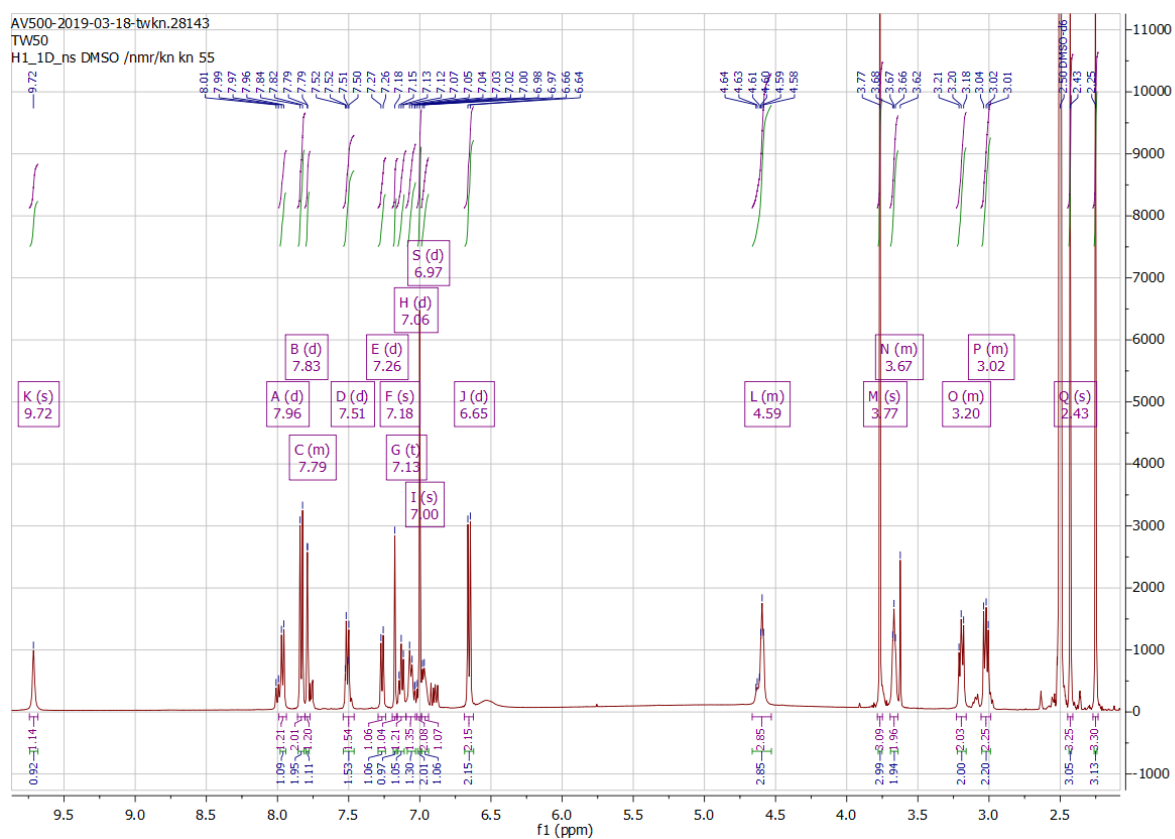
TW52\_B1 #1-11 RT: 0.00-0.74 AV: 11 NL: 1.61E6  
T: FTMS + p MALDI Full ms [550.00-750.00]

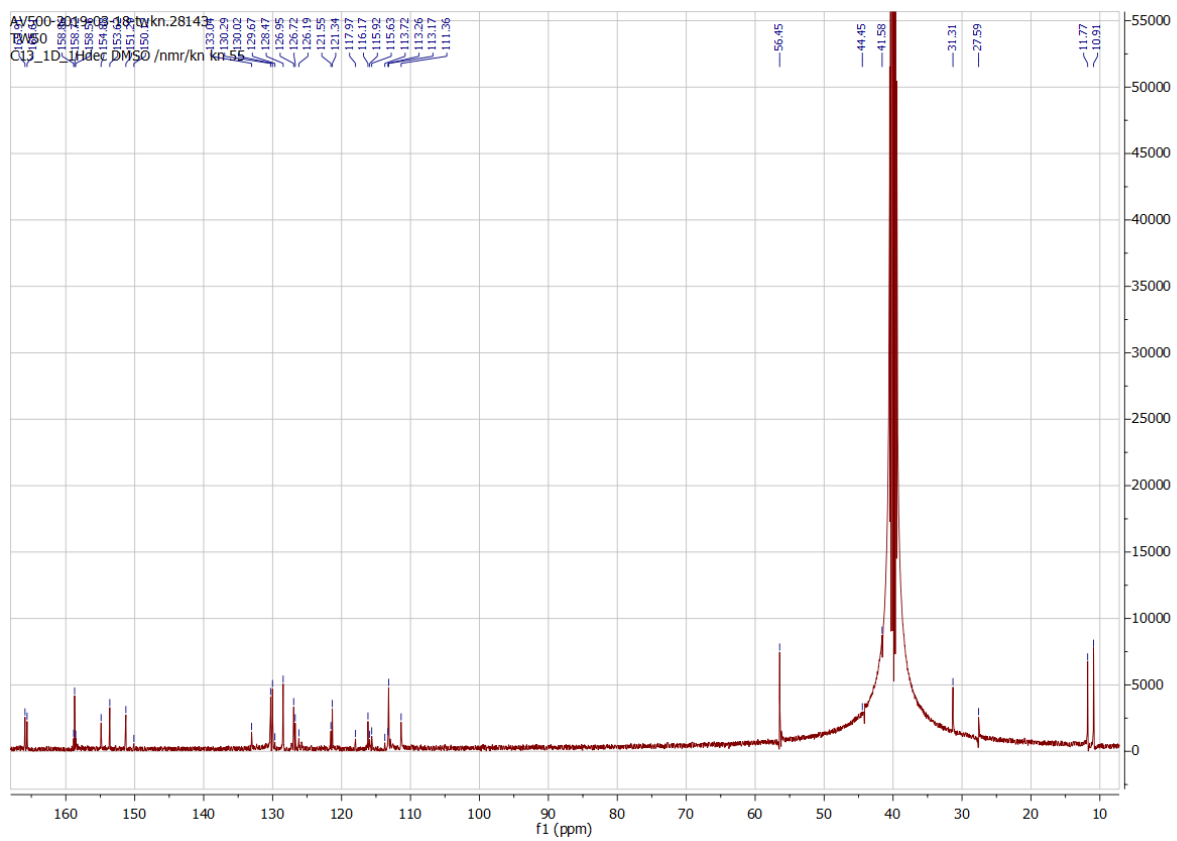


HPLC



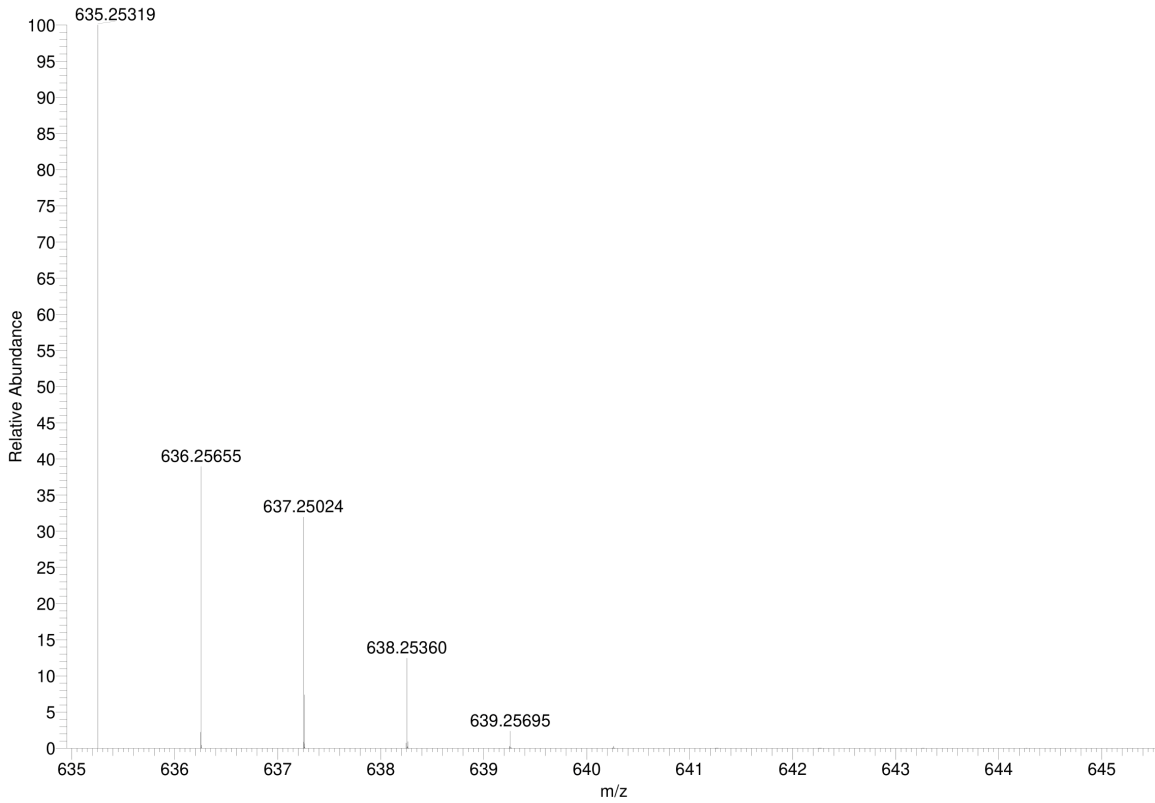
## 9.1.6. Compound 19

<sup>1</sup>H NMR

$^{13}\text{C}$  NMR

### Simulated HRMS

C<sub>36</sub>H<sub>35</sub>Cl<sub>1</sub>N<sub>6</sub>O<sub>3</sub> +H: C<sub>36</sub> H<sub>36</sub> Cl<sub>1</sub> N<sub>6</sub> O<sub>3</sub> pa Chrg 1



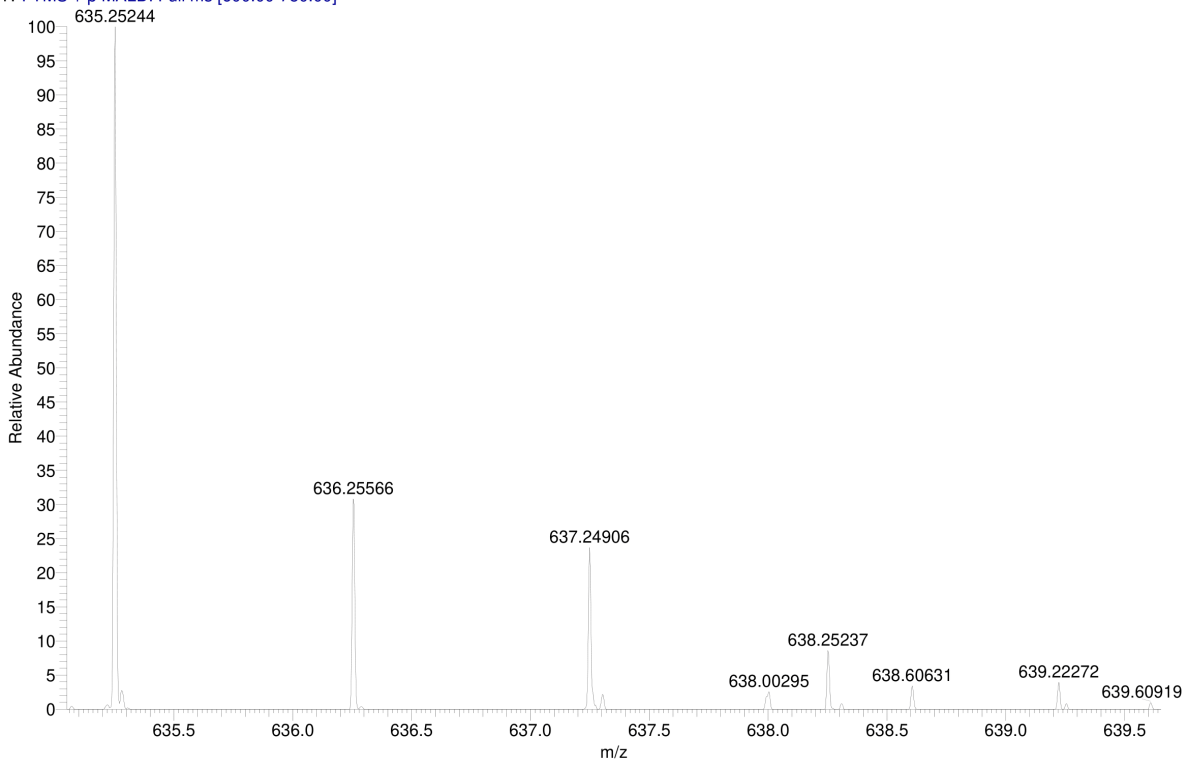
### MALDI HRMS

C:\User\...\Knapp\2019\190821\TW50\_A12

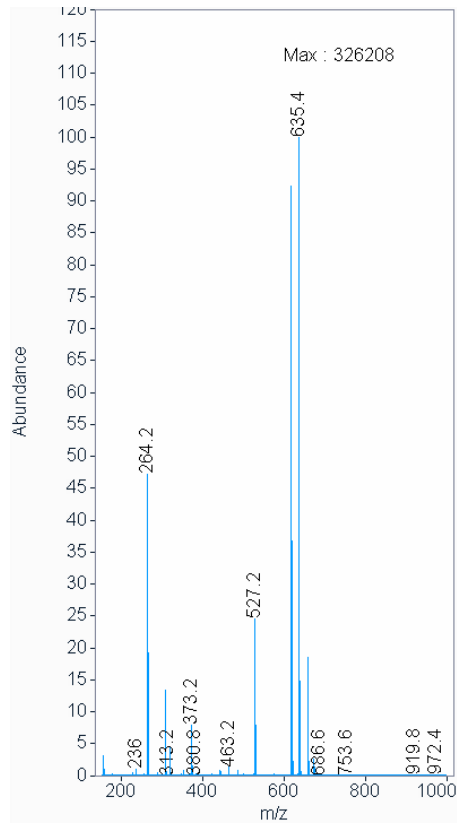
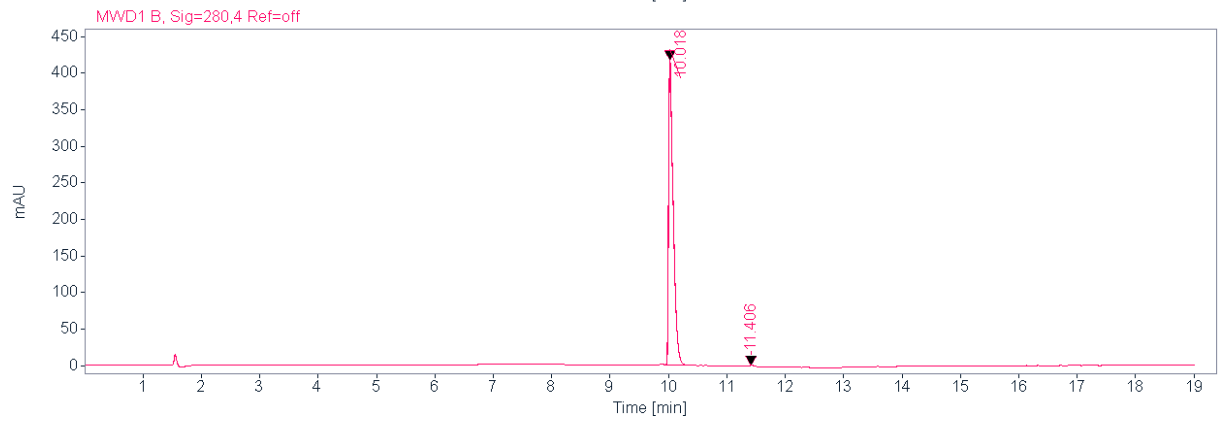
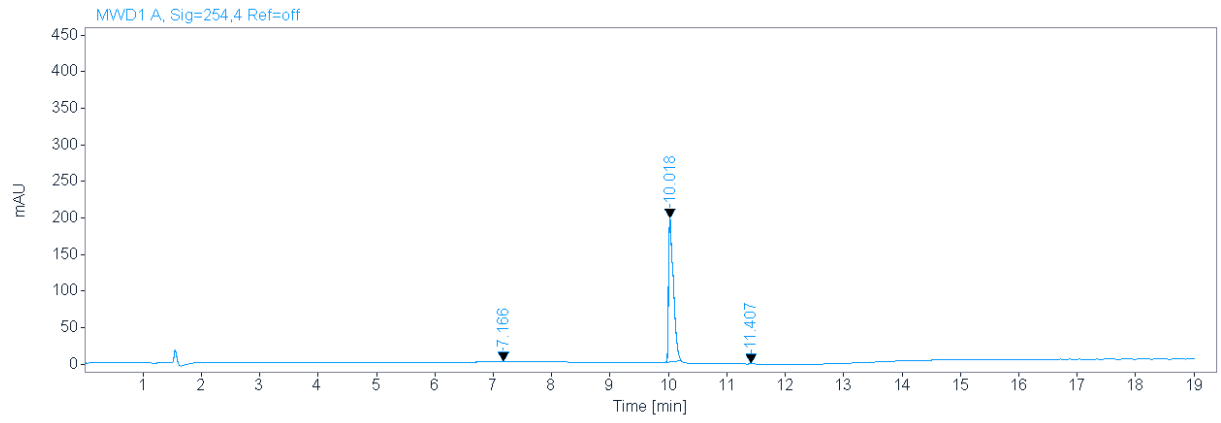
8/21/2019 4:08:14 PM

TW50 mit HCCA gemessen.

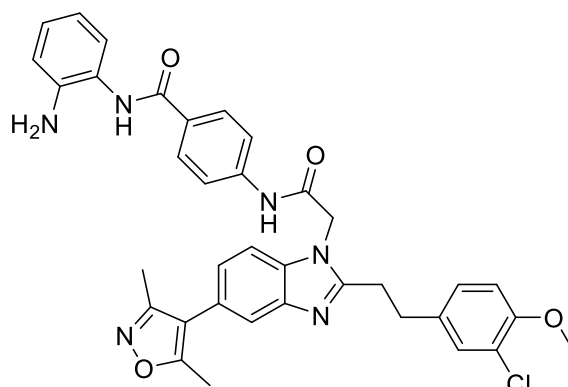
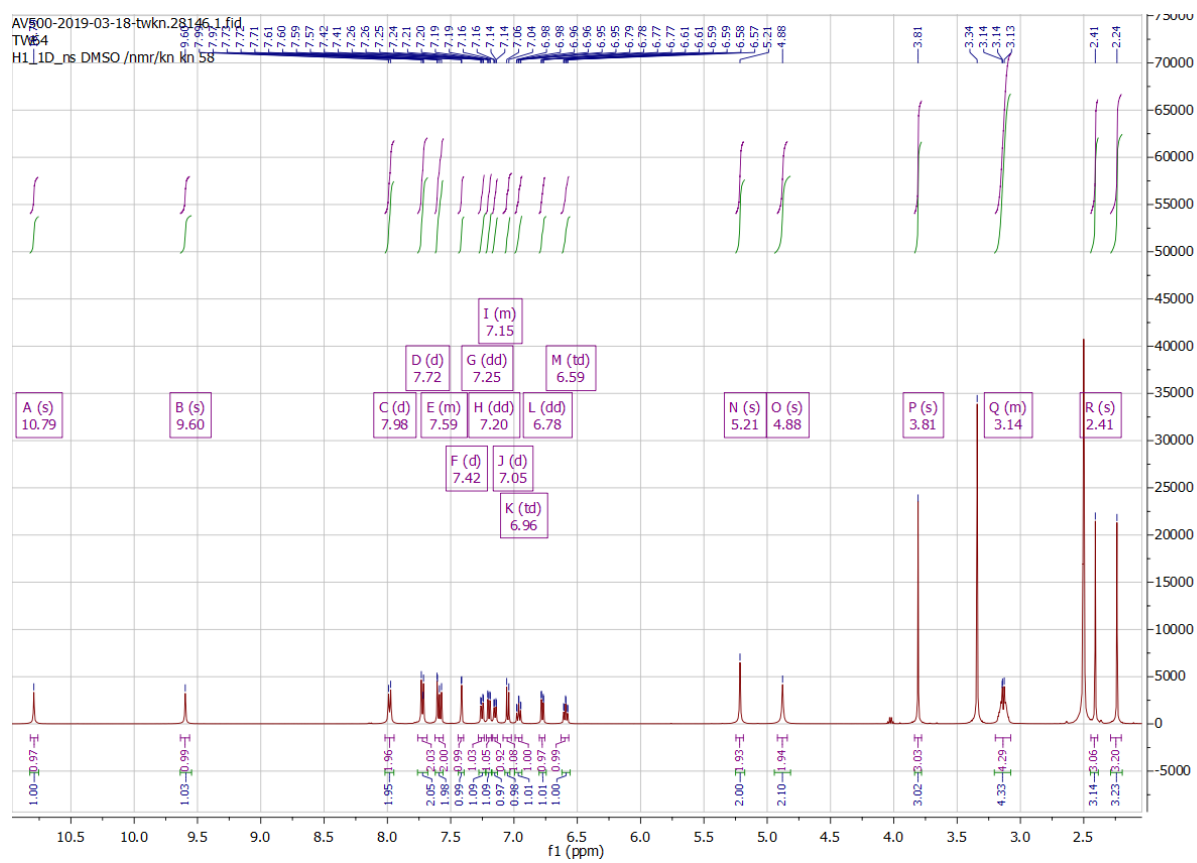
TW50\_A12 #1-7 RT: 0.01-0.58 AV: 7 NL: 4.30E5  
T: FTMS + p MALDI Full ms [600.00-750.00]



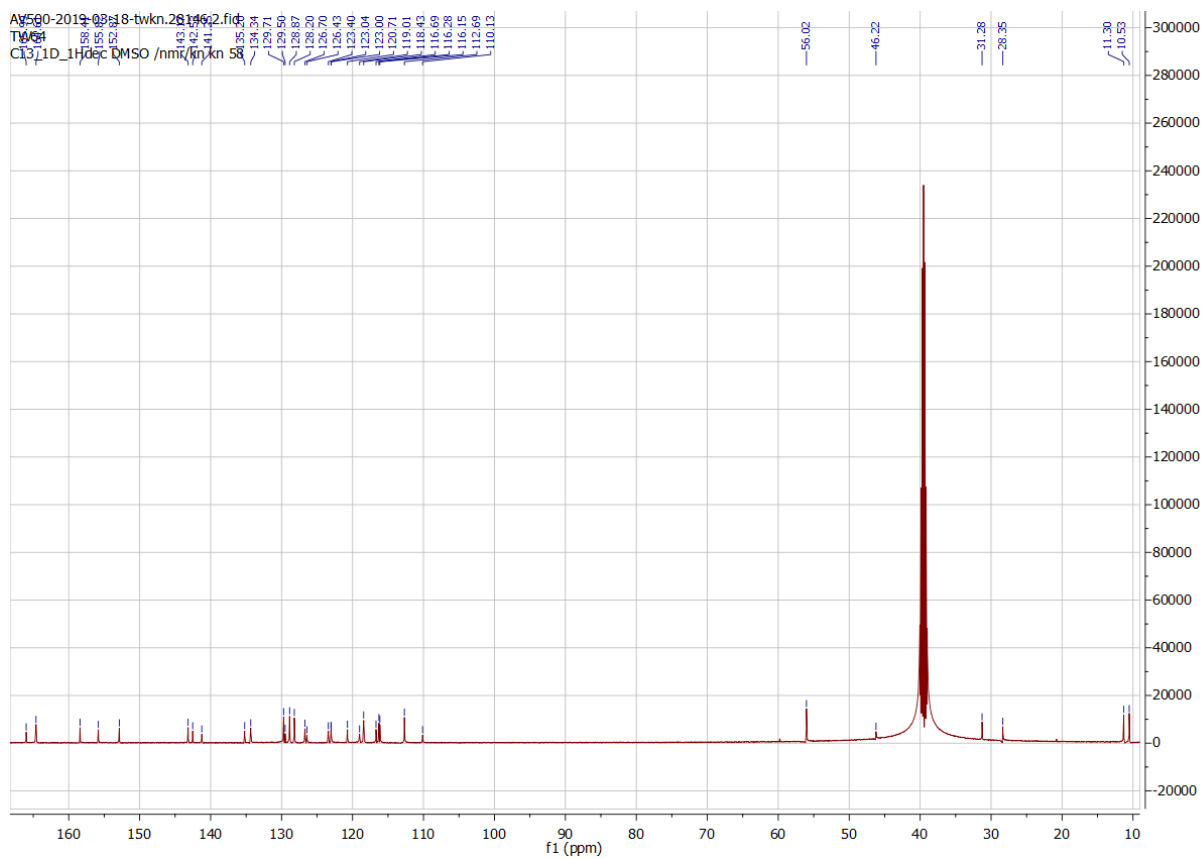
HPLC



## 9.1.7. Compound 20

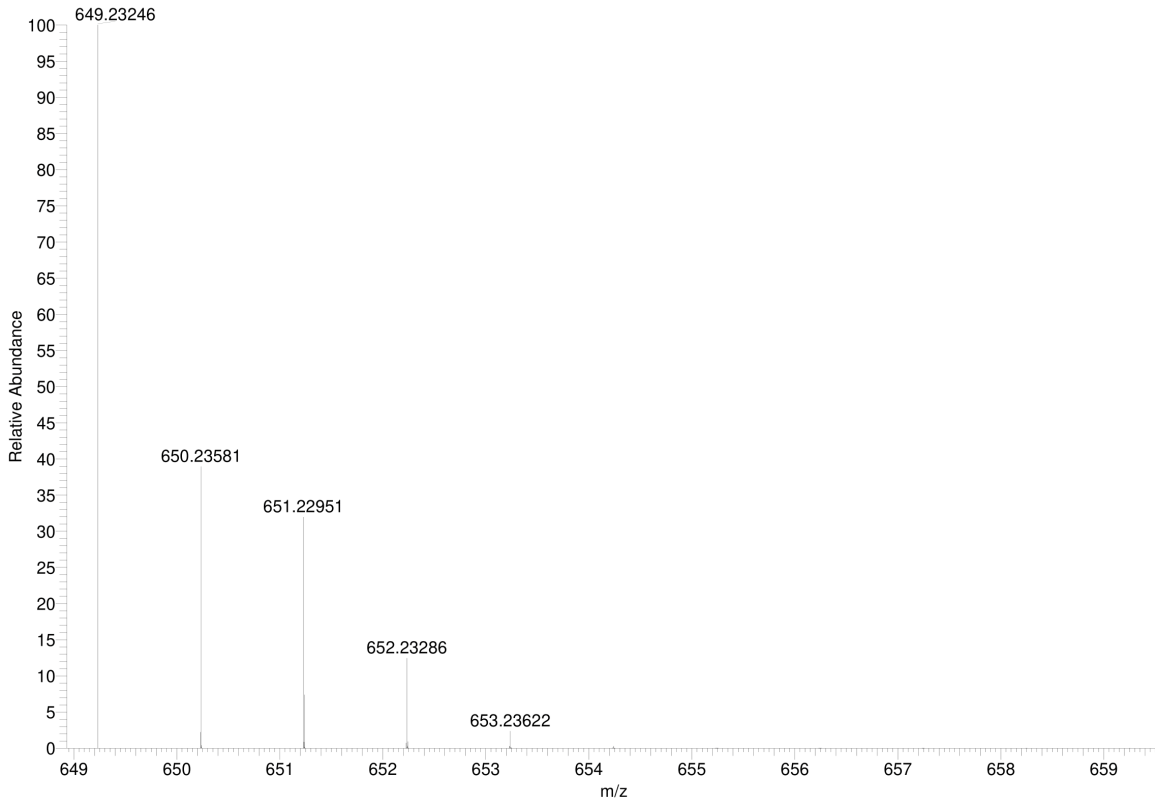
<sup>1</sup>H NMR



$^{13}\text{C}$  NMR

### Simulated HRMS

C<sub>36</sub>H<sub>33</sub>Cl<sub>1</sub>N<sub>6</sub>O<sub>4</sub> +H: C<sub>36</sub> H<sub>34</sub> Cl<sub>1</sub> N<sub>6</sub> O<sub>4</sub> pa Chrg 1



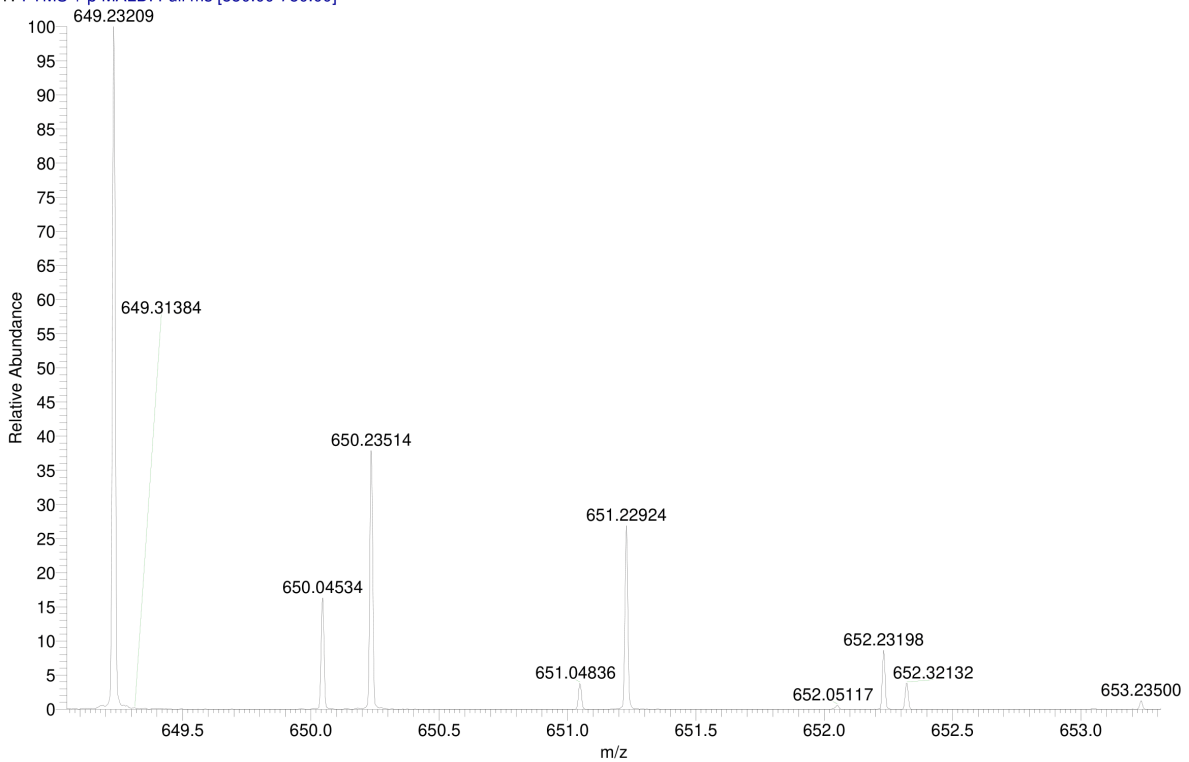
### MALDI HRMS

C:\User\...\Knapp\2019\190821\TW64\_B2

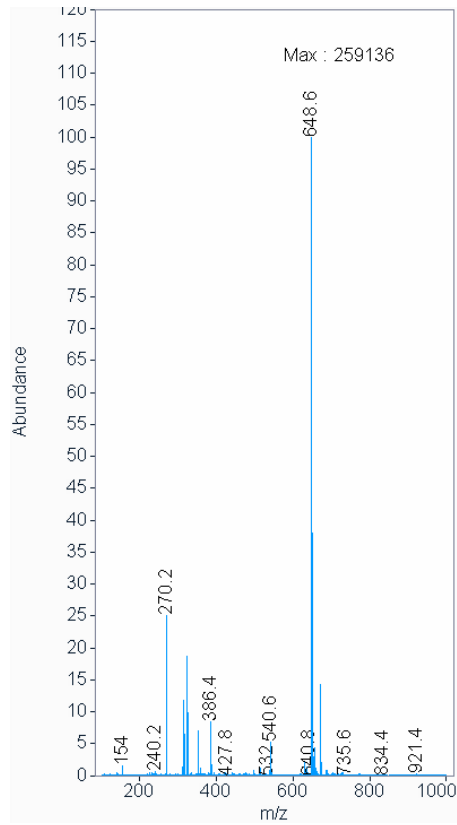
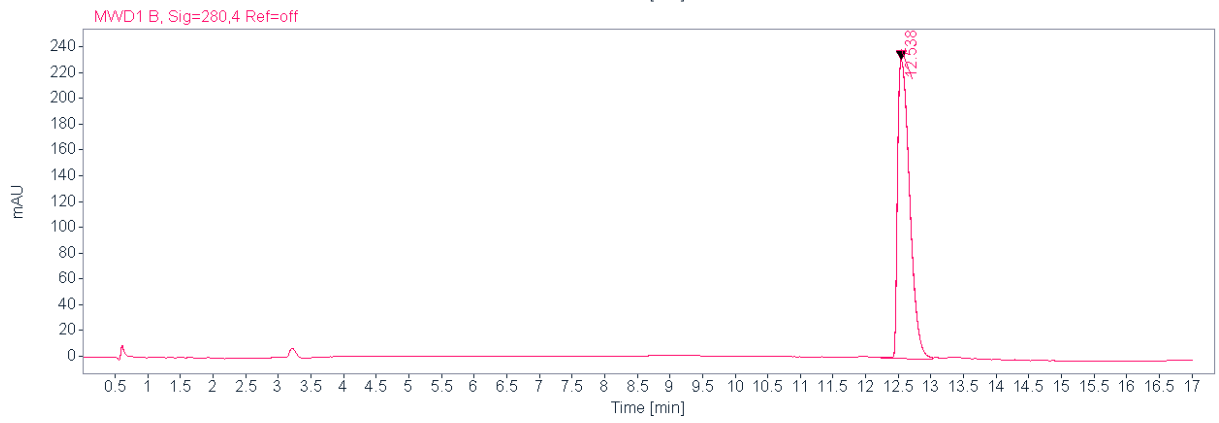
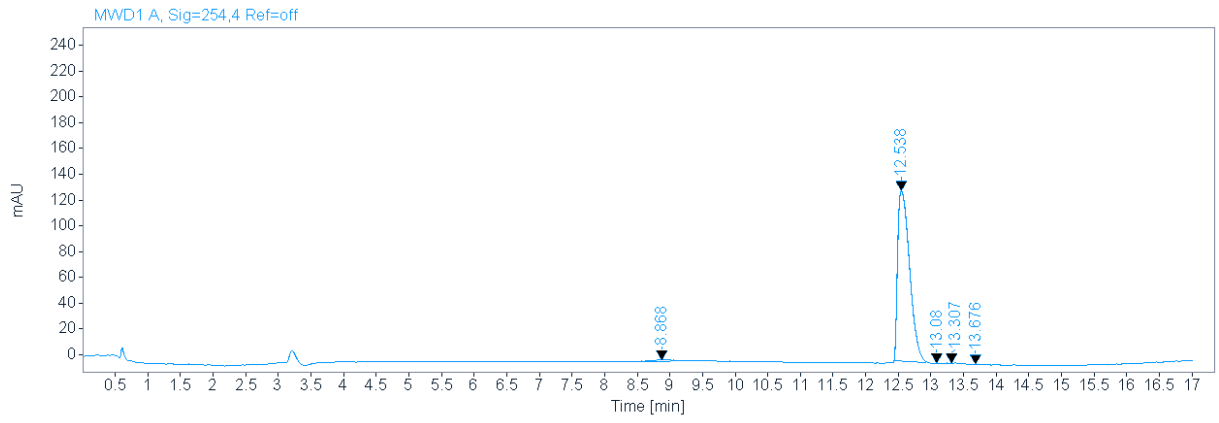
8/21/2019 4:11:19 PM

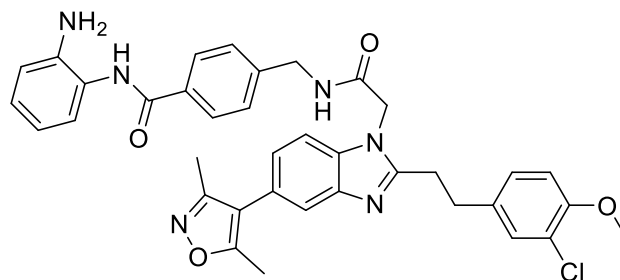
TW64 mit HCCA gemessen.

TW64\_B2 #1-16 RT: 0.00-1.56 AV: 16 NL: 2.14E6  
T: FTMS + p MALDI Full ms [550.00-750.00]

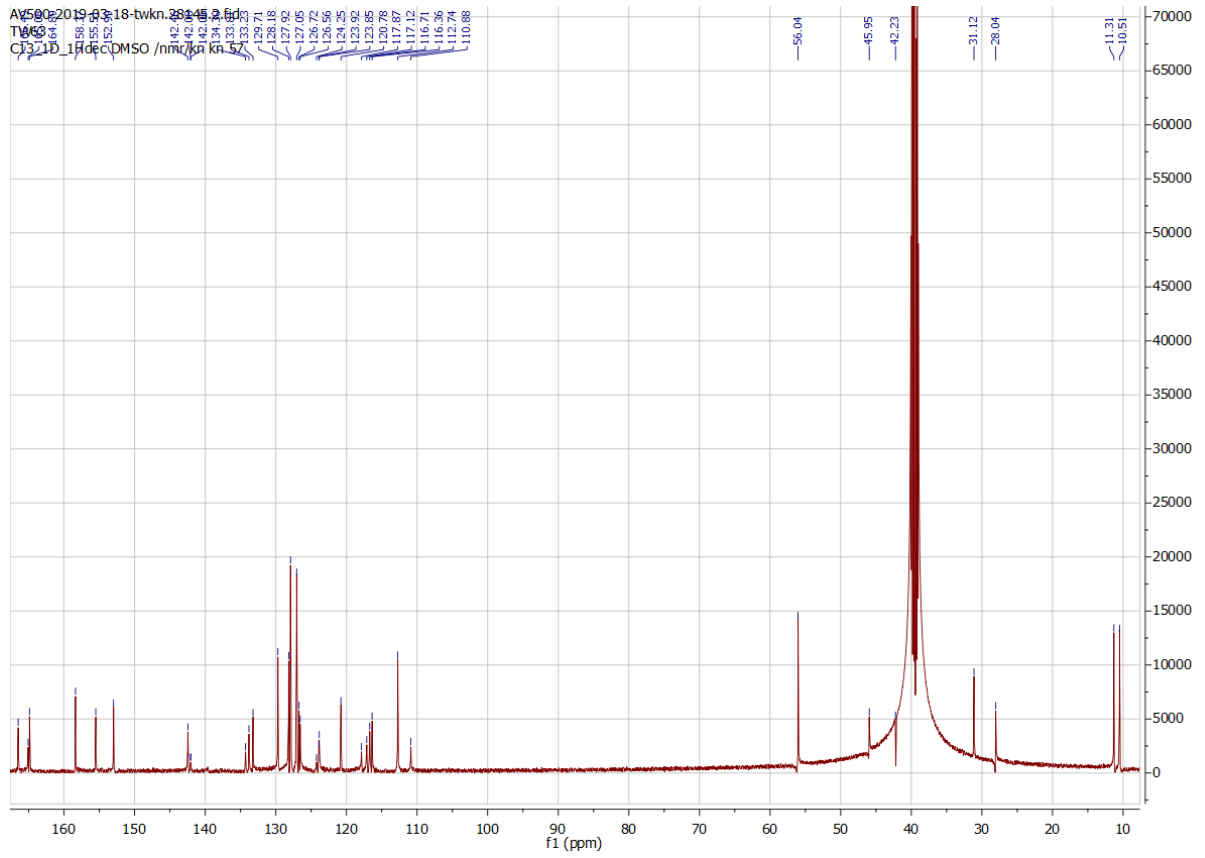


HPLC



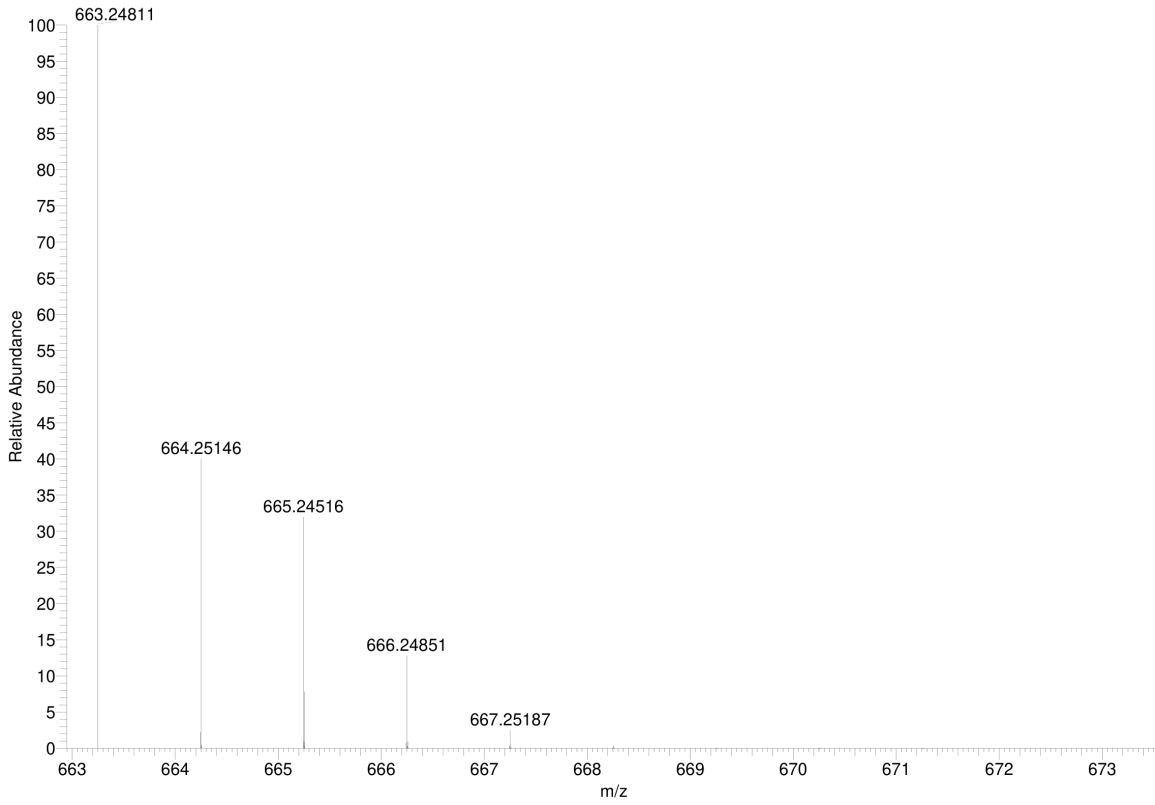
9.1.8. Compound **21**<sup>1</sup>H NMR

<sup>13</sup>C NMR



### Simulated HRMS

C<sub>37</sub>H<sub>35</sub>Cl<sub>1</sub>N<sub>6</sub>O<sub>4</sub> +H: C<sub>37</sub> H<sub>36</sub> Cl<sub>1</sub> N<sub>6</sub> O<sub>4</sub> pa Chrg 1



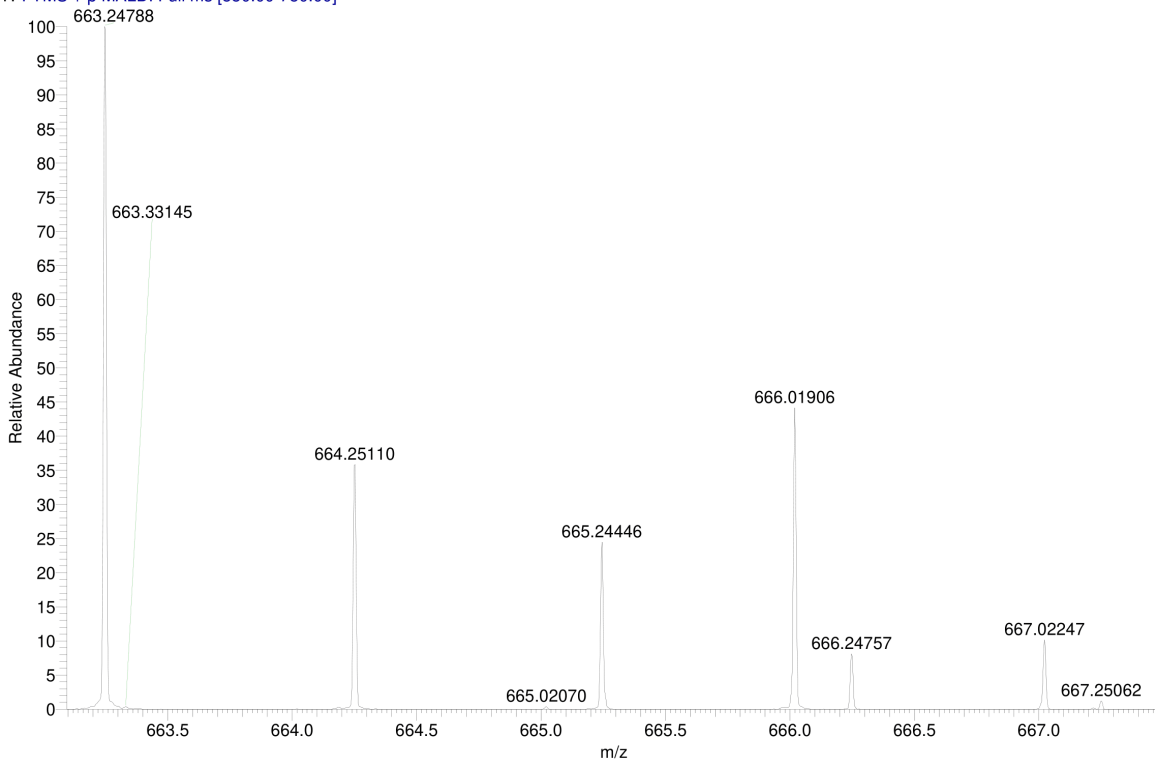
### MALDI HRMS

C:\User\...\Knapp\2019\190821\TW63\_B3

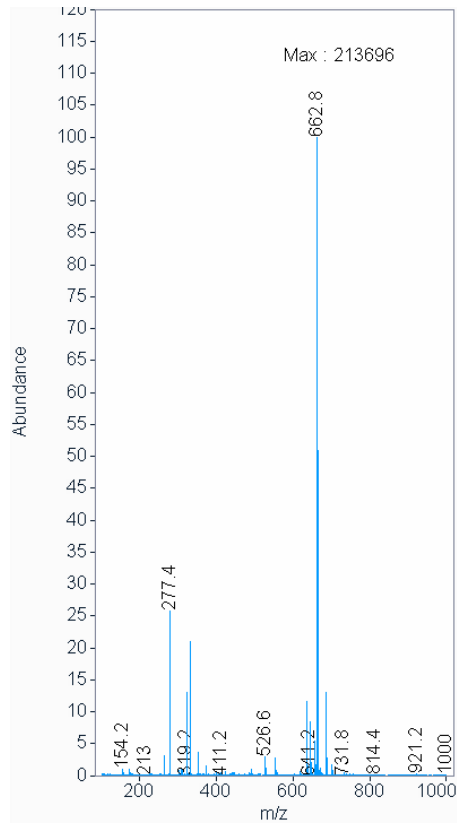
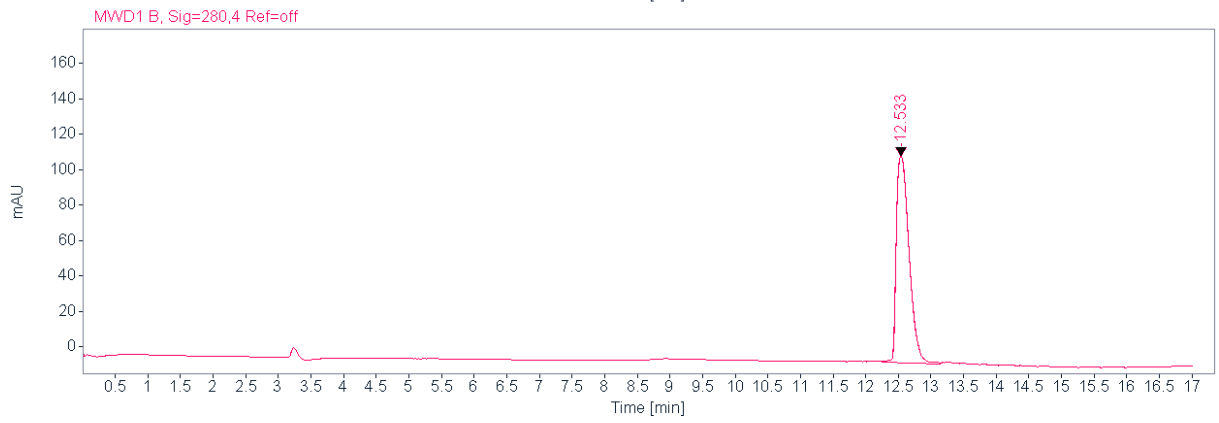
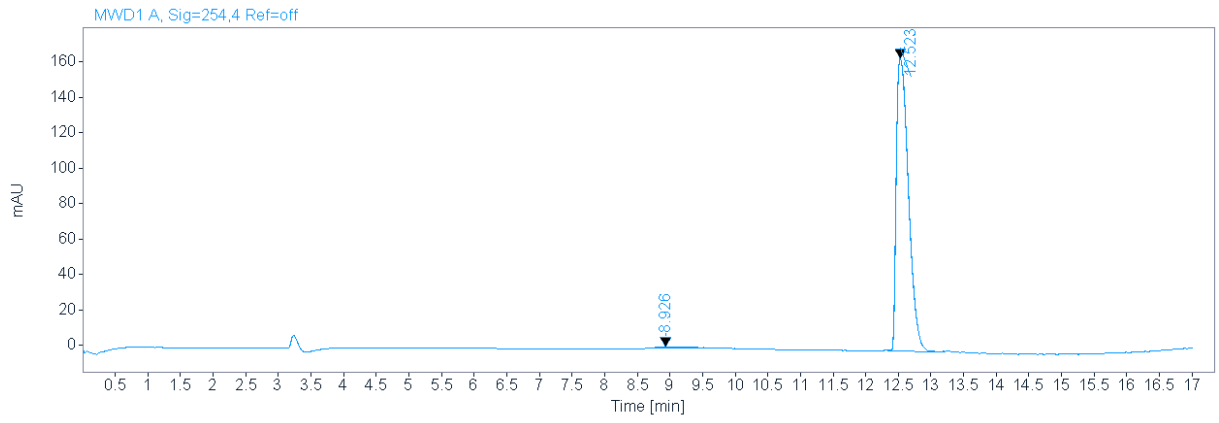
8/21/2019 4:14:05 PM

TW63 mit HCCA gemessen.

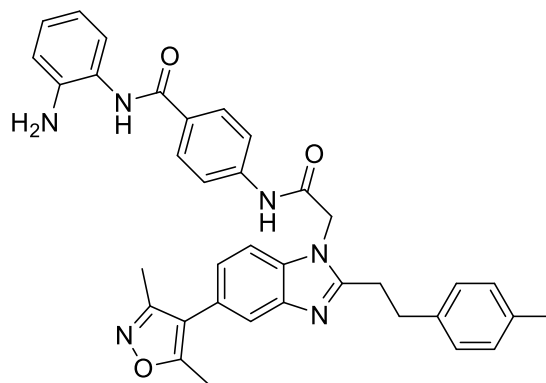
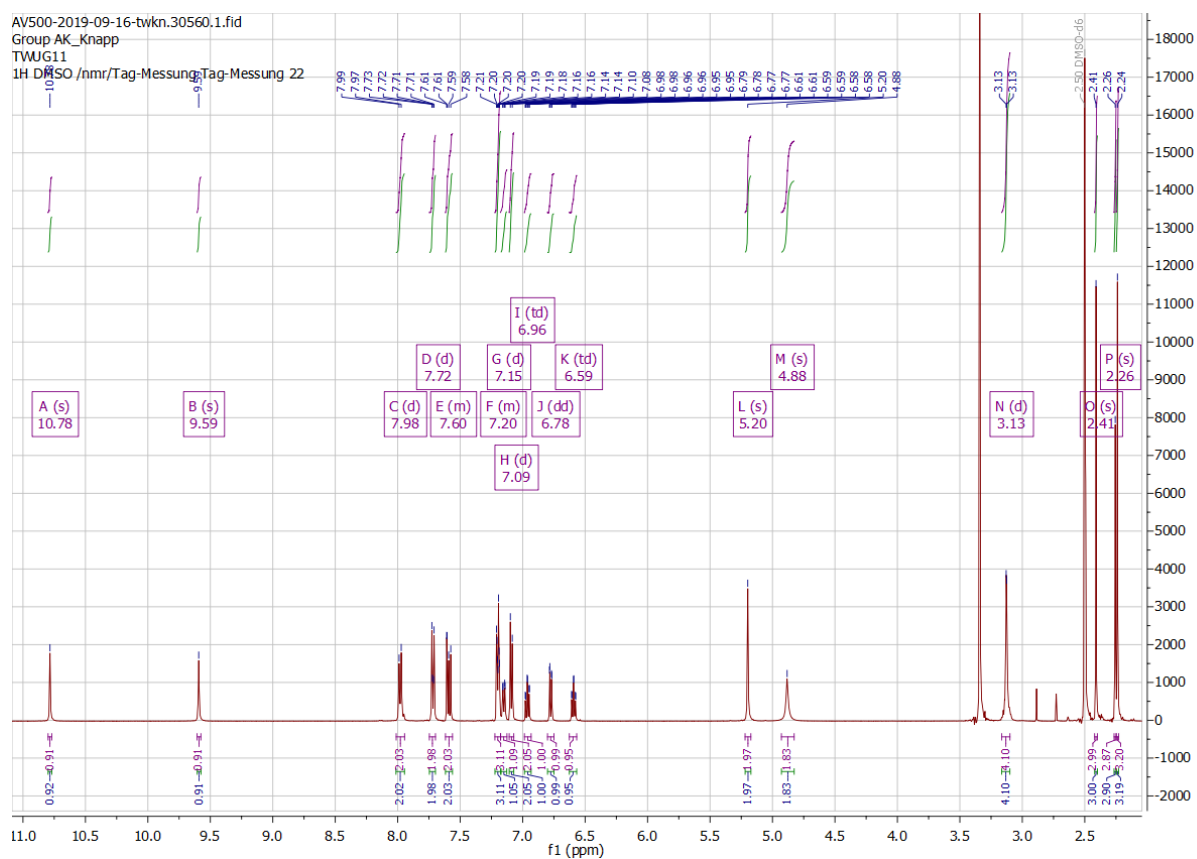
TW63\_B3 #1-14 RT: 0.00-0.89 AV: 14 NL: 2.55E6  
T: FTMS + p MALDI Full ms [550.00-750.00]



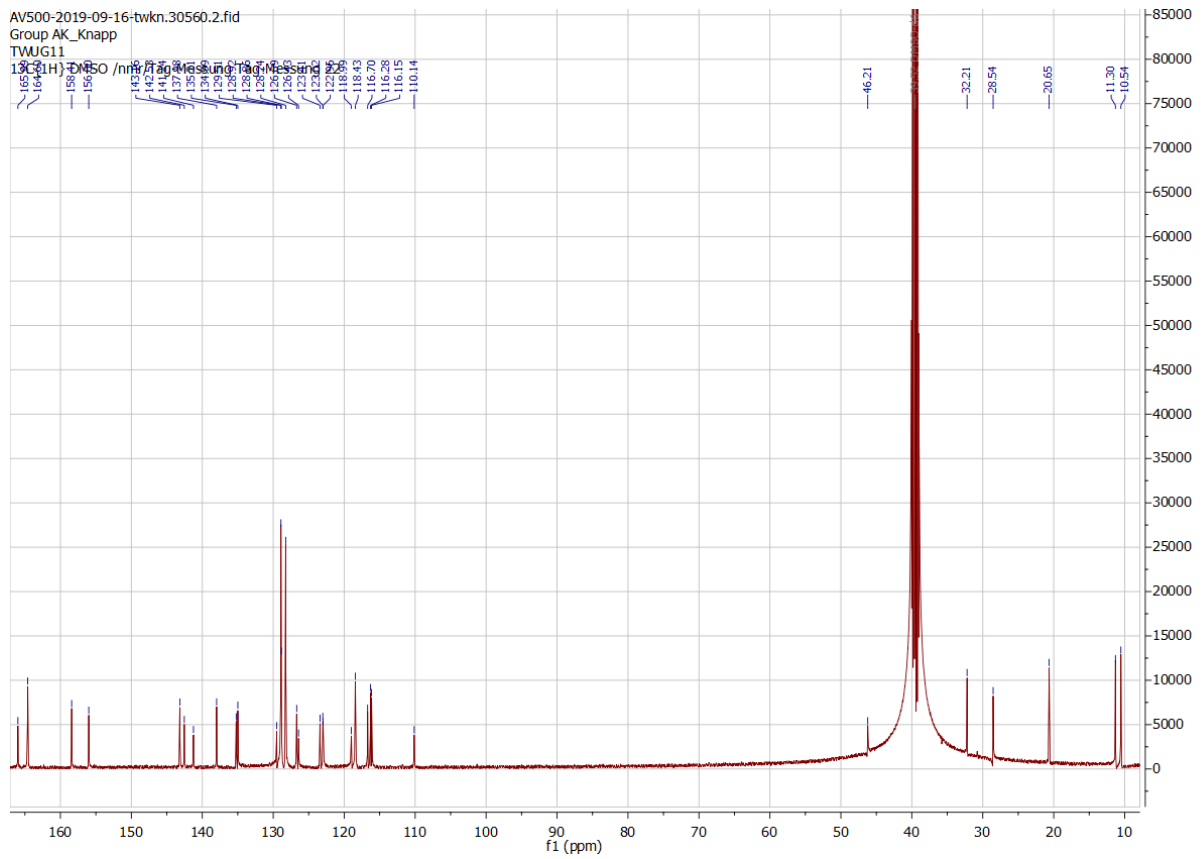
HPLC



## 9.1.9. Compound 22

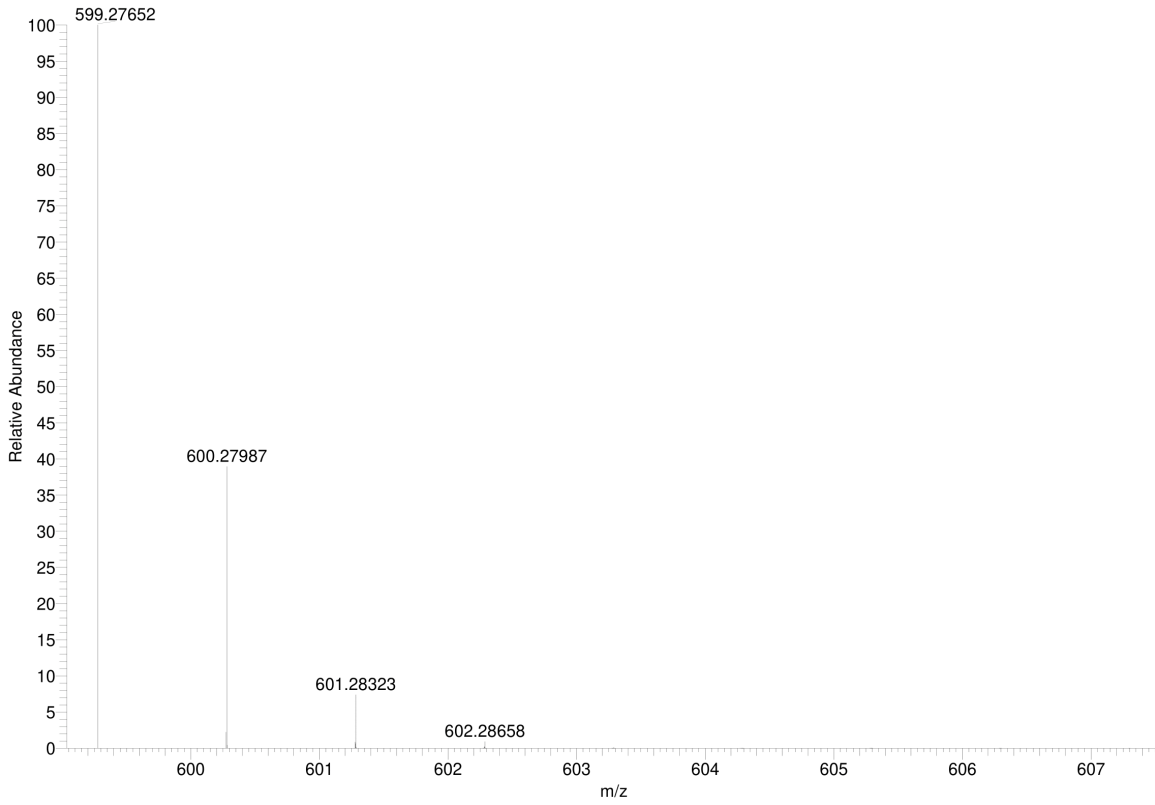
 $^1\text{H NMR}$ 



$^{13}\text{C}$  NMR

### Simulated HRMS

C<sub>36</sub>H<sub>34</sub>N<sub>6</sub>O<sub>3</sub> +H: C<sub>36</sub> H<sub>35</sub> N<sub>6</sub> O<sub>3</sub> pa Chrg 1



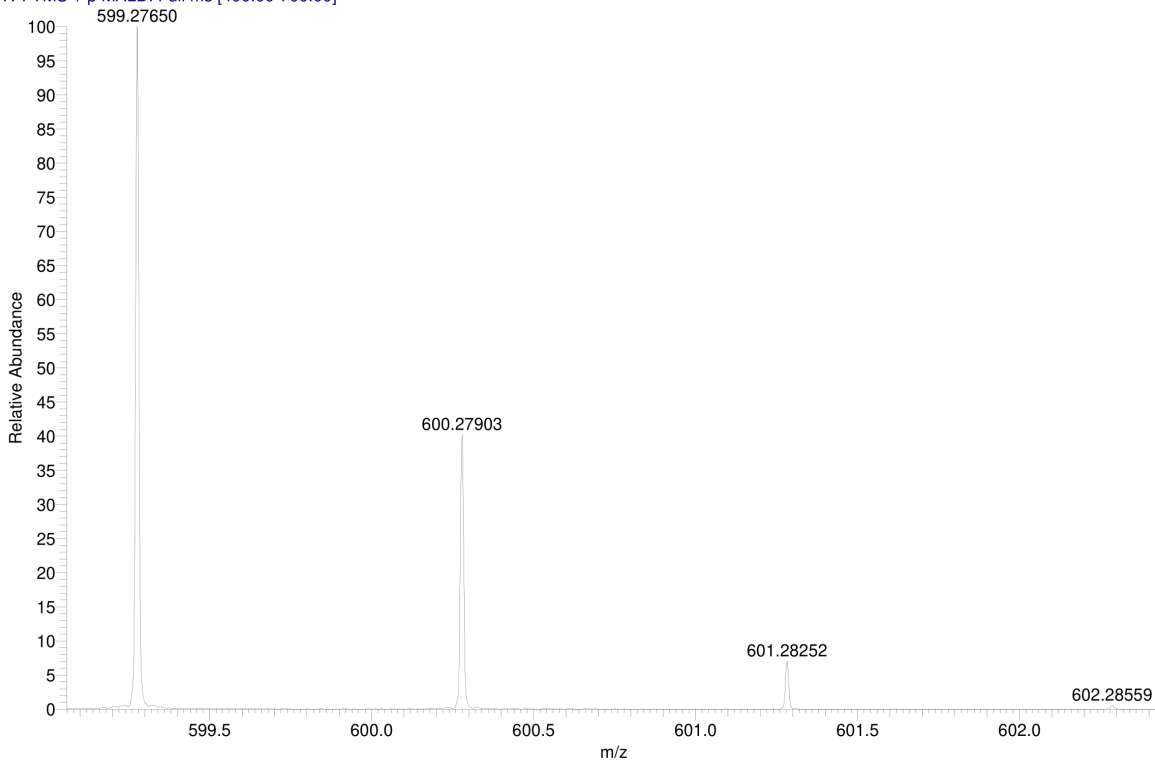
### MALDI HRMS

C:\User\...\Knapp\2019\190904\TWUG11\_D1

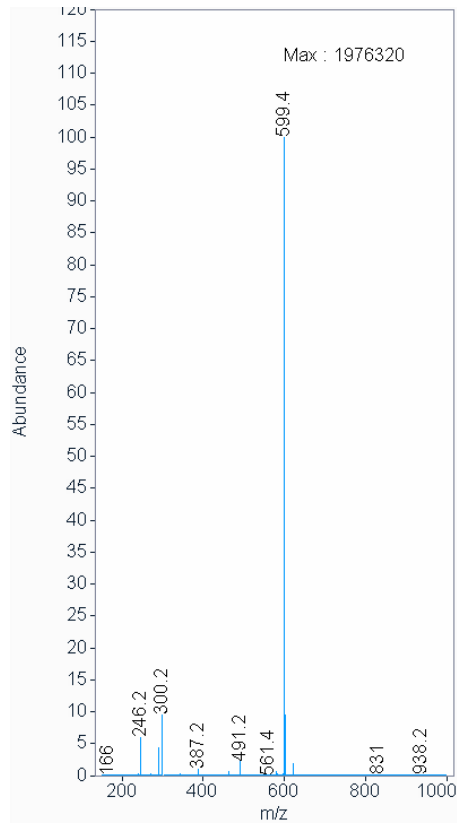
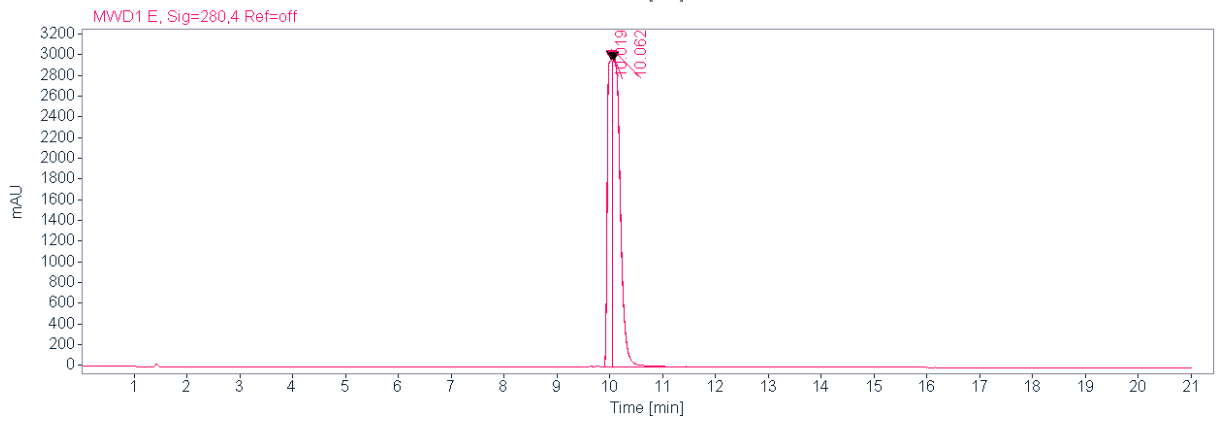
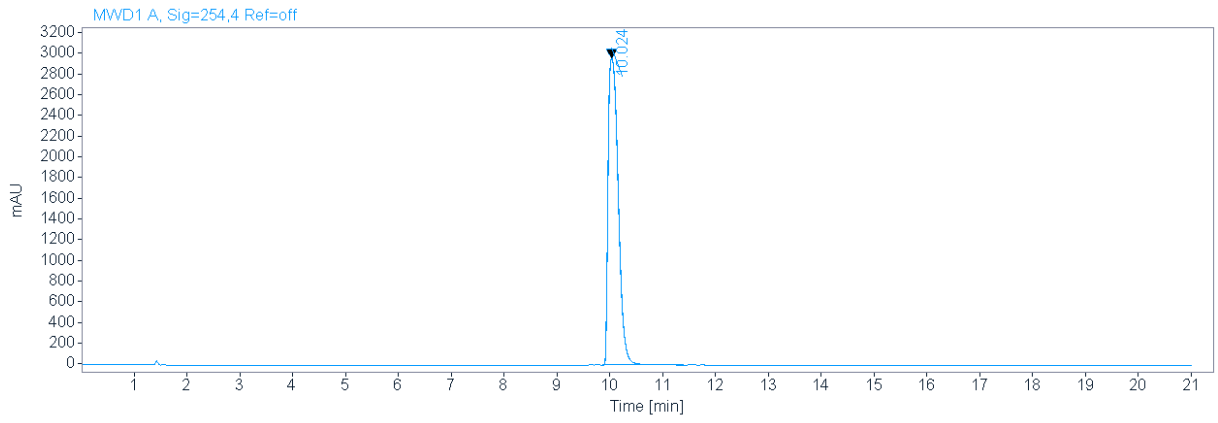
9/4/2019 9:01:41 AM

TWUG11 mit HCCA gemessen.

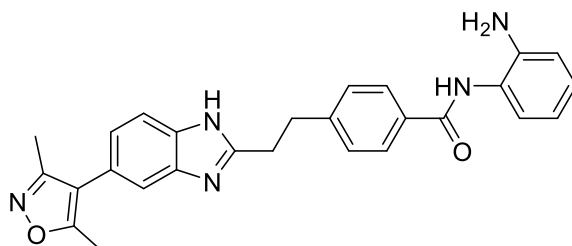
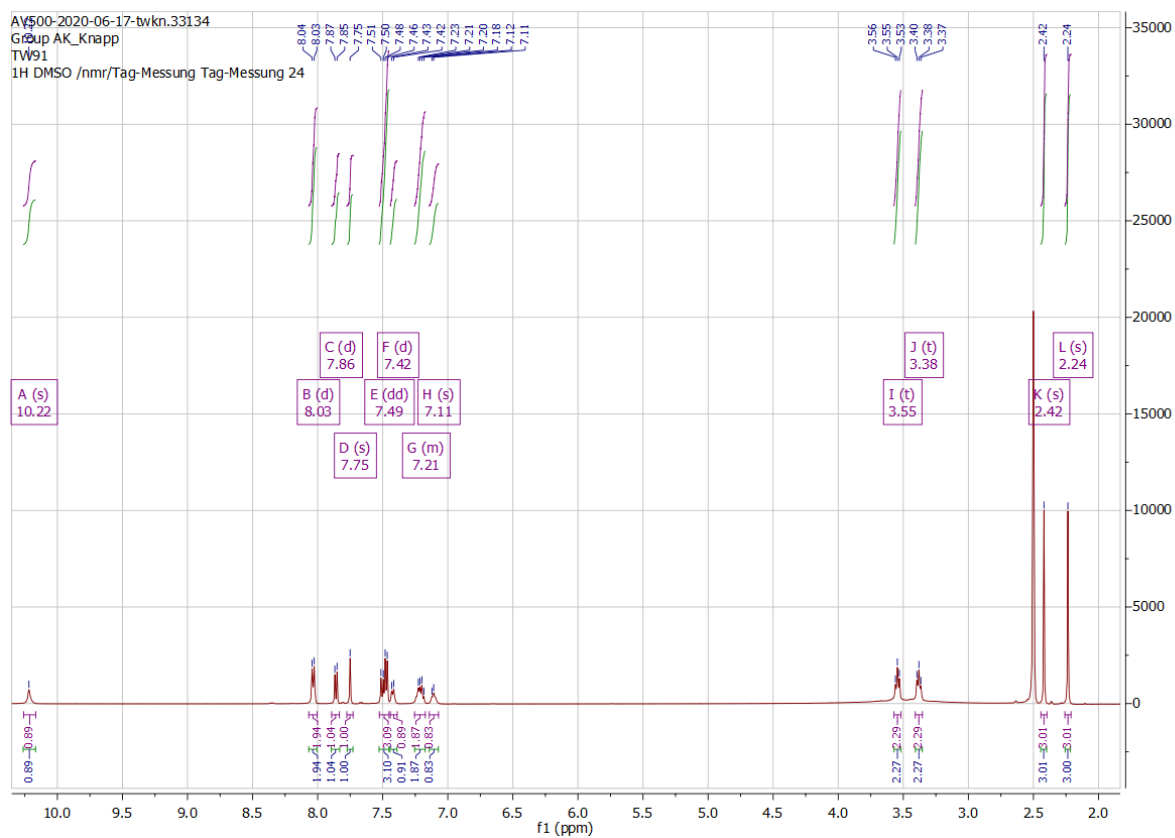
TWUG11\_D1 #1-6 RT: 0.00-0.60 AV: 6 NL: 2.96E6  
T: FTMS + p MALDI Full ms [400.00-700.00]

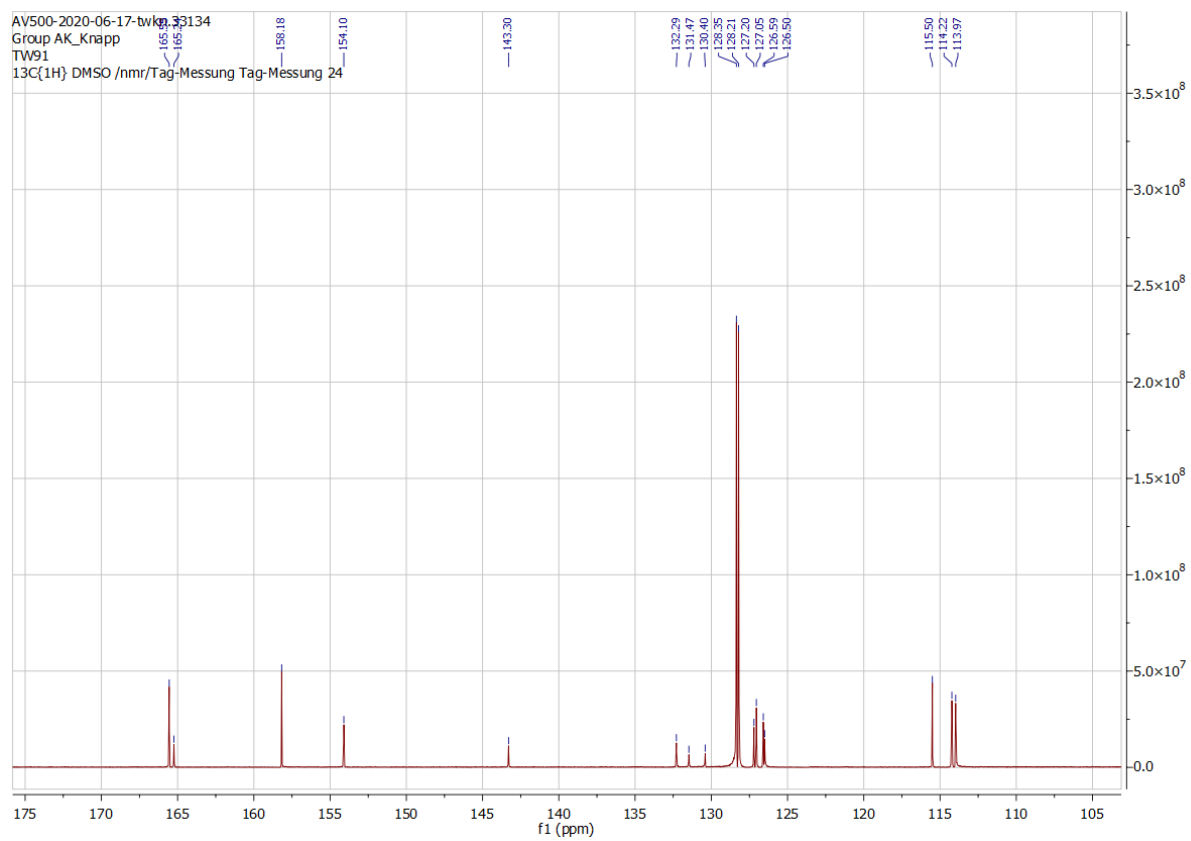


HPLC



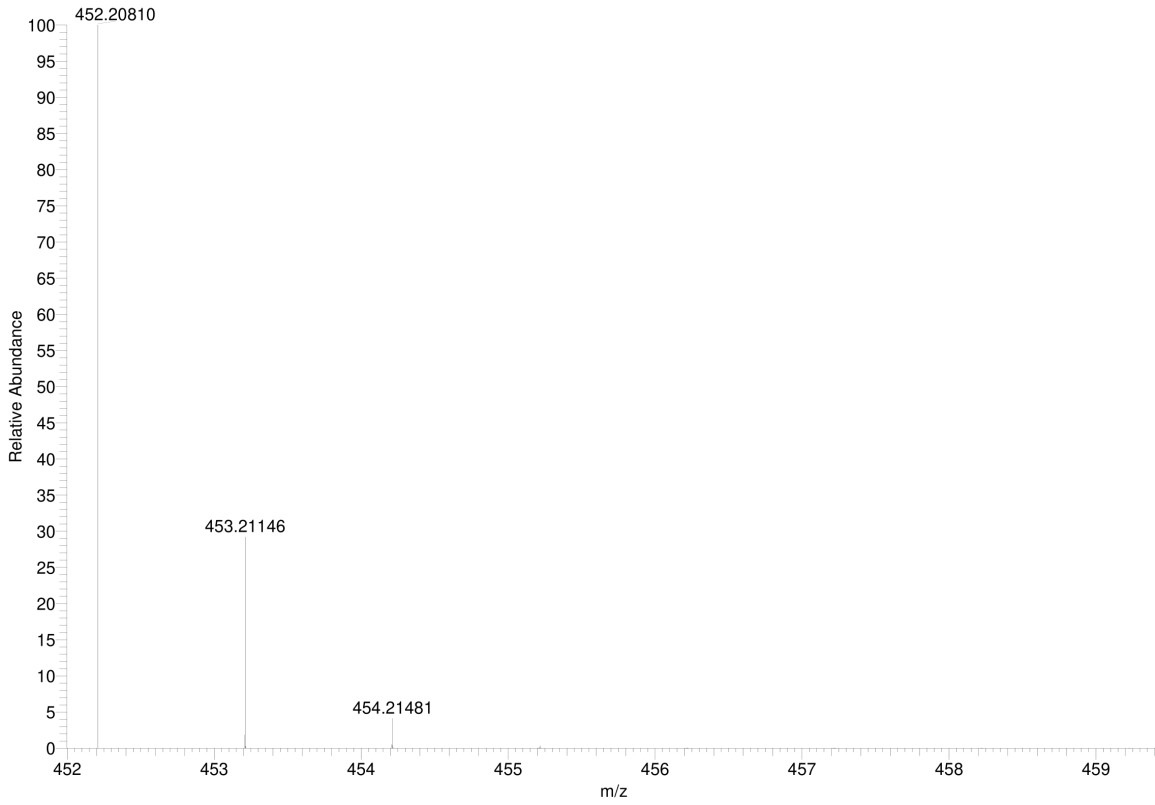
## 9.1.10. Compound 25

 $^1\text{H}$  NMR

$^{13}\text{C}$  NMR

### Simulated HRMS

C<sub>27</sub>H<sub>25</sub>N<sub>5</sub>O<sub>2</sub> +H: C<sub>27</sub> H<sub>26</sub> N<sub>5</sub> O<sub>2</sub> pa Chrg 1



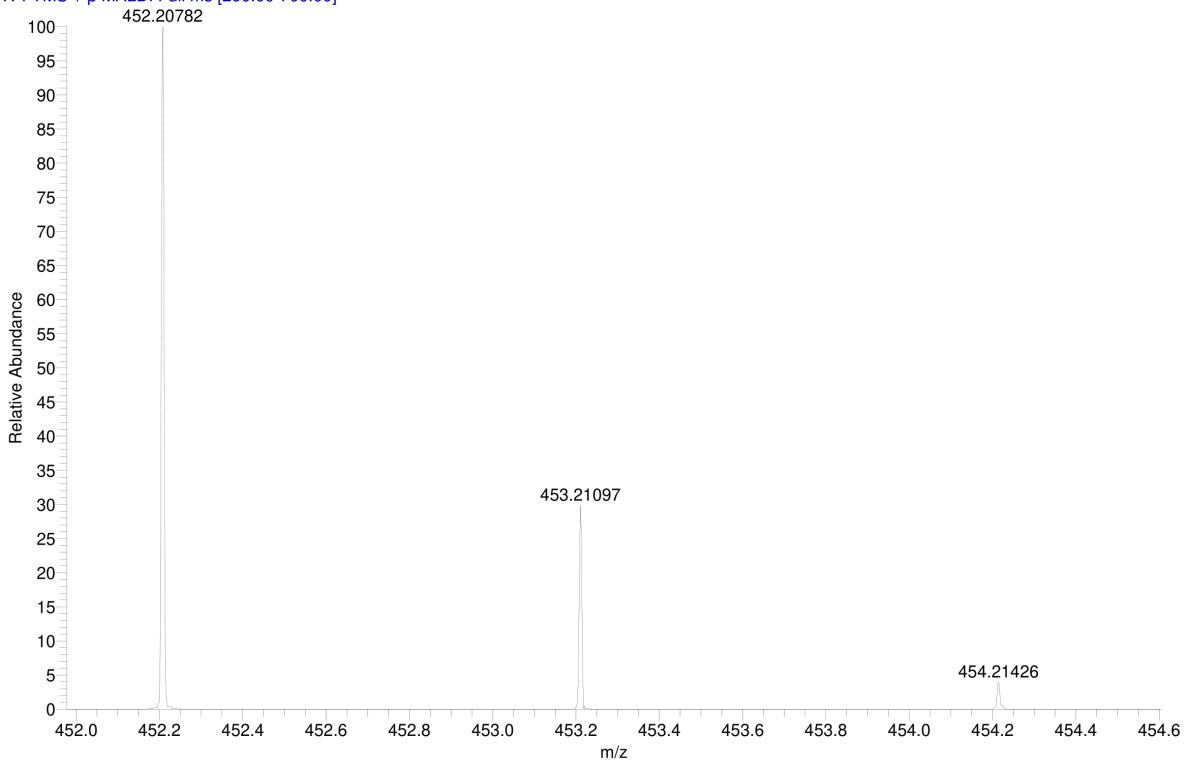
### MALDI HRMS

C:\User\...\2020\05.06.2020\TW91\_E9

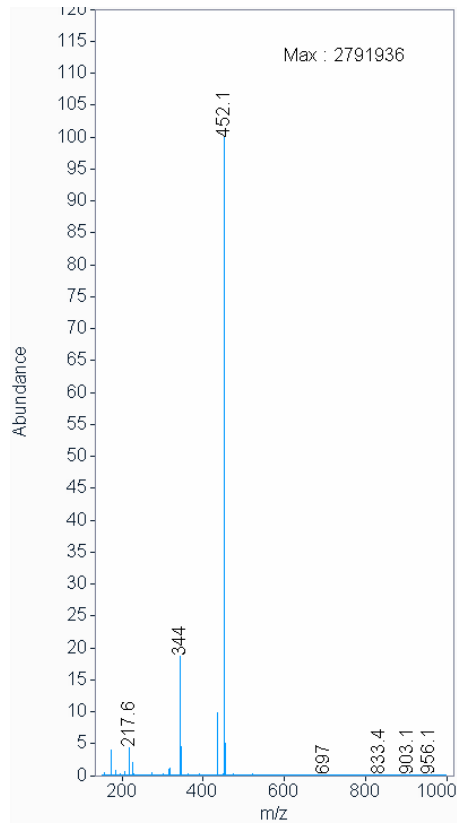
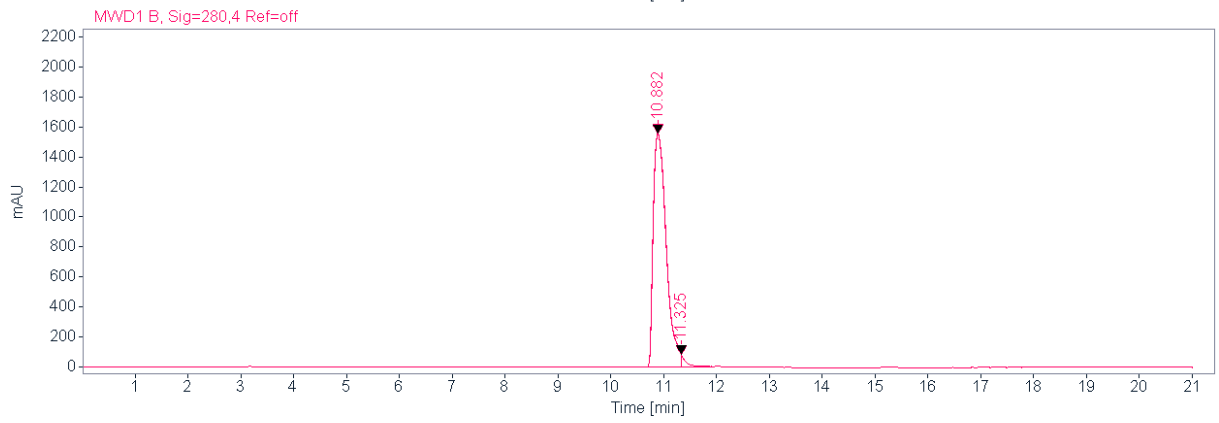
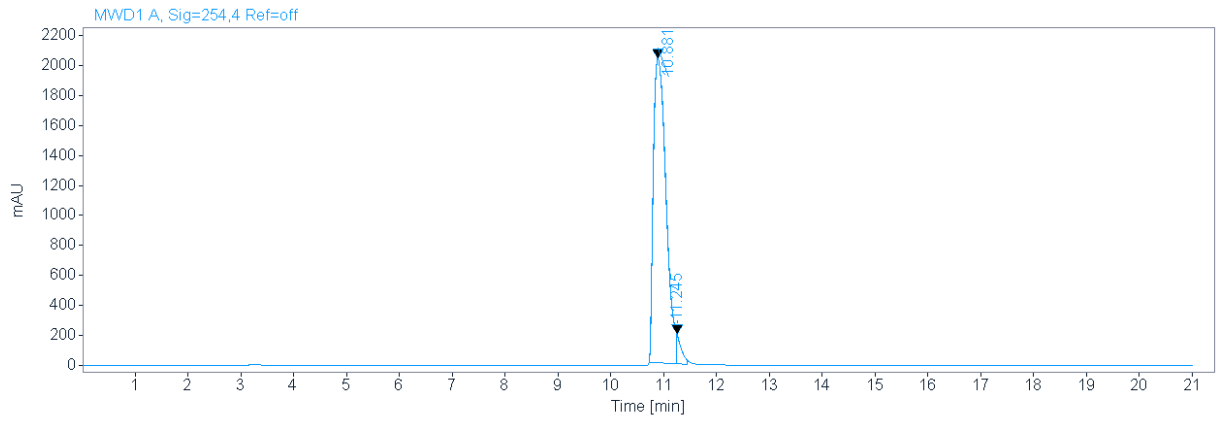
6/5/2020 9:28:30 AM

TW91 mit HCCA gemessen.

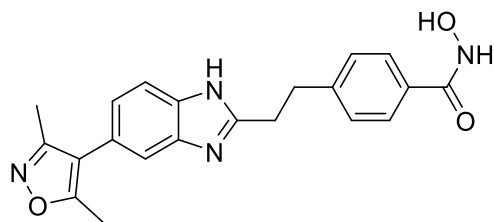
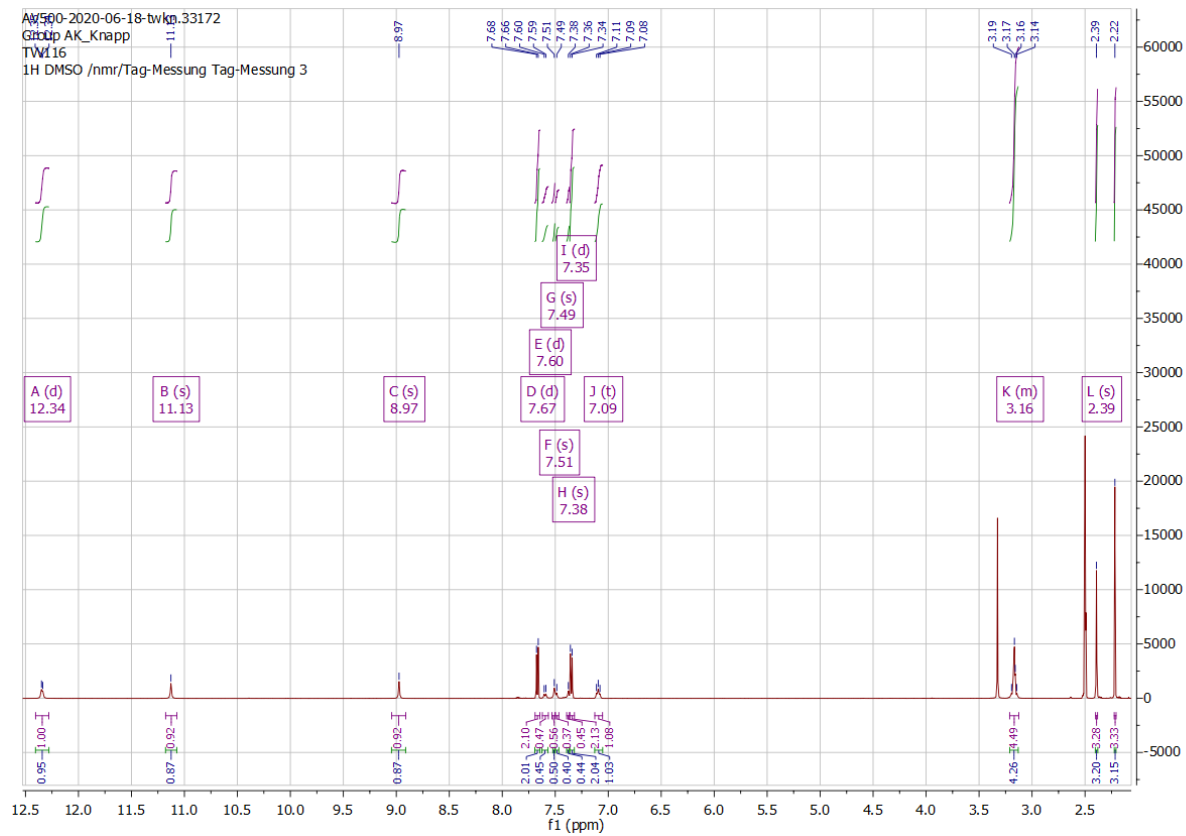
TW91\_E9 #11 RT: 0.45 AV: 1 NL: 5.92E7  
T: FTMS + p MALDI Full ms [200.00-700.00]



HPLC

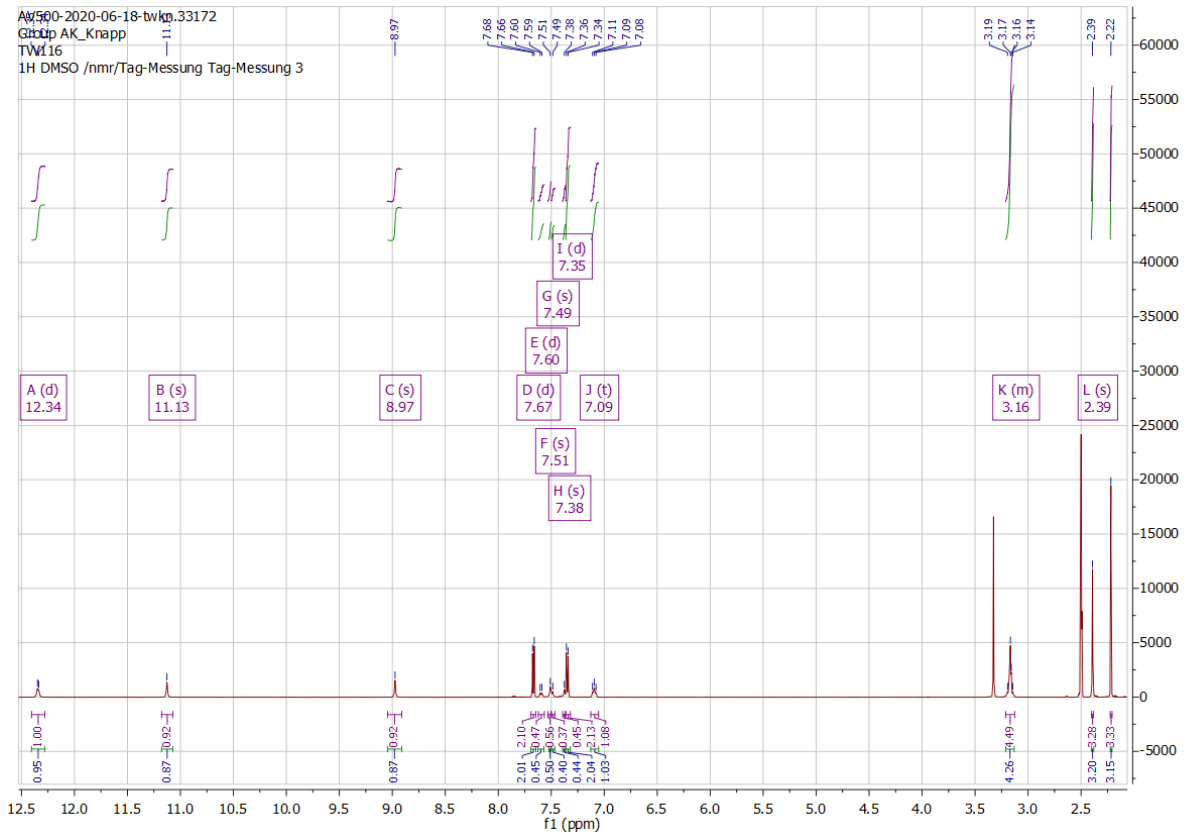


## 9.1.11. Compound 26

 $^1\text{H NMR}$ 

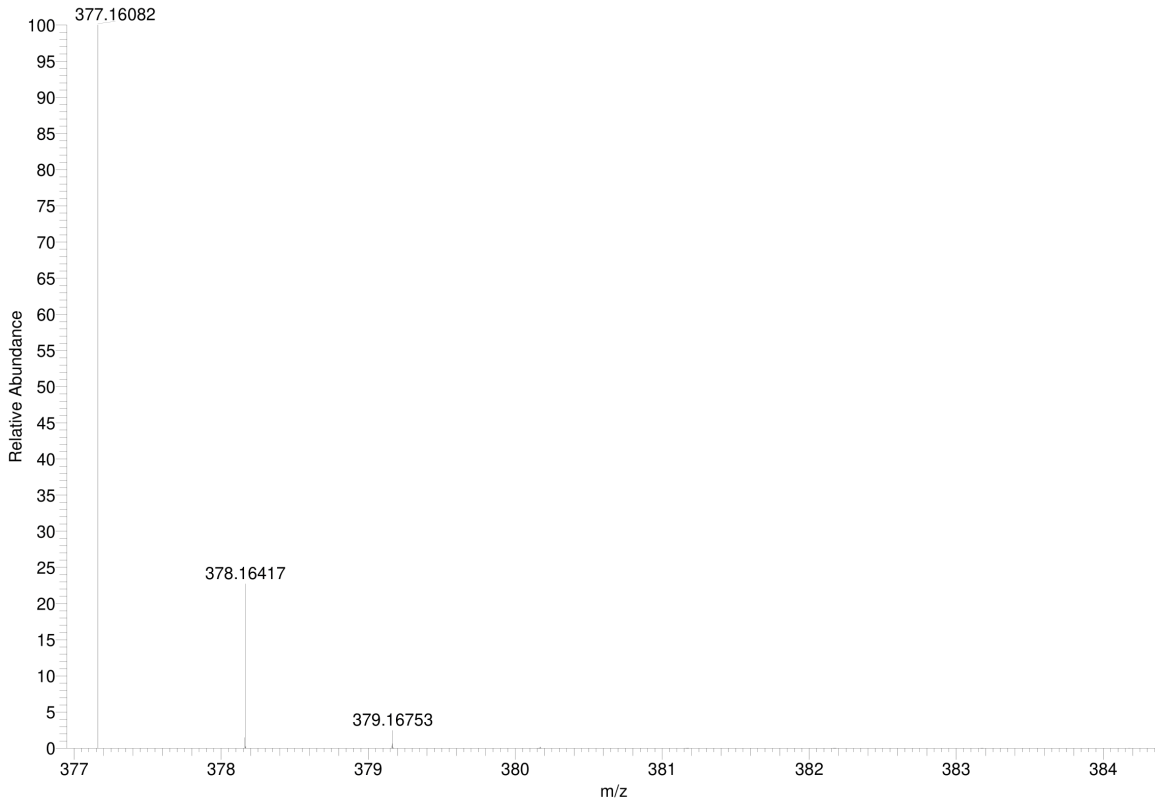


<sup>13</sup>C NMR



### Simulated HRMS

C<sub>21</sub>H<sub>20</sub>N<sub>4</sub>O<sub>3</sub> +H: C<sub>21</sub> H<sub>21</sub> N<sub>4</sub> O<sub>3</sub> pa Chrg 1



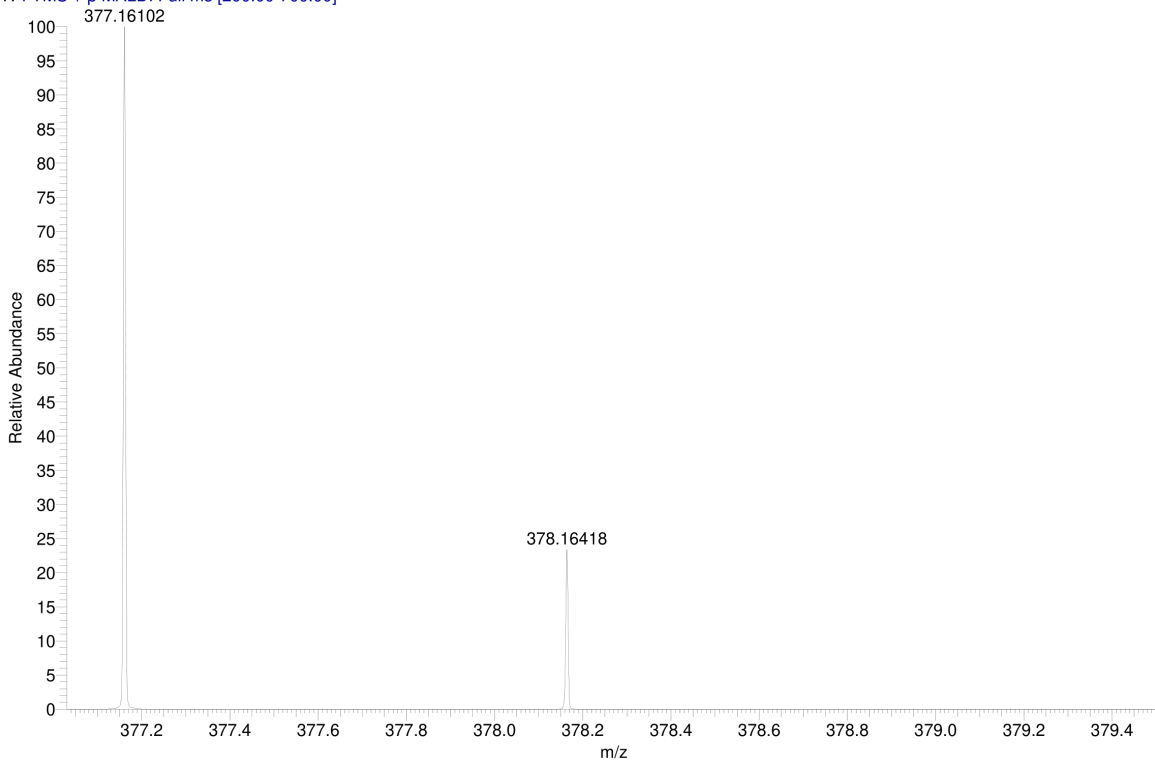
### MALDI HRMS

C:\User\...\2020\05.06.2020\TW116\_E11

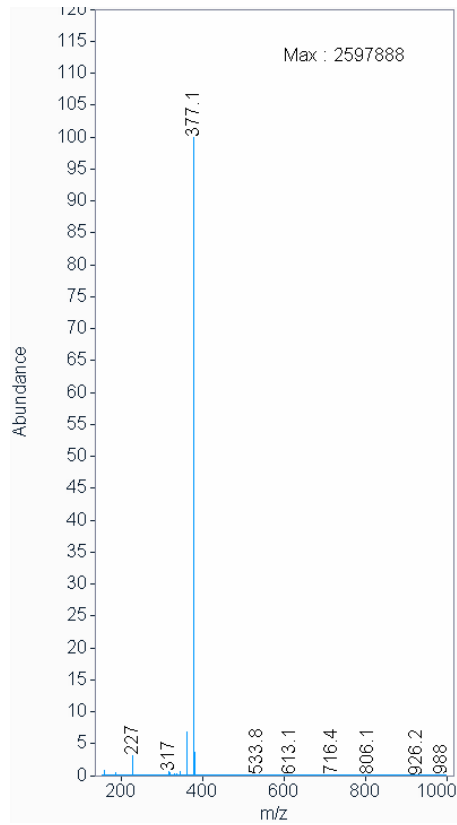
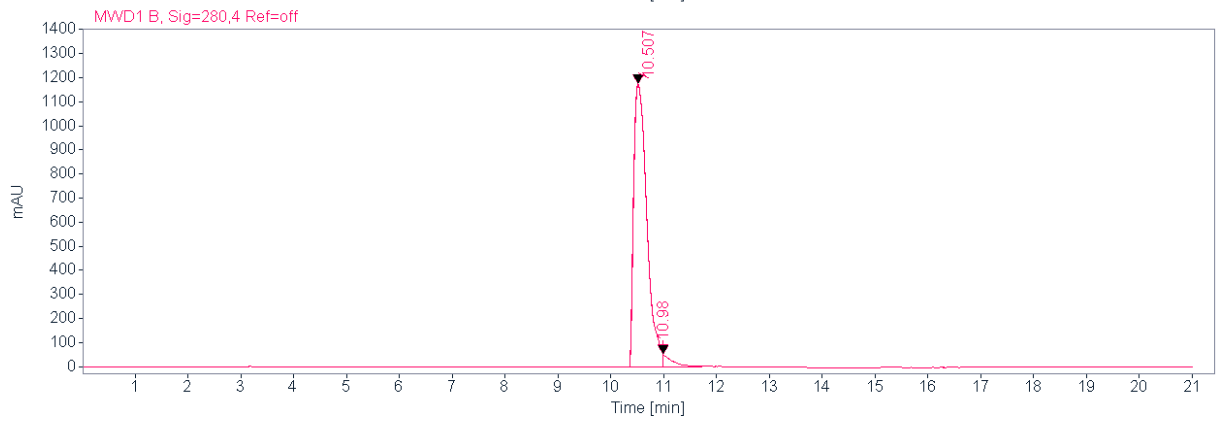
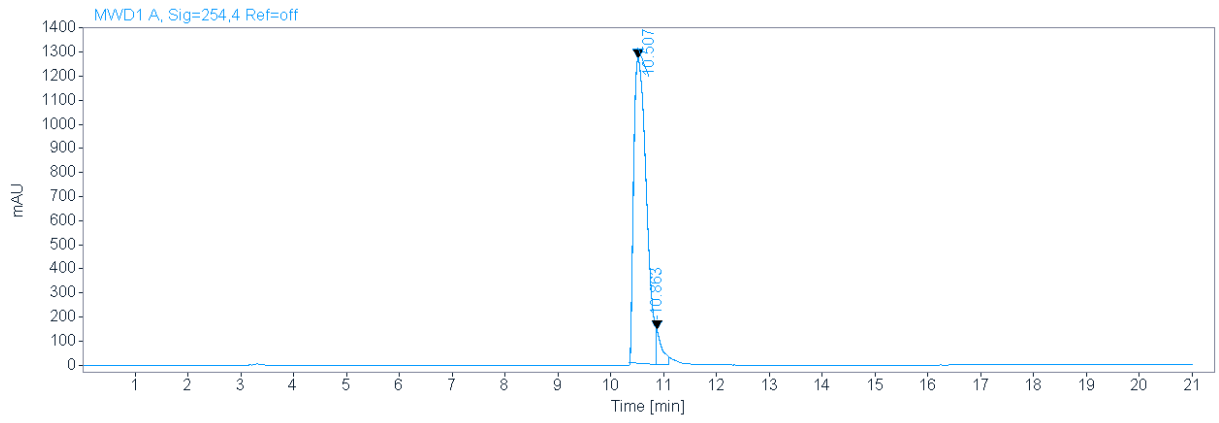
6/5/2020 9:30:50 AM

TW116 mit HCCA gemessen.

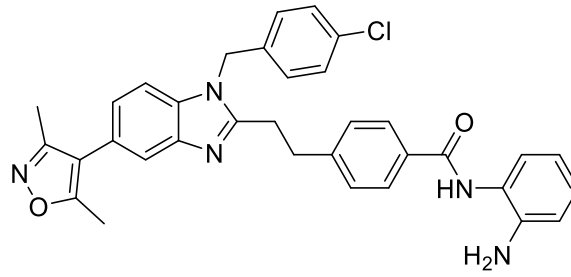
TW116\_E11 #1-10 RT: 0.01-0.42 AV: 10 NL: 4.42E7  
T: FTMS + p MALDI Full ms [200.00-700.00]



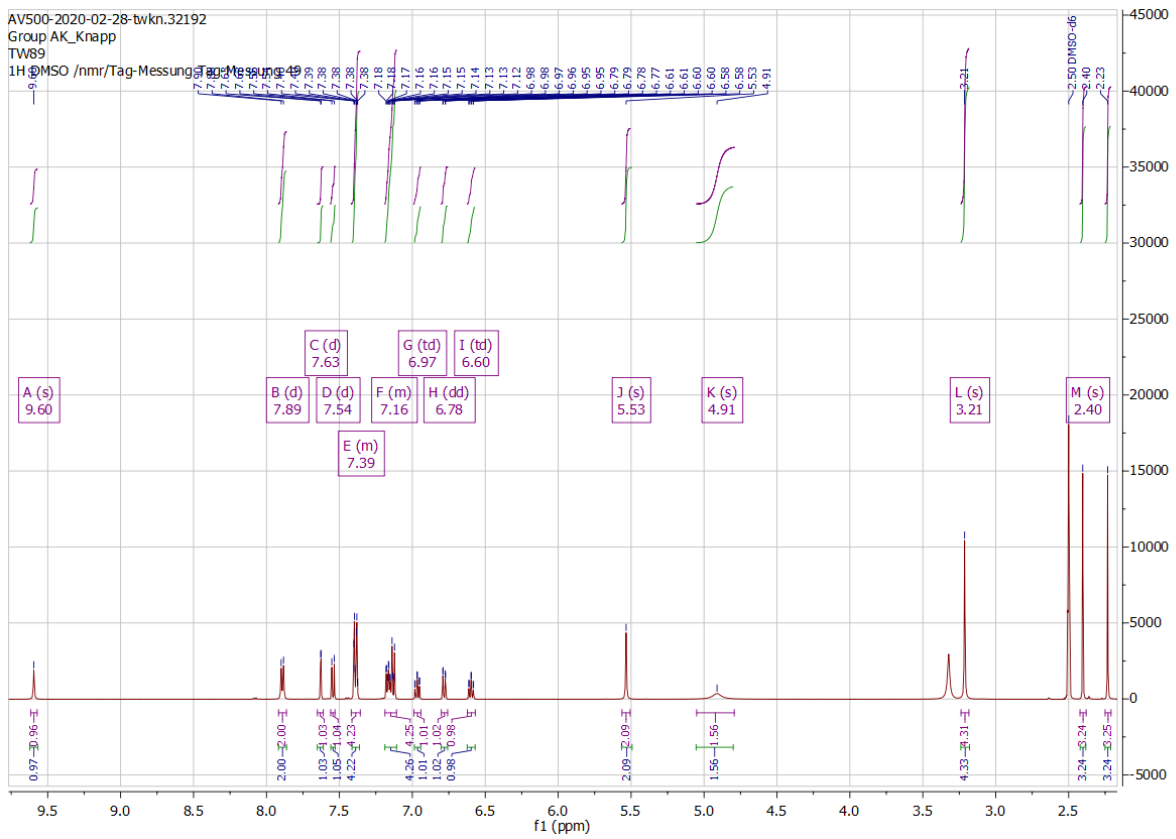
HPLC

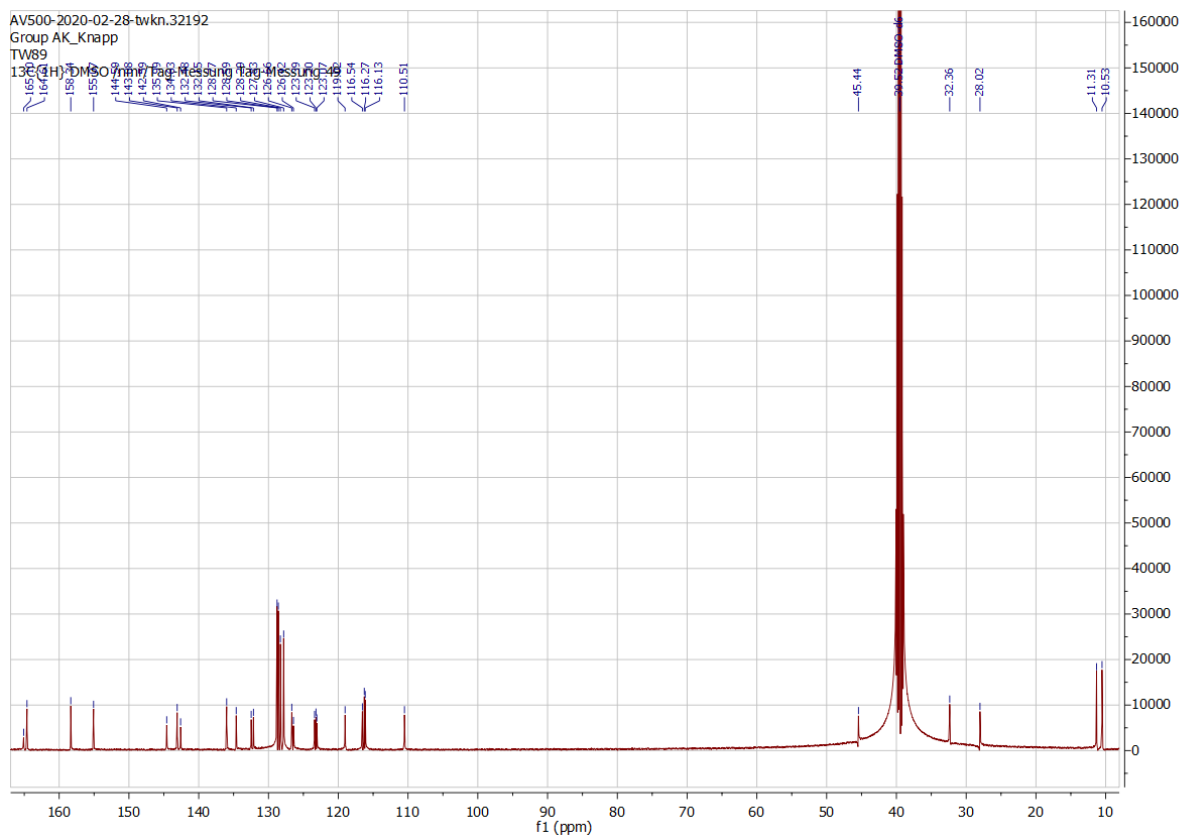


9.1.12. Compound 27



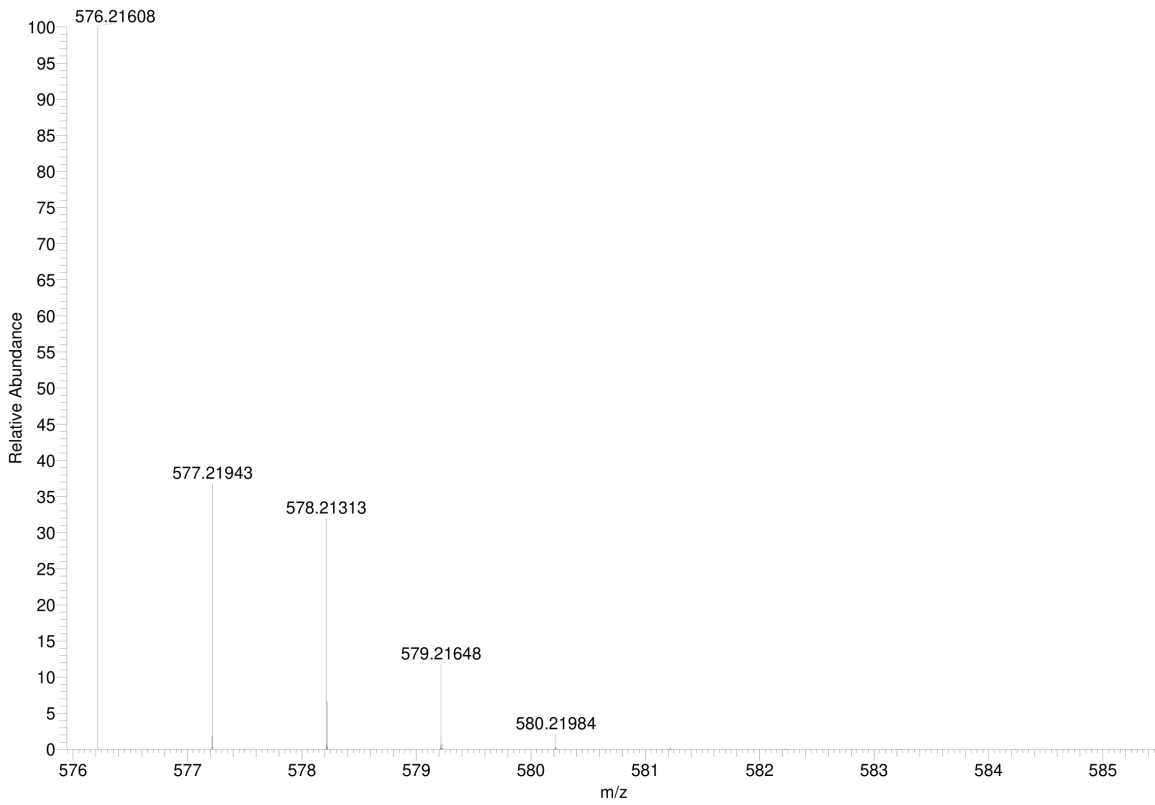
<sup>1</sup>H NMR



$^{13}\text{C}$  NMR

### Simulated HRMS

C<sub>34</sub>H<sub>30</sub>Cl<sub>1</sub>N<sub>5</sub>O<sub>2</sub> +H: C<sub>34</sub> H<sub>31</sub> Cl<sub>1</sub> N<sub>5</sub> O<sub>2</sub> pa Chrg 1



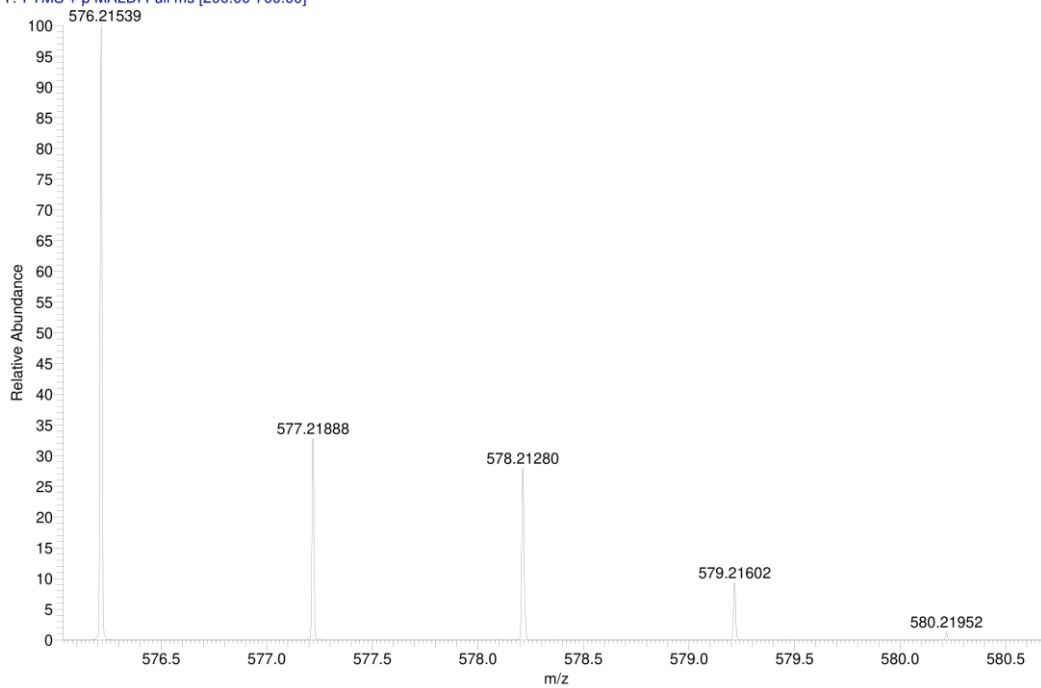
### MALDI HRMS

C:\User\...\2020\05.06.2020\TW89\_E8

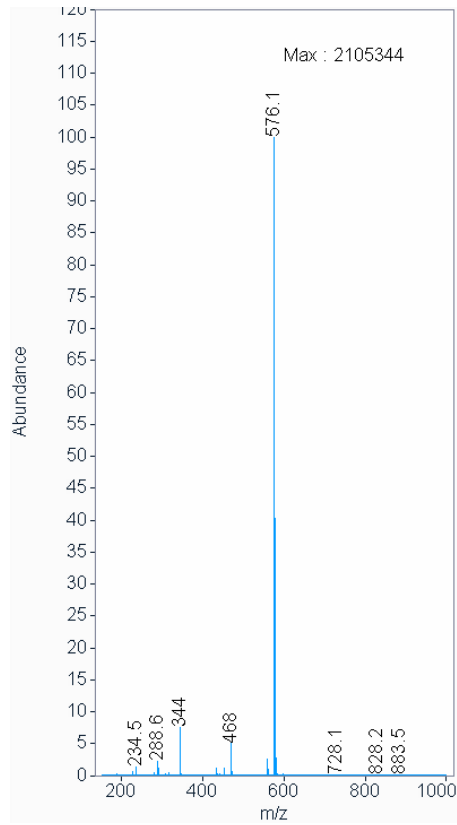
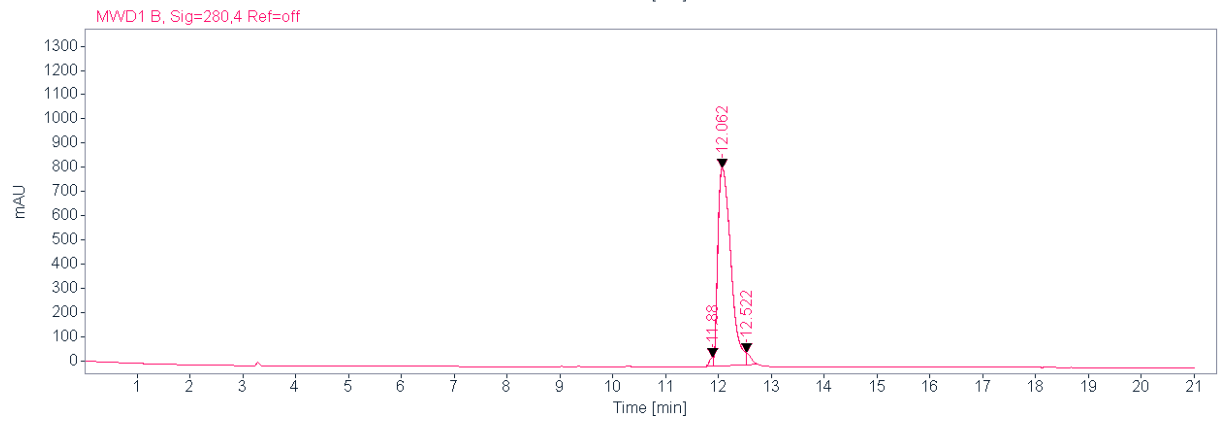
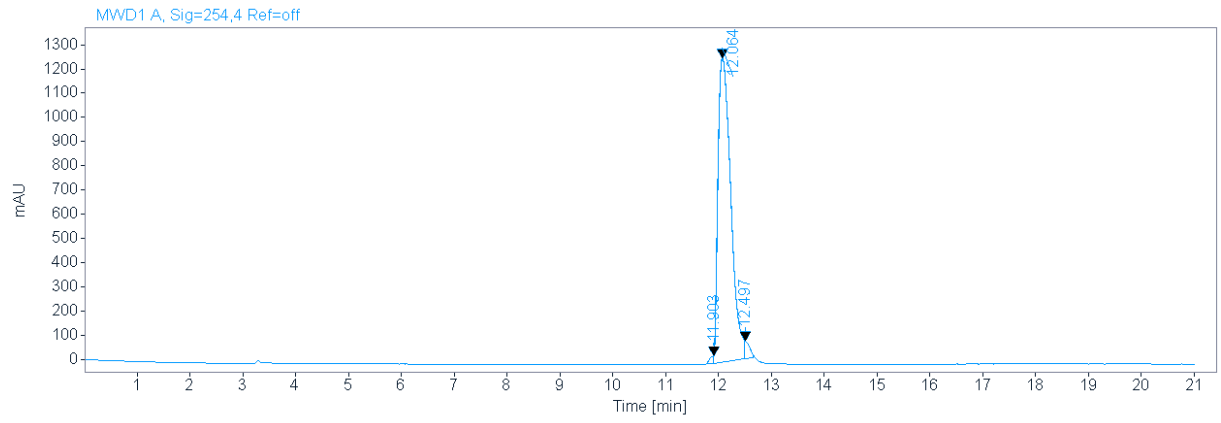
6/5/2020 9:27:42 AM

TW89 mit HCCA gemessen.

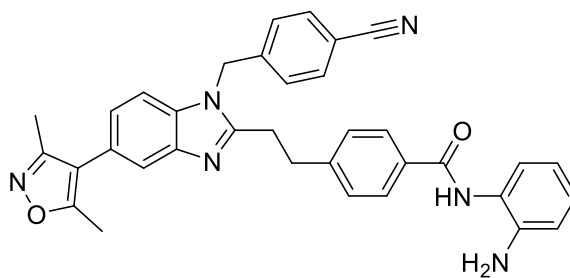
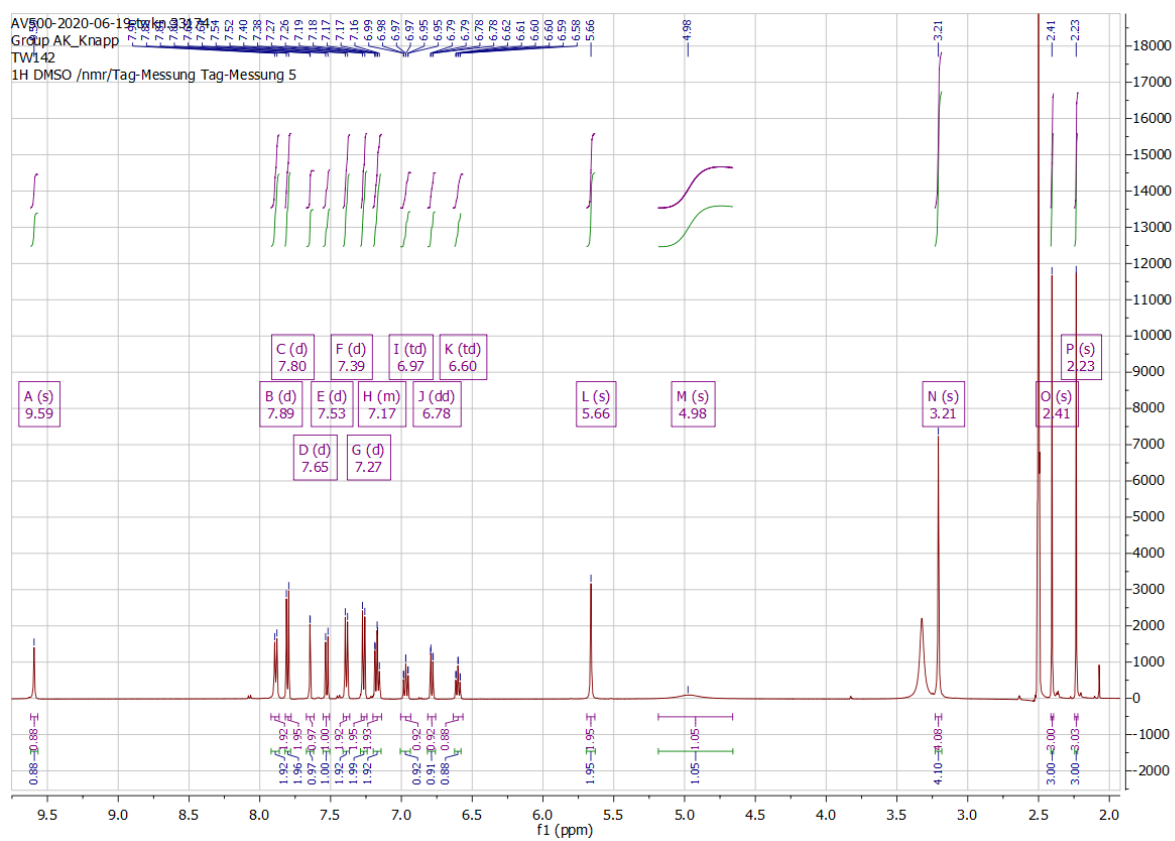
TW89\_E8 #1-9 RT: 0.00-0.36 AV: 9 NL: 1.21E7  
T: FTMS + p MALDI Full ms [200.00-700.00]



HPLC

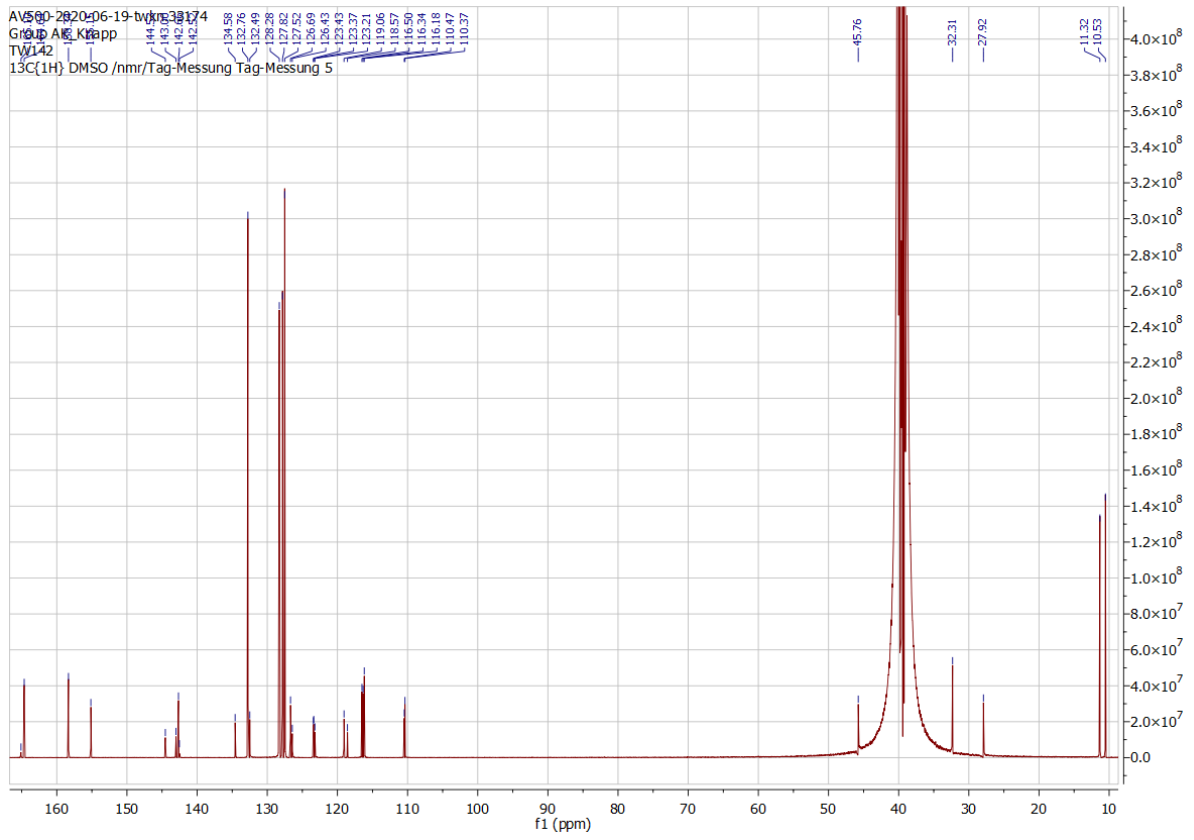


## 9.1.13. Compound 28

<sup>1</sup>H NMR

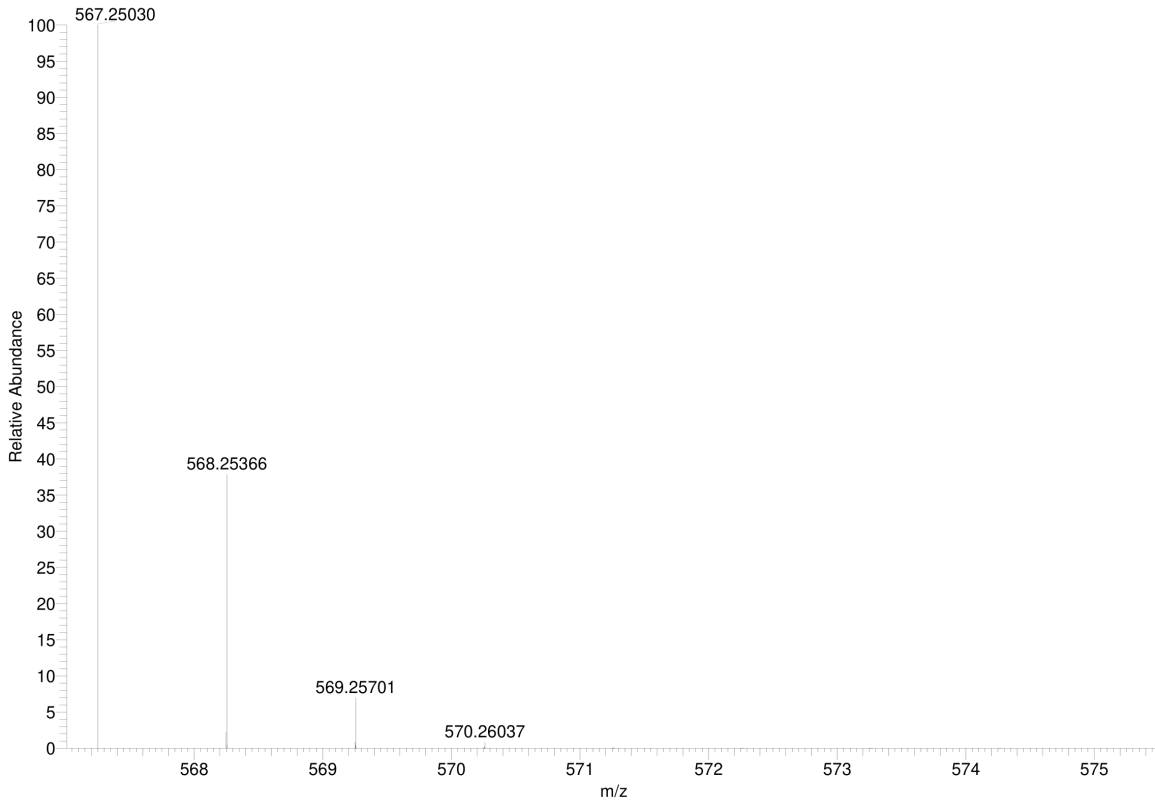


<sup>13</sup>C NMR



### Simulated HRMS

C<sub>35</sub>H<sub>30</sub>N<sub>6</sub>O<sub>2</sub> +H: C<sub>35</sub> H<sub>31</sub> N<sub>6</sub> O<sub>2</sub> pa Chrg 1



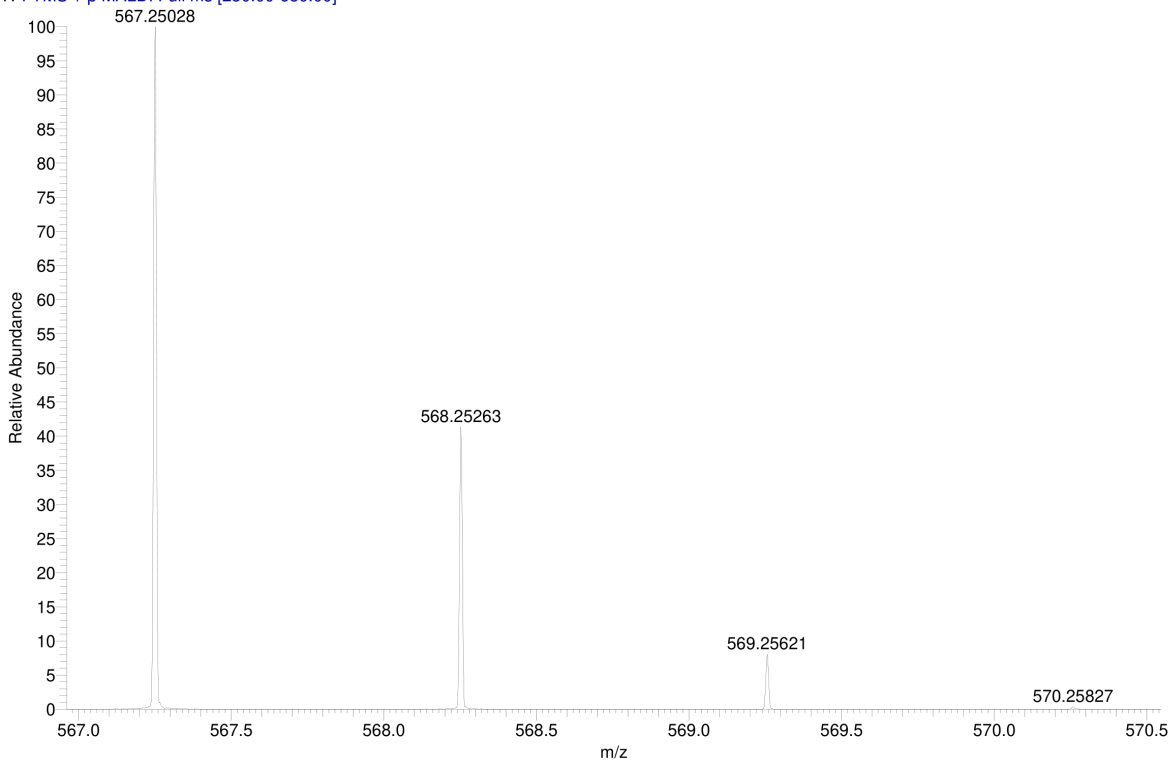
### MALDI HRMS

C:\User\...\2020\18.06.2020\TW 142\_B6

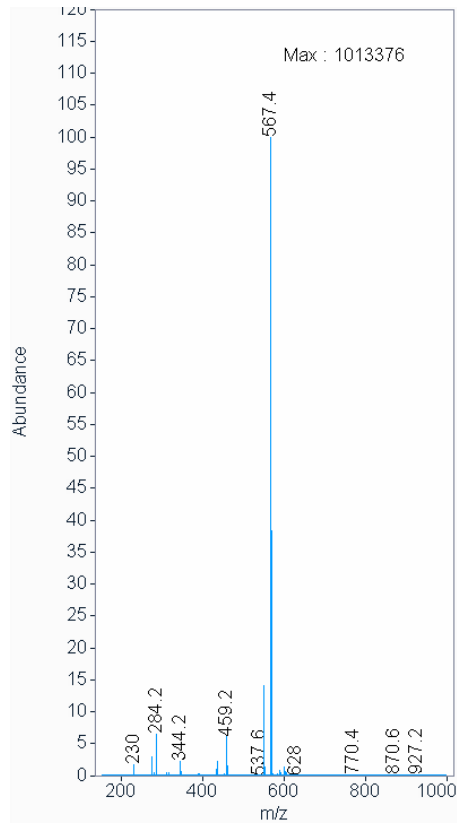
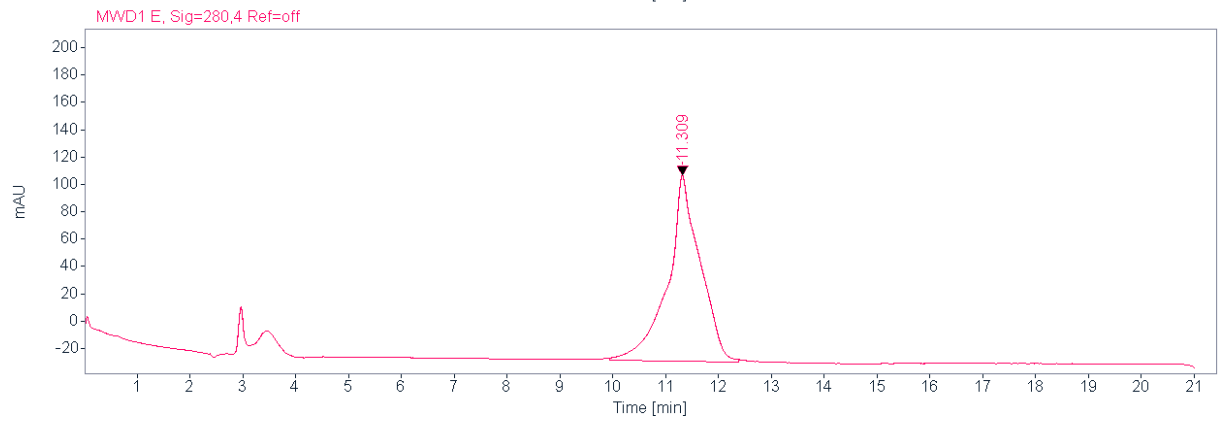
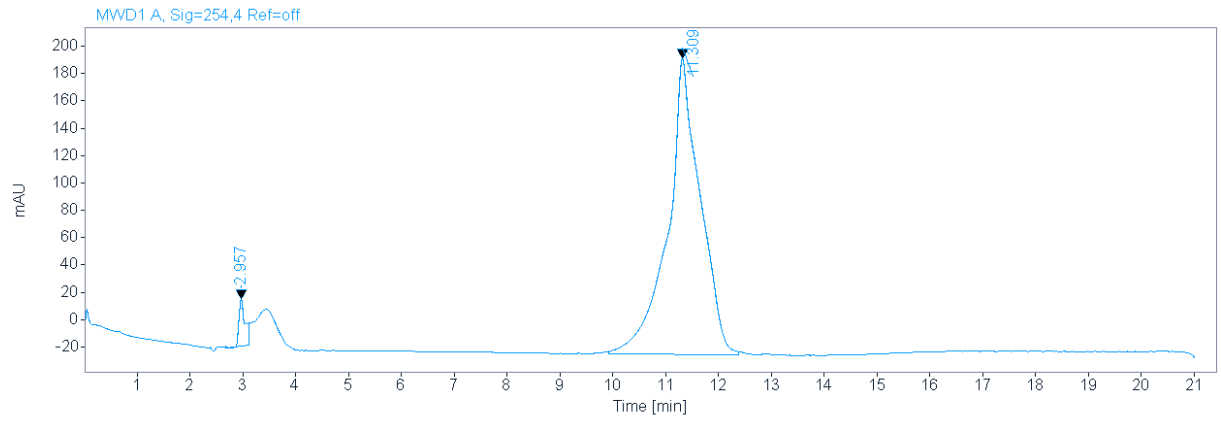
6/18/2020 6:14:25 PM

TW 142 mit HCCA gemessen.

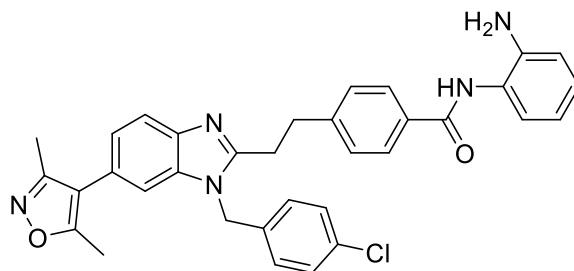
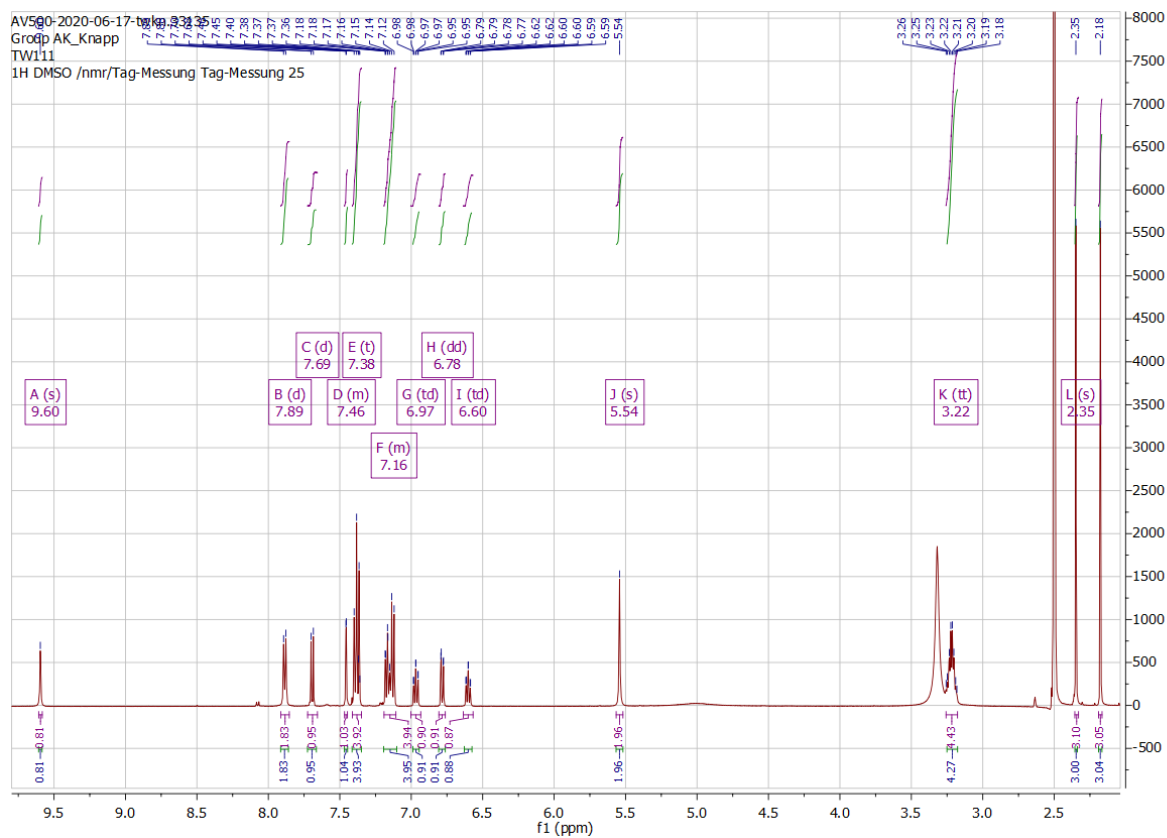
TW 142\_B6 #1-5 RT: 0.01-0.30 AV: 5 NL: 1.52E7  
T: FTMS + p MALDI Full ms [250.00-650.00]



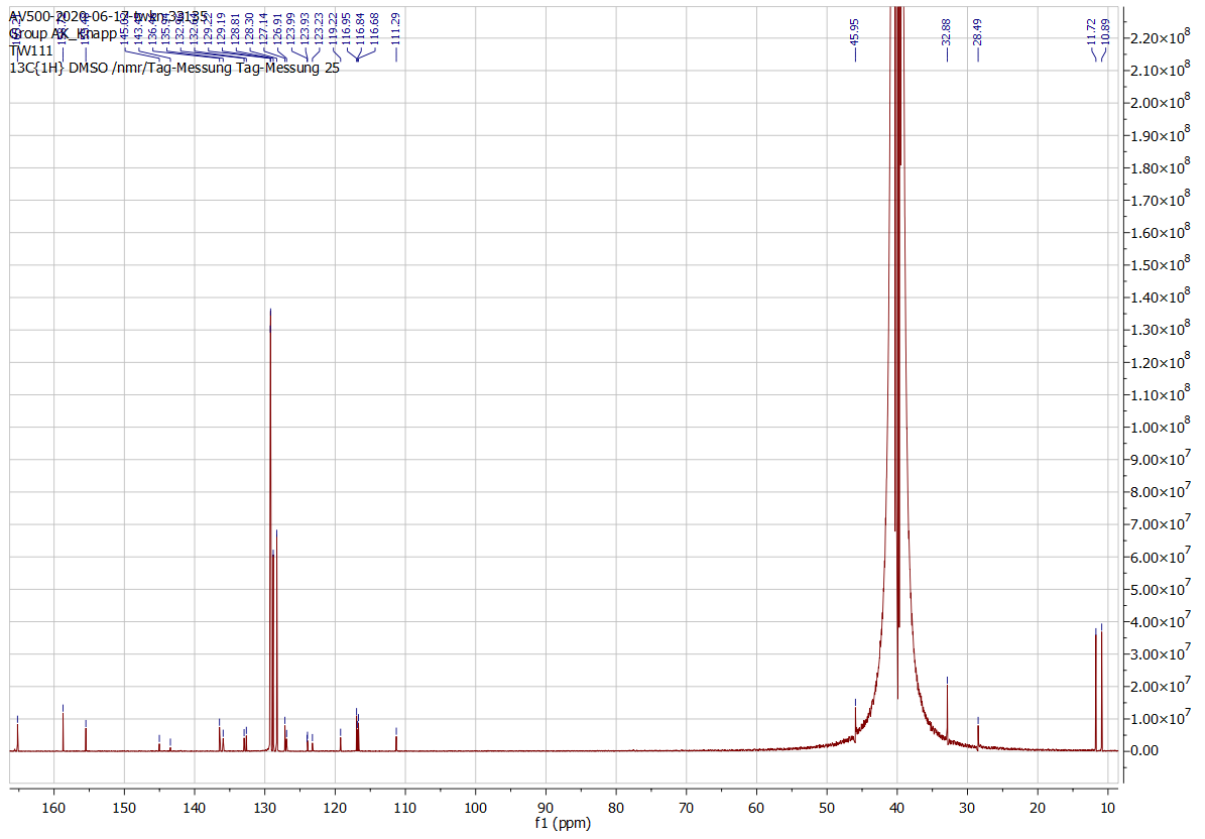
HPLC



## 9.1.14. Compound 29

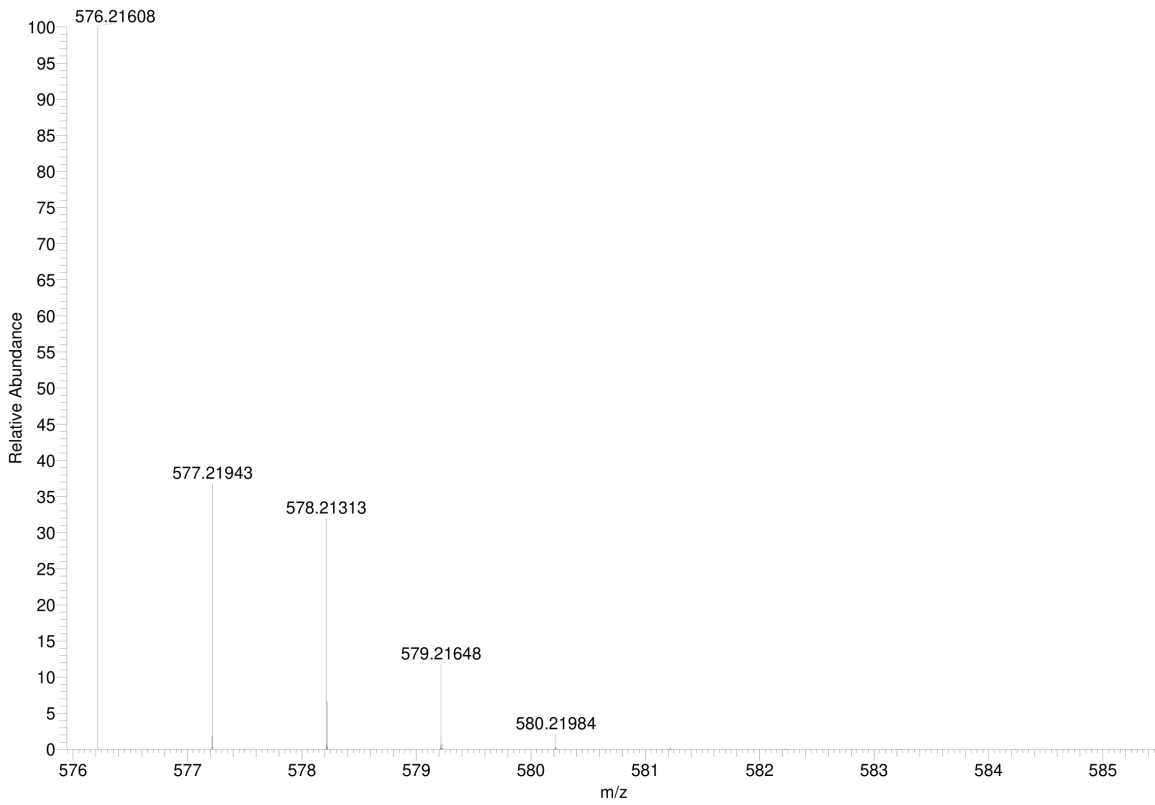
<sup>1</sup>H NMR

$^{13}\text{C}$  NMR



### Simulated HRMS

C<sub>34</sub>H<sub>30</sub>Cl<sub>1</sub>N<sub>5</sub>O<sub>2</sub> +H: C<sub>34</sub> H<sub>31</sub> Cl<sub>1</sub> N<sub>5</sub> O<sub>2</sub> pa Chrg 1



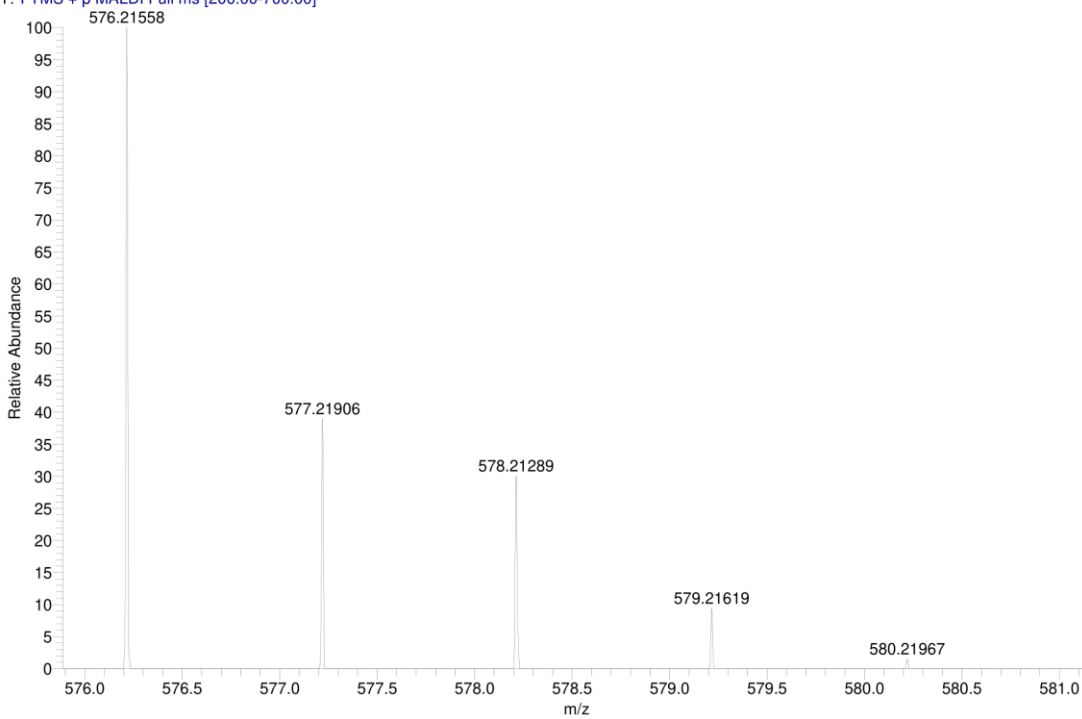
### MALDI HRMS

C:\User\...\2020\05.06.2020\TW111\_E10

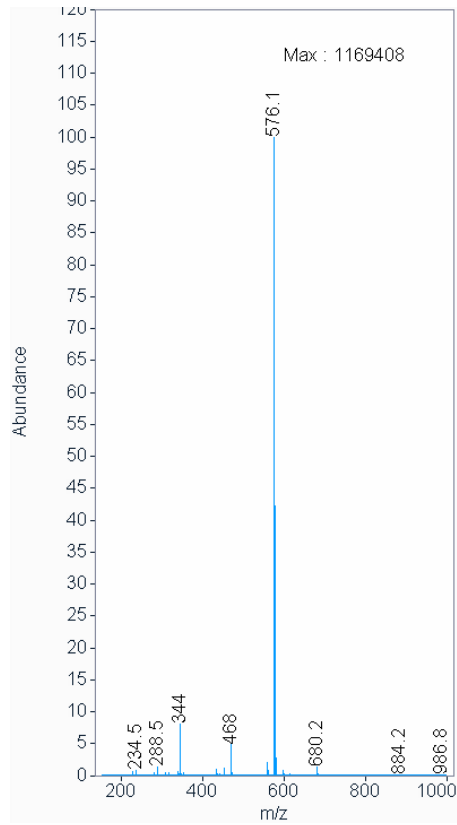
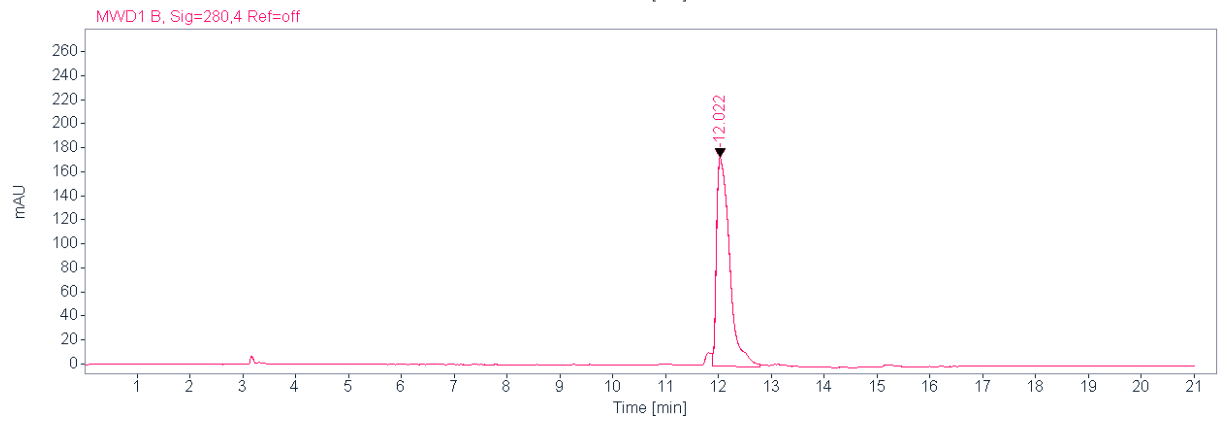
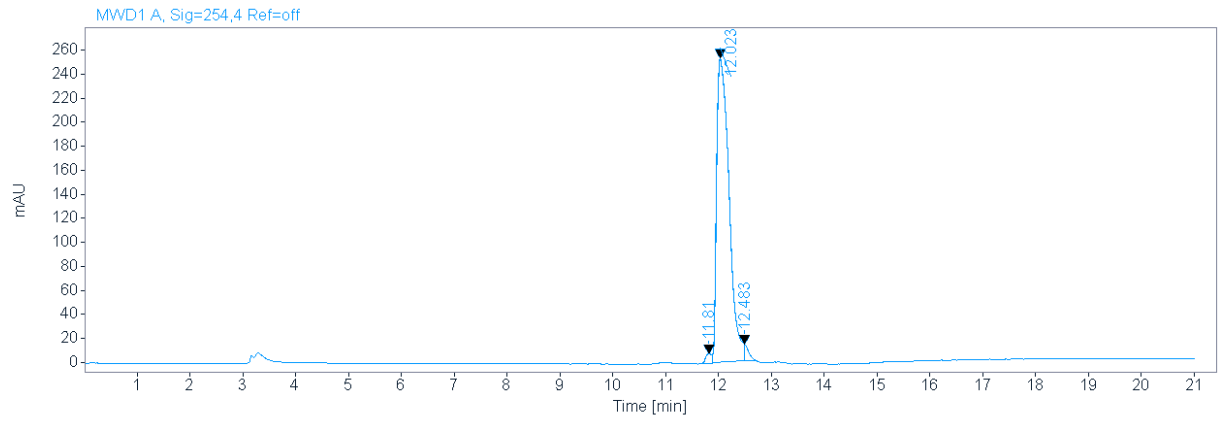
6/5/2020 9:29:45 AM

TW111 mit HCCA gemessen.

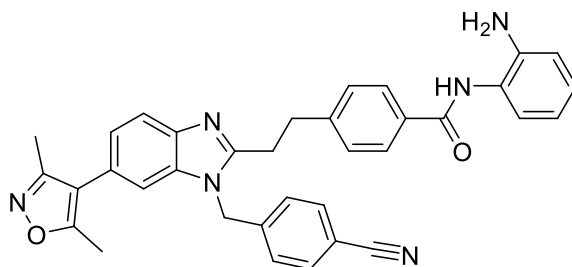
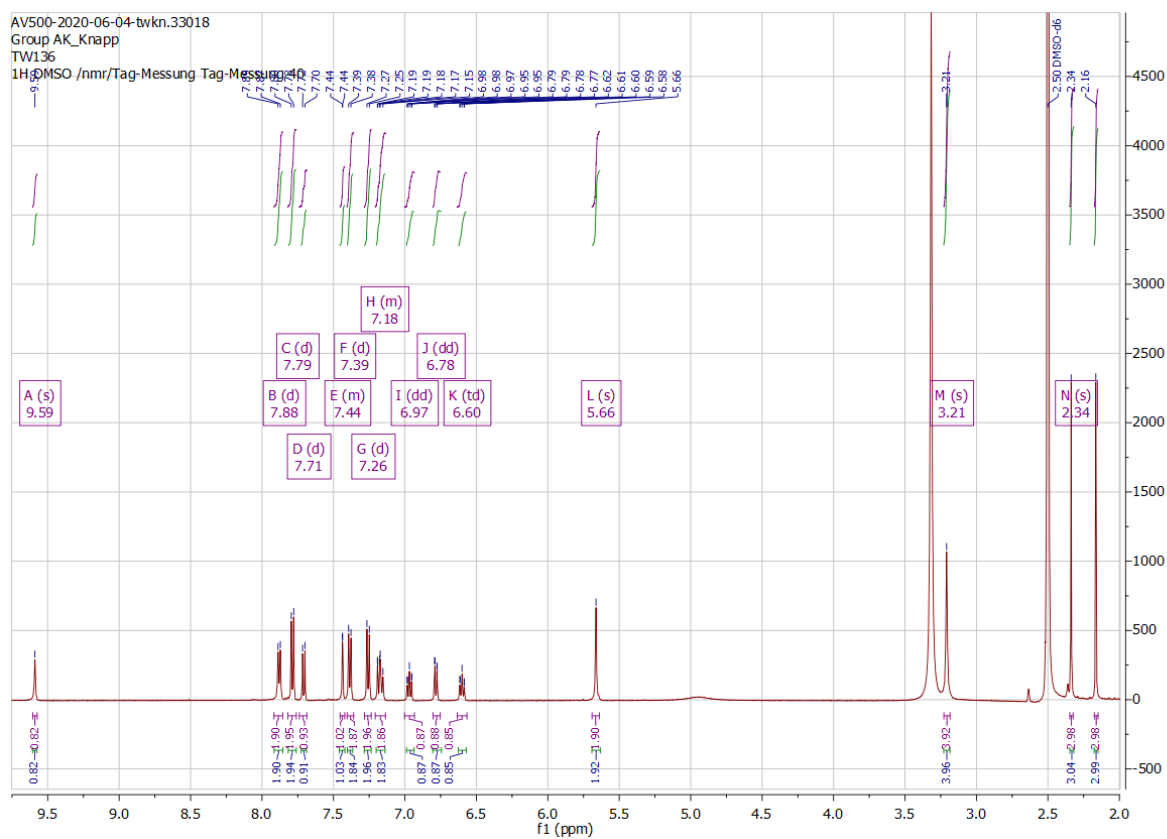
TW111\_E10 #3 RT: 0.10 AV: 1 NL: 4.37E6  
T: FTMS + p MALDI Full ms [200.00-700.00]



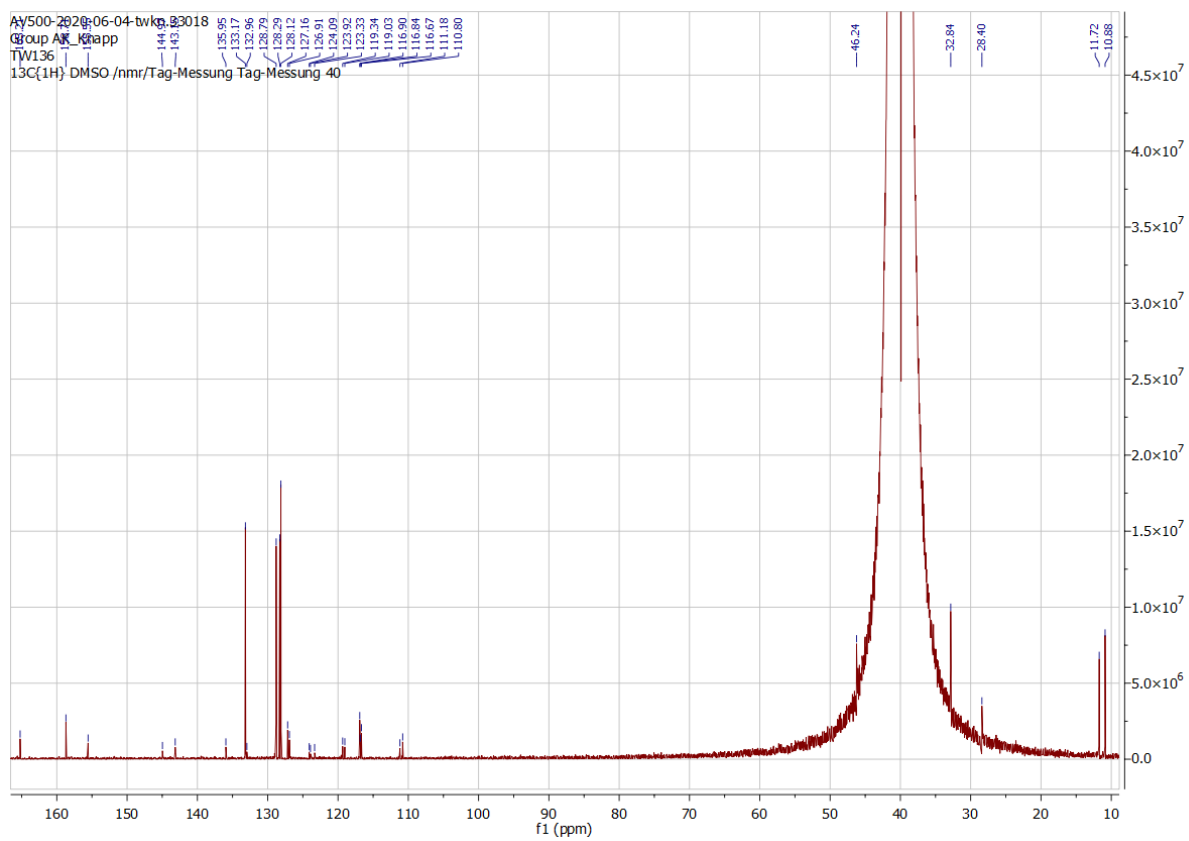
HPLC



## 9.1.15. Compound 30

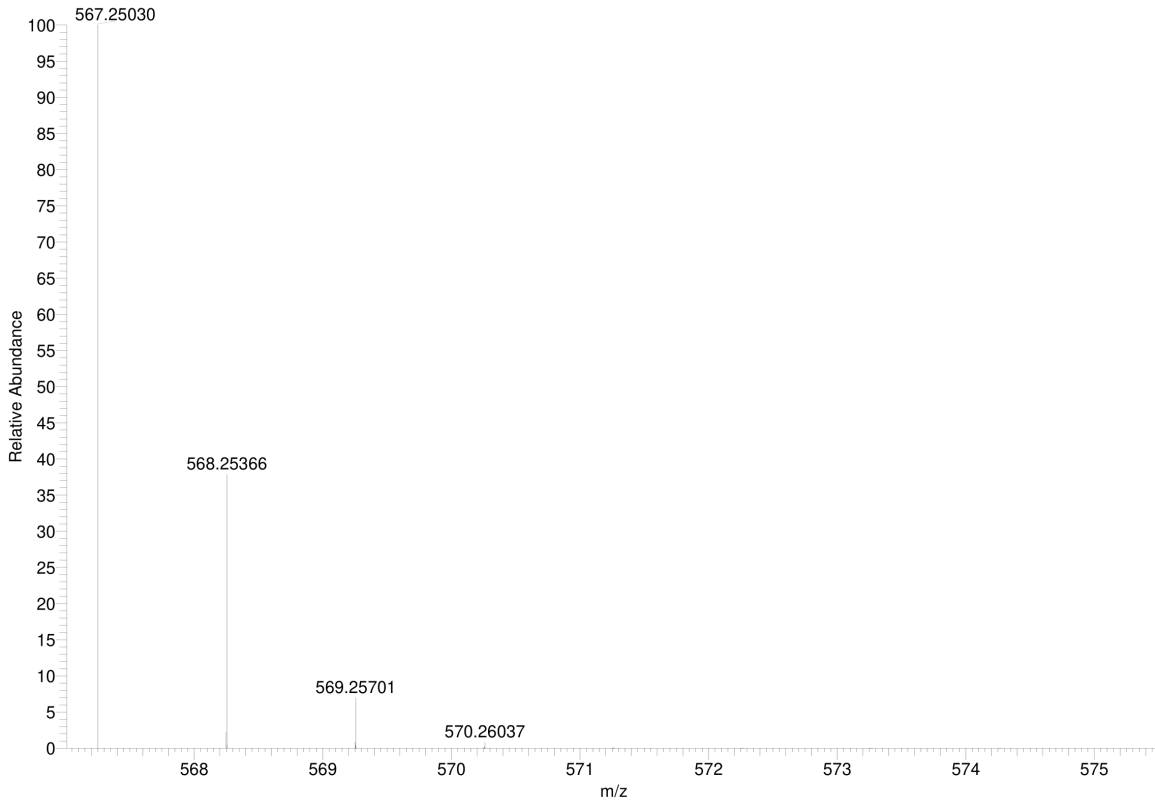
 $^1\text{H NMR}$ 



$^{13}\text{C}$  NMR

### Simulated HRMS

C<sub>35</sub>H<sub>30</sub>N<sub>6</sub>O<sub>2</sub> +H: C<sub>35</sub> H<sub>31</sub> N<sub>6</sub> O<sub>2</sub> pa Chrg 1



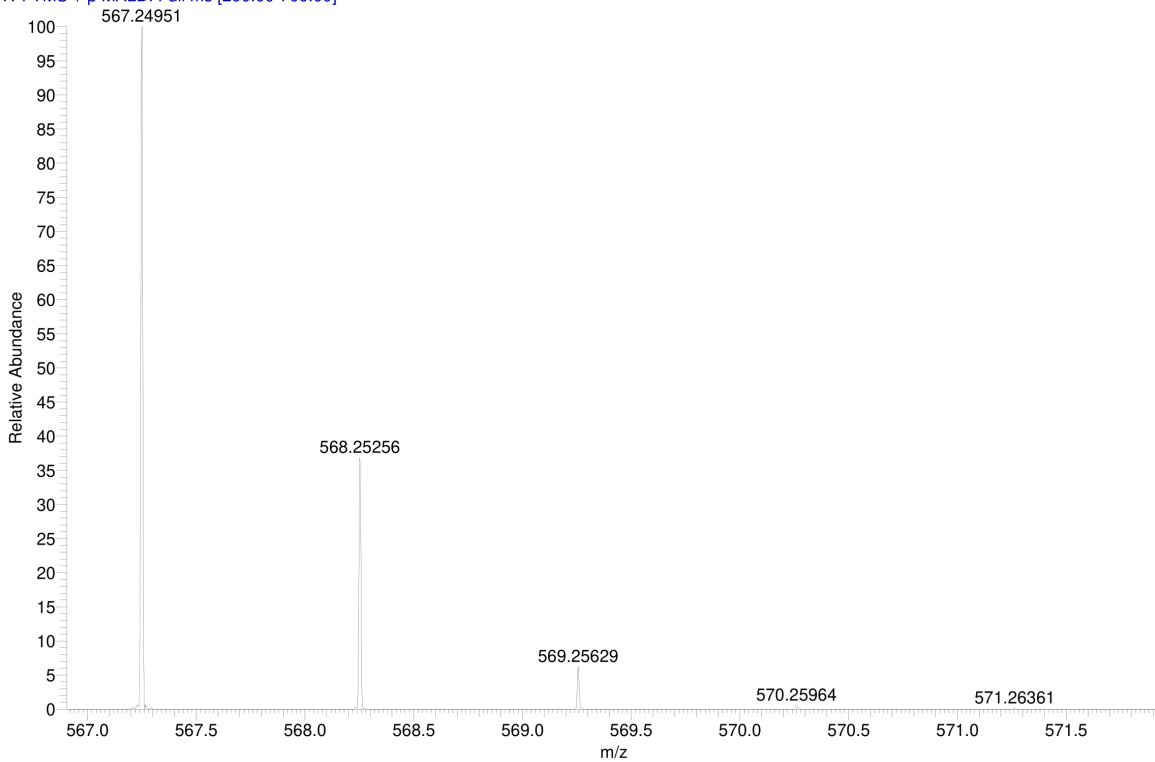
### MALDI HRMS

C:\User\...\2020\05.06.2020\TW136\_F5

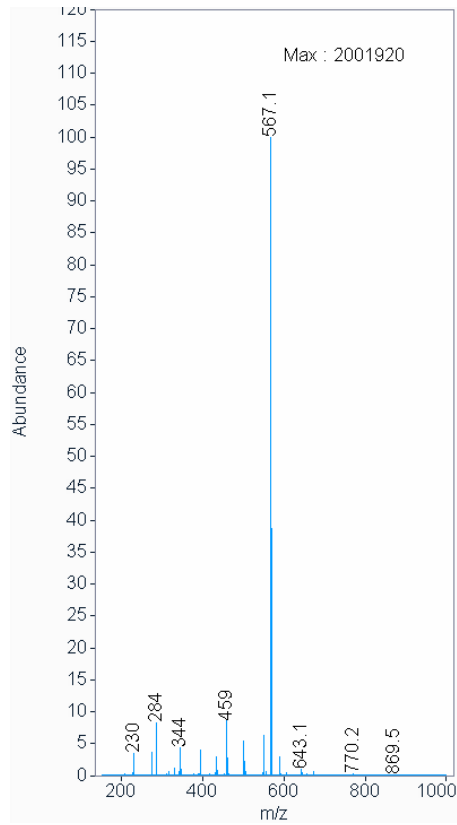
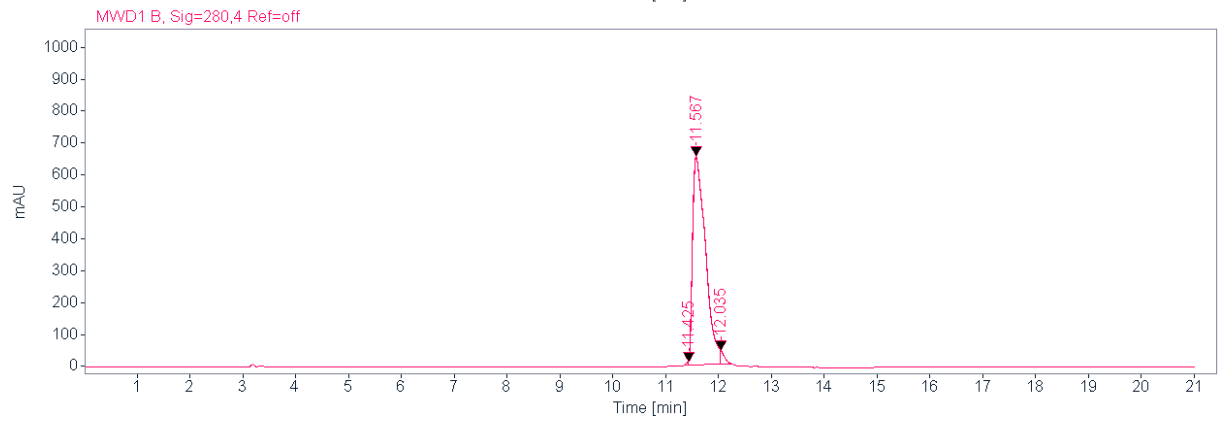
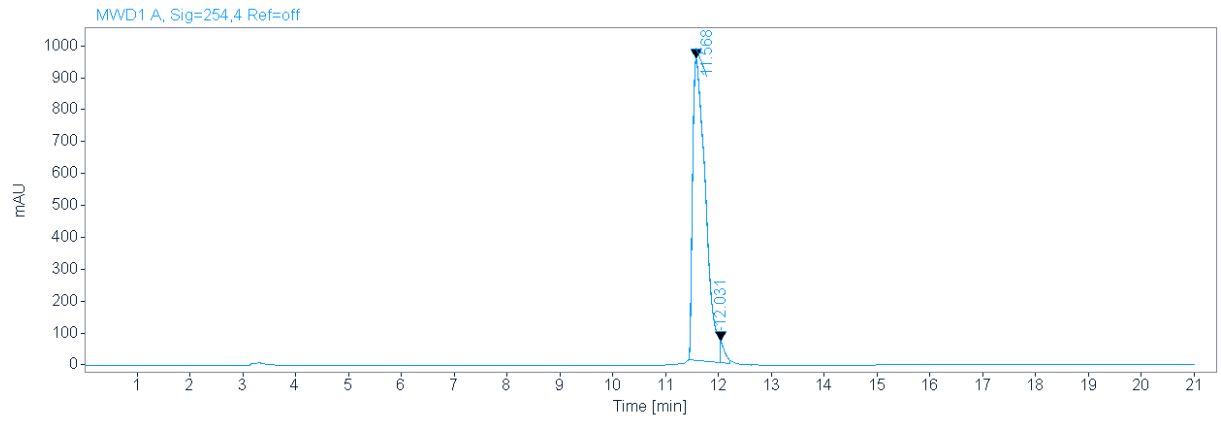
6/5/2020 9:35:17 AM

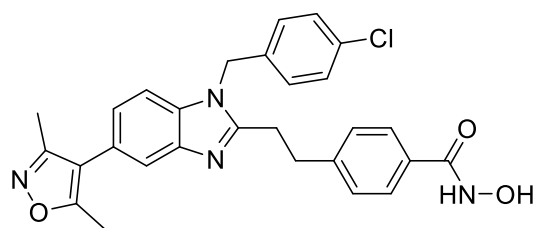
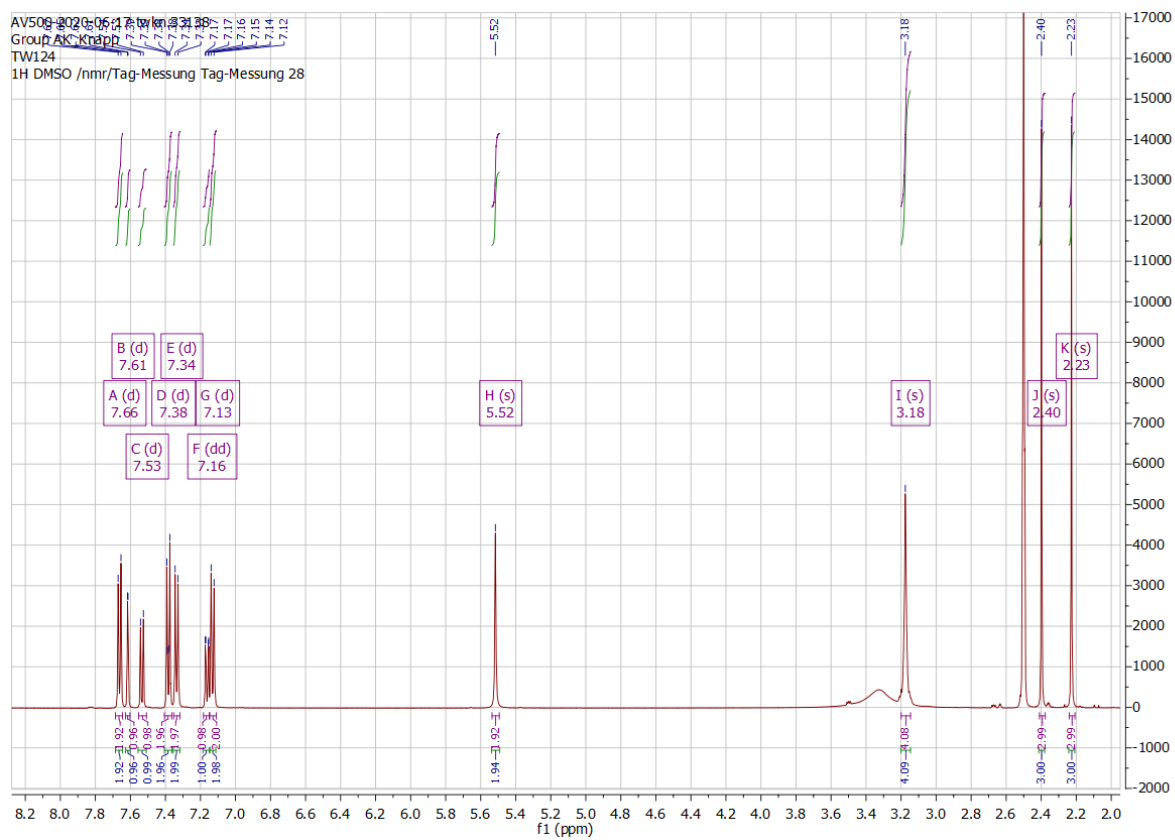
TW136 mit HCCA gemessen.

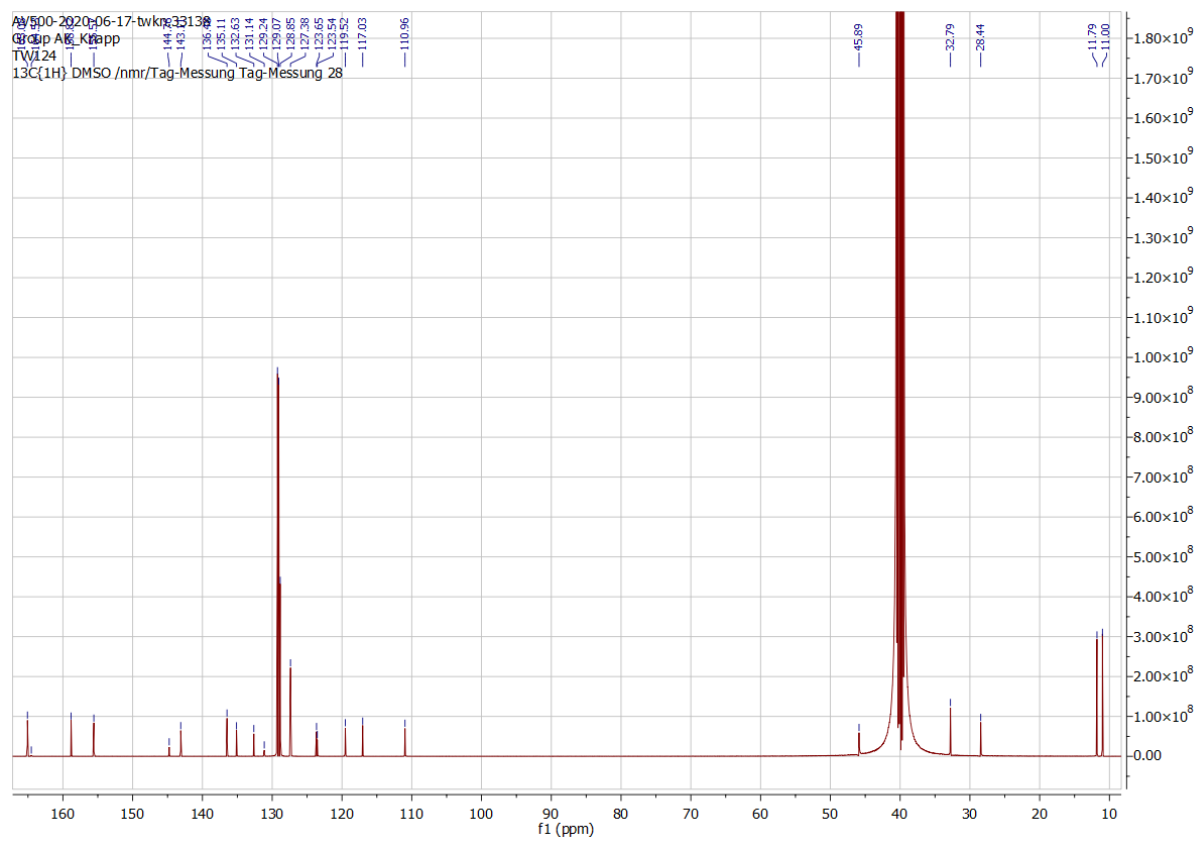
TW136\_F5 #13 RT: 0.54 AV: 1 NL: 5.35E7  
T: FTMS + p MALDI Full ms [200.00-700.00]



HPLC

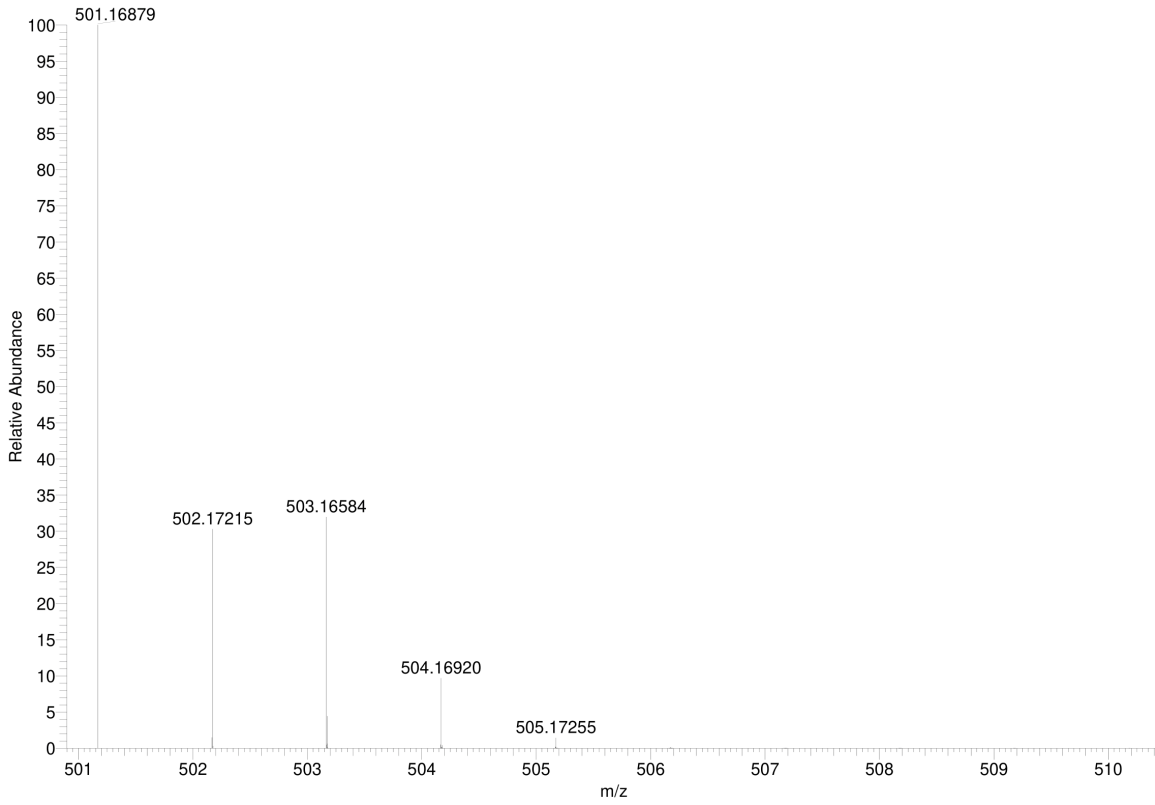


9.1.16. Compound **31**<sup>1</sup>H NMR

$^{13}\text{C}$  NMR

### Simulated HRMS

C<sub>28</sub>H<sub>25</sub>Cl<sub>1</sub>N<sub>4</sub>O<sub>3</sub> +H: C<sub>28</sub> H<sub>26</sub> Cl<sub>1</sub> N<sub>4</sub> O<sub>3</sub> pa Chrg 1



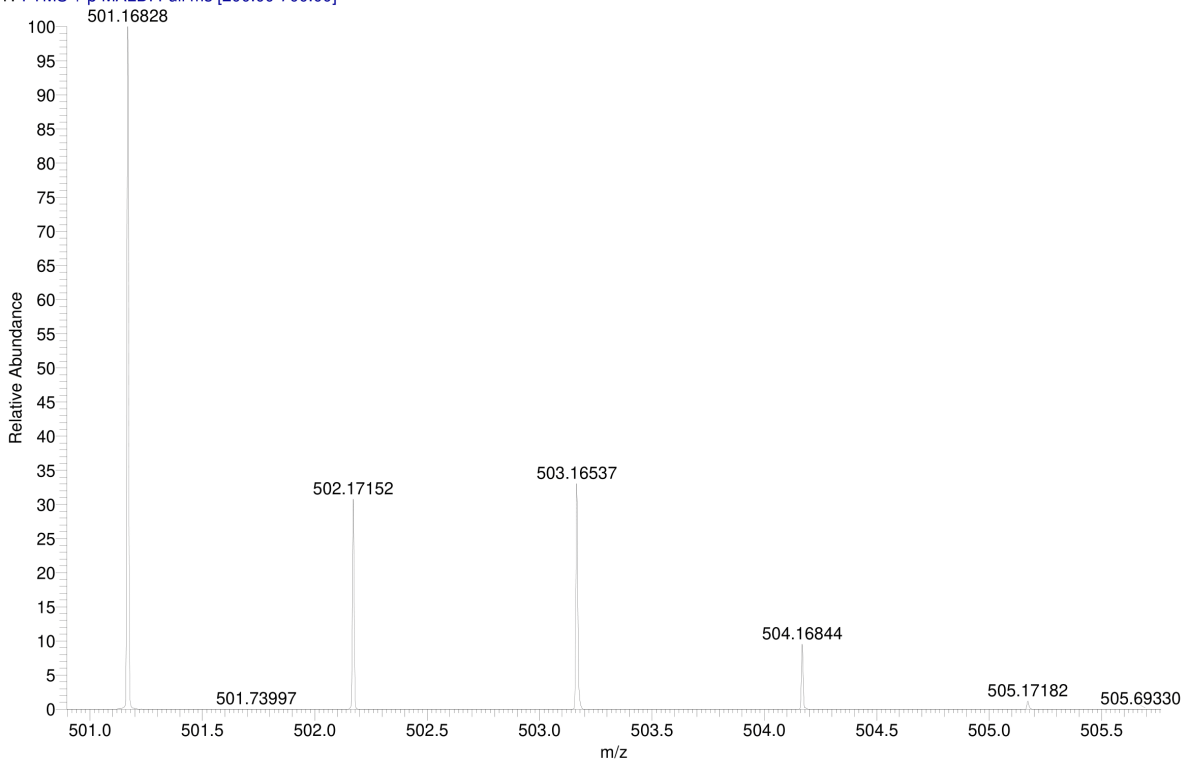
### MALDI HRMS

C:\User\...\2020\05.06.2020\TW124\_F4

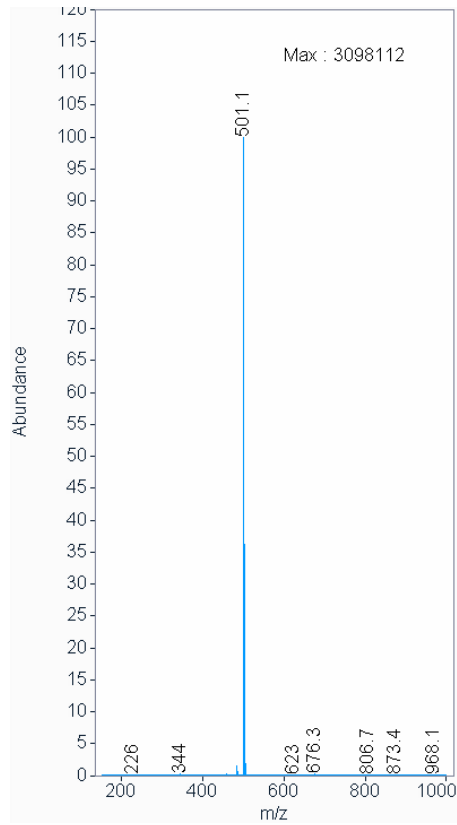
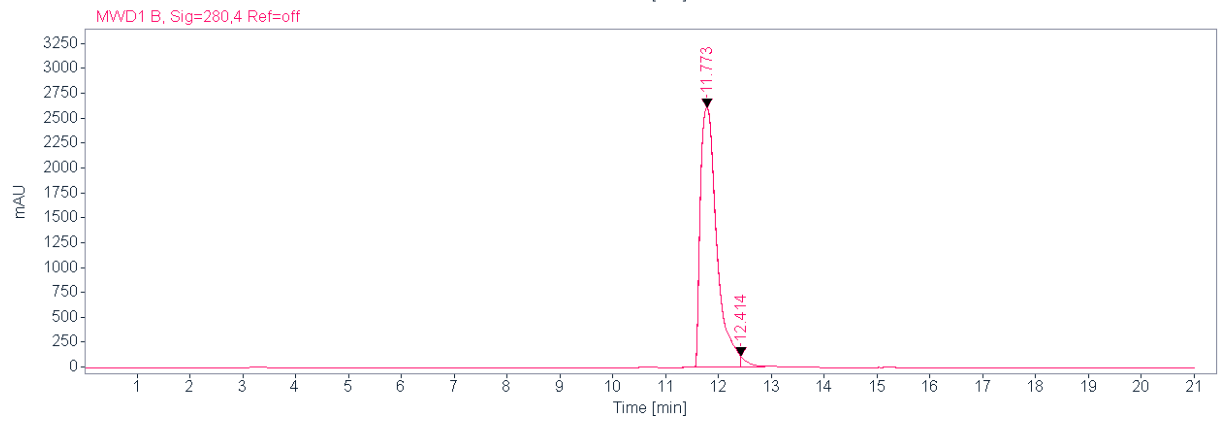
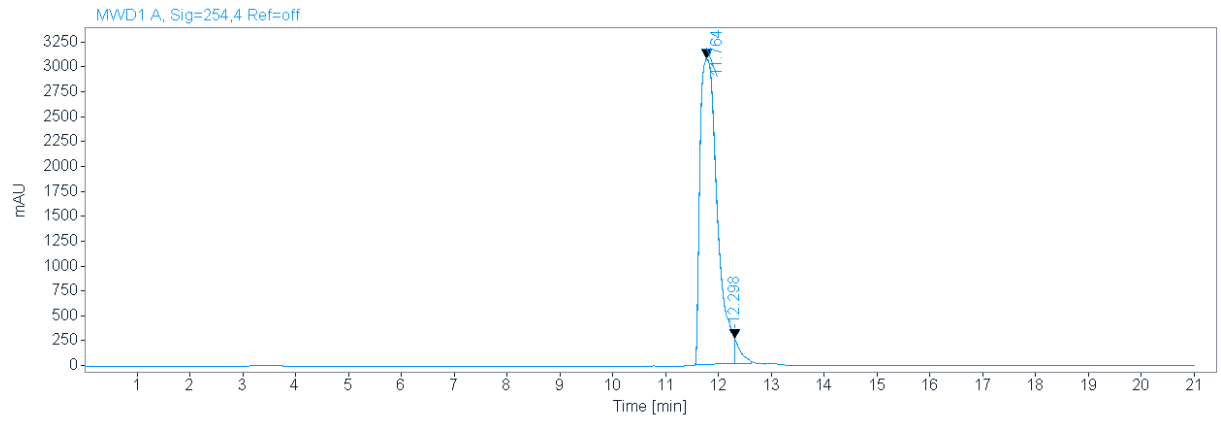
6/5/2020 9:34:08 AM

TW124 mit HCCA gemessen.

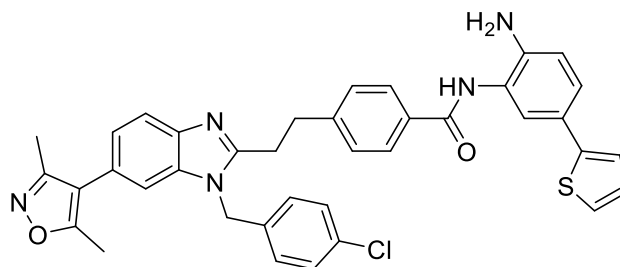
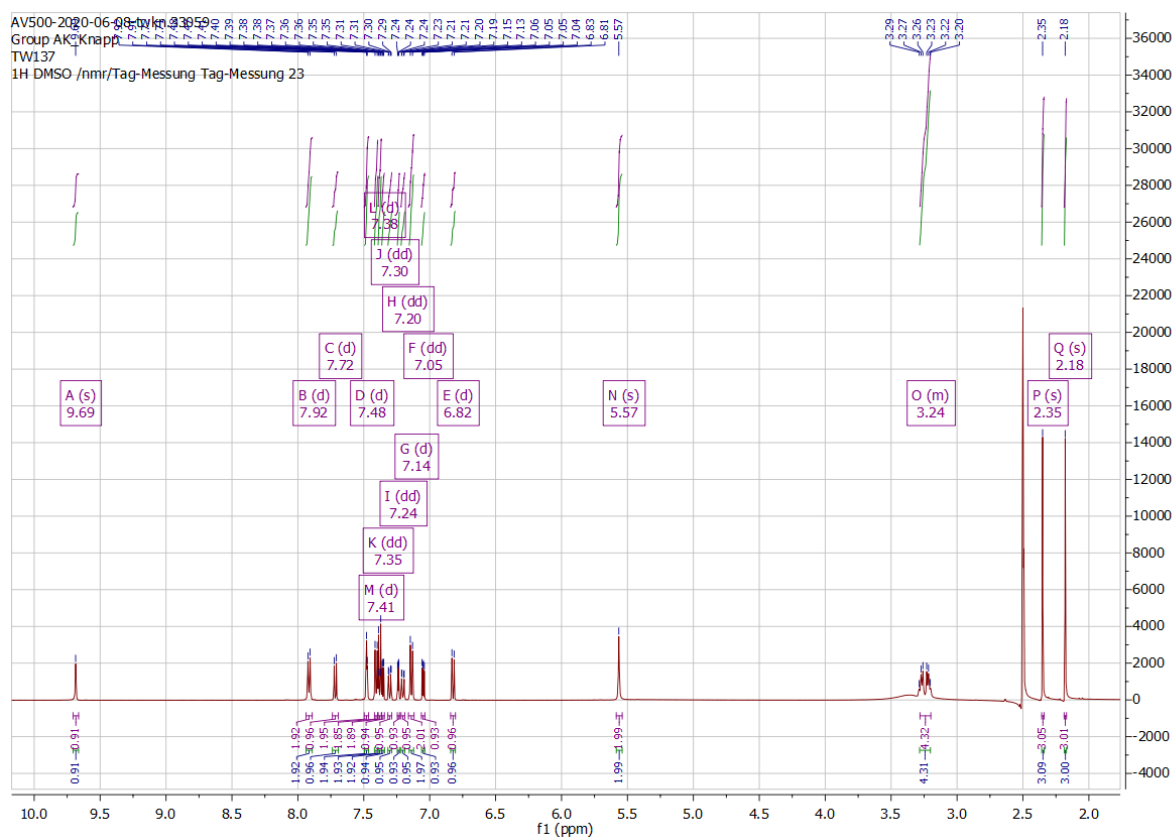
TW124\_F4 #1-12 RT: 0.01-0.50 AV: 12 NL: 3.20E7  
T: FTMS + p MALDI Full ms [200.00-700.00]



HPLC

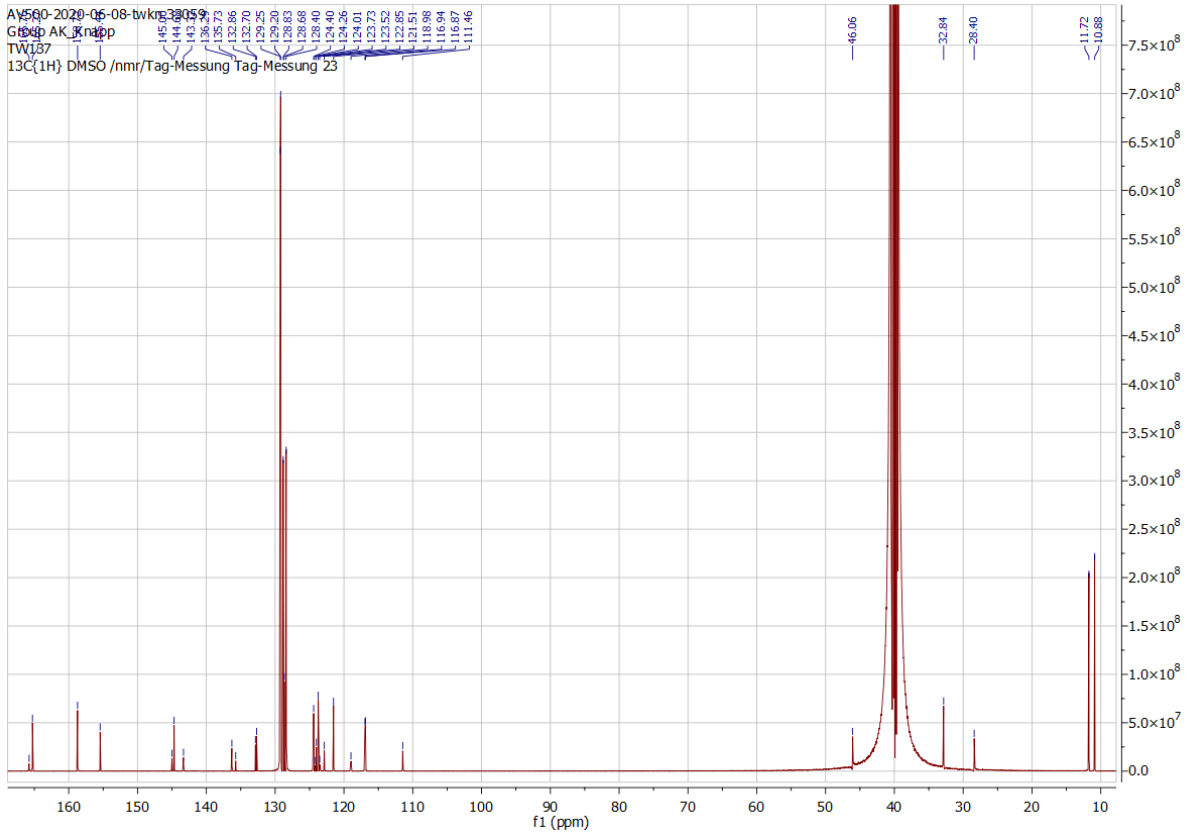


## 9.1.17. Compound 32

 $^1\text{H NMR}$ 

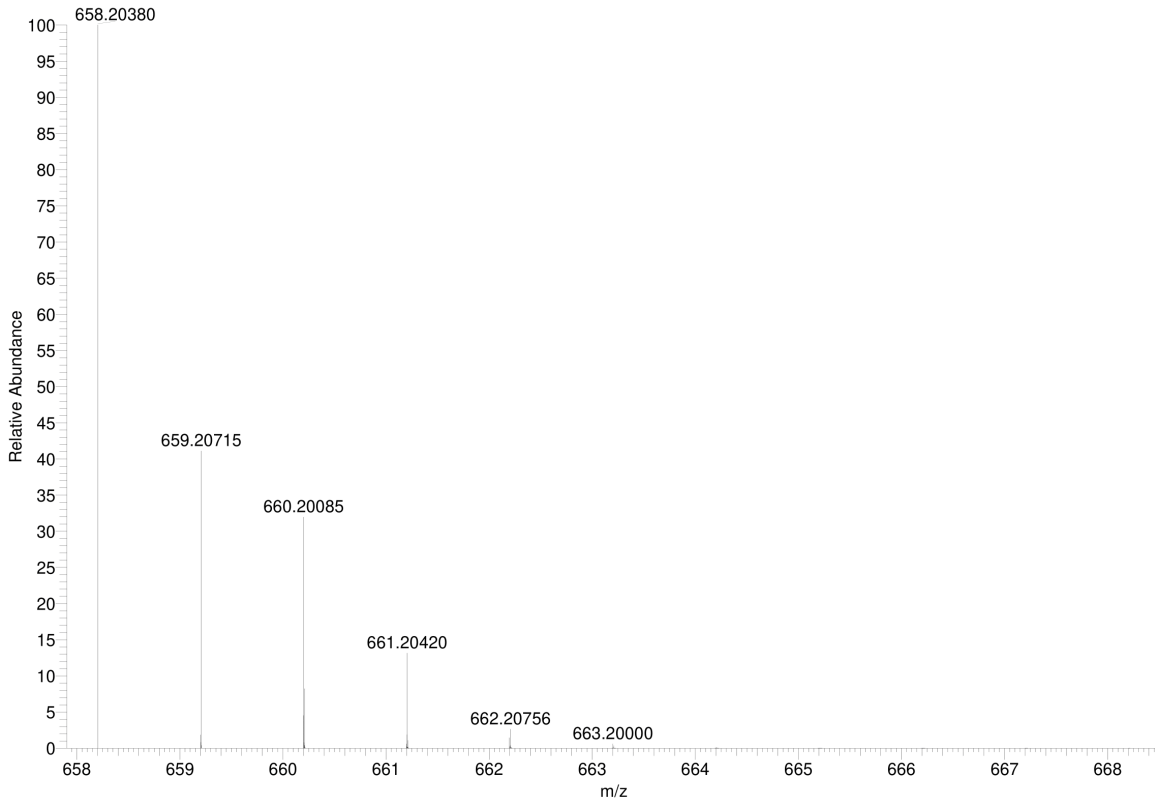


<sup>13</sup>C NMR



### Simulated HRMS

C<sub>38</sub>H<sub>32</sub>Cl<sub>1</sub>N<sub>5</sub>O<sub>2</sub>S<sub>1</sub> +H: C<sub>38</sub> H<sub>33</sub> Cl<sub>1</sub> N<sub>5</sub> O<sub>2</sub> S<sub>1</sub> pa Chrg 1



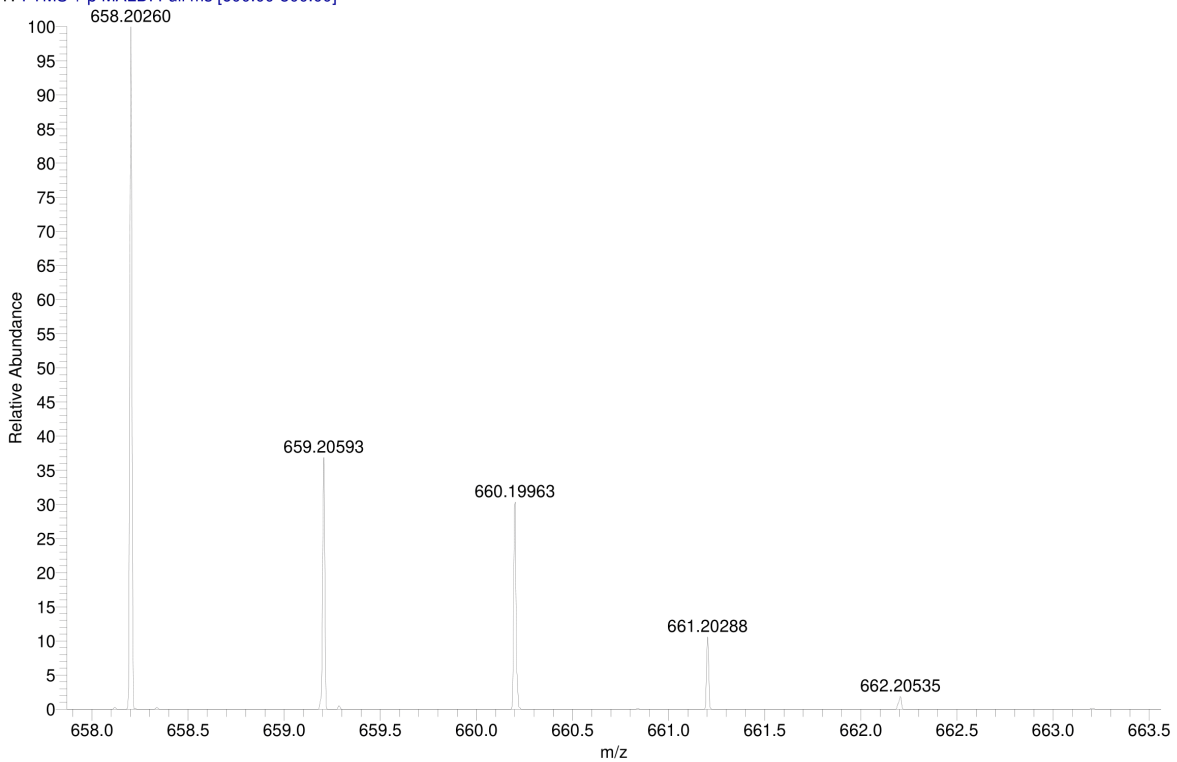
### MALDI HRMS

C:\User\...\2020\09.06.2020\TW137\_A1

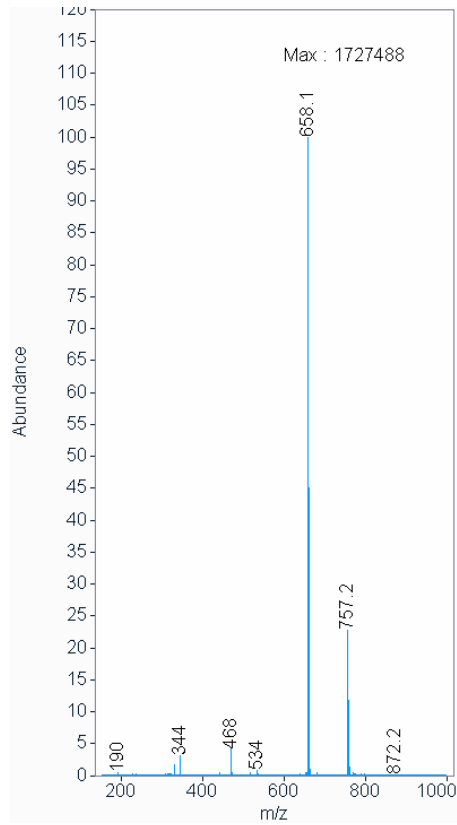
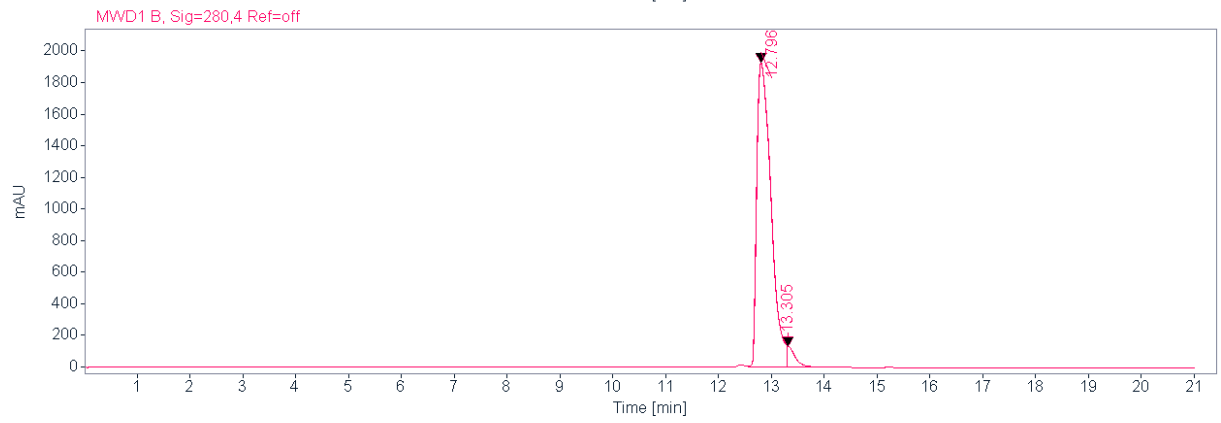
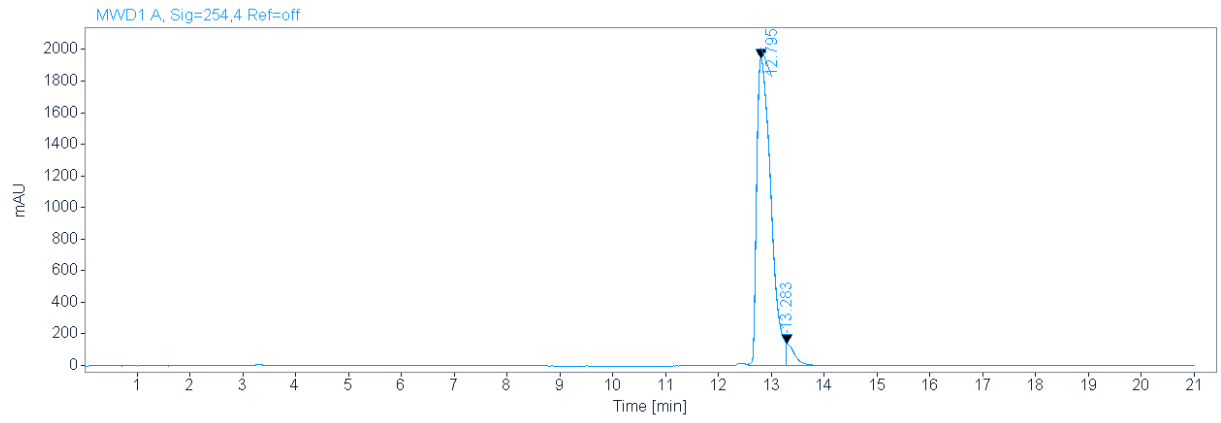
6/9/2020 8:21:22 PM

TW137 mit HCCA gemessen.

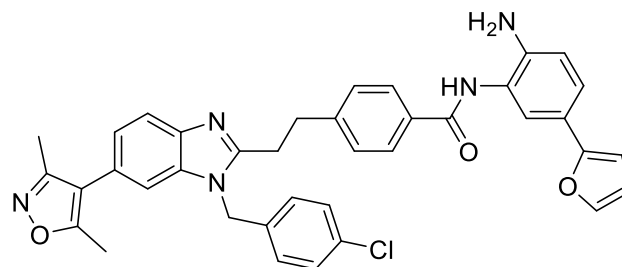
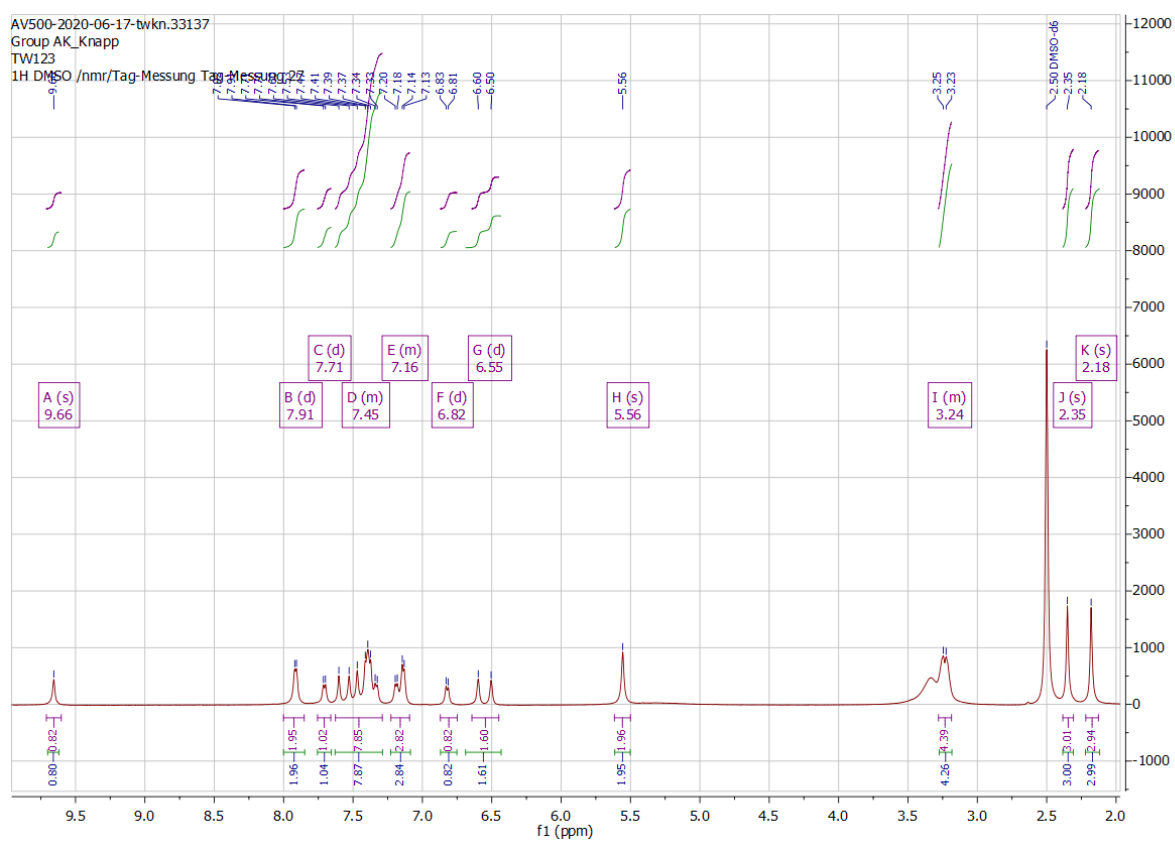
TW137\_A1 #1-6 RT: 0.00-0.22 AV: 6 NL: 9.40E6  
T: FTMS + p MALDI Full ms [600.00-800.00]

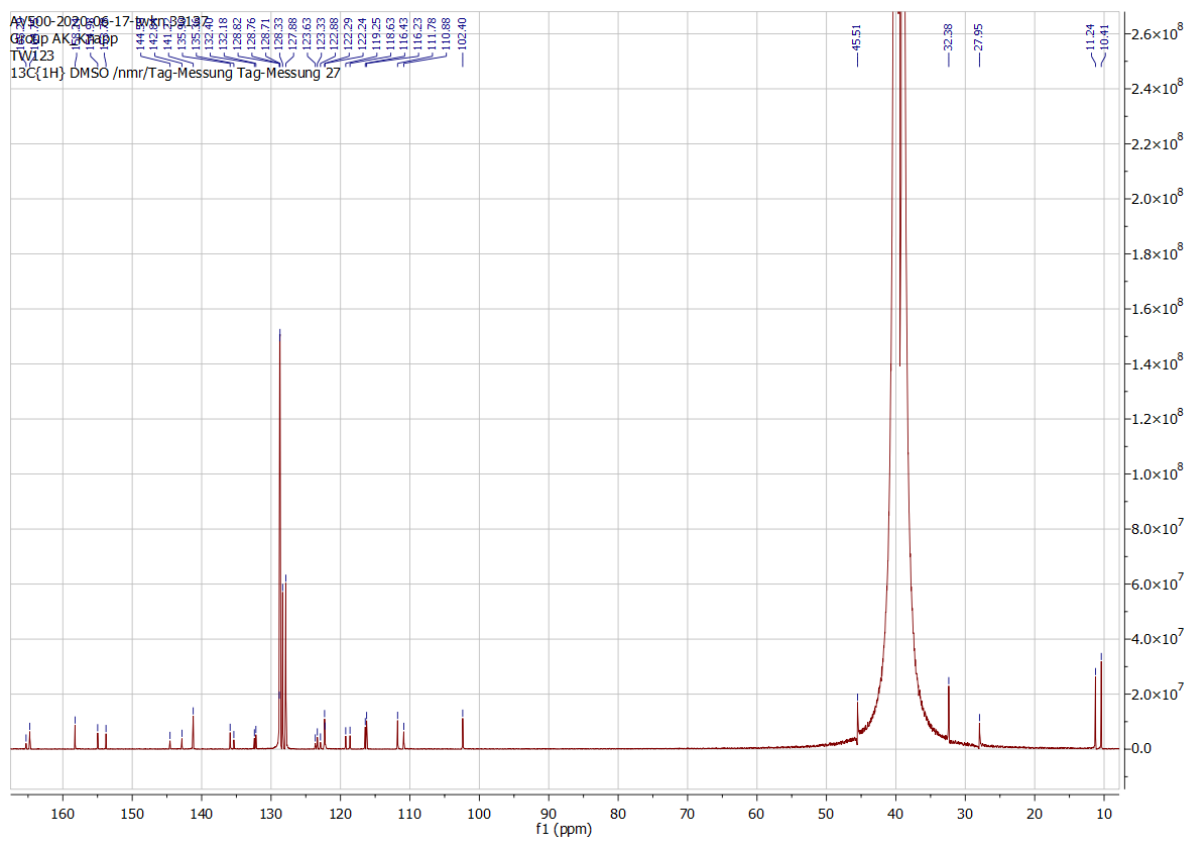


HPLC



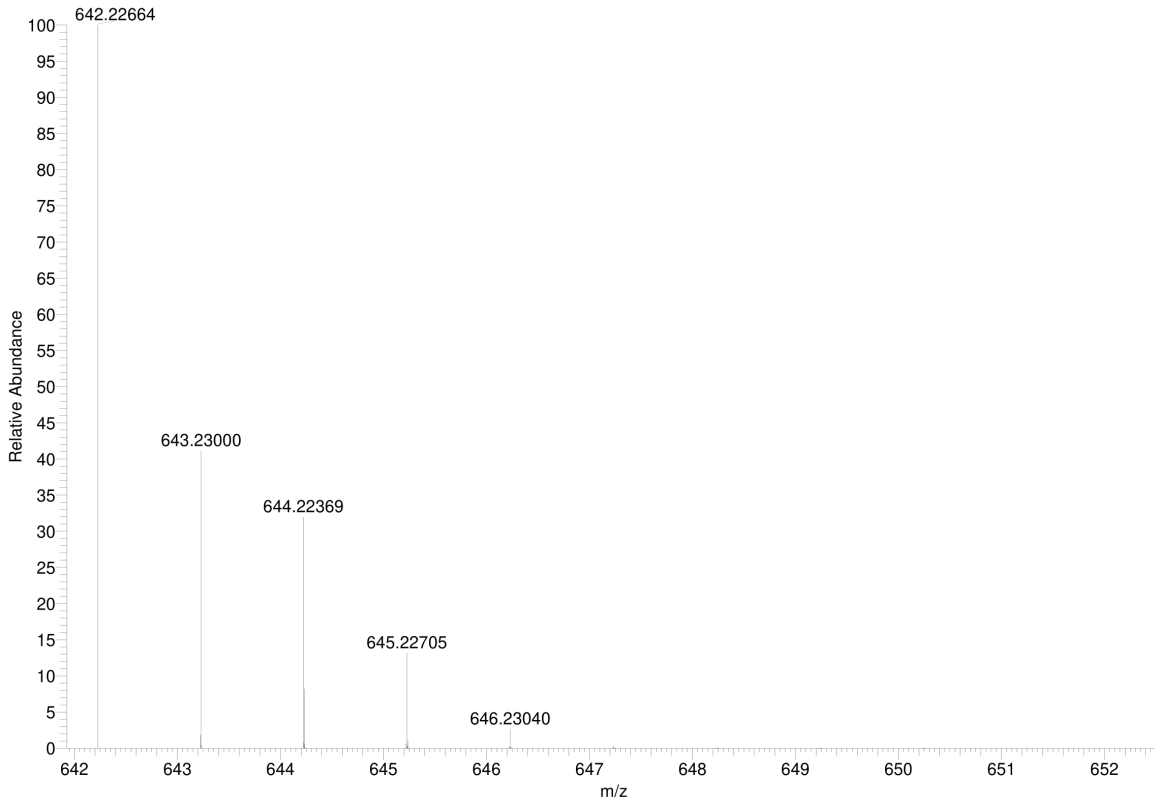
## 9.1.18. Compound 33

 $^1\text{H}$  NMR

$^{13}\text{C}$  NMR

### Simulated HRMS

C<sub>38</sub>H<sub>32</sub>Cl<sub>1</sub>N<sub>5</sub>O<sub>3</sub> +H: C<sub>38</sub> H<sub>33</sub> Cl<sub>1</sub> N<sub>5</sub> O<sub>3</sub> pa Chrg 1



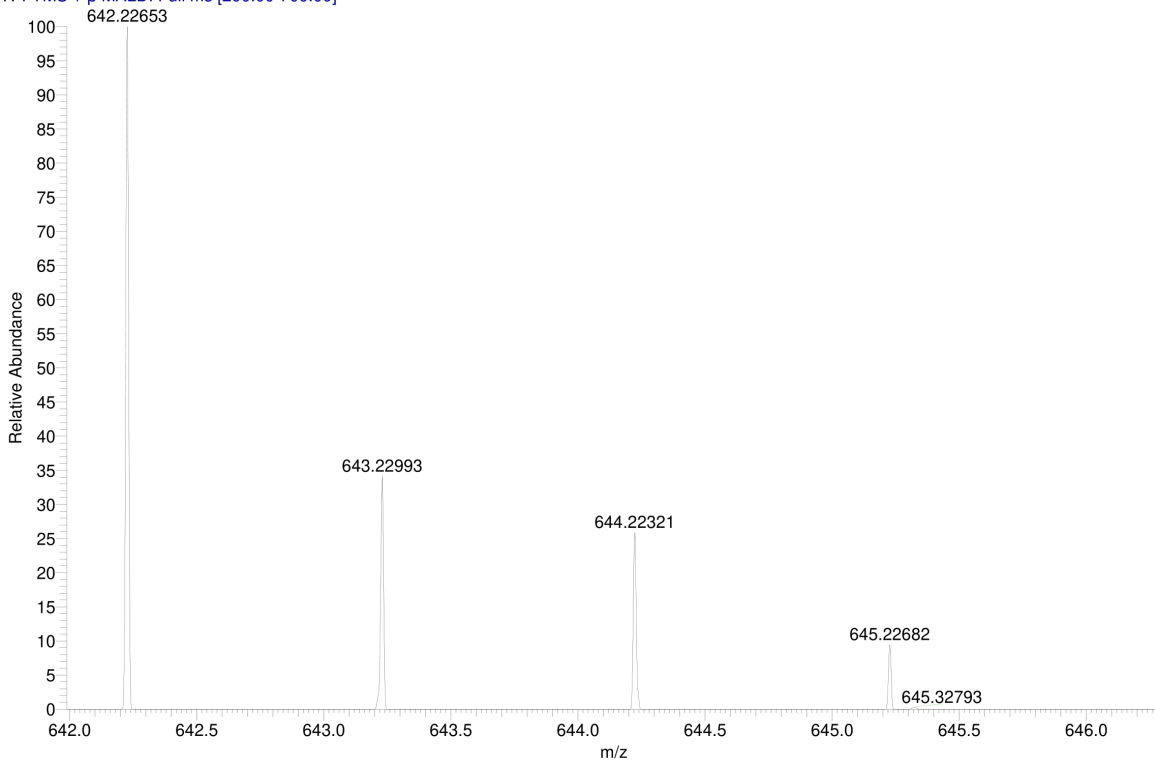
### MALDI HRMS

C:\User\...\2020\05.06.2020\TW123\_E12

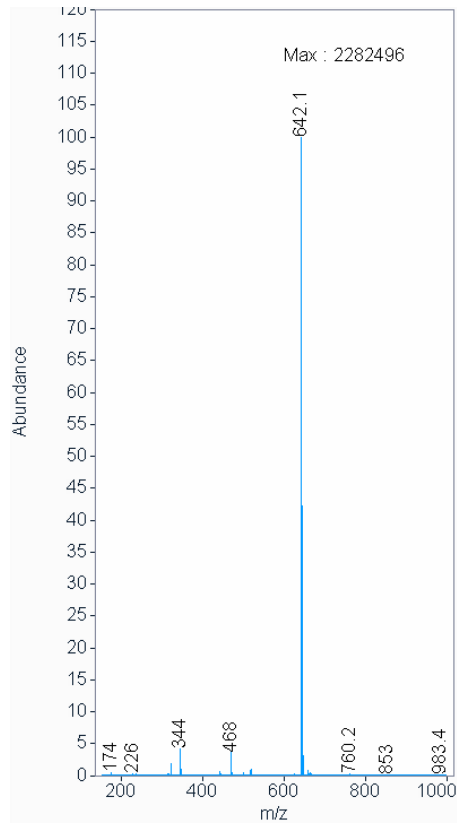
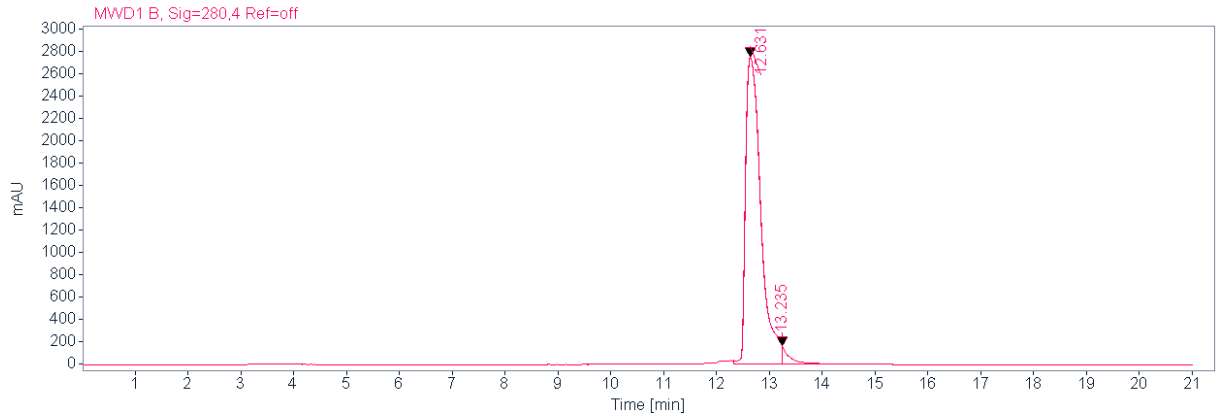
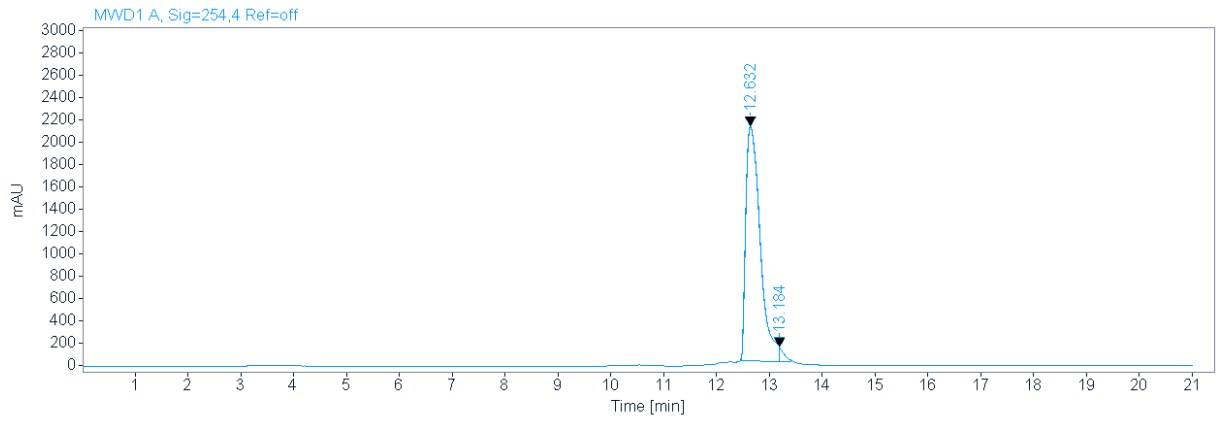
6/5/2020 9:32:22 AM

TW123 mit HCCA gemessen

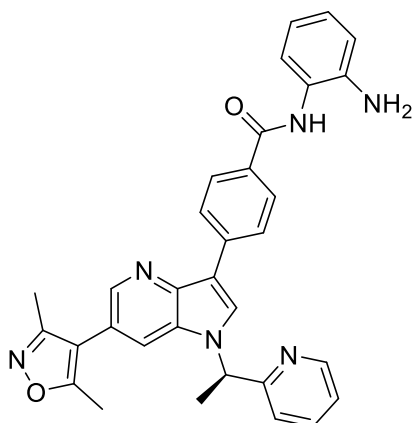
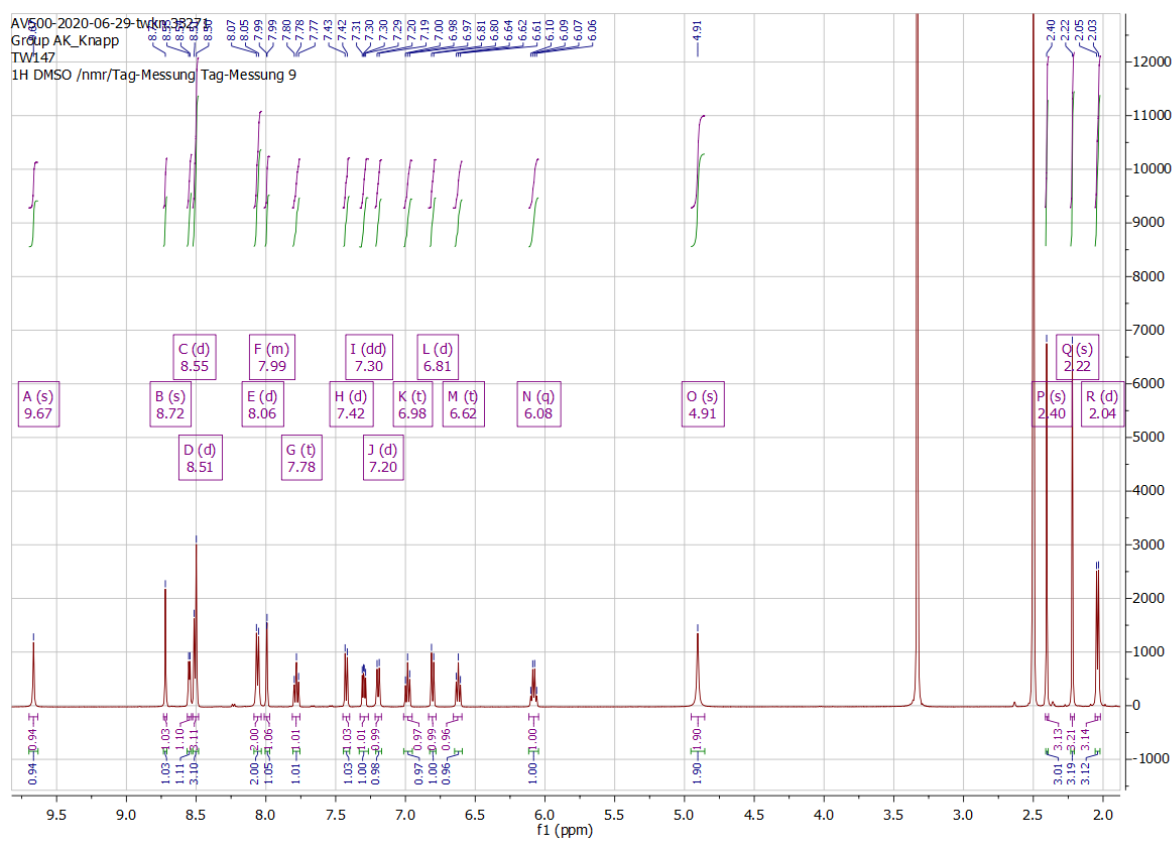
TW123\_E12 #1-18 RT: 0.01-0.75 AV: 18 NL: 1.21E6  
T: FTMS + p MALDI Full ms [200.00-700.00]



HPLC

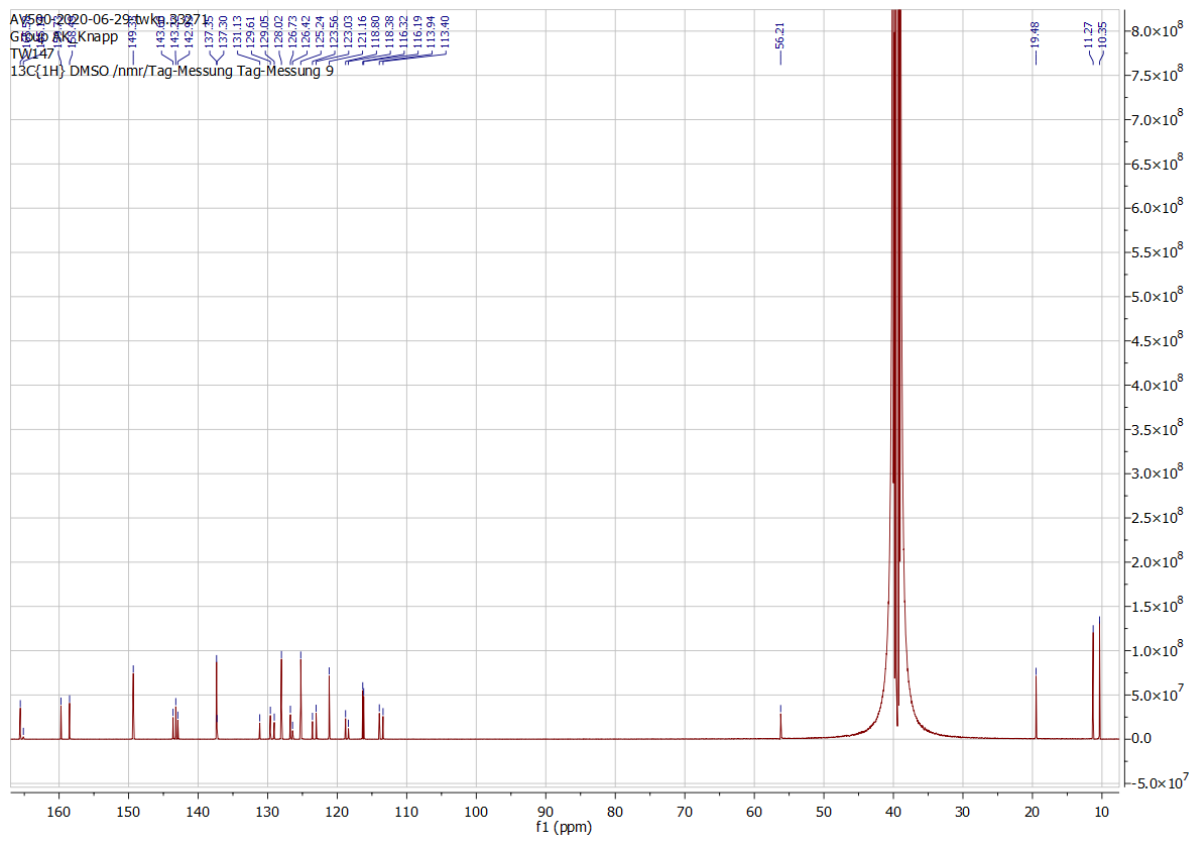


## 9.1.19. Compound 37

<sup>1</sup>H NMR

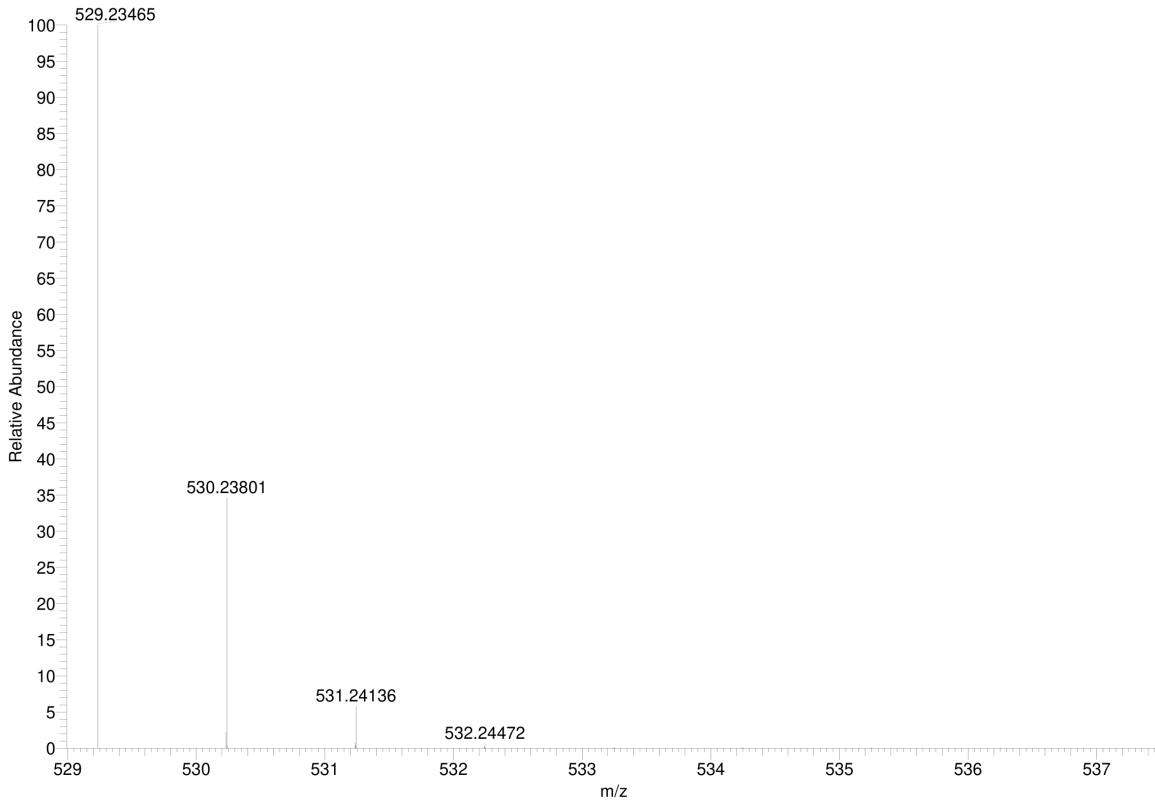


<sup>13</sup>C NMR



### Simulated HRMS

C<sub>32</sub>H<sub>28</sub>N<sub>6</sub>O<sub>2</sub> +H: C<sub>32</sub> H<sub>29</sub> N<sub>6</sub> O<sub>2</sub> pa Chrg 1



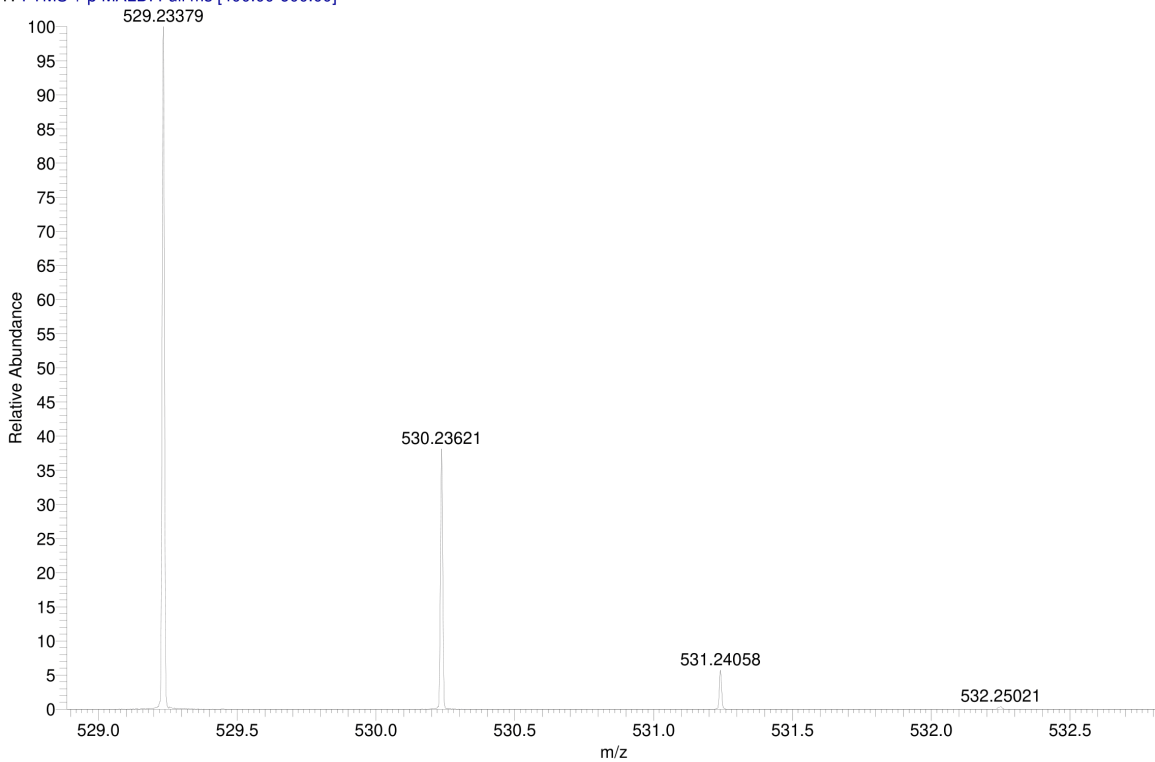
### MALDI HRMS

C:\User\...\2020\01.07.2020\TW147\_A7

7/1/2020 6:17:18 PM

TW147 mit HCCA gemessen

TW147\_A7 #1-3 RT: 0.01-0.23 AV: 3 NL: 2.15E7  
T: FTMS + p MALDI Full ms [400.00-600.00]



HPLC

